

Electronic Thesis and Dissertation Repository

---

2-4-2018 3:00 PM

## Developing Structure-Activity-Relationships for Metal-Ligand-Cooperative (MLC) Complexes using PR<sub>2</sub>NR'<sub>2</sub> Ligands

James M. Stubbs, *The University of Western Ontario*

Supervisor: Blacquiere, Johanna M., *The University of Western Ontario*

A thesis submitted in partial fulfillment of the requirements for the Doctor of Philosophy degree in Chemistry

© James M. Stubbs 2018

Follow this and additional works at: <https://ir.lib.uwo.ca/etd>

 Part of the [Inorganic Chemistry Commons](#)

---

### Recommended Citation

Stubbs, James M., "Developing Structure-Activity-Relationships for Metal-Ligand-Cooperative (MLC) Complexes using PR<sub>2</sub>NR'<sub>2</sub> Ligands" (2018). *Electronic Thesis and Dissertation Repository*. 6011. <https://ir.lib.uwo.ca/etd/6011>

This Dissertation/Thesis is brought to you for free and open access by Scholarship@Western. It has been accepted for inclusion in Electronic Thesis and Dissertation Repository by an authorized administrator of Scholarship@Western. For more information, please contact [wlsadmin@uwo.ca](mailto:wlsadmin@uwo.ca).

## Abstract

Exploring efficient and environmentally-friendly routes to synthesize molecules is critical for the pharmaceutical and fine chemical industries. One method is to study current catalytic methods to increase selectivity and performance for challenging reactions. Inclusion of an intramolecular acid/base site on the ligand of an organometallic complex has allowed for new mechanistic pathways and enhanced reactivity. This thesis delves into understanding organometallic complexes in catalysis by systematic tuning the ligand properties. Synthesis of  $P^R_2N^{R'}_2$  ligands was performed to enable the systematic tuning as R and R' alter the electronic and steric properties of the primary and secondary coordination sphere, respectively. Metalation of  $P^R_2N^{R'}_2$  ligands with Ru gave a series of MLC proton shuttling complexes for catalytic testing. From catalytic performance, structure-activity relationships were extracted for two types of reactions that exploit a proton shuttling relay: 1) the intramolecular cyclization of ethynyl amine and alcohol substrates; and 2) the acceptorless dehydrogenation of amines. Optimization for cyclization of ethynyl amines revealed sterically bulky, electron rich Ru complexes operate at turnover frequencies of above  $1500\text{ h}^{-1}$  and reach turnovers of 800, both significantly better than previous systems. Optimization for acceptorless dehydrogenation of indolines has shown sterically bulky phosphines to be beneficial. Furthermore, in both acceptorless dehydrogenation of amines and cyclization of ethynyl amines the acid/base site of the secondary coordination sphere displays a significant effect on catalytic performance. Pendent amines within the secondary coordination sphere operate best when tuned to have the same approximate basicity as the target substrate. Mechanistic analysis of both reactions revealed key catalyst deactivation routes occur as a function of the pendent amine. These findings allow for structure-activity relationships to be developed for the next generation of proton shuttling catalysts.

## Keywords

Organometallic • Homogenous Catalysis • Green Chemistry • MLC Catalysis • Acceptorless Dehydrogenation • Intramolecular Cyclization • Structure Activity Relationships • Ligand Design • Proton Shuttling

## Co-Authorship Statement

This thesis includes work from three previously published manuscripts in Chapters 2, 3, and 5. Manuscripts of the work described in chapters 4 and 5 are in preparation and will be submitted shortly.

Chapter 1 and Chapter 7 were written by JMS and edited by JMB.

The article presented in Chapter 2 was co-authored by: J. M. Stubbs, J. P. J. Bow, R. J. Hazlehurst, and J. M. Blacquiere.<sup>1</sup> JMS performed all of the synthetic and characterization work except for the optimization solvent and catalyst loadings (ca. 25% of experimental work), which was performed by JPJB. RJH collected and solved the X-ray crystallographic data. The manuscript was prepared by JMS and edited by JMB.

The article presented in Chapter 3 was co-authored by: J. M. Stubbs, D. E. Chapple, P. D. Boyle, and J. M. Blacquiere.<sup>2</sup> JMS performed all of the synthetic and characterization work except for the optimization of solvent for catalysis (ca. 5% of experimental work). PDB collected and solved the X-ray crystallographic data one of the four crystal structures. The manuscript was prepared by JMS and edited by JMB.

Chapter 4 was co-authored by: J. M. Stubbs, B. J. Bridge, and J. M. Blacquiere.<sup>3</sup> JMS performed all of the synthetic and characterization work except for preparation of a crystalline sample for X-ray diffraction and some of the catalytic experiments (ca. 3% of experimental work), which were performed by BJB. The manuscript was prepared by JMS and edited by JMB. The manuscript is complete and ready for submission.

---

<sup>1</sup> A version of this chapter has been published (J. M. Stubbs, J. P. J. Bow, R. J. Hazlehurst, and J. M. Blacquiere, *Dalton Trans.*, **2016**, 17100–17103).

<sup>2</sup> A version of this chapter has been published (J. M. Stubbs, D. E. Chapple, P. D. Boyle, and J. M. Blacquiere, *ChemCatChem*, **2018**, 3694–3702).

<sup>3</sup> A version of this chapter has been submitted for publication (J. M. Stubbs, B. J. Bridge, and J. M. Blacquiere, *ChemCatChem*, **2019**, submitted, cctc.201900104).

The article presented in Chapter 5 was co-authored by: J. M. Stubbs, R. J. Hazlehurst, P. D. Boyle, and J. M. Blacquiere.<sup>4</sup> JMS performed all of the synthetic and characterization work. RJH and PDB collected and solved the X-ray crystallographic data. The manuscript was prepared by JMS and edited by JMB.

Chapter 6 describes work performed by: J. M. Stubbs, and J. M. Blacquiere. JMS performed all of the syntheses, characterizations, and analysis. The manuscript was prepared by JMS and edited by JMB.

## Acknowledgments

First, I would like to thank my supervisor, Dr. Johanna M. Blacquiere. It has been a wonderful opportunity being part of the Blacquiere lab from the start and contributing to the growing lab. Johanna's dedication and determination are a daily inspiration to continue to push the boundaries in research. Thank you for putting up with my half-written thoughts, which were clear to me (and only me). Without your encouragement and support throughout this thesis would not have been possible. It has been a joy to work for you.

I would also like to thank all the people have come and gone through the lab while I have been here. You make the everyday new and enjoyable in your own special way. I would like to thank all the graduate students that I have gotten to work: Ava who lightened the mood of the hard days in the lab with her laughter; Richard for talking hockey; J.P. for always being down for a drink; Scott for taking everything too seriously; Devon for talking about game of thrones; Kyle for always taking the blame (you are our Mexico and we did build a wall around you); Ben for your inspiring work ethic. Additionally, many thanks to all the undergraduates that have come through the lab through the years.

I would like to take this chance to thank the great research staff at Western University. Your diligent work provides an excellent environment for research.

---

<sup>4</sup> J. M. Stubbs, R. J. Hazlehurst, P. D. Boyle, and J. M. Blacquiere, *Organometallics*, **2016**, 1692–1698.



I would like to thank all my friends over the years that have helped and supported me during my degree. A big thank you to Joe Paquette, Rebecca Yardley, Ryan Marr, Steph Barbon, Lauren Irwin, Matt Coady, Matthew Turnbull, and Joseph Turnbull.

I would like to thank my parents and parents in law for always believing in me and going the extra mile to support me.

Finally, to my wife, Meghan, I could not have done this without you. I can not find the words to thank you enough for your unconditional love, patience and support over the past four and a half years and I could not have done it without you.

# Table of Contents

Abstract.....	i
Co-Authorship Statement.....	ii
Acknowledgments.....	iii
Table of Contents.....	v
List of Tables.....	x
List of Figures.....	xi
List of Schemes.....	xvii
List of Abbreviations.....	xix
List of Complexes.....	xxiii
Chapter 1.....	1
1 Introduction.....	1
1.1 The Importance of Catalysis.....	1
1.2 Homogenous Organometallic Catalysis with Ruthenium.....	2
1.3 Metal-Ligand-Cooperative Complexes.....	4
1.4 Proton-Shuttling MLC Complexes in Organic Synthesis.....	5
1.5 Tunable $P^R_2N^{R'}_2$ Ligands and $M(P^R_2N^{R'}_2)$ Complexes.....	7
1.6 Current Methods for Cyclization to Produce Heterocycles.....	11
1.7 Current Methods of Acceptorless Dehydrogenation Catalysis.....	16
1.8 Scope of Thesis.....	23
1.9 References.....	24
Chapter 2.....	31
2 Catalytic Cyclization and Competitive Deactivation with $Ru(P^R_2N^{R'}_2)$ Complexes....	31
2.1 Introduction.....	31
2.2 Results and Discussion.....	32

2.3	Conclusion .....	36
2.4	Experimental .....	37
2.4.1	General Procedures, Materials and Instrumentation .....	37
2.4.2	Synthesis of $[\text{Ru}(\text{Cp})(\text{P}^{\text{Ph}}_2\text{N}^{\text{Bn}}_2)(\text{NCCH}_3)]\text{PF}_6$ , ( <b>2-1b</b> ).....	38
2.4.3	Synthesis of $\text{Ru}(\text{Cp})(\text{dppp})(\text{NCCH}_3)]\text{PF}_6$ , ( <b>2-3</b> ).....	38
2.4.4	Attempted Synthesis of $[\text{Ru}(\text{Cp})(\text{P}^{\text{tBu}}_2\text{N}^{\text{Bn}}_2)(-\text{C}=\text{CHC}_6\text{H}_4\text{OH})]\text{PF}_6$ , ( <b>2-5a</b> ) .....	39
2.4.5	In Situ Characterization of $[\text{Ru}(\text{Cp})(\text{P}^{\text{tBu}}_2\text{N}^{\text{Bn}}_2)(-\text{C}=\text{CHC}_6\text{H}_4\text{OH})]\text{PF}_6$ , ( <b>2-5a</b> ). .....	39
2.4.6	Representative Procedure for Catalytic Cyclization of 2-Ethynylbenzyl alcohol ( <b>EBA</b> ).....	39
2.4.7	In Situ Monitoring of Ru Species During Catalysis .....	40
2.4.8	Representative Procedure for Performing Cyclization of 2-Ethynylbenzyl alcohol with $[\text{Ru}(\text{Cp})(\text{P}^{\text{tBu}}_2\text{N}^{\text{Bn}}_2)]\text{PF}_6$ .....	40
2.5	References.....	41
Chapter 3.....		43
3	Catalyst Pendent-Base Effects on Cyclization of Alkynyl Amines .....	43
3.1	Introduction.....	43
3.2	Results and Discussion .....	46
3.2.1	Catalyst Synthesis .....	46
3.2.2	Catalytic Studies .....	48
3.3	Conclusion .....	56
3.4	Experimental .....	56
3.4.1	General Procedures, Materials and Instrumentation.....	56
3.4.2	General Procedure for the Synthesis of $\text{P}^{\text{Ph}}_2\text{N}^{\text{R}'_2}$ Ligands ( <b>1a-e</b> ).....	58
3.4.3	Synthesis of $\text{P}^{\text{Ph}}_2\text{N}^{\text{Ph}}_1$ Ligand ( <b>3-3</b> ) .....	59
3.4.4	General Procedure for the Synthesis of $\text{Ru}(\text{P}^{\text{Ph}}_2\text{N}^{\text{R}'_2})$ ( <b>2-1b</b> , <b>3-2a-d</b> ) and $\text{Ru}(\text{P}^{\text{Ph}}_2\text{N}^{\text{Ph}}_1)$ ( <b>3-4</b> ) Complexes.....	59

3.4.5	General Procedure for the Catalytic Cyclization of Substrates .....	63
3.4.6	High Throughput Catalytic Procedure .....	63
3.4.7	Stoichiometric Reactions with Complex 3-5 and Aniline .....	64
3.5	References.....	64
Chapter 4.....		66
4	Primary-Coordination Sphere Tuning of Ru-(P <sup>R</sup> <sub>2</sub> N <sup>R'</sup> <sub>2</sub> ) Cyclization Catalysts to give <i>O</i> - and <i>N</i> -Heterocycles .....	66
4.1	Introduction.....	66
4.2	Results and Discussion .....	68
4.2.1	Catalyst Synthesis .....	68
4.2.2	Catalytic Studies .....	70
4.3	Conclusions.....	81
4.4	Experimental Section .....	81
4.4.1	General Procedure, Materials and Instrumentation .....	81
4.4.2	Synthesis of P <sup>Bn</sup> <sub>2</sub> N <sup>Bn</sup> <sub>2</sub> .....	82
4.4.3	General Procedure for Synthesis of [Ru(Cp/Cp*)(P <sup>R</sup> <sub>2</sub> N <sup>R'</sup> <sub>2</sub> )(NCCH <sub>3</sub> )]PF <sub>6</sub> Complexes.....	83
4.4.4	General Procedure for the Catalytic Cyclization of Substrates .....	85
4.4.5	High Throughput Catalytic Procedure .....	85
4.4.6	General Procedure A for Sonogashira (X = I) <sup>23</sup> .....	86
4.4.7	General Procedure B for Sonogashira (X = Br) <sup>23</sup> .....	86
4.4.8	Deprotection Procedure A <sup>23</sup> .....	86
4.4.9	Deprotection Procedure B <sup>23</sup> .....	86
4.5	References.....	87
Chapter 5.....		90
5	Catalytic Acceptorless Dehydrogenation of Amines with Ru(P <sup>R</sup> <sub>2</sub> N <sup>R'</sup> <sub>2</sub> ) and Ru(dppp) Complexes.....	90

5.1	Introduction.....	90
5.2	Results and Discussion .....	91
5.3	Conclusion .....	100
5.4	Experimental Section .....	101
5.4.1	General Materials, Procedures and Instrumentation.....	101
5.4.2	Synthesis of $[\text{Ru}(\text{Cp})(\text{P}^{\text{Ph}}_2\text{N}^{\text{Bn}}_2)(\text{benzylamine})]\text{PF}_6$ (5-1).....	102
5.4.3	Synthesis of $[\text{Ru}(\text{Cp})(\text{P}^{\text{Ph}}_2\text{N}^{\text{Bn}}_2)(\text{pyrrolidine})]\text{PF}_6$ (5-2).....	103
5.4.4	General Procedure for Catalytic Dehydrogenation Reactions of Benzylamine .....	104
5.4.5	General Procedure for Catalytic Dehydrogenation Reactions of Benzylamine with Anilines.....	105
5.4.6	General Procedure for Catalytic Dehydrogenation Reactions of <i>N</i> -Heterocycles.....	105
5.4.7	General Procedure for Stoichiometric Probe Reactions with $[\text{Ru}(\text{Cp})(\text{dppp})(\text{NCMe})]\text{PF}_6$ (2-3).....	106
5.4.8	Attempted synthesis of $[\text{Ru}(\text{Cp})(\text{dppp})(\text{pyrrolidine})]\text{PF}_6$ (5-3) .....	106
5.5	References.....	106
Chapter 6.....		108
6	The Role of the 1° and 2° Coordination Spheres of MLC and Non-MLC Acceptorless Dehydrogenation Catalysts .....	108
6.1	Introduction.....	108
6.2	Results and Discussion .....	111
6.3	Conclusion .....	128
6.4	Experimental.....	129
6.4.1	General Procedures, Materials and Instrumentation.....	129
6.4.2	General Procedure for In Situ Synthesis of $[\text{Ru}(\text{Cp}/\text{Cp}^*)(\text{PP})(\text{NCCH}_3)]\text{PF}_6$ (6-1a,c, and 6-2).....	130
6.4.3	General Procedure for the Catalytic Cyclization of Substrates .....	131
6.4.4	High Throughput Catalytic Procedure .....	132

6.4.5	General Procedure for Variable Time Normalization Analysis.....	133
6.5	References.....	133
7	Summary, Conclusion and Future Work.....	136
7.1	Summary and Conclusion.....	136
7.2	Future Work.....	139
	Appendices.....	141
	Appendices A: Supplementary Information for Chapter 2.....	141
	Appendices B: Supplementary Information for Chapter 3.....	158
	Appendices C: Supplementary Information for Chapter 4.....	192
	Appendices D: Supplementary Information for Chapter 5.....	215
	Appendices E: Supplementary Information for Chapter 6.....	227
	Appendices F: Copyright Material and Permissions.....	245
	Curriculum Vitae.....	248

## List of Tables

Table 2-1. Catalyst Comparison and Substrate Scope for Cyclization <sup>[a]</sup> .....	34
Table 3-1. Catalysis of 2-Ethynylaniline ( <b>EA</b> ) using <b>2-1b</b> .....	49
Table 4-1. Cyclization of 2-ethynylaniline with catalysts 4-1b and 4-2b <sup>a</sup> .....	75
Table 4-2. Tolerance Screen using Additives for the Cyclization of 2-Ethynylaniline using Complex 4-1b <sup>[a]</sup> .....	77
Table 4-3. Substrate screen to examine different electronic and steric properties for the intramolecular cyclization of alkynes using complex 4-1b <sup>[a]</sup> .....	80
Table 5-1 Catalytic optimization for the acceptorless dehydrogenation of benzylamine. <sup>[a]</sup> ...	92
Table 5-2. Catalytic acceptorless dehydrogenation of benzylamine with aniline derivatives R-ArNH <sub>2</sub> <sup>[a]</sup> .....	94
Table 5-3. Performance of 2-1b and 2-3 toward acceptorless dehydrogenation of N-heterocycles <sup>[a]</sup> .....	97
Table 6-1. Substrate comparison to understand the effects of steric and electronic effects for substituted indolines <sup>a</sup> .....	126

## List of Figures

Figure 1-1. An energy profile for a hypothetical reaction a) without a catalyst; b) with a catalyst .....	1
Figure 1-2. A generic catalytic cycle with a transition metal catalyst (M = metal, L = ligand, Sub = substrate, Int = intermediate, Prod = product).....	2
Figure 1-3. a) A simplified mechanism for catalytic olefin metathesis using Ru; b) Ru olefin metathesis catalysts.....	4
Figure 1-4. Different types of MLC complexes: a) proton-responsive complex used in the catalytic hydrogenation of CO <sub>2</sub> and H <sub>2</sub> ; <sup>37</sup> b) electron-responsive complex causing redox switchable allosteric control; <sup>39</sup> c) photon-responsive complex enabling C-C bond formation between a tertiary amine and an imine using visible light; <sup>40</sup> d) H-bonding complex stabilizing a highly unstable Ni-OH species; <sup>41</sup> and e) molecular recognition complex producing supramolecular chirality <sup>45</sup> (L-L = cyclooctadiene) .....	5
Figure 1-5. A generic catalytic cycle with a proton shuttling MLC catalyst (M = metal, L = ligand, B = Base, Sub = substrate, Int = intermediate, Prod = product) .....	6
Figure 1-6. A proton shuttling MLC catalyst with the cooperative group (blue) positioned: a) in the primary coordination sphere; <sup>52</sup> and b) in the secondary coordination sphere <sup>28</sup> .....	7
Figure 1-7. a) The structure of a P <sup>R</sup> <sub>2</sub> N <sup>R'</sup> <sub>2</sub> ; <sup>59</sup> and b) hydrogen oxidation and production can be favoured depending on the R and R' groups on the [Ni(P <sup>R</sup> <sub>2</sub> N <sup>R'</sup> <sub>2</sub> ) <sub>2</sub> ] <sup>2+</sup> 16-18 .....	8
Figure 1-8. Two routes to synthesize P <sup>R</sup> <sub>2</sub> N <sup>R'</sup> <sub>2</sub> ligands. Route A proceeds from a primary phosphine. <sup>59, 61</sup> Route B proceeds from tris(hydroxymethyl)phosphine (THP) <sup>62</sup> .....	9
Figure 1-9. Synthesis of [Ru(Cp)(P <sup>R</sup> <sub>2</sub> N <sup>R'</sup> <sub>2</sub> )(L)]PF <sub>6</sub> complexes by two routes. Route A proceeds from Ru(Cl)(Cp)(PPh <sub>3</sub> ) <sub>2</sub> through a ligand substitution and subsequent halide abstraction. <sup>63, 64</sup> Route B proceed via ligand substitution reaction from [Ru(Cp)(NCCH <sub>3</sub> ) <sub>3</sub> ]PF <sub>6</sub> <sup>66</sup> .....	10
Figure 1-10. Deactivation of [Ru(Cp)(P <sup>t-Bu</sup> <sub>2</sub> N <sup>Bn</sup> <sub>2</sub> )(NCCH <sub>3</sub> )]PF <sub>6</sub> with phenylacetylene <sup>66</sup> .....	10



Figure 1-11. Common methods to form 5-membered heterocycles: a) Fischer-Indole synthesis; b) Larock Indole reaction; c) Paal-Knorr reaction <sup>68-73</sup> .....	12
Figure 1-12. a) Alkyne heteroatom cyclization proceeding through: b) electrophilic $\pi$ activation; and c) a metal vinylidene <sup>83</sup> .....	13
Figure 1-13. Catalytic cycle for intramolecular heteroatom cyclization for alkynes (X = O, NR) with exogenous base additive .....	14
Figure 1-14. Alkyne heteroatom cyclization non-MLC catalysts and conditions to form <i>O</i> -heterocycles by: a) Trost using Ru; <sup>91</sup> b) Saá; <sup>82</sup> and c) Trost using Rh <sup>89</sup> .....	15
Figure 1-15. Alkyne heteroatom cyclization non-MLC catalysts and conditions to form <i>O</i> -heterocycles by: a) Grotjahn catalyst; <sup>29</sup> and b) Jia catalyst <sup>94</sup> .....	16
Figure 1-16. A transfer hydrogenation reaction using high performance Fe catalyst <sup>100</sup> .....	17
Figure 1-17. a) Acceptorless dehydrogenation reaction; and b) equilibrium between metal bound H <sub>2</sub> and free H <sub>2</sub> .....	17
Figure 1-18. a) Acceptorless dehydrogenation of alcohols; <sup>26</sup> b) Milstein catalyst for acceptorless dehydrogenation of alcohols; <sup>108</sup> c) Gusev catalyst for acceptorless dehydrogenation of alcohols; <sup>19</sup> d) Beller catalyst; <sup>109</sup> and e) Grutzmacher catalyst for acceptorless dehydrogenation of methanol <sup>110</sup> .....	18
Figure 1-19. General reactions for a primary amine for AD, ADC, HB, and DAD <sup>107</sup> .....	19
Figure 1-20. Three mechanistic pathways for acceptorless dehydrogenation of amines: a) outer-sphere MLC; <sup>53</sup> b) inner-sphere MLC; <sup>112</sup> and c) inner-sphere non-MLC mechanisms <sup>113</sup> .....	20
Figure 1-21. Non-MLC catalysts for acceptorless dehydrogenation: a) Watanabe catalyst; <sup>111</sup> and b) Szymczak catalyst <sup>113</sup> .....	21
Figure 1-22. MLC catalysts for acceptorless dehydrogenation of amines: a) Albecht catalyst; <sup>106</sup> b) Yu catalyst; <sup>114</sup> c) Shvo catalyst; <sup>104</sup> and d) Huang catalyst <sup>105</sup> .....	22

Figure 1-23. Bera MLC catalysts for acceptorless dehydrogenation of benzyl amine to produce a nitrile <sup>116</sup> .....	23
Figure 2-1. a) Ruthenium MLC catalysts employed in this study; b) known deactivation of 2-1a on reaction with phenylacetylene; c) non-MLC control catalyst .....	32
Figure 2-2. a) Cyclization of EBA (150 mM) at 40 °C monitored over 24 h with [Ru] b) 5 mol% 2-1a in acetone (◆), CH <sub>2</sub> Cl <sub>2</sub> (■), THF (▲) and MeCN (●) at 60 °C; c) 5 (◆), 1 (■), 0.1 (▲) mol% 2-1a in acetone; d) 1 mol% 2-1a (■), 2-1b (●) and 2-3 (▲) in acetone .....	33
Figure 2-3. In situ observation of 2-1a (◆; <sup>31</sup> P = 53.9), 2-4a/2-4a'/2-4a" (▲; <sup>31</sup> P = 70.8), 2-5a (■; <sup>31</sup> P = 71.1) by <sup>31</sup> P{ <sup>1</sup> H} NMR spectroscopy relative to an internal standard (O=PPh <sub>3</sub> ) for 95 min at a) 40 °C and b) 50 °C .....	35
Figure 2-4. Postulated mechanism for the cyclization of 2-ethynylbenzyl alcohol (EBA) with catalyst 2-1a .....	36
Figure 3-1. Simplified probable mechanism for cyclization of 2-ethynyl aniline (EA) based on studies <sup>1e, 2a</sup> of catalytic alkyne hydration. The mechanism is depicted with an exogenous base, but an internal base on the ligand would serve the same role. The box in I indicates an open coordination site .....	44
Figure 3-2. Displacement ellipsoid plot of 3-2a. Ellipsoids are at the 50% probability level. Hydrogen atoms and PF <sub>6</sub> <sup>-</sup> were omitted for clarity.....	47
Figure 3-3. Cyclization yields of 2-ethynylaniline (EA) to indole (Ind) in THF at 55 °C after 24 h with catalysts 2-1b, 3-2a-d and 3-4 at 3 mol% (blue), 1 mol% (red), 0.5 mol% (orange) and 0.1 mol% (purple) .....	51
Figure 3-4. Cyclization yields of 2-ethynylbenzyl alcohol (EBA) to isochromene (IC) in THF at 55 °C after 24 h with catalysts 2-1b, 3-2a-d and 3-4 at 3 mol% (blue), 1 mol% (red), 0.5 mol% (orange) and 0.1 mol% (purple) .....	53
Figure 3-5. Cyclization of 2-ethynylaniline (EA) under optimal conditions (2 mol% [Ru], Me-THF, 55°C) monitored over time. [Ru] = 2-1b (R' = Bn, green), 3-2a (R' = Ph, blue), 3-2c (R' = <i>p</i> -CF <sub>3</sub> Ph, red) .....	53

Figure 3-6. Cyclization conversion over time with 2 mol% [Ru] in Me-THF of: a) 2-ethynyl-4-methoxyaniline (EA-4-OMe) at 55 °C with 3-2a (R' = Ph, blue) and 3-2d (R' = *p*-MeOPh, orange); b) 2-ethynyl-4-fluoroaniline (EA-4-F) at 55 °C with 3-2a (R' = Ph, blue) and 3-2c (R' = *p*-CF<sub>3</sub>Ph, red); and c) 2-ethynylbenzylamide (EAM) at 70 °C with 2-1b (R' = Bn, green) and 3-2a (R' = Ph, blue). In all cases conversion was quantified by <sup>1</sup>H NMR spectroscopy..... 55

Figure 4-1. Performance of previously reported catalysts A<sup>5</sup> and B<sup>6</sup> as compared to the present [Ru(Cp)(P<sup>*t*</sup>-Bu<sub>2</sub>N<sup>Ph</sup><sub>2</sub>)(MeCN)]PF<sub>6</sub> catalyst toward the cyclization of 2-ethynylaniline (EA)..... 68

Figure 4-2. Thermal displacement plot of 4-2b with ellipsoids at 50% probability. *t*-Butyl groups on P1 and P2, hydrogen atoms, along with the PF<sub>6</sub> were removed for clarity. Bond Lengths (Å): P1–Ru1 = 2.306(1); P2–Ru1 = 2.306(1); N1–Ru1 = 2.052(4). Bond Angles (°): P1–Ru1–P2 = 77.75(4); C13–N2–C14 = 108.5(3); C13–N2–C25 = 119.3(3); C14–N2–C25 = 119.3(3); C15–N3–C16 = 108.2(3); C15–N3–C31 = 124.9(3); C16–N3–C31 = 124.9(3) .... 70

Figure 4-3. a) Cyclization of 2-ethynylbenzyl alcohol (EBA) to give iso-chromene (IC). b) Yields of IC in THF at 55 °C using 2-1a,b, 4-1a and 4-2a at 0.1 (yellow), 0.5 (grey), 1 (orange), 3 (blue) mol%. Conversion data with 3 mol% 4-1a was not achieved in this screen due to inaccurate catalyst addition due to low solubility of 4-1a in the stock solution. c) Time trace of cyclization of EBA by 4-1b (blue), 4-2a (purple), and 4-2b (red) at 1 mol% at 55 °C in THF..... 72

Figure 4-4. a) Cyclization of 2-ethynylaniline (EA) to give indole (Ind). b) Yields of Ind in THF at 55 °C using 2-1a,b, 4-1a and 4-2a at 0.1 (yellow), 0.5 (grey), 1 (orange), 3 (blue) mol%. Conversion data with 3 mol% 4-1a was not achieved in this screen due to inaccurate catalyst addition due to low solubility of 4-1a in the stock solution ..... 73

Figure 4-5. Cyclization of 2-ethynylaniline (EA) in Me-THF at 70 °C with Cp catalyst 4-1b (blue) and Cp\* catalyst 4-2b (red) at loadings of 0.2 (solid) and 0.1 (dashed) mol% ..... 74

Figure 5-1. Conversion curves for the ADC of BnNH<sub>2</sub> (black) with MeO-ArNH<sub>2</sub> under the optimized conditions with catalyst a) 2-1b; and b) 2-3. Yields, determined by calibrated GC-FID analysis, of reaction products A (red), B (green), C (purple) and D (blue) are plotted.

Data points represent the average of the two runs and the error bars give the span of the conversion values of each data set. ....	95
Figure 5-2. a) Expanded section of the $^1\text{H}$ - $^1\text{H}$ ROESY NMR spectrum of 5-2; and b) Thermal displacement plot of 5-2 (right) with ellipsoids at 50% probability. Phenyl groups on P1 and P2 and the $\text{PF}_6^-$ anion were removed for clarity .....	99
Figure 5-3: Numbering scheme for $^1\text{H}$ and $^{13}\text{C}$ NMR assignment for complex 5-2.....	104
Figure 6-1. Two mechanistic pathways for the acceptorless dehydrogenation of amines. a) An inner-sphere pathway in which deprotonation can be facilitated by an exogenous base (non-MLC) or catalyst (MLC); and b) an outer-sphere pathway where deprotonation is facilitated by the catalyst (MLC) .....	109
Figure 6-2. Acceptorless dehydrogenation of benzylamine to produce nitriles <sup>26, 28</sup> .....	110
Figure 6-3. Ru complexes used in this study to divulge structure activity relationships.....	112
Figure 6-4. Catalyst comparison of the primary coordination sphere using complex 2-1a,b, 4-1a, and 4-2a for acceptorless dehydrogenation of indoline to indole at 0.5 (grey), 1 (orange) and 3 (blue) mol% .....	113
Figure 6-5. Catalyst comparison of the secondary coordination sphere using complex 2-1b ( $\text{R}' = \text{Bn}$ ), 3-2a ( $\text{R}' = \text{Ph}$ ), 3-2d ( $\text{R}' = p\text{-MeO-C}_6\text{H}_4$ ), 3-2c ( $\text{R}' = p\text{-CF}_3\text{-C}_6\text{H}_4$ ), and 3-2b ( $\text{R}' = \text{Mes}$ ) for acceptorless dehydrogenation of indoline to indole at 0.5 (grey), 1 (orange) and 3 (blue) mol% .....	114
Figure 6-6. Catalyst comparison of the Ru(P-P) complexes lacking a pendent amine in the ligand manifold using complex 6-1a (dppm), 6-1a (dppe), 6-1c (dpbz), 2-3 (dppp), and 6-2 ( $\text{Cp}^*$ , dppp) for acceptorless dehydrogenation of indoline to indole at 0.5 (grey), and 1 (orange) mol% .....	115
Figure 6-7. Catalyst comparison of the acid/base site using complex 3-2a ( $\text{Ru}(\text{P}^{\text{Ph}}_2\text{N}^{\text{Ph}}_2)$ ), 3-4 ( $\text{Ru}(\text{P}^{\text{Ph}}_2\text{N}^{\text{Ph}}_1)$ ), and 2-3 (dppp) for acceptorless dehydrogenation of indoline to indole at 0.5 (grey), 1 (orange) and 3 (blue) mol% .....	116

Figure 6-8. Reaction profile for acceptorless dehydrogenation of indoline with Ru(P <sup>R</sup> <sub>2</sub> N <sup>R'</sup> <sub>2</sub> ) (3-2a – red) and Ru(dppp) (2-3 – blue) (1 mol%) at 97 °C in anisole monitored by ReactIR .....	117
Figure 6-9. Variable time normalization analysis of catalyst at a) 0 <sup>th</sup> order; b) 1 <sup>st</sup> order; and c) 2 <sup>nd</sup> order for the acceptorless dehydrogenation of indoline (250 mM) using 3-2a (1.5 mol% – blue; 2 mol% – red) at 82 °C in anisole monitored by ReactIR.....	119
Figure 6-10. Variable time normalization analysis of catalyst at a) 0 <sup>th</sup> order; b) 1 <sup>st</sup> order; and c) 2 <sup>nd</sup> order for the acceptorless dehydrogenation of indoline (250 mM) using 2-3 (1 mol% – blue; 2 mol% – red) at 100 °C in anisole monitored by ReactIR.....	120
Figure 6-11. Variable time normalization analysis of substrate at a) 0 <sup>th</sup> order; b) 1 <sup>st</sup> order; and c) 2 <sup>nd</sup> order for the acceptorless dehydrogenation of indoline (250 mM – blue; 375 mM – red) using 1 mol% of 3-2a at 97 °C in anisole monitored by ReactIR.....	122
Figure 6-12. Variable time normalization analysis of substrate at a) 0 <sup>th</sup> order; b) negative 1 <sup>st</sup> order; d) negative 1.5 <sup>th</sup> order; and c) negative 2 <sup>nd</sup> order for the acceptorless dehydrogenation of indoline (125 mM – green; 250 mM – blue; 375 mM – red) using 1 mol% of complex 2-3 at 97 °C in anisole monitored by REACTIR.....	124
Figure 6-13. Same excess protocol for Variable time normalization analysis of substrate at 0 <sup>th</sup> order for the acceptorless dehydrogenation of indoline (125 mM – green; 375 mM – red) using 1 mol% of complex 2-3 at 97 °C in anisole monitored by REACTIR.....	124

## List of Schemes

Scheme 2-1. Catalytic cyclization of alkynyl alcohols <sup>2a-f</sup> .....	31
Scheme 3-1. Cyclization of 2-ethynylaniline (EA) with a) a non-cooperative catalyst A (10 mol% A, pyridine, 90 °C, 25 min, 84% Ind) <sup>2e</sup> and b) a cooperative catalyst B (2 mol% B, THF, 70 °C, 7 h, 87% Ind) <sup>2f</sup> .....	44
Scheme 3-2. Cyclization of 2-ethynylbenzyl alcohol (EBA) with P <sup>R</sup> <sub>2</sub> N <sup>R'</sup> <sub>2</sub> catalyst 2-1a, and catalyst deactivation product 2-2a <sup>6a</sup> .....	45
Scheme 3-3. Synthesis of P <sup>Ph</sup> <sub>2</sub> N <sup>R'</sup> <sub>2</sub> ligands used in this study. Conditions: (i) <i>p</i> -CH <sub>2</sub> O, EtOH, 78 °C, 4 h; (ii) dropwise H <sub>2</sub> NR', EtOH, 78 °C, 24 h. Yield: 3-1b = 15%; 3-1a, 3-1c-e are known <sup>5,7</sup> .....	46
Scheme 3-4. Synthesis of Ru(P <sup>Ph</sup> <sub>2</sub> N <sup>R'</sup> <sub>2</sub> ) complexes 2-1b, 3-2a-d by metalation of P <sup>Ph</sup> <sub>2</sub> N <sup>R'</sup> <sub>2</sub> ligands (3-1a-e). Complex 2-1b was previously reported <sup>6a</sup> .....	47
Scheme 3-5. Synthesis of dynamic Ru(P <sup>Ph</sup> <sub>2</sub> N <sup>Ph</sup> <sub>1</sub> ) complex 3-4. Conditions: (i) [CpRu(MeCN) <sub>3</sub> ]PF <sub>6</sub> , MeCN, RT, 4 h. Yield 3-4 = 92% .....	48
Scheme 3-6. Catalysis of 2-Ethynylaniline (EA) using 2-1b.....	49
Scheme 3-7. Stoichiometric reaction of 3-5 with aniline .....	50
Scheme 4-1. Cyclization of alkynyl amine or alcohol substrates mediated by a metal catalyst and base to promote proton shuttling. Catalysis involves a metal vinylidene for a subset of catalysts.....	67
Scheme 4-2. Synthesis of: a) [Ru(Cp)] complexes 2-1a,b, 4-1a,b; and b) [Ru(Cp*)] complexes 4-2a,b. (i) 1.05 eq P <sup>R</sup> <sub>2</sub> N <sup>R'</sup> <sub>2</sub> , MeCN, 70 °C, 4 h.....	69
Scheme 4-3. Tolerance Screen using Additives for the Cyclization of 2-Ethynylaniline using Complex 4-1b.....	77
Scheme 4-4. Substrate Screen for intramolecular cyclization of alkynes using 4-1b.....	79

Scheme 5-1. Dehydrogenation of benzylamine with 2-1b.....	91
Scheme 5-2. Acceptorless dehydrogenative coupling of benzylamine with anilines catalyzed by 2-1b or 2-3.....	93
Scheme 5-3. Acceptorless dehydrogenation of <i>N</i> -heterocycles by 0 or 1. Indoline, R = H, n = 0; 2-methylindoline (Me-Ind), R = Me, n = 0; 1,2,3,4-tetrahydroquinoline (THQ), R = H, n = 1.....	96
Scheme 5-4. Reactivity of: a) 2-1b with benzylamine or pyrrolidine; and b) 2-3 with pyrrolidine.....	98
Scheme 5-5. Possible pathways for the dehydrogenation of benzylamine with catalyst 2-1b. [Ru] = [Ru(Cp)]PF <sub>6</sub> .....	100
Scheme 5-6. Catalytic performance comparison of precatalysts 2-1b and benzylamine adduct 5-1 toward AD of benzylamine.....	100
Scheme 6-1. Acceptorless dehydrogenation of Indoline under standard conditions .....	111
Scheme 6-2. AD of Indoline for Catalyst Variable Time Normalization Analysis with 3-2a .....	118
Scheme 6-3. AD of Indoline for Catalyst Variable Time Normalization Analysis with 2-3 .....	119
Scheme 6-4. AD of Indoline for Substrate Variable Time Normalization Analysis with 3-2a .....	121
Scheme 6-5. AD of Indoline for Substrate Variable Time Normalization Analysis with 2-3 .....	123

## List of Abbreviations

AD	acceptorless dehydrogenation
ADC	acceptorless dehydrogenation coupling
Alkyl-EA	pent-4-yn-1-ol
Ar	aryl
Bn	benzyl
BnNH <sub>2</sub>	benzylamine
C $\alpha$	alpha carbon
C $\beta$	beta carbon
CDCl <sub>3</sub>	chloroform- <i>d</i>
CD <sub>2</sub> Cl <sub>2</sub>	dichloromethane- <i>d</i> <sub>2</sub>
Conv.	conversion
COSY	correlation spectroscopy
Cp	cyclopentadienyl
Cp*	pentamethylcyclopentadienyl
DAD	double acceptorless dehydrogenation
DMA	Dimethylacetamide
DMF	Dimethylformamide
DNA	Deoxyribonucleic acid
Dpbz	bis(diphenylphosphino)benzene

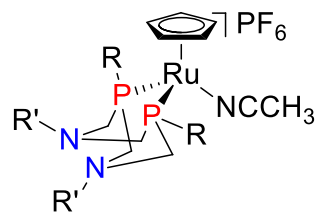


Dppe	bis(diphenylphosphino)ethane
Dppm	bis(diphenylphosphino)methane
Dppp	bis(diphenylphosphino)pentane
EA	2-ethynylaniline
EA-4-F	2-ethynyl-4-fluoroaniline
EA-4-OMe	2-ethynyl-4-methoxyaniline
EAM	2-ethynylamide
EBA	2-ethynylbenzyl alcohol
EBA-OMe	2-ethynyl-5-methoxybenzyl alcohol
Equiv.	equivalent
FTIR	Fourier-transform infrared spectroscopy
GC-FID	gas chromatography-flame ionization detector
HB	hydrogen borrowing
H-bonding	hydrogen bonding
HMBC	Heteronuclear Multiple Bond Correlation
IC	isochromene
Ind	indole
Int	intermediate
$\kappa^2$ -PP	kappa two through two phosphorus atoms
L	ligand

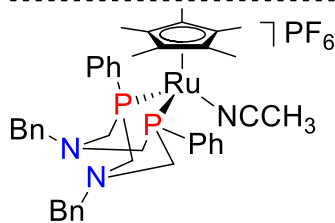
M	metal
MALDI	Matrix Assisted Laser Desorption/Ionization
Me	methyl
Me-Ind	2-methylindoline
MeCN	acetonitrile
MeO-ArNH <sub>2</sub>	4-methoxyaniline
Me-THF	2-methyltetrahydrofuran
Mes	mesityl
MLC	metal-ligand cooperative
NHC	<i>N</i> -heterocyclic carbene
NMR	nuclear magnetic resonance
Non-MLC	non-metal-ligand cooperative
ORTEP	Oak Ridge thermal ellipsoid plot
OPPh <sub>3</sub>	triphenylphosphine oxide
<i>p</i> -CF <sub>3</sub> -C <sub>6</sub> H <sub>4</sub>	4-trifluoromethylphenyl
<i>p</i> -MeO-C <sub>6</sub> H <sub>4</sub>	4-methoxyphenyl-
Ph	phenyl
P <sup>R</sup> <sub>2</sub> N <sup>R'</sup> <sub>2</sub>	1,5-diaza-3,7-diphosphacyclooctane
PP or P-P	bisphosphine
PPh <sub>3</sub>	triphenylphosphine

PR <sub>3</sub>	phosphine
P <sup>Ph</sup> <sub>2</sub> N <sup>Ph</sup> <sub>1</sub>	N,N-bis((diphenylphosphino)methyl)aniline
Prod	product
py	pyridine
ROESY	rotating-frame nuclear Overhauser effect correlation spectroscopy
Sub	substrate
tBu or <i>t</i> -Bu	tert-butyl
T <sub>0</sub>	initial time point
Temp.	temperature
THF	tetrahydrofuran
THFA	tetrahydrofurfuryl alcohol
THP	tris(hydroxymethyl)phosphine
THQ	tetrahydroquinoline
TM	transition metal
TOF	turnover frequency
TON	turnover number

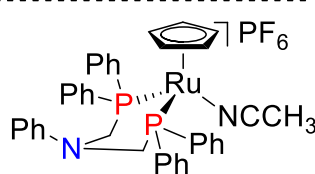
## List of Complexes



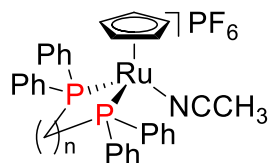
- 2-1b:** R = Ph, R' = Bn  
**2-1a:** R = <sup>t</sup>Bu, R' = Bn  
**4-1a:** R = Bn, R' = Bn  
**3-2a:** R = Ph, R' = Ph  
**3-2b:** R = Ph, R' = Mes  
**3-2c:** R = Ph, R' = *p*-CF<sub>3</sub>-C<sub>6</sub>H<sub>4</sub>  
**3-2d:** R = Ph, R' = *p*-MeO-C<sub>6</sub>H<sub>4</sub>  
**4-1b:** R = <sup>t</sup>Bu, R' = Ph



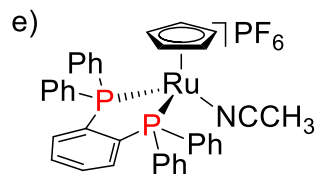
- 4-2a:** R = Ph, R' = Bn  
**4-2b:** R = <sup>t</sup>Bu, R' = Ph



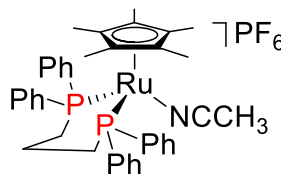
- 3-4:** R = Ph, R' = Ph



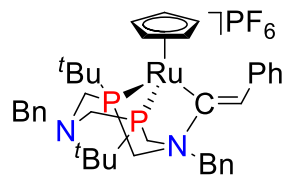
- 6-1a:** dppm (n = 1)  
**6-1b:** dppe (n = 2)  
**2-3:** dppp (n = 3)



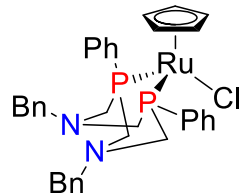
- 6-1c:** dpbz



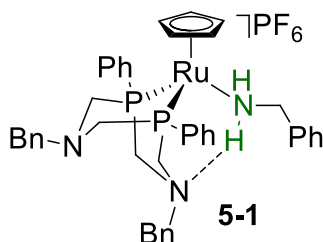
- 6-2:** dppp



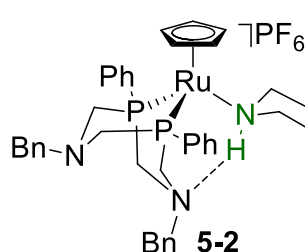
- 2-2a**



- 3-5**



- 5-1**



- 5-2**

# Chapter 1

## 1 Introduction

### 1.1 The Importance of Catalysis

From building molecular complexity to being a potential solution for energy storage, catalysis is transforming how reactions are designed and performed in modern-day chemistry.<sup>1-5</sup> A catalyst operates by lowering the activation energy of the reaction pathway to allow a substrate transformation to a desirable product through an alternative route (Figure 1-1). Typically, the catalyst will interact with a substrate, assist in a transformation, and be regenerated upon product generation. This allows the catalyst to mediate the formation of many mol of product per mol of catalyst.<sup>4, 6, 7</sup> The two main categories for catalysis are homogenous and heterogeneous.<sup>8,9</sup> Homogenous catalysis operates with the catalyst and substrate in the same phase as opposed to heterogeneous catalysis, which operates in difference phases (e.g. a solid and a liquid). Whilst, both homogenous and heterogenous catalysts are used in industry, heterogeneous catalysts are often preferred for large-scale processes due to the lower cost and ease of removal of catalyst typically through filtration. However, homogenous catalysts are preferred for product selectivity and in understanding a mechanism as well-defined systematic changes can be made to a uniform chemical structure. Through this understanding, the catalyst can be manipulated to enhance reactivity for optimal performance by altering the steric and electronic properties.<sup>9</sup>

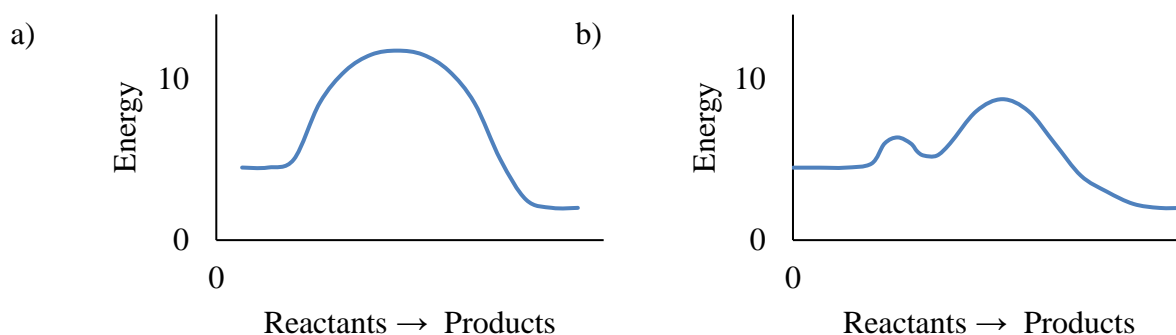


**Figure 1-1.** An energy profile for a hypothetical reaction a) without a catalyst; b) with a catalyst

Catalysis is extremely useful for facilitating many reactions to make a range of pharmaceutical and fine chemical commodities.<sup>10-12</sup> It is one way to improve efficiency and reduce the environmental impact of a reaction. Replacing stoichiometric reactions or multi-step procedures with a catalytic reaction allows for less waste production and reactions can be conducted under milder reaction conditions (lower temperatures and shorter times).<sup>4, 7</sup> However, not every reaction utilizes a catalytic system. New catalysts are needed to provide new alternative routes.<sup>13, 14</sup> Additionally, constant improvement on current catalytic reactions allows for easier bond formation at milder conditions.<sup>15</sup> One approach to developing new catalysts and improving upon previous catalytic systems is to understand the inherent factors involved in the mechanistic pathway.<sup>16-18</sup> Alternatively, numerous variants of a catalyst can be screened in a reaction to find an optimal catalytic system that drastically improves reactivity.<sup>13, 19</sup>

## 1.2 Homogenous Organometallic Catalysis with Ruthenium

Homogenous organometallic catalysis is a powerful method to perform difficult transformations selectively.<sup>20</sup> An organometallic complex consists of a metal with a metal carbon bond to an organic manifold known as a ligand. These metal-ligand bonds are referred to as the primary coordination sphere. The ligands can have different electronic and steric properties that alter the electron density at the metal centre and steric pocket around the metal. The ligand does not interact with the substrate directly and it is a spectator for the reaction. Reactivity proceeds through an open site on the metal where a substrate (the reactant) interacts with the metal centre in the primary coordination sphere. The metal causes a transformation of the substrate before releasing the product (Figure 1-2). This release of product also regenerates the catalyst allowing for more transformations to occur.<sup>6</sup>

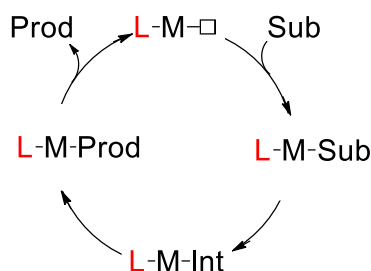


**Figure 1-2.** A generic catalytic cycle with a transition metal catalyst ( $M$  = metal,  $L$  = ligand,  $Sub$  = substrate,  $Int$  = intermediate,  $Prod$  = product)

One transition metal that has been extensively used in catalysis is ruthenium.<sup>21</sup> Ruthenium is a second row  $d^8$ -electron metal typically observed in the 0, +2, and +4 oxidation states with soft  $\sigma$ -donor ligands (phosphines) that stabilize the Ru complexes generated. These oxidation states cause ruthenium to adopt either an octahedral geometry for  $Ru^{2+}$  or tetrahedral geometry for  $Ru^{4+}$ .<sup>6</sup> Oxidation states of +1 and +3 are uncommon unless hard  $\sigma$ -donor ligands (e.g.  $O^{2-}$ ), which destabilize the bonding and anti-bonding molecular orbitals, are used to decrease the energy between the HOMO and LUMO. As the energy is decreased, a high spin electron configuration is adopted as pairing electrons becomes unfavourable.<sup>22</sup> Therefore, ruthenium does not normally perform one electron processes and remains a diamagnetic transition metal unlike the first row  $d^8$  metal iron.<sup>22-24</sup> One downside to ruthenium is cost (\$9,500 USD/kg – Dec 18<sup>th</sup> 2018) as it is quite expensive. Two potential alternatives for Ru could be the other  $d^8$  metals – iron and osmium. Iron (\$0.068 USD/kg – Dec 18<sup>th</sup> 2018) is a cheap abundant metal, but iron complexes can be paramagnetic and perform one electron processes. Osmium is electronically similar to Ru (diamagnetic), but it is far more expensive (\$14,100 USD/kg – Dec 18<sup>th</sup> 2018).<sup>12, 25</sup> Ruthenium complexes are excellent complexes for discovering and understanding reactivity due to their well-behaved electronic nature.<sup>26</sup> This leads to the generation of Ru complexes with a variety of modified ligands while the overall chemical structure deviates only at the ligand modification.<sup>26, 27</sup> These Ru complex derivatives allow for structure-activity relationships to be derived for catalyst optimization.<sup>28-30</sup> Additionally, catalyst design principles can be made for facilitating certain catalytic steps within a reaction for different catalytic reactions.<sup>31</sup>

One example of the revolutionary impact that ruthenium has had in building molecular complexity is the 2+2 transformation of combining two alkenes through a process known as olefin metathesis.<sup>32</sup> The key intermediate for this reaction is a Ru carbene (Figure 1-3a). This reaction mechanism starts with an alkene binding to ruthenium. Through back donation from the d-orbitals on the Ru centre, the alkene is activated to form a four-membered metallacycle with the ruthenium carbene. This process is reversible resulting in a new alkene followed by release of product. The Ru carbene is regenerated from the other half of the original alkene. Due to the well-behaved electronic nature of Ru, these mechanistic steps have been extensively studied to understand how the catalyst structure affects performance. This knowledge has led to substantial catalyst improvement over a span of 26 years since the first Ru olefin catalyst was reported, leading to over 60 commercial Ru olefin catalysts.<sup>11, 15</sup> For instance, in 1995 Grubbs reported a Ru complex for ring closing metathesis catalysis (Figure 1-3b). However, this Grubbs I catalyst was limited to high catalytic loadings due to catalyst deactivation. Through catalytic

optimization, the Hoveyda II catalyst was able to remove this challenge improving reactivity resulting in higher performance with a much broader substrate scope (Figure 1-3b).<sup>33</sup> Olefin metathesis is now used to synthesize pharmaceutical drugs to create large ring sizes, polymerization for high performance rubbers, and in the biorefinery of plant oils to produce renewable feedstock chemicals.<sup>11, 34</sup>

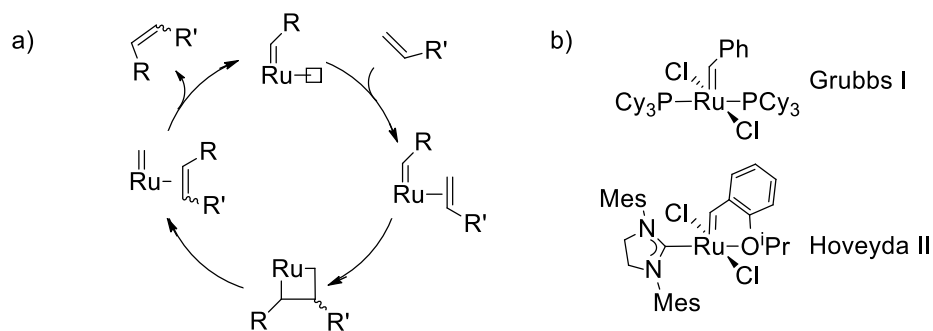


**Figure 1-3.** a) A simplified mechanism for catalytic olefin metathesis using Ru; b) Ru olefin metathesis catalysts

### 1.3 Metal-Ligand-Cooperative Complexes

Metal-ligand cooperative (MLC) complexes take the concept of organometallic catalysis one step further. The ligand in a MLC complex actively assists in the transformation through secondary interactions, which can improve performance or selectivity over traditional transition metal catalysts.<sup>4, 24, 35</sup> These multifunctional ligands possess a cooperative group that can be found in the primary or secondary coordination sphere. As opposed to the primary coordination sphere, the secondary coordination sphere is not bound to the metal centre and exists in backbone of the ligand surrounding the metal. The cooperative group can assist the metal centre in different ways depending on the moiety incorporated onto the ligand.<sup>24, 36</sup> One common method used to improve reactivity is to include a cooperative group that causes the properties of the ligand to change when simple stimulus is applied.<sup>24</sup> Protons, electrons or photons can be used as stimuli (Figure 1-4a-c).<sup>37-40</sup> This change in ligand properties can cause a favourable change in catalytic rate. Inclusion of a hydrogen-bonding group has also been used to stabilize unfavourable catalytic transition states with the substrate resulting in increased product selectivity and complex stability (Figure 1-4d).<sup>41, 42</sup> Additionally, this effect can be extended to generate molecular recognition catalysts where the ligands utilize H-bonding to self-assemble the complex.<sup>43-45</sup> Tuning of the cooperative group can result in improved performance.



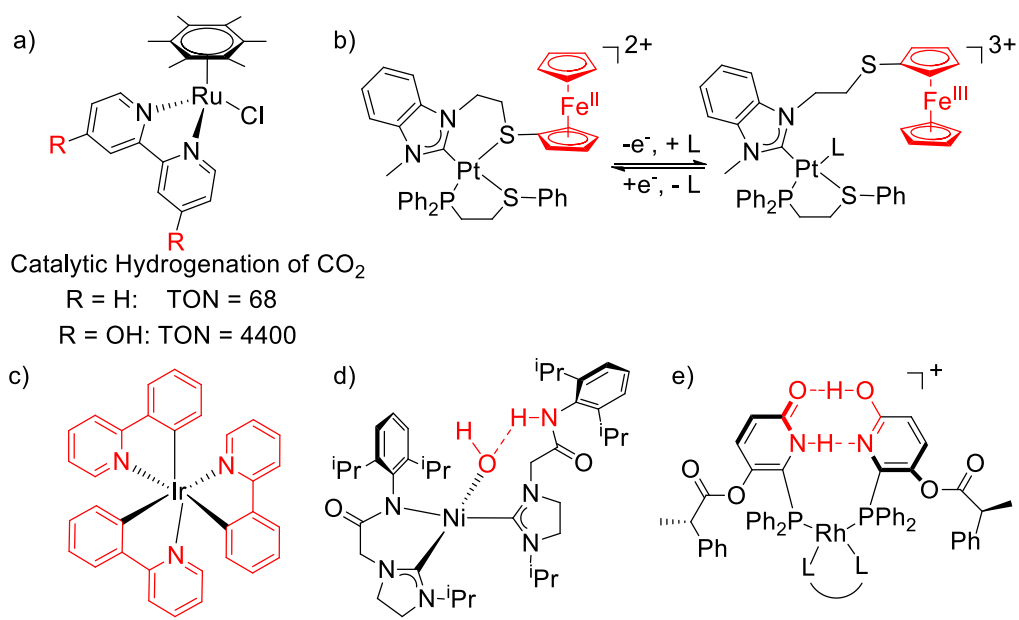


**Figure 1-4.** Different types of MLC complexes: a) proton-responsive complex used in the catalytic hydrogenation of CO<sub>2</sub> and H<sub>2</sub>;<sup>37</sup> b) electron-responsive complex causing redox switchable allosteric control;<sup>39</sup> c) photon-responsive complex enabling C-C bond formation between a tertiary amine and an imine using visible light;<sup>40</sup> d) H-bonding complex stabilizing a highly unstable Ni-OH species;<sup>41</sup> and e) molecular recognition complex producing supramolecular chirality<sup>45</sup> (L-L = cyclooctadiene)

## 1.4 Proton-Shuttling MLC Complexes in Organic Synthesis

Another subset of MLC complexes is proton-shuttling complexes.<sup>3, 24, 46, 47</sup> These complexes have a cooperative group on the ligand to facilitate rapid protonation and deprotonation steps that increase catalytic performance compared to non-MLC complexes.<sup>47</sup> Therefore, the reactivity of the primary coordination sphere reactivity is not limited by the availability of an intermolecular base/acid. Proton shuttling complexes require an acidic or basic site on the ligand to enable the proton transfer (Scheme 1-5).<sup>48, 49</sup> The acid/base site of the ligand, just like the metal centre, can be structurally altered to provide a higher degree of tunability to improve catalytic performance and/or selectivity.<sup>18, 50</sup> From differences in performance, structure-activity relationships can be made to produce new design principles for the primary and secondary coordination spheres of MLC catalysts for certain pathways.<sup>48, 51</sup>

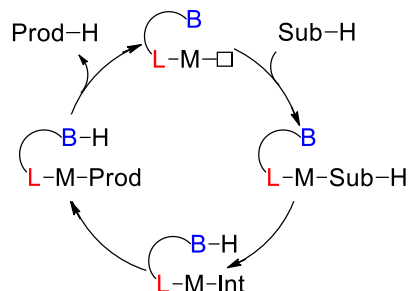


**Figure 1-5.** A generic catalytic cycle with a proton shuttling MLC catalyst (M = metal, L = ligand, B = Base, Sub = substrate, Int = intermediate, Prod = product)

Two different types of acid/base sites exist for proton shuttling catalysts. The first, made famous by the Noyori catalyst, is the use of a bidentate ligand with a strong base in the primary coordination sphere.<sup>2, 52</sup> In the Noyori system, the strong base is an anionic nitrogen that assists ruthenium in the removal of a unit of H<sub>2</sub> from isopropanol to produce acetone (Figure 1-6a).<sup>52</sup> The hydroxy group is deprotonated by the base while a hydride is transferred to the ruthenium from the adjacent carbon.<sup>53</sup> Therefore, the MLC cooperative group has two distinct modes, protonated and deprotonated, which alters the donor ligands electronic properties.<sup>37, 38</sup> This change in donor properties upon protonation alters the properties of the primary coordination as the nitrogen donates less electron density to the metal. In order to draw structure activity relationships, the effects of cooperative group and metal centre must be differentiated, which is difficult when the acid/base site are intertwined with the properties of the primary coordination sphere.

The second type of proton shuttling acid/base site is positioned in the secondary coordination sphere as to not interfere with the primary coordination sphere. The Grotjahn catalyst incorporates a pyridine derivative into the secondary coordination sphere instead of a phenyl group of a simple triphenylphosphine ligand (Figure 1-6b).<sup>28</sup> This structural change increases the rate for hydration of alkynes and facilitates the reaction under milder conditions.<sup>28, 48, 54</sup> Incorporation of the acid/base site of the ligand away from the metal allows for structure activity relationships to be distinguished from the primary coordination sphere based on the performance of catalyst derivatives with different properties. However, producing a ligand family of sterically and electronically different derivatives can be synthetically challenging as R was restricted to sterically bulky alkyl groups for reactivity to occur and to prevent the acid/base site from binding to the metal.<sup>28, 55</sup>

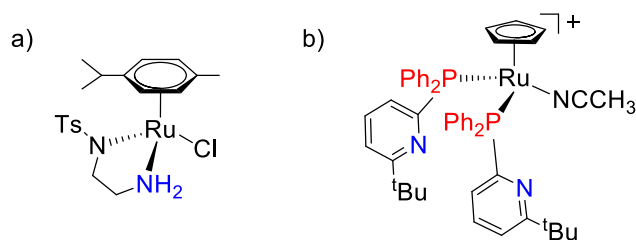


**Figure 1-6.** A proton shuttling MLC catalyst with the cooperative group (blue) positioned: a) in the primary coordination sphere;<sup>52</sup> and b) in the secondary coordination sphere<sup>28</sup>

An ideal MLC catalyst would have a high degree of tunability of the sterics and electronics in the first and second coordination spheres with the cooperative group of the ligand site positioned in the secondary coordination sphere.<sup>3, 56, 57</sup> The relationship between structure and catalyst performance for the primary and secondary coordination spheres could be deconvoluted for a MLC reaction. An in-depth understanding of the structure-activity relationships would allow new processes to be designed and allow increased performance for many MLC processes, such as hydration, hydrogenation/dehydrogenation, cyclization, etc.<sup>47, 49, 58</sup>

## 1.5 Tunable $P^R_2N^{R'}_2$ Ligands and $M(P^R_2N^{R'}_2)$ Complexes

A ligand that has demonstrated cooperativity and tunability is the 1,5-diaza-3,7-diphosphacyclooctane ( $P^R_2N^{R'}_2$ ) ligand.<sup>3, 50</sup> These ligands consist of an eight membered ring with two phosphine atoms in the 1,5-positions and two nitrogen atoms in the 3,7-positions. Linking the heteroatoms are methylene groups (Scheme 1-7a).<sup>59</sup> The tunability of the ligand arises from the R and R' groups that allows for the tuning of the steric and electronic properties<sup>17, 18, 50</sup> Typically the phosphine atoms chelate to a metal causing the R group to effect the electron density of the metal centre and steric environment of the substrate binding pocket within the primary coordination sphere.<sup>18</sup> The R' groups directly affect the basicity of the nitrogen atoms and steric environment of the amine, which are essential for a pendant base to facilitate proton shuttling effectively in second coordination sphere.<sup>17</sup> Utilization of these ligands on Ni has produced excellent electrocatalysts for  $H_2$  oxidation and production (Figure 1-7b).<sup>16, 46</sup> Use of electron rich R groups, such as cyclohexyl, causes an increase in electron density at the Ni centre via donation from the phosphine. Increased electron density at the Ni centre results in a lower  $pK_a$  for the Ni bound  $H_2$  molecule, which is favourable in  $H_2$  oxidation. Incorporation of a *t*-Bu group as the R' makes the pendent amine very basic but also sterically encumbered. After  $H_2$  binding,

deprotonation by the pendent amine is facile and due to sterics the conjugate acid of the pendent amine undergoes a conformational change to move away from the Ni hydride. Switching to  $R = \text{Ph}$  and  $R' = \text{Bn}$  inverts the direction of reactivity from  $\text{H}_2$  oxidation to  $\text{H}_2$  production.  $\text{H}_2$  generation is now favourable since the metal is less electron rich causing the Ni hydride to be more basic and the conjugate acid of the pendent amine is less sterically hindered allowing it to deliver a proton to the hydride. The direction for the electrocatalytic process is dependent on the type of  $R$  and  $R'$  groups present and thus tuning of the  $R$  and  $R'$  groups can switch a catalyst to favour either  $\text{H}_2$  production or oxidation.<sup>3, 46, 60</sup>

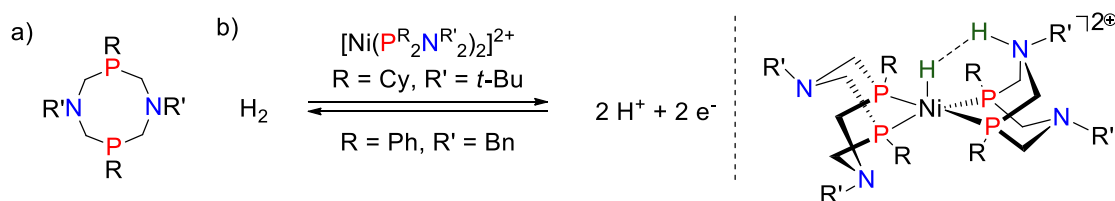


**Figure 1-7.** a) The structure of a  $\text{P}^{\text{R}}_2\text{N}^{\text{R}'_2}$ ,<sup>59</sup> and b) hydrogen oxidation and production can be favoured depending on the  $R$  and  $R'$  groups on the  $[\text{Ni}(\text{P}^{\text{R}}_2\text{N}^{\text{R}'_2})_2]^{2+}$ <sup>16-18</sup>

There are two known synthetic routes to access  $\text{P}^{\text{R}}_2\text{N}^{\text{R}'_2}$  ligands (Figure 1-8). Route A utilizes a primary phosphine that is treated with paraformaldehyde to generate an alkyl/aryl-bis(hydroxymethyl)phosphine intermediate (A). Two equivalents of this intermediate cyclize with an equimolar amount of a primary amine through four condensation reactions to give the desired  $\text{P}^{\text{R}}_2\text{N}^{\text{R}'_2}$  ligand.<sup>59, 61</sup> Route B exploits the same phosphine intermediate, which is instead formed by reacting tris(hydroxymethyl)phosphine (THP) and an alkyl chloride via a  $\text{S}_{\text{N}}2$  reaction to produce a cationic phosphonium salt. A hydroxymethyl group is then removed by adding  $\text{NEt}_3$  causing the production of  $[\text{HNEt}_3]\text{X}$ , one molecule of formaldehyde and one molecule of A. Intermediate A can then be cyclized as in Route A. Route A is a faster, more direct synthesis and can generate aryl and alkyl phosphine intermediates in high yields, but the route requires primary phosphines that are pyrophoric. Additionally, primary phosphines can be difficult to synthesize preventing access to a wide variety of derivatives. Route B is a generalized procedure from THP, a less hazardous starting material, but requires longer reaction times and is limited to  $\text{sp}^3$  alkyl carbon  $R$  substituents. Increasing the bulk of the  $\text{sp}^3$  carbon decreases reactivity leading to low yields of  $\text{P}^{\text{R}}_2\text{N}^{\text{R}'_2}$  ligands.<sup>62</sup>

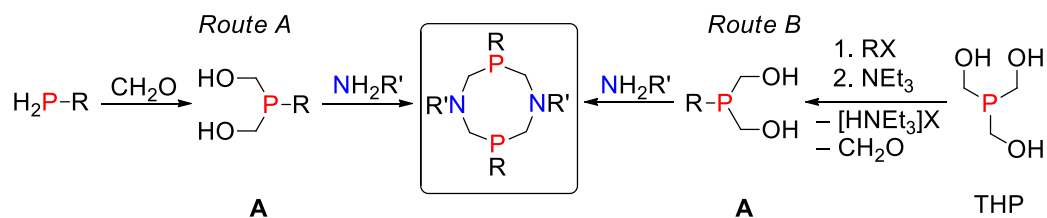


**Figure 1-8.** Two routes to synthesize  $\text{P}^{\text{R}}_2\text{N}^{\text{R}'_2}$  ligands. Route A proceeds from a primary phosphine.<sup>59</sup>  
<sup>61</sup> Route B proceeds from tris(hydroxymethyl)phosphine (THP)<sup>62</sup>

Utilization of the tunable  $\text{P}^{\text{R}}_2\text{N}^{\text{R}'_2}$  ligand with Ru generates a family of  $[\text{Ru}(\text{Cp}/\text{Cp}^*)(\text{P}^{\text{R}}_2\text{N}^{\text{R}'_2})(\text{X}/\text{L})]\text{PF}_6$  complexes. These piano-stool complexes have a chelating  $\text{P}^{\text{R}}_2\text{N}^{\text{R}'_2}$  ligand bound to the Ru metal centre with a cyclopentadienyl (Cp) or pentamethylcyclopentadienyl ( $\text{Cp}^*$ ) ligand. A halide or solvent molecule (X/L) occupies the 6<sup>th</sup> coordination site. The 6<sup>th</sup> coordination ligand is easily displaced to generate an open coordination site for substrate to bind during catalysis. The Mayer group and the Bullock group have previously synthesized derivatives of these complexes utilizing precursors  $\text{Ru}(\text{Cl})(\text{Cp})(\text{PPh}_3)_2$  or  $[\text{Ru}(\text{Cp}^*)(\text{Cl})_4]$  (Figure 1-9, Route A).<sup>63-65</sup> In order to generate an open coordination site  $\text{TiPF}_6$  must be used to perform a halide abstraction, which results in toxic  $\text{TiCl}$  byproduct (Figure 9, Route A). Both groups investigated the electrochemical properties of  $[\text{Ru}(\text{Cp}/\text{Cp}^*)(\text{P}^{\text{R}}_2\text{N}^{\text{R}'_2})(\text{X}/\text{L})]\text{PF}_6$  with  $\text{O}_2$ . Protonation of the pendent amine of  $[\text{Ru}(\text{Cp}/\text{Cp}^*)(\text{P}^{\text{R}}_2\text{N}^{\text{R}'_2})(\text{O}_2)]\text{PF}_6$  complexes led to a hydrogen bonding interaction between bound  $\text{O}_2$  and the pendent amine. This interaction demonstrates the metallacycles property to ring flip and interact with a potential substrate. The Blacquiere group has previously synthesized  $[\text{Ru}(\text{Cp})(\text{P}^{\text{R}}_2\text{N}^{\text{R}'_2})(\text{NCCH}_3)]\text{PF}_6$  ( $\text{R} = t\text{-Bu}, \text{Ph}; \text{R}' = \text{Bn}$ ) by ligand substitution with  $[\text{Ru}(\text{Cp})(\text{NCMe})_3]\text{PF}_6$  (Figure 1-9, Route B).<sup>66</sup> Ligand substitution is a fast, high yield reaction to synthesize new  $\text{Ru}-(\text{P}^{\text{R}}_2\text{N}^{\text{R}'_2})$  complexes for catalytic testing.<sup>66</sup>

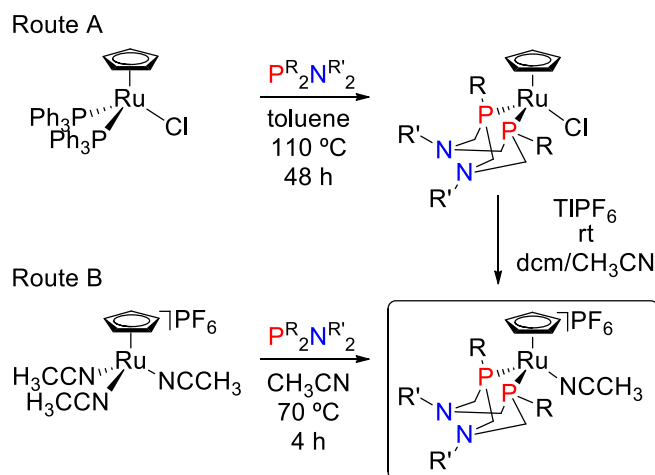


**Figure 1-9.** Synthesis of  $[\text{Ru}(\text{Cp})(\text{P}^{\text{R}}_2\text{N}^{\text{R}'_2})(\text{L})]\text{PF}_6$  complexes by two routes. Route A proceeds from  $\text{Ru}(\text{Cl})(\text{Cp})(\text{PPh}_3)_2$  through a ligand substitution and subsequent halide abstraction.<sup>63, 64</sup> Route B proceed via ligand substitution reaction from  $[\text{Ru}(\text{Cp})(\text{NCCH}_3)_3]\text{PF}_6$ <sup>66</sup>

Preliminary catalytic testing for hydration of alkynes with  $[\text{Ru}(\text{Cp})(\text{P}^{\text{t-Bu}}_2\text{N}^{\text{Bn}}_2)(\text{NCCH}_3)]\text{PF}_6$  showed no catalysis. This was unexpected due to the Ru complex possessing similar attributes to the previously reported hydration catalysts. A ruthenium vinylidene species, the key intermediate within the catalytic cycle, was expected to be formed between the alkyne and Ru complex. However, a stoichiometric reaction between phenylacetylene and  $[\text{Ru}(\text{Cp})(\text{P}^{\text{t-Bu}}_2\text{N}^{\text{Bn}}_2)(\text{NCCH}_3)]\text{PF}_6$  revealed a Ru-vinyl ammonium complex (**B**) was produced instead (Figure 1-10). Species **B** can be formed from nucleophilic attack of the Ru vinylidene with the pendent amine from the  $\text{P}^{\text{t-Bu}}_2\text{N}^{\text{Bn}}_2$  ligand. Addition of strong nucleophiles, such as Grignard reagents, revealed the complex **B** to be a thermodynamic energy sink and the reaction to be irreversible. A new approach is needed to overcome deactivation.<sup>66</sup>

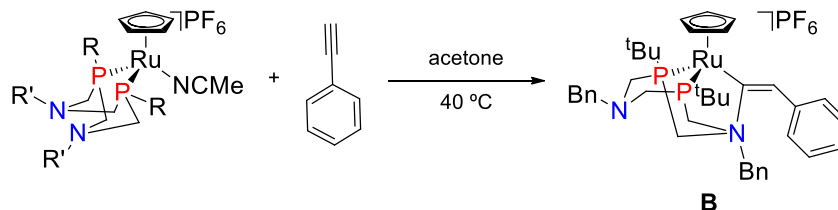


**Figure 1-10.** Deactivation of  $[\text{Ru}(\text{Cp})(\text{P}^{\text{t-Bu}}_2\text{N}^{\text{Bn}}_2)(\text{NCCH}_3)]\text{PF}_6$  with phenylacetylene<sup>66</sup>

## 1.6 Current Methods for Cyclization to Produce Heterocycles

Heterocycles play a key role in nature being found in DNA (e.g. adenosine), proteins (e.g. tryptophan), and chemical signaling (e.g. serotonin as a neurotransmitter). Current pharmaceuticals utilize derivatives of heterocycles since their structure inherently promotes or inhibits specific functions.<sup>67</sup> Some current routes to 5-membered *N*-heterocyclic structures use the Fischer-indole, Larock indole, or Paal-Knorr reactions.<sup>68-73</sup> The Fischer-indole reaction is a versatile reaction for producing indoles using phenylhydrazine and a ketone in an acidic solution (Scheme 11a). Buchwald-Hartwig amination can be coupled with the Fischer-indole reaction to use aryl bromides and hydrazones to produce functionalized hydrazines that can undergo the [3,3] sigmatropic rearrangement. Some functional groups are not tolerant of acidic conditions the high temperatures (>100 °C) that are essential for the reaction to proceed. Additionally, synthesis of certain substituents, such as C3 substituted indoles or electrophilic substituents resulting in competitive nucleophilicity at the nitrogen, cause the Fischer-indole reaction to fail and remains a challenge.<sup>70, 74, 75</sup> The Larock-indole reaction is an alternative synthesis for producing indoles (Scheme 1-11b). This Pd catalyzed reaction proceeds using a 2-iodoaniline derivative and an alkyne. It is complimentary to the Fischer-indole synthesis as it operates under basic conditions to allow a route for acid sensitive functional groups to be tolerated.<sup>71</sup> The Paal-Knorr reaction is also a widespread method for producing 5-membered rings. This reaction utilizes the aldol condensation of 1,4-diketone under acidic conditions to form furans, pyrroles (if a primary amine reagent is present), or thiophenes (if phosphorus pentasulfide reagent is present).<sup>73</sup> These methods represent cheap, efficient, and selective pathways that are used in fine chemical synthesis and the pharmaceutical industry.<sup>69, 73</sup> Future challenges within the pharmaceutical industry are to increase the structural diversity of the heterocyclic ring and expand the structural space of the heterocycle from planar (like aromatic rings) to non-planar (like cyclohexyl rings)” to find new drug opportunities. One drawback with the above methods is the lack of ring diversity synthetically possible. 5-Membered one heteroatom aromatized heterocycles, such as indoles, are the most common heterocyclic moieties. New complimentary methods are needed for heterocyclic diversity, and large membered rings, such as the azaindole or tetrahydropyran derivatives, respectively.<sup>76, 77</sup>

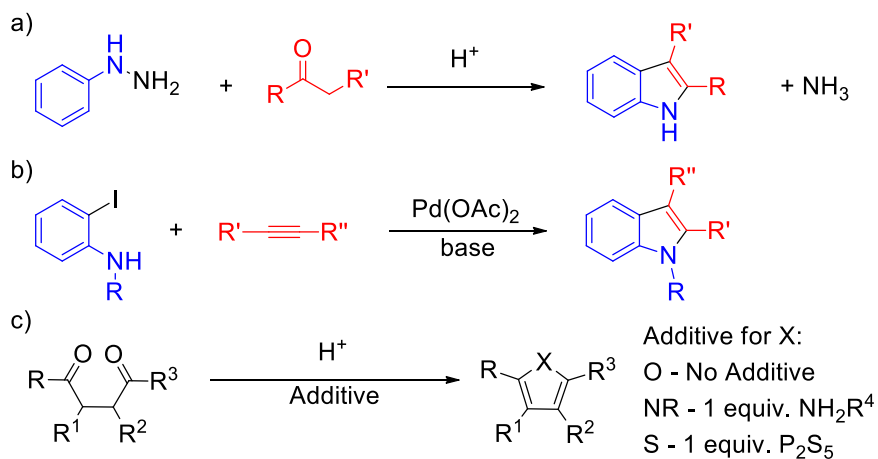


**Figure 1-11.** Common methods to form 5-membered heterocycles: a) Fischer-Indole synthesis; b) Larock Indole reaction; c) Paal-Knorr reaction<sup>68-73</sup>

Alkyne heteroatom cyclization is an alternative, atom-efficient process to access a greater diversity of heterocycles, including those with larger ring sizes.<sup>78, 79</sup> These reactions proceed through alkyne activation and subsequent cyclization using an intramolecular nucleophile. Two products can be formed as the alkyne can undergo nucleophilic attack at either carbon. The *exo-dig* product is produced when the nucleophile attacks the internal carbon of the alkyne while the *endo-dig* product is produced when the nucleophile attacks the terminal carbon (Scheme 1-12).<sup>78</sup> Generally, these reactions follow one of two main mechanisms each requiring a transition metal catalyst. The first route proceeds through  $\pi$ -coordination of an alkyne to the metal centre (Ru, Rh, Os) followed by a rearrangement to form a metal vinylidene.<sup>79-82</sup> A metal vinylidene is when a carbon atom, known as the alpha carbon ( $C\alpha$ ), forms a double bond with both a metal and another carbon atom. Cyclization selectivity is not an issue with Ru, Rh or Os complexes that proceed through a metal vinylidene intermediate since nucleophilic attack occurs only at the  $C\alpha$  (Scheme 1-12c). The selectivity is controlled by the difference in electrophilicity between the  $C\alpha$  and  $C\beta$  of the metal vinylidene.<sup>83, 84</sup> Incomplete backbonding of a pair of electron to form the double bond between the metal and the  $C\alpha$  causes the  $C\alpha$  to be more electrophilic in nature and thus the preferred site of nucleophilic attack.<sup>85</sup> Utilization of a Ru vinylidene produces the *endo-dig* product allowing for 5-, 6-, and 7-membered rings to be formed.<sup>29, 30</sup> Alternatively, electrophilic activation through  $\pi$ -coordination of an alkyne to an electrophilic metal (e.g. Au) can weaken the triple bond resulting in nucleophilic attack by an intramolecular alcohol or amine (Scheme 1-12b).<sup>78, 86-88</sup> Selectivity is difficult with this method as both carbon atoms of the triple bond are electrophilically activated which results in both the *exo-dig* and *endo-dig* products. Additionally, 5-membered rings are



favoured over 6 membered rings that cause a preferential formation of smaller membered heterocycles.<sup>87</sup>

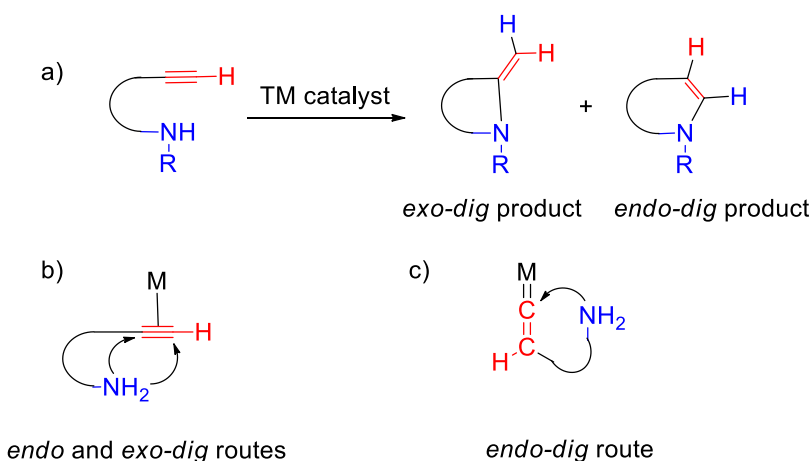


**Figure 1-12.** a) Alkyne heteroatom cyclization proceeding through: b) electrophilic  $\pi$  activation; and c) a metal vinylidene<sup>83</sup>

The mechanism for alkyne heteroatom cyclization is based on the same mechanism as intermolecular hydration of alkynes (Figure 1-13). It proceeds with the alkyne forming a sigma bond through  $\pi$ -donation to a metal centre (Figure 1-13: II). For ruthenium, the terminal proton of the alkyne is transferred to the metal. A 1,2 insertion of the alkyne into the Ru hydride then occurs producing the ruthenium vinylidene intermediate (III). The intramolecular nucleophile (X) then attacks the electrophilic  $C\alpha$  forming the *endo-dig* ring (IV). Protonation of the  $C\alpha$  is required release product and regenerate the starting catalyst. An exogenous base is critical to reactivity as deprotonation of the nucleophile and protonation of the  $C\alpha$  is required for product generation and release. Typically, strong exogenous bases are used in excess for bimolecular reaction to overcome the entropic challenge of the transition state required to facilitate proton transfer steps.<sup>30, 89</sup>

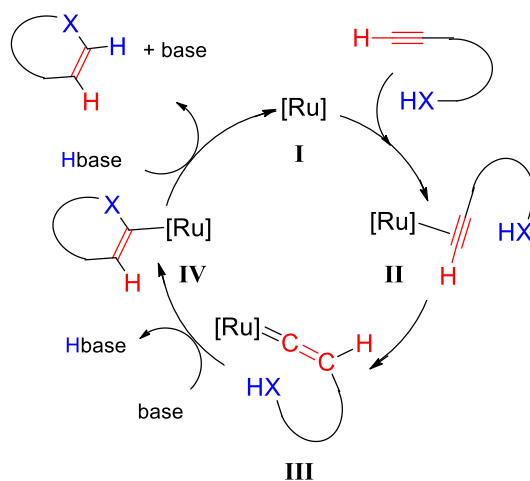


**Figure 1-13.** Catalytic cycle for intramolecular heteroatom cyclization for alkynes (X = O, NR) with exogenous base additive

Trost et al. in 1999 first reported the intramolecular cyclization of alkynyl alcohols with stoichiometric oxidant to produce lactones using 15 mol% of  $\text{Ru}(\text{Cl})(\text{Cp})(\text{PPh}_3)_2$  and an intermolecular base at 95 °C in a mixture of DMF and water. Use of small, electron withdrawing phosphine ligands, such as tri(2-furyl)phosphine, allowed for a decrease in catalytic loading to 4 mol% resulting in 93% conversion after 29 h.<sup>90</sup> Further advances with  $\text{RuCl}(\text{Cp})(\text{PR}_3)_2$  revealed that with an increase of electron density of the aryl substituent on the phosphine shifts the product selectivity from lactones to produce dihydropyrans. However, an oxidant and excess base were still necessary for the reaction to proceed (Figure 1-14a).<sup>91</sup> Similar reactivity was also reported by Trost using  $\text{Rh}(\text{Cl})(\text{PPh}_3)_3$  generated in situ where the best reactivity was observed with electron withdrawing aryl phosphine ligands (Figure 1-14c).<sup>92</sup> A later report in 2007 discussed the use of a  $[\text{Rh}(\text{cod})\text{Cl}]_2$  complex with triphenylphosphine capable of performing alkyne cyclization on 4-chloro-2-ethynylaniline and 4,6-dichloro-2-ethynylphenol forming oxygen and nitrogen heterocycles. Catalysis was most effective at low concentrations of substrate (200 mM) using 5 mol% of catalyst at 85 °C in DMF.<sup>89</sup> None of the catalysts above possess a cooperative ligand to facilitate the proton transfer steps. Instead, proton transfer steps are mediated by solvent, an oxidant, or exogenous base is used to facilitate these processes resulting in high catalytic loadings and high temperatures.

Further exploitation of  $\text{Ru}(\text{Cl})(\text{Cp})(\text{PPh}_3)_2$  was performed by Saá in 2009, 2011 and 2012.<sup>81, 82, 93</sup> Saá expanded the substrate scope using  $\text{RuCl}(\text{Cp})(\text{PPh}_3)_2$  with n-butylamine as the solvent at 90 °C. While this is an improvement as an oxidant is not required for the reaction to proceed, a high catalytic loading

of 10 mol% with the solvent acting as the excess intermolecular base at high temperatures is still necessary. Both oxygen and nitrogen 5- and 6-membered heterocycles with a variety of functional groups can be obtained. Additionally, switching to  $[\text{Os}(\text{Cp})(\text{py})_3]\text{PF}_6$  allowed for the generation of 7-membered *N*-heterocycles.<sup>79</sup>

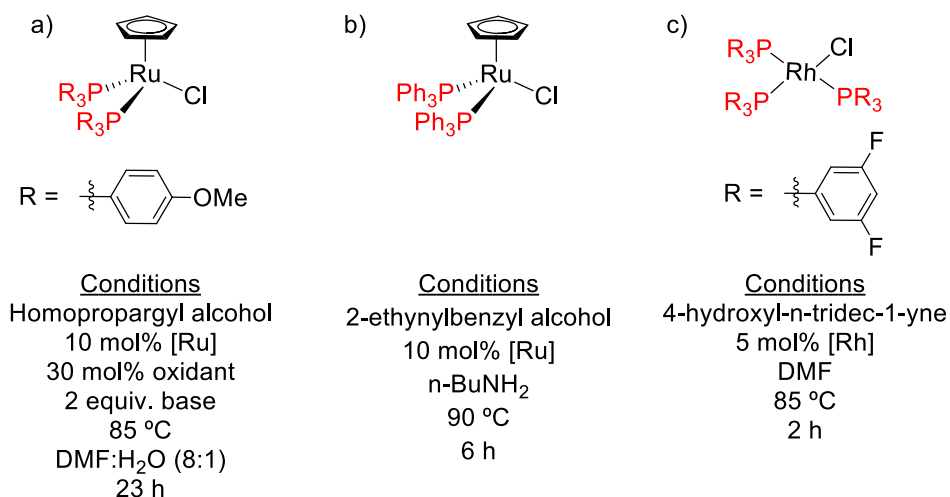


**Figure 1-14.** Alkyne heteroatom cyclization non-MLC catalysts and conditions to form *O*-heterocycles by: a) Trost using Ru;<sup>91</sup> b) Saá;<sup>82</sup> and c) Trost using Rh<sup>89</sup>

One method used to increase catalyst performance under milder reaction conditions is to include a cooperative ligand to facilitate proton shuttling. Grotjahn synthesized a complex based on  $\text{RuCl}(\text{Cp})(\text{PPh}_3)_2$  with the incorporation of a functional group into the secondary coordination sphere of the ligand (Figure 1-15a).<sup>28</sup>  $[\text{Ru}(\text{Cp})(\text{PPh}_2\text{Ar})_2(\text{NCCH}_3)]\text{PF}_6$  (Ar = 6-(tert-butyl)pyridin-2-yl) was found to operate in a cooperative manner due to the acid/base site, which increased performance for the hydration of alkynes to aldehydes.<sup>54</sup> In 2010, Grotjahn utilized this catalyst for alkyne heteroatom cyclization to generate indoles and benzopyrans. The MLC Ru catalyst was able to operate at 70 °C with 2 mol% catalyst in THF or acetone.<sup>29,30</sup> These conditions are much lower than Saá catalytic system of 10 mol% catalyst at 90 °C in exogenous base. However, the substrate scope was limited to 5-membered *O*- and *N*-heterocycles. Similar reaction conditions for heteroatom cyclization were reported by Jia using a  $[\text{Ru}(\text{N}_3\text{P})(\text{OAc})]\text{BF}_4$  complex ( $\text{N}_3\text{P}$  = tetradentate ligand) (Figure 1-15b). This complex cyclizes alkynyl alcohols to produce 5-, 6- and 7-membered *O*-heterocycles at 1-5 mol% at 80 °C in THF. Based on stoichiometric reactivity, the mechanism is expected to proceed through the ruthenium vinylidene intermediate with the acetate ligand potentially acting as a proton shuttle.<sup>94</sup>

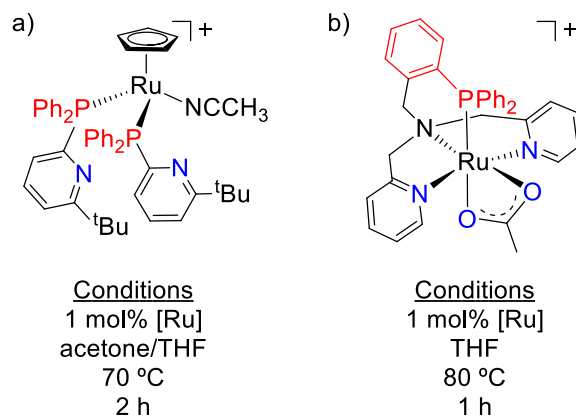


**Figure 1-15.** Alkyne heteroatom cyclization non-MLC catalysts and conditions to form *O*-heterocycles by: a) Grotjahn catalyst;<sup>29</sup> and b) Jia catalyst<sup>94</sup>

Currently, MLC Ru catalysts require high catalytic loadings (2 mol%) and operate at high temperatures (70 °C) to access simple substrates. More challenging 5-, 6- and 7-membered rings with greater substitution requires more forcing conditions to obtain high yields of product.

## 1.7 Current Methods of Acceptorless Dehydrogenation Catalysis

One area of catalysis often used in fine chemical synthesis is hydrogenation and dehydrogenation transformations.<sup>95</sup> Hydrogenation and dehydrogenation are also useful processes for chemical H<sub>2</sub> storage for the hydrogen fuel cell.<sup>96</sup> Transfer hydrogenation is a reaction that utilizes a MLC catalyst to perform dehydrogenation (of isopropanol) and hydrogenation (of ketones) to access chiral alcohols.<sup>97-99</sup> Typically, the ligand will accept a proton while the metal accepts a hydride from isopropanol to produce one unit of acetone. The acid/base site of the ligand is usually attached to the metal, which causes the electronic properties of the primary coordination sphere to significantly change following protonation. The hydride and proton can then be used to hydrogenate a ketone/imine substrate to a chiral alcohol/amine.<sup>53, 97</sup> Current transfer hydrogenation catalysts utilize Fe and are extremely efficient as they are able to reach high turnover numbers (5,000) under mild conditions (room temperature) (Figure 1-16).<sup>100</sup>

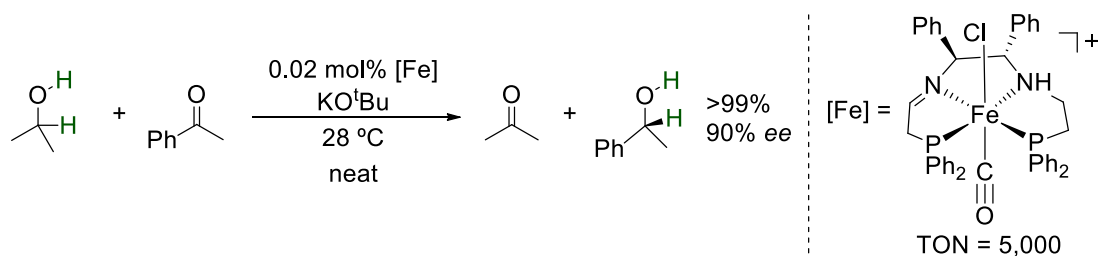


**Figure 1-16.** A transfer hydrogenation reaction using high performance Fe catalyst<sup>100</sup>

Until recently, catalytic dehydrogenation for the oxidation of amines or alcohols to imines, nitriles or ketones needed a H<sub>2</sub> acceptor to promote reactivity. Dehydrogenation is typically thermodynamically unfavourable since the formation of double/triple bonds is enthalpically unfavourable compared to the starting materials (Figure 1-17a). Use of stoichiometric H<sub>2</sub> acceptors can make dehydrogenation more thermodynamically favourable as the reaction products are more enthalpically favourable. Additionally, H<sub>2</sub> release is entropically favourable and can increase the favourability of the reaction. Stoichiometric H<sub>2</sub> acceptors can be eliminated by altering the equilibrium between the catalyst and the reversible process of H<sub>2</sub> release and binding to favour H<sub>2</sub> release (Figure 1-17b).<sup>101-106</sup> As dehydrogenation proceeds to completion, the H<sub>2</sub> pressure increases resulting in an increase in rate of H<sub>2</sub> binding to the metal centre until equilibrium is reached resulting in incomplete conversion. Use of an open vessel is one way to relieve the H<sub>2</sub> pressure and prevent H<sub>2</sub> from re-binding.<sup>102, 107</sup>

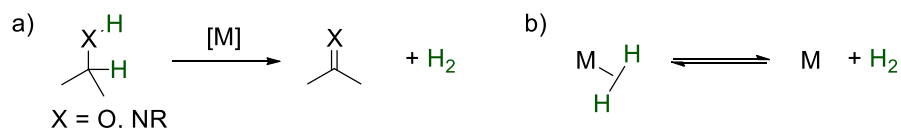


**Figure 1-17.** a) Acceptorless dehydrogenation reaction; and b) equilibrium between metal bound H<sub>2</sub> and free H<sub>2</sub>

Acceptorless dehydrogenation of alcohols is a useful synthetic tool for coupling polar groups such as amines and alcohols with each other without the use of an oxidant or base. Milstein in 2005 reported the successful dehydrogenation of alcohols, such as benzyl alcohol, to produce esters due to a nucleophilic attack of the aldehyde by starting material to generate a hemiacetal (Figure 1-18a).<sup>26, 108</sup> A second unit of H<sub>2</sub> is subsequently removed from the hemiacetal to form an ester. Harsh reaction conditions were required for the reaction (115 °C, 0.1 mol% [Ru], 0.1 mol% KOH, neat) for 72 h under open conditions. Increasing the temperature to 157 °C improved the rate of the reaction and led to a shorter reaction time (24 h). The MLC catalyst consisted of a Ru metal with a tridentate PNP pincer

ligand where methylene adjacent to the pyridyl group of the ligand is acting cooperatively (Figure 1-18b).<sup>108</sup> Further advances in performance were demonstrated by Gusev have shown that an Os(PNN) pincer complex operates at low catalytic loadings (0.05 mol%) with high conversion and low times (1.6 h) albeit high temperatures (158 °C) compared to Ru(PNN) analogues (Figure 1-18c).<sup>19</sup> In 2013, Beller and Grutzmacher separately reported the dehydrogenation of methanol and water to carbon dioxide and three units of H<sub>2</sub> gas. Both reports utilize a Ru catalyst at high temperatures (90 °C).<sup>109, 110</sup> Beller used a tridentate PNP pincer ligand where the amine acts as the acid/base site on the ligand for proton transfer steps (Figure 1-18d).<sup>109</sup> Grutzmacher also used a cooperative ligand. However, his ligand was the tetradentate trop<sub>2</sub>dad ligand. Both amines act as proton acceptors while the ethylene backbone and metal accepts the hydride to facilitate the MLC process (Figure 1-18e).<sup>110</sup>

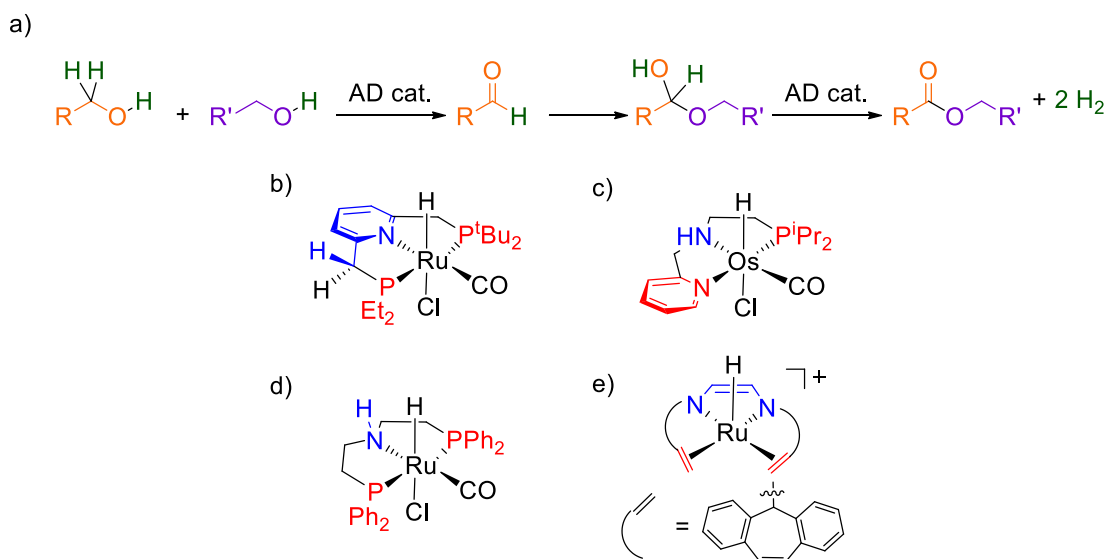


**Figure 1-18.** a) Acceptorless dehydrogenation of alcohols;<sup>26</sup> b) Milstein catalyst for acceptorless dehydrogenation of alcohols;<sup>108</sup> c) Gusev catalyst for acceptorless dehydrogenation of alcohols;<sup>19</sup> d) Beller catalyst;<sup>109</sup> and e) Grutzmacher catalyst for acceptorless dehydrogenation of methanol<sup>110</sup>

Amines present a difficult, but rewarding dehydrogenation substrate as a target for both H<sub>2</sub> storage and fine chemical synthesis.<sup>26</sup> The current catalysts for AD of amines operate under harsh conditions and can produce many side products due to competitive routes such as acceptorless dehydrogenative coupling (ADC), hydrogen borrowing (HB) and double acceptorless dehydrogenation (DAD) (Figure 1-19).<sup>35</sup> These alternative routes can be useful, but only if the catalyst is operating selectively. Primary amines can act as a source of up to two equivalents of H<sub>2</sub> and nitriles.<sup>102, 107</sup> However, coupling of the imine intermediate with a second amine substrate can lead to the ADC product. Benzylamine is

commonly used as a benchmark to compare catalyst selectivity. Possible products that can arise from benzylamine are the AD product, phenylmethanimine, the ADC product, 1-(phenylmethyl)-*N*-phenylmethanimine, the DAD product, benzonitrile, and the HB product, dibenzylamine.<sup>107</sup> Indoline is commonly used to evaluate catalyst performance since only one product (indole) is typically produced.<sup>111</sup>

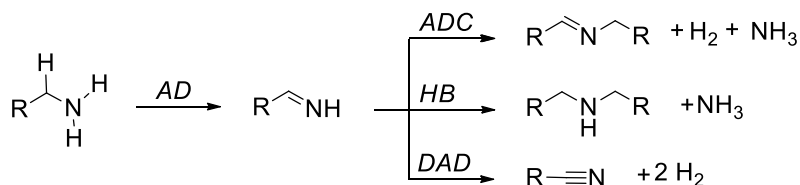


**Figure 1-19.** General reactions for a primary amine for AD, ADC, HB, and DAD<sup>107</sup>

Three main plausible mechanistic routes exist for acceptorless dehydrogenation of amines: 1) outer-sphere MLC (Figure 1-20a); 2) inner-sphere MLC (Figure 1-20b); and 3) inner-sphere non-MLC (Figure 1-20c). These three mechanisms are based on the related mechanisms developed and studied for hydrogenation chemistry.<sup>53, 112</sup> In an outer-sphere MLC mechanism, a hydride is transferred to the metal centre from the carbon adjacent to the amine, while the ligand accepts a proton from the amine. The hydride transfer and deprotonation steps can occur in a stepwise or concerted process. The metal-hydride is then protonated by the ligand and H<sub>2</sub> is released from the metal centre.<sup>53</sup> An inner-sphere mechanism proceeds through binding of the substrate through the lone pair of the amine.  $\beta$ -Hydride elimination can then occur to produce an imine and a ruthenium hydride. Deprotonation of the substrate can occur before or after  $\beta$ -hydride elimination. If the ligand acts as the base the route is cooperative.<sup>112</sup> Whereas, if an external base (i.e. another unit of substrate or another unit of catalyst in the M-H form) deprotonates the substrate, the route is non-MLC.<sup>113</sup>

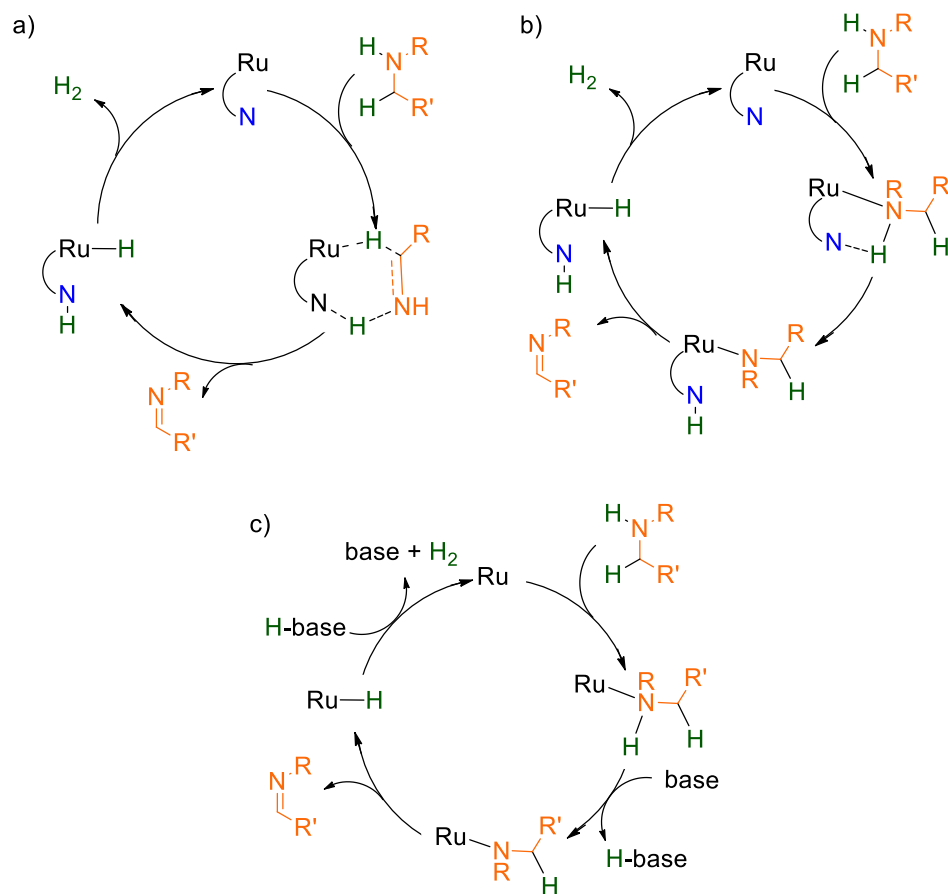


**Figure 1-20.** Three mechanistic pathways for acceptorless dehydrogenation of amines: a) outer-sphere MLC;<sup>53</sup> b) inner-sphere MLC;<sup>112</sup> and c) inner-sphere non-MLC mechanisms<sup>113</sup>

In 1990, Watanabe published the first example of acceptorless dehydrogenation of an amine with a homogenous catalyst. The catalyst comparison found that  $\text{RuCl}_2(\text{PPh}_3)_3$  had the highest performance of a non-MLC complex toward AD of indoline at 2 mol% at 110 °C in toluene. Complete conversion was observed after 6 h (Figure 1-21a).<sup>111</sup> A Ru complex that operates under similar conditions was produced by Szymczak in 2013. This catalyst consists of a tridentate NNN pincer ligand, two triphenylphosphine ligands and a ruthenium hydride that performs acceptorless dehydrogenation of alkyl amines to nitriles at 1 mol% at 110 °C in toluene after 24 h under closed conditions (Figure 1-21b).<sup>102</sup> The NNN pincer ligand has the potential to be cooperative. However, mechanistic investigation revealed the most plausible pathway for protonation of the hydride was by the substrate causing  $\text{H}_2$  release. Substrate deprotonation generates an anionic amine substrate, which binds to the metal centre.  $\beta$ -Hydride elimination then occurs regenerating the hydride (Figure 1-20c).<sup>113</sup>



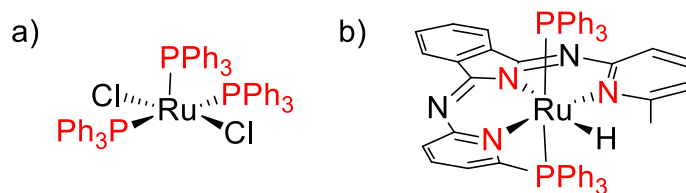


**Figure 1-21.** Non-MLC catalysts for acceptorless dehydrogenation: a) Watanabe catalyst;<sup>111</sup> and b) Szymczak catalyst<sup>113</sup>

Other examples of AD typically use a Ru catalyst above 120 °C and with catalytic loadings of 1 – 5 mol% for over 24 h in toluene.<sup>102, 105, 106</sup> Albrecht utilized a *p*-cymene piano-stool Ru catalyst with either a strongly electron donating *N*-heterocyclic carbene (NHC) or triazolidene ligand (Figure 1-22a). Acceptorless dehydrogenation of benzyl amine to give the ADC product selectively using harsh conditions of 5 mol% of catalyst in toluene at 150 °C for 12 h is required to reach completion under closed conditions. The mechanism for this catalyst is unknown but it is possible that an amine on the NHC/triazolidene ligand could act as the acid/base site for an inner or outer-sphere MLC pathway.<sup>106</sup> Yu exploited a Ru(NNN) pincer complex to perform acceptorless dehydrogenation of indoline at 2 mol% in *o*-xylene at 140 °C under open conditions reaching complete conversion to indole after 48 h (Figure 1-22b).<sup>114</sup> The proposed mechanism suggests that the Ru(NNN) pincer ligand operates in an inner-sphere non-MLC pathway. However, the exact mechanistic route has not been fully investigated. The central nitrogen could accept a proton from substrate supported by an aromatization/dearomatization mechanism while the metal accepts the hydride providing a route for an inner or outer-sphere MLC pathway. The Shvo catalyst can also perform acceptorless dehydrogenation of indoline at high temperature (165 °C) in mesitylene with a catalyst loading of 2.5 mol% under closed conditions for 24 h (Figure 1-22c). The Shvo catalyst is a Ru piano stool dimer, in which a hydride ligand is able bridge the two Ru centres due to hydrogen bonding stabilization between the hydroxyl groups of the two cyclopentadiene ligands. Indole is formed through an inner-sphere MLC pathway with the alcohol on the Cp of the catalyst acting as the acid/base site.<sup>104</sup> In 2012, Huang reported a Ru(PNP) pincer catalyst for acceptorless dehydrogenation of benzylamine (Figure 22d). The reaction was selective for the ADC product with 1 mol% catalyst at 115 °C in toluene under open conditions. The Ru(PNP) pincer catalyst is thought to operate through an outer-sphere MLC mechanism with the imine in the backbone of the ligand acting as the acid/base site.<sup>105</sup> Even though some of these catalysts are thought to proceed through a MLC mechanism, the overall performance remains low compared to

the benefit of an MLC systems observed in other areas of catalysis. The potential scope for both alcohols and amines is limited since the reaction requires high temperatures to proceed with electronically biased substrate due to the thermodynamic driving force of aromaticity.<sup>105, 106</sup>

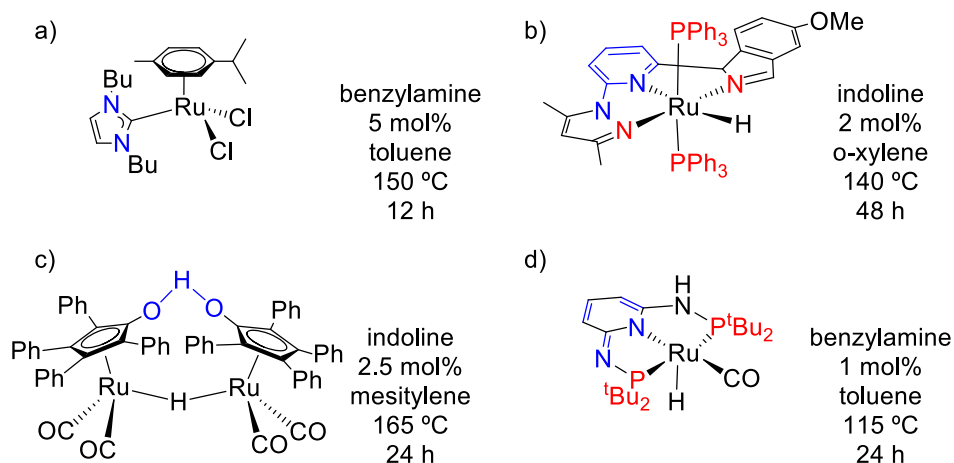


**Figure 1-22.** MLC catalysts for acceptorless dehydrogenation of amines: a) Albrecht catalyst;<sup>106</sup> b) Yu catalyst;<sup>114</sup> c) Shvo catalyst;<sup>104</sup> and d) Huang catalyst<sup>105</sup>

One recent example has demonstrated the benefit of a MLC catalytic system toward acceptorless dehydrogenation of amines. Bera reported the acceptorless dehydrogenation of benzyl amine at a much lower temperature (70 °C vs. >110 °C) than previous Ru catalysts under similar catalytic loading (2 mol%) after 24 h (Figure 1-23). Benzonitrile was produced in 89% yield employing an open system to prevent H<sub>2</sub> binding. This catalyst possesses a Ru centre and it features a pyrazole group within the secondary coordination sphere. Methylation of the pyrazole cooperative site causes a significant decrease in catalytic performance as the acid/base site of the secondary coordination sphere cannot act as a base. Computational data of the reaction mechanism suggests an outer-sphere MLC mechanism (Figure 1-20a). Additionally, an intermolecular base was used to deprotonate the pyrazole to initiate catalysis.<sup>115</sup> These findings reveal the need a strong base in the secondary coordination sphere of the ligand to increase catalytic performance. When the reaction was conducted under closed conditions, a significant decrease in reactivity was also observed. Therefore, H<sub>2</sub> release is still in equilibrium with H<sub>2</sub> binding.

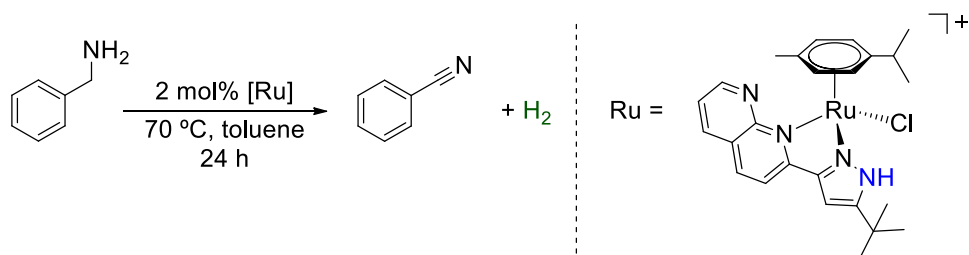


**Figure 1-23.** Bera MLC catalysts for acceptorless dehydrogenation of benzyl amine to produce a nitrile<sup>116</sup>

## 1.8 Scope of Thesis

A family of MLC catalysts is needed to develop design principles for new MLC catalysts to facilitate certain reaction steps. Systematic structure-activity relationships provide a way to understand the favourable properties required for optimal performance by comparing differences in catalyst performance to a standard. A series of  $[\text{Ru}(\text{Cp})(\text{P}^{\text{R}}_2\text{N}^{\text{R}'_2})(\text{NCMe})]\text{PF}_6$  complexes was prepared to probe the electronic and steric properties of the primary ( $\text{R} = \text{Ph}, t\text{-Bu}, \text{Bn}; \text{R}' = \text{Bn}$ ) and secondary coordination sphere ( $\text{R} = \text{Ph}; \text{R}' = \text{Bn}, \text{Ph}, \text{Mes}, p\text{-CH}_3\text{O-C}_6\text{H}_4, p\text{-CF}_3\text{-C}_6\text{H}_4$ ). These complexes are used to investigate the reactivity for two different types of organic reactions: 1) intramolecular heteroatom cyclization of alkynes; and 2) acceptorless dehydrogenation of amines.

In chapter two, the balance between productive catalysis and deactivation is explored for cyclization. The first successful application of the  $\text{P}^{\text{R}}_2\text{N}^{\text{R}'_2}$  ligand family toward an organic transformation is described. The cationic pre-catalysts  $[\text{Ru}(\text{Cp})(\text{P}^{\text{R}}_2\text{N}^{\text{Bn}_2})(\text{MeCN})]\text{PF}_6$  ( $\text{R} = t\text{-Bu}$  and  $\text{Ph}$ ) are active toward the cyclization of 2-ethynylbenzyl alcohol at low catalyst loading and moderate temperatures. Catalyst performance however is limited by both low conscription of the pre-catalyst into the catalytic cycle and by competitive deactivation of a key vinylidene intermediate. A control complex was synthesized to determine if the  $\text{P}^{\text{R}}_2\text{N}^{\text{R}'_2}$  ligands are acting cooperatively in cyclization.

In chapter three, the effects of altering the properties of the acid/base site in the secondary coordination sphere were explored for the cyclization of heterocycles. Utilization of the tunable  $\text{P}^{\text{R}}_2\text{N}^{\text{R}'_2}$  ligands, a new array of  $\text{Ru}(\text{P}^{\text{R}}_2\text{N}^{\text{R}'_2})$  complexes ( $\text{R} = \text{Ph}; \text{R}' = \text{Ph}, \text{Mes}, p\text{-CH}_3\text{O-C}_6\text{H}_4, p\text{-CF}_3\text{-C}_6\text{H}_4$ ) were synthesized. Additionally, the benefit of one and two acid/base sites were compared. The catalytic performance was evaluated with 2-ethynylbenzyl alcohol and 2-ethynylaniline. Structure-activity

relationships were developed for understanding the importance of the sterics and basicity of the pendant amine in the secondary coordination sphere.

In chapter four, a series of piano-stool  $[\text{Ru}(\text{P}^{\text{R}}_2\text{N}^{\text{R}'_2})]$  complexes (Cp/Cp\*; R = *t*-Bu, Ph, Bn; R' = Ph or Bn) were synthesized and compared to determine the structure-activity relationships of the primary coordination sphere for the cyclization of alkynes via intramolecular attack by amines and alcohols to produce 5- and 6-membered heterocycles. An optimal catalyst displayed excellent performance (TON = 802, 70 °C, 2 h) relative to previous catalytic systems (TON = 49, 70 °C, 7 h). The robustness and scope of this optimal catalyst was examined through use of additives during catalysis and cyclization of several substrate derivatives.

In chapter five,  $[\text{Ru}(\text{Cp})(\text{P}^{\text{Ph}}_2\text{N}^{\text{Bn}}_2)(\text{MeCN})]\text{PF}_6$  and  $[\text{Ru}(\text{Cp})(\text{dppp})(\text{MeCN})]\text{PF}_6$  complexes were determined to be active for the acceptorless dehydrogenation of benzylamine ( $\text{BnNH}_2$ ) and nitrogen heterocycles. The two catalysts have similar activity, but different selectivity for dehydrogenation products. Independent synthesis of a  $[\text{Ru}(\text{Cp})(\text{P}^{\text{Ph}}_2\text{N}^{\text{Bn}}_2)(\text{NH}_2\text{Bn})]\text{PF}_6$  adduct reveals the presence of a hydrogen bond between the bound amine and the pendant base of the  $\text{P}^{\text{Ph}}_2\text{N}^{\text{Bn}}_2$  ligand. Preliminary mechanistic studies reveal the benzylamine adduct is not an on-cycle catalyst intermediate.

In chapter six, a catalyst comparison of  $[\text{Ru}(\text{P}^{\text{R}}_2\text{N}^{\text{R}'_2})]$ ,  $[\text{Ru}(\text{P}^{\text{R}}_2\text{N}^{\text{R}'_1})]$ , and  $[\text{Ru}(\text{P}-\text{P})]$  complexes for acceptorless dehydrogenation catalysis of indoline was performed. Through the tunability of the primary coordination sphere (R = Ph, *t*-Bu, Bn), the effects of electronic and steric properties surrounding the Ru centre are explored. The importance of the pendant amines present in the secondary coordination sphere is explored through varying the number of basic functional groups. Additionally, the sterics and basicity of the pendant amine was investigated to understand the optimum factors for proton shuttling. Furthermore, a kinetic analysis to determine reaction order was conducted for indoline, with MLC and non-MLC Ru complexes. Finally, altering the electronics and sterics of substituents on the substrate allow for mechanistic insight into the reaction pathway.

## 1.9 References

1. Grubbs, R. H., *Handbook of Metathesis*. Wiley-VCH: Weinheim, 2003.
2. Noyori, R.; Yamakawa, M.; Hashiguchi, S., *J. Org. Chem.* **2001**, *66* (24), 7931-7944.
3. DuBois, D. L.; Bullock, R. M., *Eur. J. Inorg. Chem.* **2011**, *2011* (7), 1017-1027.
4. Anastas, P.; Eghbali, N., *Chem. Soc. Rev.* **2010**, *39* (1), 301-312.

5. Meijere, A. D.; Diederich, F. O., *Metal-catalyzed cross-coupling reactions*. Wiley-VCH: Weinheim; Chichester, **2004**; Vol. 2nd.
6. Crabtree, R. H., *The Organometallic Chemistry of the Transition Metals*. Wiley-Interscience: Hoboken, N.J, **2005**; Ed. 4th.
7. Anastas, P. T.; Kirchhoff, M. M., *Acc. Chem. Res.* **2002**, *35* (9), 686-694.
8. Dach, R.; Song, J. J.; Roschangar, F.; Samstag, W.; Senanayake, C. H., *Org. Process Res. Dev.* **2012**, *16* (11), 1697-1706.
9. Copéret, C.; Chabanas, M.; Petroff Saint-Arroman, R.; Basset, J.-M., *Angew. Chem. Int. Ed.* **2003**, *42* (2), 156-181.
10. Brown, D. G.; Boström, J., *J. Med. Chem.* **2016**, *59* (10), 4443-4458.
11. Higman, C. S.; Lummiss, J. A. M.; Fogg, D. E., *Angew. Chem. Int. Ed.* **2016**, *55* (11), 3552-3565.
12. E.B. Bauer, R. B. B., P.B. Brenner, P.-A.R. Breuil, G.J.P. Britovsek, B. Burcher, C. Darcel, D.P. de Sousa, S. Gaillard, M. Grau, M. Itazaki, H. Keipour, L. Magna, C.J. McKenzie, H. Nakazawa, H. Olivier-Bourbigou, T. Ollevier, J.-L. Renaud, J.-B. Sortais, *Iron Catalysis II*. Springer: Cham, **2015**.
13. Monfette, S.; Blacquiere, J. M.; Fogg, D. E., *Organometallics* **2011**, *30* (1), 36-42.
14. Constable, D. J. C.; Dunn, P. J.; Hayler, J. D.; Humphrey, G. R.; Leazer, J. J. L.; Linderman, R. J.; Lorenz, K.; Manley, J.; Pearlman, B. A.; Wells, A.; Zaks, A.; Zhang, T. Y., *Green Chem.* **2007**, *9* (5), 411-420.
15. Doppiu, A.; Caijo, F.; Tripoteau, F.; Bompard, S.; Crévisy, C.; Mauduit, M., *Top. Catal.* **2014**, *57* (17-20), 1351-1358.
16. Bullock, R. M.; Helm, M. L., *Acc. Chem. Res.* **2015**, *48* (7), 2017-2026.
17. Kilgore, U. J.; Roberts, J. A. S.; Pool, D. H.; Appel, A. M.; Stewart, M. P.; DuBois, M. R.; Dougherty, W. G.; Kassel, W. S.; Bullock, R. M.; DuBois, D. L., *J. Am. Chem. Soc.* **2011**, *133* (15), 5861-5872.
18. Kilgore, U. J.; Stewart, M. P.; Helm, M. L.; Dougherty, W. G.; Kassel, W. S.; DuBois, M. R.; DuBois, D. L.; Bullock, R. M., *Inorg. Chem.* **2011**, *50* (21), 10908-10918.
19. Spasyuk, D.; Smith, S.; Gusev, D. G., *Angew. Chem. Int. Ed.* **2012**, *51* (11), 2772-2775.
20. Magano, J.; Dunetz, J. R., *Chem. Rev.* **2011**, *111* (3), 2177-2250.
21. M. Akita, P. G. A., E. Balaraman, M. Beller, C. Bruneau, V. Cadierno, B. Chaudret, P. Crochet, S. De'rien, P.H. Dixneuf, C. González-Rodríguez, R.H. Grubbs, M.B. Herbert, H. Junge, T. Koike, B. Li, P. Lignier, V.M. Marx, D. Mellmann, D. Milstein, K. Philippot, L.E. Rosebrugh, C. Saa', J.A. Varela, *Ruthenium in Catalysis*. Springer: Cham, **2014**.
22. Emsley, J., *Nature's Building Blocks: An A-Z Guide to the Elements*. 2nd Edition ed.; Oxford University Press: New York, **2011**.
23. Griffith, W. P., *Ruthenium Oxidation Complexes: Their Uses as Homogenous Organic Catalysts*. Springer: Dordrecht, **2011**.

24. Crabtree, R. H., Multifunctional ligands in transition metal catalysis. *New J. Chem.* **2011**, *35* (1), 18-23.
25. van der Vlugt, J. I., *Eur. J. Inorg. Chem.* **2012**, *2012* (3), 363-375.
26. Gunanathan, C.; Milstein, D., *Science* **2013**, *341* (6143), 1229712.
27. Michrowska, A.; Bujok, R.; Harutyunyan, S.; Sashuk, V.; Dolgonos, G.; Grela, K., *J. Am. Chem. Soc.* **2004**, *126* (30), 9318-9325.
28. Grotjahn, D. B., *Chem. Eur. J.* **2005**, *11* (24), 7146-7153.
29. Nair, R. N.; Lee, P. J.; Grotjahn, D. B., *Top. Catal.* **2010**, *53* (15), 1045-1047.
30. Nair, R. N.; Lee, P. J.; Rheingold, A. L.; Grotjahn, D. B., *Chem. Eur. J.* **2010**, *16* (27), 7992-7995.
31. Grotjahn, D. B., *Dalton Trans.* **2008**, *46*, 6497-6508.
32. Grubbs, R. H., *Angew. Chem., Int. Ed.* **2006**, *45* (23), 3760-3765.
33. Ritter, T.; Hejl, A.; Wenzel, A. G.; Funk, T. W.; Grubbs, R. H., *Organometallics* **2006**, *25* (24), 5740-5745.
34. Yee, N. K.; Farina, V.; Houpis, I. N.; Haddad, N.; Frutos, R. P.; Gallou, F.; Wang, X.-J.; Wei, X.; Simpson, R. D.; Feng, X.; Fuchs, V.; Xu, Y.; Tan, J.; Zhang, L.; Xu, J.; Smith-Keenan, L. L.; Vitous, J.; Ridges, M. D.; Spinelli, E. M.; Johnson, M.; Donsbach, K.; Nicola, T.; Brenner, M.; Winter, E.; Kreye, P.; Samstag, W., *J. Org. Chem.* **2006**, *71* (19), 7133-7145.
35. Döbereiner, G. E.; Crabtree, R. H., *Chem. Rev.* **2010**, *110* (2), 681-703.
36. Cook, S. A.; Borovik, A. S., *Acc. Chem. Res.* **2015**, *48* (8), 2407-2414.
37. Himeda, Y.; Onozawa-Komatsuzaki, N.; Sugihara, H.; Kasuga, K., *Organometallics* **2007**, *26* (3), 702-712.
38. Onishi, N.; Xu, S.; Manaka, Y.; Suna, Y.; Wang, W.-H.; Muckerman, J. T.; Fujita, E.; Himeda, Y., *Inorg. Chem.* **2015**, *54* (11), 5114-5123.
39. Cheng, H. F.; d'Aquino, A. I.; Barroso-Flores, J.; Mirkin, C. A., *J. Am. Chem. Soc.* **2018**, *140* (44), 14590-14594.
40. Michelin, C.; Hoffmann, N., *ACS Catal.* **2018**, *8* (12), 12046-12055.
41. Samantaray, M. K.; Shaikh, M. M.; Ghosh, P., *Organometallics* **2009**, *28* (7), 2267-2275.
42. Esteruelas, M. A.; Fernández-Alvarez, F. J.; Oliván, M.; Oñate, E., *Organometallics* **2009**, *28* (7), 2276-2284.
43. Breit, B.; Gellrich, U.; Li, T.; Lynam, J. M.; Milner, L. M.; Pridmore, N. E.; Slattery, J. M.; Whitwood, A. C., *Dalton Trans.* **2014**, *43* (29), 11277-11285.
44. Chevallier, F.; Breit, B., *Angew. Chem. Int. Ed.* **2006**, *45* (10), 1599-1602.
45. Wenz, K. M.; Leonhardt-Lutterbeck, G.; Breit, B., *Angew. Chem. Int. Ed.* **2018**, *57* (18), 5100-5104.
46. Bullock, R. M.; Appel, A. M.; Helm, M. L., *Chem. Commun.* **2014**, *50* (24), 3125-3143.

47. Grotjahn, D. B., *Top. Catal.* **2010**, *53* (15-18), 1009-1014.
48. Grotjahn, D. B.; Incarvito, C. D.; Rheingold, A. L., *Angew. Chem. Int. Ed.* **2001**, *40* (20), 3884-3887.
49. Sues, P. E.; Demmans, K. Z.; Morris, R. H., *Dalton Trans.* **2014**, *43* (21), 7650-7667.
50. Wiedner, E. S.; Yang, J. Y.; Dougherty, W. G.; Kassel, W. S.; Bullock, R. M.; DuBois, M. R.; DuBois, D. L., *Organometallics* **2010**, *29* (21), 5390-5401.
51. O, W. W. N.; Lough, A. J.; Morris, R. H., *Organometallics* **2012**, *31* (6), 2137-2151.
52. Noyori, R.; Hashiguchi, S., *Acc. Chem. Res.* **1997**, *30* (2), 97-102.
53. Samec, J. S. M.; Backvall, J.-E.; Andersson, P. G.; Brandt, P., *Chem. Soc. Rev.* **2006**, *35* (3), 237-248.
54. Grotjahn, D. B.; Lev, D. A., *J. Am. Chem. Soc.* **2004**, *126* (39), 12232-12233.
55. Hintermann, L.; Xiao, L.; Labonne, A. I.; Englert, U., *Organometallics* **2009**, *28* (19), 5739-5748.
56. Chirik, P. J., Modern Alchemy: Replacing Precious Metals with Iron in Catalytic Alkene and Carbonyl Hydrogenation Reactions. In *Catalysis without Precious Metals*, Bullock, R. M., Ed. Wiley-VCH: Weinheim, **2010**.
57. Prokopchuk, D. E.; Morris, R. H., *Organometallics* **2012**, *31* (21), 7375-7385.
58. Boeck, F.; Kribber, T.; Xiao, L.; Hintermann, L., *J. Am. Chem. Soc.* **2011**, *133* (21), 8138-8141.
59. G. Märkl, V.; Jin, G. Y.; Schoerner, C., *Tetrahedron Lett.* **1980**, *21* (15), 1409-1412.
60. Weiss, C. J.; Das, P.; Miller, D. L.; Helm, M. L.; Appel, A. M., *ACS Catal.* **2014**, *4* (9), 2951-2958.
61. Frazee, K.; Wilson, A. D.; Appel, A. M.; Rakowski DuBois, M.; DuBois, D. L., *Organometallics* **2007**, *26* (16), 3918-3924.
62. Doud, M. D.; Grice, K. A.; Lilio, A. M.; Seu, C. S.; Kubiak, C. P., *Organometallics* **2012**, *31* (3), 779-782.
63. Tronic, T. A.; Kaminsky, W.; Coggins, M. K.; Mayer, J. M., *Inorg. Chem.* **2012**, *51* (20), 10916-10928.
64. Tronic, T. A.; Rakowski DuBois, M.; Kaminsky, W.; Coggins, M. K.; Liu, T.; Mayer, J. M., *Angew. Chem. Int. Ed.* **2011**, *50* (46), 10936-10939.
65. Liu, T.; DuBois, M. R.; DuBois, D. L.; Bullock, R. M., *Energy & Environ. Sci.* **2014**, *7* (11), 3630-3639.
66. Bow, J.-P. J.; Boyle, P. D.; Blacquiere, J. M., *Eur. J. Inorg. Chem.* **2015**, *2015* (25), 4162-4166.
67. Quin, L. D.; Tyrell, J. A., *Fundamentals of Heterocyclic Chemistry: Importance in Nature and in the Synthesis of Pharmaceuticals*. John Wiley & Sons Inc.: Hoboken, New Jersey, **2010**; p 327.

68. Barden, T. C., Indoles: Industrial, Agricultural and Over-the-Counter Uses. In *Heterocyclic Scaffolds II: Reactions and Applications of Indoles*, Gribble, G. W., Ed. Springer Berlin Heidelberg: Berlin, Heidelberg, **2010**; pp 31-46.
69. Gribble, G. W., *Indole Ring Synthesis: From Natural Products to Drug Discovery*. John Wiley & Sons Ltd.: Chichester, **2016**.
70. Wagaw, S.; Yang, B. H.; Buchwald, S. L., *J. Am. Chem. Soc.* **1999**, *121* (44), 10251-10263.
71. Zeni, G.; Larock, R. C., *Chem. Rev.* **2006**, *106* (11), 4644-4680.
72. Humphrey, G. R.; Kuethe, J. T., *Chem. Rev.* **2006**, *106* (7), 2875-2911.
73. Li, J. J.; Li, R. C., *Heterocyclic Chemistry in Drug Discovery*. John Wiley & Sons, Incorporated: Oxford, United States, **2013**.
74. Simmons, B. J.; Hoffmann, M.; Champagne, P. A.; Picazo, E.; Yamakawa, K.; Morrill, L. A.; Houk, K. N.; Garg, N. K., *J. Am. Chem. Soc.* **2017**, *139* (42), 14833-14836.
75. Çelebi-Ölçüm, N.; Boal, B. W.; Hutters, A. D.; Garg, N. K.; Houk, K. N., *J. Am. Chem. Soc.* **2011**, *133* (15), 5752-5755.
76. Blakemore, D. C.; Castro, L.; Churcher, I.; Rees, D. C.; Thomas, A. W.; Wilson, D. M.; Wood, A., *Nat. Chem.* **2018**, *10* (4), 383-394.
77. Boström, J.; Brown, D. G.; Young, R. J.; Keserü, G. M., *Nat. Rev. Drug Discov.* **2018**, *17*, 709.
78. Godoi, B.; Schumacher, R. F.; Zeni, G., *Chem. Rev.* **2011**, *111* (4), 2937-2980.
79. Varela-Fernández, A.; García-Yebra, C.; Varela, J. A.; Esteruelas, M. A.; Saá, C., *Angew. Chem. Int. Ed.* **2010**, *49* (25), 4278-4281.
80. Kanno, H.; Nakamura, K.; Noguchi, K.; Shibata, Y.; Tanaka, K., *Org. Lett.* **2016**, *18* (7), 1654-1657.
81. Varela-Fernández, A.; González-Rodríguez, C.; Varela, J. A.; Castedo, L.; Saá, C., *Org. Lett.* **2009**, *11* (22), 5350-5353.
82. Varela-Fernández, A.; Varela Jesús, A.; Saá, C *Adv. Synth. Catal.* **2011**, *353* (11-12), 1933-1937.
83. Ogunlana, A. A.; Zou, J.; Bao, X., *J. Organomet. Chem.* **2018**, *864*, 160-168.
84. Álvarez-Pérez, A.; González-Rodríguez, C.; García-Yebra, C.; Varela, J. A.; Oñate, E.; Esteruelas, M. A.; Saá, C., *Angew. Chem. Int. Ed.* **2015**, *54* (45), 13357-13361.
85. Grotjahn, D. B., *Pure Appl. Chem.* **2010**, *82*, 635-647.
86. Arcadi, A.; Bianchi, G.; Marinelli, F., Application of gold catalysis in the synthesis of heterocyclic systems. *Targets in Heterocyclic Systems* **2004**, *8*, 82-119.
87. Dorel, R.; Echavarren, A. M., *Chem. Rev.* **2015**, *115* (17), 9028-9072.
88. Trost, B. M., *Acc. Chem. Res.* **1990**, *23*, 34.
89. Trost, B. M.; McClory, A., *Angew. Chem. Int. Ed.* **2007**, *46* (12), 2074-2077.
90. Trost, B. M.; Rhee, Y. H., *J. Am. Chem. Soc.* **1999**, *121* (50), 11680-11683.



91. Trost, B. M.; Rhee, Y. H., *J. Am. Chem. Soc.* **2002**, *124* (11), 2528-2533.
92. Trost, B. M.; Rhee, Y. H., *J. Am. Chem. Soc.* **2003**, *125* (25), 7482-7483.
93. Varela-Fernandez, A.; Varela, J. A.; Saá, C., *Synthesis* **2012**, *44* (21), 3285-3295.
94. Liu, P. N.; Su, F. H.; Wen, T. B.; Sung, H. H. Y.; Williams, I. D.; Jia, G., *Chem. Eur. J.* **2010**, *16* (26), 7889-7897.
95. Chen, B.; Wang, L.; Gao, S., *ACS Catal.* **2015**, *5* (10), 5851-5876.
96. DuBois, D. L., *Inorg. Chem.* **2014**, *53* (8), 3935-3960.
97. Ell, A. H.; Samec, J. S. M.; Brasse, C.; Backvall, J.-E., *Chem. Commun.* **2002**, (10), 1144-1145.
98. Gu, X.-Q.; Chen, W.; Morales-Morales, D.; Jensen, C. M., *J. Mol. Catal. A: Chem.* **2002**, *189* (1), 119-124.
99. Bernskoetter, W. H.; Brookhart, M., *Organometallics* **2008**, *27* (9), 2036-2045.
100. Zuo, W.; Morris, R. H., *Nat. Protoc.* **2015**, *10*, 241.
101. Fujita, K.-i.; Tanaka, Y.; Kobayashi, M.; Yamaguchi, R., *J. Am. Chem. Soc.* **2014**, *136* (13), 4829-4832.
102. Tseng, K.-N. T.; Rizzi, A. M.; Szymczak, N. K., *J. Am. Chem. Soc.* **2013**, *135* (44), 16352-16355.
103. Wu, J.; Talwar, D.; Johnston, S.; Yan, M.; Xiao, J., *Angew. Chem. Int. Ed.* **2013**, *52* (27), 6983-6987.
104. Muthaiah, S.; Hong, S. H., *Adv. Synth. Catal.* **2012**, *354* (16), 3045-3053.
105. He, L.-P.; Chen, T.; Gong, D.; Lai, Z.; Huang, K.-W., *Organometallics* **2012**, *31* (14), 5208-5211.
106. Prades, A.; Peris, E.; Albrecht, M., *Organometallics* **2011**, *30* (5), 1162-1167.
107. Tseng, K. N. T.; Szymczak, N. K., *Synlett* **2014**, *25* (17), 2385-2389.
108. Zhang, J.; Leitus, G.; Ben-David, Y.; Milstein, D., *J. Am. Chem. Soc.* **2005**, *127* (31), 10840-10841.
109. Nielsen, M.; Alberico, E.; Baumann, W.; Drexler, H.-J.; Junge, H.; Gladiali, S.; Beller, M., *Nature* **2013**, *495* (7439), 85-89.
110. Rodríguez-Lugo, R. E.; Trincado, M.; Vogt, M.; Tewes, F.; Santiso-Quinones, G.; Grützmacher, H., *Nat. Chem.* **2013**, *5* (4), 342-347.
111. Tsuji, Y.; Kotachi, S.; Huh, K. T.; Watanabe, Y., Ruthenium-catalyzed dehydrogenative N-heterocyclization. *J. Org. Chem.* **1990**, *55* (2), 580-584.
112. Sandoval, C. A.; Ohkuma, T.; Muñiz, K.; Noyori, R., *J. Am. Chem. Soc.* **2003**, *125* (44), 13490-13503.
113. Tseng, K.-N. T.; Kampf, J. W.; Szymczak, N. K., *ACS Catal.* **2015**, *5* (9), 5468-5485.
114. Wang, Q.; Chai, H.; Yu, Z., *Organometallics* **2018**, *37* (4), 584-591.

115. Dutta, I.; Yadav, S.; Sarbajna, A.; De, S.; Hölscher, M.; Leitner, W.; Bera, J. K., *J. Am. Chem. Soc.* **2018**, *140* (28), 8662-8666.
116. Gunanathan, C.; Ben-David, Y.; Milstein, D., *Science* **2007**, *317* (5839), 790-792.

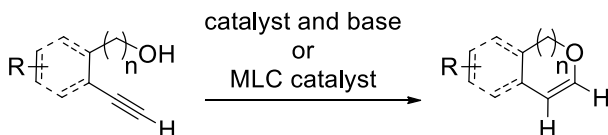
## Chapter 2

### 2 Catalytic Cyclization and Competitive Deactivation with $\text{Ru}(\text{P}^{\text{R}_2}\text{N}^{\text{R}'_2})$ Complexes

The first successful application of the  $\text{P}^{\text{R}_2}\text{N}^{\text{R}'_2}$  (3,7-R'-1,5-R-3,7-diaza-1,5-diphosphacyclooctane) ligand family toward an organic transformation is described. The cationic precatalysts  $[\text{Ru}(\text{Cp})(\text{P}^{\text{R}_2}\text{N}^{\text{Bn}_2})(\text{MeCN})]\text{PF}_6$  are active toward the cyclization of ethynylbenzyl alcohol at low catalyst loading and moderate temperatures. Catalyst performance however is limited by both low consumption, due to acetonitrile lability, and by competitive deactivation, caused by nucleophilic deactivation of the Ruthenium vinylidene by the pendent amine.

#### 2.1 Introduction

Oxygen heterocycles are important motifs in a variety of natural products and are used extensively as building blocks in synthesis.<sup>1</sup> Oxygen-containing iso-chromenes can be accessed through atom-economic catalytic cyclization of alkynyl alcohols (Scheme 2-1).<sup>2</sup> Mechanistically, this involves isomerization of a terminal alkyne to a metal vinylidene, followed by nucleophilic attack of the alcohol at the carbon alpha to the metal.<sup>2c</sup> Early examples of this transformation used a large excess of a base additive to mediate the required proton-transfer steps.<sup>2a</sup> Improved catalyst loadings and higher performance can be achieved by using a base as the solvent.<sup>2c, 2d</sup> An intermolecular base can be avoided completely if the catalyst contains an acid/base group on the ligand to shuttle protons in an intramolecular fashion.<sup>2f</sup> Such metal-ligand cooperative (MLC) catalysts require low catalyst loadings and operate at moderate temperatures.



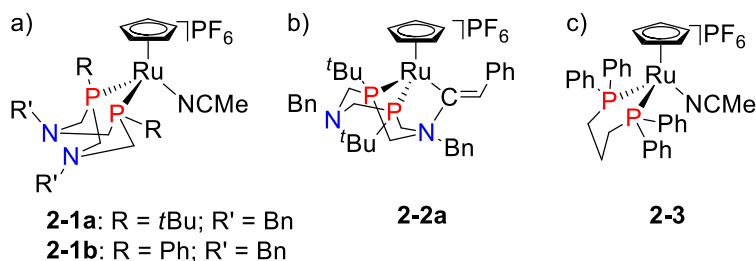
**Scheme 2-1.** Catalytic cyclization of alkynyl alcohols<sup>2a-f</sup>

The bisphosphine  $\text{P}^{\text{R}_2}\text{N}^{\text{R}'_2}$  (3,7-R'-1,5-R-3,7-diaza-1,5-diphosphacyclooctane) MLC ligand family is highly tunable through the R and R' substituents.<sup>3</sup> This property is exploited extensively in electrocatalytic transformations, including  $\text{H}_2$  oxidation and production. Despite the growth of MLC catalytic processes used in organic synthesis,<sup>4</sup> the  $\text{P}^{\text{R}_2}\text{N}^{\text{R}'_2}$  ligands are yet to be exploited successfully

in this realm. In an effort to address this, we recently studied the reactivity of  $[\text{Ru}(\text{Cp})(\text{P}^{\text{t-Bu}}_2\text{N}^{\text{Bn}}_2)(\text{MeCN})]\text{PF}_6$  (**2-1a**, Figure 2-1) with phenylacetylene.<sup>5</sup> The complex readily reacts with the alkyne to give a putative vinylidene, which is immediately and irreversibly deactivated at C $\alpha$  by attack of the Lewis basic pendent nitrogen to give **2-2a**. This precludes the use of **2-1a** in catalytic alkyne functionalization strategies<sup>6</sup> that rely on intermolecular nucleophilic attack at this C $\alpha$  position. However, we reasoned that cyclization via intramolecular nucleophilic attack would compete with deactivation. Herein, we report the first successful use of  $\text{M}(\text{P}^{\text{R}}_2\text{N}^{\text{R}'_2})$  complexes in a transformation for organic synthesis, specifically cyclization of alkynyl alcohols.

## 2.2 Results and Discussion

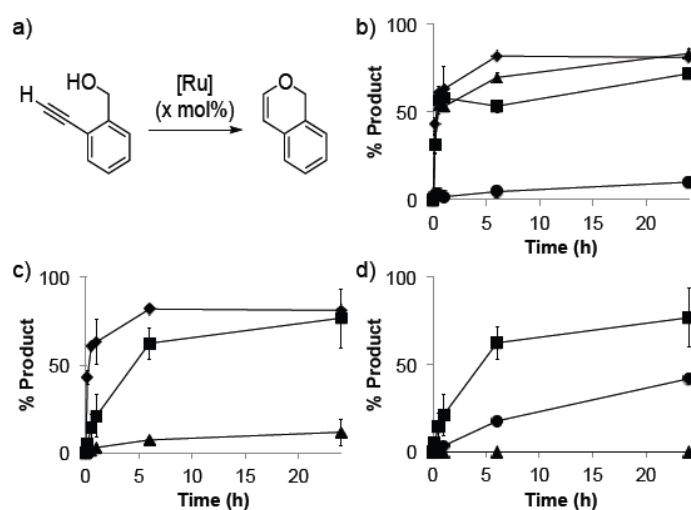
In addition to **2-1a**, the MLC complex **2-1b** and a control complex **2-3** – that lacks a pendent base in the dppp ligand backbone (dppp = 1,3-bisdiphenylphosphinopropane) – were prepared by ligand exchange with the ruthenium precursor  $[\text{Ru}(\text{Cp})(\text{MeCN})_3]\text{PF}_6$ . Complexes **2-1b** and **2-3** exhibited  $\delta^{31\text{P}}$  of 38.4 and 37.4, respectively, that are in accord with previously reported **2-1a**<sup>7</sup> and  $\text{RuCl}(\text{Cp})(\text{dppp})$ <sup>8</sup> (cf. 52.6 and 38.7 ppm, respectively). The structure of **2-1b** and **2-3** were further characterized by  $^1\text{H}$  and  $^{13}\text{C}\{^1\text{H}\}$  NMR spectroscopy and MALDI mass spectrometry. A crystal structure of **2-1b** was also obtained (See Figure A-23).



**Figure 2-1.** a) Ruthenium MLC catalysts employed in this study; b) known deactivation of **2-1a** on reaction with phenylacetylene; c) non-MLC control catalyst

Cyclization catalysis was assessed with ethynylbenzyl alcohol (**EBA**) with 5 mol% **2-1a** at 40 °C in acetone,  $\text{CH}_2\text{Cl}_2$  and THF, and at 60 °C in MeCN (Figure 2-2). Gratifyingly, the MLC catalyst **2-1a** is active in the intramolecular cyclization reaction. Optimal catalyst performance was observed in acetone where a maximum conversion of 82% of isochromene (**IC**) was achieved within 6 h. Conversion was slower in  $\text{CH}_2\text{Cl}_2$  and THF, but final 24 h values were similar to acetone. Poor performance in MeCN

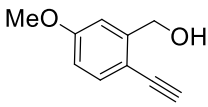
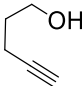
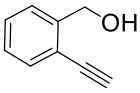
(max 10% conv.) is likely due to suppressed lability of the coordinating MeCN ligand preventing substrate binding. Lowering the loading of **2-1a** to 1 and 0.1 mol% in acetone reveals that reasonable performance is achieved with the former amount. The catalyst loadings are in the range of the best known cyclization catalysts (1 – 5 mol%)<sup>2b, 2f</sup> whilst operating at a lower temperature (cf. 70 – 90 °C for known<sup>2a-f</sup> systems). A comparison of catalyst performance was conducted under optimal conditions of 1 mol% catalyst at 40 °C in acetone (Figure 2-2d). Catalyst **2-1b** with phenyl substituents on the phosphine donors leads to lower catalyst activity relative to the *t*-Bu-substituted **2-1a**. No product is observed on treating **EBA** with the dppp catalyst **2-3**, which is strong support that the pendent base of **2-1a** and **2-1b** is required for catalysis. The role of the base is likely to act as the proton shuttle, required for a MLC mechanism.



**Figure 2-2.** a) Cyclization of EBA (150 mM) at 40 °C monitored over 24 h with [Ru] b) 5 mol% **2-1a** in acetone (◆), CH<sub>2</sub>Cl<sub>2</sub> (■), THF (▲) and MeCN (●) at 60 °C; c) 5 (◆), 1 (■), 0.1 (▲) mol% **2-1a** in acetone; d) 1 mol% **2-1a** (■), **2-1b** (●) and **2-3** (▲) in acetone

Using the optimal conditions of 1 mol% **2-1a** or **2-1b** at 40 °C the substrate scope was evaluated with the more challenging methoxy-substituted (**EBA-OMe**) and alkyl-linked ethynyl alcohol (**alkyl-EA**) substrates (Table 2-1, Entries 1-4). In both cases, poor or no product yield was observed with either catalyst, which prompted catalytic testing at increased temperatures. Surprisingly, no improvement in yield is observed on conducting cyclization of **EBA** at 54 °C (Table 2-1, Entries 5-8). In the case of the dppp catalyst **2-3**, the higher temperature still did not promote productive turnover (Table 2-1, Entries 9-10).

**Table 2-1.** Catalyst Comparison and Substrate Scope for Cyclization<sup>[a]</sup>

Entry	Substrate	[Ru]	Temp. (°C)	Yield (%) <sup>[b]</sup>
1		1a	40	22
2	<b>EBA-OMe</b>	1b	40	12
3		1a	40	0
4	<b>alkyl-EA</b>	1b	40	0
5	 <b>EBA</b>	1a	40	77
6		1a	54	52 <sup>[c]</sup>
7		1b	40	42
8		1b	54	34
9		3	40	0
10		3	54	0

[a] Conditions: 150 mM **EBA**, 1 mol% [Ru], acetone, 24 h. [b] Determined by <sup>1</sup>H NMR spectroscopy by relative integration to an internal standard (dimethyl terephthalate). [c] Time = 2 h at which point max conversion is reached.

The poor conversion to cyclization product **IC** at higher temperatures suggested a competitive deactivation process is promoted under these conditions. To confirm this, ruthenium speciation was monitored by <sup>31</sup>P{<sup>1</sup>H} NMR spectroscopy during catalysis (Figure 2-3). Reactions were conducted at 40 and 50 °C in acetone-*d*<sub>6</sub> with a slightly higher loading of **2-1a** (1.5 mol%) to achieve reasonable signal to noise. At 40 °C the signal for precatalyst **2-1a** is the dominant species over 95 min, representing ca. 71% of the initial integration. Therefore, conscription of **2-1a** into the catalytic cycle is low, presumably due to poor MeCN lability. Two minor species are observed at 70.8 and 71.1 ppm each in

ca. 10% yield. At 50 °C entry of **1a** into the catalytic cycle is increased as the proportion of the precatalyst is reduced significantly to ca. 30%. By 95 minutes the species found at 71.1 and 70.8 ppm are present in a 43 and 9% yield, respectively. We assign the dominant ruthenium species as the deactivation product **2-5a**, an analogue of the previously characterized deactivation species **2-2a** that has a very similar  $^{31}\text{P}$  chemical shift (cf.  $\delta^{31}\text{P} = 71.5$  for **2-2a**).<sup>5</sup> The third species found at 70.8 is tentatively assigned as an on-cycle catalyst intermediate that could be a  $\pi$ -bound alkyne species (**2-4a**), a Ru–vinylidene (**2-4a'**) or Ru–vinyloxonium species (**2-4a''**) (Figure 4). We favour assignment as **2-4a''** since analogues of **2-4a** and **2-4a'** were not observed as intermediates on reaction of **2-1a** with phenylacetylene.<sup>5</sup>

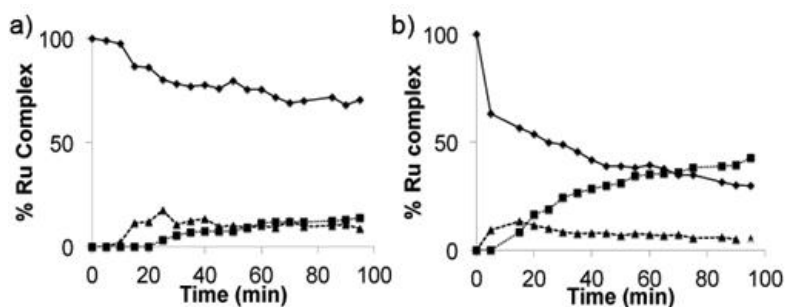


**Figure 2-3.** In situ observation of **2-1a** (♦;  $\delta^{31}\text{P} = 53.9$ ), **2-4a/2-4a'/2-4a''** (▲;  $\delta^{31}\text{P} = 70.8$ ), **2-5a** (■;  $\delta^{31}\text{P} = 71.1$ ) by  $^{31}\text{P}\{^1\text{H}\}$  NMR spectroscopy relative to an internal standard (O=PPh<sub>3</sub>) for 95 min at a) 40 °C and b) 50 °C

In situ  $^1\text{H}$ - $^1\text{H}$  COSY,  $^1\text{H}$ - $^{13}\text{C}$  HMBC NMR experiments were performed on **2-5a** under catalytic conditions of 1 mol % at 25 °C in acetone-*d*<sub>6</sub>. A similar pattern to **2-2a** is observed.<sup>5</sup> Correlations are observed for the vinyl proton (7.48 ppm) to the alpha vinyl carbon (196.9 ppm) and the proximal benzyl protons (4.85 ppm -  $^1\text{H}$ - $^1\text{H}$  COSY) and carbon (62.0 ppm -  $^1\text{H}$ - $^{13}\text{C}$  HMBC). These signals are consistent with a vinyl ammonium decomposition species rather than an on cycle species. Unlike **2-2a**, attempts to isolate **2-5a** were unsuccessful.

We postulated rapid turnover with minimal deactivation could be achieved at low temperature by generating the active catalyst by halide abstraction. The active catalyst would be the dominant species at low temperatures, which would avoid the elevated temperatures required to promote acetonitrile dissociation from the precatalysts **2-1a/2-1b**. Cyclization of **EBA** at 40 °C was conducted with 1 mol% of the neutral precatalyst RuCl(Cp)(P<sup>t</sup>Bu<sub>2</sub>N<sup>Bn</sup><sub>2</sub>) treated with TIPF<sub>6</sub> to abstract the halide in situ. A

maximum conversion of 79% product **2-5a** was reached within 1 h, considerably faster than catalyst **2-1a** that requires 6 h to reach a similar conversion. However, the maximum conversion does not exceed that found for **2-1a** (cf. 77% at 24 h). Thus, halide abstraction from pre-catalyst  $\text{RuCl}(\text{Cp})(\text{P}^{\text{tBu}}_2\text{N}^{\text{Bn}}_2)$  gives faster catalysis via improved initiation, but overall yields are not improved as deactivation remains problematic. Rapid initiation and deactivation is likewise found at room temperature.

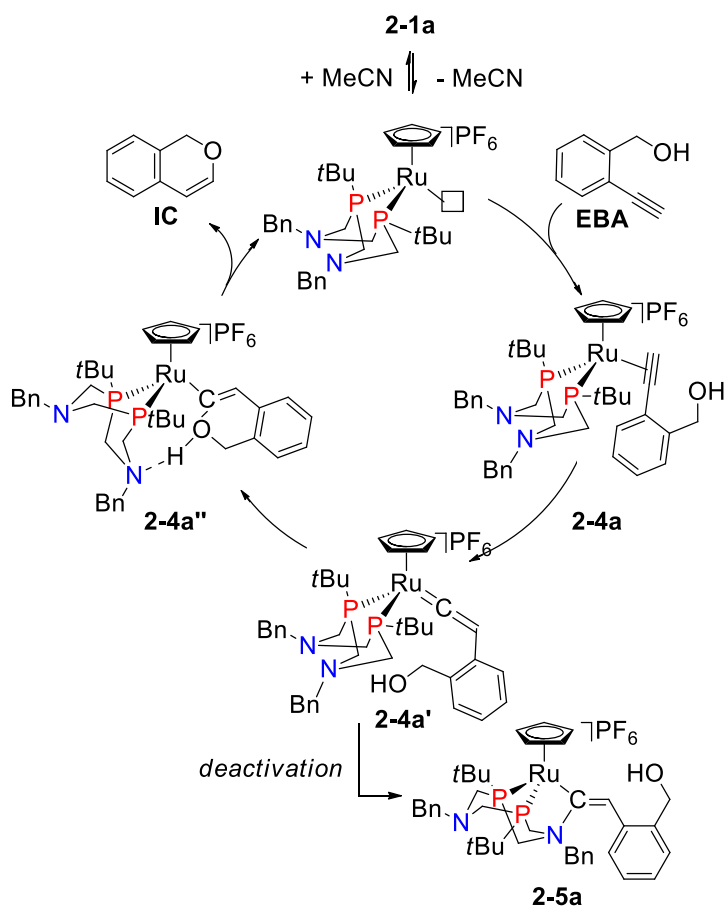


**Figure 2-4.** Postulated mechanism for the cyclization of 2-ethynylbenzyl alcohol (**EBA**) with catalyst **2-1a**

## 2.3 Conclusion

The cationic precatalysts  $[\text{Ru}(\text{Cp})(\text{P}^{\text{R}}_2\text{N}^{\text{Bn}}_2)(\text{MeCN})]\text{PF}_6$  (**2-1a**:  $\text{R} = t\text{-Bu}$ ; **2-1b**:  $\text{R} = \text{Ph}$ ) are active for the cyclization of ethynylbenzyl alcohol (**EBA**) under milder conditions than known catalysts. The work discussed in this chapter represents the first successful example of the MLC  $\text{P}^{\text{R}}_2\text{N}^{\text{R}'_2}$  ligand family used in an organic transformation. In situ catalyst studies revealed that competitive catalyst deactivation



is a major challenge to increasing performance and expanding the substrate scope. Thus, the pendent amine of the  $P^{R_2}N^{R'_2}$  ligand is both beneficial by promoting cooperative catalysis and detrimental by deactivating the active vinylidene intermediate. The balance of these two roles must be considered for future catalyst designs and in other applications of these complexes.

## 2.4 Experimental

### 2.4.1 General Procedures, Materials and Instrumentation

All reactions were manipulated under  $N_2$  using standard Schlenk or glovebox techniques. All glassware was oven dried prior to use. Triphenylphosphine oxide (99%) was obtained from Alfa Aesar. Bis(diphenylphosphino)propane (dppp; 98%), pyrene (98%), 2-ethynylbenzyl alcohol (99%), and 4-pentyn-1-ol (97%) were obtained from Sigma-Aldrich. Thallium hexafluorophosphate (97%) was obtained from Strem. Chloroform-*d* (99.8%) and acetone-*d*<sub>6</sub> (99.9%) were obtained from Cambridge Isotope Laboratories.  $[Ru(Cp)(MeCN)_3]PF_6$ ,<sup>9</sup>  $P^{Ph_2}N^{Bn_2}$ ,<sup>10</sup>  $[Ru(Cp)(P^{tBu_2}N^{Bn_2})(NCMe)]PF_6$ ,<sup>5</sup>  $Ru(Cp)(P^{tBu_2}N^{Bn_2})Cl$ <sup>7</sup> and 2-ethynyl-5-methoxybenzyl alcohol<sup>2c</sup> were synthesized following literature procedures.  $P^{tBu_2}N^{Bn_2}$  was used as gifted. Dry and degassed solvents were obtained from an Innovative Technology 400-5 Solvent Purification System and stored over 4 Å molecular sieves (Fluka and activated at 150 °C for 12 h) under  $N_2$  unless otherwise noted. Acetone was dried with  $Cs_2CO_3$  and degassed by bubbling with  $N_2$ . Chloroform-*d* was dried with 4 Å molecular sieves and degassed by bubbling with  $N_2$ . All other chemicals were used as received. All NMR spectra were recorded on either an Inova 600 MHz or Mercury 400 MHz instrument.  $^1H$  and  $^{13}C$  { $^1H$ } spectra acquired were referenced internally against the residual solvent signal to TMS at 0 ppm.  $^{31}P$  spectra were referenced externally to 85% phosphoric acid at 0.00 ppm. Infrared spectra were collected on solid samples using a PerkinElmer UATR TWO FTIR spectrometer. Elemental analysis was performed by Laboratoire d'Analyse Élémentaire de l'Université de Montréal. MALDI-TOF mass spectra were collected using an AB Sciex 5800 TOF/TOF mass spectrometer using pyrene as the matrix in a 20:1 molar ratio with the sample. The instrument is equipped with a 349 nm OptiBeam On-Axis laser. The laser pulse rate was 400 Hz and data were collected in reflectron positive mode. Reflectron mode was externally calibrated at 50 ppm mass tolerance. Each mass spectrum was collected as a sum of 500 shots.

## 2.4.2 Synthesis of [Ru(Cp)(P<sup>Ph</sup><sub>2</sub>N<sup>Bn</sup><sub>2</sub>)(NCCH<sub>3</sub>)]PF<sub>6</sub>, (**2-1b**)

[RuCp(NCMe)<sub>3</sub>]PF<sub>6</sub> (461 mg, 1.06 mmol, 1 equiv.) and P<sup>Ph</sup><sub>2</sub>N<sup>Bn</sup><sub>2</sub> (511 mg, 1.06 mmol, 1 equiv.) were combined in a 100 mL Schlenk flask with acetonitrile (5 mL) and heated to 70°C for 4 h. The ligand solubilizes on heating causing the solution to turn yellow. After cooling to room temperature, the solvent was removed under vacuum to afford a yellow air-sensitive powder. X-ray quality crystals were grown by vapor diffusion in THF and diethyl ether. Yield: 841 mg (95%). <sup>1</sup>H NMR (600 MHz, CDCl<sub>3</sub>): δ 7.64-5.8 (m, Ph-*H*, 4H), 7.53-7.46 (m, Ph-*H*, 6H), 7.38-7.17 (m, Ph-*H*, 10H), 4.71 (s, Cp-*H*, 5H), 3.81 (s, PhCH<sub>2</sub>N, 2H), 3.66 (s, PhCH<sub>2</sub>N, 2H), 3.22-3.05 (m, PCH<sub>2</sub>N, 4H), 2.98-2.88 (m, PCH<sub>2</sub>N, 2H), 2.81-2.73 (m, PCH<sub>2</sub>N, 2H), 2.26 (s, RuNCCH<sub>3</sub>, 3H). <sup>31</sup>P{<sup>1</sup>H} NMR (243 MHz, CDCl<sub>3</sub>): δ 38.4 (s, RuP), -144.2 (sept, <sup>1</sup>J<sub>P-F</sub> = 714 Hz, PF<sub>6</sub>). <sup>13</sup>C{<sup>1</sup>H} NMR (151.5 MHz, CDCl<sub>3</sub>): δ 137.0 (s, CH<sub>2</sub>C-Ar), 136.5 (s, CH<sub>2</sub>C-Ar), 134.3 (dd, <sup>1</sup>J<sub>C-P</sub> = 21.4 Hz, <sup>3</sup>J<sub>C-P</sub> = 21.4 Hz, PC-Ar), 131.6-128.2 and 128.0 (C-Ar), 128.1 (s, RuNCCH<sub>3</sub>), 81.7 (s, Cp), 65.5 (s, NCH<sub>2</sub>Ph), 52.5 (dd, <sup>1</sup>J<sub>C-P</sub> = 18.1 Hz, <sup>3</sup>J<sub>C-P</sub> = 18.1 Hz, NCH<sub>2</sub>PPh), 51.7 (dd, <sup>1</sup>J<sub>C-P</sub> = 18.1 Hz, <sup>3</sup>J<sub>C-P</sub> = 18.1 Hz, NCH<sub>2</sub>PPh), 4.2 (s, CH<sub>3</sub>CNRu). Anal. Calc. for C<sub>37</sub>H<sub>40</sub>F<sub>6</sub>N<sub>3</sub>P<sub>3</sub>Ru•0.25 hexanes: C, 54.00; H, 5.12; N, 4.91. Found: C, 54.34; H, 4.93; N, 4.76. MALDI MS (pyrene matrix): Calc. m/z 649.1 [RuCp(P<sup>Ph</sup><sub>2</sub>N<sup>Bn</sup><sub>2</sub>)]<sup>+</sup>, Obs. m/z 649.2.

## 2.4.3 Synthesis of Ru(Cp)(dppp)(NCCH<sub>3</sub>)]PF<sub>6</sub>, (**2-3**)

[RuCp(NCMe)<sub>3</sub>]PF<sub>6</sub> (81 mg, 0.19 mmol, 1 equiv.) and dppp (77 mg, 0.19 mmol, 1 equiv.) were combined in a pre-weighed vial in the glovebox with acetonitrile (5 mL) and stirred for 4 h at room temperature causing the solution to turn yellow from orange. The solvent was removed under vacuum to give a pure yellow solid. Yield: 145 mg (96%). <sup>1</sup>H NMR (600 MHz, CDCl<sub>3</sub>): δ 7.48-7.40 (m, Ph-*H*, 12H), 7.25 (dd, <sup>3</sup>J<sub>Hg-P</sub> = 7.2 Hz, <sup>3</sup>J<sub>Hg-Hh</sub> = 7.2 Hz, Ph-*H*, 4H), 7.12 (m, Ph-*H*, 4H), 4.60 (s, H-Cp, 5H), 2.62 (m, P-*CHH'*, 2H), 2.45 (m, CH<sub>2</sub>-*CHH'*, 1H), 2.36 (s, CH<sub>3</sub>CN, 3H), 2.30 (m, P-*CHH'*, 2H), 1.71 (m, P-*CHH'*, 1H). <sup>31</sup>P{<sup>1</sup>H} NMR (242.9 MHz, CDCl<sub>3</sub>): δ 37.4 (s, P-C), -144.4 (sept, <sup>1</sup>J<sub>P-F</sub> = 714 Hz, PF<sub>6</sub>). <sup>13</sup>C{<sup>1</sup>H} NMR (150.9 MHz, CDCl<sub>3</sub>): δ 138.6 (m, P-*C<sub>Ar</sub>*), 137.2 (m, P-*C<sub>Ar</sub>*), 132.5 (d, <sup>3</sup>J<sub>C-P</sub> = 5.7 Hz, *m-C<sub>Ar</sub>*), 132.5 (d, <sup>3</sup>J<sub>C-P</sub> = 5.7 Hz, *m-C<sub>Ar</sub>*), 131.7 (d, <sup>3</sup>J<sub>C-P</sub> = 5.3 Hz, *m-C<sub>Ar</sub>*), 131.7 (d, <sup>3</sup>J<sub>C-P</sub> = 5.3 Hz, *m-C<sub>Ar</sub>*), 130.2 (s, *p-C<sub>Ar</sub>*), 130.1 (s, *p-C<sub>Ar</sub>*), 129.0 (d, <sup>2</sup>J<sub>C-P</sub> = 5.0 Hz, *o-C<sub>Ar</sub>*), 129.0 (d, <sup>2</sup>J<sub>C-P</sub> = 5.0 Hz, *o-C<sub>Ar</sub>*), 129.0 (s, CN), 128.6 (d, <sup>2</sup>J<sub>C-P</sub> = 5.0 Hz, *o-C<sub>Ar</sub>*), 82.8 (s, Cp), 26.9 (dd, <sup>1</sup>J<sub>C-P</sub> = 15.3 Hz, <sup>3</sup>J<sub>C-P</sub> = 15.3 Hz, P-CH<sub>2</sub>), 20.8 (s, CH<sub>2</sub>-CH<sub>2</sub>), 4.4 (s, CH<sub>3</sub>). Anal. Calc. for C<sub>34</sub>H<sub>34</sub>F<sub>6</sub>NP<sub>3</sub>Ru•0.08 dppp: C, 54.45; H, 4.56; N, 1.76. Found: C, 54.84; H, 4.60; N, 1.43. MALDI MS (pyrene matrix): Calc. m/z 579.0 [RuCp(dppp)]<sup>+</sup>, Obs. m/z 579.1.

#### 2.4.4 Attempted Synthesis of $[\text{Ru}(\text{Cp})(\text{P}^{\text{tBu}}_2\text{N}^{\text{Bn}}_2)(-\text{C}=\text{CHC}_6\text{H}_4\text{OH})]\text{PF}_6$ , (**2-5a**)

$[\text{Ru}(\text{Cp})(\text{P}^{\text{tBu}}_2\text{N}^{\text{Bn}}_2)(\text{NCMe})]\text{PF}_6$  (14 mg, 0.018 mmol, 1.5 mM, 1 equiv.) and 2-ethynylbenzyl alcohol (239 mg, 1.81 mmol, 150 mM, 100 equiv.) were combined in a 100 mL Schlenk with acetone (12 mL) and heated to 54 °C for 5 days.  $^{31}\text{P}\{^1\text{H}\}$  NMR spectra indicate a maximum conversion of 77% to **2-5a** from **2-1a** (23% remaining). The reaction was cooled and the solvent was removed under vacuum to produce a brownish yellow solid. The solid was washed with hexanes (3 × 15 mL) and dried under vacuum. Analysis by  $^{31}\text{P}\{^1\text{H}\}$  NMR spectroscopy in  $\text{CDCl}_3$  revealed the presence of multiple unknown species.

#### 2.4.5 In Situ Characterization of $[\text{Ru}(\text{Cp})(\text{P}^{\text{tBu}}_2\text{N}^{\text{Bn}}_2)(-\text{C}=\text{CHC}_6\text{H}_4\text{OH})]\text{PF}_6$ , (**2-5a**).

In a glovebox, substrate **EBA** (171 mg, 1.30 mmol) and catalyst **2-1a** (10 mg, 0.013 mmol) were combined in a vial in acetone- $d_6$  (1 mL) with a stir bar. The initial concentrations of the species were: **EBA** (1.30 M) and **2-1a** (0.013 mM). The vial was heated and stirred for 7 h at 54 °C.  $^{31}\text{P}\{^1\text{H}\}$  NMR spectroscopy revealed one new signal found at 71.2 ppm at 84% with the balance being **2-1a**.  $^1\text{H}$ ,  $^{31}\text{P}\{^1\text{H}\}$ ,  $^1\text{H}-^1\text{H}$  COSY, and  $^1\text{H}-^{13}\text{C}$  gHMBCAD NMR spectra were collected. Diagnostic  $^1\text{H}$  and  $^{13}\text{C}$  NMR signals are identified to confirm assignment as **2-5a**.  $^1\text{H}$  NMR (600 MHz,  $(\text{CD}_3)_2\text{CO}$ ):  $\delta$  7.48 (Ru- $\text{C}_\alpha(\text{NCH}_2\text{Ph})=\text{CHAr}$ ), 4.85 (Ru- $\text{C}_\alpha(\text{NCH}_2\text{Ph})=\text{CHAr}$ ).  $^{13}\text{C}\{^1\text{H}\}$  NMR (150.9 MHz,  $(\text{CD}_3)_2\text{CO}$ ):  $\delta$  196.9 (Ru- $\text{C}_\alpha$ ), 62.0 (Ru- $\text{C}_\alpha(\text{NCH}_2\text{Ph})=\text{CHAr}$ ).  $^{31}\text{P}\{^1\text{H}\}$  NMR (242.9 MHz,  $\text{CDCl}_3$ ):  $\delta$  71.2 (s, Ru- $P$ ), -144.4 (sept,  $^1J_{\text{P-F}} = 714$  Hz,  $\text{PF}_6$ ).

#### 2.4.6 Representative Procedure for Catalytic Cyclization of 2-Ethynylbenzyl alcohol (**EBA**)

In a glovebox, the following stock solutions were prepared: **EBA** (159 mg, 1.20 mmol, 0.300 M) and dimethyl terephthalate (38 mg, 0.19 mmol, 0.049 M) in acetone (4.01 mL); **2-1a** (6 mg, 0.007 mmol, 6 mM) in acetone (1.15 mL); **2-1b** (6 mg, 0.007 mmol, 6 mM) in acetone (1.12 mL); **2-3** (7 mg, 0.009 mmol, 6 mM) in acetone (1.50 mL). Four sets (A-D) of 5 vials (20 vials total) containing stir bars were charged with the **EBA**/dimethyl terephthalate stock solution (250  $\mu\text{L}$ ) and additional acetone (125  $\mu\text{L}$ ). To each vial of set A was added the **2-1a** stock solution (125  $\mu\text{L}$ ) giving a final volume of 500  $\mu\text{L}$ . To each vial of set B was added the **2-1b** stock solution (125  $\mu\text{L}$ ) giving a final volume of 500  $\mu\text{L}$ . To each vial of set D,  $\text{NEt}_3$  was added (6  $\mu\text{L}$ ). To each vial of sets C and D was added the **2-3**

stock solution (125  $\mu\text{L}$ ) giving a final volume of 500  $\mu\text{L}$ . The final concentrations for all vials were 0.150 M in substrate. A final vial was charged with substrate/internal standard stock solution (100  $\mu\text{L}$ ) for use as the time = 0 sample, required for accurate quantification of substrate and product. The vials were capped and removed from the glove box and heated to 40  $^{\circ}\text{C}$  (sets A-D) with stirring. After 0.167, 0.5, 1, 6, and 24 hours one vial from each of the sets was removed from heat, cooled, and exposed to air to quench. The solvent was then removed in vacuo; the remaining residue was dissolved in  $\text{CDCl}_3$  and analyzed by  $^1\text{H}$  NMR spectroscopy. Substrate consumption and product formation was determined relative to the internal standard (dimethyl terephthalate).

#### 2.4.7 In Situ Monitoring of Ru Species During Catalysis

In a glovebox, the following stock solutions were prepared: **EBA** (1.60 M, 1.13 mmol) with dimethyl terephthalate (0.388 M, 0.275 mmol) in acetone- $d_6$  in a vial with a septum cap; **2-1a** (35 mM, 0.011 mmol) with triphenylphosphine oxide (35 mM, 0.011 mmol) in acetone- $d_6$  in a septum capped NMR tube. A  $^{31}\text{P}\{^1\text{H}\}$  NMR spectrum was acquired at time = 0. The INOVA 600 NMR spectrometer was heated to the appropriate temperature (313 K or 323 K). The substrate stock solution (0.450 mL) was injected in the septum capped NMR tube. The NMR tube was shaken and immediately placed in the instrument.  $^1\text{H}$  and  $^{31}\text{P}\{^1\text{H}\}$  NMR spectra were collected every 5 minutes for 90 minutes. The initial concentrations of the species were: **EBA** (960 mM); dimethyl terephthalate (233 mM); **2-1a** (14 mM);  $\text{OPPh}_3$  (14 mM).

#### 2.4.8 Representative Procedure for Performing Cyclization of 2-Ethynylbenzyl alcohol with $[\text{Ru}(\text{Cp})(\text{P}^{\text{tBu}}_2\text{N}^{\text{Bn}}_2)]\text{PF}_6$

$\text{TIPF}_6$  was used in this procedure. Thallium is extremely TOXIC and due care is needed. Solid waste and solution waste contaminated with thallium were placed in a separate containers marked for thallium waste. Glassware contaminated with thallium were heated in water to dissolve residual thallium salts. In a glovebox, the following stock solutions were prepared: 2-Ethynylbenzyl alcohol **EBA** (226 mg, 1.70 mmol, 0.300 M) and dimethyl terephthalate (50 mg, 0.25 mmol, 0.050 M) in acetone (5.710 mL);  $\text{Ru}(\text{Cp})(\text{P}^{\text{tBu}}_2\text{N}^{\text{Bn}}_2)\text{Cl}$  (3.7 mg, 0.006 mmol, 3 mM) and  $\text{TIPF}_6$  (4.0 mg, 0.011, 6 mM) in acetone (1.915 mL). Four sets (A-D) of 5 vials (20 vials total) containing stir bars were charged with the **EBA**/dimethyl terephthalate stock solution (150  $\mu\text{L}$ ). To each vial in set A and B the **2-1a** stock solution (150  $\mu\text{L}$ ) was added giving a final volume of 300  $\mu\text{L}$ . To each vial in set C and D was added the **2-1a** stock solution (15  $\mu\text{L}$ ) and acetone (135  $\mu\text{L}$ ) giving a final volume of 300  $\mu\text{L}$ . The final concentrations for all vials

were 0.150 M in substrate. A final vial was charged with substrate/internal standard stock solution (150  $\mu$ L) for use as the time = 0 sample, required for accurate quantification of substrate and product. The vials were capped and removed immediately after catalyst stock solution was added from the glove box and heated to 25 °C (set A and C) and 40 °C (sets B and D) with stirring. After 0.167, 0.5, 1, 6, and 24 hours one vial from each of the sets was removed from heat, cooled, and exposed to air to quench. The solvent was then removed in vacuo; the remaining residue was dissolved in CDCl<sub>3</sub> and analyzed by <sup>1</sup>H NMR spectroscopy. The starting material and/or product was referenced internally to dimethyl terephthalate.

## 2.5 References

- (a) N. Majumdar, N. D. Paul, S. Mandal, B. de Bruin, W. D. Wulff, *ACS Catal.* **2015**, *5*, 2329-2366; (b) L. D. Quin, J. A. Tyrell, *Fundamentals of Heterocyclic Chemistry: Importance in Nature and in the Synthesis of Pharmaceuticals*, John Wiley & Sons Inc., Hoboken, New Jersey, **2010**.
- (a) B. M. Trost, Y. H. Rhee, *J. Am. Chem. Soc.* **2002**, *124*, 2528-2533; (b) P. N. Liu, F. H. Su, T. B. Wen, H. H. Y. Sung, I. D. Williams, G. Jia, *Chem. Eur. J.* **2010**, *16*, 7889-7897; (c) A. Varela-Fernández, C. González-Rodríguez, J. A. Varela, L. Castedo, C. Saá, *Org. Lett.* **2009**, *11*, 5350-5353; (d) A. Varela-Fernández, C. García-Yebra, J. A. Varela, M. A. Esteruelas, C. Saá, *Angew. Chem. Int. Ed.* **2010**, *49*, 4278-4281; (e) R. N. Nair, P. J. Lee, D. B. Grotjahn, *Top. Catal.* **2010**, *53*, 1045-1047; (f) R. N. Nair, P. J. Lee, A. L. Rheingold, D. B. Grotjahn, *Chem. Eur. J.* **2010**, *16*, 7992-7995; (g) J. A. Varela, C. González-Rodríguez, C. Saá, in *Ruthenium in Catalysis* (Eds.: H. P. Dixneuf, C. Bruneau), Springer International Publishing, Cham, **2014**, pp. 237-287.
- (a) R. M. Bullock, M. L. Helm, *Acc. Chem. Res.* **2015**, *48*, 2017-2026; (b) D. L. DuBois, *Inorg. Chem.* **2014**, *53*, 3935-3960; (c) R. M. Bullock, A. M. Appel, M. L. Helm, *Chem. Commun.* **2014**, *50*, 3125-3143; (d) S. Raugei, M. L. Helm, S. Hammes-Schiffer, A. M. Appel, M. O'Hagan, E. S. Wiedner, R. M. Bullock, *Inorg. Chem.* **2016**, *55*, 445-460.
- (a) J. R. Khusnutdinova, D. Milstein, *Angew. Chem. Int. Ed.* **2015**, *54*, 12236-12273; (b) C. Gunanathan, D. Milstein, *Acc. Chem. Res.* **2011**, *44*, 588-602; (c) H. Grützmacher, *Angew. Chem. Int. Ed.* **2008**, *47*, 1814-1818; (d) J. I. van der Vlugt, *Eur. J. Inorg. Chem.* **2012**, *3*, 363-375; (e) D. B. Grotjahn, *Chem. Eur. J.* **2005**, *11*, 7146-7153.
- J.-P. J. Bow, P. D. Boyle, J. M. Blacquiere, *Eur. J. Inorg. Chem.* **2015**, *25*, 4162-4166.
- (a) B. M. Trost, F. D. Toste, A. B. Pinkerton, *Chem. Rev.* **2001**, *101*, 2067-2096; (b) D. B. Grotjahn, *Pure Appl. Chem.* **2010**, *82*, 635-647; (c) L. Hintermann, A. Labonne, *Synthesis* **2007**, 1121-1150.
- T. A. Tronic, W. Kaminsky, M. K. Coggins, J. M. Mayer, *Inorg. Chem.* **2012**, *51*, 10916-10928.
- D. S. Perekalin, E. E. Karslyan, E. A. Trifonova, A. I. Konovalov, N. L. Loskutova, Y. V. Nelyubina, A. R. Kudinov, *Eur. J. Inorg. Chem.* **2013**, *4*, 481-493.
- E. P. Kündig, F. R. Monnier, *Adv. Synth. Catal.* **2004**, *346*, 901-904.

10. K. Frazee, A. D. Wilson, A. M. Appel, M. Rakowski DuBois, D. L. DuBois, *Organometallics* **2007**, *26*, 3918-3924.

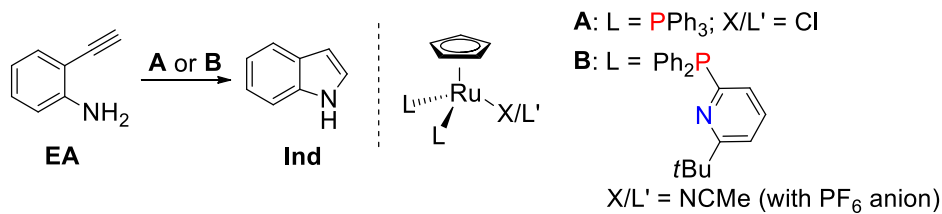
## Chapter 3

### 3 Catalyst Pendent-Base Effects on Cyclization of Alkynyl Amines

A family of [CpRu(PP)(MeCN)]PF<sub>6</sub> complexes (**2-1b**, **3-2a-d** and **3-4**) was prepared in which the bis-phosphine ligand contains a pendent tertiary amine in the second-coordination sphere. **2-1b**, **3-2a-d** contain P<sup>Ph</sup><sub>2</sub>N<sup>R'</sup><sub>2</sub> ligands with two amine groups as the pendent base. Complex **3-4** has the P<sup>Ph</sup><sub>2</sub>N<sup>Ph</sup><sub>1</sub> ligand with only one pendent amine. The catalytic performance of **2-1b**, **3-2a-d** and **3-4** was assessed in the cyclization of 2-ethynyl aniline and 2-ethynylbenzyl alcohol. It was revealed that the positioning of the pendent amine near the metal active site is essential for high catalyst performance. A comparison of P<sup>Ph</sup><sub>2</sub>N<sup>R'</sup><sub>2</sub> catalysts (**2-1b**, **3-2a-d**) showed minimal difference in performance as a function of pendent amine basicity. Rather, only a threshold basicity – in which the pendent amine was more basic than the substrate – was required for high performance.

#### 3.1 Introduction

Metal-ligand cooperative (MLC) catalysts employ ligands that work in concert with the metal to convert substrate to product.<sup>1</sup> The most common subset of these catalysts contain a Brønsted acidic or basic site on the ligand that shuttle protons in an intramolecular fashion, allowing for high performance in a variety of transformations such as hydrogenation, dehydrogenation, dehydrogenative coupling and hydration reactions. Cyclization of alkynyl amines or alcohols gives *N*- and *O*-heterocycles respectively,<sup>2</sup> which are important motifs in a variety of natural products and pharmaceuticals.<sup>3</sup> Cyclization of the benchmark substrate 2-ethynylaniline (**EA**) to indole (**Ind**) showcases the benefit of MLC catalysts over non-cooperative catalysts (Scheme 3-1).<sup>2e, 2f</sup> The non-cooperative catalyst CpRuCl(PPh<sub>3</sub>)<sub>2</sub> (**A**) achieves complete conversion with short reaction times, but the solvent is limited to pyridine, which is required as an intermolecular base to mediate proton-transfer steps.<sup>2e</sup> The MLC catalyst **B**, with a pendent pyridyl group on the phosphine ligand, gives **Ind** in more typical solvents (i.e. THF) and with lower catalyst loadings (2 mol% **B** vs. 10 mol% for **A**).<sup>2f</sup>



**Scheme 3-1.** Cyclization of 2-ethynylaniline (**EA**) with a) a non-cooperative catalyst **A** (10 mol% **A**, pyridine, 90 °C, 25 min, 84% **Ind**)<sup>2e</sup> and b) a cooperative catalyst **B** (2 mol% **B**, THF, 70 °C, 7 h, 87% **Ind**)<sup>2f</sup>

The mechanism for alkynyl amine cyclization is expected to follow a similar route to the related intermolecular hydration of alkynes.<sup>1e, 2a</sup> The simplified mechanism for cyclization includes reaction of the low-coordinate active catalyst (**I**) with the alkyne to give a vinylidene intermediate (**II**) (Figure 3-1). Nucleophilic attack at C $\alpha$  by the substrate amine, and proton shuttling by exogenous or internal base, will give intermediate (**III**). Protonolysis of the Ru-C bond by the protonated base releases the product and regenerates **I**. Experimental and computational studies of hydration reactions indicate that the highest-barrier steps include proton-transfer events.<sup>1e, 2a</sup> Therefore, it is expected that the pK<sub>a</sub>/pK<sub>b</sub> and sterics of the acidic/basic site of cyclization catalysts will influence catalyst performance and that these properties offer an additional dimension for ligand tuning.

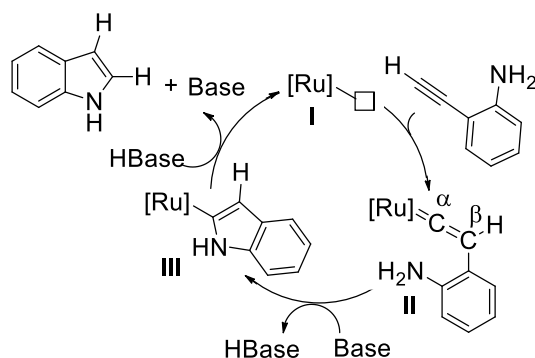
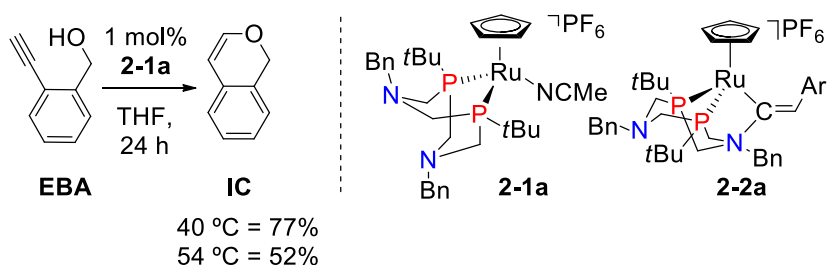


**Figure 3-1.** Simplified probable mechanism for cyclization of 2-ethynylaniline (**EA**) based on studies<sup>1e, 2a</sup> of catalytic alkyne hydration. The mechanism is depicted with an exogenous base, but an internal base on the ligand would serve the same role. The box in **I** indicates an open coordination site

Systematic studies that evaluate the effects of the second-coordination sphere properties on catalyst performance are scarce. Such studies are challenging since many MLC ligand motifs have the acidic or



basic site in the primary coordination sphere, where any changes in basicity will inevitably strongly affect the optimal steric/electronic properties for metal-mediated catalytic steps. Several ligands have the acidic or basic site in the secondary-coordination sphere (i.e. the ligand backbone), but in many cases extensive synthetic variation is non-trivial. Conversely, the  $P^{R_2}N^{R'_2}$  (3,7- $R'$ -1,5- $R$ -3,7-diaza-1,5-diphosphacyclooctane) ligand class contains a tertiary amine in the secondary-coordination sphere that is readily synthetically varied (e.g. see ligand in **2-1a**, Scheme 3-2).<sup>4</sup> In the case of  $[Ni(P^{R_2}N^{R'_2})_2]^{2+}$  electrocatalysts, tuning the properties of the pendent base significantly altered the rates of  $H_2$  oxidation/production.<sup>4b,5</sup> We have previously demonstrated that these ligands can be used to give MLC catalysts of the type  $[CpRu(P^{R_2}N^{R'_2})(MeCN)]PF_6$ , where derivative **2-1a** exhibits similar performance to **B** in the cyclization of 2-ethynylbenzyl alcohol (Scheme 3-2). Unfortunately, this catalyst easily deactivates at elevated temperatures to give the vinyl ammonium species **2-2a**.<sup>6</sup> Deactivation occurs by nucleophilic attack of the ligand pendent amine, rather than the oxygen nucleophile of the substrate, on  $C\alpha$  of the vinylidene intermediate (i.e. **II**). We hypothesize that a more nucleophilic substrate, such as an amine, will preferentially undergo productive turnover, rather than decomposition. Therefore, we have elected to employ 2-ethynylaniline and related compounds as representative cyclization substrates to elucidate the optimal steric and electronic parameters of the ligand basic site in MLC cyclization catalysts. Thus, we have prepared a group of  $[CpRu(P^{Ph_2}N^{R'_2})(MeCN)]PF_6$  complexes that differ in the substituent on the pendent amine ( $R'$ ) to systematically compare ligand structure to catalyst performance.

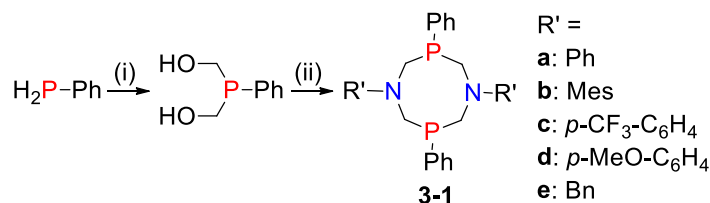


**Scheme 3-2.** Cyclization of 2-ethynylbenzyl alcohol (**EBA**) with  $P^{R_2}N^{R'_2}$  catalyst **2-1a**, and catalyst deactivation product **2-2a**<sup>6a</sup>

## 3.2 Results and Discussion

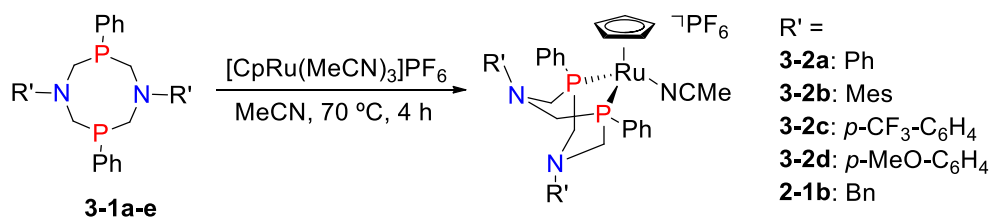
### 3.2.1 Catalyst Synthesis

A group of five  $P^R_2N^{R'}_2$  ligands were synthesized that have the same phosphine substituent ( $R = Ph$ ) but differ in the amine substituent  $R'$  (Scheme 3-3). The amine substituents were selected to evaluate both steric ( $R'$ : **3-1e** = Bn, **3-1a** = Ph, **3-1b** = Mes) and electronic ( $R'$ : **3-1c** = *p*-CF<sub>3</sub>-C<sub>6</sub>H<sub>4</sub>, **3-1a** = Ph, **3-1d** = *p*-MeO-C<sub>6</sub>H<sub>4</sub>) properties. The ligands were synthesized using modified literature procedures starting from phenyl phosphine, paraformaldehyde and the respective amine (Scheme 3-3).<sup>5, 7</sup> Derivative **3-1b** is a new entry into this ligand family and it was synthesized as a white solid in a poor yield (15%). Cyclization to give the 8-membered ligand is sensitive to the steric bulk of the amine since a related ligand with  $R' = t$ -Bu was reported to have a similarly low yield (cf. 26%).<sup>8</sup> X-ray quality crystals were obtained for **3-1c** and **3-1d** ( $R' = p$ -CF<sub>3</sub>-C<sub>6</sub>H<sub>4</sub> and *p*-MeO-C<sub>6</sub>H<sub>4</sub>, respectively). The P1-C1 bond lengths (**3-1c** = 1.832(2) Å; **3-1d** = 1.829(1) Å) are similar to that of  $R' = Ph$  ligand **3-1a** (1.828-1.833 Å).<sup>9</sup> This suggests that the substitution at  $R'$  has minimal long-range influence on the phosphine.



**Scheme 3-3.** Synthesis of  $P^{Ph}_2N^{R'}_2$  ligands used in this study. Conditions: (i) paraformaldehyde, EtOH, 78 °C, 4 h; (ii) dropwise  $H_2NR'$ , EtOH, 78 °C, 24 h. Yield: **3-1b** = 15%; **3-1a**, **3-1c-e** are known<sup>5, 7</sup>

Reaction of ligands **3-1a-e** with [CpRu(NCMe)<sub>3</sub>]PF<sub>6</sub> in acetonitrile at 70 °C for 4 h produced the known complex **2-1b**<sup>6a</sup> and new derivatives **3-2a-d** in good to excellent yields (79–98%; Scheme 3-4). All of the complexes were characterized by <sup>1</sup>H, <sup>13</sup>C{<sup>1</sup>H}, <sup>31</sup>P{<sup>1</sup>H} NMR and IR spectroscopies and MALDI mass spectrometry. The <sup>31</sup>P{<sup>1</sup>H} NMR signals are all found at ca. 40 ppm for **2-1b**, **3-2a-d**, suggesting the phosphine environment is not significantly influenced by the different  $R'$  substituents of the pendent amine.



**Scheme 3-4.** Synthesis of Ru(P<sup>Ph</sup><sub>2</sub>N<sup>R'</sup>)<sub>2</sub> complexes **2-1b**, **3-2a-d** by metalation of P<sup>Ph</sup><sub>2</sub>N<sup>R'</sup><sub>2</sub> ligands (**3-1a-e**). Complex **2-1b** was previously reported<sup>6a</sup>

Single crystals of **3-2a** were obtained and X-ray crystallography confirmed the expected structure (Figure 3-2). The Ru-P bond lengths are 2.251(2) and 2.260(2) Å (Ru-P1 and Ru-P2, respectively), which are very similar to the analogous values found for **2-1b**<sup>6a</sup> (2.2589(6) and 2.2605(6) Å). The distances between ruthenium and the Cp carbon atoms are likewise similar to **2-1b**. This shows that changing the R' substituent from Bn to Ph (**2-1b** and **3-2a**, respectively) has very little impact on the solid-state bonding parameters of the primary-coordination sphere.

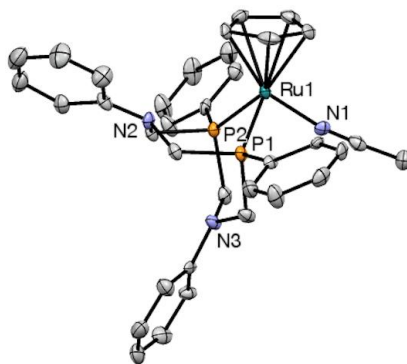
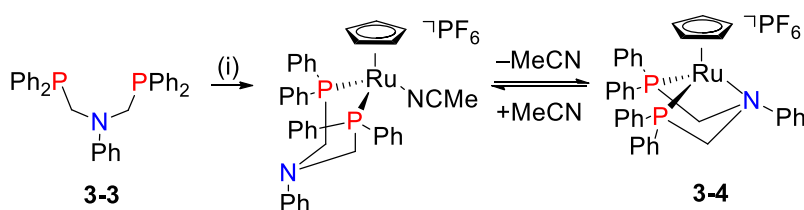


**Figure 3-2.** Displacement ellipsoid plot of **3-2a**. Ellipsoids are at the 50% probability level. Hydrogen atoms and PF<sub>6</sub><sup>-</sup> were omitted for clarity

While the P<sup>R</sup><sub>2</sub>N<sup>R'</sup><sub>2</sub> ligands contain two pendent basic sites, only the amine proximal to the acetonitrile ligand (i.e. the metal active site) in **2-1b**, **3-2a-d** should participate productively in cyclization catalysis. To evaluate the necessity of the second pendent base, the known<sup>10</sup> bisphosphine ligand P<sup>Ph</sup><sub>2</sub>N<sup>Ph</sup><sub>1</sub> (**3-3**), with one backbone pendent amine, was prepared. Metalation of **3-3** with [CpRu(NCMe)<sub>3</sub>]PF<sub>6</sub> gave **3-4** in high yield (Scheme 3-5). Instead of the typical yellow/orange solid observed for **2-1b**, **3-2a-d**, complex **3-4** is a vibrant red solid on solvent removal. This distinct colour is also observed following halide abstraction from CpRuCl(P<sup>R</sup><sub>2</sub>N<sup>R'</sup>) and Cp<sup>\*</sup>RuCl(P<sup>R</sup><sub>2</sub>N<sup>R'</sup>) complexes in non-coordinating

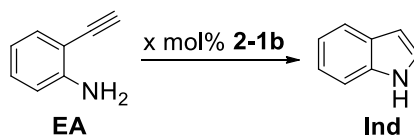
solvent.<sup>6b, 11</sup> The colour in these reactions was presumed to be a consequence of ligand coordination in a  $\kappa^3$ -PPN mode. The appearance of the  $^{31}\text{P}\{^1\text{H}\}$  NMR spectrum of isolated **3-4** in non-coordinating  $\text{CD}_2\text{Cl}_2$  is highly dependent on the presence of excess acetonitrile. Rigorous removal of  $\text{CH}_3\text{CN}$  gives a spectrum with broad signals between 48.9–56.0 ppm and a minor (ca. 15%) sharp singlet at 34.3 ppm. Cooling exhibited some sharpening of the broad signals, but the sample precipitated before the signals could be fully resolved. When **3-4** is dissolved in  $\text{CD}_3\text{CN}$ , only the sharp singlet at 34.6 ppm is observed, which is similar to the analogous signals in **2-1b**, **3-2a-d**. Additionally, dissolution in  $\text{CD}_3\text{CN}$  causes a colour change from red to orange and all of the  $^1\text{H}$  NMR signals are sharper than in  $\text{CD}_2\text{Cl}_2$ . Therefore, this indicates that acetonitrile coordinates to **3-4** and the  $\text{P}^{\text{Ph}}_2\text{N}^{\text{Ph}}_1$  ligand changes its coordination mode to  $\kappa^2$ -PP.



**Scheme 3-5.** Synthesis of dynamic  $\text{Ru}(\text{P}^{\text{Ph}}_2\text{N}^{\text{Ph}}_1)$  complex **3-4**. Conditions: (i)  $[\text{CpRu}(\text{MeCN})_3]\text{PF}_6$ , MeCN, RT, 4 h. Yield **3-4** = 92%

### 3.2.2 Catalytic Studies

The benchmark substrate 2-ethynylaniline (**EA**) was employed to optimize catalytic cyclization conditions with **2-1b** (Scheme 3-6). Very little difference in conversion was observed for cyclization conducted at 40 °C in a range of solvents (Table 3-1, Entry 1-7). Minor amounts of side products were observed in carbonyl-containing solvents, thus THF was selected as the optimal solvent for ongoing studies. Extending the reaction time from 1 to 24 h increased the yield of indole (**Ind**) from 12 to 73% (Entry 9). The temperature was increased to 55 °C and complete conversion was observed at 6 h (Table 3-1, Entry 11). Lowering the catalyst loading to 1 mol% gave 91% **Ind** after 6 h and >99% conversion was reached after 24 h. Further reduction in catalyst loading to 0.1 mol% gives a cyclization yield of 37%, which corresponds to a turnover number of 370 (Table 3-1, Entry 13). Increasing the temperature further to 70 °C gave quantitative conversion to **Ind** with 1 mol% **2-1b** within 2 h (Table 3-1, Entry 14).



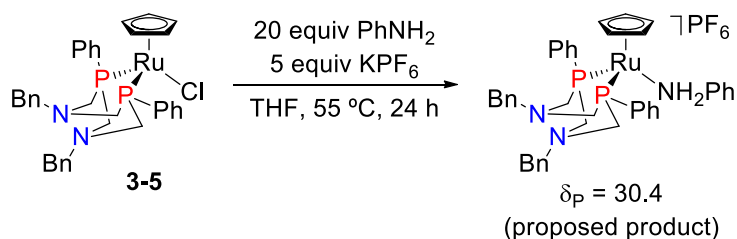
**Scheme 3-6.** Catalysis of the cyclization of 2-ethynylaniline (**EA**) using **2-1b**

**Table 3-1.** Catalysis of the cyclization of 2-ethynylaniline (**EA**) using **2-1b**

Entry	mol%	Solvent	Temp (°C)	Time (h)	Yield <b>Ind</b> (%) <sup>[a]</sup>
1	2	Acetone	40	1	13
2	2	Dioxane	40	1	8
3	2	THF	40	1	12
4	2	EtOAc	40	1	13
5	2	Anisole	40	1	10
6	2	DMF	40	1	8
7	2	DMA	40	1	15
8	2	THF	40	16	30
9	2	THF	40	24	73
10	2	THF	55	24	>99
11	2	THF	55	6	>99
12	1	THF	55	6	91
13	0.1	THF	55	24	37
14 <sup>[b]</sup>	1	Me-THF	70	2	≥99

<sup>[a]</sup> All yields are in situ values, determined by <sup>1</sup>H NMR spectroscopy by quantification of **EA** and **Ind** relative to the internal standard, dimethyl terephthalate. Reactions were conducted in proteo solvents, which were removed under vacuum and the residues redissolved in CDCl<sub>3</sub> for NMR analysis. <sup>[b]</sup> Yield of **Ind** was determined by calibrated GC-FID and the yield was determined relative to the internal standard, tetralin.

The high yield of **Ind** at elevated temperatures suggests that catalyst **2-1b** preferentially undergoes productive catalysis rather than deactivation, such as to a vinyl ammonium complex (i.e. an analog of **2-2a**). To confirm this, cyclization of **EA** was monitored by  $^{31}\text{P}\{^1\text{H}\}$  NMR spectroscopy under catalytic conditions (1.5 mol% of **2-1b** in THF at 50 °C). Throughout the experiment (up to 2 h), no new signal appeared in the downfield region (55-75 ppm) where **2-2a** and related vinyl ammonium species were previously<sup>6</sup> observed. At 2 h, the reaction composition is comprised of pre-catalyst **2-1b** (85%) and a new minor species (ca. 10%) observed as a singlet at 30.6 ppm. The minor signal is in a similar location to a known benzylamine adduct formed with **2-1b** that has  $\delta_{\text{P}} = 29.2$ .<sup>12</sup> With the goal in mind of identifying the structure of this minor resting state species, the chloro complex  $\text{CpRuCl}(\text{P}^{\text{Ph}}_2\text{N}^{\text{Bn}}_2)$ , **3-5**, was synthesized and characterized by  $^1\text{H}$ ,  $^{31}\text{P}\{^1\text{H}\}$ ,  $^{13}\text{C}\{^1\text{H}\}$  NMR and IR spectroscopies, MALDI mass spectrometry and X-ray crystallography. Complex **3-5** was reacted with  $\text{KPF}_6$  in THF in the presence of aniline (Scheme 3-7). Only one new product signal was observed by  $^{31}\text{P}\{^1\text{H}\}$  spectroscopy and it is a singlet at 30.4 ppm. The close similarity of this shift to that of the minor species observed under catalytic conditions with **2-1b**, suggests that the latter is a Ru-NH<sub>2</sub>Ar adduct. Evidence of a deactivated vinyl ammonium compound (analogous to **2-2a**), or other deactivation species, is not observed. Rather, the catalyst predominantly exists as pre-catalyst and an amine-adduct, which are both off-cycle resting states.



**Scheme 3-7.** Stoichiometric reaction of **3-5** with aniline

With optimal conditions identified, a screen of catalysts was undertaken using **2-1b**, **3-2a-d** and **3-4**. Cyclization of **EA** was conducted in THF, at 55 °C with 0.1, 0.5, 1, and 3 mol% catalyst loadings (Figure 3-3). Conversion to **Ind** was quantified by GC-FID analysis of reaction solutions after a 24 h reaction time. All of the complexes were active cyclization catalysts, except the  $\text{P}^{\text{Ph}}_2\text{N}^{\text{Ph}}_1$  complex **3-4**. Even at 3 mol% **3-4** shows no conversion, while its closest  $\text{P}^{\text{R}}_2\text{N}^{\text{R}'}_2$  comparator **3-2a** gives 31% **Ind** at only 0.1 mol% loading. This corresponds to a higher activity of **3-2a** over **3-4** by at least an order of magnitude. Thus, the second metallacycle ring and pendent amine is critical for high catalyst activity.

In the case of  $[\text{Ni}(\text{P}^{\text{R}'_2\text{N}^{\text{R}'_2})_2]^{2+}$  electrocatalysts, steric repulsions between the two metallacycle rings enforced the close positioning of one pendent base to the metal centre.<sup>4b,4c</sup> This positioning was deemed essential to achieve high catalytic rates.<sup>13</sup> A similar importance of pendent amine positioning is likely at play here and is the reason for the superior performance of  $\text{P}^{\text{Ph}_2\text{N}^{\text{R}'_2}$  catalysts **2-1b**, **3-2a-d** over  $\text{P}^{\text{Ph}_2\text{N}^{\text{Ph}_1}$  catalyst **3-4**.

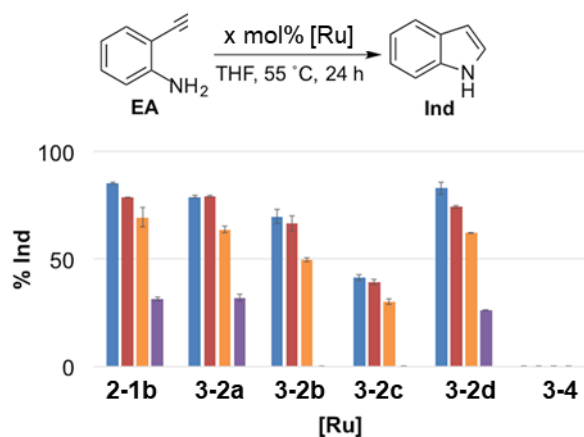


**Figure 3-3.** Cyclization yields of 2-ethynylaniline (**EA**) to indole (**Ind**) in THF at 55 °C after 24 h with catalysts **2-1b**, **3-2a-d** and **3-4** at 3 mol% (blue), 1 mol% (red), 0.5 mol% (orange) and 0.1 mol% (purple)

A comparison of  $\text{P}^{\text{Ph}_2\text{N}^{\text{R}'_2}$  catalysts **2-1b**, **3-2a-d** with a 0.5 mol% catalyst loading (Figure 3, orange bars) reveals that the order of activity in **EA** cyclization follows **2-1b**  $\approx$  **3-2a**  $\approx$  **3-2d** > **3-2b** > **3-2c** ( $\text{R}' = \text{Bn} \approx \text{Ph} \approx p\text{-MeO-C}_6\text{H}_4 > \text{Mes} > p\text{-CF}_3\text{-C}_6\text{H}_4$ ). The yield of **Ind** is ca. 15% lower with **3-2b** relative to **3-2a** ( $\text{R}' = \text{Mes}$  and  $\text{Ph}$ , respectively). Thus, the reaction is tolerant of the increase in steric bulk at the pendent amine despite the likely steric hindrance during proton-transfer steps. Also notable from the performance trend is the poor conversion with **3-2c**, which has the least basic pendent amine. A comparison of ammonium  $\text{p}K_{\text{a}}$  values gives a rough guide to relative acidities of the substrates, possible intermediates and the protonated pendent amine of the ligand. None of ligands in **2-1b**, **3-2a-d** have a pendent amine that is sufficiently basic to deprotonate aniline. Therefore, it is most likely that the ligand deprotonates the substrate after, or in concert with, nucleophilic attack on the vinylidene intermediate **II** (see Figure 3-1). The pendent amine of **3-2c** is less basic than the substrate **EA** ( $\text{p}K_{\text{a}}$ : [ $p\text{-CF}_3\text{C}_6\text{H}_4\text{NH}_3$ ] $^+ = 8.16$ , [ $\text{PhNH}_3$ ] $^+ = 10.6$ ).<sup>[14]</sup> In contrast, catalysts **2-1b**, **3-2a,d** are all of similar or higher basicity ( $\text{p}K_{\text{a}}$ : [ $p\text{-OMeC}_6\text{H}_4\text{NH}_3$ ] $^+ = 12.05$ , [ $\text{BnNH}_3$ ] $^+ = 16.76$ , [ $\text{PhNH}_3$ ] $^+ = 10.6$ )<sup>14</sup> and these

three catalysts have equivalent activity. We hypothesize that, to achieve high activity, the basicity of the ligand need only be above a threshold defined by the basicity of the substrate.

A similar catalyst performance study for **2-1b**, **3-2a-d** and **3-4** was conducted with **EBA** as the substrate (Figure 4). All of the catalysts **2-1b**, **3-2a-d** showed lower performance than in cyclization of **EA**; the highest yield of isochromene (**IC**) was 32%, which was achieved with 3 mol% **2-1b**. The trend in activity of the  $\text{P}^{\text{Ph}}_2\text{N}^{\text{R}'_2}$  catalysts followed a very similar trend to that found with **EA** where **2-1b**  $\approx$  **3-2a**  $\approx$  **3-2d**  $>$  **3-2c**  $>$  **3-2b** ( $\text{R}' = \text{Bn} \approx \text{Ph} \approx p\text{-MeO-C}_6\text{H}_4 > p\text{-CF}_3\text{-C}_6\text{H}_4 > \text{Mes}$ ). In all cases the pendent amine is more basic than the substrate alcohol functionality,<sup>15</sup> indicating that all catalysts should be equally competent at deprotonation of an intermediate formed after nucleophilic attack of the alcohol on the vinylidene. We hypothesize that the low yields of **IC** are due to competing formation of deactivation compounds, including those similar to **2-2a**, as was confirmed previously in the cyclization of **EBA** with catalyst **2-1a**. To confirm that deactivation, rather than low catalyst initiation, limits activity, cyclization of **EBA** was conducted with 1 mol% **2-1b**, **3-2a-d** at 70 °C. Complexes **2-1b**, **3-2a,b,d** gave <5% **IC** with no increase in product after 1h, which is lower than the yields observed at 55 °C. Catalyst **3-2c** was slightly improved at the higher temperature, but the yield of **IC** only reached 15%. We had previously hypothesized that a sterically hindered or a poorly nucleophilic pendent amine would be less susceptible to vinyl ammonium deactivation. However, catalysts **3-2b** and **3-2c** ( $\text{R}' = \text{Mes}$  and  $p\text{-CF}_3\text{-C}_6\text{H}_4$ , respectively), which were designed with these characteristics in mind, showed the lowest activity of **2-1b**, **3-2a-d**. Therefore, preventing deactivation through steric or electronic tuning of the ligand was insufficient to effectively cyclize **EBA**.



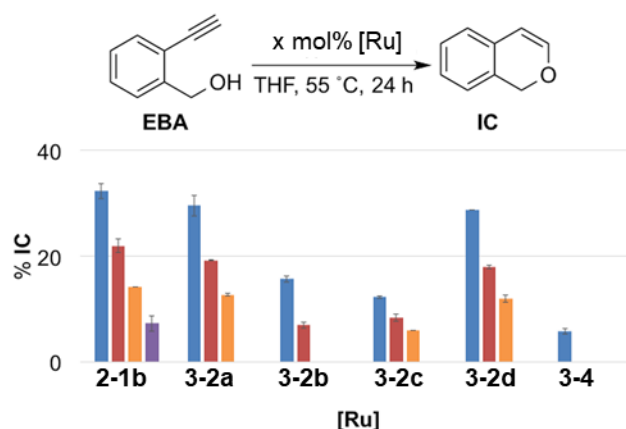


**Figure 3-4.** Cyclization yields of 2-ethynylbenzyl alcohol (**EBA**) to isochromene (**IC**) in THF at 55 °C after 24 h with catalysts **2-1b**, **3-2a-d** and **3-4** at 3 mol% (blue), 1 mol% (red), 0.5 mol% (orange) and 0.1 mol% (purple)

The conversion of **EA** to **Ind** was monitored over time with 2 mol% **2-1b**, and **3-2a,c** at 55 °C (Figure 3-5). In the above studies it was observed that catalysts **2a** and **2b** ( $R' = \text{Bn}$  and  $\text{Ph}$ ) have similar 24 h conversion. Here it is clear that their rates are very similar and that they both reach complete conversion to **Ind** within 6 h. The activity is superior to the previously reported catalysts **A** (Scheme 3-1) that requires higher catalyst loading (10 mol% **A**) and the conditions are milder than those used with catalysts **A** and **B** that operate at higher temperatures (**A**: 90 °C; **B**: 70 °C).<sup>2e, 2f</sup> Notably, heating 1 mol% **3-2a** to 70 °C gives complete conversion to **Ind** within 2 h (Table 3-1, Entry 14), which is more rapid than the MLC catalyst **B** (2 mol%). At short reaction times (<2 h) catalyst **3-2c** ( $R' = p\text{-CF}_3\text{-C}_6\text{H}_4$ ) also has similar performance, but shows lower conversion than **2-1b** and **3-2a** at longer times.

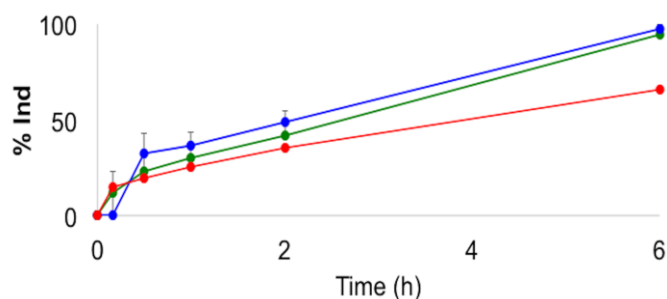


**Figure 3-5.** Cyclization of 2-ethynylaniline (**EA**) under optimal conditions (2 mol% [Ru], Me-THF, 55 °C) monitored over time. [Ru] = **2-1b** ( $R' = \text{Bn}$ , green), **3-2a** ( $R' = \text{Ph}$ , blue), **3-2c** ( $R' = p\text{-CF}_3\text{-C}_6\text{H}_4$ , red)

We proposed above that, for amine substrates, the pendent amine of the  $\text{P}^{\text{Ph}}_2\text{N}^{\text{R}'_2}$  catalysts must only be more basic than the substrate to give productive turnover. To probe this hypothesis, the cyclization of three additional substrates – 2-ethynyl-4-methoxyaniline (**EA-4-OMe**), 2-ethynyl-4-fluoroaniline (**EA-4-F**) and 2-ethynylbenzamide (**EAM**) – was conducted (Figure 3-6). In all cases, 2 mol% [Ru] was employed and reactions were conducted in Me-THF at 55 or 70 °C. Substrate **EA-4-OMe** was effectively cyclized by both catalysts **3-2a** and **3-2d** ( $\text{R}' = \text{Ph}$  and  $p\text{-MeO-C}_6\text{H}_4$ , respectively) within 48 h at 55 °C. Catalyst **3-2a** is estimated to be similar or slightly less basic than the substrate ( $\text{p}K_{\text{a}}$ ,  $[\text{PhNH}_3]^+ = 10.6$ ,  $[\text{PhNMe}_2\text{H}]^+ = 12.30$ :  $[p\text{-OMeC}_6\text{H}_4\text{NH}_3]^+ = 12.05$ ),<sup>14</sup> which could account for the slightly slower rate of **3-2a** relative to **3-2d**. The less basic aniline substrate **EA-4-F** is cyclized to ca. 85% with both **3-2a** and **3-2c** ( $\text{R}' = \text{Ph}$  and  $p\text{-CF}_3\text{-C}_6\text{H}_4$ , respectively) within 48 h at 55 °C. The **EA-4-F** conversion curves for **3-2a** and **3-2c** are nearly indistinguishable, which is in contrast to cyclization of **EA** with these two catalysts where **3-2a** was superior to **3-2c** (Figure 3-5). This supports the hypothesis that a threshold basicity of the pendent amine is important for catalyst performance. Cyclization of amide substrate **EAM** was attempted with **2-1b** and **3-2a** ( $\text{R}' = \text{Bn}$  and  $\text{Ph}$ , respectively) at 55 °C, but <15% 1(2H)-isoquinolinone (**IQO**) was observed after 48 h. At 70 °C, **2-1b** gave complete conversion to **IQO** by 48 h, but conversion with **3-2a** reached only 15%. The poor performance of **3-2a** is surprising since the pendent amine in this catalyst is significantly more basic than **EAM** ( $\text{p}K_{\text{a}}$ :  $[\text{PhNH}_3]^+ = 10.6$ ,  $[\text{PhCONH}_3]^+ = 3.7$ ).<sup>14, 16</sup> The nucleophilicity of the amide functionality in **EAM** is expected to be lower than that of the aniline substrates. Thus, the lower performance of **3-2a** may be a consequence of competitive deactivation through a vinyl ammonium species of type **2-2a**. Alternatively, the mechanistic pathway, and/or rate determining step, may be different for this substrate. Further mechanistic analysis is required to fully understand the limitations of **3-2a** as compared to **2-1b** when extending the scope beyond aniline-type substrates.

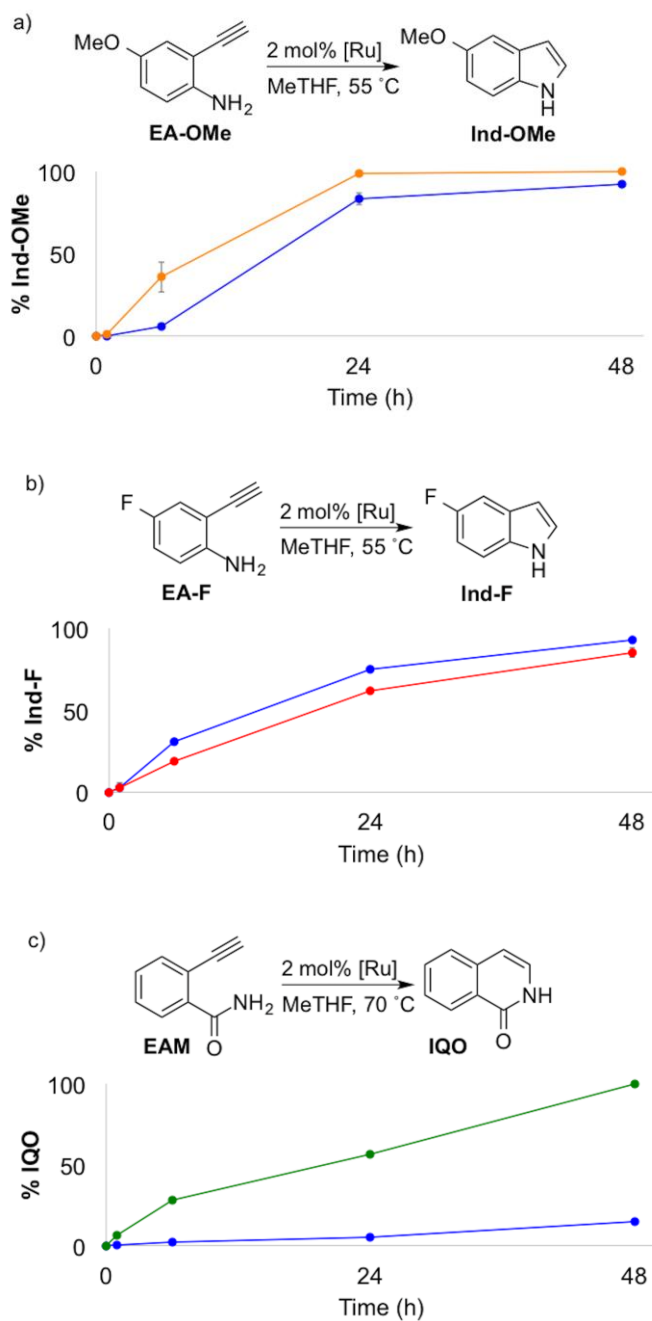


**Figure 3-6.** Cyclization conversion over time with 2 mol% [Ru] in Me-THF of: a) 2-ethynyl-4-methoxyaniline (**EA-4-OMe**) at 55 °C with **3-2a** (R' = Ph, blue) and **3-2d** (R' = *p*-MeO-C<sub>6</sub>H<sub>4</sub>, orange); b) 2-ethynyl-4-fluoroaniline (**EA-4-F**) at 55 °C with **3-2a** (R' = Ph, blue) and **3-2c** (R' = *p*-CF<sub>3</sub>-C<sub>6</sub>H<sub>4</sub>, red); and c) 2-ethynylbenzylamide (EAM) at 70 °C with **2-1b** (R' = Bn, green) and **3-2a** (R' = Ph, blue). In all cases conversion was quantified by <sup>1</sup>H NMR spectroscopy

### 3.3 Conclusion

We have synthesized a new group of  $[\text{CpRu}(\text{P}^{\text{Ph}}_2\text{N}^{\text{R}'_2})(\text{NCMe})]\text{PF}_6$  complexes (**2-1b**, **3-2a-d**) that differ in the steric and electronic properties of the pendent amine. These complexes were tested as catalysts in the cyclization of alkynyl amines and alcohol to give *N*- and *O*-heterocycles, respectively. This class of catalyst showed much higher activity toward aniline-type, as compared to alcohol-type, substrates. Indeed, the optimal catalysts (**2-1b**, **3-2a,d**) generate indole under milder conditions and shorter reaction times than previously reported catalysts. The superior performance of the  $\text{P}^{\text{Ph}}_2\text{N}^{\text{R}'_2}$  catalysts (**2-1b**, **3-2a-d**) over the  $\text{P}^{\text{Ph}}_2\text{N}^{\text{Ph}}_1$  catalyst **3-4**, suggests that a positioned pendent amine is essential to achieve high performance. Catalyst comparison in the cyclization of 2-ethynylaniline derivatives revealed that the yield and rates are very similar for  $\text{R}' = \text{Bn}$ ,  $\text{Ph}$ , *p*-MeO-C<sub>6</sub>H<sub>4</sub> derivatives **2-1b**, **3-2a** and **3-2d**, respectively. The less basic catalyst **3-2c** ( $\text{R}' = p\text{-CF}_3\text{-C}_6\text{H}_4$ ) showed inferior performance, except with the relatively low-basicity substrate 2-ethynyl-4-fluoroaniline where it had comparable performance to **3-2a**. This suggests that to achieve high catalyst performance, the ligand pendent base should be similar or more basic than the substrate amine of aniline substrates. Proton shuttling during catalysis is somewhat tolerant of steric bulk at the pendent amine since catalyst **3-2b** ( $\text{R}' = \text{Mes}$ ) shows only a minor reduction in activity as compared to **3-2a** ( $\text{R}' = \text{Ph}$ ) in the cyclization of 2-ethynyl aniline. Surprisingly, only catalyst **2-1b** was competent in the cyclization of 2-ethynylamide, indicating that there are still important aspects to the mechanism that are yet to be elucidated. We are currently extending this investigation to study the mechanism and the role of the primary-coordination sphere (i.e. the phosphine substituents, R) on catalyst performance.

### 3.4 Experimental

#### 3.4.1 General Procedures, Materials and Instrumentation

All air and water-sensitive reactions were manipulated under N<sub>2</sub> using standard Schlenk or glovebox techniques unless otherwise stated. All glassware was oven dried prior to use. BnNH<sub>2</sub> (>98%), aniline (>99%), mesitylene amine (98%), and triphenylphosphine oxide (99%) were obtained from Alfa Aesar. Phenylphosphine (99%) was obtained from Strem. 4-Trifluoroaniline (99%), tetrahydronaphthalene (99%), 2-ethynylaniline (98%), and 2-methyltetrahydrofuran (Me-THF) (>99% anhydrous) were obtained from Sigma-Aldrich. 4-methoxyaniline (98%) was obtained from Oakwood Chemicals. Chloroform-*d*<sub>1</sub> (99.8%), and dichloromethane-*d*<sub>2</sub> (99.8%) were obtained from Cambridge Isotope

Laboratories. Paraformaldehyde was prepared by filtration of formaldehyde (37% by weight solution in water with 10-15% methanol) to remove any solids, removing methanol and water under vacuum until a white gel is produced.  $[\text{Ru}(\text{Cp})(\text{MeCN})_3]\text{PF}_6$ ,<sup>[17]</sup>  $\text{P}^{\text{Ph}}_2\text{N}^{\text{R}'_2}$  (**1a,c,d,e**),<sup>5, 7</sup> and  $[\text{Ru}(\text{Cp})(\text{P}^{\text{Ph}}_2\text{N}^{\text{Bn}_2})(\text{NCMe})]\text{PF}_6$  (**2-1b**)<sup>6a</sup> were synthesized following literature procedures. Substrates 2-ethynyl-4-methoxyaniline (**EA-4-OMe**), 2-ethynyl-4-fluoroaniline (**EA-4-F**), and 2-ethynylamide (**EAM**) were synthesized following literature procedures.<sup>2d, 18</sup> Dry and degassed tetrahydrofuran (THF), diethyl ether, toluene, dichloromethane (DCM), hexanes, dimethylformamide (DMF), dioxane and acetonitrile (MeCN) were obtained from an Innovative Technology 400-5 Solvent Purification System and stored under  $\text{N}_2$ . These dry and degassed solvents, except for MeCN, were stored over 4 Å molecular sieves (Fluka and activated at 150 °C under vacuum for over 12 h). Acetone was dried with  $\text{Cs}_2\text{CO}_3$  and degassed by bubbling with  $\text{N}_2$ . Tetrahydrofuran was distilled from  $\text{CaH}_2$  and degassed by bubbling  $\text{N}_2$ . Absolute ethanol was deoxygenated by bubbling with  $\text{N}_2$ . *N,N*-Dimethylacetamide and chloroform-*d*<sub>1</sub> were dried with 4 Å molecular sieves and degassed by bubbling with  $\text{N}_2$ . Benzylamine was dried with NaOH, distilled under vacuum and stored under  $\text{N}_2$ . All other chemicals were used as received.

Charge-transfer Matrix Assisted Laser Desorption/Ionization (MALDI) mass spectrometry data were collected on an AB Sciex 5800 TOF/TOF mass spectrometer using pyrene as the matrix in a 20:1 molar ratio to metal complex. Samples were spotted on the target plate as solutions in DCM. All NMR spectra were recorded on either a Varian Inova 400 or 600 MHz, a Varian Mercury 400 MHz or Bruker 400 MHz NMR spectrometer. <sup>1</sup>H and <sup>13</sup>C{<sup>1</sup>H} spectra acquired in  $\text{CDCl}_3$  were referenced internally against the residual solvent signal ( $\text{CHCl}_3$ ) to TMS at 0 ppm. <sup>31</sup>P spectra were referenced externally to 85% phosphoric acid at 0.00 ppm. Infrared spectra were collected on solid samples using a PerkinElmer UATR TWO FTIR spectrometer. Elemental analysis of **5** was performed by Canadian Microanalytical Service Ltd. in Delta, BC. Satisfactory elemental analyses of **3-2a-d** and **3-4** were not obtained due to persistent minor, but variable, amounts of MeCN in the samples. Quantification of catalytic conversion of **EBA** or **EA** was achieved using an Agilent 7890a gas chromatography with a flame ionization detector (GC-FID), fitted with a HP-5 column. Calibration curves for **EA**, **Ind**, **EBA**, **IC** were prepared to determine the response factors. The amount of each species was quantified, relative to the internal standard (tetrahydronaphthalene), using area counts corrected with the response factors.

### 3.4.2 General Procedure for the Synthesis of $P^{Ph_2}N^{R'_2}$ Ligands (**1a-e**)

A modified literature procedure<sup>7a</sup> was followed. These reactions were manipulated under argon. Phenylphosphine (1.00g, 9.08 mmol) was added to 100 mL Schlenk flask in a glovebox. On the Schlenk line, a 2-neck 500 mL Schlenk flask containing: a stir bar, freshly made ( $\leq 1$  week) paraformaldehyde (3 g, 0.1 mol), and 200 mL EtOH, was fit with a reflux condenser under argon. Degassed EtOH (50 mL) was added via cannula to the 100 mL Schlenk with the primary phosphine. The primary phosphine solution was then added to the 500 mL Schlenk via cannula at room temperature. Degassed EtOH (50 mL) was added via cannula to the 100 mL Schlenk to rinse the flask and this was added to the 500 mL reaction flask. The reaction flask was heated to reflux for 4 h after which an aliquot was transferred to a degassed NMR tube by syringe. The solution was analyzed by  $^{31}P\{^1H\}$  NMR spectroscopy (unlocked) to determine if any  $PhPH_2$  ( $\delta = ca. -120$ ) remained. Once the  $PhPH_2$  was consumed (ca. 4 h), the primary amine (1.05 eq) was added to the solution (still heated to 70 °C) dropwise by syringe at a rate of ca. 1 drop/10 seconds. Liquid amines ( $RNH_2$ : R = Bn, Ph, Mes, *p*-CF<sub>3</sub>Ph) were added neat and solid amines ( $RNH_2$ : R = *p*-OMePh) were added as solutions in EtOH (25 mM). White precipitate was observed on addition of each drop, but did not persist. The reaction was left to stir at 70 °C for 24 h and then cooled to room temperature. Reactions giving ligands **1a-e** afforded a white precipitate, which was isolated by filtration through a filter frit and washed with acetonitrile (3 × 5 mL). Reactions to give ligands **1c-d** did not give significant precipitate on cooling to room temperature. In these cases, the ligand (**1c-d**) was precipitated after addition of acetonitrile (15 mL) and cooling to -35 °C. The ligands **1c-d** were isolated through decanting the mother liquor and washing the solid with cold acetonitrile (5-10 mL).

**$P^{Ph_2}N^{Ph_2}$  (3-1a)**: Yield = 87%.  $^1H$  and  $^{31}P\{^1H\}$  NMR spectra matched literature values.<sup>7b</sup>

**$P^{Ph_2}N^{Mes_2}$  (3-1b)** Yield = 15%.  $^1H$  NMR (600 MHz,  $CD_2Cl_2$ ):  $\delta$  7.34–7.27 (m, Ph-*H*, 3H), 7.27–7.15 (m, Ph-*H*, 7H), 6.88–6.84 (br, Ph-*H*, 1H), 6.84–6.82 (br, Ph-*H*, 2H), 6.78–6.73 (br, Ph-*H*, 1H), 4.54–4.46 (m,  $PCH_2N$ , 2H), 4.12–4.05 (m,  $PCH_2N$ , 2H), 3.84–3.77 (m,  $PCH_2N$ , 2H), 3.69–3.61 (m,  $PCH_2N$ , 2H), 2.67 (s,  $CH_3$ , 3H), 2.39 (s,  $CH_3$ , 6H), 2.20 (m,  $CH_3$ , 9H).  $^{31}P\{^1H\}$  NMR (243 MHz,  $CD_2Cl_2$ ):  $\delta$  -22.4 (s,  $P^{Ph_2}N^{Mes_2}$ ), -27.0 (s,  $P^{Ph_2}N^{Mes_2}$ ).  $^{13}C\{^1H\}$  NMR (151.5 MHz,  $CD_2Cl_2$ ):  $\delta$  150.4–150.3 (m,  $C_{Ar}$ -N), 137.4 ( $C_{Ar}$ ), 136.7 ( $C_{Ar}$ ), 136.5 ( $C_{Ar}$ ), 135.5 ( $C_{Ar}$ ), 135.3 ( $C_{Ar}$ ), 132.5–132.2 ( $C_{Ar}$ ), 132.1 (d,  $^2J_{C-P} = 16.1$  Hz,  $C_{Ar}$ ), 131.6 (d,  $^2J_{C-P} = 16.1$  Hz,  $C_{Ar}$ ), 130.2 ( $C_{Ar}$ ), 130.0 ( $C_{Ar}$ ), 129.5 ( $C_{Ar}$ ), 128.8–128.6 ( $C_{Ar}$ ), 128.5 (d,  $^3J_{C-P} = 6.1$  Hz,  $C_{Ar}$ ), 128.3 (d,  $^3J_{C-P} = 6.1$  Hz,  $C_{Ar}$ ), 62.3–62.0 (m,  $PCH_2N$ ), 58.2–57.9 (m,

PCH<sub>2</sub>N), 20.9–20.7 (CH<sub>3</sub>), 20.0 (CH<sub>3</sub>), 19.9 (CH<sub>3</sub>), 19.3 (CH<sub>3</sub>). MALDI MS (pyrene matrix): Calc. m/z 538.3 [C<sub>34</sub>H<sub>39</sub>N<sub>2</sub>P<sub>2</sub>]<sup>+</sup>, Obs. m/z 638.3.

**P<sup>Ph</sup><sub>2</sub>N<sup>C<sub>6</sub>H<sub>4</sub>-CF<sub>3</sub></sup><sub>2</sub> (3-1c)**: Yield = 75%. <sup>1</sup>H and <sup>31</sup>P{<sup>1</sup>H} NMR spectra matched literature values.<sup>5</sup> X-ray quality crystals formed from a chilled (–35 °C) solution of **1d** in MeCN.

**P<sup>Ph</sup><sub>2</sub>N<sup>C<sub>6</sub>H<sub>4</sub>-OMe</sup><sub>2</sub> (3-1d)**: Yield = 90%. <sup>1</sup>H and <sup>31</sup>P{<sup>1</sup>H} NMR spectra matched literature values.<sup>5</sup> X-ray quality crystals formed from a chilled (–35 °C) solution of **1e** in MeCN.

**P<sup>Ph</sup><sub>2</sub>N<sup>Bn</sup><sub>2</sub> (3-1e)**: Yield = 83%. <sup>1</sup>H and <sup>31</sup>P{<sup>1</sup>H} NMR spectra matched literature values.<sup>7a</sup>

### 3.4.3 Synthesis of P<sup>Ph</sup><sub>2</sub>N<sup>Ph</sup><sub>1</sub> Ligand (**3-3**)

A modified procedure of the literature reported method<sup>19</sup> was followed. The reaction was manipulated under argon. Diphenylphosphine (1.05 g, 5.64 mmol) was added to 100 mL Schlenk flask in a glovebox. On the Schlenk line, a 2-neck 500 mL Schlenk flask containing: a stir bar, freshly made (≤1 week) paraformaldehyde (3.00 g, 0.100 mol, 18 equiv.), and 200 mL EtOH was fit with a reflux condenser under argon. Degassed EtOH (50 mL) was added via cannula to the 100 mL Schlenk with the primary phosphine. The primary phosphine solution was then added to the 500 mL Schlenk via cannula at room temperature. Degassed EtOH (50 mL) was added via cannula to the 100 mL Schlenk to rinse the flask and this was added to the 500 mL reaction flask. The reaction flask was heated under reflux for 4 h after which an aliquot was transferred to a degassed NMR tube by syringe. The solution was analyzed by <sup>31</sup>P{<sup>1</sup>H} NMR spectroscopy (unlocked) to determine if any PhPH<sub>2</sub> remained. Once the PhPH<sub>2</sub> was consumed (4 h), the primary amine (1.05 equiv) was added neat dropwise by syringe at a rate of ca. 1 drop/10 seconds, while the reaction remained at 70 °C. White precipitate was observed on addition of each drop but did not persist. The reaction was left to stir at 70 °C for 24 h and then cooled to room temperature. The reaction afforded a white precipitate, which was isolated by filtration through a filter frit and washed with acetonitrile (3 × 5 mL). Yield = 95%. <sup>1</sup>H and <sup>31</sup>P{<sup>1</sup>H} NMR spectra matched literature values.

### 3.4.4 General Procedure for the Synthesis of Ru(P<sup>Ph</sup><sub>2</sub>N<sup>R'</sup><sub>2</sub>) (**2-1b, 3-2a-d**) and Ru(P<sup>Ph</sup><sub>2</sub>N<sup>Ph</sup><sub>1</sub>) (**3-4**) Complexes

To a 100 mL Schlenk flask with a stir bar, [CpRu(NCMe)<sub>3</sub>]PF<sub>6</sub> (0.100-0.120 mmol), ligand P<sup>Ph</sup><sub>2</sub>N<sup>R'</sup><sub>2</sub> or P<sup>Ph</sup><sub>2</sub>N<sup>R'</sup><sub>1</sub> (0.105-1.26 mmol, 1.05 equiv.) and acetonitrile (20 mL) was added. The flask was heated to

65 °C for 4 hours with stirring. The solvent was removed under vacuum and the remaining solid was triturated with pentane (3 × 2 mL). Acetonitrile (2 mL) was added and the resulting suspension was filtered. The solid was washed with acetonitrile until the washings were colourless. The solvent of the filtrate was removed under vacuum to produce a solid that was washed with toluene (3 x 2 mL) and diethyl ether (5 mL). The product was dried under vacuum to produce clean product. Reprecipitation of **2-1b**, and **3-2a-d** from acetonitrile gave minor by-products, as judged by <sup>1</sup>H NMR spectroscopy, that are assigned to κ<sup>3</sup>-(PPN) derivatives. To avoid mixtures, purification by reprecipitation was avoided for **2-1b**, and **3-2a-d**.

**[Ru(Cp)(P<sup>Ph</sup><sub>2</sub>N<sup>Bn</sup><sub>2</sub>)(NCMe)]PF<sub>6</sub> (**2-1b**):** <sup>1</sup>H and <sup>31</sup>P{<sup>1</sup>H} NMR spectra matched literature values in CDCl<sub>3</sub>.<sup>6a</sup> Spectral data in CD<sub>2</sub>Cl<sub>2</sub> is provided here to ease comparisons between the various catalysts **2a-e**. <sup>1</sup>H NMR (600 MHz, CD<sub>2</sub>Cl<sub>2</sub>): δ 7.69–7.60 (m Ph-*H*, 4H), 7.56–7.48 (m, Ph-*H*, 6H), 7.41–7.16 (m, Ph-*H*, 10H), 4.78 (s, Cp-*H*, 5H), 3.89 (s, PhCH<sub>2</sub>N, 2H), 3.71 (s, PhCH<sub>2</sub>N, 2H), 3.29–3.17 (m, PCH<sub>2</sub>N, 4H), 3.04–2.96 (m, PCH<sub>2</sub>N, 2H), 2.77–2.70 (m, PCH<sub>2</sub>N, 2H), 2.22 (s, NCCH<sub>3</sub>, 3H). <sup>31</sup>P{<sup>1</sup>H} NMR (243 MHz, CD<sub>2</sub>Cl<sub>2</sub>): δ 38.7 (s, RuP), –144.4 (sept, <sup>1</sup>J<sub>P-F</sub> = 712 Hz, PF<sub>6</sub><sup>-</sup>).

**[Ru(Cp)(P<sup>Ph</sup><sub>2</sub>N<sup>Ph</sup><sub>2</sub>)(NCMe)]PF<sub>6</sub> (**3-2a**):** Yield = 89%. <sup>1</sup>H NMR (600 MHz, CD<sub>2</sub>Cl<sub>2</sub>): δ 7.93–7.87 (m, Ph-*H*, 4H), 7.69–7.61 (m, Ph-*H*, 6H), 7.29 (dd, <sup>3</sup>J<sub>H-H</sub> = 8.0 Hz, <sup>3</sup>J<sub>H-H</sub> = 8.0 Hz, Ph-*H*, 2H), 7.25 (dd, <sup>3</sup>J<sub>H-H</sub> = 8.0 Hz, <sup>3</sup>J<sub>H-H</sub> = 8.0 Hz, Ph-*H*, 2H), 7.02–6.95 (m, Ph-*H*, 3H), 6.88–6.83 (m, Ph-*H*, 3H), 4.79 (s, Cp-*H*, 5H), 4.25–4.13 (m, PCH<sub>2</sub>N, 4H), 4.00–3.91 (m, PCH<sub>2</sub>N, 2H), 3.63–3.57 (m, PCH<sub>2</sub>N, 2H), 2.28 (s, NCCH<sub>3</sub>, 3H). <sup>31</sup>P{<sup>1</sup>H} NMR (243 MHz, CD<sub>2</sub>Cl<sub>2</sub>): δ 39.7 (s, RuP), –144.4 (sept, <sup>1</sup>J<sub>P-F</sub> = 712 Hz, PF<sub>6</sub><sup>-</sup>). <sup>13</sup>C{<sup>1</sup>H} NMR (151.5 MHz, CD<sub>2</sub>Cl<sub>2</sub>): δ 152.5 (t, <sup>3</sup>J<sub>C-P</sub> = 8 Hz, C<sub>Ar</sub>-N), 151.2 (t, <sup>3</sup>J<sub>C-P</sub> = 6 Hz, <sup>3</sup>J<sub>C-P</sub> = 6 Hz, C<sub>Ar</sub>-N), 133.6 (dd, <sup>1</sup>J<sub>C-P</sub> = 19.7 Hz, <sup>3</sup>J<sub>C-P</sub> = 19.7 Hz, C<sub>Ar</sub>-P), 132.3–132.0 (C<sub>Ar</sub>), 130.3–129.8 (C<sub>Ar</sub>), 128.8 (CN), 122.4 (C<sub>Ar</sub>), 120.9 (C<sub>Ar</sub>), 118.5 (C<sub>Ar</sub>), 116.8 (C<sub>Ar</sub>), 82.3 (C<sub>Cp</sub>), 52.8 (dd, <sup>1</sup>J<sub>C-P</sub> = 17 Hz, <sup>3</sup>J<sub>C-P</sub> = 17 Hz, PCH<sub>2</sub>N), 51.1 (dd, <sup>1</sup>J<sub>C-P</sub> = 22 Hz, <sup>3</sup>J<sub>C-P</sub> = 22 Hz, PCH<sub>2</sub>N), 4.7 (CH<sub>3</sub>). MALDI MS (pyrene matrix): Calc. m/z 621.1 [Ru(Cp)(P<sup>Ph</sup><sub>2</sub>N<sup>Ph</sup><sub>2</sub>)]<sup>+</sup>, Obs. m/z 621.1. X-ray quality crystals were formed from a concentrated solution of **2b** in DCM to which was added toluene until the solution was slight cloudy and the solution was chilled (–35 °C).

**[Ru(Cp)(P<sup>Ph</sup><sub>2</sub>N<sup>Mes</sup><sub>2</sub>)(NCMe)]PF<sub>6</sub> (**3-2b**):** Yield = 79%. <sup>1</sup>H NMR (400 MHz, CD<sub>2</sub>Cl<sub>2</sub>): δ 7.92–7.77 (m, C<sub>Ar</sub>-*H*, 4H), 7.68–7.54 (m, C<sub>Ar</sub>-*H*, 6H), 7.35–7.24 (m, C<sub>Ar</sub>-*H*, 2H), 6.98–6.84 (m, C<sub>Ar</sub>-*H*, 2H), 5.04 (s, Cp-*H*, 5H), 4.74–4.64 (m, PCH<sub>2</sub>N, 2H), 3.80–3.63 (m, PCH<sub>2</sub>N, 4H), 3.40–3.30 (m, PCH<sub>2</sub>N, 2H), 2.44 (s, CH<sub>3</sub>, 3H), . <sup>31</sup>P{<sup>1</sup>H} NMR (243 MHz, CD<sub>2</sub>Cl<sub>2</sub>): δ 37.8 (s, RuP), –144.4 (sept, <sup>1</sup>J<sub>P-F</sub> = 712 Hz, PF<sub>6</sub><sup>-</sup>).



$^{13}\text{C}\{^1\text{H}\}$  NMR (151.5 MHz,  $\text{CD}_2\text{Cl}_2$ ):  $\delta$  146.7 (t,  $^3J_{\text{C-P}} = 10.1$  Hz,  $C_{\text{Ar-N}}$ ), 145.1 ( $C_{\text{Ar-N}}$ ), 137.0 ( $C_{\text{Ar}}$ ), 135.7, ( $C_{\text{Ar}}$ ), 133.6 (t,  $^1J_{\text{C-P}} = 34.2$  Hz,  $^3J_{\text{C-P}} = 34.2$  Hz,  $C_{\text{Ar}}$ ), 132.0 (d,  $^3J_{\text{C-P}} = 9.8$  Hz,  $C_{\text{Ar}}$ ), 132.0 (d,  $^2J_{\text{C-P}} = 9.8$  Hz,  $C_{\text{Ar-P}}$ ), 131.8 ( $C_{\text{Ar}}$ ), 130.9–130.2 ( $C_{\text{Ar}}$ ), 129.6 (d,  $^3J_{\text{C-P}} = 8.2$  Hz,  $C_{\text{Ar}}$ ), 129.5 (d,  $^3J_{\text{C-P}} = 8.2$  Hz,  $C_{\text{Ar}}$ ), 129.4 (CN), 83.1 ( $C_{\text{Cp}}$ ), 52.6 (dd,  $^1J_{\text{C-P}} = 15.7$  Hz,  $^3J_{\text{C-P}} = 15.7$  Hz,  $\text{PCH}_2\text{N}$ ), 51.8 (dd,  $^1J_{\text{C-P}} = 22.2$  Hz,  $^3J_{\text{C-P}} = 22.2$  Hz,  $\text{PCH}_2\text{N}$ ), 22.5 ( $\text{PhCH}_3$ ), 21.3–19.8 ( $\text{PhCH}_3$ ), 5.4 ( $\text{CH}_3$ ). MALDI MS (pyrene matrix): Calc.  $m/z$  705.2 [ $\text{Ru}(\text{Cp})(\text{P}^{\text{Ph}_2\text{N}^{\text{Mes}_2})}]^+$ , Obs.  $m/z$  705.2.

**[Ru(Cp)(P<sup>Ph<sub>2</sub>N<sup>p-CF<sub>3</sub>-C<sub>6</sub>H<sub>4</sub>)<sub>2</sub>(NCMe)]PF<sub>6</sub> (3-2c)</sup></sup>**: Yield = 98%.  $^1\text{H}$  NMR (600 MHz,  $\text{CD}_2\text{Cl}_2$ ):  $\delta$  8.04–7.90 (m,  $C_{\text{Ar-H}}$ , 4H), 7.81–7.66 (m,  $C_{\text{Ar-H}}$ , 6H), 7.58 (d,  $^3J_{\text{H-F}} = 7.6$  Hz,  $C_{\text{Ar-H}}$ , 2H), 7.50 (d,  $^3J_{\text{H-F}} = 7.5$  Hz,  $C_{\text{Ar-H}}$ , 2H), 7.08 (d,  $^3J_{\text{H-F}} = 7.1$  Hz,  $C_{\text{Ar-H}}$ , 2H), 6.86 (d,  $^3J_{\text{H-F}} = 6.9$  Hz,  $C_{\text{Ar-H}}$ , 2H), 4.79 (s,  $\text{Cp-H}$ , 5H), 4.42–4.32 (m,  $\text{PCH}_2\text{N}$ , 2H), 4.26–4.12 (m,  $\text{PCH}_2\text{N}$ , 4H), 3.80–3.69 (m,  $\text{PCH}_2\text{N}$ , 2H), 2.33 (s,  $\text{CH}_3$ , 3H).  $^{31}\text{P}\{^1\text{H}\}$  NMR (243 MHz,  $\text{CD}_2\text{Cl}_2$ ):  $\delta$  40.6 (s,  $\text{RuP}$ ), –144.4 (sept,  $^1J_{\text{P-F}} = 712$  Hz,  $\text{PF}_6^-$ ).  $^{19}\text{F}\{^1\text{H}\}$  NMR (376.3 MHz,  $\text{CD}_2\text{Cl}_2$ ):  $\delta$  –61.9 (s,  $\text{CF}_3$ ), –62.0 (s,  $\text{CF}_3$ ), –72.3 (d,  $^1J_{\text{F-P}} = 712$  Hz,  $\text{PF}_6^-$ ).  $^{13}\text{C}\{^1\text{H}\}$  NMR (151.5 MHz,  $\text{CD}_2\text{Cl}_2$ ):  $\delta$  154.4–154.2 (m,  $C_{\text{Ar-N}}$ ), 152.8–152.6, (m,  $C_{\text{Ar-N}}$ ), 132.9 (d,  $^1J_{\text{C-P}} = 19.2$  Hz,  $^3J_{\text{C-P}} = 19.2$  Hz,  $C_{\text{Ar-P}}$ ), 132.7 (d,  $^1J_{\text{C-P}} = 19.2$  Hz,  $C_{\text{Ar-P}}$ ), 132.5 ( $C_{\text{Ar}}$ ), 132.2 (d,  $^2J_{\text{C-P}} = 6.1$  Hz,  $C_{\text{Ar}}$ ), 132.1 (d,  $^2J_{\text{C-P}} = 6.1$  Hz,  $C_{\text{Ar}}$ ), 130.2 (d,  $^3J_{\text{C-P}} = 5.1$  Hz,  $C_{\text{Ar}}$ ), 130.1 (d,  $^3J_{\text{C-P}} = 5.1$  Hz,  $C_{\text{Ar}}$ ), 129.5 (CN), 127.6 (quartet,  $^3J_{\text{C-F}} = 4.7$  Hz,  $C_{\text{Ar}}$ ), 127.4 (quartet,  $^3J_{\text{C-F}} = 4.0$  Hz,  $C_{\text{Ar}}$ ), 123.1 (found through correlation,  $\text{CCF}_3$ ), 121.4 (found through correlation,  $\text{CCF}_3$ ), 117.9 (m,  $\text{CF}_3$ ), 116.9 ( $C_{\text{Ar}}$ ), 116.2 (m,  $\text{CF}_3$ ), 114.8 ( $C_{\text{Ar}}$ ), 82.4 ( $C_{\text{Cp}}$ ), 51.6 (dd,  $^1J_{\text{C-P}} = 16.2$  Hz,  $^3J_{\text{C-P}} = 16.2$  Hz,  $\text{PCH}_2\text{N}$ ), 49.9 (dd,  $^1J_{\text{C-P}} = 21.7$  Hz,  $^3J_{\text{C-P}} = 21.7$  Hz,  $\text{PCH}_2\text{N}$ ), 4.7 ( $\text{CH}_3$ ). MALDI MS (pyrene matrix): Calc.  $m/z$  757.1 [ $\text{Ru}(\text{Cp})(\text{P}^{\text{Ph}_2\text{N}^{\text{PhCF}_3})}]^+$ , Obs.  $m/z$  757.1.

**[Ru(Cp)(P<sup>Ph<sub>2</sub>N<sup>p-MeO-C<sub>6</sub>H<sub>4</sub>)<sub>2</sub>(NCMe)]PF<sub>6</sub> (3-2d)</sup></sup>**: Yield = 95%.  $^1\text{H}$  NMR (600 MHz,  $\text{CD}_2\text{Cl}_2$ ):  $\delta$  7.92–7.82 (m,  $C_{\text{Ar-H}}$ , 4H), 7.65–7.58 (m,  $C_{\text{Ar-H}}$ , 6H), 7.04–6.99 (m,  $C_{\text{Ar-H}}$ , 2H), 6.96–6.91 (m,  $C_{\text{Ar-H}}$ , 2H), 6.87–6.82 (m,  $C_{\text{Ar-H}}$ , 4H), 4.88 (s,  $\text{Cp-H}$ , 5H), 4.18–4.12 (m,  $\text{PCH}_2\text{N}$ , 2H), 3.96–3.91 (m,  $\text{PCH}_2\text{N}$ , 2H), 3.77–3.66 (m,  $\text{PCH}_2\text{N}$  and  $\text{OCH}_3$ , 8H), 3.53–3.46 (m,  $\text{PCH}_2\text{N}$ , 2H), 2.37 (s,  $\text{NCCCH}_3$ , 3H).  $^{31}\text{P}\{^1\text{H}\}$  NMR (243 MHz,  $\text{CD}_2\text{Cl}_2$ ):  $\delta$  39.9 (s,  $\text{RuP}$ ), –144.4 (sept,  $^1J_{\text{P-F}} = 712$  Hz,  $\text{PF}_6^-$ ).  $^{13}\text{C}\{^1\text{H}\}$  NMR (151.5 MHz,  $\text{CD}_2\text{Cl}_2$ ):  $\delta$  156.2 ( $\text{COCH}_3$ ), 155.2 ( $\text{COCH}_3$ ), 147.0–146.7 (m,  $C_{\text{Ar-N}}$ ), 146.3–145.8, (m,  $C_{\text{Ar-N}}$ ), 133.8 (t,  $^1J_{\text{C-P}} = 18.2$  Hz,  $^3J_{\text{C-P}} = 18.2$  Hz,  $C_{\text{Ar-P}}$ ), 132.8–131.5 ( $C_{\text{Ar}}$ ), 130.1–129.4 ( $C_{\text{Ar}}$ ), 128.8 (CN), 121.6 ( $C_{\text{Ar}}$ ), 120.3 ( $C_{\text{Ar}}$ ), 115.8–114.4 (m,  $C_{\text{Ar}}$ ), 82.1 ( $C_{\text{Cp}}$ ), 55.9 ( $\text{OCH}_3$ ), 54.0 (found through correlation due to overlap with  $\text{CD}_2\text{Cl}_2$ ,  $\text{PCH}_2\text{N}$ ), 52.7 (dd,  $^1J_{\text{C-P}} = 21$  Hz,  $^3J_{\text{C-P}} = 21$  Hz,  $\text{PCH}_2\text{N}$ ), 4.8 ( $\text{CH}_3$ ). MALDI MS (pyrene matrix): Calc.  $m/z$  681.1 [ $\text{Ru}(\text{Cp})(\text{P}^{\text{Ph}_2\text{N}^{\text{PhOMe}_2})}]^+$ , Obs.  $m/z$  681.2.

**[Ru(Cp)(P<sup>Ph</sup><sub>2</sub>N<sup>Ph</sup><sub>1</sub>)]PF<sub>6</sub> (3-4):** Yield = 92%. <sup>1</sup>H NMR (400 MHz, CD<sub>2</sub>Cl<sub>2</sub>): δ 8.17–6.87 (br, C<sub>Ar</sub>-H, 23H), 6.72–6.37 (br, C<sub>Ar</sub>-H, 2H), 5.81–5.17 (br, C<sub>Ar</sub>-H, 2H), 4.97–4.37 (br, Cp-H and PCH<sub>2</sub>N, 7H), 4.03–3.57 (br, PCH<sub>2</sub>N, 2H). <sup>31</sup>P{<sup>1</sup>H} NMR (243 MHz, CD<sub>2</sub>Cl<sub>2</sub>): δ 48.9–56.0 (br, RuP, 85% rel. integration), 34.6 (s, RuP, 15% rel. integration), –144.5 (sept, <sup>1</sup>J<sub>P-F</sub> = 712 Hz, PF<sub>6</sub><sup>-</sup>). <sup>1</sup>H NMR (400 MHz, CD<sub>3</sub>CN): δ 7.80–7.26 (br, C<sub>Ar</sub>-H, 19H), 7.22–7.10 (br, C<sub>Ar</sub>-H, 2H), 7.00–6.85 (br, C<sub>Ar</sub>-H, 1H), 6.69–6.46 (br, C<sub>Ar</sub>-H, 3H), 4.78–4.68 (m, Cp-H, 5H), 4.68–4.51 (m, PCH<sub>2</sub>N, 2H), 3.96–3.78 (m, PCH<sub>2</sub>N, 2H), 2.34 (br, CH<sub>3</sub>). <sup>31</sup>P{<sup>1</sup>H} NMR (243 MHz, CD<sub>3</sub>CN): 34.6 (s, RuP), –144.6 (sept, <sup>1</sup>J<sub>P-F</sub> = 706 Hz, PF<sub>6</sub><sup>-</sup>). <sup>13</sup>C{<sup>1</sup>H} NMR (151.5 MHz, CD<sub>3</sub>CN): δ 152.7 (through <sup>1</sup>H–<sup>13</sup>C HMBC, C<sub>Ar</sub>-N), 137.8 (through <sup>1</sup>H–<sup>13</sup>C HMBC, C<sub>Ar</sub>-P), 133.9–133.5 (m, C<sub>Ar</sub>), 131.6 (C<sub>Ar</sub>), 131.4 (C<sub>Ar</sub>), 130.3 (C<sub>Ar</sub>), 129.3 (d, <sup>2</sup>J<sub>C-P</sub> = 5.1 Hz, C<sub>Ar</sub>), 129.2 (d, <sup>2</sup>J<sub>C-P</sub> = 5.1 Hz, C<sub>Ar</sub>), 123.2 (C<sub>Ar</sub>), 120.2 (C<sub>Ar</sub>), 83.7 (C<sub>Cp</sub>), 56.3 (dd, <sup>1</sup>J<sub>C-P</sub> = 21.2 Hz, <sup>3</sup>J<sub>C-P</sub> = 21.2 Hz, PCH<sub>2</sub>N). MALDI MS (pyrene matrix): Calc. m/z 656.1 [Ru(Cp)(P<sup>Ph</sup><sub>2</sub>N<sup>Ph</sup><sub>1</sub>)]<sup>+</sup>, Obs. m/z 656.1.

**Ru(Cl)(Cp)(P<sup>Ph</sup><sub>2</sub>N<sup>Bn</sup><sub>2</sub>) (3-5):** RuCl(Cp)(PPh<sub>3</sub>)<sub>2</sub> (300 mg, 0.412 mmol) and P<sup>Ph</sup><sub>2</sub>N<sup>Bn</sup><sub>2</sub> (200 mg, 0.415 mmol) were combined under N<sub>2</sub> in a 100 mL Schlenk flask. Toluene (50 mL) was added via cannula. The reaction was heated to reflux and stirred for 42 h. The reaction was cooled, and the toluene was removed under vacuum. The resulting solid was triturated with hexanes (3 × 30 mL). Hexanes were added (30 mL) and the suspension was filtered under air to give an orange solid. Yield: 299 mg (87%). <sup>1</sup>H NMR (400 MHz, CD<sub>2</sub>Cl<sub>2</sub>): δ 7.82–7.76 (m, Ph-H, 4H), 7.45–7.38 (m, Ph-H, 6H), 7.36–7.22 (m, Ph-H, 10H), 4.53 (s, Cp-H, 5H), 3.87 (s, PhCH<sub>2</sub>N, 2H), 3.59 (s, PhCH<sub>2</sub>N), 3.53–3.49 (m, PCH<sub>2</sub>N, 2H), 3.19–3.11 (m, PCH<sub>2</sub>N, 4H), 2.63–2.56 (m, PCH<sub>2</sub>N, 2H). <sup>31</sup>P{<sup>1</sup>H} (162 MHz, CD<sub>2</sub>Cl<sub>2</sub>): δ 39.3 (s, RuP). <sup>13</sup>C{<sup>1</sup>H} NMR (101 MHz, CD<sub>2</sub>Cl<sub>2</sub>): 138.0 (s, C<sub>Ar</sub>), 137.9 (s, C<sub>Ar</sub>), 136.9 (d, <sup>1</sup>J<sub>C-P</sub> = 12.1 ppm, C<sub>Ar</sub>), 136.8 (d, <sup>1</sup>J<sub>C-P</sub> = 12.1 ppm, C<sub>Ar</sub>), 131.5 (d, <sup>3</sup>J<sub>C-P</sub> = 4.0 ppm, C<sub>Ar</sub>), 131.5 (d, <sup>3</sup>J<sub>C-P</sub> = 4.0 ppm, C<sub>Ar</sub>), 129.9 (s, C<sub>Ar</sub>), 128.4–128.2 (C<sub>Ar</sub>), 127.5 (s, C<sub>Ar</sub>), 127.3 (s, C<sub>Ar</sub>), 79.5 (s, Cp), 66.1 (t, <sup>3</sup>J<sub>C-P</sub> = 8.1 Hz, NCH<sub>2</sub>Ph), 65.5 (t, <sup>3</sup>J<sub>C-P</sub> = 9.1 Hz, NCH<sub>2</sub>Ph), 52.1 (t, <sup>1</sup>J<sub>C-P</sub> = 16.2 Hz, PCH<sub>2</sub>N), 50.7 (t, <sup>1</sup>J<sub>C-P</sub> = 14.1, PCH<sub>2</sub>N). Anal. Calc. for C<sub>41</sub>H<sub>48</sub>F<sub>6</sub>N<sub>3</sub>P<sub>3</sub>Ru•0.1(CH<sub>2</sub>Cl<sub>2</sub>): C, 60.86; H, 5.41; N, 4.04. Found: C, 60.78; H, 5.80; N, 3.85. MALDI MS (pyrene matrix): Calc. m/z 684.1 [RuCp(P<sup>Ph</sup><sub>2</sub>N<sup>Bn</sup><sub>2</sub>)Cl]<sup>+</sup>, 649.1 [RuCp(P<sup>Ph</sup><sub>2</sub>N<sup>Bn</sup><sub>2</sub>)]<sup>+</sup>, Obs. m/z 684.1, 649.1. Anal. Calc. for C<sub>41</sub>H<sub>48</sub>F<sub>6</sub>N<sub>3</sub>P<sub>3</sub>Ru: C, 61.45; H, 5.45; N, 4.09. Found: C, 60.78; H, 5.80; C, 3.85. Orange X-ray quality crystals formed following vapor diffusion of hexanes into a concentrated solution of **5** in DCM.

### 3.4.5 General Procedure for the Catalytic Cyclization of Substrates

In a glovebox, the following stock solutions were prepared: **EA** (246 mg, 2.10 mmol, 0.300 M) and tetralin (185 mg, 1.4 mmol, 0.2 M) in THF (14.00 mL); **2-1b** (10 mg, 0.012 mmol, 6 mM) in THF (2.00 mL); **3-2a** (10 mg, 0.012 mmol, 6 mM) in THF (2.07 mL); **3-2b** (10 mg, 0.011 mmol, 6 mM) in THF (1.87 mL); **3-2c** (10 mg, 0.011 mmol, 6 mM) in THF (1.77 mL); **3-2d** (10 mg, 0.012 mmol, 6 mM) in THF (1.92 mL). Five sets (A-E) of 5 4 mL vials (25 vials total) containing stir bars were charged with the **EA**/tetralin stock solution (250  $\mu$ L) and additional THF (125  $\mu$ L). To each vial was added catalyst stock solution (125  $\mu$ L, set A = **2-1b**, B = **3-2a**, C = **3-2b**, D = **3-2c**, E = **3-2d**) giving a final volume of 500  $\mu$ L. The final concentrations for all vials were 0.150 M in substrate and 1.5 mM in catalyst. A final vial was charged with substrate/internal standard stock solution (100  $\mu$ L) for use as the time = 0 sample, required for accurate quantification of substrate and product. The vials were capped and removed from the glove box and heated to 55 °C (sets A-E) with stirring. After 0.167, 0.5, 1, 6, and 24 hours one vial from each of the sets was removed from heat, cooled, and exposed to air to quench. A 20  $\mu$ L aliquot was diluted to 3 mM (0.980  $\mu$ L) in acetonitrile and analyzed by GC-FID. A 10  $\mu$ L aliquot of the T<sub>0</sub> sample was diluted with acetonitrile (990  $\mu$ L) and analyzed by GC-FID.

### 3.4.6 High Throughput Catalytic Procedure

A representative procedure is given for **EA**. In a glovebox, the following stock solutions were prepared: **EA** (435 mg, 3.72 mmol, 0.300 M) and tetralin (328 mg, 2.48 mmol, 0.200 M) in THF (12.39 mL). Stock solutions of catalysts (9 mM and 1.5 mM) were prepared as above. Reaction components were added to a cooled (0 °C) 8  $\times$  12 reaction plate in the following order: catalyst, solvent, then substrate. Stock solutions of catalysts were robotically dispensed to their appropriate concentration amounts: 0.15, 0.75, 1.50, and 3.00 mM (0.1, 0.5, 1, 3 mol%). Solvent and substrate were added by Eppendorf pipette to the well plate and to a T<sub>0</sub> sample. Final conditions: 150 mM Substrate, 0.1/0.5/1/3 mol% catalyst, 100  $\mu$ L reaction volume in THF. The 96 well plate was sealed with a Teflon sheet, a rubber sheet and an aluminium cover, to minimize evaporation, and the plate was heated to 55 °C for 24 h. After the plate had cooled, the solutions were daughtered into a second plate and diluted to 2.5 mM (based on the starting concentration of 2-ethynylaniline) in acetonitrile for GC-FID analysis. A 10  $\mu$ L aliquot of the T<sub>0</sub> sample was diluted with acetonitrile (990  $\mu$ L) and analyzed by GC-FID.

### 3.4.7 Stoichiometric Reactions with Complex 3-5 and Aniline

In a glovebox Ru(Cp)(Cl)(P<sup>Ph</sup><sub>2</sub>N<sup>Bn</sup><sub>2</sub>) (7 mg, 0.01 mmol) was dissolved with OPPh<sub>3</sub> (3 mg, 0.01 mmol) in THF. An initial time = 0 (T<sub>0</sub>) spectrum was acquired by externally referenced <sup>31</sup>P{<sup>1</sup>H} NMR spectroscopy. KPF<sub>6</sub> (10 mg, 0.05, 5 eq) and aniline (20 mg, 0.21 mmol, 20 eq) were added to the NMR tube, which was then heated at 55 °C in an oil bath. After times of 3 and 24 h, the tube was removed from the bath, cooled and <sup>31</sup>P{<sup>1</sup>H} NMR spectra were acquired.

## 3.5 References

- (a) J. R. Khusnutdinova, D. Milstein, *Angew. Chem. Int. Ed.* **2015**, *54*, 12236-12273; (b) S. Werkmeister, J. Neumann, K. Junge, M. Beller, *Chem. Eur. J.* **2015**, *21*, 12226-12250; (c) V. T. Annibale, D. Song, *RSC Adv.* **2013**, *3*, 11432-11449; (d) R. H. Crabtree, *New J. Chem.* **2011**, *35*, 18-23; (e) D. B. Grotjahn, *Top. Catal.* **2010**, *53*, 1009-1014; (f) H. Grützmacher, *Angew. Chem. Int. Ed.* **2008**, *47*, 1814-1818; (g) H. Li, B. Zheng, K.-W. Huang, *Coord. Chem. Rev.* **2015**, *293-294*, 116-138; (h) J. I. van der Vlugt, *Eur. J. Inorg. Chem.* **2012**, *2012*, 363-375.
- (a) A. J. Arita, J. Cantada, D. B. Grotjahn, A. L. Cooksy, *Organometallics* **2013**, *32*, 6867-6870; (b) B. Godoi, R. F. Schumacher, G. Zeni, *Chem. Rev.* **2011**, *111*, 2937-2980; (c) A. Álvarez-Pérez, C. González-Rodríguez, C. García-Yebra, J. A. Varela, E. Oñate, M. A. Esteruelas, C. Saá, *Angew. Chem. Int. Ed.* **2015**, *54*, 13357-13361; (d) A. Varela-Fernandez, J. A. Varela, C. Saá, *Synthesis* **2012**, *44*, 3285-3295; (e) A. Varela-Fernández, A. Varela Jesús, C. Saá, *Adv. Synth. Catal.* **2011**, *353*, 1933-1937; (f) R. N. Nair, P. J. Lee, A. L. Rheingold, D. B. Grotjahn, *Chem. Eur. J.* **2010**, *16*, 7992-7995.
- (a) M. Ishikura, T. Abe, T. Choshi, S. Hibino, *Nat. Prod. Rep.* **2013**, *30*, 694-752; (b) L. D. Quin, J. A. Tyrell, *Fundamentals of Heterocyclic Chemistry: Importance in Nature and in the Synthesis of Pharmaceuticals*, John Wiley & Sons Inc., Hoboken, New Jersey, **2010**; (c) A. J. Kochanowska-Karamyan, M. T. Hamann, *Chem. Rev.* **2010**, *110*, 4489-4497.
- (a) R. M. Bullock, M. L. Helm, *Acc. Chem. Res.* **2015**, *48*, 2017-2026; (b) R. M. Bullock, A. M. Appel, M. L. Helm, *Chem. Commun.* **2014**, *50*, 3125-3143; (c) S. Raugei, M. L. Helm, S. Hammes-Schiffer, A. M. Appel, M. O'Hagan, E. S. Wiedner, R. M. Bullock, *Inorg. Chem.* **2016**, *55*, 445-460.
- U. J. Kilgore, J. A. S. Roberts, D. H. Pool, A. M. Appel, M. P. Stewart, M. R. DuBois, W. G. Dougherty, W. S. Kassel, R. M. Bullock, D. L. DuBois, *J. Am. Chem. Soc.* **2011**, *133*, 5861-5872.
- (a) J. M. Stubbs, J. P. J. Bow, R. J. Hazlehurst, J. M. Blacquiere, *Dalton Trans.* **2016**, *45*, 17100-17103; (b) J.-P. J. Bow, P. D. Boyle, J. M. Blacquiere, *Eur. J. Inorg. Chem.* **2015**, *2015*, 4162-4166.
- (a) K. Frazee, A. D. Wilson, A. M. Appel, M. Rakowski DuBois, D. L. DuBois, *Organometallics* **2007**, *26*, 3918-3924; (b) V. G. Märkl, G. Y. Jin, C. Schoerner, *Tetrahedron Lett.* **1980**, *21*, 1409-1412.

8. J. A. Franz, M. O'Hagan, M.-H. Ho, T. Liu, M. L. Helm, S. Lense, D. L. DuBois, W. J. Shaw, A. M. Appel, S. Raugei, R. M. Bullock, *Organometallics* **2013**, *32*, 7034-7042.
- 9 B. A. Arbuzov, O. A. Erastov, G. N. Nikonov, I. A. Litvinov, D. S. Yiufit, Y. T. Struchov, *Doklady Akademii Nauk SSSR* **1981**, *257*, 127-131 (CCDC #: 1105714).
10. S. E. Durran, M. R. J. Elsegood, N. Hawkins, M. B. Smith, S. Talib, *Tetrahedron Lett.* **2003**, *44*, 5255-5257.
11. T. A. Tronic, M. Rakowski DuBois, W. Kaminsky, M. K. Coggins, T. Liu, J. M. Mayer, *Angew. Chem. Int. Ed.* **2011**, *50*, 10936-10939.
12. J. M. Stubbs, R. J. Hazlehurst, P. D. Boyle, J. M. Blacquiere, *Organometallics* **2017**, *36*, 1692-1698.
13. M. L. Helm, M. P. Stewart, R. M. Bullock, M. R. DuBois, D. L. DuBois, *Science* **2011**, *333*, 863.
14. I. Kaljurand, A. Kütt, L. Sooväli, T. Rodima, V. Mäemets, I. Leito, I. A. Koppel, *J. Org. Chem.* **2005**, *70*, 1019-1028.
15. K. Izutsu, *Acid-Base Dissociation Constants in Dipolar Aprotic Solvents*, Blackwell Scientific, Oxford, UK, **1990**.
16. I. M. Kolthoff, M. K. Chantooni, *J. Am. Chem. Soc.* **1973**, *95*, 8539-8546.
17. E. P. Kündig, F. R. Monnier, *Adv. Synth. Catal.* **2004**, *346*, 901-904.
18. Z.-Y. Liao, P.-Y. Liao, T.-C. Chien, *Chem. Commun.* **2016**, *52*, 14404-14407.
19. A. L. Balch, M. M. Olmstead, S. P. Rowley, *Inorg. Chim. Acta* **1990**, *168*, 255-264.

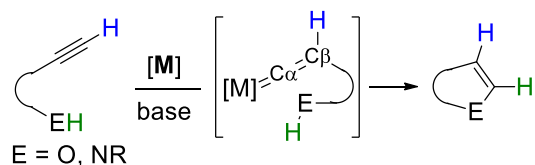
## Chapter 4

### 4 Primary-Coordination Sphere Tuning of Ru-(P<sup>R</sup><sub>2</sub>N<sup>R'</sup><sub>2</sub>) Cyclization Catalysts to give O- and N- Heterocycles

A series of [Ru(Cp/Cp\*)(P<sup>R</sup><sub>2</sub>N<sup>R'</sup><sub>2</sub>)(MeCN)]PF<sub>6</sub> complexes was prepared, in which the steric and electronic properties of the primary coordination were varied (R = Ph, *t*-Bu, Bn; and Cp vs Cp\*). These complexes were tested as catalysts in the cyclization of alkynyl amines or alcohol substrates to produce 5- and 6-membered heterocycles. Based on the elucidated structure-activity relationships, an optimal catalyst was identified as [Ru(Cp)(P<sup>*t*-Bu</sup><sub>2</sub>N<sup>Ph</sup><sub>2</sub>)(MeCN)]PF<sub>6</sub>. This catalyst was >1 order of magnitude more active than previous catalysts in the cyclization of the benchmark substrate 2-ethynylaniline. This catalyst is tolerant of a diverse group of functional groups and it is competent in the cyclization to give various substituted indoles.

#### 4.1 Introduction

Oxygen- and nitrogen-containing heterocycles of varying ring sizes are important motifs in many classes of molecules, including: natural products, pharmaceuticals and conjugated polymers.<sup>1</sup> An atom-economic route into such structures is the catalytic cyclization of an alkyne with an alcohol or amine (1° or 2°) functionality.<sup>2</sup> Transition metal catalysts that mediate this reaction either activate the alkyne by  $\pi$ -coordination or through formation of a vinylidene intermediate.<sup>3</sup> The latter class of catalysts promotes nucleophilic attack at the C $\alpha$ , selectively giving endo cyclized products (Scheme 4-1). A Brønsted base additive is an essential component of such catalyst systems, which is needed to shuttle protons during several steps of the proposed catalytic cycle.<sup>4</sup> Pyridine can effectively act as the proton shuttle in conjunction with the ruthenium bis-phosphine catalyst **A** for the cyclization of the benchmark substrate 2-ethynylaniline (Figure 4-1).<sup>5</sup> While the catalyst exhibits fast rates, the turnover numbers are low and pyridine must be used in significant excess (i.e. as the solvent). The related complex **B** has a pyridyl group incorporated into the ligand framework and this results in an ca. 5 fold increase in catalyst turnover number (Figure 4-1).<sup>6</sup> The intramolecular proton shuttle eliminates the need for an exogenous Brønsted base and allows reactions to be conducted in common organic solvents. However, the turnover numbers remain modest, which limits uptake and application to a broader range of more challenging substrates.



**Scheme 4-1.** Cyclization of alkynyl amine or alcohol substrates mediated by a metal catalyst and base to promote proton shuttling. Catalysis involves a metal vinylidene for a subset of catalysts

Transition metal catalysts that contain an intramolecular base are a type of metal-ligand cooperative (MLC) catalyst.<sup>4a, 7</sup> A wide range of MLC ligands have been reported over the last decade, but few allow for systematic and independent tuning of the Brønsted base and the Lewis basic donor groups. Such structural modifications have been achieved with the  $P^{R_2}N^{R'_2}$  ligand family (see ligand in **4-1b**, Figure 1), in which modification of the substituents of the Brønsted basic amine ( $R'$ ) and the Lewis basic phosphine ( $R$ ) can dramatically alter MLC catalyst performance.<sup>8</sup> Recently, we exploited  $P^{R_2}N^{R'_2}$  ligands for the synthesis of piano-stool ruthenium complexes,  $[Ru(Cp)(P^{Bn_2}N^{R'_2})(MeCN)]PF_6$  ( $Cp$  = cyclopentadienyl), which are analogous to **A** and **B**.<sup>9</sup> Within this series of catalysts the primary coordination sphere was held constant ( $R = Bn$ ) while the substitution of the secondary coordination sphere ( $R'$ ) was modified. A comparison of performance in the cyclization of 2-ethynylaniline and related substrates revealed that the  $P^{R_2}N^{R'_2}$  amine must meet or exceed the basicity of the substrate amine. Additionally, a sterically encumbered basic site ( $R' = Mes$ ) is detrimental to catalysis. This led to the conclusion that  $R'$  substituents  $Bn$  or  $Ph$  are optimal for cyclization catalysis with  $[Ru(Cp)(P^{R_2}N^{R'_2})(NCCH_3)]PF_6$  complexes. In the present study we continue the evaluation of optimal structure for the  $Ru-(P^{R_2}N^{R'_2})$  class of catalysts through modification of the primary coordination sphere.

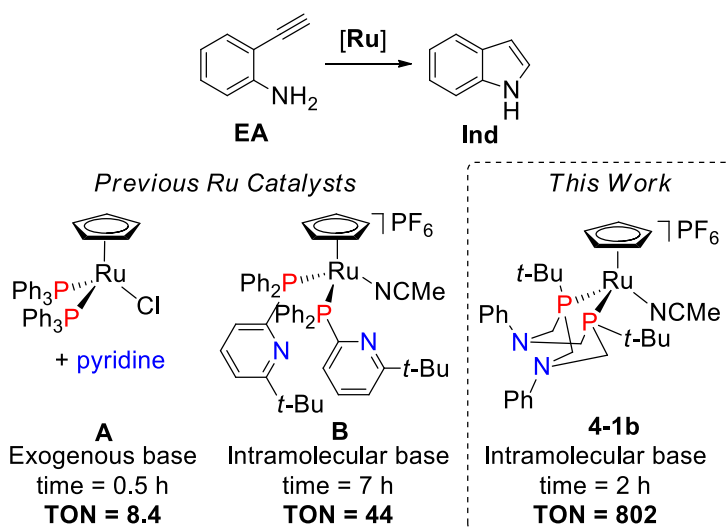


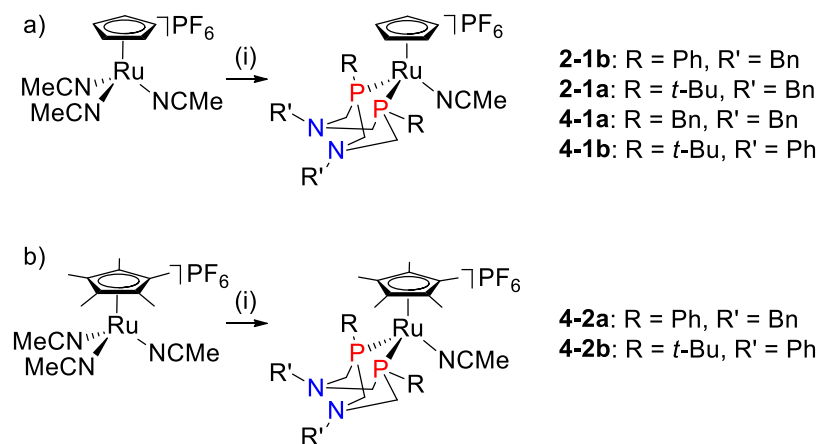
**Figure 4-1.** Performance of previously reported catalysts **A**<sup>5</sup> and **B**<sup>6</sup> as compared to the present  $[\text{Ru}(\text{Cp})(\text{P}^{t\text{-Bu}}_2\text{N}^{\text{Ph}}_2)(\text{MeCN})]\text{PF}_6$  catalyst toward the cyclization of 2-ethynylaniline (**EA**)

## 4.2 Results and Discussion

### 4.2.1 Catalyst Synthesis

A group of complexes was prepared that have the same substituent on the pendent amine of the  $\text{P}^{\text{R}}_2\text{N}^{\text{R}'_2}$  ligand ( $\text{R}' = \text{Bn}$ ), but differ in the substituent of the phosphine (Cp, R: **2-1b** = Ph; **2-1a** = *t*-Bu; **4-1a** = Bn) and in the nature of the placeholder ligand (Cp\* R: **4-2a** = Ph; Cp\* = pentamethylcyclopentadienyl). Our previous evaluation of related catalysts revealed that R' benzyl and phenyl substituents give similar cyclization performance. Given the easier synthetic accessibility of ligands containing phenyl versus benzyl substituents, two additional catalysts (Cp, R = *t*-Bu) were prepared with a phenyl substituent on the pendent amine (**4-1b** and **4-2b**). Each complex was prepared by coordination of a  $\text{P}^{\text{R}}_2\text{N}^{\text{R}'_2}$  ligand to the metal precursors  $[\text{Ru}(\text{Cp})(\text{MeCN})_3]\text{PF}_6$  or  $[\text{Ru}(\text{Cp}^*)(\text{MeCN})_3]\text{PF}_6$  to give Cp (**2-1a,b**, **4-1a,b**) and Cp\* (**4-2a,b**) complexes, respectively (Scheme 4-2). Complexes **4-1a,b** and **4-2a,b** are new entries into the  $[\text{Ru}(\text{Cp}/\text{Cp}^*)(\text{P}^{\text{R}}_2\text{N}^{\text{R}'_2})(\text{MeCN})]\text{PF}_6$  family of catalysts and each was obtained in excellent yield (**4-1a**: 87%, **4-1b**: 90%, **4-2a**: 99%, **4-2b**: 95%).





**Scheme 4-2.** Synthesis of: a) [Ru(Cp)] complexes **2-1a,b**, **4-1a,b**; and b) [Ru(Cp\*)] complexes **4-2a,b**.

(i) 1.05 eq  $\text{P}^{\text{R}}_2\text{N}^{\text{R}'}_2$ , MeCN, 70 °C, 4 h

Complexes **4-1a,b** and **4-2a,b** were characterized by  $^1\text{H}$ ,  $^{31}\text{P}\{^1\text{H}\}$ , and  $^{13}\text{C}\{^1\text{H}\}$  NMR spectroscopy, MALDI mass spectrometry, and IR spectroscopy. Successful ligand coordination was confirmed in each case by MALDI MS, which revealed a major signal for a  $[\text{M-MeCN}]^+$  fragment signal that is consistent with previously synthesized complexes of this type.<sup>9a, 9b</sup> One singlet is observed in the  $^{31}\text{P}\{^1\text{H}\}$  NMR spectra of **4-1b**, **4-2a** and **4-2b** at room temperature. In contrast, the Bn derivative **4-1a** has several signals at room temperature. Coalescence to one major signal is observed in the  $^{31}\text{P}\{^1\text{H}\}$  NMR on cooling to  $-90\text{ }^\circ\text{C}$  in  $\text{CH}_2\text{Cl}_2$ . These observations are consistent with a dynamic structure for **4-1a**, due to changes in conformation of the  $\text{Ru-P}^{\text{Bn}}_2\text{N}^{\text{Bn}}_2$  metallocyclic rings and the benzyl substituents. The chemical shift for the Cp\* complexes are ca. 8-15 ppm upfield from the corresponding signal for the Cp analogue (**2-1b**: 38.4 ppm; **4-2a**: 30.7 ppm; **2-1a**: 55.5 ppm; **4-2b**: 40.7 ppm in  $\text{CD}_2\text{Cl}_2$ ). This difference is due to the greater donor properties of Cp\* vs. Cp, which attenuates the donation of the phosphines to the Ru centre.

Single crystals of **4-2b** were obtained and the X-ray structure confirmed the expected connectivity (Figure 4-2). The Ru-P(1)/P(2) bond lengths (both 2.306(1) Å) and P(1)-Ru-P(2) angle ( $77.75(4)^\circ$ ) are similar to those in the closely related chloro complex  $\text{RuCl(Cp}^*\text{)(P}^{\text{t-Bu}}_2\text{N}^{\text{Ph}}_2\text{)}$  (Ru-P = 2.3077(4) and 2.3001(4) Å; P-Ru-P =  $78.272(15)^\circ$ ).<sup>10</sup> However, the solid-state structure of **4-2b** reveals two unusual features as compared to related complexes. First, both of the R' phenyl substituents are coplanar with the lone pair of the amine of the  $\text{P}^{\text{t-Bu}}_2\text{N}^{\text{Ph}}_2$  ligand. The coplanar arrangement suggests that the nitrogen lone pair is delocalized into the  $\pi$ -system, which is supported by the planar geometry found for N3 (sum

of bonding angles =  $359.05^\circ$ ). Second, the two six-membered metallacycles are both in a boat conformation, positioning one pendent amine (N3) close to the bound acetonitrile ligand (i.e. the active site of the catalyst). The close proximity of the pendent amine to the acetonitrile is uncommon for solid-state structures of  $[\text{Ru}(\text{Cp}/\text{Cp}^*)(\text{P}^{\text{R}}_2\text{N}^{\text{R}'_2})]^+$  complexes, which generally crystallize with this proximal metallacycle in a chair conformation, positioning the tertiary amine away from the active site. Previous instances in which the  $[\text{Ru}(\text{Cp}/\text{Cp}^*)(\text{P}^{\text{R}}_2\text{N}^{\text{R}'_2})]^+$  complexes that have been crystallized with the proximal pendent amine close to the active site have relied on H-bonding interactions to stabilize this conformation. In the case of **4-2b**, a stabilizing C-H/ $\pi$  hydrogen-bonding interaction<sup>11</sup> between the acetonitrile methyl group and the aryl of the amine substituent is proposed. The distance between the plane of the aryl ring and H2A is 2.74(1) Å, which is within the 3.05 Å distance that is the typical maximum for such interactions.<sup>11a</sup> Additionally, the angle between the centre of the aryl ring, H2A and C2 is  $124.0(2)^\circ$ , which is also within the expected range of  $112\text{--}168^\circ$ .<sup>11b</sup> Two weaker CH/ $\pi$  interactions may also exist between the distal pendent amine and the C-H groups of the Cp\* ligand (C25-C30 and H9C on C9 3.04 Å,  $178.6^\circ$ ); and C25-C26 and H8B on C8 (3.06 Å,  $174.2^\circ$ ).

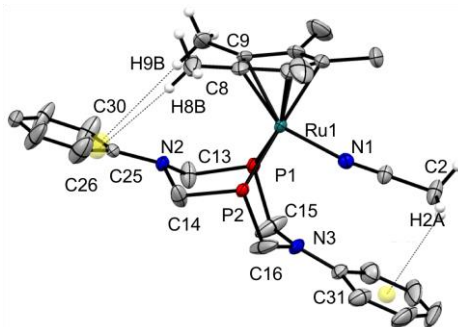


**Figure 4-2.** Thermal displacement plot of **4-2b** with ellipsoids at 50% probability. *t*-Butyl groups on P1 and P2, hydrogen atoms, along with the PF<sub>6</sub> were removed for clarity. Bond Lengths (Å): P1–Ru1 = 2.306(1); P2–Ru1 = 2.306(1); N1–Ru1 = 2.052(4). Bond Angles (°): P1–Ru1–P2 = 77.75(4); C13–N2–C14 = 108.5(3); C13–N2–C25 = 119.3(3); C14–N2–C25 = 119.3(3); C15–N3–C16 = 108.2(3); C15–N3–C31 = 124.9(3); C16–N3–C31 = 124.9(3)

## 4.2.2 Catalytic Studies

The catalytic activity of complexes **2-1a,b**, **4-1a** and **4-2a** was tested for the cyclization of 2-ethynylbenzyl alcohol (**EBA**) at 55 °C in THF at catalytic loadings of 0.1, 0.5, 1, and 3 mol% (Figure 4-3). Incomplete conversion to isochromene (**IC**) was observed with all catalysts and loadings and

increasing the loading from 1 to 3 mol% had minimal effect on conversion in each case. Therefore, incomplete conversion is likely due to competitive formation of a vinyl ammonium deactivation complex by nucleophilic attack of the pendent amine on the vinylidene alpha carbon. Such deactivation was previously established for catalyst **2-1a** and deactivation was favoured at temperatures  $>55\text{ }^{\circ}\text{C}$ .<sup>9b</sup> The relative activity of the four catalysts **2-1a,b**, **4-1a** and **4-2a**, is consistent at each loading. Since the highest turnover numbers are achieved at 1 mol% (Figure 4-3b, red bars), the 1 mol% data will be discussed to compare performance. Consistent with a previous study,<sup>9b</sup> the R = *t*-Bu derivative **2-1a** gave approximately double the yield of **IC** as compared to the Ph complex **2-1b**. The benzyl derivative **4-1a** has the lowest performance giving only 12% conversion. Therefore, the trend in activity as a function of R substituent is *t*-Bu > Ph > Bn. Switching the Cp ligand in **2-1b** for Cp\* in **4-2a** doubles the yield of **IC**. The higher performance with the *t*-Bu phosphine substituent or Cp\* suggests that a sterically encumbered metal centre is favourable for this reaction. The donor ability of the ligands appears to be less critical given that performance does not track with phosphine donor strength.

The combined beneficial properties of the R = *t*-Bu substituent and the Cp\* ligand was evaluated using catalyst **4-2b**. The performance of this catalyst was compared to analogues with a Cp ligand (**4-1b**) or R = Ph substituent (**4-2a**) by monitoring the formation of **IC** over time (Figure 4-3c). The Cp\* catalysts, **4-2a** and **4-2b**, reached a plateau in conversion by ca. 1 h with a maximum conversion of 47 and 62%, respectively. The higher conversion of **4-2b** vs. **4-2a** confirms that the performance trend of the R substituent is *t*-Bu > Ph. The Cp catalyst **4-1b** did not reach a plateau in conversion within 6 h, and the **IC** yield at this point is only 31%. Catalyst turnover frequencies at the 10 min reaction time were determined to be: 270, 101 and 30 h<sup>-1</sup> for **4-2b**, **4-2a** and **4-1b**, respectively. These numbers clearly show that Cp\* ligand accelerates catalysis as compared to Cp. Presumably this is due to increased MeCN lability and thus initiation of the catalyst into the cycle. This could be a consequence of either the improved donor strength or greater steric bulk of the Cp\* ligand. Therefore, the C-H/ $\pi$  interaction observed in the solid-state structure of **4-2b** does not hinder MeCN lability

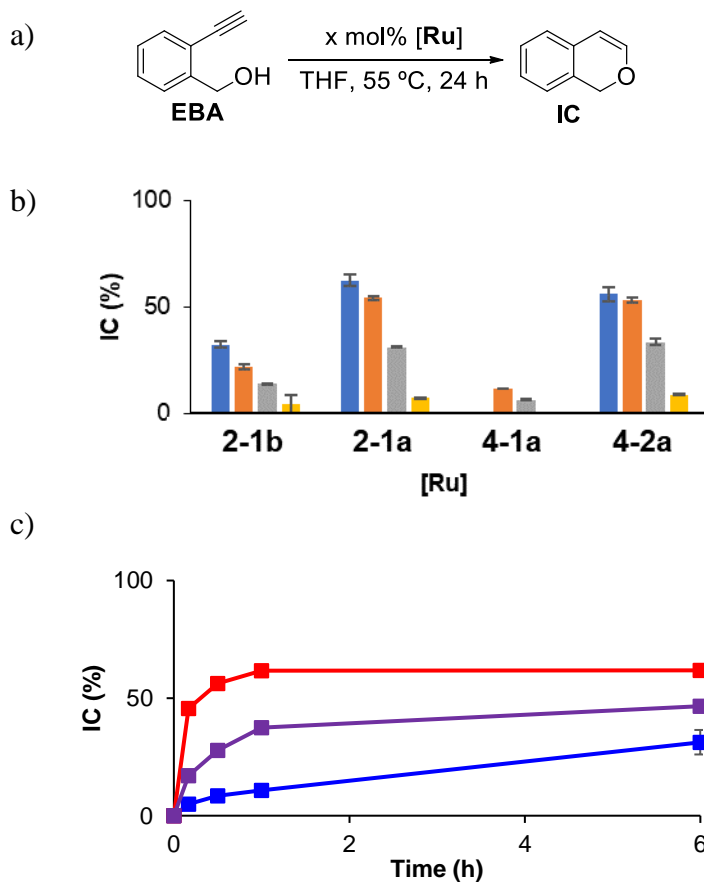


**Figure 4-3.** a) Cyclization of 2-ethynylbenzyl alcohol (**EBA**) to give isochromene (**IC**). b) Yields of **IC** in THF at 55 °C using **2-1a,b**, **4-1a** and **4-2a** at 0.1 (yellow), 0.5 (grey), 1 (orange), 3 (blue) mol%. Conversion data with 3 mol% **4-1a** was not achieved in this screen due to inaccurate catalyst addition due to low solubility of **4-1a** in the stock solution. c) Time trace of cyclization of **EBA** by **4-1b** (blue), **4-2a** (purple), and **4-2b** (red) at 1 mol% at 55 °C in THF

The catalytic activity of complexes **2-1a,b**, **4-1a** and **4-2a** was also tested for the cyclization of 2-ethynylaniline (**EA**) at 55 °C in THF at catalyst loadings of 0.1, 0.5, 1, and 3 mol% (Figure 4-4). Catalysts **2-1a** and **4-2a** achieve quantitative conversion at loadings  $\geq 0.5$  mol%, which shows that cyclization to give the 5-membered indole (**Ind**) is much easier than the 6-membered isochromene. The trend in catalyst activity at 0.1 mol% is **4-2a** > **2-1a** > **2-1b** > **4-1a**, which is consistent with the trends observed with **EBA**.

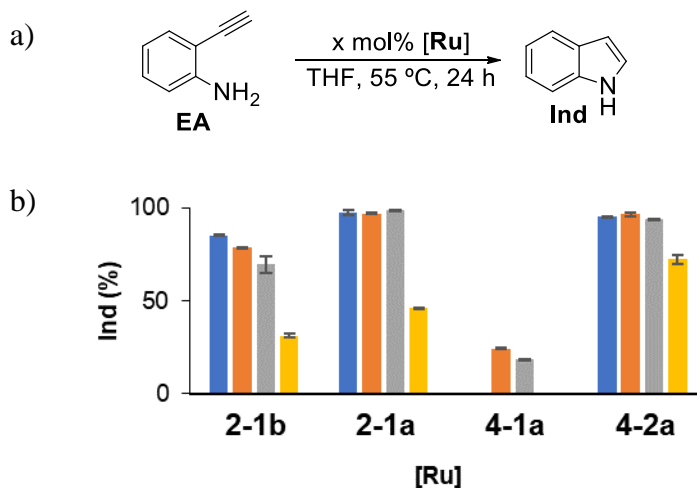


**Figure 4-4.** a) Cyclization of 2-ethynylaniline (**EA**) to give indole (**Ind**). b) Yields of **Ind** in THF at 55 °C using **2-1a,b**, **4-1a** and **4-2a** at 0.1 (yellow), 0.5 (grey), 1 (orange), 3 (blue) mol%. Conversion data with 3 mol% **4-1a** was not achieved in this screen due to inaccurate catalyst addition due to low solubility of **4-1a** in the stock solution

The combined insight from the catalyst screen above and our previous study<sup>9a</sup> indicated that the optimal  $\text{P}^{\text{R}}_2\text{N}^{\text{R}'_2}$  ligand for cyclization of **EA** should have  $\text{R} = t\text{-Bu}$  and  $\text{R}' = \text{Ph}$  or  $\text{Bn}$ . Given the more facile synthesis of  $\text{R}' = \text{Ph}$  derivatives, the  $\text{P}^{t\text{-Bu}}_2\text{N}^{\text{Ph}}_2$  catalysts **4-1b** (Cp) and **4-2b** (Cp\*) were favoured for forward studies. The influence of Cp vs Cp\* was evaluated by conducting cyclization of **EA** under a variety of conditions and the conversion to **Ind** was monitored over time (Table 4-1). At 55 °C and a 0.5 mol% loading, both catalysts achieved nearly quantitative conversion of **EA** (Entries 1-2). The two catalysts had the same overall conversion at lower loadings of 0.2 and 0.1 mol%, but **4-2b** reached a conversion plateau at only 6 h as compared to 24 h for **4-1b** (Table 4-1, Entries 3-6). The faster rate of the Cp\* catalyst as compared to the Cp version is consistent with the performance of these catalysts in the cyclization of **EBA** (Figure 4-3c). Lowering the temperature to 40 °C gave **Ind** yields of 23 and 91% with 0.5 mol% **4-1b** and **4-2b**, respectively (Table 4-1, Entries 7-8). This notable difference can be attributed to the lower thermal initiation barrier of the Cp\* complex **4-2b** relative to the Cp analogue. The hypothesis that the thermal initiation was higher for the Cp analogue (**4-1b**) was further supported by the observation that complete conversion with both **4-1b** and **4-2b** was achieved within 10 min when catalysis was conducted at 70 °C (Table 4-1, Entries 9-10). Rapid initiation was maintained at this temperature with lower loadings of 0.2 and 0.1 mol% (Table 4-1, Entries 11-14). Under both of these conditions, the Cp catalyst **4-1b** gives higher conversion, while the Cp\* catalyst **4-2b** is faster (Figure

4-5). At 0.1 mol%, the conversion is limited by catalyst lifetime so the turnover number (TON) and turnover frequency (TOF) were calculated at these conditions. The TON values for **4-1b** and **4-2b** of 802 and 330, respectively, indicate that the lifetime of the Cp catalyst is approximately double that of the Cp\* catalyst. The longer-lifetime catalyst **4-1b** has a TON value for **EA** cyclization that is ca. 100 and 20 times greater than catalysts **A** and **B**, respectively. This improvement in catalyst performance is a showcase for the beneficial impact of facile and systematic ligand tuning. The TOF values for **4-1b** and **4-2b** were calculated at the shortest time point (10 min). At this point **4-1b** affords <50% of the total conversion, but **4-2b** has nearly reached a plateau at this time and therefore the TOF value for this catalyst is a lower limit. Despite this, it is evident that the Cp\* catalyst (**4-2b**) is faster with a TOF of >1662 h<sup>-1</sup> as compared to 1500 h<sup>-1</sup> for the Cp complex (**4-1b**).

Cyclization of **EA** was conducted in the presence of 5 equiv of water with 0.2 mol% **4-1b** or **4-2b** (Table 4-1, Entries 15-16). The yield of **Ind** was 9 and 7% lower with **4-1b** and **4-2b**, respectively than under dry conditions (Table 4-1, Entries 3-4). No evidence of competitive alkyne hydration was observed, a reaction in which catalyst **B** is particularly effective.<sup>12</sup> A reaction solution with catalyst **4-1b** was bubbled with O<sub>2</sub> prior to catalysis and a decrease of 38% in **Ind** yield was observed as compared to the reaction under N<sub>2</sub> (Table 4-1, Entry 17 vs. 9). While these catalysts should be used under inert atmosphere, these results indicate that they should be tolerant of solvents that are not dried prior to use.

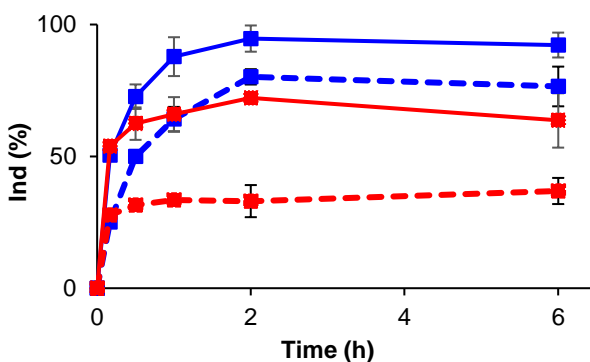


**Figure 4-5.** Cyclization of 2-ethynylaniline (**EA**) in Me-THF at 70 °C with Cp catalyst **4-1b** (blue) and Cp\* catalyst **4-2b** (red) at loadings of 0.2 (solid) and 0.1 (dashed) mol%

**Table 4-1.** Cyclization of 2-ethynylaniline with catalysts **4-1b** and **4-2b**<sup>a</sup>

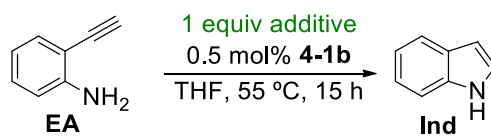
	[Ru]	mol%	Temp. (°C)	Time (h)	Ind (%)
1	<b>4-1b</b>	0.5	55	24	98
2	<b>4-2b</b>	0.5	55	24	93
3	<b>4-1b</b>	0.2	55	24	46
4	<b>4-2b</b>	0.2	55	6	48
5	<b>4-1b</b>	0.1	55	24	15
6	<b>4-2b</b>	0.1	55	6	21
7 <sup>[b]</sup>	<b>4-1b</b>	0.5	40	24	23
8 <sup>[b]</sup>	<b>4-2b</b>	0.5	40	24	91
9	<b>4-1b</b>	0.5	70	0.17	97
10	<b>4-2b</b>	0.5	70	0.17	99
11	<b>4-1b</b>	0.2	70	2	95
12	<b>4-2b</b>	0.2	70	2	72
13	<b>4-1b</b>	0.1	70	2 (1500 h <sup>-1</sup> ) <sup>[c]</sup>	80 (802) <sup>[d]</sup>
14	<b>4-2b</b>	0.1	70	1 (>1662 h <sup>-1</sup> ) <sup>[c]</sup>	33 (330) <sup>[d]</sup>
15 <sup>[e]</sup>	<b>4-1b</b>	0.2	55	24	37
16 <sup>[e]</sup>	<b>4-2b</b>	0.2	55	6	41
17 <sup>[f]</sup>	<b>4-1b</b>	0.5	70	15	62

[a] Conditions: 2-ethynylaniline (150 mM) and tetralin (50 mM) as an internal standard in Me-THF. Reactions were monitored over time and %**Ind** are in-situ values determined by calibrated GC-FID. [b] Solvent = THF. [c] TOF calculated based on the conversion at 10 min. [d] TON calculated from the maximum conversion value. [e] With 5 equiv. H<sub>2</sub>O additive relative to substrate. [f] Reaction bubbled with dry O<sub>2</sub> prior to heating.

The robustness<sup>13</sup> of the optimal catalyst **4-1b** was evaluated by conducting the cyclization of **EA** in the presence of additives with a diverse set of functional groups (Table 4-2). In all cases, cyclization was

conducted with 0.5 mol% **4-1b** in the presence of 1 equivalent of additive relative to substrate and the conversion was evaluated after 15 h. A control reaction without additive afforded 40% **Ind** (Table 4-2, Entry 1), which is an ideal value to observe either a significant decrease or increase in yield in the presence of an additive. Dimethyl terephthalate contains methyl ester groups and this molecule is frequently used as an internal standard in  $^1\text{H}$  NMR spectroscopy experiments. Encouragingly this additive had no effect on catalyst performance (Table 4-2, Entry 2). Likewise, a negligible impact on yield (<13% change relative to control, which is within  $\pm$  5% **Ind** yield) was observed with: PhX (X = F, Cl, Br, I), diphenylacetic acid, benzophenone, benzyl alcohol, dimethylformamide, styrene and diphenyl acetylene (Table 4-2, Entries 3-9). This indicates that catalyst **4-1b** is tolerant of aryl halides, carboxylic acids, ketones, alcohols, amides, alkenes and internal alkynes, all groups that are useful for downstream functionalization. A number of additives were significantly detrimental to catalyst activity (>50% change in activity relative to control), including: benzyl amine, benzonitrile, sodium iodide, phenyl acetylene, and 1,2-ethanedithiol (Table 4-2, Entries 10-15). Thus, catalyst **4-1b** is not compatible with functional groups that have a propensity to bind to the metal centre, such as primary amines, nitriles, halide salts, terminal alkynes and thiols. A smaller, but still negative impact (15-50% change relative to control) on catalysis is observed for the additives: potassium carbonate, triethylamine, benzaldehyde, trifluoromethylbenzene, nitrobenzene and *p*-tolylboronic acid (Table 4-2, Entries 15-20). The poor compatibility of **4-1b** toward the bases  $\text{K}_2\text{CO}_3$  and  $\text{NEt}_3$  is notable given that these are commonly employed in synthesis and could be present as contaminants. Unfortunately, **4-1b** has limited compatibility with aldehyde, nitro, trifluoromethyl and boronic acid functional groups.





**Scheme 4-3.** Tolerance Screen using Additives for the Cyclization of 2-Ethynylaniline using Complex **4-1b**

**Table 4-2.** Tolerance Screen using Additives for the Cyclization of 2-Ethynylaniline using Complex **4-1b**<sup>[a]</sup>

Entry	Additive	Ind (%)	%Change (%) <sup>[b]</sup>
1	None	40	–
2	Dimethyl terephthalate	40	0
3	PhF, PhCl, PhBr, PhI	40	0
4	Ph <sub>2</sub> CHCOOH	41	+3
5	Benzophenone	35	–13
6	Benzyl alcohol	43	+8
7	DMF	37	–8
8	Styrene	36	–10
9	diphenylacetylene	37	–8
10	Benzylamine	5	–88
11	Benzonitrile	6	–85
12	NaI	4	–90

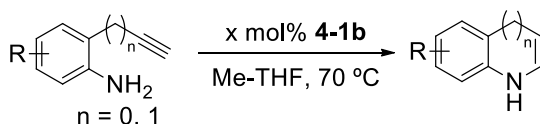
13	Phenyl acetylene	5	-88
14	1,2-Ethandithiol	7	-83
15	K <sub>2</sub> CO <sub>3</sub>	13	-68
16	NEt <sub>3</sub>	31	-23
17	Benzaldehyde	20	-50
18	Trifluoromethylbenzene	30	-25
19	Nitrobenzene	31	-23
20	<i>p</i> -Tolylboronic acid	28	-30

---

[a] Conditions: 2-Ethynylaniline (150 mM), additive (150 mM), and tetralin (50 mM), as an internal standard, in THF at 55 °C. Samples were analysed after 15 h and in-situ %conv. values were determined by calibrated GC-FID. [b] % Change =  $((\% \text{Ind}_{\text{Additive}} - \% \text{Ind}_{\text{Control}}) / \% \text{Ind}_{\text{Control}}) * 100$ .

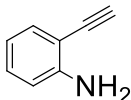
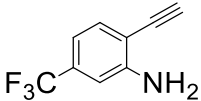
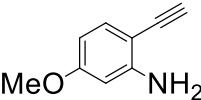
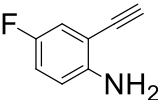
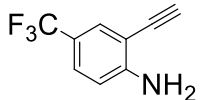
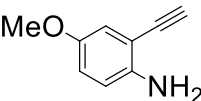
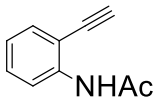
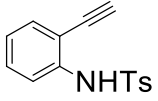
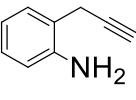
The scope of catalyst **4-1b** was evaluated in the cyclization of a variety of *ortho*-alkyne aniline substrates (Table 4-3). In all cases, cyclization was conducted at 70 °C with both 0.5 and 1 mol% **4-1b**. At 0.5 mol% the conversion of all the substrates was lower than for the benchmark **EA** (Table 4-3, Entry 1) indicating that any substitution on the substrate results in a decrease in both conversion and rate. Electron withdrawing (CF<sub>3</sub>) and donating (OMe) groups *para* to the alkyne gave 42 and 58% product yields, respectively (Table 4-3, Entries 2-3). In both cases, 1 mol% produced good conversions of 74 and 80% for the CF<sub>3</sub> and OMe substrate *para* to the alkyne, respectively. Catalyst performance is less sensitive to withdrawing (F and CF<sub>3</sub>) and donating (OMe) groups *para* to the amine giving yields of 85, 42, 69%, respectively with 0.5 mol% **4-1b** (Table 4-3, Entries 4-6). Each of these three substrates were cyclized to a product in >95% yield when the catalyst loading was increased to 1 mol%. Electronic changes to the alkyne have a pronounced effect on catalyst performance possibly because many reaction steps (vinylidene rearrangement, intramolecular nucleophilic attack, and product release) are all affected. Previous work to develop structure-activity relationships for the secondary coordination sphere revealed that when the pK<sub>a</sub> of the substrate is matched to the acid/base site of the ligand, optimal catalytic performance can occur. The rearrangement of the alkyne is additionally affected since proton

shuttling has been proposed to increase the rate of vinylidene rearrangement.<sup>3c</sup> Furthermore, using an increased catalytic loading of 1 mol% of **4-1b**, good to excellent yields of CF<sub>3</sub> derivatives can be obtained (Table 4-3, Entries 2,5) despite poor functional group tolerance (Table 4-2, Entry 18). Mono-protection of the amine with acetyl or tosyl groups resulted in poor yields at both 0.5 (Ac: 9%; Ts: 17%) or 1 (Ac: 20%; Ts: 30%) mol% **4-1b** (Table 4-3, Entries 7-8). The low yields with these secondary amine substrates could be explained by the decreased nucleophilicity or increased steric hinderance of the amine. We hypothesize that sterics may be the dominant factor given that the non-cooperative catalyst **A** can cyclize both of these substrates with pyridine as the exogenous base, albeit at a 10 mol% catalyst loading.<sup>5</sup> Attempted cyclization of 2-(prop-2-ynyl)-aniline with 0.5 or 1 mol% **4-1b** resulted in minor substrate consumption and trace amounts of 6-membered heterocycles dihydroisoquinoline and isoquinoline (Table 4-3, Entry 9). The latter is likely formed following dehydrogenation<sup>14</sup> of the expected cyclization product dihydroisoquinoline. The difficulty in cyclizing 6-membered *N*-heterocycles relative to 5-membered is acknowledged with related catalysts (**A** and **B**).<sup>5, 15</sup> Both **A** and **B** can achieve cyclization to give related 6-membered *O*- and *N*-heterocycles. While the P<sup>R</sup><sub>2</sub>N<sup>R'</sup><sub>2</sub> catalyst **4-1b** reported here operates at a lower loading than **A** and **B**, the low performance toward 6-membered *N*-heterocycle products is a current limitation of this catalyst family. The low conversion of 2-(prop-2-ynyl)-aniline may be due to the greater flexibility of the substrate that slows the rate of nucleophilic attack on the vinylidene alpha carbon. This slow step would in turn allow catalyst deactivation, possibly via a vinyl ammonium compound,<sup>9b, 9c</sup> that competes with productive catalysis.



**Scheme 4-4.** Substrate screen for intramolecular cyclization of alkynes using **4-1b**

**Table 4-3.** Substrate screen to examine different electronic and steric properties for the intramolecular cyclization of alkynes using complex **4-1b**<sup>[a]</sup>

Entry	Substrate	Loading <b>4-1b</b> (mol%)	Conv. (%)	
			1 h	6 h
1		0.5	100	100
2		0.5	7	42
		1	–	74
3		0.5	39	58
		1	–	80
4		0.5	57	8
		1	–	96
5		0.5	27	42
		1	–	93
6		0.5	42	69
		1	–	99
7		0.5	3	9
		1	20 (24 h)	
		5	78%	
8		0.5	13	17
		1	–	30
		5	–	97%
9		0.5	0	3 <sup>[b]</sup>
		1	–	6 <sup>[b]</sup>

[a] Conditions: Substrate (150 mM) and trimethoxybenzene (25 mM), as an internal standard, in Me-THF at 70 °C. Samples were monitored by <sup>1</sup>H NMR spectroscopy and in-situ %conv. values are listed. [b] Mixture of dihydroisoquinoline and isoquinoline in a 2:1 and 1:1 ratio at 0.5 and 1 mol% respectively.

## 4.3 Conclusions

A group of [Ru(Cp/Cp\*)(P<sup>R</sup><sub>2</sub>N<sup>R'</sup><sub>2</sub>)(MeCN)]PF<sub>6</sub> complexes was prepared in which the nature of the primary coordination sphere was varied systematically. The performance of the complexes was assessed in metal-ligand cooperative cyclization catalysis to give *O*- and *N*-heterocycles. Catalyst activity increased as a function of the steric bulk of the phosphine substituent (R: *t*-Bu > Ph > Bn). The placeholder ligand Cp gave catalysts with higher turnover numbers, while Cp\* promoted faster catalysis. This systematic ligand tuning afforded [Ru(Cp)(P<sup>*t*-Bu</sup><sub>2</sub>N<sup>Ph</sup><sub>2</sub>)(MeCN)]PF<sub>6</sub> (**4-1b**), which cyclized the benchmark substrate 2-ethynylaniline with a turnover number that is one and two orders of magnitude higher than previous cooperative (**B**) and non-cooperative (**A**) ruthenium catalysts, respectively. A robustness screen revealed that catalyst **4-1b** is not compatible with additives that can competitively coordinate to the metal, but it is tolerant of a wide range of functional groups including: alcohols, carboxylic acids and aryl halides. A scope analysis indicated that **4-1b** is tolerant of electron donating or withdrawing groups *para* to either the alkyne or amine functionality of the substrate. Cyclization to give 6-membered heterocycles remains a challenge for this catalyst family and ongoing studies are focused on overcoming this limitation.

## 4.4 Experimental Section

### 4.4.1 General Procedure, Materials and Instrumentation

All air- and water-sensitive reactions were manipulated under Ar or N<sub>2</sub> using standard Schlenk or glovebox techniques, respectively, unless otherwise stated. All glassware was oven dried prior to use. Benzylamine (>98%), and triphenylphosphine oxide (99%) was obtained from Alfa Aesar. Triethylamine (99%) was obtained from Caledon Laboratory Chemicals. Pyrene (98%), benzyl chloride (99%), 2-ethynylaniline (98%), 2-ethynylbenzyl alcohol (95%), tetrahydronaphthalene (99%), and 2-methyltetrahydrofuran (Me-THF; >99% anhydrous) were obtained from Sigma-Aldrich. Chloroform-*d*<sub>1</sub> (99.8%), acetonitrile-*d*<sub>3</sub> (99.8%), toluene-*d*<sub>8</sub> (99.5%), benzene-*d*<sub>6</sub> (99.6%), and dichloromethane-*d*<sub>2</sub> (99.8%) were obtained from Cambridge Isotope Laboratories. 4-Fluoro-2-iodoaniline (97%), 4-amino-

3-bromobenzotrifluoride (95%), 3-amino-4-bromobenzotrifluoride (95%), 2-Bromo-4-methoxyaniline (95%) were obtained from Oakwood Chemicals.  $[\text{Ru}(\text{Cp})(\text{MeCN})_3]\text{PF}_6$ ,<sup>16</sup>  $[\text{Ru}(\text{Cp})(\text{P}^{\text{Ph}}_2\text{N}^{\text{Bn}}_2)(\text{MeCN})]\text{PF}_6$  (**2-1b**),<sup>9b</sup>  $[\text{Ru}(\text{Cp})(\text{P}^{\text{tBu}}_2\text{N}^{\text{Bn}}_2)(\text{MeCN})]\text{PF}_6$  (**2-1a**),<sup>9c</sup>  $\text{P}^{\text{tBu}}_2\text{N}^{\text{Ph}}_2$ ,<sup>17</sup> 2-(prop-2-ynyl)-aniline,<sup>18</sup> 2-ethynyl-N-tosylaniline,<sup>19</sup> 2-iodo-N-acetylaniline,<sup>20</sup> and 2-iodo-m-anisidine<sup>21</sup> were synthesized following literature procedures. Dry and degassed tetrahydrofuran (THF), diethyl ether, toluene, dichloromethane (DCM), hexanes, pentane and acetonitrile (MeCN) were obtained from an Innovative Technology 400-5 Solvent Purification System and stored under  $\text{N}_2$ . These dry and degassed solvents, except for MeCN, were stored over 4 Å molecular sieves (Fluka and activated at 150 °C for over 12 h). Acetone was dried with  $\text{Cs}_2\text{CO}_3$  and degassed by bubbling with  $\text{N}_2$ . THF was further dried with  $\text{CaH}_2$  and distilled under Ar. Triethylamine and ethanol were dried with 4 Å molecular sieves and degassed by bubbling with  $\text{N}_2$ . Chloroform-*d*<sub>1</sub> was dried with 4 Å molecular sieves and degassed by bubbling with  $\text{N}_2$ . Benzylamine was dried with NaOH, distilled under vacuum and stored under  $\text{N}_2$ . All other chemicals were used as received.

Charge-transfer Matrix Assisted Laser Desorption/Ionization (MALDI) mass spectra were collected on an AB Sciex 5800 TOF/TOF mass spectrometer using pyrene as the matrix in a 20:1 molar ratio to metal complex. Samples were spotted on the target plate as solutions in DCM. All NMR spectra were recorded on either an Inova 400 or 600 MHz, or Mercury/Bruker 400 MHz instrument.  $^1\text{H}$  and  $^{13}\text{C}\{^1\text{H}\}$  spectra acquired in  $\text{CDCl}_3$  were referenced internally against the residual solvent signal ( $\text{CHCl}_3$ ) to TMS at 0 ppm.  $^{31}\text{P}\{^1\text{H}\}$  spectra were referenced externally to 85% phosphoric acid at 0.00 ppm. Infrared spectra were collected on solid samples using a PerkinElmer UATR TWO FTIR spectrometer. Elemental analysis was performed by Canadian Microanalytical Service Ltd. Quantification of catalytic reactivity was achieved using an Agilent 7890a gas chromatography with a flame ionization detector (GC-FID), fitted with a HP-5 column. Calibration curves for 2-ethynylbenzyl alcohol, isochromene, 2-ethynylaniline, indole, and were prepared to determine the response factors relative to tetralin. The amount of each species was quantified, relative to the internal standard (tetralin), using area counts corrected with the response factors.

#### 4.4.2 Synthesis of $\text{P}^{\text{Bn}}_2\text{N}^{\text{Bn}}_2$

This procedure was based on the synthesis of  $\text{P}^{\text{Me}}_2\text{N}^{\text{Ph}}_2$ .<sup>22</sup> Tris(hydroxymethyl)phosphine (THP) (0.976 g, 7.87 mmol, 2 equiv.) was added to a 100 mL Schlenk flask with a stir bar, and THF (ca. 5 mL) was added by cannula. The solution was cooled to  $-40$  °C and  $\text{BnCl}$  (8.84 mmol, 2.2 equiv.) was added

dropwise by syringe whilst stirring. The reaction was left to warm to room temperature overnight while stirring. The solvent was removed under vacuum and  $\text{NEt}_3$  (~20 mL) was added by cannula to the transparent oil. The solution was left to stir at room temperature for 72 h. The reaction was filtered via cannula to remove  $\text{NEt}_3 \cdot \text{HBr}$ . The remaining  $\text{NEt}_3$  was removed from the filtrate under vacuum. To the resulting transparent oil was added EtOH (50 mL) and  $\text{BnNH}_2$  (8.26 mmol, 2.1 equiv.) by cannula and syringe, respectively. The reaction was heated at reflux and stirred for 24 h, at which point the reaction was cooled to room temperature and left to stir for an additional 48 h without precipitation occurring. EtOH was removed under vacuum to produce a white residue. The residue was dissolved in acetonitrile and cooled to  $-35\text{ }^\circ\text{C}$  to force precipitation after one week. The solution was decanted to isolate the white precipitate which was dried under vacuum for 24 h. Crude yield: 7%.  $^{31}\text{P}\{^1\text{H}\}$  (400 MHz,  $\text{CDCl}_3$ )  $\delta$ : 60.0 (broad, *P*).

#### 4.4.3 General Procedure for Synthesis of $[\text{Ru}(\text{Cp}/\text{Cp}^*)(\text{P}^{\text{R}}_2\text{N}^{\text{R}'})_2(\text{NCCH}_3)]\text{PF}_6$ Complexes

To a 100 mL Schlenk flask with a stir bar,  $[\text{Ru}(\text{Cp})(\text{NCCH}_3)_3]\text{PF}_6$  or  $[\text{Ru}(\text{Cp}^*)(\text{NCCH}_3)_3]\text{PF}_6$  (1 equiv.), ligand  $\text{P}^{\text{R}}_2\text{N}^{\text{R}'})_2$  (1.05 equiv.) and acetonitrile (20 mL) were added. The flask was heated to  $65\text{ }^\circ\text{C}$  for 4 hours with stirring. The solvent was removed under vacuum and the remaining solid was triturated with pentane ( $3 \times 2$  mL). Acetonitrile (2 mL) was added and the resulting suspension was filtered. The solid was washed with acetonitrile until the washings were colourless. The solvent volume of the filtrate was reduced under vacuum to ca. 0.5 mL and diethyl ether (5 mL) was added to precipitate the product. The solvent was decanted off and the product was dried under vacuum.

**$[\text{Ru}(\text{Cp})(\text{P}^{\text{Bn}}_2\text{N}^{\text{Bn}})_2(\text{NCCH}_3)]\text{PF}_6$  (4-1a)**: Yield: 87%.  $^1\text{H}$  NMR (400 MHz,  $\text{CD}_2\text{Cl}_2$ ,  $-75\text{ }^\circ\text{C}$ )  $\delta$ : 7.94-6.63 (m,  $\text{C}_{\text{Ar}}\text{-H}$ , 20H) 6.47 (broad, 1H), 5.83 (broad, 1H), 5.33 (s,  $\text{Cp}\text{-H}$ , 5H), 4.70-4.45 (m, 1H), 4.21-4.00 (m, 1H), 3.97-1.29 (m 10H).  $^{31}\text{P}\{^1\text{H}\}$  NMR (162 MHz,  $\text{CD}_2\text{Cl}_2$ )  $\delta$ : 36.6 (s,  $\text{P}^{\text{Bn}}$ , major species),  $-144.3$  (sept,  $^1\text{J}_{\text{P-F}} = 711.2$  Hz,  $\text{PF}_6$ ). MALDI MS (pyrene matrix): Calc.  $m/z$  677.2  $[\text{Ru}(\text{Cp})(\text{P}^{\text{Bn}}_2\text{N}^{\text{Bn}})_2]^+$ , Obs.  $m/z$  677.2.

**$[\text{Ru}(\text{Cp})(\text{P}^{\text{tBu}}_2\text{N}^{\text{Ph}})_2(\text{NCCH}_3)]\text{PF}_6$  (4-1b)**: Yield: 90%.  $^1\text{H}$  NMR (400 MHz,  $\text{CD}_2\text{Cl}_2$ )  $\delta$ : 7.35-7.26 (m,  $\text{Ph}\text{-H}$ , 4H), 7.01-6.85 (m,  $\text{Ph}\text{-H}$ , 6H), 4.87 (s,  $\text{Cp}\text{-H}$ , 5H), 3.93-3.85 (m,  $\text{CH}_2$ , 2H), 3.74-3.59 (m,  $\text{CH}_2$ , 4H), 3.58-3.51 (m,  $\text{CH}_2$ , 2H), 2.03 (s,  $\text{NCCH}_3$ , 3H), 1.46-1.29 (m,  $\text{P}(\text{CH}_3)_3$ , 18H).  $^{31}\text{P}\{^1\text{H}\}$  NMR (162 MHz,  $\text{CD}_2\text{Cl}_2$ )  $\delta$ : 55.3 (s,  $\text{P}^{\text{tBu}}$ ),  $-144.3$  (sept,  $^1\text{J}_{\text{P-F}} = 711.2$  Hz,  $\text{PF}_6$ ).  $^{13}\text{C}\{^1\text{H}\}$  NMR (101 MHz,  $\text{CD}_2\text{Cl}_2$ )

$\delta$ : 152.8 (t,  $^3J_{C-P} = 6.1$  Hz, N- $C_{Ar}$ ), 151.7 (t,  $^3J_{C-P} = 5.1$  Hz, N- $C_{Ar}$ ), 130.4 (s,  $C_{Ar}$ ), 130.3 (s,  $C_{Ar}$ ), 128.7 (s, Ru-CNCH<sub>3</sub>), 121.6 (s,  $C_{Ar}$ ), 121.0 (s,  $C_{Ar}$ ), 117.4 (s,  $C_{Ar}$ ), 116.9 (s,  $C_{Ar}$ ), 80.4 (s, Cp), 48.8 (d,  $^1J_{C-P} = 17.2$  Hz, P-CH<sub>2</sub>-N), 48.6 (d,  $^1J_{C-P} = 16.2$  Hz, P-CH<sub>2</sub>-N), 47.0 (d,  $^1J_{C-P} = 14.2$  Hz, P-CH<sub>2</sub>-N), 46.8 (d,  $^1J_{C-P} = 14.1$  Hz, P-CH<sub>2</sub>-N), 35.7 (t,  $^1J_{C-P} = 10.1$  Hz,  $^3J_{C-P} = 10.1$  Hz, PC(CH<sub>3</sub>)<sub>3</sub>), 27.2 (s, (CH<sub>3</sub>)<sub>3</sub>CP), 4.3 (s, CH<sub>3</sub>CN). Anal. Calc. for C<sub>31</sub>H<sub>44</sub>F<sub>6</sub>N<sub>3</sub>P<sub>3</sub>Ru: C, 48.56; H, 5.78; N, 5.48. Found: C, 48.89; H, 6.05; N, 5.48. MALDI MS (pyrene matrix): Calc. m/z 581.2 [Ru(Cp)(P<sup>tBu</sup><sub>2</sub>N<sup>Ph</sup><sub>2</sub>)]<sup>+</sup>, Obs. m/z 581.2.

**[Ru(Cp\*)(P<sup>Ph</sup><sub>2</sub>N<sup>Bn</sup><sub>2</sub>)(NCCH<sub>3</sub>)]PF<sub>6</sub> (4-2a)**: Yield: 99%. <sup>1</sup>H NMR (600 MHz, CD<sub>2</sub>Cl<sub>2</sub>)  $\delta$ : 7.57-7.37 (m, Ph-H, 16H), 7.24-7.18 (m, Ph-H, 2H), 6.94-6.90 (m, Ph-H, 2H), 4.07-4.05 (m, Ph-CH<sub>2</sub>-N, 2H), 3.53-3.47 (m, Ph-CH<sub>2</sub>-N and P-CH<sub>2</sub>-N, 4H), 3.18-3.12 (m, P-CH<sub>2</sub>-N, 2H), 2.83-2.74 (m, P-CH<sub>2</sub>-N, 2H), 2.46 (s, NCCH<sub>3</sub>, 3H), 1.35 (t,  $^4J_{H-P} = 1.9$  Hz, Cp-CH<sub>3</sub>, 15H). <sup>31</sup>P{<sup>1</sup>H} NMR (243 MHz, CD<sub>2</sub>Cl<sub>2</sub>)  $\delta$ : 30.7 (s, P<sup>Ph</sup>), -144.4 (sept,  $^1J_{P-F} = 712.0$  Hz, PF<sub>6</sub>). <sup>13</sup>C{<sup>1</sup>H} NMR (151.5 MHz, CD<sub>2</sub>Cl<sub>2</sub>)  $\delta$ : 136.9 (s,  $C_{Ar}$ -CH<sub>2</sub>N), 135.6 (s,  $C_{Ar}$ -CH<sub>2</sub>N), 132.3 (t,  $^1J_{C-P} = 19.6$  Hz,  $^3J_{C-P} = 19.6$  Hz, N- $C_{Ar}$ ), 131.1 (s,  $C_{Ar}$ ), 130.6 (d,  $^2J_{C-P} = 5.17$  Hz,  $C_{Ar}$ ), 130.6 (d,  $^2J_{C-P} = 5.2$  Hz,  $C_{Ar}$ ), 129.9-129.7 (m,  $C_{Ar}$ ), 129.1 (s,  $C_{Ar}$ ), 129.0 (s,  $C_{Ar}$ ), 128.7 (s,  $C_{Ar}$ ), 128.2 (s,  $C_{Ar}$ ), 126.5 (s, Ru-CNCH<sub>3</sub>), 93.1 (s, Cp-CH<sub>3</sub>), 66.8 (t,  $^3J_{C-P} = 12.3$  Hz, Ph-CH<sub>2</sub>-N), 66.5 (t,  $^3J_{C-P} = 11.0$  Hz, Ph-CH<sub>2</sub>-N), 54.8 (d,  $^1J_{C-P} = 17.5$  Hz, P-CH<sub>2</sub>-N), 54.7 (d,  $^1J_{C-P} = 18.8$  Hz, P-CH<sub>2</sub>-N), 47.4 (d,  $^1J_{C-P} = 22.4$  Hz, P-CH<sub>2</sub>-N), 47.2 (d,  $^1J_{C-P} = 25.4$  Hz, P-CH<sub>2</sub>-N), 35.6 (t,  $^1J_{C-P} = 10.1$  Hz,  $^3J_{C-P} = 10.1$  Hz, PC(CH<sub>3</sub>)<sub>3</sub>), 27.4 (t,  $^2J_{C-P} = 2.0$  Hz, (CH<sub>3</sub>)<sub>3</sub>CP), 10.0 (s, CH<sub>3</sub>-Cp), 4.9 (s, CH<sub>3</sub>CN). MALDI MS (pyrene matrix): Calc. m/z 719.2 [Ru(Cp)(P<sup>Ph</sup><sub>2</sub>N<sup>Ph</sup><sub>2</sub>)]<sup>+</sup>, Obs. m/z 719.2.

**[Ru(Cp\*)(P<sup>tBu</sup><sub>2</sub>N<sup>Ph</sup><sub>2</sub>)(NCCH<sub>3</sub>)]PF<sub>6</sub> (4-2b)**: Yield: 95%. <sup>1</sup>H NMR (400 MHz, CD<sub>2</sub>Cl<sub>2</sub>)  $\delta$ : 7.35-7.24 (m, Ph-H, 4H), 7.04-6.95 (m, Ph-H, 3H), 6.93-6.84 (m, Ph-H, 3H), 3.82-3.73 (m, CH<sub>2</sub>, 4H), 3.65-3.55 (m, CH<sub>2</sub>, 2H), 3.28-3.21 (m, CH<sub>2</sub>, 2H), 1.95 (s, NCCH<sub>3</sub>, 3H), 1.77 (t,  $^4J_{H-P} = 1.5$  Hz, Cp-CH<sub>3</sub>, 15H), 1.41-1.35 (m, P(CH<sub>3</sub>)<sub>3</sub>, 18H). <sup>31</sup>P{<sup>1</sup>H} NMR (162 MHz, CD<sub>2</sub>Cl<sub>2</sub>)  $\delta$ : 40.7 (s, P<sup>tBu</sup>), -144.5 (sept,  $^1J_{P-F} = 709.6$  Hz, PF<sub>6</sub>). <sup>13</sup>C{<sup>1</sup>H} NMR (101 MHz, CD<sub>2</sub>Cl<sub>2</sub>)  $\delta$ : 172.6 (s, Ru-CNCH<sub>3</sub>), 154.1 (t,  $^3J_{C-P} = 7.6$  Hz, N- $C_{Ar}$ ), 151.8 (t,  $^3J_{C-P} = 6.1$  Hz, N- $C_{Ar}$ ), 130.4 (s,  $C_{Ar}$ ), 130.2 (s,  $C_{Ar}$ ), 121.5 (s,  $C_{Ar}$ ), 120.4 (s,  $C_{Ar}$ ), 118.8 (s,  $C_{Ar}$ ), 115.9 (s,  $C_{Ar}$ ), 90.1 (s, Cp-CH<sub>3</sub>), 49.1 (d,  $^1J_{C-P} = 17.2$  Hz, P-CH<sub>2</sub>-N), 48.9 (d,  $^1J_{C-P} = 17.2$  Hz, P-CH<sub>2</sub>-N), 48.7 (d,  $^1J_{C-P} = 14.1$  Hz, P-CH<sub>2</sub>-N), 48.5 (d,  $^1J_{C-P} = 13.1$  Hz, P-CH<sub>2</sub>-N), 35.6 (t,  $^1J_{C-P} = 10.1$  Hz,  $^3J_{C-P} = 10.1$  Hz, PC(CH<sub>3</sub>)<sub>3</sub>), 27.4 (t,  $^2J_{C-P} = 2.0$  Hz, (CH<sub>3</sub>)<sub>3</sub>CP), 12.5 (s, CH<sub>3</sub>-Cp), 4.3 (s, CH<sub>3</sub>CN). Anal. Calc. for C<sub>36</sub>H<sub>54</sub>F<sub>6</sub>N<sub>3</sub>P<sub>3</sub>Ru: C, 51.67; H, 6.50; N, 5.02. Found: C, 51.37; H, 6.86; N, 5.39. MALDI MS (pyrene matrix): Calc. m/z 651.3 [Ru(Cp\*)(P<sup>tBu</sup><sub>2</sub>N<sup>Ph</sup><sub>2</sub>)]<sup>+</sup>, Obs. m/z 651.3.



#### 4.4.4 General Procedure for the Catalytic Cyclization of Substrates

In a glovebox, the following stock solutions were prepared: 2-ethynylaniline (246 mg, 2.10 mmol, 0.300 M) and tetralin (185 mg, 1.4 mmol, 0.2 M) in THF (14.00 mL); **2-1b** (10 mg, 0.012 mmol, 6 mM) in THF (2.00 mL); **2-1a** (10 mg, 0.013 mmol, 6 mM) in THF (2.10 mL); **4-1a** (10 mg, 0.012 mmol, 6 mM) in THF (1.93 mL); **4-1b** (10 mg, 0.013 mmol, 6 mM) in THF (2.17 mL); **4-2a** (10 mg, 0.011 mmol, 6 mM) in THF (1.84 mL); **4-2b** (10 mg, 0.012 mmol, 6 mM) in THF (1.99 mL). Five sets (A-F) of five 4 mL vials (30 vials total) containing stir bars were charged with the 2-ethynylaniline/tetralin stock solution (250  $\mu$ L) and additional THF (125  $\mu$ L). To each vial was added catalyst stock solution (125  $\mu$ L, set A = **2-1b**, B = **2-1a**, C = **4-1a**, D = **4-1b**, E = **4-2a**, F = **4-2b**) giving a final volume of 500  $\mu$ L. The final concentrations for all vials were 0.150 M in substrate and 0.75 mM in catalyst. A final vial was charged with substrate/internal standard stock solution (100  $\mu$ L) for use as the time = 0 sample, required for accurate quantification of substrate and product. The vials were capped and removed from the glove box and heated to 55 °C (sets A-F) with stirring. After 0.167, 0.5, 1, 2, 6, and 24 hours one vial from each of the sets was removed from heat, cooled, and exposed to air to quench. A 20  $\mu$ L aliquot was diluted to 3 mM (0.980  $\mu$ L) in acetonitrile and analyzed by GC-FID. A 10  $\mu$ L aliquot of the T<sub>0</sub> sample was diluted with acetonitrile (990  $\mu$ L) and analyzed by GC-FID.

#### 4.4.5 High Throughput Catalytic Procedure

A representative procedure is given for 2-ethynylaniline. In a glovebox, the following stock solutions were prepared: 2-ethynylaniline (435 mg, 3.72 mmol, 0.300 M) and tetralin (328 mg, 2.48 mmol, 0.200 M) in THF (12.390 mL). Stock solutions of catalysts (9 mM and 1.5 mM) were prepared as above. Reaction components were added to a cooled (0 °C) 8  $\times$  12 reaction plate in the following order: catalyst, solvent, then substrate. Stock solutions of catalysts were robotically dispensed to their appropriate concentration amounts: 0.15, 0.75, 1.50, and 3.00 mM (0.1, 0.5, 1, 3 mol%). Solvent and substrate were added by Eppendorf pipette to the well plate and to a T<sub>0</sub> sample. Final conditions: 150 mM Substrate, 0.1/0.5/1/3 mol% catalyst, 100  $\mu$ L reaction volume in THF. The 96 well plate was sealed with a Teflon sheet, a rubber sheet and an aluminium cover, to minimize evaporation, and the plate was heated to 55 °C for 24 h. After the plate had cooled, the solutions were daughtered into a second plate and diluted to 2.5 mM (based on the starting concentration of 2-ethynylaniline) in acetonitrile for GC-FID analysis. A 10  $\mu$ L aliquot of the T<sub>0</sub> sample was diluted with acetonitrile (990  $\mu$ L) and analyzed by GC-FID.

#### 4.4.6 General Procedure A for Sonogashira (X = I)<sup>23</sup>

To a 200 mL Schlenk flask, Pd(PPh<sub>3</sub>)<sub>2</sub>Cl<sub>2</sub> (0.01 equiv.), CuI (0.05 equiv.), 2-iodoaniline derivative (500 mM, 1 equiv.) in THF:NEt<sub>3</sub> (1:1). Trimethylsilyl acetylene (1.25 equiv.) was added to the reaction by syringe at room temperature while stirring resulting in almost immediate colour change. The reaction was left for 4 h and an aliquot was checked by <sup>1</sup>H NMR spectroscopy to ensure reaction had proceeded to completion. Upon completion, the reaction was filter through a plug of silica under air and the filtrate was evaporated to dryness. The residue was dissolved in ethyl acetate (20 mL) and washed with brine (3 x 40 mL). The product was dried with Na<sub>2</sub>SO<sub>4</sub>, filtered, and then dried under vacuum. The product was then subsequently used in the next step without further purification.

#### 4.4.7 General Procedure B for Sonogashira (X = Br)<sup>23</sup>

To a 200 mL Schlenk flask, Pd(PPh<sub>3</sub>)<sub>2</sub>Cl<sub>2</sub> (0.03 equiv.), CuI (0.05 equiv.), 2-iodoaniline derivative (500 mM, 1 equiv.) in THF:NEt<sub>3</sub> (1:1). Trimethylsilyl acetylene (1.25 equiv.) was added to the reaction by syringe at room temperature while stirring resulting in almost immediate colour change. The reaction was refluxed at 90 °C for 24 h when an aliquot was checked by <sup>1</sup>H NMR spectroscopy to ensure reaction had proceeded to completion. Upon completion, the reaction was filter through a plug of silica under air and the filtrate was evaporated to dryness. The residue was dissolved in ethyl acetate (20 mL) and washed with brine (3 x 40 mL). The product was dried with Na<sub>2</sub>SO<sub>4</sub>, filtered, and then dried under vacuum. The product was then subsequently used in the next step without further purification.

#### 4.4.8 Deprotection Procedure A<sup>23</sup>

In a 200 mL round bottom under air, the TMS-protected substrate was deprotected in MeOH (50 mL) using K<sub>2</sub>CO<sub>3</sub> (1 equiv.). The reaction was stirred for 1 h. The solvent was evaporated to dryness. The residue was dissolved in ethyl acetate (20 mL) and washed with water (3x30 mL). The substrate was evaporated to dryness. Further purification was performed using a silica gel flash column using a gradient ethyl acetate-hexane solvent system increasing from a ratio of 1:99.

#### 4.4.9 Deprotection Procedure B<sup>23</sup>

In a 200 mL Schlenk flask, the TMS-protected substrate was dissolved in THF (30 mL). The reaction mixture was cooled to – 25 °C and TBAF (1M, 1 equiv.) was added dropwise whilst stirred. The reaction was left to warm to room temperature and then quenched with water (1 mL). The solvent was evaporated

to dryness. The residue was dissolved in ethyl acetate (20 mL) and washed with water (3x30 mL). The substrate was evaporated to dryness. Further purification was performed using a silica gel flash column using a gradient ethyl acetate-hexane solvent system increasing from a ratio of 1:99.

**2-Ethynyl-4-fluoroaniline:** Sonogashira A; Deprotection A. <sup>1</sup>H NMR spectra matched literature values.<sup>24</sup>

**2-Ethynyl-4-methoxyaniline:** Sonogashira B; Deprotection A. <sup>1</sup>H NMR spectra matched literature values.<sup>25</sup>

**2-Ethynyl-4-trifluoromethylaniline:** Sonogashira B; Deprotection A. <sup>1</sup>H NMR spectra matched literature values.<sup>26</sup>

**2-Ethynyl-5-methoxyaniline:** Sonogashira A; Deprotection B. <sup>1</sup>H NMR spectra matched literature values.<sup>27</sup>

**2-Ethynyl-5-trifluoromethylaniline:** Sonogashira B; Deprotection A. <sup>1</sup>H NMR spectra matched literature values.<sup>28</sup>

**2-Ethynyl-N-acetylaniline:** Sonogashira A, Deprotection A. <sup>1</sup>H NMR spectra matched literature values.<sup>27</sup>

## 4.5 References

- (a) M. Ishikura, T. Abe, T. Choshi, S. Hibino, *Nat. Prod. Rep.* **2013**, *30*, 694-752; (b) A. J. Kochanowska-Karamyan, M. T. Hamann, *Chem. Rev.* **2010**, *110*, 4489-4497; (c) N. Majumdar, N. D. Paul, S. Mandal, B. de Bruin, W. D. Wulff, *ACS Catal.* **2015**, *5*, 2329-2366; (d) L. D. Quin, J. A. Tyrell, *Fundamentals of Heterocyclic Chemistry: Importance in Nature and in the Synthesis of Pharmaceuticals*, John Wiley & Sons Inc., Hoboken, New Jersey, **2010**; (e) O. Gidron, M. Bendikov, *Angew. Chem. Int. Ed.* **2014**, *53*, 2546-2555.
- B. Godoi, R. F. Schumacher, G. Zeni, *Chem. Rev.* **2011**, *111*, 2937-2980.
- (a) H. Kanno, K. Nakamura, K. Noguchi, Y. Shibata, K. Tanaka, *Org. Lett.* **2016**, *18*, 1654-1657; (b) L.H. Chung, C.Y. Wong, *Organometallics* **2013**, *32*, 3583-3586; (c) A. A. Ogunlana, J. Zou, X. Bao, *J. Organomet. Chem.* **2018**, *864*, 160-168.
- (a) D. B. Grotjahn, *Top. Catal.* **2010**, *53*, 1009-1014; (b) A. J. Arita, J. Cantada, D. B. Grotjahn, A. L. Cooksy, *Organometallics* **2013**, *32*, 6867-6870.

5. A. Varela-Fernández, A. Varela Jesús, C. Saá, *Adv. Synth. Catal.* **2011**, *353*, 1933-1937.
6. R. N. Nair, P. J. Lee, A. L. Rheingold, D. B. Grotjahn, *Chem. Eur. J.* **2010**, *16*, 7992-7995.
7. (a) J. R. Khusnutdinova, D. Milstein, *Angew. Chem. Int. Ed.* **2015**, *54*, 12236-12273; (b) S. Werkmeister, J. Neumann, K. Junge, M. Beller, *Chem. Eur. J.* **2015**, *21*, 12226-12250; (c) V. T. Annibale, D. Song, *RSC Adv.* **2013**, *3*, 11432-11449; (d) R. H. Crabtree, *New J. Chem.* **2011**, *35*, 18-23; (e) H. Grützmacher, *Angew. Chem. Int. Ed.* **2008**, *47*, 1814-1818; (f) H. Li, B. Zheng, K.-W. Huang, *Coord. Chem. Rev.* **2015**, *293-294*, 116-138; (g) J. I. van der Vlugt, *Eur. J. Inorg. Chem.* **2012**, *2012*, 363-375.
8. (a) R. M. Bullock, M. L. Helm, *Acc. Chem. Res.* **2015**, *48*, 2017-2026; (b) R. M. Bullock, A. M. Appel, M. L. Helm, *Chem. Commun.* **2014**, *50*, 3125-3143; (c) U. J. Kilgore, M. P. Stewart, M. L. Helm, W. G. Dougherty, W. S. Kassel, M. R. DuBois, D. L. DuBois, R. M. Bullock, *Inorg. Chem.* **2011**, *50*, 10908-10918; (d) U. J. Kilgore, J. A. S. Roberts, D. H. Pool, A. M. Appel, M. P. Stewart, M. R. DuBois, W. G. Dougherty, W. S. Kassel, R. M. Bullock, D. L. DuBois, *J. Am. Chem. Soc.* **2011**, *133*, 5861-5872.
9. (a) J. M. Stubbs, D. E. Chapple, P. D. Boyle, J. M. Blacquiere, *ChemCatChem* **2018**, *10*, 3694-3702; (b) J. M. Stubbs, J. P. J. Bow, R. J. Hazlehurst, J. M. Blacquiere, *Dalton Trans.* **2016**, *45*, 17100-17103; (c) J.-P. J. Bow, P. D. Boyle, J. M. Blacquiere, *Eur. J. Inorg. Chem.* **2015**, *2015*, 4162-4166.
10. T. A. Tronic, W. Kaminsky, M. K. Coggins, J. M. Mayer, *Inorg. Chem.* **2012**, *51*, 10916-10928.
11. (a) M. Nishio, *CrystEngComm* **2004**, *6*, 130-158; (b) H. Suezawa, S. Ishihara, Y. Umezawa, S. Tsuboyama, M. Nishio, *Eur. J. Org. Chem.* **2004**, *2004*, 4816-4822.
12. D.B. Grotjahn, C. D. Incarvito, A. L. Rheingold, *Angew. Chem, Int. Ed.* **2001**, *40*, 3884-3887; (b) D. B. Grotjahn, D. A. Lev, *J. Am. Chem. Soc.* **2004**, *126*, 12232-12233.
13. K. D. Collins, F. Glorius, *Nat. Chem.* **2013**, *5*, 597-601.
14. J. M. Stubbs, R. J. Hazlehurst, P. D. Boyle, J. M. Blacquiere, *Organometallics* **2017**, *36*, 1692-1698.
15. R. N. Nair, P. J. Lee, D. B. Grotjahn, *Top. Catal.* **2010**, *53*, 1045-1047.
16. E. P. Kündig, F. R. Monnier, *Adv. Synth. Catal.* **2004**, *346*, 901-904.
17. E. S. Wiedner, J. Y. Yang, W. G. Dougherty, W. S. Kassel, R. M. Bullock, M. R. DuBois, D. L. DuBois, *Organometallics* **2010**, *29*, 5390-5401.
18. B. Das, P. Kundu, C. Chowdhury, *Org. Biomol. Chem.* **2014**, *12*, 741-748.
19. A. Varela-Fernández, A. Varela Jesús, C. Saá, *Synthesis* **2012**, *44*, 3285-3295.
20. H. Shen, J. Fu, H. Yuan, J. Gong, Z. Yang, *J. Org. Chem.* **2016**, *81*, 10180-10192.
21. A. Wetzels, F. Gagosz, *Angew. Chem, Int. Ed.* **2011**, *50*, 7354-7358.
22. M. D. Doud, K. A. Grice, A. M. Lilio, C. S. Seu, C. P. Kubiak, *Organometallics* **2012**, *31*, 779-782.
23. Z.-Y. Liao, P.-Y. Liao, T.-C. Chien, *Chem. Commun.* **2016**, *52*, 14404-14407.
24. N. Sakai, K. Annaka, T. Konakahara, *J. Org. Chem.* **2006**, *71*, 3653-3655.

25. A. Carpita, A. Ribecai, P. Stabile, *Tetrahedron* **2010**, *66*, 7169-7178.
26. J. H. Lee, B. S. Lee, H. Shin, D. H. N. Nam, D. Y. Chi, *Synlett* **2006**, *1*, 65-68.
27. N. Sakai, K. Annaka, A. Fujita, A. Sato, T. Konakahara, *J. Org. Chem.* **2008**, *73*, 4160-4165.
28. N. Sakai, K. Tamura, K. Shimamura, R. Ikeda, T. Konakahara, *Org. Lett.* **2012**, *14*, 836-839.

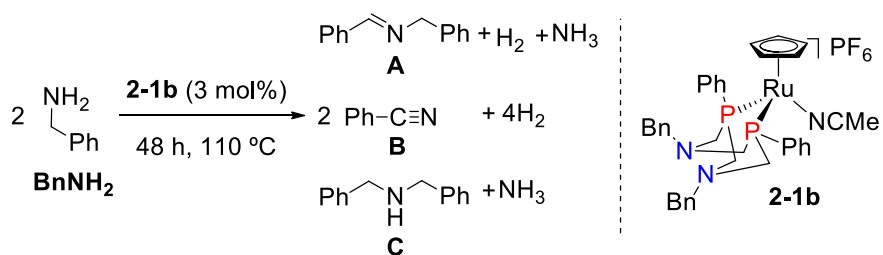
## Chapter 5

### 5 Catalytic Acceptorless Dehydrogenation of Amines with Ru(P<sup>R</sup><sub>2</sub>N<sup>R'</sup><sub>2</sub>) and Ru(dppp) Complexes

[Ru(Cp)(P<sup>Ph</sup><sub>2</sub>N<sup>Bn</sup><sub>2</sub>)(MeCN)]PF<sub>6</sub> (**2-1b**; P<sup>Ph</sup><sub>2</sub>N<sup>Bn</sup><sub>2</sub> = 1,5-benzyl-3,7-phenyl-1,5-diaza-3,7-diphosphacyclooctane) and [Ru(Cp)(dppp)(MeCN)]PF<sub>6</sub> (**2-3**; dppp = 1,3-bis(diphenylphosphino)propane) are both active toward the acceptorless dehydrogenation of benzylamine (**BnNH<sub>2</sub>**) and *N*-heterocycles. The two catalysts have similar activity, but different selectivity for dehydrogenation products. Independent synthesis of a [Ru(Cp)(P<sup>Ph</sup><sub>2</sub>N<sup>Bn</sup><sub>2</sub>)(NH<sub>2</sub>Bn)]PF<sub>6</sub> adduct (**5-1**) reveals the presence of a hydrogen bond between the bound amine and the pendent base of the P<sup>Ph</sup><sub>2</sub>N<sup>Bn</sup><sub>2</sub> ligand. Preliminary mechanistic studies reveal the benzylamine adduct is not an on-cycle catalyst intermediate.

#### 5.1 Introduction

Acceptorless dehydrogenation (AD) and acceptorless dehydrogenative coupling (ADC) have recently emerged as atom economic routes to versatile functionalities such as aldehydes, esters, carboxylic acids, amides, imines and amines.<sup>1</sup> Generally, these reactions involve dehydrogenation of an alcohol moiety, typically followed by nucleophilic attack by another alcohol or amine molecule. Relatively few catalysts have been reported for amine dehydrogenation,<sup>2</sup> but the reaction represents a low-waste synthesis of imines that is an alternative to common oxidative strategies.<sup>3</sup> Additionally, release of chemically stored H<sub>2</sub> from amines to give nitriles is desirable for alternative fuel applications.<sup>4</sup> One of the more successful systems for acceptorless dehydrogenation is the pincer catalysts developed by Milstein.<sup>1b, 5</sup> The Milstein pincer catalyst is proposed to operate through a cooperative<sup>6</sup> H<sub>2</sub> removal mechanism that involves proton transfer to the ligand and hydride transfer to the metal.<sup>7</sup> The success of such a catalyst inspired us to test the established<sup>8</sup> cooperative P<sup>R</sup><sub>2</sub>N<sup>R'</sup><sub>2</sub> (3,7-R<sup>1</sup>-1,5-R<sup>2</sup>-3,7-diaza-1,5-diphosphacyclooctane) ligand family. Similar to dehydrogenation, electrocatalytic H<sub>2</sub> formation (and the reverse H<sub>2</sub> oxidation) is promoted with a number of Ni, Fe and Ru complexes, where the pendent amine of the P<sup>R</sup><sub>2</sub>N<sup>R'</sup><sub>2</sub> ligand acts as an intramolecular base to shuttle protons to/from the metal. Herein, we evaluate the catalytic performance toward amine dehydrogenation and preliminary mechanistic details of the known<sup>9</sup> [Ru(Cp)(P<sup>Ph</sup><sub>2</sub>N<sup>Bn</sup><sub>2</sub>)(MeCN)]PF<sub>6</sub> (**2-1b**) complex (Scheme 5-1).



**Scheme 5-1.** Dehydrogenation of benzylamine with **2-1b**

## 5.2 Results and Discussion

Benzylamine (**BnNH<sub>2</sub>**) was chosen as the benchmark substrate that has three possible dehydrogenation products **A-C** (Scheme 1). Imine **A** is formed following dehydrogenation of **BnNH<sub>2</sub>** and coupling with a second substrate molecule (also called transamination), nitrile **B** is formed through two successive dehydrogenations, and dibenzylamine **C** forms through hydrogenation of imine **A** (termed hydrogen borrowing<sup>10</sup>). Catalysis with **2-1b** (3 mol%) was evaluated at 110 °C in a variety of solvents (Table 5-1). Insolubility of **2-1b** limited performance in toluene, a common solvent for other<sup>2a-d</sup> AD catalysts (Entry 1). Polar solvents DMF and DMA give improved solubility and consumption of **BnNH<sub>2</sub>**, but AD products are not observed and a control reaction without **2-1b** likewise results in the consumption of **BnNH<sub>2</sub>**. The dominant reactivity is ascribed to a competitive, uncatalyzed, coupling with the solvent (Entries 2-3). Other high-boiling polar solvents afford improved product formation (Entries 4-6) with the sustainable<sup>11</sup> solvent anisole giving the best performance. A conversion of 75% is achieved after 2 days and nearly complete consumption of **BnNH<sub>2</sub>** is reached after 4 days. This performance is similar to known catalysts<sup>2a-c</sup> that reach maximum conversion with similar catalyst loadings (1-5 mol%) and shorter times (ca. 24 h), but at higher temperatures (115-150 °C). The products generated with **2-1b** are imine **A** and nitrile **B** in a ca. 3:1 ratio, which is distinct from most reported catalysts that commonly<sup>10, 12</sup> form hydrogen borrowing product **C**, though catalysts for selective production of **A** or **B** are known.<sup>2a-c, 2i</sup> Release of the generated H<sub>2</sub> under a flow of N<sub>2</sub> does not lead to improved conversion or product selectivity. Treatment of **2-1b** with amine **C** gives poor conversion suggesting secondary amines are challenging substrates (Entry 8). Addition of mercury to test for heterogenous Ru nanoparticles does not negatively impact catalyst activity (Entry 9), supporting the homogeneity of the dehydrogenation catalyst.

The non-cooperative complex [Ru(Cp)(dppp)(MeCN)]PF<sub>6</sub>, **2-3** is also catalytically active toward dehydrogenation of **BnNH<sub>2</sub>** (Entry 10; dppp = 1,3-bis(diphenylphosphino)propane). Despite the absence of an internal base in the ligand backbone, **2-3** shows very good conversion (91%) under the optimized conditions. Again, the major product is imine **A**, but both nitrile **B** and secondary amine **C** are observed as minor products. Thus, an internal base is not required, suggesting that in the case of **2-3** the substrate acts as a suitable intermolecular base. Indeed, addition of NEt<sub>3</sub> as an exogenous base for catalyst **2-3** had no impact on the performance (Entry 11).

**Table 5-1 Catalytic optimization for the acceptorless dehydrogenation of benzylamine.<sup>[a]</sup>**

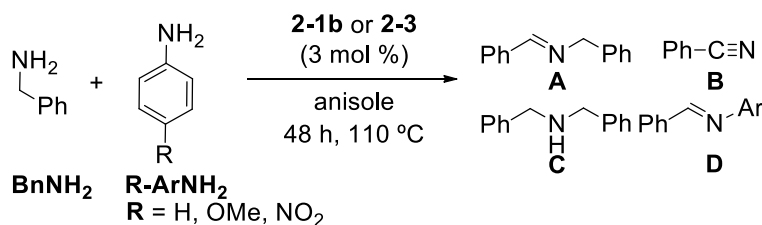
Entry	[Ru]	Solvent <sup>[b]</sup>	Conv. (%) <sup>[c]</sup>	A (%)	B (%)	C (%)
1	<b>2-1b</b>	Toluene	7	6	0	0
2	<b>2-1b</b>	DMF	99	2	0	0
3	<b>2-1b</b>	DMA	71	19	17	1
4	<b>2-1b</b>	THFA	32	22	10	1
5	<b>2-1b</b>	2,4,6-collidine	64	44	3	0
6	<b>2-1b</b>	Anisole	76	54	20	3
7 <sup>[d]</sup>	<b>2-1b</b>	Anisole	95	69	18	8
8 <sup>[e]</sup>	<b>2-1b</b>	Anisole	18	1	0	–
9 <sup>[f]</sup>	<b>2-1b</b>	Anisole	94	34	50	0
10	<b>2-3</b>	Anisole	91	65	18	10
11 <sup>[g]</sup>	<b>2-3</b>	Anisole	87	52	18	10

<sup>[a]</sup> Conditions: 250 mM BnNH<sub>2</sub>, 3 mol% [Ru], 110 °C, 48 h, in a sealed vial. Quantification was conducted by calibrated GC-FID using an internal standard and values are an average of two runs and



errors are  $<\pm 5\%$ . <sup>[b]</sup> DMF = dimethylformamide; DMA = dimethylacetamide; THFA = tetrahydrofurfuryl alcohol. <sup>[c]</sup> Amount of **BnNH<sub>2</sub>** consumed. <sup>[d]</sup> 96 h. <sup>[e]</sup> Substrate is **C**. <sup>[f]</sup> 100  $\mu\text{L}$  of elemental mercury was added. <sup>[g]</sup> 15 mol% NEt<sub>3</sub>.

To further probe the scope and distinction between the P<sup>Ph</sup><sub>2</sub>N<sup>Bn</sup><sub>2</sub> (**2-1b**) and dppp (**2-3**) catalysts, AD of benzylamine was conducted in the presence of para-substituted anilines, **R-ArNH<sub>2</sub>**, to give coupled products **D** (Scheme 5-2). In all cases, the major product with **2-1b** or **2-3** after 24 h is the homo-coupled product **A** (Figure 5-1). At this time in all cases,  $>75\%$  consumption of **BnNH<sub>2</sub>** is observed and the amount of heterocoupled product **D** is  $<10\%$ . Formation of **D** at longer reaction times (vide infra) likely proceeds following nucleophilic attack of the aniline on **A**, rather than on the primary imine (PhHC=NH) generated after AD of **BnNH<sub>2</sub>**. A comparison of product yields at 48 h reveals distinct selectivity for the two catalysts **2-1b** and **2-3** (Table 5-2). With the **MeO-ArNH<sub>2</sub>** substrate, catalyst **1** gives the aniline coupled ADC product **D** as the major species with minor amounts of **A** and nitrile **B** (Figure 5-1a; Table 5-2, Entry 1). Comparison to reaction of **2-1b** with **BnNH<sub>2</sub>** alone (Table 5-1, Entry 6) shows a similar distribution of dehydrogenation products **B** and **C**. The role of the aniline is predominantly as a nucleophile to convert the homocoupled product **A** to heterocoupled product **D**. In contrast, catalyst **2-3** gives only ca. 10% of **D** (Figure 5-1b; Table 2, Entry 2). While the aniline shows minimal participation as a nucleophile, it dramatically alters the product distribution as compared to ADC with **BnNH<sub>2</sub>** alone (Table 5-1, Entry 10). The Brønsted basicity of **MeO-ArNH<sub>2</sub>** diverts the selectivity of **2** from ADC product **A** to hydrogen borrowing product **C**.



**Scheme 5-2.** Acceptorless dehydrogenative coupling of benzylamine with anilines catalyzed by **2-1b** or **2-3**.

**Table 5-2.** Catalytic acceptorless dehydrogenation of benzylamine with aniline derivatives **R-ArNH<sub>2</sub>**<sup>[a]</sup>

Entry	<b>R</b> <sup>[b]</sup>	<b>[Ru]</b>	Conv. (%)	<b>A</b> (%)	<b>B</b> (%)	<b>C</b> (%)	<b>D</b> (%)
1	OMe	<b>2-1b</b>	98	15	24	0	53
2		<b>2-3</b>	100	7	10	58	8
3	H	<b>2-1b</b>	98	42	38	0	19
4		<b>2-3</b>	100	23	34	8	34
5	NO <sub>2</sub>	<b>2-1b</b>	98	73	32	0	0
6		<b>2-3</b>	100	48	24	24	0

[a] Conditions: 250 mM BnNH<sub>2</sub>, 250 mM **R-ArNH<sub>2</sub>**, 3 mol% [Ru], 110 °C, 48 h, in a sealed vial. Quantification was conducted by calibrated GC-FID using an internal standard and values are an average of two runs and errors are <±5%, conversion curves are included in the S.I. [b] R of aniline substrates **R-ArNH<sub>2</sub>**.

With the less nucleophilic aniline **H-ArNH<sub>2</sub>** an unselective mixture of products is observed for both catalysts **2-1b** and **2-3** (Table 5-2, Entries 3-4). Notably, the dppp catalyst **2-3** gives only minor amounts of hydrogen borrowing product **C**, but the aniline coupling product **D** is generated as a major product (along with nitrile **B**). This increase in **D** despite the lower nucleophilicity of the aniline relative to **MeO-ArNH<sub>2</sub>** is attributed to the lower Brønsted basicity of **H-ArNH<sub>2</sub>**. The P<sup>Ph</sup><sub>2</sub>N<sup>Bn</sup><sub>2</sub> catalyst **2-1b** mediates ADC in the presence of **BnNH<sub>2</sub>** and **H-ArNH<sub>2</sub>** to give **A** as the dominant product. This difference in selectivity relative to the reaction with **MeO-ArNH<sub>2</sub>** is expected based on the lower nucleophilicity of **H-ArNH<sub>2</sub>**, which decreases the yield of **D**. While proton shuttling by the aniline cannot be excluded for catalyst **2-1b**, it should be noted that the participation of an external base does not necessarily preclude a cooperative mechanism for the P<sup>Ph</sup><sub>2</sub>N<sup>Bn</sup><sub>2</sub> catalyst. Extensive mechanistic studies of [Ni(P<sup>R</sup><sub>2</sub>N<sup>R'</sup><sub>2</sub>)<sub>2</sub>]<sup>2+</sup> electrocatalysts reveals that a pK<sub>a</sub> matched external base dramatically improves catalyst performance by shuttling protons to the correctly positioned pendent amine.<sup>13</sup> ADC with **NO<sub>2</sub>-ArNH<sub>2</sub>** does not give any of the heterocoupled product **D** with either catalyst **2-1b** or **2-3**

(Table 5-2, Entries 5-6). The electron-withdrawing nitro moiety decreases the nucleophilicity of the aniline sufficiently to inhibit coupling. The  $P^{Ph_2}N^{Bn_2}$  catalyst gives **A** and **B** in a higher yield, but similar ratio (ca. 2.3:1; Table 2 Entry 5) to that observed without the aniline present (cf. 3:1; Table 5-1, Entry 6). Catalyst **2-3** also has similar conversion, but ca. 15% higher yield of the hydrogen borrowing product **C** is found (Table 5-2, Entry 6) relative to reaction without the aniline (Table 5-1, Entry 10). Overall, the added aniline substrates alter the dehydrogenation selectivity with both the  $P^{Ph_2}N^{Bn_2}$  (**2-1b**) and dppp (**2-3**) catalysts. The Brønsted basicity of the aniline is a dominant indicator of selectivity for **2-3**, while the nucleophilic character most important for **2-1b**.

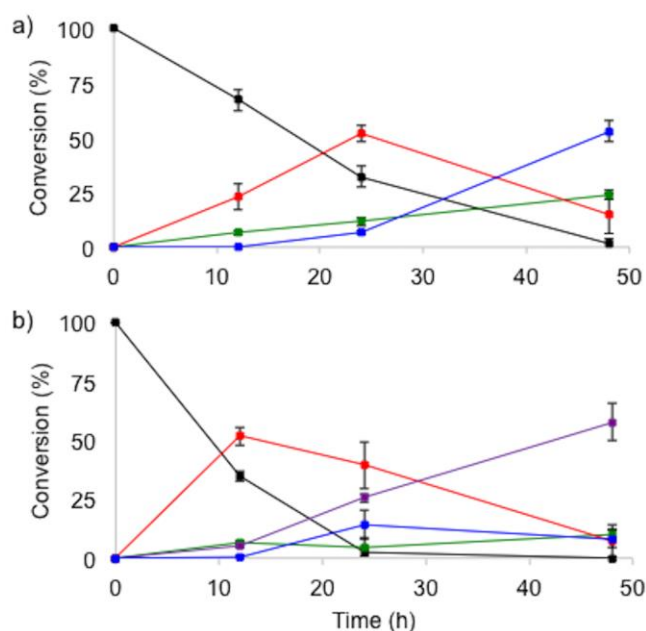
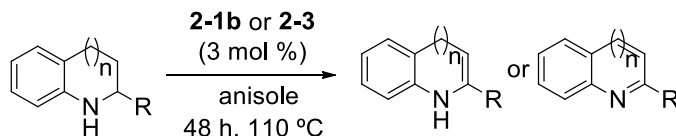


**Figure 5-1.** Conversion curves for the ADC of  $BnNH_2$  (black) with  $MeO-ArNH_2$  under the optimized conditions with catalyst a) **2-1b**; and b) **2-3**. Yields, determined by calibrated GC-FID analysis, of reaction products **A** (red), **B** (green), **C** (purple) and **D** (blue) are plotted. Data points represent the average of the two runs and the error bars give the span of the conversion values of each data set.

Complexes **2-1b** and **2-3** are also competent catalysts for the acceptorless dehydrogenation of 5- and 6-membered heterocycles to give indole and quinoline products (Scheme 5-3, Table 5-3). Both catalysts dehydrogenate ca. 90% indoline under the optimized catalytic conditions (Entries 1-2), with a faster rate than observed for **2-1b**. By comparison, hydride catalysts  $RuH_2CO(PPh_3)_3$ ,  $RuH_2(PPh_3)_3$  and the Shvo catalyst each give >90% conversion of indoline to indole at a higher catalyst loading (5 mol%) and higher temperature (165 °C).<sup>2g</sup> Similar performance is also found for  $RuCl_2(PPh_3)_3$  at conditions (2

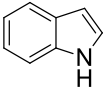
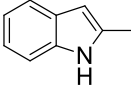
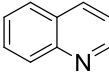
mol% and 110 °C) that are closer to those used for **2-1b** and **2-3**.<sup>14</sup> These prior studies and the results presented here show little distinction in catalyst performance in the AD of indoline between established cooperative (i.e. **2-1b** and the Shvo catalyst) and non-cooperative catalysts. However, the P<sup>Ph</sup><sub>2</sub>N<sup>Bn</sup><sub>2</sub> catalyst **2-1b** outperforms dppp catalyst **2-3** in the dehydrogenation of **Me-Ind** to give 2-methylindole (Table 3, Entries 3-4). This suggests **2-1b** is more tolerant of steric bulk at the site of dehydrogenation than **2-3**. Both catalysts show poor performance in the AD of the 6-membered heterocycle 1,2,3,4-tetrahydroquinoline (**THQ**; Entries 5-6).



**Scheme 5-3.** Acceptorless dehydrogenation of *N*-heterocycles by 0 or 1. Indoline, R = H, n = 0; 2-methylindoline (**Me-Ind**), R = Me, n = 0; 1,2,3,4-tetrahydroquinoline (**THQ**), R = H, n = 1.

The different overall activity and selectivity of P<sup>Ph</sup><sub>2</sub>N<sup>Bn</sup><sub>2</sub> catalyst **2-1b** and dppp catalyst **2-3** led us to question the role of the pendent amine of **2-1b** in the dehydrogenation mechanism. Stoichiometric reactions of **2-1b** were thus conducted to identify potential catalytic intermediates (Scheme 5-4). Treatment of **2-1b** with 5 equiv. benzylamine at 65 °C does not give catalytic turnover, but a new product is formed as judged by the ca. 10 ppm upfield shift of the <sup>31</sup>P{<sup>1</sup>H} NMR signal. In a larger-scale reaction, the product is isolated (85% yield) and is identified as amine-adduct **5-1** (Scheme 5-2a). Benzylamine coordination is supported by MALDI mass spectrometry that gives a signal with an isotope pattern and *m/z* value (757.2) that match to simulated values for [5-1-PF<sub>6</sub>+H]<sup>+</sup>. The new methylene and aryl signals in the <sup>1</sup>H NMR spectrum overlap with existing signals, but their presence is evident by a change in integration. The signal for the amine Ru-NH<sub>2</sub>Bn moiety is observed at 4.91 ppm, which is ca. 1 ppm downfield as compared to other [Ru]-NH<sub>2</sub>Bn complexes.<sup>15</sup> We hypothesize that the downfield shift may be due to a hydrogen-bonding interaction between the N-H moiety of the benzylamine ligand and the pendent tertiary amine of the P<sup>Ph</sup><sub>2</sub>N<sup>Bn</sup><sub>2</sub> ligand. Identification of through space interactions from the N-H signal to the methylene of the P<sup>Ph</sup><sub>2</sub>N<sup>Bn</sup><sub>2</sub> benzyl moiety by <sup>1</sup>H-<sup>1</sup>H ROESY NMR analysis are inconclusive due to the overlap of the latter signal with the methylene of the benzylamine ligand.

**Table 5-3.** Performance of **2-1b** and **2-3** toward acceptorless dehydrogenation of N-heterocycles<sup>[a]</sup>

Entry	Sub.	[Ru]	Conv. (%)	Prod.	Yield (%)
1	Indoline	<b>2-1b</b>	94		88
2	Indoline	<b>2-3</b>	91		91
3	Me-Ind	<b>2-1b</b>	93		78
4	Me-Ind	<b>2-3</b>	68		54
5	THQ	<b>2-1b</b>	20		11
6	THQ	<b>2-3</b>	27		24

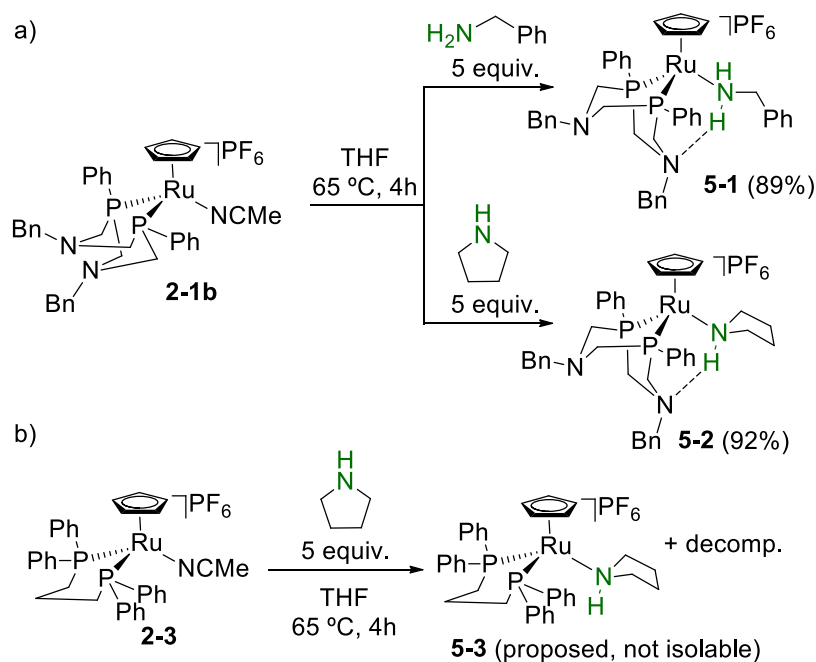
<sup>[a]</sup> Conditions: 250 mM Sub., 3 mol% [Ru], 110 °C, anisole, 48 h, in a sealed vial. Quantification was conducted by calibrated GC-FID using an internal standard and values are an average of two runs and errors are  $\leq \pm 5\%$

Compound **5-2**, the pyrrolidine analogue of **5-1**, was synthesized to evaluate the potential for hydrogen bonding between the metal-bound amine and the pendent amine of the  $\text{P}^{\text{Ph}}_2\text{N}^{\text{Bn}}_2$  ligand (Scheme 5-4a). At the lower temperature used for the synthesis of **5-2** (65 °C) relative to catalysis (110 °C), no evidence of dehydrogenated pyrrolidine was observed.  $^1\text{H}$ - $^1\text{H}$  ROESY analysis of **5-2** reveals two notable correlations between one of the  $\text{P}^{\text{Ph}}_2\text{N}^{\text{Bn}}_2$  N-Bn substituents and the pyrrolidine ligand: 1)  $\text{H}_s$  to  $\text{H}_j$ ; and 2)  $\text{H}_i$  to  $\text{H}_v$  (Figure 5-2a). These suggest that, in the solution-state, the pendent amine is positioned close to the bound pyrrolidine. By contrast, no correlation is found between the  $\text{P}^{\text{Ph}}_2\text{N}^{\text{Bn}}_2$  N-Bn methylene and the methyl protons of the acetonitrile ligand in **2-1b**. The location of the NH signal for **5-2** (6.30 ppm) is shifted significantly downfield relative to related Ru(II)-amine complexes (ca. 3-4 ppm)<sup>15a, 16</sup> and further supports the presence of a hydrogen-bond in solution.

Single crystals of **5-2** were successfully obtained and the aforementioned intramolecular hydrogen-bonding interaction is evident from the solid-state structure (Figure 5-2b). The N1-N3 distance of 2.953(7) Å is in the expected range for similar intramolecular N-H-N hydrogen-bonding distances (2.7 – 3.0 Å).<sup>17</sup> The proximal six-membered metallacycle of the  $\text{P}^{\text{Ph}}_2\text{N}^{\text{Bn}}_2$  ligand is in a boat conformation,

pointing toward the pyrrolidine ligand. By comparison, the metallocyclic ring in all crystallized  $\text{Ru}(\text{Cp}/\text{Cp}^*)(\text{P}^{\text{R}}_2\text{N}^{\text{R}'_2})(\text{L})$  complexes is in a chair conformation with the pendent base pointed away from ligand L ( $\text{X} = \text{MeCN}, \text{Cl}, \text{O}_2$ ), unless the amine is protonated and hydrogen bonds to L (i.e.  $\text{N-H}\cdots\text{O}_2$ ).<sup>9</sup>

18



**Scheme 5-4.** Reactivity of: a) **2-1b** with benzylamine or pyrrolidine; and b) **2-3** with pyrrolidine

Attempts to synthesize a pyrrolidine adduct with dppp complex **2-3** also afforded a new product tentatively assigned as **5-3** in a 27% yield after 4 h as judged by  $^{31}\text{P}\{^1\text{H}\}$  NMR spectroscopy (Scheme 5-4b). The product is unstable to isolation and it is accompanied by significant decomposition as is evidenced by formation of solids and a loss of  $^{31}\text{P}$  integration over time. As amine adducts **5-1** and **5-2** are isolable and **5-3** is not further supports that a hydrogen bond is a stabilizing force.

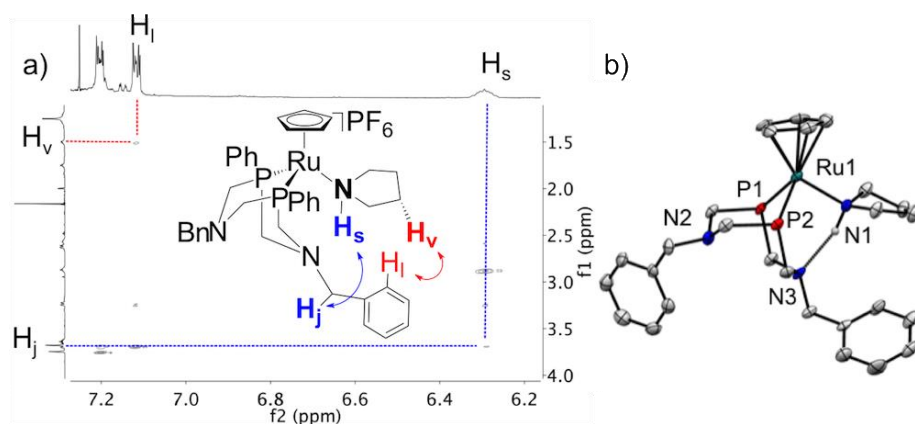
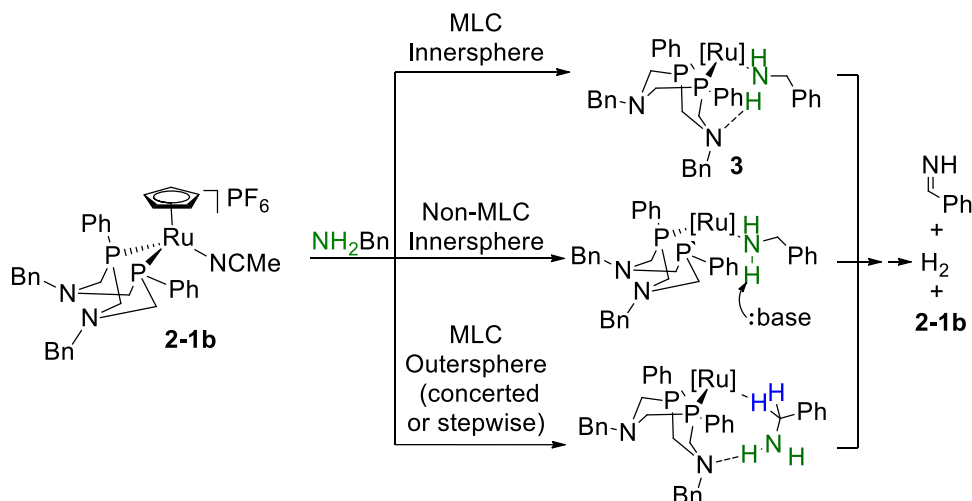


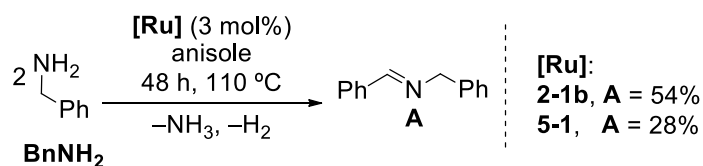
**Figure 5-2.** a) Expanded section of the  $^1\text{H}$ - $^1\text{H}$  ROESY NMR spectrum of **5-2**; and b) Thermal displacement plot of **5-2** (right) with ellipsoids at 50% probability. Phenyl groups on P1 and P2 and the  $\text{PF}_6^-$  anion were removed for clarity

The catalytic mechanism for **2-1b** could follow one of three possible general paths: cooperative inner-sphere; non-cooperative inner-sphere or cooperative outer-sphere (Scheme 5-5). Amine coordination, to give the isolated compound **5-1**, is the first step in either a cooperative or non-cooperative inner-sphere pathway. The cooperative route would involve substrate deprotonation by the pendent base and  $\beta$ -H elimination from the bound amido. These steps would give a Ru-H that would be protonated by the pendent group to release  $\text{H}_2$ . In such a route complex **5-1** would be an on-cycle catalytic species and a precursor to deprotonation. Thus, it should have the same, or higher, activity toward amine dehydrogenation as compared to precatalyst **2-1b** that must dissociate MeCN prior to entering the cycle. The non-cooperative route is similar, except an exogenous base (i.e. a second equivalent of substrate) deprotonates the bound substrate and shuttles the proton back to the hydride. Finally, proton and hydride can be transferred to the catalyst through an outer-sphere route (either concerted or stepwise) without coordination of the amine nitrogen to the metal centre.



**Scheme 5-5.** Possible pathways for the dehydrogenation of benzylamine with catalyst **2-1b**. [Ru] = [Ru(Cp)]PF<sub>6</sub>

Catalytic testing of **5-1** under the optimized conditions revealed that the amine adduct has significantly lower activity than **2-1b**, with only 28% imine formed over 48 h (Scheme 5-6; see Appendices D10 for conversion curve). This suggests that the benzylamine adduct **5-1** is not an on-cycle intermediate and that dehydrogenation does not proceed through an inner-sphere cooperative mechanism. Instead, **5-1** is an off-cycle species that enters the catalytic cycle by amine dissociation to follow a cooperative outersphere pathway or by cleavage of the hydrogen bond to follow a non-cooperative mechanism, which would be operative for the dppp catalyst **2-3**.



**Scheme 5-6.** Catalytic performance comparison of precatalysts **2-1b** and benzylamine adduct **5-1** toward AD of benzylamine

### 5.3 Conclusion

The complex [Ru(Cp)(P<sup>Ph</sup><sub>2</sub>N<sup>Bn</sup><sub>2</sub>)(NCMe)]PF<sub>6</sub> (**2-1b**) is an active acceptorless dehydrogenation catalyst toward benzylamine and it preferentially forms imine and nitrile products. The related complex [Ru(Cp)(dppp)(NCMe)]PF<sub>6</sub> (**2-3**) shows competitive activity, but selectivity favours the hydrogen



borrowing product (Bn<sub>2</sub>NH). Both catalysts show similar activity, but different selectivity, toward AD of benzylamine and coupling with various anilines. They are both competitive catalysts for the dehydrogenation of 5-membered *N*-heterocycles. This comparison of the cooperative P<sup>Ph</sup><sub>2</sub>N<sup>Bn</sup><sub>2</sub> and non-cooperative dppp ligands reveals that product selectivity is the dominant difference between the catalysts. While the dppp catalyst must follow a non-cooperative pathway, the mode of action of the pendent amine in **2-3** is less obvious. Isolation and characterization of Ru-benzylamine and Ru-pyrrolidine adducts (**5-1** and **5-2**, respectively) reveals that these species are stabilized by a hydrogen bond formed with the P<sup>Ph</sup><sub>2</sub>N<sup>Bn</sup><sub>2</sub> ligand. Poor catalytic performance of the benzylamine adduct **5-1** indicates that it is not a precursor to substrate deprotonation and is not an on-cycle catalyst intermediate. This study excludes an inner-sphere cooperative mechanism for **2-1b**, leaving an outer-sphere cooperative or non-cooperative mechanisms as possible routes. Since the aniline basicity in ADC reactions with **2-1b** has minimal impact on the dehydrogenation selectivity (only the subsequent coupling), a non-cooperative (base assisted) route is less likely for the P<sup>Ph</sup><sub>2</sub>N<sup>Bn</sup><sub>2</sub> catalyst. Elucidation of the dominant pathway in acceptorless dehydrogenation with **2-1b** will be investigated in due course.

## 5.4 Experimental Section

### 5.4.1 General Materials, Procedures and Instrumentation

All reactions were manipulated under N<sub>2</sub> using standard Schlenk or glovebox techniques unless otherwise stated. All glassware was oven dried prior to use. Benzylamine (>98%), triphenylphosphine oxide (99%), aniline (>99%) and 2,4,6-collidine (99%) were obtained from Alfa Aesar. Pyrrolidine (>99%) was obtained from Fluka. NEt<sub>3</sub> (99%) was obtained from Caledon Laboratory Chemicals. Pyrene (98%), anisole (99%), dimethylacetamide (99%) and tetrahydrofurfuryl alcohol (THFA) (99%) were obtained from Sigma-Aldrich. *p*-Anisidine (99%) and *p*-nitroaniline (99%) were obtained from Oakwood Chemicals. Chloroform-*d* (99.8%) was obtained from Cambridge Isotope Laboratories. [Ru(Cp)(P<sup>Ph</sup><sub>2</sub>N<sup>Bn</sup><sub>2</sub>)(NCMe)]PF<sub>6</sub>, (**2-1b**) and [Ru(Cp)(dppp)(NCMe)]PF<sub>6</sub> (**2-3**) were synthesized following literature procedures.<sup>9</sup> Dry and degassed tetrahydrofuran (THF), toluene, dichloromethane (DCM), hexanes, dimethylformamide (DMF), dioxane and acetonitrile (MeCN) were obtained from an Innovative Technology 400-5 Solvent Purification System and stored under N<sub>2</sub>. These dry and degassed solvents, except for MeCN, were stored over 4 Å molecular sieves (Fluka and activated at 150 °C for over 12 h). Triethylamine was dried with 4 Å molecular sieves and degassed by bubbling with N<sub>2</sub>. Chloroform-*d* was dried with 4 Å molecular sieves and degassed by bubbling with N<sub>2</sub>. Benzylamine

was dried with NaOH, distilled under vacuum and stored under N<sub>2</sub>. All other chemicals were used as obtained.

Charge-transfer Matrix Assisted Laser Desorption/Ionization mass spectrometry (MALDI) data were collected on an AB Sciex 5800 TOF/TOF mass spectrometer using pyrene as the matrix in a 20:1 molar ratio to complex. Solutions were prepared in DCM and spotted on a sample plate under an inert atmosphere and transferred to the instrument in a sealed Ziplock<sup>®</sup> bag. The instrument is equipped with a 349 nm OptiBeam On-Axis laser. The laser pulse rate was 400 Hz and data were collected in reflectron positive mode. Reflectron mode was externally calibrated at 50 ppm mass tolerance. Each mass spectrum was collected as a sum of 500 shots. All NMR spectra were recorded on either an Inova 400 or 600 MHz, or Mercury 400 MHz instrument. <sup>1</sup>H and <sup>13</sup>C spectra acquired in CDCl<sub>3</sub> were referenced internally against residual solvent signals (CHCl<sub>3</sub>) to TMS at 0 ppm. <sup>31</sup>P spectra were referenced externally to 85% phosphoric acid at 0.00 ppm. Infrared spectra were collected on a PerkinElmer UATR TWO FTIR spectrometer. Elemental analysis was performed by Laboratoire d'Analyse Élémentaire de l'Université de Montréal. Quantification of catalytic reactivity was achieved using an Agilent 7890a gas chromatograph with a flame ionization detector (GC-FID). A HP-5 column was used. Benzylamine, phenyl-N-(phenylmethyl)-methanimine, dibenzylamine, and benzonitrile were calibrated relative to the internal standard (tetrahydronaphthalene).

#### 5.4.2 Synthesis of [Ru(Cp)(P<sup>Ph</sup><sub>2</sub>N<sup>Bn</sup><sub>2</sub>)(benzylamine)]PF<sub>6</sub> (5-1).

[Ru(Cp)(P<sup>Ph</sup><sub>2</sub>N<sup>Bn</sup><sub>2</sub>)(NCMe)]PF<sub>6</sub> (**2-1b**) (101 mg, 0.121 mmol, 1 equiv.) was added to a 100 mL Schlenk flask with a stir bar in the glovebox. Dry THF (10 mL) and **BnNH<sub>2</sub>** (13 μL, 0.12 mmol, 1 equiv.) were added by micropipette and micro syringe, respectively. The Schlenk flask was fitted with a condenser was heated to reflux on the Schlenk line for 4 h. The solvent was removed under vacuum to afford a brown powder that was washed with Et<sub>2</sub>O. Yield: 98 mg (89%). <sup>1</sup>H NMR (600 MHz, CDCl<sub>3</sub>): δ 7.64-7.59 (m, Ph-*H*, 4H), 7.55-7.48 (m, Ph-*H*, 6H), 7.36-7.28 (m, Ph-*H*, 6H), 7.25-7.17 (m, Ph-*H*, 3H), 7.14-7.09 (m, Ph-*H*, 2H), 7.08-7.03 (m, Ph-*H*, 2H), 6.94-6.88 (m, Ph-*H*, 2H), 4.91 (broad, BnNH<sub>2</sub>, 2H), 4.73 (s, Cp-*H*, 5H), 3.66-3.60 (m, NCH<sub>2</sub>P, NCH<sub>2</sub>Ph, RuNH<sub>2</sub>CH<sub>2</sub>Ph, 8H), 3.47 (s, NCH<sub>2</sub>Ph, 2H), 3.09 (m, NCH<sub>2</sub>P, 2H), 2.47 (m, NCH<sub>2</sub>P, 2H). <sup>31</sup>P{<sup>1</sup>H} NMR (243 MHz, CDCl<sub>3</sub>): δ 29.2 (s, RuP), -144.3 (sept, <sup>1</sup>J<sub>P-F</sub> = 715 Hz, PF<sub>6</sub><sup>-</sup>). <sup>13</sup>C{<sup>1</sup>H} NMR (151.5 MHz, CDCl<sub>3</sub>): δ 139.7 (Ph-*C* ring), 136.5 (Ph-*C* ring), 134.2 (Ph-*C* ring), 134.1 (Ph-*C* ring), 131.4 (Ph-*C* ring), 131.2 (Ph-*C* ring), 130.0 (Ph-*C* ring), 129.6 (Ph-*C* ring), 129.1-128.5 (Ph-*C* ring), 128.4-127.9 (Ph-*C* ring), 81.1 (s, Cp), 67.4 (s, NCH<sub>2</sub>Ph) and

64.7 (s, NCH<sub>2</sub>Ph), 60.1 (s, NH<sub>2</sub>CH<sub>2</sub>Ph), 58.3 (s, NCH<sub>2</sub>P) and 55.2 (s, NCH<sub>2</sub>P). MALDI MS (pyrene matrix): Calc.  $m/z$  757.2 [**5-1** – PF<sub>6</sub> + H]<sup>+</sup>, Obs.  $m/z$  757.2. A crystalline sample was obtained following vapor diffusion of Et<sub>2</sub>O into a concentrated solution of **5-1** in acetone. Anal. Calc. for C<sub>42</sub>H<sub>46</sub>F<sub>6</sub>N<sub>3</sub>P<sub>3</sub>Ru: C, 56.00; H, 5.15; N, 4.66. Found: C, 56.47; H, 5.25; N, 4.62.

### 5.4.3 Synthesis of [Ru(Cp)(P<sup>Ph</sup><sub>2</sub>N<sup>Bn</sup><sub>2</sub>)(pyrrolidine)]PF<sub>6</sub> (**5-2**)

[Ru(Cp)(P<sup>Ph</sup><sub>2</sub>N<sup>Bn</sup><sub>2</sub>)(NCMe)]PF<sub>6</sub> (**2-1b**) (150 mg, 0.180 mmol, 1 equiv.) was added to a 100 mL Schlenk flask with a stir bar. Dry THF (10 mL) and pyrrolidine (60 μL, 0.90 mmol, 5 equiv.) were added by micropipette and micro syringe, respectively. The reaction was heated to reflux on the Schlenk line for 4 h. The solvent was removed under vacuum to afford a brown product that was washed with Et<sub>2</sub>O. Yield: 142 mg (92%). Purity = 90% by NMR. Single crystals were formed following vapor diffusion of Et<sub>2</sub>O into a concentrated solution of product in acetone. Upon dissolving single crystals of **5-2** in THF or CDCl<sub>3</sub>, ca. 10% decomposition is observed by <sup>1</sup>H and <sup>31</sup>P NMR spectroscopy in 10–15 min, after which not further decomposition is observed. <sup>1</sup>H NMR (600 MHz, CDCl<sub>3</sub>): δ 7.62 (m, *H<sub>a</sub>*, 4H), 7.53–7.47 (m, *H<sub>b</sub>*, *H<sub>c</sub>*, 6H), 7.36–7.30 (m, *H<sub>m</sub>*, *H<sub>n</sub>*, *H<sub>r</sub>*, *H<sub>q</sub>*, 6H), 7.21 (m, *H<sub>l</sub>*, 2H), 7.13 (m, *H<sub>p</sub>*, 2H), 6.30 (broad, *H<sub>s</sub>*, 1H), 4.72 (s, Cp-*H*, 5H), 3.76 (s, *H<sub>i</sub>*, 2H), 3.71 (m, N-*CH<sub>g</sub>*-P, 2H), 3.70 (s, *H<sub>j</sub>*, 2H), 3.65 (m, N-*CH<sub>e</sub>*-P, 2H), 3.23 (m, N-*CH<sub>g</sub>*-P, 2H), 2.88 (m, *H<sub>t</sub>*, 2H), 2.63 (m, N-*CH<sub>f</sub>*-P, 2H), 2.58 (m, *H<sub>u</sub>*, 2H), 1.76 (m, *H<sub>w</sub>*, 2H), 1.51 (m, *H<sub>v</sub>*, 2H). <sup>31</sup>P{<sup>1</sup>H} NMR (243 MHz, CDCl<sub>3</sub>): δ 29.3 (s, *P*-Ph), –144.3 (sept, <sup>1</sup>*J*<sub>P-F</sub> = 713 Hz, PF<sub>6</sub><sup>–</sup>). <sup>13</sup>C{<sup>1</sup>H} NMR (151.5 MHz, CDCl<sub>3</sub>): δ 136.8 (s, *C<sub>o</sub>*), 135.2 (s, *C<sub>k</sub>*), 134.0 (dd, <sup>1</sup>*J*<sub>C-P</sub> = 19.9 Hz, <sup>3</sup>*J*<sub>C-P</sub> = 19.9 Hz, *C<sub>d</sub>*), 131.3 (m, *C<sub>a</sub>*), 129.9 (s, *C<sub>c</sub>*, *C<sub>l</sub>*, *C<sub>p</sub>*), 126.6 (m, *C<sub>b</sub>*), 129.1 (s, *C<sub>q</sub>*), 129.0 (s, *C<sub>m</sub>*), 128.5 (s, *C<sub>r</sub>*), 128.1 (s, *C<sub>n</sub>*), 81.6 (s, *C<sub>p</sub>*), 66.4 (s, *C<sub>j</sub>*), 65.4 (s, *C<sub>i</sub>*), 62.4 (s, *C<sub>t</sub>*), 58.5 (dd <sup>1</sup>*J*<sub>C-P</sub> = 26.3 Hz, <sup>3</sup>*J*<sub>C-P</sub> = 26.3 Hz, *C<sub>e</sub>*), 55.8 (dd', <sup>1</sup>*J*<sub>C-P</sub> = 17.7 Hz, <sup>3</sup>*J*<sub>C-P</sub> = 17.7 Hz, *C<sub>g</sub>*), 26.1 (s, *C<sub>w</sub>*). MALDI MS (anthracene matrix): Calc.  $m/z$  717.2 [**5-2** – PF<sub>6</sub> – 3H]<sup>+</sup>, Obs.  $m/z$  717.2. Anal. Calc. for C<sub>39</sub>H<sub>46</sub>F<sub>6</sub>N<sub>3</sub>P<sub>3</sub>Ru: C, 54.17; H, 5.36; N, 4.86. Found for a crystalline sample: C, 54.61; H, 5.43; N, 4.77.

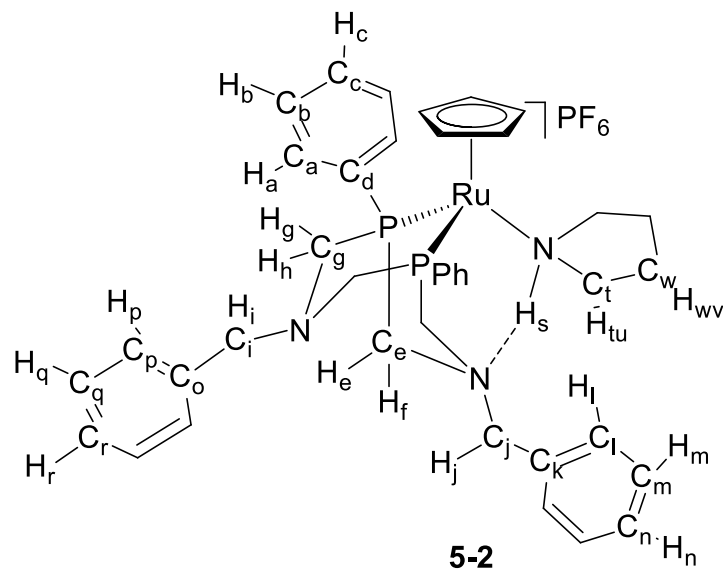


**Figure 5-3:** Numbering scheme for  $^1\text{H}$  and  $^{13}\text{C}$  NMR assignment for complex **5-2**.

#### 5.4.4 General Procedure for Catalytic Dehydrogenation Reactions of Benzylamine

In a glovebox, the following stock solutions were prepared: benzylamine (322 mg, 3.00 mmol, 1 M) and tetrahydronaphthalene (159 mg, 1.20 mmol, 400 mM) in anisole (3.00 mL); **2-1b** (7.5 mg, 0.011 mmol, 15 mM) in anisole (0.750 mL); **2-3** (14 mg, 0.019 mmol, 15 mM) in anisole (1.250 mL). Four sets, A-D, of 2 vials (8 vials total) containing stir bars were charged with the benzylamine stock solution (125  $\mu\text{L}$ ). To each of these vials the catalyst stock **2-1b** (250  $\mu\text{L}$  to set A), and **2-3** (250  $\mu\text{L}$  to set B and C) along with additional anisole solvent (125  $\mu\text{L}$  for A-C, 375  $\mu\text{L}$  for D) were added. Triethylamine (1.1  $\mu\text{L}$ , 0.76 mmol) was added to each vial in set C. The final concentrations for vials in sets A-D were 0.25 M in benzyl amine with 3 mol% catalyst loading (A-C), and set D contained no catalyst. A final vial was charged with substrate/internal standard stock solution (100  $\mu\text{L}$ ) for use as the initial time = 0 ( $T_0$ ) sample for GC-FID analysis. The vials (except  $T_0$  sample) were capped and removed from the glove box and heated to 110  $^\circ\text{C}$  with stirring. After 24 and 48 hours one vial from each of the sets was removed from heat, cooled, and exposed to air to quench. An aliquot (40  $\mu\text{L}$ ) was diluted to 10 mM benzylamine with MeCN (960  $\mu\text{L}$ ) and analyzed by GC-FID. A 20  $\mu\text{L}$  aliquot of the  $T_0$  sample was diluted with solvent (980  $\mu\text{L}$ ) and analyzed by GC-FID.

#### 5.4.5 General Procedure for Catalytic Dehydrogenation Reactions of Benzylamine with Anilines

In a glovebox, the following stock solutions were prepared: benzylamine (322 mg, 3.00 mmol, 1 M) and tetrahydronaphthalene (159 mg, 1.20 mmol, 400 mM) in anisole (3.00 mL); aniline (279 mg, 3 mmol, 1M) in anisole (3.00 mL); **2-1b** (15 mg, 0.22 mmol, 15 mM) in anisole (1.50 mL); **2-3** (17 mg, 0.022 mmol, 15 mM) in anisole (1.500 mL). Benzylamine and aniline stock solutions were combined (500 mM). Two sets, A-B, of 3 vials (6 vials total) containing stir bars were charged with the benzylamine/aniline stock solution (250  $\mu$ L). To each of these vials the catalyst stock **2-1b** (250  $\mu$ L to set A), and **2-3** (250  $\mu$ L) to set B. The final concentrations for vials in sets A-B were 0.25 M in benzylamine with 3 mol% catalyst loading (A-B). A final vial was charged with substrate/internal standard stock solution (100  $\mu$ L) for use as the initial time = 0 ( $T_0$ ) sample for GC-FID analysis. The vials (except  $T_0$  sample) were capped and removed from the glove box and heated to 110 °C with stirring. After 12, 24 and 48 hours one vial from each of the sets was removed from heat, cooled, and exposed to air to quench. An aliquot (40  $\mu$ L) was diluted to 10 mM benzylamine with MeCN (960  $\mu$ L) and analyzed by GC-FID. A 20  $\mu$ L aliquot of the  $T_0$  sample was diluted with solvent (980  $\mu$ L) and analyzed by GC-FID.

#### 5.4.6 General Procedure for Catalytic Dehydrogenation Reactions of *N*-Heterocycles

In a glovebox, the following stock solutions were prepared: indoline (357 mg, 3.00 mmol, 500 mM) and tetrahydronaphthalene (80 mg, 0.60 mmol, 200 mM) in anisole (6.00 mL); **2-1b** (15 mg, 0.022 mmol, 15 mM) in anisole (1.50 mL); **2-3** (17 mg, 0.022 mmol, 15 mM) in anisole (1.500 mL). Two sets, A-B, of 5 vials (10 vials total) containing stir bars were charged with the indoline stock solution (250  $\mu$ L). To each vial in set A, 250  $\mu$ L of the catalyst stock **2-1b** was added. To each vial in set B, 250  $\mu$ L of the catalyst stock **2-3** was added. The final concentrations for vials in sets A-B were 0.25 M in indoline with 3 mol% catalyst loading (A-B). A final vial was charged with substrate/internal standard stock solution (100  $\mu$ L) for use as the initial time = 0 ( $T_0$ ) sample for GC-FID analysis. The vials (except  $T_0$  sample) were capped and removed from the glove box and heated to 110 °C with stirring. After 1, 4, 12, 24 and 48 hours one vial from each of the sets was removed from heat, cooled, and exposed to air to quench. An aliquot (200  $\mu$ L) was diluted to 50 mM indoline with MeCN (800  $\mu$ L) and analyzed by GC-FID. A 100  $\mu$ L aliquot of the  $T_0$  sample was diluted with solvent (900  $\mu$ L) and analyzed by GC-FID.

#### 5.4.7 General Procedure for Stoichiometric Probe Reactions with [Ru(Cp)(dppp)(NCMe)]PF<sub>6</sub> (2-3)

Complex **2-3** (8 mg, 0.01 mmol, 1 equiv.) and triphenylphosphine oxide (3 mg, 0.01 mmol, 1 equiv.) were added to a vial with a stir bar. THF (0.800 mL) was added by micropipette. The solution was transferred to a NMR tube and an initial (time = 0) <sup>31</sup>P{<sup>1</sup>H} NMR spectrum was obtained. The tube contents were transferred back to the vial containing the stir bar and substrate (benzylamine or pyrrolidine) (0.5 mmol, 5 equiv.) was added. The vial was stirred and heated to 65 °C in an aluminum heating block for 4 h. The contents were transferred back into a clean NMR tube and a <sup>31</sup>P{<sup>1</sup>H} NMR spectrum was obtained. If more time points were obtained, the process of heating in the vial and transfer to NMR tube were repeated for each subsequent time point.

#### 5.4.8 Attempted synthesis of [Ru(Cp)(dppp)(pyrrolidine)]PF<sub>6</sub> (5-3)

Complex **2-3** (77 mg, 0.1 mmol, 1 equiv.) was added to a 100 mL Schlenk flask with a stir bar and THF (8 mL) was added. To the Schlenk flask, pyrrolidine (36 mg, 0.5 mmol, 5 equiv.) was added. The Schlenk flask was stirred and heated to 65 °C for 45 h. The reaction was monitored over time until all of complex **2-3** producing black particles. The solvent was removed under vacuum and the <sup>31</sup>P{<sup>1</sup>H} NMR spectra were obtained in either proteo-THF or CDCl<sub>3</sub> revealing full decomposition in both solvents.

## 5.5 References

1. (a) Gunanathan, C.; Milstein, D., *Chem. Rev.* **2014**, *114*, 12024-12087; (b) Gunanathan, C.; Milstein, D., *Acc. Chem. Res.* **2011**, *44*, 588-602.
2. (a) Tseng, K.-N. T.; Rizzi, A. M.; Szymczak, N. K., *J. Am. Chem. Soc.* **2013**, *135*, 16352-16355; (b) He, L.-P.; Chen, T.; Gong, D.; Lai, Z.; Huang, K.-W., *Organometallics* **2012**, *31*, 5208-5211; (c) Prades, A.; Peris, E.; Albrecht, M., *Organometallics* **2011**, *30*, 1162-1167; (d) Ho, H.-A.; Manna, K.; Sadow, A. D., *Angew. Chem. Int. Ed.* **2012**, *51*, 8607-8610; (e) Fujita, K.-i.; Tanaka, Y.; Kobayashi, M.; Yamaguchi, R., *J. Am. Chem. Soc.* **2014**, *136*, 4829-4832; (f) Wu, J.; Talwar, D.; Johnston, S.; Yan, M.; Xiao, J., *Angew. Chem. Int. Ed.* **2013**, *52*, 6983-6987; (g) Muthaiah, S.; Hong, S. H., *Adv. Synth. Catal.* **2012**, *354*, 3045-3053; (h) Chakraborty, S.; Brennessel, W. W.; Jones, W. D., *J. Am. Chem. Soc.* **2014**, *136*, 8564-8567; (i) Myers, T. W.; Berben, L. A., *J. Am. Chem. Soc.* **2013**, *135*, 9988-9990.
3. LARGERON, M., *Eur. J. Org. Chem.* **2013**, *2013*, 5225-5235.
4. GRELLIER, M.; SABO-ETIENNE, S., *Dalton Trans.* **2014**, *43*, 6283-6286.
5. ZELL, T.; MILSTEIN, D., *Acc. Chem. Res.* **2015**, *48*, 1979-1994.

6. (a) Khusnutdinova, J. R.; Milstein, D., *Angew. Chem. Int. Ed.* **2015**, *54*, 12236-12273; (b) Crabtree, R. H., *New J. Chem.* **2011**, *35*, 18-23; (c) Grützmacher, H., *Angew. Chem. Int. Ed.* **2008**, *47*, 1814-1818.
7. (a) Sun, Y.; Koehler, C.; Tan, R.; Annibale, V. T.; Song, D., *Chem. Commun.* **2011**, *47*, 8349-8351; (b) Zhang, J.; Leitus, G.; Ben-David, Y.; Milstein, D., *Angew. Chem. Int. Ed.* **2006**, *45*, 1113-1115; (c) Ben-Ari, E.; Leitus, G.; Shimon, L. J. W.; Milstein, D., *J. Am. Chem. Soc.* **2006**, *128*, 15390-15391; (d) Hou, C.; Zhang, Z.; Zhao, C.; Ke, Z., *Inorg. Chem.* **2016**, *55*, 6539-6551; (e) Cho, D.; Ko, K. C.; Lee, J. Y., *Organometallics* **2013**, *32*, 4571-4576; (f) Yang, X.; Hall, M. B., *J. Am. Chem. Soc.* **2010**, *132*, 120-130.
8. (a) Bullock, R. M.; Helm, M. L., *Acc. Chem. Res.* **2015**, *48*, 2017-2026; (b) Bullock, R. M.; Appel, A. M.; Helm, M. L., *Chem. Commun.* **2014**, *50*, 3125-3143; (c) Liu, T.; DuBois, M. R.; DuBois, D. L.; Bullock, R. M., *Energy Environ. Sci.* **2014**, *7*, 3630-3639.
9. Stubbs, J. M.; Bow, J. P. J.; Hazlehurst, R. J.; Blacquiere, J. M., *Dalton Trans.* **2016**, *45*, 17100-17103.
10. Dobereiner, G. E.; Crabtree, R. H., *Chem. Rev.* **2010**, *110*, 681-703.
11. Alder, C. M.; Hayler, J. D.; Henderson, R. K.; Redman, A. M.; Shukla, L.; Shuster, L. E.; Sneddon, H. F., *Green Chem.* **2016**, *18*, 3879-3890.
12. Bui The, K.; Concilio, C.; Porzi, G., *J. Organomet. Chem.* **1981**, *208*, 249-251.
13. (a) Raugei, S.; Helm, M. L.; Hammes-Schiffer, S.; Appel, A. M.; O'Hagan, M.; Wiedner, E. S.; Bullock, R. M., *Inorg. Chem.* **2016**, *55*, 445-460; (b) O'Hagan, M.; Ho, M.-H.; Yang, J. Y.; Appel, A. M.; DuBois, M. R.; Raugei, S.; Shaw, W. J.; DuBois, D. L.; Bullock, R. M., *J. Am. Chem. Soc.* **2012**, *134*, 19409-19424.
14. Tsuji, Y.; Kotachi, S.; Huh, K. T.; Watanabe, Y., *J. Org. Chem.* **1990**, *55*, 580-584.
15. (a) Nyawade, E. A.; Friedrich, H. B.; Omondi, B.; Mpungose, P., *Organometallics* **2015**, *34*, 4922-4931; (b) Sortais, J.-B.; Pannetier, N.; Holuigue, A.; Barloy, L.; Sirlin, C.; Pfeffer, M.; Kyritsakas, N., *Organometallics* **2007**, *26*, 1856-1867.
16. (a) Lummiss, J. A. M.; Ireland, B. J.; Sommers, J. M.; Fogg, D. E., *ChemCatChem* **2014**, *6*, 459-463; (b) Fogg, D. E.; James, B. R., *Inorg. Chem.* **1995**, *34*, 2557-2561.
17. (a) Dabb, S. L.; Messerle, B. A.; Wagler, J., *Organometallics* **2008**, *27*, 4657-4665; (b) Prokopchuk, D. E.; Lough, A. J.; Morris, R. H., *Dalton Trans.* **2011**, *40*, 10603-10608.
18. (a) Tronic, T. A.; Kaminsky, W.; Coggins, M. K.; Mayer, J. M., *Inorg. Chem.* **2012**, *51*, 10916-10928; (b) Tronic, T. A.; Rakowski DuBois, M.; Kaminsky, W.; Coggins, M. K.; Liu, T.; Mayer, J. M., *Angew. Chem. Int. Ed.* **2011**, *50*, 10936-10939.

## Chapter 6

### 6 The Role of the 1° and 2° Coordination Spheres of MLC and Non-MLC Acceptorless Dehydrogenation Catalysts

A catalyst comparison of  $[\text{Ru}(\text{P}^{\text{R}}_2\text{N}^{\text{R}'}_2)]$ ,  $[\text{Ru}(\text{P}^{\text{R}}_2\text{N}^{\text{R}'}_1)]$ , and  $[\text{Ru}(\text{P}-\text{P})]$  complexes for acceptorless dehydrogenation catalysis was performed with indoline. Through tunability of the primary coordination sphere ( $\text{R} = \text{Ph}, t\text{-Bu}, \text{Bn}$ ), the effects of electronic and steric properties surrounding the Ru centre were explored. The importance of the pendent amines present in the secondary coordination sphere is explored through varying their number. The sterics and basicity of the pendent amine was investigated to understand the optimum factors for proton shuttling. Furthermore, a variable time normalization analysis was conducted to understand how the substrate and catalyst are interacting for both the MLC,  $[\text{Ru}(\text{P}^{\text{R}}_2\text{N}^{\text{R}'}_2)]^+$ , and non-cooperative,  $[\text{Ru}(\text{dppp})]^+$ , complexes. Finally, altering the electronics and sterics of substituents on the substrate allow for mechanistic insight into the reaction pathway.

#### 6.1 Introduction

Metal-ligand-cooperative (MLC) complexes have revolutionized catalytic reactivity allowing for powerful transformations to occur through previously unfavourable pathways.<sup>1-6</sup> These MLC complexes utilize the primary reactivity of the metal centre along with complementary reactivity from a functional group on the ligand to assist in the transformation.<sup>7-10</sup> One type of MLC system is called proton transfer complexes.<sup>8</sup> These complexes have a functional group present to assist with deprotonation and protonation steps that otherwise would need to be mediated by an exogenous base.<sup>11-15</sup> Incorporation of these acid/base sites on to the ligand of a transition metal complex has been shown to assist in hydrogenation/dehydrogenation catalysis (e.g. Noyori or Milstein catalysts).<sup>16-18</sup> However, the acid/base sites are often bound to the metal centre and directly affect the primary coordination sphere. Therefore, altering the steric and electronic environment of the acid/base site also directly effects the primary coordination sphere.<sup>19, 20</sup> Thereby, construction of structure-activity relationships for the primary coordination sphere and the acid/base site are often very difficult to achieve.<sup>21</sup>

Acceptorless dehydrogenation of amines is a growing area of interest as an atom efficient alternative route to produce imines and nitriles along with the energy vector  $\text{H}_2$ .<sup>2, 3, 22-27</sup> Current catalysts for acceptorless dehydrogenation utilize Ru or Os and are proposed to operate through both cooperative



and non-cooperative pathways.<sup>22, 26, 28</sup> One pathway proceeds through an inner-sphere route where the substrate binds through the amine to the metal centre. Deprotonation of the amine by a basic site on the catalyst or exogenous base and  $\beta$ -hydride elimination can then occur in a stepwise process (Figure 6-1a).<sup>28, 29</sup> Alternatively, an outer-sphere process is possible. For this pathway, the substrate does not bind to the metal centre through the amine. Instead, a metal hydride interaction occurs between the metal and the hydrogen of the carbon adjacent to the amine. A hydride is then transferred from the substrate to the metal centre after or simultaneously with deprotonation of the amine (Figure 6-1b).<sup>18, 30</sup> These mechanistic pathways are based on the reverse reaction pathway for hydrogenation.

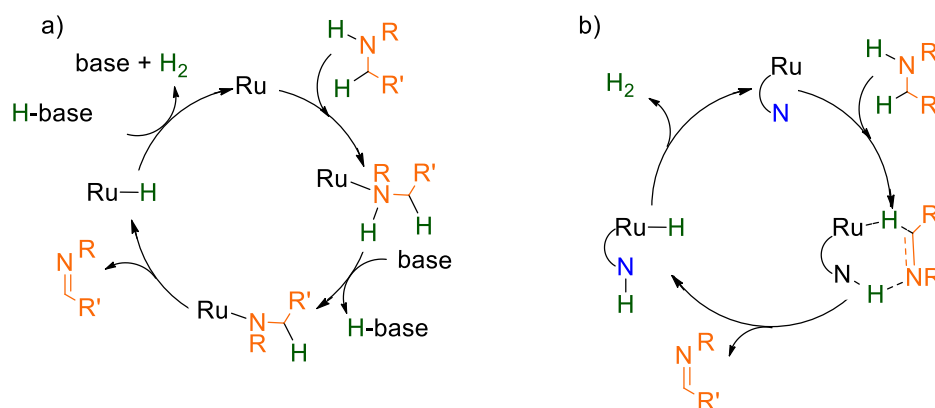


**Figure 6-1.** Two mechanistic pathways for the acceptorless dehydrogenation of amines. a) An inner-sphere pathway in which deprotonation can be facilitated by an exogenous base (non-MLC) or catalyst (MLC); and b) an outer-sphere pathway where deprotonation is facilitated by the catalyst (MLC)

Harsh conditions are important for the generation of double and triple bonds as both products are enthalpically unfavourable.<sup>10, 25, 31-34</sup> The entropic release of  $H_2$  from the catalyst is used to make acceptorless dehydrogenation more favourable.<sup>25, 26, 31, 32</sup> However,  $H_2$  release and  $H_2$  binding are in equilibrium. As the reaction proceeds in a closed (capped) system, the  $H_2$  pressure increases until the rate of  $H_2$  binding is equal to the rate of  $H_2$  release causing an incomplete reaction.<sup>26</sup> Open conditions, under a flow of  $N_2$ , can be employed to release  $H_2$  and allow AD reactions to go to completion.<sup>25, 26, 31, 32</sup> Current Ru catalysts typically operate at high temperatures (110-145 °C) with high catalytic loadings (1-3 mol%).<sup>10, 25, 33</sup> Optimization of the catalyst based on the known mechanistic pathway can allow for a reduction in reaction conditions (temperature, catalyst loading, reaction time). Two reports provide mechanistic insight for acceptorless dehydrogenation of amines (Figure 6-2). Szymczak reported a potential MLC catalyst for acceptorless dehydrogenation of benzylamine with 1 mol% [Ru] at 110 °C. However, mechanistic investigation revealed the catalyst to proceed through an inner-sphere non-

cooperative pathway.<sup>28</sup> Bera recently used a MLC catalyst that operated under milder conditions than previous systems (2 mol% at 70 °C). Mechanistic insight revealed the catalyst to likely proceed through an outer-sphere MLC pathway.<sup>26</sup> Therefore, catalyst structure is critical to the mechanistic pathway. Understanding how these reactions proceed and how structure effects activity would be an asset to improve performance and design new catalysts for acceptorless dehydrogenation of amines.

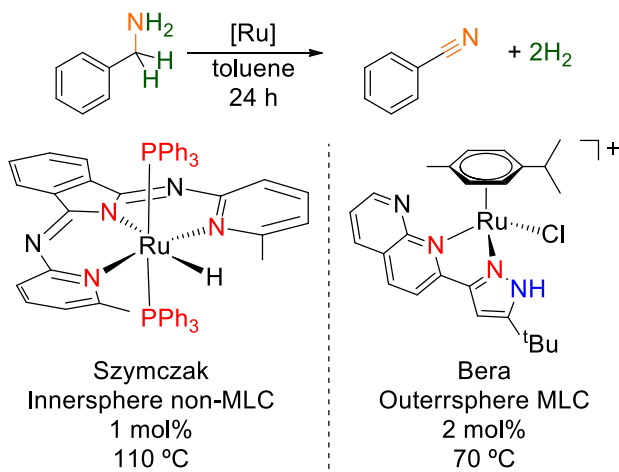


**Figure 6-2.** Acceptorless dehydrogenation of benzylamine to produce nitriles<sup>26, 28</sup>

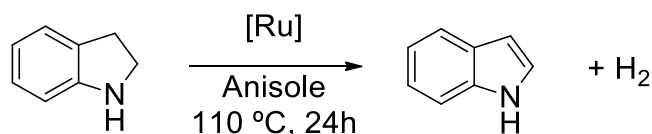
[Ru(Cp)(P<sup>Ph</sup><sub>2</sub>N<sup>Bn</sup><sub>2</sub>)(NCCH<sub>3</sub>)]PF<sub>6</sub> (**2-1b**) was recently reported to be active for the acceptorless dehydrogenation of benzylamine at 110 °C at 1 mol% in anisole.<sup>35</sup> Only two main products are observed with **2-1b** – the acceptorless dehydrogenative coupling product, *N*-benzyl-phenylimine, and double acceptorless dehydrogenation product, benzonitrile. Mechanistic insight suggested an outer-sphere MLC pathway for producing *N*-benzyl-phenylimine. A non-cooperative inner-sphere mechanistic pathway was found to be active for [Ru(Cp)(dppp)(NCCH<sub>3</sub>)]PF<sub>6</sub> (**2-3**) toward the acceptorless dehydrogenation of benzylamine. The substrate is thought to facilitate the proton transfer steps in the reaction as no exogenous base was added.

The Ru-(P<sup>R</sup><sub>2</sub>N<sup>R'</sup><sub>2</sub>) system represents an opportunity to deconvolute the effects of the primary and secondary coordination sphere upon acceptorless dehydrogenation through systematic tuning of the ligand. Structure-activity relationships can be constructed to allow for catalyst optimization. However, a simpler substrate system is necessary to focus on catalyst activity without additional selectivity effects. Herein, we discuss the acceptorless dehydrogenation of indoline with 14 different catalyst to understand the importance of the primary and secondary coordination sphere effects and give mechanistic insight of the role of the pendent amine.

## 6.2 Results and Discussion

Three main derivatives of the Cp and Cp\* analogues of  $[\text{Ru}(\text{P-P})(\text{NCCH}_3)]\text{PF}_6$  were used in this study. The first set (**2-1a,b**, **3-1a-d**, **4-1a**) use the Cp ligand with a  $\text{P}^{\text{R}_2}\text{N}^{\text{R}'_2}$  ligand wherein the R group effects the steric environment and electron density at the metal and R' alters the steric environment and basicity of the pendent amine (Figure 6-3a). The other two types of derivatives vary by the number of pendent amines that are present within the ligand. A  $\text{P}^{\text{R}_2}\text{N}^{\text{R}'_1}$  ligand (Figure 6-3c) and bis(diphenylphosphine) ligands (P-P: dppe, dppe, dppp, dpbz) (Figure 3d,e) were utilized to generate Ru(Cp) derivatives (**3-4** and **2-3**, **6-1a-c** respectively) to investigate the role of the pendent amine. Derivatives with a Cp\* ligand (**4-2** and **6-2**) was also used as a comparison to the Cp analogues (**2-1b** and **2-3**) (Figure 6-3b,f). A series of bis(phosphino) complexes – **6-1a** (dppm), **6-1c** (dpbz), and **6-2** (Cp\*, dppp) – are new entries into this class of compounds and they were characterized by  $^1\text{H}$ ,  $^{31}\text{P}\{^1\text{H}\}$ ,  $^{13}\text{C}\{^1\text{H}\}$  NMR spectroscopy, MALDI mass spectrometry, and IR spectroscopy.

A screen of 14 catalyst derivatives was performed under standard conditions of 110 °C in anisole using 0.5, 1, and 3 mol% catalytic loading under closed conditions (Scheme 6-1). Indoline was chosen as the substrate since only one product (indole) can be formed following acceptorless dehydrogenation. Indoline is additionally not as thermodynamically challenging as other AD substrates due to the aromatization of the heterocyclic ring system. The conversion was calculated after 24 h.



**Scheme 6-1.** Acceptorless dehydrogenation of Indoline under standard conditions

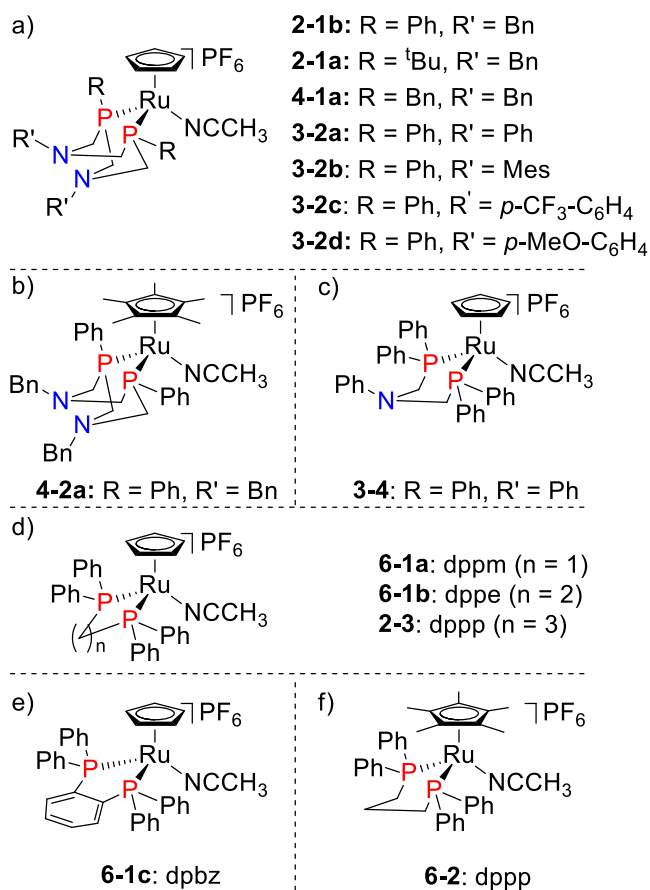


**Figure 6-3.** Ru complexes used in this study to divulge structure activity relationships

A catalyst comparison of the primary coordination sphere was performed under standard conditions through a change to the R group of the  $P^{R_2}N^{R'_2}$  ligand (R = Ph, *t*-Bu, Bn) while the secondary coordination sphere was held constant (R' = Bn) (Figure 6-4). Therefore, complexes **2-1b**, **2-1a**, **4-1a** and **4-2a** were used for the acceptorless dehydrogenation of indoline to produce indole under standard conditions. Complete conversion was not achieved for any catalyst. However, catalyst **2-1b** and **2-1a** reached similar conversion values at 3 mol%. Therefore, 1 mol% and 3 mol% loading results were used to compare performance among the catalysts. At 1 mol%, **2-1b** (R = Ph) and **2-1a** (R = *t*-Bu) outperform **4-1a** (R = Bn) resulting in turnover numbers of 56 (**2-1b**) vs. 76 (**2-1a**) vs. 6 (**4-1a**). An increase in the steric environment of the phosphine appears to be more important (R = *t*-Bu > Ph > Bn) than the effect of the electron density of the phosphine (R = *t*-Bu > Bn < Ph). Bulky phosphine groups would cause the substrate to align with the pendent amine more easily as substrate rotation could be encumbered in either an inner-sphere or outer-sphere mechanism. At 3 mol%, the Cp analogue (**2-1b**) substantially outperformed the Cp\* analogue (**4-2a**) (TON = 25 vs. 3, respectively). Therefore, the Cp analogues

display higher catalytic activity. This result reveals that a less electron rich Ru centre has higher performance. However, the steric environment of the Cp analogue has decreased in comparison to Cp\* analogue. Ru(Cl)(Cp/Cp\*)(P<sup>R</sup><sub>2</sub>N<sup>R'</sup><sub>2</sub>) derivatives were used for the attempted reduction of dioxygen. Reactions with substrate showed that the steric environment of the Cp and Cp\* analogues did not effect the open coordination site when forming [Ru(Cp/Cp\*)(P<sup>R</sup><sub>2</sub>N<sup>R'</sup><sub>2</sub>)(O<sub>2</sub>)]<sup>+</sup> complexes.<sup>36, 37</sup> Therefore, this steric change may not be significant as the methyl groups of the Cp\* are further from the catalytic site and would not affect the steric environment of the open site in acceptorless dehydrogenation. A small alkyl derivative (R = Me) was synthesized in an attempt to deconvolute the effects of steric and electronic properties. This complex was tested for acceptorless dehydrogenation of indoline but showed no catalytic reactivity. However, the Ru complex does not exhibit the same chemical structure as other Ru(P<sup>R</sup><sub>2</sub>N<sup>R'</sup><sub>2</sub>) complexes as observed by <sup>1</sup>H and <sup>31</sup>P{<sup>1</sup>H} NMR spectroscopy possibly due to either decomposition or different conformations existing as many <sup>31</sup>P {<sup>1</sup>H} signals are observed (3-20 ppm) upfield of the typical Ru(P<sup>R</sup><sub>2</sub>N<sup>R'</sup><sub>2</sub>) singlet observed between 33-54 ppm. Therefore, the observed lack of reactivity does not provide insight into the effects of steric and electronic properties. Overall, the primary coordination sphere benefits from the less electron rich Cp ligand and sterically bulky R groups on the phosphine.

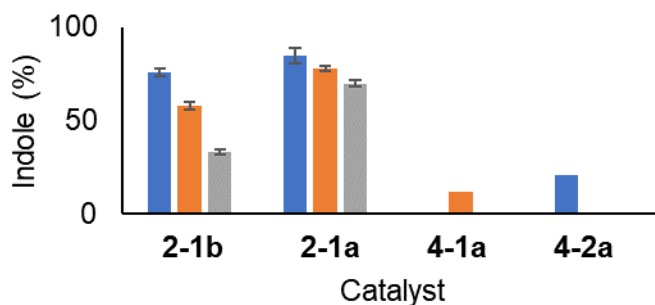


**Figure 6-4.** Catalyst comparison of the primary coordination sphere using complex **2-1a,b**, **4-1a**, and **4-2a** for acceptorless dehydrogenation of indoline to indole at 0.5 (grey), 1 (orange) and 3 (blue) mol%

A catalyst screen of the secondary coordination sphere was examined by altering the R' group of the P<sup>R</sup><sub>2</sub>N<sup>R'</sup><sub>2</sub> ligand but keeping the primary coordination sphere constant (Cp, R = Ph). The AD of indoline was conducted under standard conditions and complete conversion with complexes **2-1b** (R' = Bn), **3-2a** (R' = Ph), **3-2d** (R' = *p*-CH<sub>3</sub>O-C<sub>6</sub>H<sub>4</sub>), **3-2c** (R' = *p*-CF<sub>3</sub>-C<sub>6</sub>H<sub>4</sub>), **3-2b** (R' = Mes) was not achieved (Figure 6-5). At 3 mol%, complexes **2-1b**, **3-2a-d** produced approximately the same amount of indole (76-83%). However, complex **3-2b** produced significantly less indole (32%). This low yield of indole

for the sterically bulky pendent amine reveals that the pendent amine must be accessible for proton shuttling in order to achieve high conversion. The basicity of the pendent amine was increased and decreased by using catalysts **2-1b**, **3-2a,c,d**. All of these catalysts were compared at 0.5 mol% as all had similar performance at 1 and 3 mol%. Complex **3-2a** ( $R' = \text{Ph}$ , TON = 162) and **3-2d** ( $R' = p\text{-CH}_3\text{O-C}_6\text{H}_4$ , TON = 140) produced the most indole at 0.5 mol%. Complex **2-1b** ( $R' = \text{Bn}$ , TON = 66) and complex **3-1c** ( $R' = p\text{-CF}_3\text{-C}_6\text{H}_4$ , TON = 64) produced less than half as much as **3-2a** and **3-2d**. When ordering these complexes in terms of approximate  $\text{pK}_a$  of the conjugate acid of the pendent amine, the most basic would be  $R' = \text{Bn} > p\text{-CH}_3\text{O-C}_6\text{H}_4 > \text{Ph} > p\text{-CF}_3\text{-C}_6\text{H}_4$ . Comparing the turnover numbers in order of basicity reveals that catalytic performance does not track with reactivity –  $\text{Bn}$  (TON = 66) <  $p\text{-CH}_3\text{O-C}_6\text{H}_4$  (140) <  $\text{Ph}$  (162) >  $p\text{-CF}_3\text{-C}_6\text{H}_4$  (64). A Goldilocks situation exists where performance decreases if the basicity of the pendent amine is too high or too low and it will not cooperate optimally with the metal centre. Optimal catalytic performance was observed with a  $R'$  of  $\text{Ph}$  on the pendent amine. The structure of the pendent amine  $R' = \text{Ph}$  closely resembles the structure of indoline and therefore the respective anilinium and indolium cation conjugate acids would have similar  $\text{pK}_a$ . Optimal basicity of the pendent amine is likely intertwined with the basicity substrate. A previous MLC-substrate relationship was observed with  $\text{Ru-P}^{\text{R}}_2\text{N}^{\text{R}'_2}$  complexes for intramolecular cyclization of amino alkynes as a threshold basicity was required for optimal performance.<sup>21</sup> As the basicity of the pendent amine has a significant influence on catalytic performance of acceptorless dehydrogenation, this effect strongly suggests a MLC mechanistic pathway for  $\text{Ru-(P}^{\text{R}}_2\text{N}^{\text{R}'_2})$  catalysts.

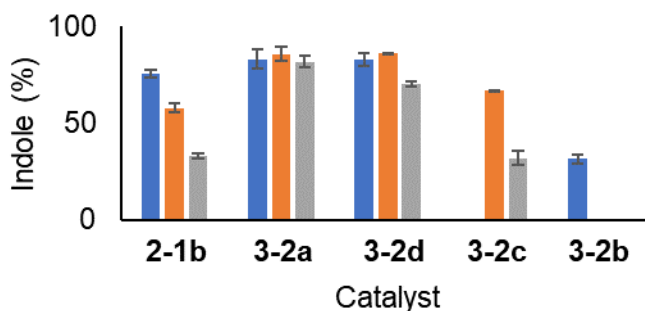


**Figure 6-5.** Catalyst comparison of the secondary coordination sphere using complex **2-1b** ( $R' = \text{Bn}$ ), **3-2a** ( $R' = \text{Ph}$ ), **3-2d** ( $R' = p\text{-MeO-C}_6\text{H}_4$ ), **3-2c** ( $R' = p\text{-CF}_3\text{-C}_6\text{H}_4$ ), and **3-2b** ( $R' = \text{Mes}$ ) for acceptorless dehydrogenation of indoline to indole at 0.5 (grey), 1 (orange) and 3 (blue) mol%

A screen of  $\text{Ru}(\text{Cp})$  (**2-3**, **6-1a-c**) and  $\text{Ru}(\text{Cp}^*)$  (**6-2**) complexes with non-MLC P-P ligands was performed to determine the optimal metallacycle ring size (Figure 6-6). These catalysts were used with

loadings of 0.5 and 1 mol% in the AD of indoline under standard conditions. Indole was observed in all cases except with catalyst **6-1d** (P–P = dpbz), which did not consume any starting material. The P–P ligands dppm (**6-1a**), dppe (**6-1b**), and dppp (**2-3**) resulted in TONs of 39, 58 and 70, respectively. The amount of indole produced increases with the number of carbons in the linker chain of the catalyst. For analogous Ru(Cp)(H)(P–P) complexes, the bite angle of the chelating bis(phosphine) ligand increases with the number of carbon atoms in the linker (72.01° for dppm, 84.50° for dppe, and 93.96° for dppp). Hydrogenation of iminium cations with these Ru–H catalysts revealed that as the bite angle is increased, the rate of hydride transfer and thus catalysis decreases.<sup>30</sup> The HOMO of the Ru–H complex closely resembles the LUMO of [Ru(Cp)(P–P)]<sup>+</sup>. Therefore, the rate is linked to the stability of the LUMO. As the bite angle increases, the stability of [Ru(Cp)(P–P)]<sup>+</sup> increases.<sup>30</sup> The most stable [Ru(Cp)(P–P)]<sup>+</sup> screened was **2-3**, which has the highest performance for acceptorless dehydrogenation of indoline. Catalyst **2-3** has a much larger bite angle when compared to [Ru(P<sup>R</sup><sub>2</sub>N<sup>R'</sup><sub>2</sub>)]<sup>+</sup> complexes that typically have a bite angle between 77–80° due to the restrictive metallacycles. Complex **6-2** is the Cp\* analogue of **2-3** and its performance was also assessed under standard conditions. However, a significant decrease in performance was observed (TON = 15) at 1 mol%. This result is consistent with the Cp and Cp\* analogues for [Ru(P<sup>Ph</sup><sub>2</sub>N<sup>Bn</sup><sub>2</sub>)]<sup>+</sup> complexes.

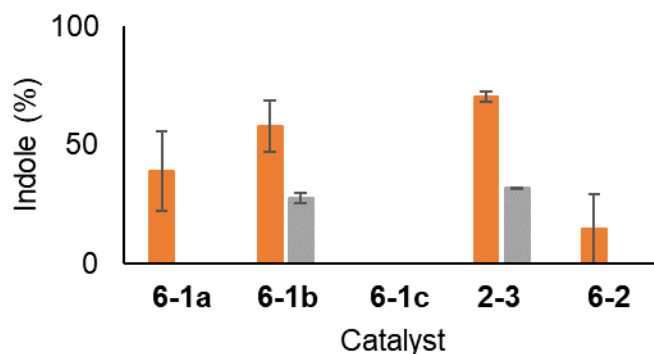


**Figure 6-6.** Catalyst comparison of the Ru(P–P) complexes lacking a pendent amine in the ligand using complex **6-1a** (dppm), **6-1a** (dppe), **6-1c** (dpbz), **2-3** (dppp), and **6-2** (Cp\*, dppp) for acceptorless dehydrogenation of indoline to indole at 0.5 (grey), and 1 (orange) mol%

The three types of derivatives have different number of acid/base sites within the ligand. A screen of Ru-(P<sup>Ph</sup><sub>2</sub>N<sup>Ph</sup><sub>2</sub>) (**3-2a**), Ru-(P<sup>Ph</sup><sub>2</sub>N<sup>Ph</sup><sub>1</sub>) (**3-4**), and Ru-(dppp) (**2-3**) was performed to determine the role of the pendent amine (Figure 6-6). These catalysts were used with loadings of 0.5 and 1 mol% for the acceptorless dehydrogenation of indoline with under standard conditions. The P<sup>Ph</sup><sub>2</sub>N<sup>Ph</sup><sub>2</sub>, P<sup>Ph</sup><sub>2</sub>N<sup>Ph</sup><sub>1</sub>, and

dppp ligands possess two, one and zero pendent amines within the secondary coordination sphere, respectively. This difference allows for a direct comparison of a potential cooperative and non-cooperative ligand system. At 1 mol%, the complex with the  $P^{Ph_2}N^{Ph_2}$  ligand (**3-2a**, TON = 86) outperforms  $P^{Ph_2}N^{Ph_1}$  ligand (**3-4**, TON = 74) and dppp ligand (**2-3**, TON = 70) (Figure 7). Dropping the catalyst loading to 0.5 mol%, pronounces the difference between the catalysts. Once again, use of the  $P^{Ph_2}N^{Ph_2}$  ligand (**3-2a**) outperforms  $P^{Ph_2}N^{Ph_1}$  (**3-4**) and dppp ligand (**2-3**) (TON = 162 vs. 66 vs. 62). Complex  $Ru(P^{Ph_2}N^{Ph_1})$  (**3-4**) slightly outperforms  $Ru(dppp)$  (**2-3**) at both 0.5 mol% and 1 mol%. The impact of a dual 6-membered metallacycles on  $Ru(P^{Ph_2}N^{Ph_2})$  (**3-2a**) likely causes improved performance due to the proximal pendent amine being closer to the open coordination site than the more flexible  $Ru(P^{Ph_2}N^{Ph_1})$  (**3-4**). If the intramolecular pendent amine has too much flexibility, it will have to overcome the same entropic challenges as an intermolecular base.  $Ru(dppp)$  (**2-3**) has to proceed through a non-MLC pathway, which requires an external base. Therefore, the use of one flexible pendent amine results in only a slight improvement for  $Ru(P^{Ph_2}N^{Ph_1})$  (**3-4**) over  $Ru(dppp)$  (**2-3**) at both 0.5 and 1 mol%. Overall, a drastic improvement in catalyst performance is observed when utilizing  $P^{Ph_2}N^{Ph_2}$  ligand.

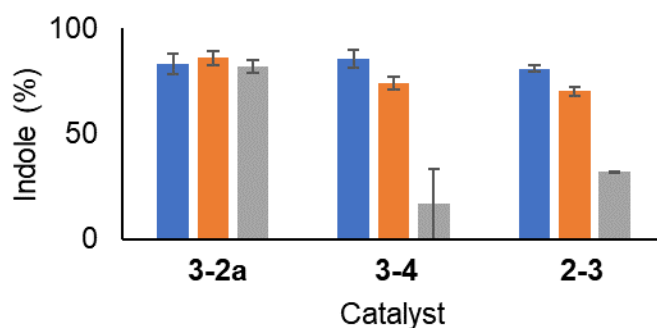


**Figure 6-7.** Catalyst comparison of the acid/base site using complex **3-2a** ( $Ru(P^{Ph_2}N^{Ph_2})$ ), **3-4** ( $Ru(P^{Ph_2}N^{Ph_1})$ ), and **2-3** (dppp) for acceptorless dehydrogenation of indoline to indole at 0.5 (grey), 1 (orange) and 3 (blue) mol%

A comparison of the rate of reaction for best  $Ru(P^{R_2}N^{R'_2})$  (**3-2a**) and  $Ru(dppp)$  (**2-3**) in the acceptorless dehydrogenation of indoline was performed at 1 mol% at 97 °C in anisole. The reaction was monitored by REACTIR and conversion was corrected after the reaction was complete by GC-FID (Figure 6-8). The  $Ru(P^{R_2}N^{R'_2})$  (**3-2a**) complex reacts much faster than  $Ru(dppp)$  (**2-3**) with a turnover frequency = 61  $h^{-1}$  compared to 9  $h^{-1}$ . Therefore, the pendent amine increases the rate of reaction for **3-2a** demonstrating the benefit of an MLC catalyst over a non-MLC catalyst. Additionally, other acceptorless



dehydrogenation catalysts require much longer reaction times (24-48 h) at similar catalytic loadings (1-5 mol%). Use of a tunable MLC catalyst allows for superior performance through optimization of the primary and secondary coordination spheres.

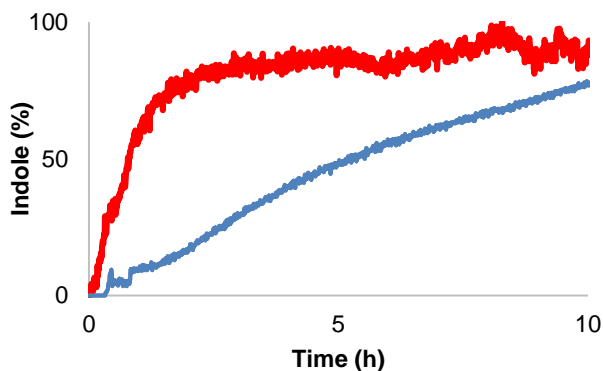
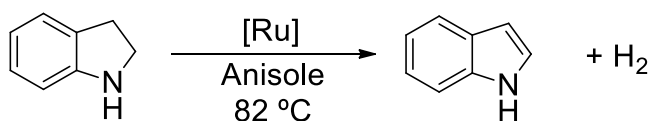


**Figure 6-8.** Reaction profile for acceptorless dehydrogenation of indoline with Ru( $P^{R_2}N^{R'_2}$ ) (**3-2a** – red) and Ru(dppp) (**2-3** – blue) (1 mol%) at 97 °C in anisole monitored by ReactIR

To understand how indoline interacts with the complexes Ru-( $P^{Ph_2}N^{Ph_2}$ ) (**3-2a**) and Ru-(dppp) (**2-3**), a mechanistic investigation of the reaction pathway was undertaken to deconvolute the effect of the pendent amine. Previous work with Ru-( $P^{Ph_2}N^{Bn_2}$ ) for acceptorless dehydrogenation of benzyl amine suggests a MLC mechanistic pathway. Additionally, the basicity of the pendent amine significantly influences catalytic performance of indoline. Therefore, Ru-( $P^{Ph_2}N^{Ph_2}$ ) (**3-2a**) is highly likely to perform acceptorless dehydrogenation through an inner or outer-sphere mechanism. Whereas it is proposed that **2-3** relies upon additional units of substrate to act as an intermolecular base as no exogenous base was added to the reaction. Therefore, the rate law for these two complexes may not be the same. A variable time normalization analysis was performed to elucidate the order in both catalyst and substrate.<sup>38, 39</sup> To perform a variable time normalization analysis, a full reaction profile must be obtained, in which the concentration of the species of interest is varied whilst other reagents are kept constant. By graphing the conversion of product against the summation of the concentration of the species of interest and time ( $\sum[A]^{reaction\ order\ of\ A} \Delta t$ ), a visual interpretation of which rate law is correct can be obtained. The rate order for catalyst for the acceptorless dehydrogenation of indoline (250 mM) was probed using the variable time normalization analysis for **3-2a** and **2-3**. Complex **3-2a** was analysed at 1.5 and 2 mol% at 82 °C in anisole (Scheme 6-2) and complex **2-3** was probed at 1 and 2 mol% at 100 °C in anisole (Scheme 6-3). The reaction was monitored by REACTIR and conversion corrected after the reaction was complete by GC-FID analysis relative to tetrahydronaphthalene. Even with a temperature

difference of 18 °C, both reactions reach completion at 10 h at 2 mol% (**3-2a**: 91% vs. **2-3**: 94%). This reaction with **3-2a** is yet another example of the benefits of a tunable MLC system as only one other report has achieved similar performance (Bera: 2 mol% [Ru], 70 °C, open conditions).<sup>26</sup> The x-axis was adjusted using the order of the catalyst ( $[\text{Ru}]^{\text{reaction order of Ru}} \Delta t$ ). As the order of the reaction for catalyst is increased from zero to one, the two reaction profiles (1.5 mol% vs. 2 mol% Ru-(P<sup>Ph</sup><sub>2</sub>N<sup>Bn</sup><sub>2</sub>)) merge (Figure 6-9). After the order of the reaction is increased from one to two, the reaction profiles delineated again. A similar relationship is observed for Ru-(dppp) (Figure 6-10). Therefore, the reaction order for catalyst is one and one molecule of catalyst is involved in the rate-determining step for Ru-(P<sup>Ph</sup><sub>2</sub>N<sup>Bn</sup><sub>2</sub>) (**3-2a**) and Ru-(dppp) (**2-3**).



**Scheme 6-2.** AD of indoline for catalyst variable time normalization analysis with **3-2a**

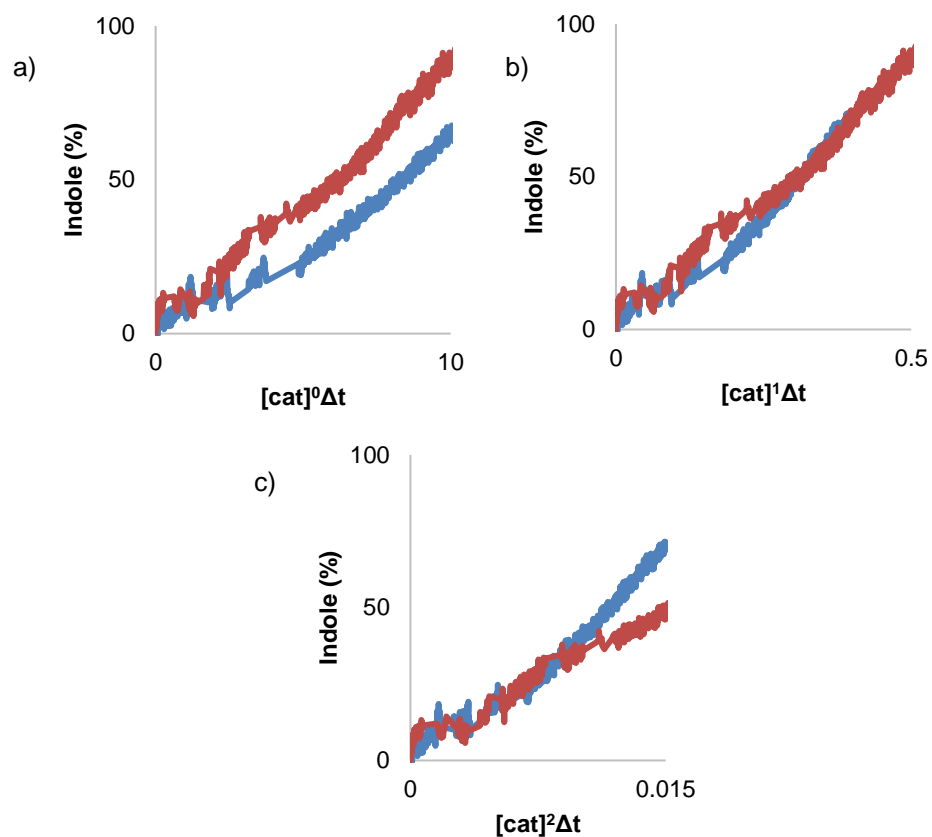
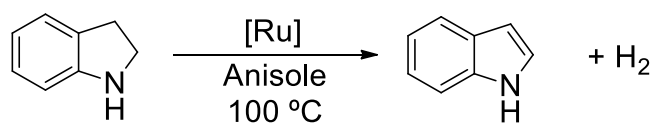


**Figure 6-9.** Variable time normalization analysis of catalyst at a) 0<sup>th</sup> order; b) 1<sup>st</sup> order; and c) 2<sup>nd</sup> order for the acceptorless dehydrogenation of indoline (250 mM) using **3-2a** (1.5 mol% – blue; 2 mol% – red) at 82 °C in anisole monitored by ReactIR



**Scheme 6-3.** AD of indoline for catalyst variable time normalization analysis with **2-3**

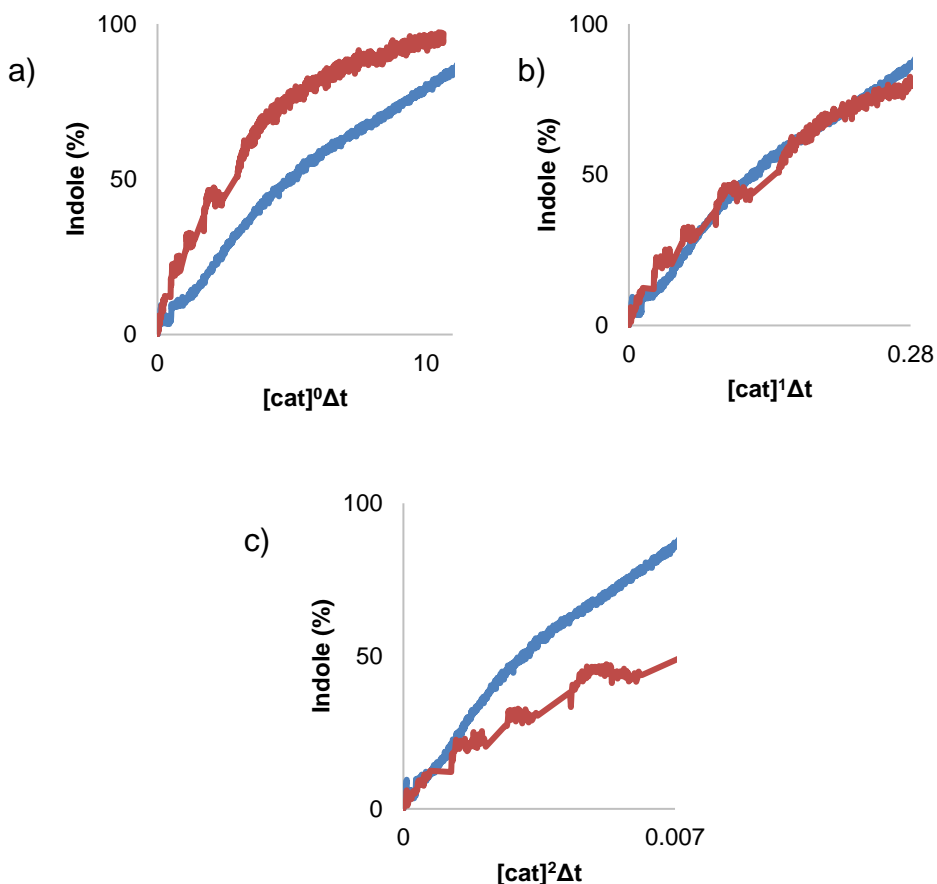
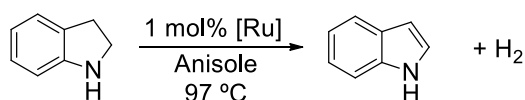


**Figure 6-10.** Variable time normalization analysis of catalyst at a) 0<sup>th</sup> order; b) 1<sup>st</sup> order; and c) 2<sup>nd</sup> order for the acceptorless dehydrogenation of indoline (250 mM) using **2-3** (1 mol% – blue; 2 mol% – red) at 100 °C in anisole monitored by ReactIR

A variable time normalization analysis was performed for acceptorless dehydrogenation of indoline at 250 mM and 375 mM for **3-2a** (1 mol%) at 97 °C in anisole under open conditions (Scheme 6-4). The rate of reaction for indoline at 375 mM was faster than at 250 mM (TOF = 77 vs. 61 h<sup>-1</sup>). As expected the rate is dependent on substrate. This substrate dependency indicates that H<sub>2</sub> formation or release is not rate determining. The x-axis was adjusted using the order of the substrate ( $\sum[\text{Sub}]^{\text{reaction order of Sub}} \Delta t$ ). As the order of the reaction for substrate is increased from zero to one, the two reaction profiles (250 mM vs. 375 mM indoline) merge (Figure 6-11). After the order of the reaction is increased from one to two, the reaction profiles delineated again. As the two reaction profiles merge at 1, reaction order of indoline is 1. An equilibrium exists between pre-catalyst, active catalyst and substrate bound catalyst. This equilibrium lies heavily towards the pre-catalyst or the substrate bound catalyst as the active

catalyst has an open coordination site. As the reaction is performed open, acetonitrile (b.p. = 82 °C) would boil away after dissociation has occurred. This results in an equilibrium heavily favouring the substrate bound metal complex. For an inner-sphere mechanistic pathway, the substrate bound metal is an on cycle intermediate. Due to the strong equilibrium, the substrate is kinetically saturated, which results in a reaction order of zero for the substrate. An outer-sphere mechanism, however, requires a hydride to be transferred without the amine bonding to the metal centre. This rate-determining step would require one molecule of substrate and one molecule of catalyst. A reaction order of 1 for indoline and Ru-(P<sup>Ph</sup><sub>2</sub>N<sup>Ph</sup><sub>2</sub>) (**3-2a**) is required to facilitate acceptorless dehydrogenation likely through an outer-sphere mechanistic pathway. Additionally, the approximate pK<sub>a</sub> of the substrate would be greater than that of the conjugate acid of any of the pendent amine functional groups.<sup>21</sup> Therefore, deprotonation of the substrate does not occur until an interaction with the metal exists. As a result, the deprotonation step must be concerted. Therefore, Ru-(P<sup>Ph</sup><sub>2</sub>N<sup>Ph</sup><sub>2</sub>) (**3-2a**) likely proceeds through an MLC outer-sphere concerted mechanism. Further mechanistic studies are needed to confirm this pathway.



**Scheme 6-4.** AD of indoline for substrate variable time normalization analysis with **3-2a**

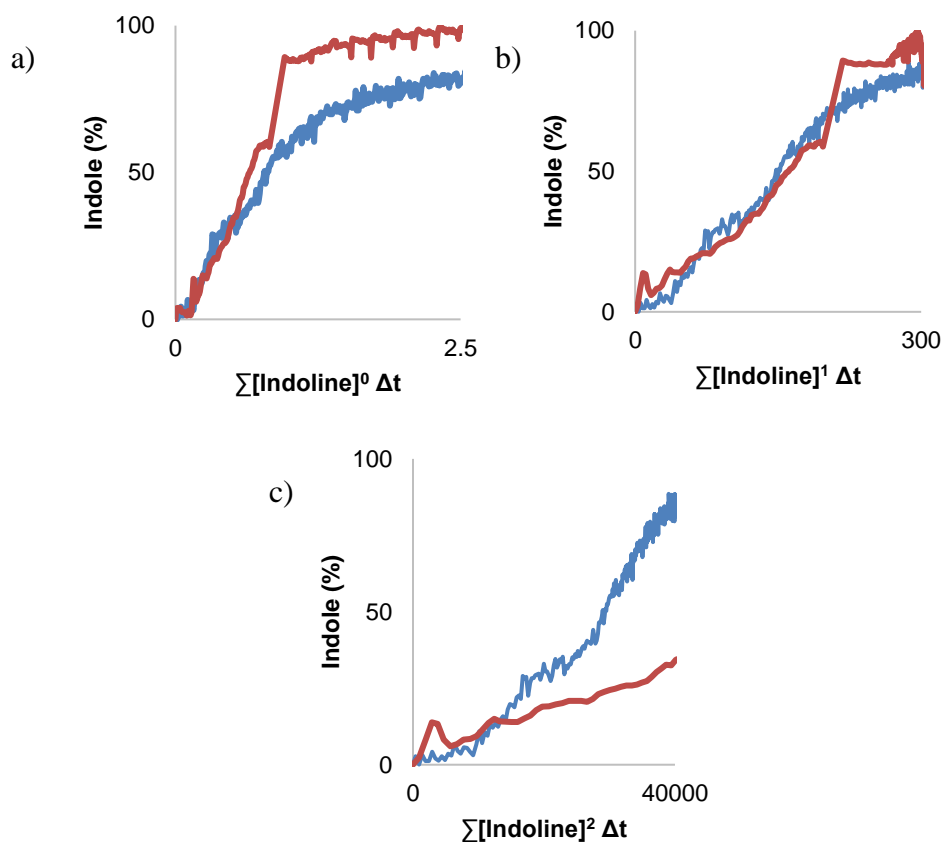
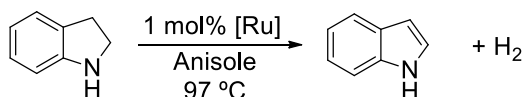


**Figure 6-11.** Variable time normalization analysis of substrate at a) 0<sup>th</sup> order; b) 1<sup>st</sup> order; and c) 2<sup>nd</sup> order for the acceptorless dehydrogenation of indoline (250 mM – blue; 375 mM – red) using 1 mol% of **3-2a** at 97 °C in anisole monitored by ReactIR

A variable time normalization analysis was also performed for Ru-(dppp) (**2-3**) (1 mol%) with indoline (125 mM, 250 mM, 375 mM) at 97 °C in anisole (Scheme 6-5). Increasing substrate concentration should increase rate as an inner-sphere mechanism would favour binding of the substrate to the Ru centre and deprotonation from an intermolecular base. The reaction was found to proceed at a faster rate at low concentrations of indoline (125 mM > 250 mM > 375 mM) (Figure 6-12a). However, after ca. 20% conversion for the reactions with high substrate concentration (250 and 375 mM), the rate of reaction profiles displays a dramatic increase. This behaviour is consistent with catalyst inhibition due to high concentrations of substrate. Variable time normalization analysis of these reactions revealed no perfect rate order match (Figure 6-12). Separating the catalyst inhibition and productive rates is not trivial due to the overall rate law changing over time. The reaction order of catalyst inhibition appears to be -2 in substrate (Figure 6-12c). As mentioned with **3-2a**, a strong pre-equilibrium favours the

formation of the substrate bound catalyst. For a non-MLC catalyst, a unit of substrate is thought to facilitate proton transfer. Thus, a reaction order of one is expected for an inner-sphere non-MLC mechanism. Use of same-excess protocol manipulates the x-axis to align reaction profiles at a starting concentration ( $T_0 = 125$  mM indoline) (Figure 6-13).<sup>40</sup> A variable time normalization analysis can now be performed to extract the rate order unaffected by pre-equilibrium steps. The reaction order of indoline was found to be zero for Ru-(dppp) (**2-3**). Therefore, substrate is not facilitating proton transfer. It is possible that the bisphosphine ligand is facilitating the proton transfer steps if the ligand is hemilabile. While not always thought of as bases, phosphines can act as bases and have a  $pK_a$  for the protonated phosphine between 2.7-10.4 for  $PPh_3$  and  $P(t-Bu)_3$ .<sup>41</sup> This  $pK_a$  range is close to the approximated  $pK_a$  range of **3-2c,d** (8.2-12.1).<sup>21, 42</sup> For the dppp ligand to act as the acid/base site, the ligand must be hemilabile. As the catalyst is inhibited at high concentrations of substrate, it is possible that the substrate displaces the ligand entirely. Further mechanistic studies are needed to investigate this potential route.



**Scheme 6-5.** AD of indoline for substrate variable time normalization analysis with **2-3**

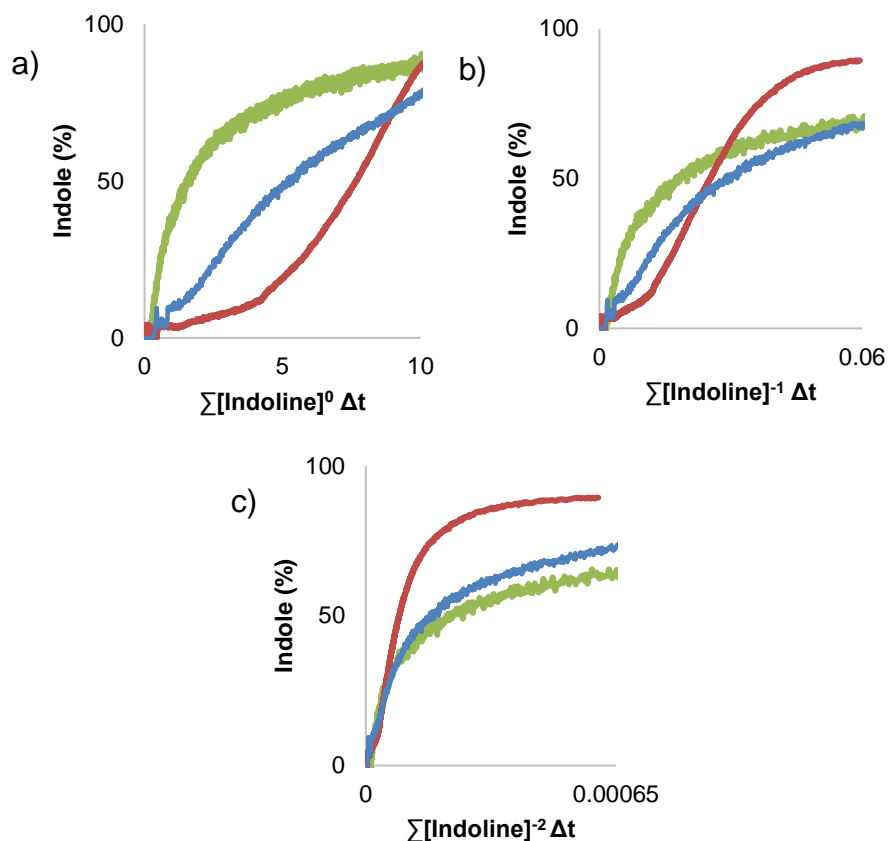


**Figure 6-12.** Variable time normalization analysis of substrate at a) 0<sup>th</sup> order; b) negative 1<sup>st</sup> order; and c) negative 2<sup>nd</sup> order for the acceptorless dehydrogenation of indoline (125 mM – green; 250 mM – blue; 375 mM – red) using 1 mol% of complex **2-3** at 97 °C in anisole monitored by REACTIR

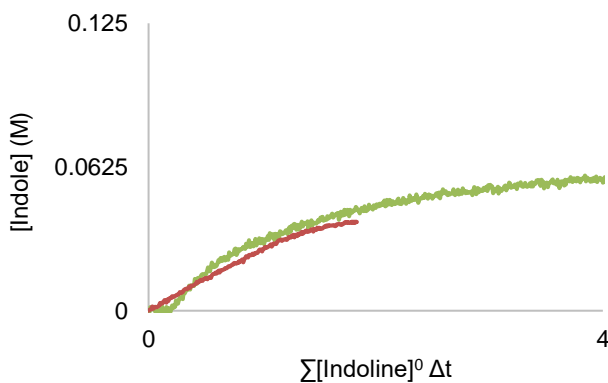


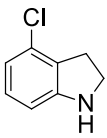
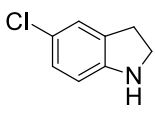
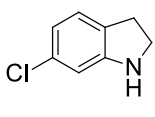
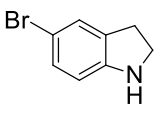
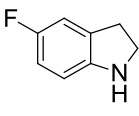
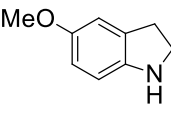
**Figure 6-13.** Same excess protocol for Variable time normalization analysis of substrate at 0<sup>th</sup> order for the acceptorless dehydrogenation of indoline (125 mM – green; 375 mM – red) using 1 mol% of complex **2-3** at 97 °C in anisole monitored by REACTIR

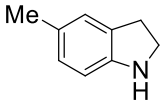
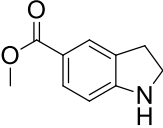
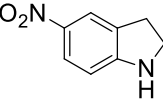
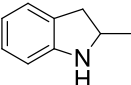
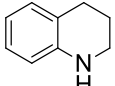
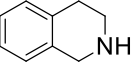


A substrate screen of functionalized indoline derivatives was performed using complex **3-1a** to test the functional group tolerance for acceptorless dehydrogenation. The substituents can alter the electronic properties of the amine and the donor ability of the hydridic C-H of indoline. Therefore, the effects of electron donating and withdrawing groups can be studied for mechanistic insight. Substrates were initially reacted at 1 mol% under standard conditions. Altering the position of a Cl group from 4, 5, and 6 resulted in drastic conversion differences (5%, 43% and 15%, respectively; Table 6-1, Entries 1a, 2a, 3a). Therefore, substrates with electron withdrawing groups in the 4- and 6-positions are more difficult than the 5-position. Increasing the temperature to 125 °C in a closed system did cause an increase in conversion, but did not result in full conversion (Table 6-1, Entries 1b, 2b and 3b). An open system was employed to allow H<sub>2</sub> release in case an equilibrium exists between H<sub>2</sub> binding and release for the Ru complex (**3-2a**). Use of an open system to release H<sub>2</sub> pressure did not cause a significant increase in conversion (Table 6-1, Entries 1c, 2c, 3c). Functional groups para to the amine of the substrate have a stronger effect than functional groups in the meta position due to resonance. Other substrates with functional groups on the phenyl ring at the 5-position (para to the nitrogen) were therefore attempted. With other halogen substituents, a greater amount of product was produced at 110 °C than with the 5-Cl substituent (5-Br = 84%; 5-F = 58%; Entry 4-5). Increasing the temperature to 125 °C within a closed system did not result in a significantly higher conversion in a closed system (5-Br = 79%, 5-F = 63%). In an open system at 125 °C, the substituted 5-F indole was produced almost quantitatively (98%). The 5-Br indoline was fully consumed at 125 °C in both the open and closed systems. However, in an open system only 30% of 5-Br indole was produced. Two new unidentified species were also present as detected by GC-FID that were not present under milder conditions. Use of substituents such as 5-MeO and 5-Me produced adequate amounts of indole product at 110 °C (5-MeO = 44%; 5-Me = 51%; Table 6-1, Entry 6-7). Increasing the temperature to 125 °C resulted in very good to excellent yields (80–99%) in open or closed systems. Use of electron-withdrawing substituents such as 5-COOMe and 5-NO<sub>2</sub> resulted in poor yields (3-16%) at 110 or 125 °C under open or closed conditions (Entry 8-9). A sterically encumbered substrate would be challenging for an inner-sphere mechanism as the deprotonation and binding would become more difficult. Increasing the sterics at the 2 position was achieved through use of 2-Me. This sterically challenging substrate produced 43% after 24 h at 110 °C in anisole (Table 6-1, Entry 10). Increasing the temperature to 125 °C under closed conditions increased the conversion to 50% after 4 h. Use of an open vessel improved the conversion to 79%. Six membered *N*-heterocycles were also attempted using tetrahydroquinoline and

tetrahydroisoquinoline. However, at 110 °C and 125 °C in a closed and open system, only trace amounts of substrate were consumed (Entry 11-12). Further work is needed to develop catalysts to perform acceptorless dehydrogenation of larger rings.

**Table 6-1. Substrate comparison to understand the effects of steric and electronic effects for substituted indolines<sup>a</sup>**

Entry	Substrate	Method	Time (h)	Conv. (%)
1a	 4-Cl	A	24	5
1b		B	24	31
1c		C	24	31
2a	 5-Cl	A	24	43
2b		B	12	51
2c		C	12	67
3a	 6-Cl	A	24	15
3b		B	18	11
3c		C	18	11
4a	 5-Br	A	24	84
4b		B	4	79 <sup>b</sup>
4c		C	4	30 <sup>b</sup>
5a	 5-F	A	24	58
5b		B	24	63
5c		C	24	98
6a	 5-MeO	A	24	44
6b		B	25	99
6c		C	25	89
7a		A	24	51

7b	 5-Me	B	3	80
7c		C	3	88
8a	 5-COOMe	A	24	16
8b		B	4.5	9
8c		C	4.5	16
9a	 5-NO <sub>2</sub>	A	24	6
9b		B	16	7
9c		C	16	3
10a	 2-Me	A	24	43
10b		B	4	50
10c		C	4	79
11a		A	24	0
11b		B	2	trace
11c		C	2	trace
12a		A	24	0
12b		B	12	7
12c		C	12	7

(a) Reactions were performed in replicate (+/- 5%) using 1 mol% **3-2a** in anisole with substrate (250 mM) and tetralin (100 mM) as an internal standard and monitored by GC-FID. Method A operated at 110 °C under closed conditions. Method B operated at 125 °C under closed conditions. Method C operated at 125 °C under open conditions. (b) Full consumption of starting material was observed.

## 6.3 Conclusion

A catalyst comparison of the steric and electronic properties of the primary and secondary coordination spheres for acceptorless dehydrogenation was undertaken. Systematic changes to the primary coordination sphere showed an increase in conversion as the steric environment of the R group of the  $P^{R_2}N^{R'_2}$  ligand is increased. However, increasing the electron density and steric bulk of the Ru centre through use of a Cp\* analogue resulted in poor reactivity. Further studies are needed to deconvolute the steric environment of the open site and electronics of the metal centre. Changing the properties of the secondary coordination sphere resulted in a Goldilocks situation where the pendent amine operates best at a basicity similar to the substrate. Increasing or decreasing the  $pK_a$  of the pendent amine renders the proton shuttling moiety less effective and thus limits turnovers. Additionally, increasing the steric bulk of the proton shuttling moiety is detrimental.

A comparison of the number of pendent amines present (0-2) on the bis(phosphine) ligand revealed  $[Ru(Cp)(P^{Ph_2}N^{Ph_2})(NCCH_3)]PF_6$  (**3-2a**), which has two pendent amines, to be best catalyst. Additionally, MLC complex (**3-2a**) operates at a faster rate and lower temperatures than a non-MLC  $[Ru(Cp)(dppp)(NCCH_3)]PF_6$  complex (**2-3**). Variable time normalization analysis was used to investigate the reaction order of substrate and catalyst during the rate-determining step to help differentiate mechanistic pathways. Ru- $(P^{Ph_2}N^{Ph_2})$  catalyst (**3-1a**) for acceptorless dehydrogenation of indoline behaves in a first order manner for both catalyst and substrate. Therefore, the rate-determining step proceeds through an outer-sphere concerted MLC pathway. Ru-(dppp) catalyst (**2-3**) similarly operates in a first order manner for catalyst. Parsing out the reaction order for indoline reveals the substrate is not facilitating proton transfer. An alternative mechanism is proposed in which the bisphosphine ligand is hemilabile. This hemilability results in the phosphine performing the proton transfer steps. Additionally, due to the necessity for the phosphine to be hemilabile, indoline displaces the bisphosphine resulting in catalyst inhibition. Further studies are needed to confirm the concerted outer-sphere mechanistic pathway for **3-2a** and fully elucidate the mechanistic pathway for **2-3**.

The different substituents on indoline was investigated to understand the effects of altering the steric and electronic properties of the substrate on acceptorless dehydrogenation. Electron-donating and neutral substituents did not effect overall reactivity resulting in high yields of indoles being produced. Electron-withdrawing groups resulted in a significant decrease in catalyst activity. Increasing the sterics

of the carbon adjacent to the N (2-Me) had little impact compared to methylation of the 5 position (79 vs. 88%).

## 6.4 Experimental

### 6.4.1 General Procedures, Materials and Instrumentation

All air/water-sensitive reactions were manipulated under N<sub>2</sub> using standard Schlenk or glovebox techniques unless otherwise stated. All glassware was oven dried prior to use. Indoline (>98%), and indole (99%) were obtained from Alfa Aesar. Pyrene (98%), tetrahydronaphthalene (99%), anisole (>99.7% anhydrous), bis(diphenylphosphino)methane (97%), bis(diphenylphosphino)benzene (97%), bis(diphenylphosphino)propane (97%), tetrahydroisoquinoline (98%), and 5-chloroindoline were obtained from Sigma-Aldrich. Chloroform-*d* (99.8%) were obtained from Cambridge Isotope Laboratories. 4-Chloroindoline (>95%), 4-chloroindole (95%), 5-chloroindole (95%), 6-chloroindoline (95%), 6-chloroindole (98%), 5-fluoroindoline (97%), 5-fluoroindole (97%), 5-bromoindoline (>95%), 5-bromoindole (98%), 5-methoxyindoline (95%), 5-methoxyindole (99%), 5-methylindoline (95%), 5-methylindole (98%), 5-nitroindoline (95%), 5-nitroindole (98%), methyl 5-indoline carboxylate (xx%), methyl 5-indole carboxylate (98%), 2-methylindoline (98%), 2-methylindole (>98%), tetrahydroquinoline (99%), quinoline (98%), and isoquinoline (97%) were obtained from Oakwood Chemicals. [Ru(Cp)(MeCN)<sub>3</sub>]PF<sub>6</sub>, [Ru(Cp\*)(MeCN)<sub>3</sub>]PF<sub>6</sub>, [Ru(Cp)(P<sup>Ph</sup><sub>2</sub>N<sup>R'</sup><sub>2</sub>)(NCCH<sub>3</sub>)]PF<sub>6</sub> (R' = Bn, Ph, *p*-CF<sub>3</sub>-C<sub>6</sub>H<sub>4</sub>, *p*-CH<sub>3</sub>O-C<sub>6</sub>H<sub>4</sub>, Mes), [Ru(Cp)(P<sup>tBu</sup><sub>2</sub>N<sup>Bn</sup><sub>2</sub>)(NCCH<sub>3</sub>)]PF<sub>6</sub>, [Ru(Cp\*)(P<sup>Ph</sup><sub>2</sub>N<sup>Bn</sup><sub>2</sub>)(NCCH<sub>3</sub>)]PF<sub>6</sub> in situ generation of [Ru(Cp)(P<sup>Bn</sup><sub>2</sub>N<sup>Bn</sup><sub>2</sub>)(NCCH<sub>3</sub>)]PF<sub>6</sub>, P<sup>Ph</sup><sub>2</sub>N<sup>Bn</sup><sub>2</sub> were synthesized following literature procedures. (Kundig 2004 Adv. Synth. Catal.; Stubbs Dalton, Bow, DuBois OM 2010, Kubiak OM 2012). Dry and degassed diethyl ether, and acetonitrile (MeCN) were obtained from an Innovative Technology 400-5 Solvent Purification System and stored under N<sub>2</sub>. Diethyl was stored over 4 Å molecular sieves (Fluka and activated at 150 °C for over 12 h). Substrates received under air were degassed prior to use. All other chemicals were used as received.

Charge-transfer Matrix Assisted Laser Desorption/Ionization (MALDI) mass spectrometry data were collected on an AB Sciex 5800 TOF/TOF mass spectrometer using pyrene as the matrix in a 20:1 molar ratio to metal complex. Samples were spotted on the target plate as solutions in DCM. All NMR spectra were recorded on a Bruker 400 MHz instrument. <sup>1</sup>H and <sup>13</sup>C spectra acquired in CDCl<sub>3</sub> were referenced

internally against the residual solvent signal ( $\text{CHCl}_3$ ) to TMS at 0 ppm.  $^{31}\text{P}$  spectra were referenced externally to 85% phosphoric acid at 0.00 ppm. Quantification of catalytic reactivity was achieved using an Agilent 7890a gas chromatography with a flame ionization detector (GC-FID), fitted with a HP-5 column. The amount of each species was quantified, relative to tetrahydronaphthalene, using area counts corrected with the response factors. Reaction profiles were monitored in situ using a Toledo-Mettler ReactIR 15 with a silicon probe.

#### 6.4.2 General Procedure for In Situ Synthesis of $[\text{Ru}(\text{Cp}/\text{Cp}^*)(\text{PP})(\text{NCCH}_3)]\text{PF}_6$ (6-1a,c, and 6-2)

To a 100 mL Schlenk flask with a stir bar,  $[\text{Ru}(\text{Cp}/\text{Cp}^*)(\text{NCCH}_3)_3]\text{PF}_6$  (1 equiv., 5 mM), ligand P-P (1.05 equiv., 5 mM) and acetonitrile (20 mL) was added. The flask was heated to 65 °C for 4 hours with stirring. The solvent was removed under vacuum and the remaining solid was triturated with pentane ( $3 \times 2$  mL). Acetonitrile (2 mL) was added and the resulting suspension was filtered. The solid was washed with acetonitrile until the washings were colourless. The solvent volume of the filtrate was reduced under vacuum to ca. 0.5 mL and diethyl ether (5 mL) was added to precipitate the product. The solvent was decanted off and the product was dried under vacuum.

**$[\text{Ru}(\text{Cp})(\text{dppm})(\text{NCCH}_3)]\text{PF}_6$  (6-1a):** Yield: 86%.  $^1\text{H}$  NMR (400 MHz,  $\text{CDCl}_3$ )  $\delta$ : 7.75-7.60 (m,  $\text{C}_{\text{Ar}}\text{-H}$ , 3H), 7.54-7.11 (m,  $\text{C}_{\text{Ar}}\text{-H}$ , 17H), 5.32-4.43 (m, Cp-H, 5H), 2.81 (s  $\text{NCCH}_3$ , 3H), 1.70 (t,  $\text{PCH}_2\text{P}$ , 2H).  $^{31}\text{P}\{^1\text{H}\}$  NMR (162 MHz,  $\text{CDCl}_3$ )  $\delta$ : 10.1 (s,  $\text{PPh}_2$ ), -144.2 (sept,  $^1\text{J}_{\text{P-F}} = 711.2$  Hz,  $\text{PF}_6$ ).  $^{13}\text{C}\{^1\text{H}\}$  NMR (101 MHz,  $\text{CDCl}_3$ )  $\delta$ : 135.7 (dd,  $^1\text{J}_{\text{C-P}} = 22.6$  Hz,  $\text{C}_{\text{Ar}}$ ), 132.9 (dd,  $^2\text{J}_{\text{C-P}} = 9.7$  Hz,  $\text{C}_{\text{Ar}}$ ), 132.5 (dd,  $^3\text{J}_{\text{C-P}} = 6.0$  Hz,  $\text{C}_{\text{Ar}}$ ), 131.4 (s,  $\text{C}_{\text{Ar}}$ ), 131.1 (s,  $\text{C}_{\text{Ar}}$ ), 131.0 (s,  $\text{C}_{\text{Ar}}$ ), 130.9 (s,  $\text{C}_{\text{Ar}}$ ), 130.9 (s,  $\text{C}_{\text{Ar}}$ ), 129.2 (dd,  $^3\text{J}_{\text{C-P}} = 5.7$  Hz,  $\text{C}_{\text{Ar}}$ ), 128.8 (dd,  $^3\text{J}_{\text{C-P}} = 3.9$  Hz,  $\text{C}_{\text{Ar}}$ ), 128.8 (s,  $\text{C}_{\text{Ar}}$ ), 128.5 (t,  $^3\text{J}_{\text{C-P}} = 3.6$  Hz,  $\text{C}_{\text{Ar}}$ ), 128.3 (s, CN-Ru), 130.9 (s,  $\text{C}_{\text{Ar}}$ ), 80.2 (s, Cp), 49.9 (t,  $^1\text{J}_{\text{C-P}} = 23.1$  Hz, P- $\text{CH}_2$ -P), 3.6 (s, Ru-NC- $\text{CH}_3$ ). MALDI MS (pyrene matrix): Calc. m/z 551.1  $[\text{Ru}(\text{Cp})(\text{dppm})]^+$ , Obs. m/z 551.1.

**$[\text{Ru}(\text{Cp})(\text{dpbz})(\text{NCCH}_3)]\text{PF}_6$  (6-1c):** Yield: 57%.  $^1\text{H}$  NMR (400 MHz,  $\text{CDCl}_3$ )  $\delta$ : 7.63-7.58 (m,  $\text{C}_{\text{Ar}}\text{-H}$ , 3H), 7.53-7.35 (m,  $\text{C}_{\text{Ar}}\text{-H}$ , 18H), 7.29-7.20 (m,  $\text{C}_{\text{Ar}}\text{-H}$ , 3H), 4.64 (s, Cp-H, 5H).  $^{31}\text{P}\{^1\text{H}\}$  NMR (162 MHz,  $\text{CDCl}_3$ ). MALDI MS (pyrene matrix): Calc. m/z 613.1  $[\text{Ru}(\text{Cp})(\text{dpbz})]^+$ , Obs. m/z 613.1.

**$[\text{Ru}(\text{Cp}^*)(\text{dppp})(\text{NCCH}_3)]\text{PF}_6$  (6-2):** Yield: 89%.  $^1\text{H}$  NMR (400 MHz,  $\text{CDCl}_3$ )  $\delta$ : 7.51-7.39 (m,  $\text{C}_{\text{Ar}}\text{-H}$ , 8H), 7.38-7.24 (m,  $\text{C}_{\text{Ar}}\text{-H}$ , 8H), 7.24-7.17 (m,  $\text{C}_{\text{Ar}}\text{-H}$ , 4H), 2.69 (t,  $^4\text{J}_{\text{H-P}} = 1.2$  Hz,  $\text{NCCH}_3$ , 3H), 1.70 (t,  $\text{PCH}_2\text{P}$ , 2H), 2.65-2.50 (m, P- $\text{CHH}'$ , 2H), 2.30 (t,  $^3\text{J}_{\text{H-P}} = 12.8$  Hz, P- $\text{CHH}'$ , 2H), 1.68-1.50 (m, P-

CH<sub>3</sub>H, 2H), 1.30 (t, <sup>4</sup>J<sub>H-P</sub> = 1.6 Hz, Cp-CH<sub>3</sub>, 15H). <sup>31</sup>P{<sup>1</sup>H} NMR (162 MHz, CDCl<sub>3</sub>) δ: 19.0 (s, PPh<sub>2</sub>), -144.3 (sept, <sup>1</sup>J<sub>P-F</sub> = 711.18 Hz, PF<sub>6</sub>). <sup>13</sup>C{<sup>1</sup>H} NMR (101 MHz, CDCl<sub>3</sub>) δ: 133.9 (t, J = 6.1 Hz, C<sub>Ar</sub>), 131.9 (t, J = 5.1 Hz, C<sub>Ar</sub>), 130.5 (s, C<sub>Ar</sub>), 130.3 (s, C<sub>Ar</sub>), 128.7 (t, J = 6.06 Hz, C<sub>Ar</sub>), 128.6 (s, Ru-NC), 128.2 (t, J = 5.1 Hz, C<sub>Ar</sub>), 92.4 (s, Cp), 60.1 (P-CH<sub>2</sub>-P), 48.1 (P-CH<sub>2</sub>-P), 9.6 (s, Cp-CH<sub>3</sub>), 4.2 (s, Ru-NC-CH<sub>3</sub>). MALDI MS (pyrene matrix): Calc. m/z 649.2 [Ru(Cp\*)(dppp)]<sup>+</sup>, Obs. m/z 649.2.

### 6.4.3 Synthesis of [Ru(Cp)(P<sup>Me</sup><sub>2</sub>N<sup>Bn</sup><sub>2</sub>)(NCMe)]PF<sub>6</sub>

[Ru(Cp)(NCMe)<sub>3</sub>]PF<sub>6</sub> (257 mg, 0.592 mmol, 1 equiv.) and P<sup>Me</sup><sub>2</sub>N<sup>Bn</sup><sub>2</sub> (213 mg, 0.595 mmol, 1 equiv.) were combined in a 100 mL Schlenk flask with acetonitrile (10 mL) and heated at 70 °C for 4 h. A bright orange solution formed. The solvent was removed under vacuum to afford an orange powder. Yield: 414 mg (98%). <sup>1</sup>H NMR (400 MHz, acetone-*d*<sub>6</sub>) δ: 7.82-7.23 (m, Ph-*H*, 10H), 4.88 (s, Cp-*H*, 5H), 4.03 (s, NCH<sub>2</sub>Ph, 2H), 3.76 (s, NCH<sub>2</sub>Ph), 3.41 (m, CH<sub>3</sub>P, 6H), 3.17 (m, NCH<sub>2</sub>P, 4H), 2.97 (m, NCH<sub>2</sub>P, 4H), 2.43 (s, RuCNCH<sub>3</sub>, 3H). <sup>31</sup>P{<sup>1</sup>H} NMR (162 MHz, acetone-*d*<sub>6</sub>) δ: 39.2 (s, RuP), -144.2 (sept, <sup>1</sup>J<sub>P-F</sub> = 707 Hz, PF<sub>6</sub>). <sup>13</sup>C{<sup>1</sup>H} NMR (101 MHz, CDCl<sub>3</sub>) δ: 138.5 (s, CH<sub>2</sub>(Ph-C)), 137.8 (s, CH<sub>2</sub>(Ph-C)), 132.6, 131.8, 130.5, 129.8, 129.3, and 128.5 (s, Ph-C), 129.0 (s, RuCNCH<sub>3</sub>), 82.2 (s, Cp), 65.7 (s, NCH<sub>2</sub>Ph), 64.9 (s, NCH<sub>2</sub>Ph), 53.1 (NCH<sub>2</sub>P), 52.5 (NCH<sub>2</sub>P), 52.3 (CH<sub>3</sub>P), 4.2 (s, CH<sub>3</sub>CN). \*This species would convert to another under mild conditions in solvent (quickly) and as a solid (slowly).

### 6.4.4 General Procedure for the Catalytic Cyclization of Substrates under Closed Conditions

A representative procedure is given for one substrate. In a glovebox, the following stock solutions were prepared: 4-chloroindoline (77 mg, 0.50 mmol, 1.00 M) and tetrahydronaphthalene (26 mg, 0.2 mmol, 0.4 M) in anisole (0.50 mL); **3-1a** (10 mg, 0.011 mmol, 5 mM) in anisole (2.20 mL). In a 4 mL vial containing a stir bar, the substrate/tetrahydronaphthalene stock solution (125 μL, 4-chloroindoline) and additional anisole (125 μL). To the vial, **3-1a** stock solution (250 μL) was added giving a final volume of 500 μL. The final concentrations for all the vial were 0.250 M in substrate and 2.5 mM in catalyst. A final vial was charged with substrate/internal standard stock solution (100 μL) for use as the time = 0 sample, required for accurate quantification of substrate and product. The vial was tightly capped under N<sub>2</sub>, electrical taped, and removed from the glove box and heated to 110 °C with stirring. After 24 hours all the vial was removed from the heat, cooled, and exposed to air to quench. A 40 μL aliquot was diluted to 10 mM (960 μL) in acetonitrile and analyzed by GC-FID. A 10 μL aliquot of the T<sub>0</sub> sample was diluted with acetonitrile (990 μL) and analyzed by GC-FID.

### 6.4.5 General Procedure for the Catalytic Cyclization of Substrates under Open Conditions

A representative procedure is given for one substrate. In a glovebox, the following stock solutions were prepared: 4-chloroindoline (77 mg, 0.50 mmol, 1.00 M) and tetrahydronaphthalene (26 mg, 0.2 mmol, 0.4 M) in anisole (0.50 mL); **3-1a** (10 mg, 0.011 mmol, 5 mM) in anisole (2.20 mL). To a 100 mL Schlenk tube containing a stir bar, the substrate/tetrahydronaphthalene stock solution (200  $\mu$ L, 4-chloroindoline) and additional anisole (200  $\mu$ L). To the 100 mL Schlenk tube, **3-1a** stock solution (400  $\mu$ L) was added giving a final volume of 800  $\mu$ L. The final concentrations for the Schlenk tube were 0.250 M in substrate and 2.5 mM in catalyst. A final vial was charged with substrate/internal standard stock solution (100  $\mu$ L) for use as the time = 0 sample, required for accurate quantification of substrate and product. The Schlenk tube was removed from the glove box and put under a flow of N<sub>2</sub>. Following set up of the ReactIR and an initial IR spectrum, the Schlenk tube was heated to 125 °C with stirring. After 24 hours, the Schlenk tube was removed from the heat, cooled, and exposed to air to quench. A 40  $\mu$ L aliquot was diluted to 10 mM (960  $\mu$ L) in acetonitrile and analyzed by GC-FID. A 10  $\mu$ L aliquot of the T<sub>0</sub> sample was diluted with acetonitrile (990  $\mu$ L) and analyzed by GC-FID.

### 6.4.6 High Throughput Catalytic Procedure

A representative procedure is given for indoline. In a glovebox, the following stock solutions were prepared: indoline (634 mg, 5.32 mmol, 0.500 M) and tetrahydronaphthalene (246 mg, 1.86 mmol, 0.175 M) in anisole (10.64 mL). Stock solutions of catalysts (15 mM and 2.5 mM) were prepared as above. Reaction components were added to a cooled (0 °C) 8  $\times$  12 reaction plate in the following order: catalyst, solvent, then substrate. Stock solutions of catalysts were robotically dispensed to their appropriate concentration amounts: 0.25, 1.25, 2.50, and 7.50 mM (0.1, 0.5, 1, 3 mol%). Solvent and substrate were added by Eppendorf pipette to the well plate and to a T<sub>0</sub> sample. Final conditions: 250 mM Substrate, 0.1/0.5/1/3 mol% catalyst, 100  $\mu$ L reaction volume in anisole. The 96 well plate was sealed with a Teflon sheet, a rubber sheet and an aluminium cover, to minimize evaporation, and the plate was heated to 110 °C for 24 h. After the plate had cooled, the solutions were daughtered into a second plate and diluted to 2.5 mM (based on the starting concentration of indoline) in acetonitrile for GC-FID analysis. A 10  $\mu$ L aliquot of the T<sub>0</sub> sample was diluted with acetonitrile (990  $\mu$ L) and analyzed by GC-FID.



## 6.4.7 General Procedure for Variable Time Normalization Analysis

A representative procedure is given for a run. In a glovebox, the following stock solutions were prepared: indoline (120 mg, 1.00 mmol, 0.500 M) and tetrahydronaphthalene (46 mg, 0.35 mmol, 0.18 M) in anisole (2.00 mL). A stock solution of **3-1a** (10 mg, 0.012 mmol, 15 mM) in anisole (0.83 mL) was prepared. A 100 mL Schlenk tube was charged with 0.75 mL of indoline stock solution, 0.25 mL of **3-1a** stock solution, and 0.50 mL of anisole. The final concentrations for this set of conditions were indoline at 250 mM, and **3-1a** at 2.5 mM (1 mol%) in 1.50 mL of anisole. The Schlenk tube was removed from the glovebox and setup on a Schlenk line under a flow of N<sub>2</sub>. The pre-zeroed silicon probe of the REACTIR and the reaction was started with a scan rate of 1 scan per 15 seconds. After 1 minute, the reaction was immersed into a pre-heated oil bath with a thermometer (not a thermocouple) and wavenumbers of interest monitored until completion. At completion, the Schlenk tube was removed from the oil bath and left to cool. A 40 µL aliquot was diluted to 10 mM (960 µL) in acetonitrile and analyzed by GC-FID. A 10 µL aliquot of the T<sub>0</sub> sample (stock solution of indoline) was diluted with acetonitrile (990 µL) and analyzed by GC-FID.

## 6.5 References

1. Gunanathan, C.; Milstein, D., *Science* **2013**, *341*, 1229712.
2. Chen, B.; Wang, L.; Gao, S., *ACS Catal.* **2015**, *5*, 5851-5876.
3. Spasyuk, D.; Vicent, C.; Gusev, D. G., *J. Am. Chem. Soc.* **2015**, *137*, 3743-3746.
4. Grotjahn, D. B.; Lev, D. A., *J. Am. Chem. Soc.* **2004**, *126*, 12232-12233.
5. O'Hagan, M.; Ho, M.-H.; Yang, J. Y.; Appel, A. M.; DuBois, M. R.; Raugei, S.; Shaw, W. J.; DuBois, D. L.; Bullock, R. M., *J. Am. Chem. Soc.* **2012**, *134*, 19409-19424.
6. Zuo, W.; Morris, R. H., *Nat. Protoc.* **2015**, *10*, 241.
7. Khusnutdinova, J. R.; Milstein, D., *Angew. Chem. Int. Ed.* **2015**, *54*, 12236-12273.
8. Crabtree, R. H., *New J. Chem.* **2011**, *35*, 18-23.
9. Noyori, R.; Yamakawa, M.; Hashiguchi, S., *J. Org. Chem.* **2001**, *66*, 7931-7944.
10. Muthaiah, S.; Hong, S. H., *Adv. Synth. Catal.* **2012**, *354*, 3045-3053.
11. Grotjahn, D. B., *Chem. Eur. J.* **2005**, *11*, 7146-7153.
12. O'Hagan, M.; Shaw, W. J.; Raugei, S.; Chen, S.; Yang, J. Y.; Kilgore, U. J.; DuBois, D. L.; Bullock, R. M., *J. Am. Chem. Soc.* **2011**, *133*, 14301-14312.
13. Varela-Fernández, A.; González-Rodríguez, C.; Varela, J. A.; Castedo, L.; Saá, C., *Org. Lett.* **2009**, *11*, 5350-5353.
14. Varela-Fernández, A.; Varela Jesús, A.; Saá, C., *Adv. Synth. Catal.* **2011**, *353*, 1933-1937.

15. Varela-Fernandez, A.; Varela, J. A.; Saá, C., *Synthesis* **2012**, *44*, 3285-3295.
16. Sandoval, C. A.; Ohkuma, T.; Muñiz, K.; Noyori, R., *J. Am. Chem. Soc.* **2003**, *125*, 13490-13503.
17. Morris, R. H., *Acc. Chem. Res.* **2015**, *48*, 1494-1502.
18. Samec, J. S. M.; Backvall, J.-E.; Andersson, P. G.; Brandt, P., *Chem. Soc. Rev.* **2006**, *35*, 237-248.
19. Himeda, Y.; Onozawa-Komatsuzaki, N.; Sugihara, H.; Kasuga, K., *Organometallics* **2007**, *26*, 702-712.
20. Onishi, N.; Xu, S.; Manaka, Y.; Suna, Y.; Wang, W.-H.; Muckerman, J. T.; Fujita, E.; Himeda, Y., *Inorg. Chem.* **2015**, *54*, 5114-5123.
21. Stubbs, J. M.; Chapple, D. E.; Boyle, P. D.; Blacquiere, J. M., *ChemCatChem* **2018**, *10*, 3694-3702.
22. Spasyuk, D.; Smith, S.; Gusev, D. G., *Angew. Chem. Int. Ed.* **2012**, *51*, 2772-2775.
23. Zell, T.; Milstein, D., *Acc. Chem. Res.* **2015**, *48*, 1979-1994.
24. Tseng, K. N. T.; Szymczak, N. K., *Synlett* **2014**, *25*, 2385-2389.
25. Wang, Q.; Chai, H.; Yu, Z., *Organometallics* **2018**, *37*, 584-591.
26. Dutta, I.; Yadav, S.; Sarbajna, A.; De, S.; Hölscher, M.; Leitner, W.; Bera, J. K., *J. Am. Chem. Soc.* **2018**, *140*, 8662-8666.
27. Werkmeister, S.; Neumann, J.; Junge, K.; Beller, M., *Chem. Eur. J.* **2015**, *21*, 12226-12250.
28. Tseng, K.-N. T.; Kampf, J. W.; Szymczak, N. K., *ACS Catal.* **2015**, *5*, 5468-5485.
29. Noyori, R., *Angew. Chem. Int. Ed.* **2002**, *41*, 2008-2022.
30. Guan, H.; Iimura, M.; Magee, M. P.; Norton, J. R.; Janak, K. E., *Organometallics* **2003**, *22*, 4084-4089.
31. He, L.-P.; Chen, T.; Gong, D.; Lai, Z.; Huang, K.-W., *Organometallics* **2012**, *31*, 5208-5211.
32. Gu, X.-Q.; Chen, W.; Morales-Morales, D.; Jensen, C. M., *J. Mol. Cat. A: Chem.* **2002**, *189*, 119-124.
33. Tseng, K.-N. T.; Rizzi, A. M.; Szymczak, N. K., *J. Am. Chem. Soc.* **2013**, *135*, 16352-16355.
34. Prades, A.; Peris, E.; Albrecht, M., *Organometallics* **2011**, *30*, 1162-1167.
35. Stubbs, J. M.; Hazlehurst, R. J.; Boyle, P. D.; Blacquiere, J. M., *Organometallics* **2017**, *36*, 1692-1698.
36. Tronic, T. A.; Kaminsky, W.; Coggins, M. K.; Mayer, J. M., *Inorg. Chem.* **2012**, *51*, 10916-10928.
37. Tronic, T. A.; Rakowski DuBois, M.; Kaminsky, W.; Coggins, M. K.; Liu, T.; Mayer, J. M., *Angew. Chem. Int. Ed.* **2011**, *50*, 10936-10939.
38. Burés, J., *Angew. Chem. Int. Ed.* **2016**, *55*, 2028-2031.

39. Burés, J., *Angew. Chem. Int. Ed.* **2016**, *55*, 16084-16087.
40. Baxter, R. D.; Sale, D.; Engle, K. M.; Yu, J.-Q.; Blackmond, D. G., *J. Am. Chem. Soc.* **2012**, *134*, 4600-4606.
41. Allman, T.; Goel, R. G., *Can. J. Chem.* **1982**, *60*, 716-722.
42. Kilgore, U. J.; Roberts, J. A. S.; Pool, D. H.; Appel, A. M.; Stewart, M. P.; DuBois, M. R.; Dougherty, W. G.; Kassel, W. S.; Bullock, R. M.; DuBois, D. L., *J. Am. Chem. Soc.* **2011**, *133*, 5861-5872.

## 7 Summary, Conclusion and Future Work

### 7.1 Summary and Conclusion

A family of metal-ligand cooperative (MLC) catalysts were synthesized to achieve the primary goal of developing structure-activity relationships for MLC reactions. Systematic structural derivatives allowed for a comparison of the properties of the primary and secondary coordination spheres. These MLC complexes have been utilized for 1) intramolecular cyclization of 2-ethynylbenzyl alcohol and 2-ethynylaniline and derivatives; and 2) acceptorless dehydrogenation of benzylamine and indoline.

In chapter two, the first successful application of the  $P^{R_2}N^{R'_2}$  ligand family toward an organic transformation is described. The cationic pre-catalysts  $[Ru(Cp)(P^{R_2}N^{Bn_2})(NCMe)]PF_6$  ( $R = t\text{-Bu}$  – **2-1a**; and  $Ph$  – **2-1b**) exhibit better performance at lower temperatures than the previous generation of proton transfer catalysts for 2-ethynylbenzyl alcohol. A control complex ( $[Ru(Cp)(dppp)(NCMe)]PF_6$  (**2-3**) lacking an acid/base site was synthesized. Comparison of the  $Ru-(P^{R_2}N^{R'_2})$  and  $Ru-(dppp)$  complexes under similar conditions showed the control complex exhibited no catalytic activity confirming the cooperative nature of the MLC  $P^{R_2}N^{R'_2}$  ligand for heteroatom cyclization. However,  $Ru-(P^{R_2}N^{R'_2})$  catalysts were not tolerant of other 6-membered *O*-heterocycles and were limited to 2-ethynylbenzyl alcohol as more difficult oxygen based substrates required increased reaction temperatures to proceed. At higher temperatures a decrease in yield was observed. In situ  $^{31}P$   $\{^1H\}$  NMR revealed catalyst performance was limited by both low conscription of the pre-catalyst into the catalytic cycle and by competitive deactivation of a key vinylidene intermediate. Spectroscopic data for the deactivation species revealed similarities to the previously reported  $Ru$ -(vinyl ammonium) deactivation. Use of  $RuCl(Cp)(P^{tBu_2}N^{Bn_2})$  (**2-4**) with  $TIPF_6$  allowed full conscription of the pre-catalyst causing an increase in rate. However, overall conversion remained similar to the cationic MeCN analogue, **2-1a**.

In chapter three, a new series of  $Ru-(P^{R_2}N^{R'_2})$  derivatives ( $R = Ph$ ;  $R' = Ph$  – **3-2a**,  $Mes$  – **3-2b**,  $p\text{-CF}_3\text{-C}_6\text{H}_4$  – **3-2c**,  $p\text{-CH}_3\text{O-C}_6\text{H}_4$  – **3-2d**) and a  $Ru-(P^{Ph_2}N^{Ph_1})$  complex (**3-3**) were synthesized. These  $Ru-(P^{R_2}N^{R'_2})$  derivatives were found to be active for the cyclization of 2-ethynylaniline. In situ monitoring of the catalyst structure under catalytic conditions coupled with stoichiometric reactivity revealed no observable  $Ru$ -(vinyl ammonium) deactivation to occur. The steric environment around the pendent amine was evaluated by comparison of the catalytic performance for derivatives in which  $R'$  is varied,

Bn (**2-1b**), Ph (**3-2a**), and Mes (**3-2b**). Cyclization of 2-ethynylaniline showed that an increase in steric environment around the pendent amine was detrimental to reactivity, which suggests that the MLC proton transfer steps cannot be performed quickly. The electronic environment around the pendent amine was evaluated by comparison of the catalytic performance for derivatives in which R' is varied, derivatives Ph (**3-2a**), *p*-CF<sub>3</sub>-C<sub>6</sub>H<sub>4</sub> (**3-2c**), and *p*-CH<sub>3</sub>O-C<sub>6</sub>H<sub>4</sub> (**3-2d**). Cyclization of 2-ethynylaniline showed that a basicity threshold was required for optimal MLC proton transfer steps. The basicity threshold is substrate dependent but can be anticipated based on the p*K*<sub>a</sub> value of the substrate to the relative p*K*<sub>a</sub> of the conjugate acid of the pendent amine. Additionally, these Ru-(P<sup>Ph</sup><sub>2</sub>N<sup>R'</sup><sub>2</sub>) derivative were evaluated as catalysts for 2-ethynylbenzyl alcohol cyclization since an increased steric environment (R' = Mes: **3-2b**) or less nucleophilic pendent amine (R' = *p*-CF<sub>3</sub>-C<sub>6</sub>H<sub>4</sub>: **3-2c**) had the potential to limit catalyst deactivation. A similar trend, however, was observed for 2-ethynylbenzyl alcohol as for 2-ethynylaniline. At increased temperatures (70 °C), however, a longer lifetime was observed for Ru-(P<sup>Ph</sup><sub>2</sub>N<sup>R'</sup><sub>2</sub>) (R' = *p*-CF<sub>3</sub>-C<sub>6</sub>H<sub>4</sub>: **3-2c**) compared to other derivatives but minimal amounts of product were found in all cases (> 20%). Furthermore, a comparison of the benefit of one (**3-3**) and two (**3-1a**) acid/base sites was performed, which showed substantially better catalytic performance for two acid/base sites.

In chapter four, a series of Ru-(P<sup>R</sup><sub>2</sub>N<sup>R'</sup><sub>2</sub>) derivatives were synthesized to probe the steric and electronic properties of the primary coordination sphere (Cp, R: *t*-Bu – **2-1a**, Ph – **2-1b**, Bn – **4-1a**; or Cp\*, R = Ph: **4-2a**) while the secondary coordination sphere was kept constant (R' = Bn). The steric environment around the phosphine was evaluated by comparison of the catalytic performance for derivatives in which R' is varied, *t*-Bu (**2-1a**), Ph (**2-1b**), and Bn (**4-1a**). A Cyclization of 2-ethynylaniline showed that an increase in sterics to be beneficial (*t*-Bu > Ph > Bn). However, the optimal electronic effects of the phosphine and Cp/Cp\* remain unclear (*t*-Bu > Ph but Ph > Bn) suggesting the steric environment of the phosphines could be more important than the electronic effects. Additionally, Cp and Cp\* Ru-(P<sup>R</sup><sub>2</sub>N<sup>R'</sup><sub>2</sub>) derivatives were tested under catalytic conditions for the cyclization of 2-ethynylbenzyl alcohol in an attempt to overcome deactivation. The attempt resulted in similar structure-activity relationships as with 2-ethynylaniline with catalyst deactivation still evident. Combining the effects observed in chapter 3 and 4, conditions optimization was performed for the cyclization of 2-ethynylaniline utilizing Cp and Cp\* Ru-(P<sup>*t*Bu</sup><sub>2</sub>N<sup>Ph</sup><sub>2</sub>) catalyst analogues (**4-1b** and **4-2b**, respectively). Catalyst **4-2b** exhibits excellent reaction rates (TOF: >1600 h<sup>-1</sup>, TON: 330) while catalyst **4-1b** was shown to have excellent lifetime (TON: 802, TOF: 1500 h<sup>-1</sup>) at 70 °C reaching completion within 2 h.

Both complexes show superior activity compared to previous MLC catalytic systems (TON = 49, 70 °C, 7 h). A robustness screen was performed with a variety of additives using catalyst **4-1b** revealing a tolerance to additives with halides, carboxylic acids, esters, ketones, alcohols, amides, alkenes, and internal alkyne functional groups. Additionally, a substrate scope with different electronic properties *para* to the amine and alkyne was examined with **4-1b**. High catalytic performance of **4-1b** could be obtained at 0.5 or 1 mol%. Additionally, substituents *para* to the alkyne affected catalyst performance more than substituents *para* to the amine.

In chapter five,  $[\text{Ru}(\text{Cp})(\text{P}^{\text{Ph}}_2\text{N}^{\text{Bn}}_2)(\text{MeCN})]\text{PF}_6$  (**2-1b**) and  $[\text{Ru}(\text{Cp})(\text{dppp})(\text{MeCN})]\text{PF}_6$  (**2-3**) complexes were shown to be active for the acceptorless dehydrogenation of benzylamine ( $\text{BnNH}_2$ ) and *N*-heterocycles. The two catalysts exhibit similar catalytic performance (1 mol%, 110 °C, 48 h) but different selectivity for dehydrogenation products. Use of aniline additives further differentiates the two catalysts since use of strong aniline bases switches product selectivity with benzylamine for catalyst **2-3** but not for **2-1b**. Therefore, it is thought that  $\text{Ru}(\text{P}^{\text{Ph}}_2\text{N}^{\text{Bn}}_2)$  (**2-1b**) proceeds through an MLC mechanistic pathway while  $\text{Ru}(\text{dppp})$  (**2-3**) proceeds through an inner-sphere non-MLC pathway. Independent synthesis of a potential on-cycle  $[\text{Ru}(\text{Cp})(\text{P}^{\text{Ph}}_2\text{N}^{\text{Bn}}_2)(\text{NH}_2\text{Bn})]\text{PF}_6$  adduct reveals the presence of a hydrogen bond between the bound amine and the pendent base of the  $\text{P}^{\text{Ph}}_2\text{N}^{\text{Bn}}_2$  ligand. Preliminary mechanistic studies reveal the benzylamine adduct is not an on-cycle catalyst intermediate for the formation of the ADC product (*N*-benzyl-phenylimine) suggesting an outer-sphere MLC mechanistic pathway.

In chapter six, a catalyst comparison of  $\text{Ru}(\text{P}^{\text{R}}_2\text{N}^{\text{R}'_2})$ ,  $\text{Ru}(\text{P}^{\text{R}}_2\text{N}^{\text{R}'_1})$ , and  $\text{Ru}(\text{P}-\text{P})$  derivatives for catalytic acceptorless dehydrogenation of indoline was performed. The steric and electronic properties around the phosphine were evaluated by comparison of the catalytic performance for derivatives in which  $\text{R}'$  is varied, *t*-Bu (**2-1a**), Ph (**2-1b**), and Bn (**4-1a**). Acceptorless dehydrogenation of indoline showed an increase in reactivity as steric bulk was increased on the phosphine ( $\text{R} = t\text{-Bu} > \text{Ph} > \text{Bn}$ ). Comparing catalytic performance from an electronic viewpoint showed an inconsistent trend ( $\text{R} = t\text{-Bu} > \text{Bn} < \text{Ph}$ ). Furthermore, Cp and Cp\* analogues (**2-1b** and **4-2a**, respectively) were compared. Superior performance was observed with the less electron donating, and less sterically bulky, Cp ligand. The number of acid/base sites in the secondary coordination sphere (0-2) was compared with two acid/base sites outperforming the other catalysts (0-1 acid/base sites). Only having one acid/base site did not improve reactivity significantly over the non-MLC  $\text{Ru}(\text{dppp})$  **2-3** possibly due to ligand flexibility.

Non-MLC Ru-(P-P) ligands were also screened for catalyst optimization. However, **2-3** remained the best non-MLC catalyst. Additionally, the sterics ( $R' = \text{Bn, Ph, Mes}$ : **2-1b, 3-2a,b**, respectively) and basicity ( $R' = p\text{-CF}_3\text{-C}_6\text{H}_4, \text{Ph, } p\text{-CH}_3\text{O-C}_6\text{H}_4$ : **3-2c,a,d** respectively) of the pendent amine was investigated to understand the optimum factors for proton shuttling. While all the catalysts did work, the sterically bulky pendent amine ( $R' = \text{Mes}$ ) exhibited the lowest catalytic performance likely due to the inability of the pendent amine to perform the proton transfer steps. As the basicity of the acid/base site was altered, the catalytic performance showed a Goldilocks relationship ( $\text{Bn (TON: 66)} < p\text{-CH}_3\text{O-C}_6\text{H}_4 (140) < \text{Ph (162)} > p\text{-CF}_3\text{-C}_6\text{H}_4 (64)$ ) with the pendent amine at a similar  $pK_a$  of the conjugate acid of the substrate ( $pK_a [\text{Ru-NH}_2\text{Ph}]^+ \approx pK_a [\text{R}_2\text{NHPH}]^+$ ). Furthermore, mechanistic insight revealed a first order relationship for indoline and catalyst for Ru-( $\text{P}^{\text{Ph}}_2\text{N}^{\text{Ph}}_2$ ) **3-2a**. On the other hand, **2-3** was first order for catalyst and the order in substrate was complex. Deconvolution of the rate order for the substrate suggests a zeroth order relationship in indoline under steady state conditions. A non-MLC mechanistic pathway is extremely unlikely for Ru-( $\text{P}^{\text{Ph}}_2\text{N}^{\text{Ph}}_2$ ) (**3-2a**) due to the strong influence of pendent amine observed in catalyst performance. Therefore, Ru-( $\text{P}^{\text{Ph}}_2\text{N}^{\text{Ph}}_2$ ) (**3-2a**) likely proceeds through an outer-sphere MLC pathway. However, the mechanistic pathway for Ru-(dppp) (**2-3**) is still unclear and requires further mechanistic investigation to deduce a likely pathway.

Overall, the Ru-( $\text{P}^{\text{R}_2}\text{N}^{\text{R}'_2}$ ) complex family have been shown to dramatically increase catalytic performance compared to previous proton transfer catalysts for intramolecular alkyne heteroatom cyclization and acceptorless dehydrogenation of amines. Systematic tuning of the primary and secondary coordination sphere has enabled for catalyst structure-activity relationships to be made for these organic transformations. To obtain optimal performance in future proton-shuttling catalysis, one should consider the  $pK_a$  of substrate relative to the acid/base site for the given transformation. Additionally, the importance of sterically bulky phosphines within the primary coordination sphere reveals that the right orientation for the substrate-binding pocket could be key to promote facile proton transfer since the pendent amine and substrate would be in close proximity.

## 7.2 Future Work

Catalyst deactivation remains the main challenge before Ru-( $\text{P}^{\text{R}_2}\text{N}^{\text{R}'_2}$ ) complexes can be used widely for cyclization chemistry. Deactivation of the Ru-vinylidene intermediate by the pendent amine

limits a broader substrate scope and use of intermolecular nucleophiles. The nucleophilicity of the pendent amine needs to be decreased whilst the basicity remains similar to current proton shuttling catalysts. Next generation acid/base sites for proton transfer reactions should target amines that are less nucleophilic due to resonance such as amides or aminopyridines. Such groups should decrease the nucleophilicity of the pendent amine but retain the proton shuttling abilities.

Further optimization for acceptorless dehydrogenation is required for  $[\text{Ru}-(\text{P}^{\text{R}}_2\text{N}^{\text{R}'_2})]$  catalyst derivatives. Use of a sterically bulky mesityl-substituted phosphine could improve reactivity with indoline since sterically bulky phosphines were optimal. Additionally, most reported Ru catalysts possess a ruthenium hydride on the starting complex. The hydride ligand may accelerate reactivity as it would be an on-cycle catalytic species. Finally, further mechanistic insight is required to understand the potential outer-sphere MLC mechanism.



# Appendices

## Appendices A: Supplementary Information for Chapter 2

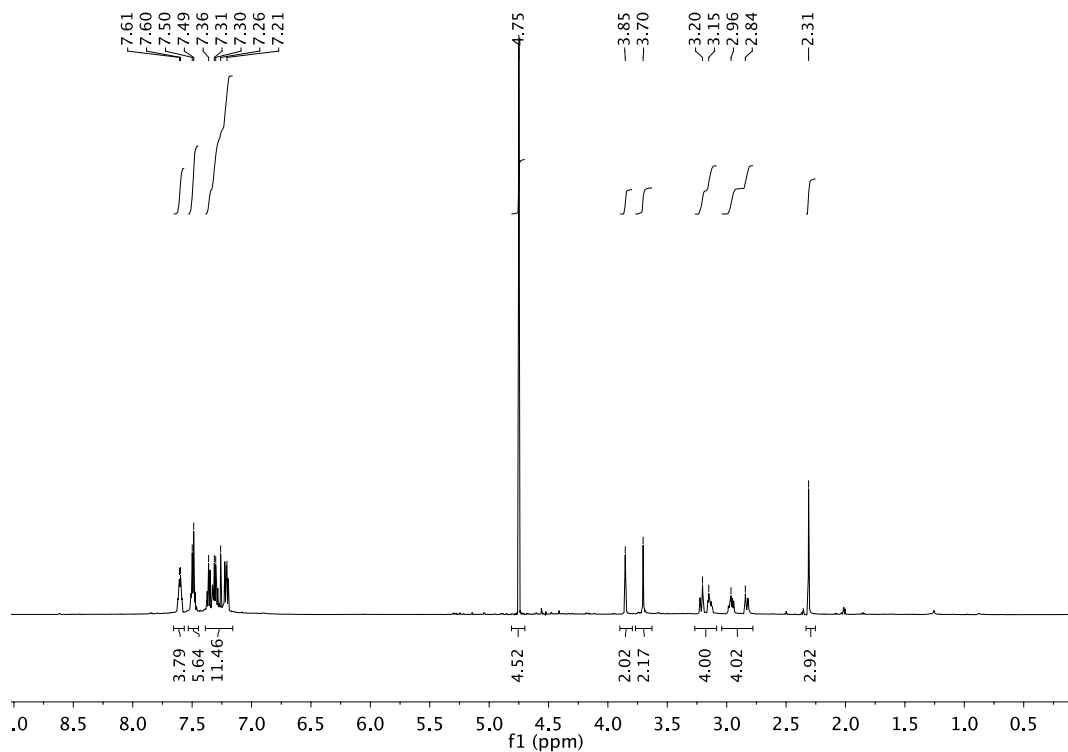


**Figure A-1.**  $^1\text{H}$  NMR spectrum of **2-1b** in  $\text{CDCl}_3$  (600 MHz).

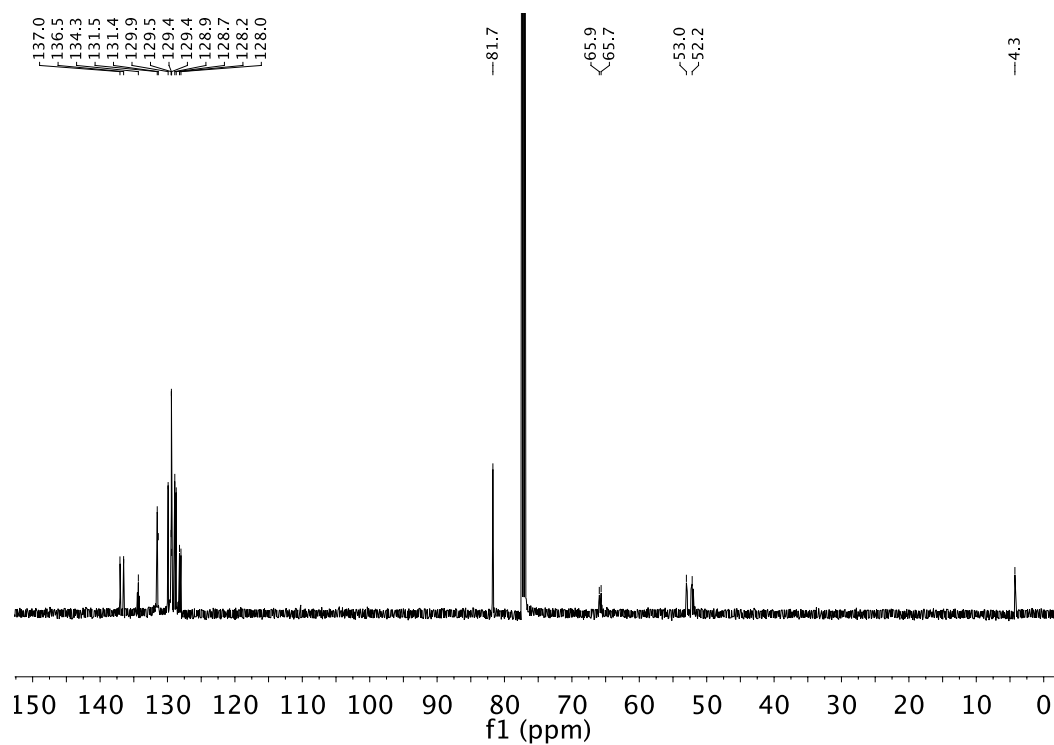


**Figure A-2.**  $^{13}\text{C}\{^1\text{H}\}$  NMR spectrum of **2-1b** in  $\text{CDCl}_3$  (151 MHz).

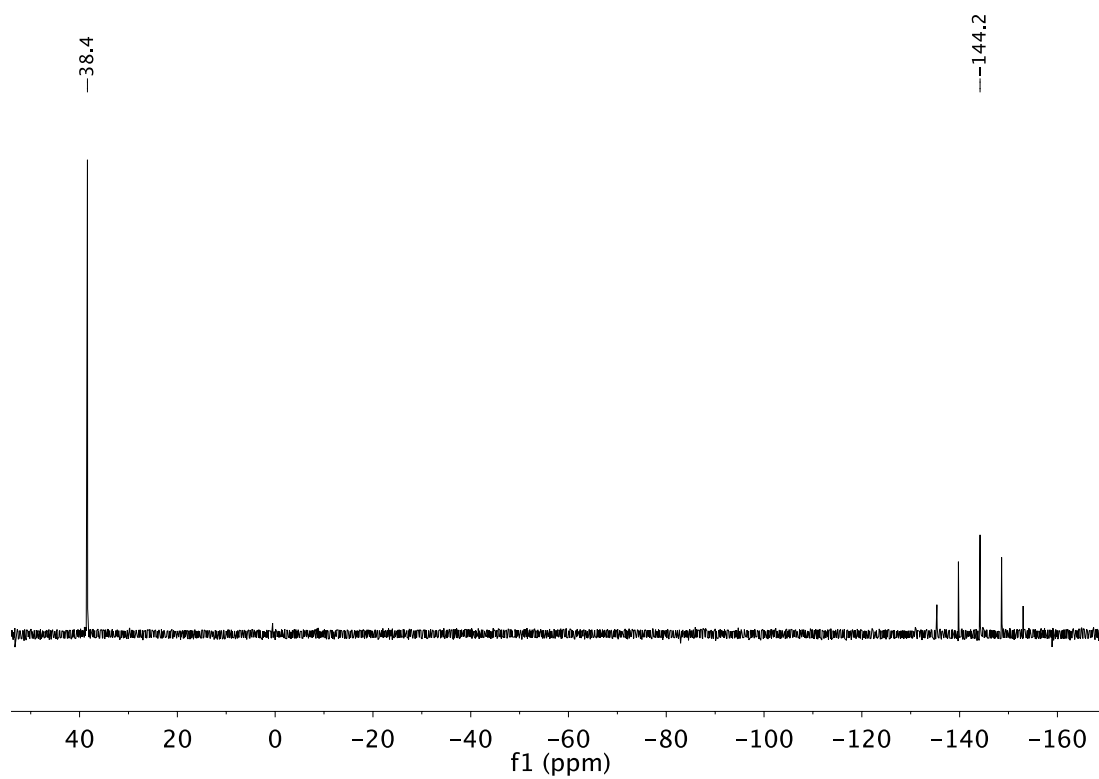


**Figure A-3.**  $^{31}\text{P}\{^1\text{H}\}$  NMR spectrum of **2-1b** in  $\text{CDCl}_3$  (243 MHz).

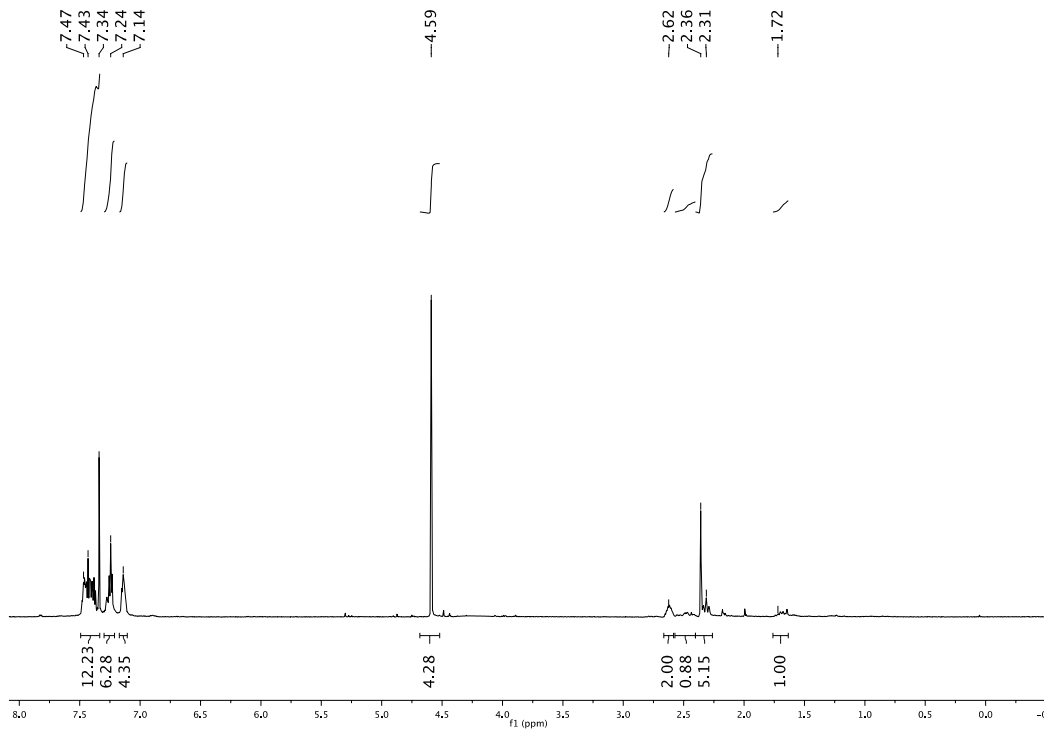


**Figure A-4.**  $^1\text{H}$  NMR spectrum of **2-3** in  $\text{CDCl}_3$  (600 MHz)

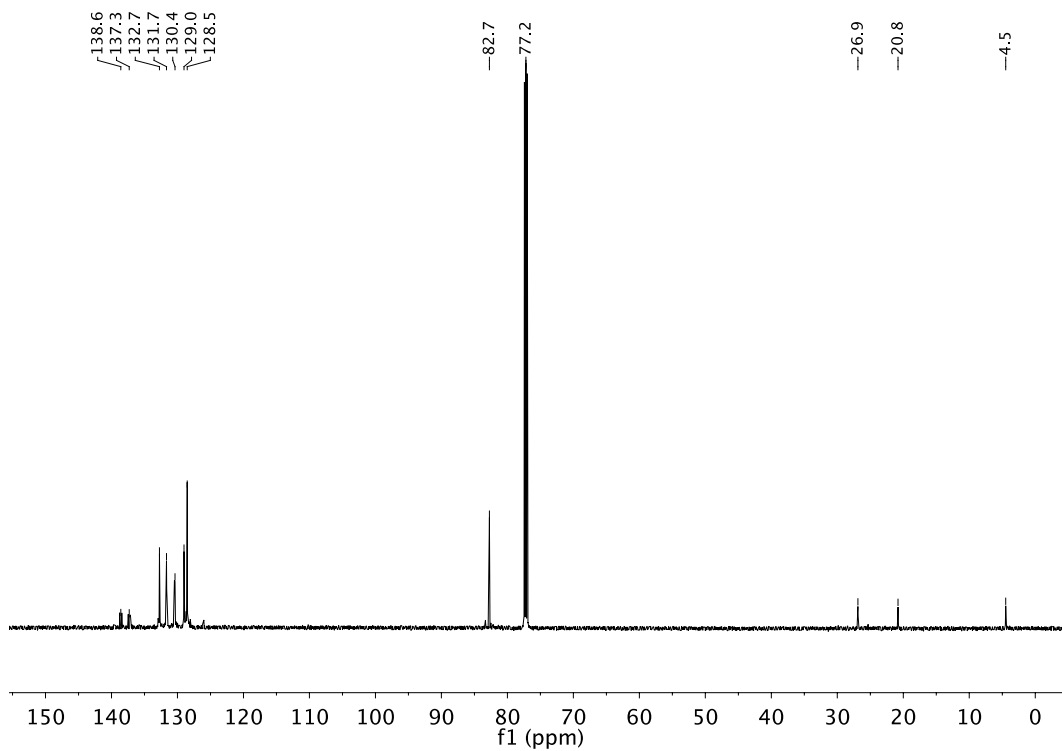


**Figure A-5.**  $^{13}\text{C}\{^1\text{H}\}$  NMR spectrum of **2-3** in  $\text{CDCl}_3$  (151 MHz).

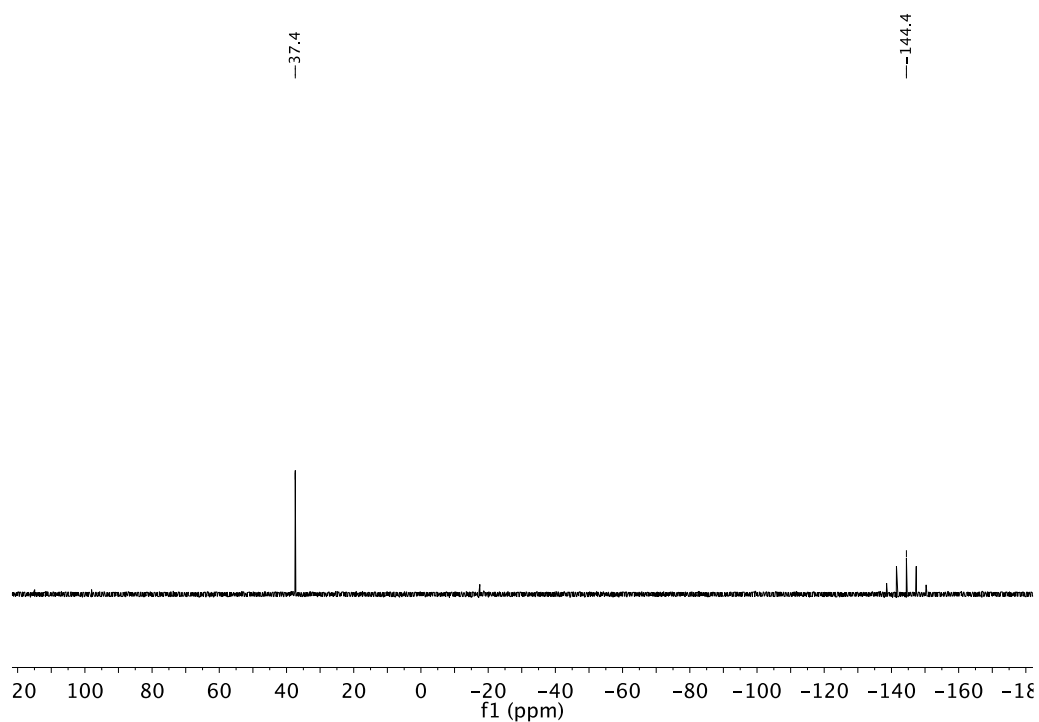


**Figure A-6.**  $^{31}\text{P}\{^1\text{H}\}$  NMR spectrum of **2-3** in  $\text{CDCl}_3$  (243 MHz).

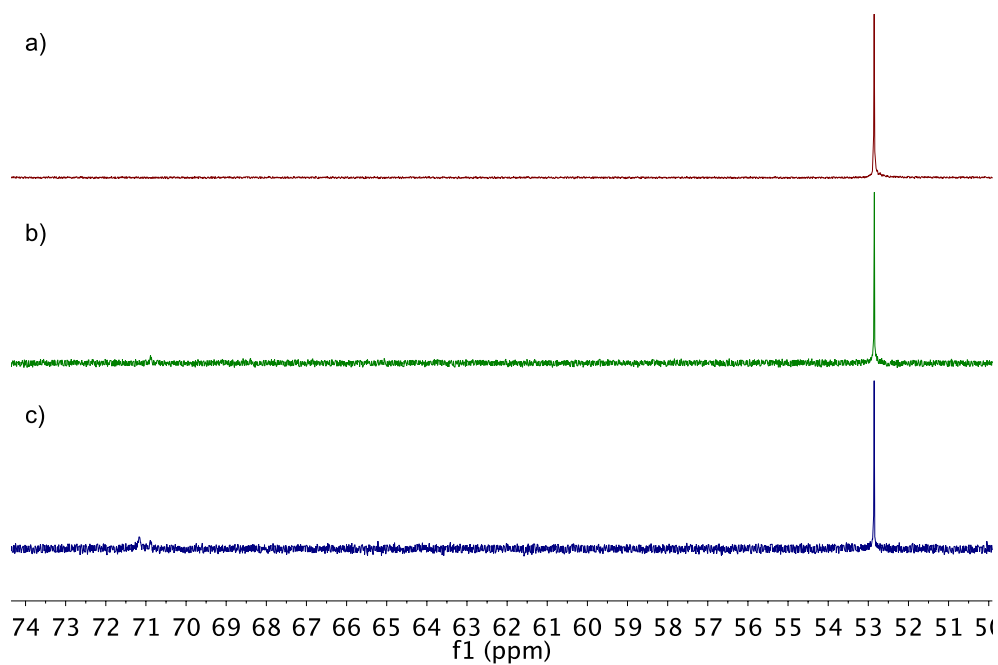


**Figure A-7.**  $^{31}\text{P}\{^1\text{H}\}$  NMR stacked spectra of the catalytic reaction of 2-ethynylbenzyl alcohol (**EBA**) with **2-1a** (1.5 mol%) at 40 °C at time points of: a) 0 min (before substrate addition); b) 15 minutes; c) 90 minutes.

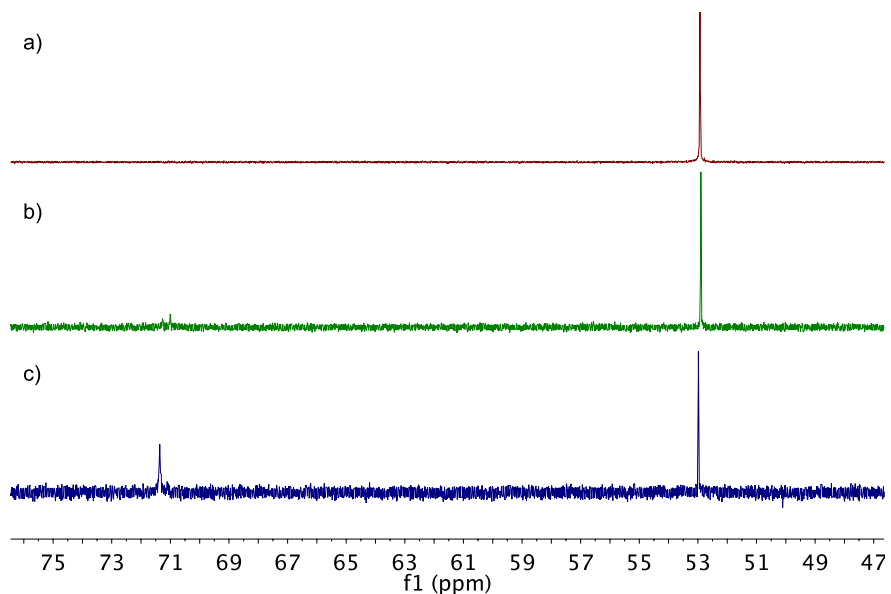


**Figure A-8.**  $^{31}\text{P}\{^1\text{H}\}$  NMR stacked spectra of the catalytic reaction of 2-ethynylbenzyl alcohol (**EBA**) with **2-1a** (1.5 mol%) at 40 °C at time points of: a) 0 min (before substrate addition); b) 15 minutes; c) 90 minutes.

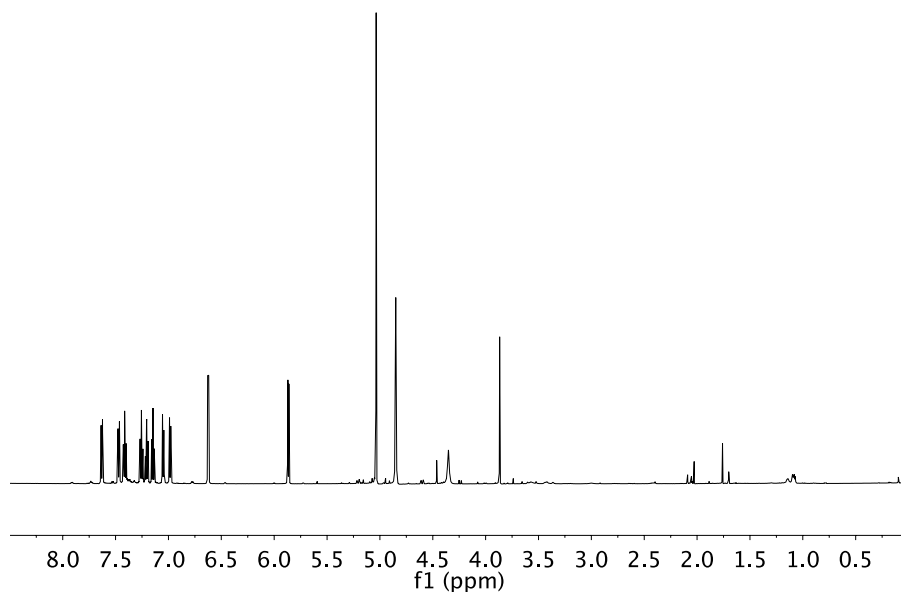


**Figure A-9.**  $^1\text{H}$  NMR spectra of the in situ characterization of **2-5a** in acetone- $d_6$  (600 MHz), formed under catalytic conditions with 100 equiv of substrate **EBA** after heating (54 °C) for 7h. The majority species observed is the cyclization product **IC**.

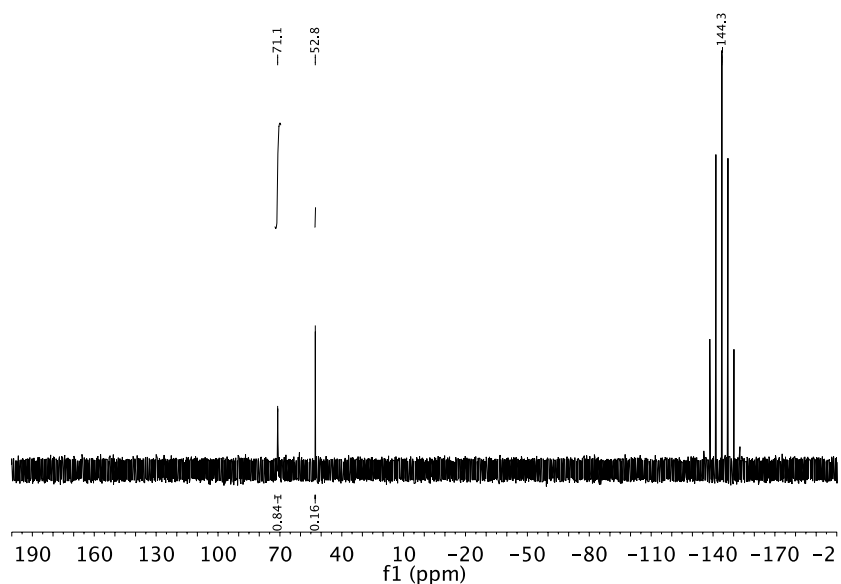


**Figure A-10.**  $^{31}\text{P} \{^1\text{H}\}$  NMR spectra of the in situ characterization of **2-5a** in acetone- $d_6$  (243 MHz), formed under catalytic conditions with 100 equiv of substrate **EBA** after heating (54 °C) for 7h. The signal for **2-1a** is found at 52.8 ppm.

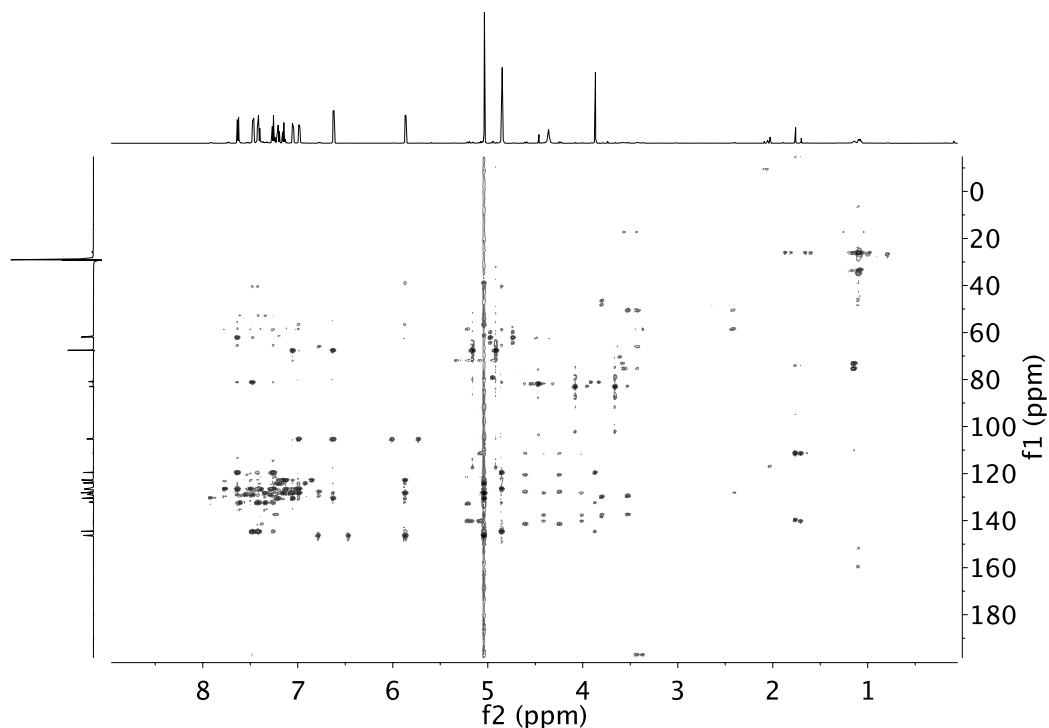


**Figure A-11.**  $^1\text{H}-^{13}\text{C}$  gHMBCAD NMR spectra of the in situ characterization of **2-5a** in acetone- $d_6$ , formed under catalytic conditions with 100 equiv of substrate **EBA** after heating (54 °C) for 7h.

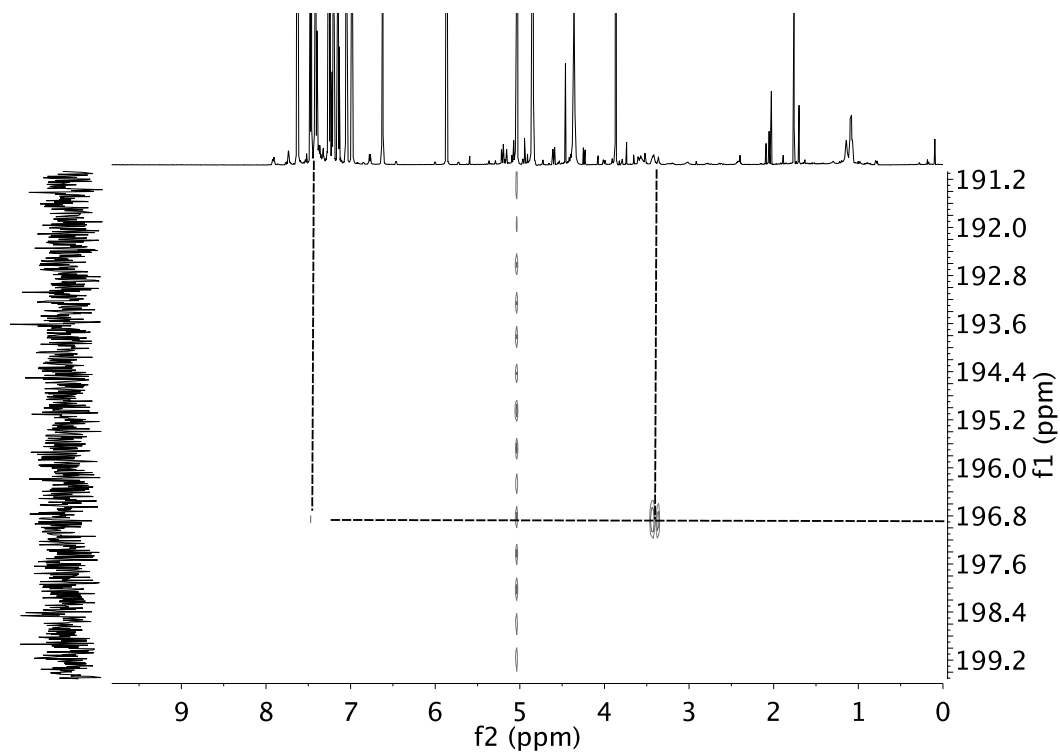


**Figure A-12.** A zoom in on the important signals in  $^1\text{H}$ - $^{13}\text{C}$  gHMBCAD NMR spectra of the in situ characterization of **2-5a** in acetone- $d_6$ , formed under catalytic conditions with 100 equiv of substrate **EBA** after heating (54 °C) for 7h.

## IR Spectra

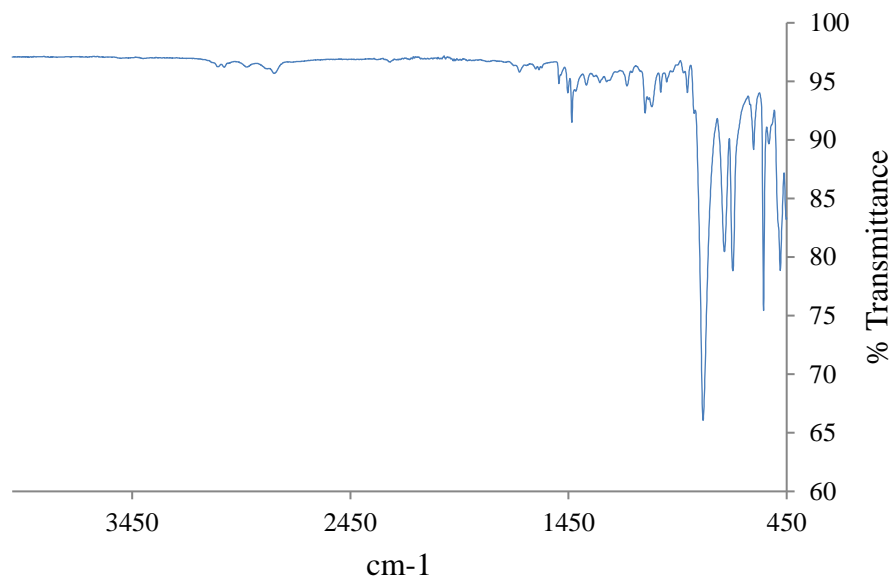


**Figure A-13.** IR spectrum of solid **2-1b** collected with a PerkinElmer UATR Two FT-IR Spectrum Two

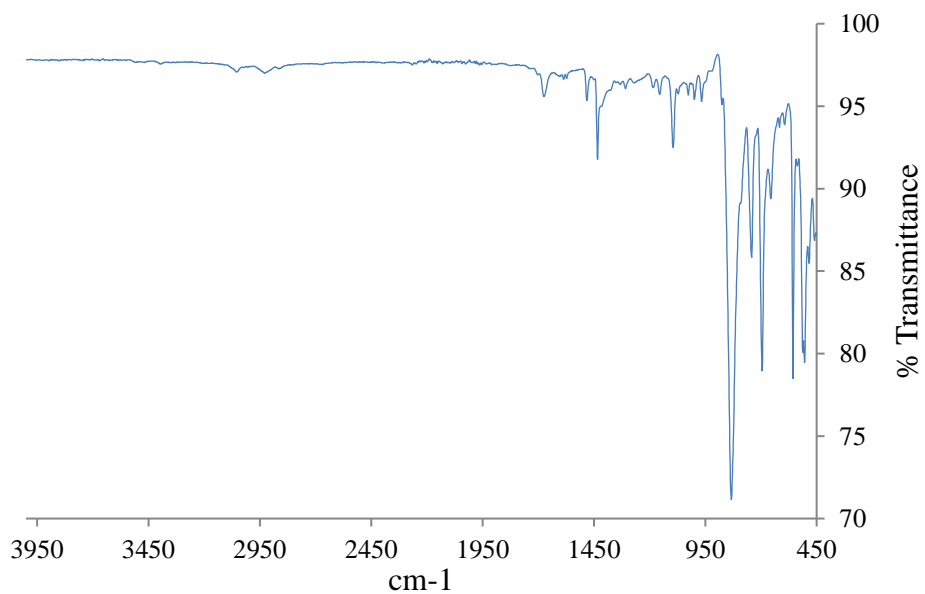


**Figure A-14.** IR spectrum of solid **2-3** collected with a PerkinElmer UATR Two FT-IR Spectrum Two



## MALDI data

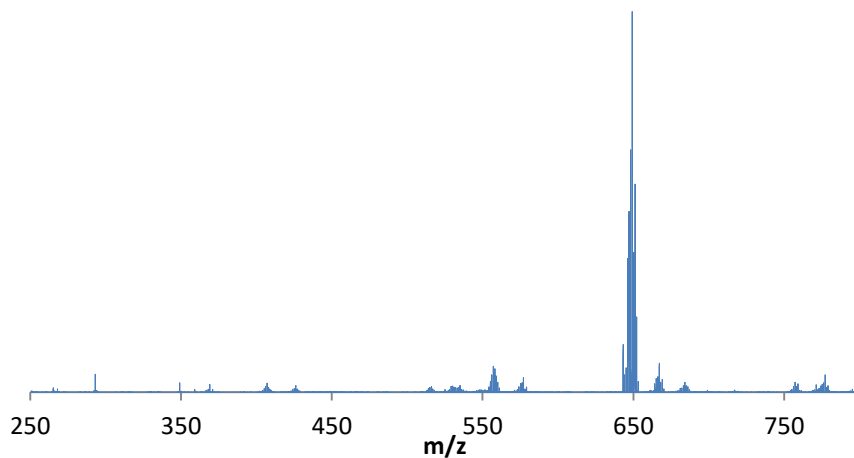


**Figure A-15.** MALDI-TOF mass spectrum of **2-1b** collected with pyrene as the matrix.

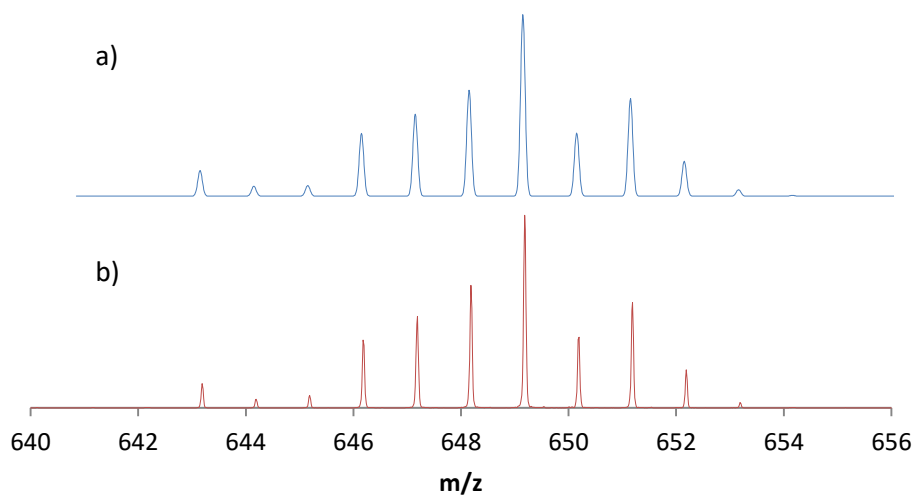


**Figure A-16.** MALDI-TOF MS isotope patterns a) Simulated for  $[2-1b-MeCN-PF_6]^+$  with  $m/z = 649.1$ ; b) expansion of the spectrum in Figure A-15 to show the observed signal found at  $m/z = 649.2$ . Observed data were acquired with pyrene as the matrix.



## Additional Catalysis Graphs

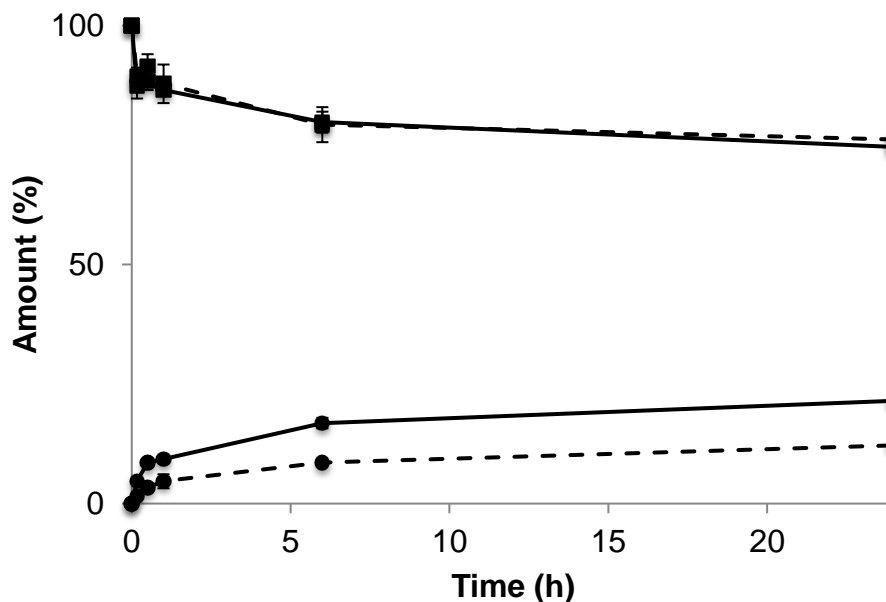


**Figure A-19.** – Cyclization of **EBA-4-OMe** (150 mM) by 1 mol% of catalyst **2-1a** (solid line) and **1b** (dashed line) at 40 °C monitored over 24 h. The quantities of substrate **EBA-4-OMe** (■) and product **IC-4-OMe** (●) are depicted. Amounts were determined by  $^1\text{H}$  NMR spectroscopy by integration of signals for **EBA-4-OMe/IC-4-OMe** relative to an internal standard. Reactions were conducted in duplicate. Data points represent the average of the two runs and the error bars give the span of the conversion values of each data set.

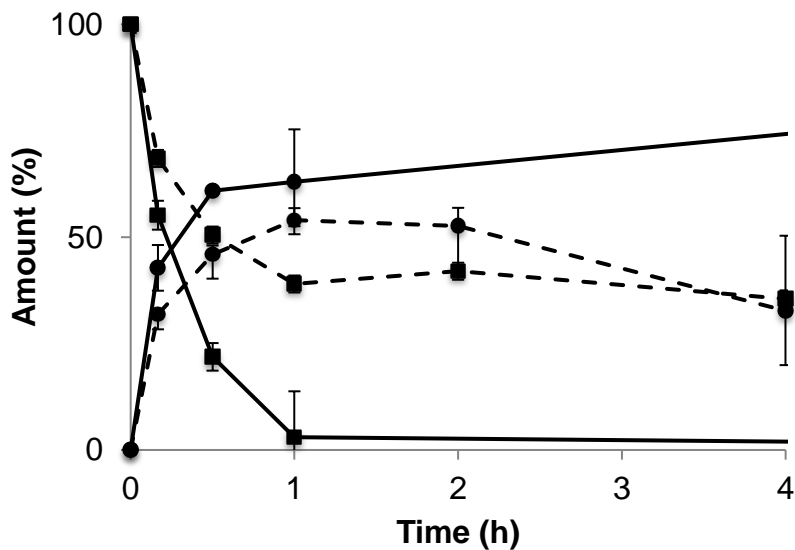


**Figure A-20.** Cyclization of **EBA** (150 mM) by 1 mol% of **2-1a** at 40 °C (solid line) and 54 °C (dashed line) monitored over 24 h. The quantities of substrate **EBA** (■) and product **IC** (●) are depicted. Amounts were determined by  $^1\text{H}$  NMR spectroscopy by integration of signals for **EBA/IC** relative to an internal standard. Reactions were conducted in duplicate. Data points represent the average of the two runs and the error bars give the span of the conversion values of each data set.

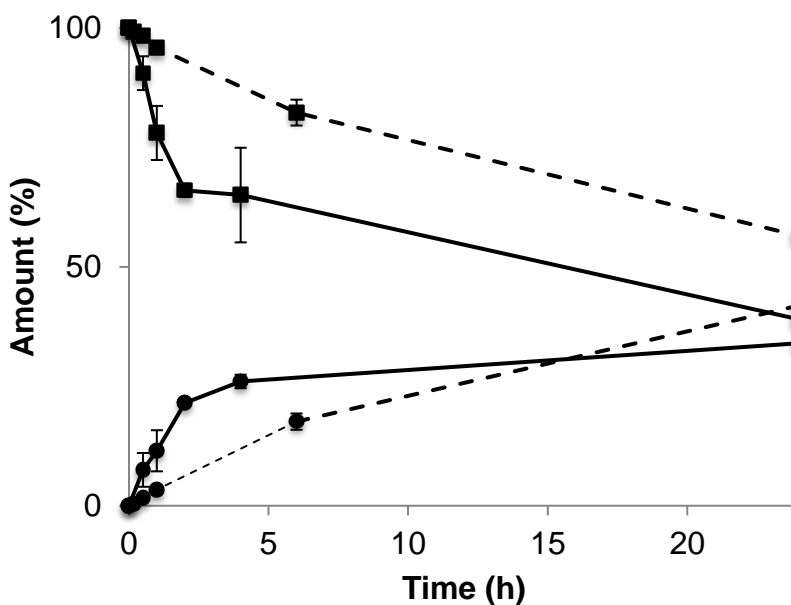


**Figure A-21.** Cyclization of **EBA** (150 mM) by 1 mol% of **2-1b** at 40 °C (solid line) and 54 °C (dashed line) monitored over 24 h. The quantities of substrate **EBA** (■) and product **IC** (●) are depicted.

Amounts were determined by  $^1\text{H}$  NMR spectroscopy by integration of signals for **EBA/IC** relative to an internal standard. Reactions were conducted in duplicate. Data points represent the average of the two runs and the error bars give the span of the conversion values of each data set.

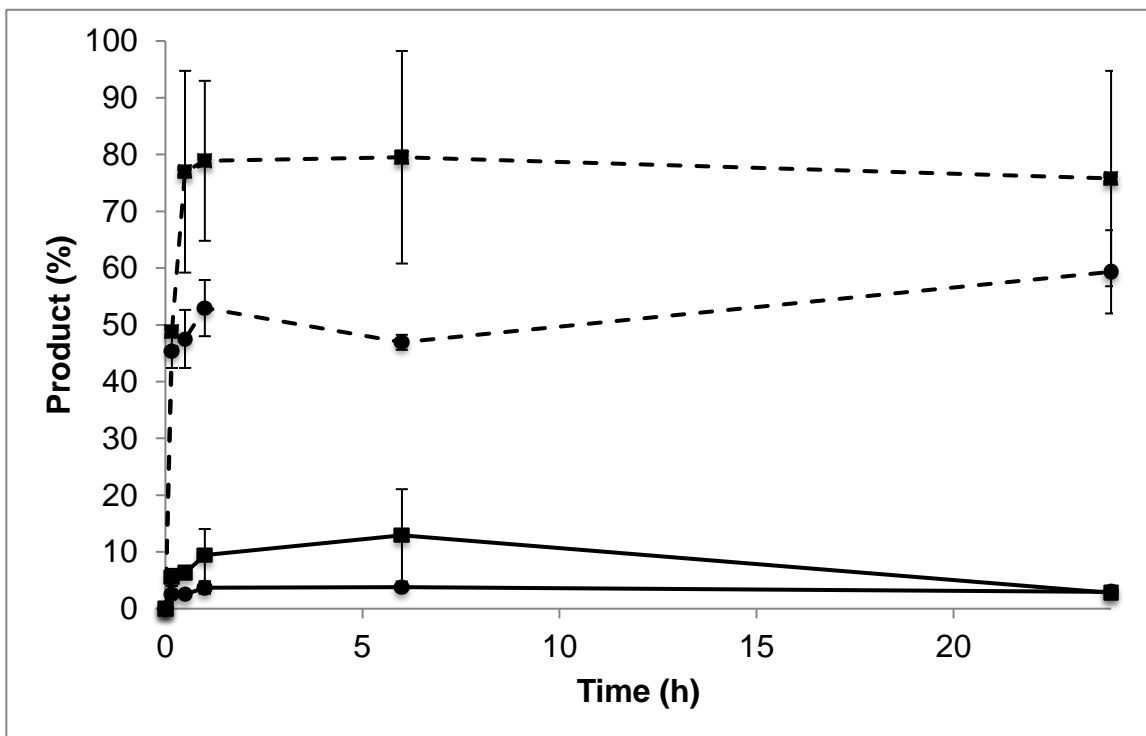


**Figure A-22.** Cyclization of **EBA** (150 mM) by 0.1 (solid line) and 1 mol% (dashed line) of precatalyst  $\text{RuCl}(\text{Cp})(\text{P}^{\text{Ph}}_2\text{N}^{\text{Bn}}_2)$  treated with  $\text{TIPF}_6$  at 25 °C (●) and 40 °C (■) over 24 h. Amounts were determined by  $^1\text{H}$  NMR spectroscopy by integration of signals for **EBA/IC** relative to an internal standard. Reactions were conducted in duplicate. Data points represent the average of the two runs and the error bars give the span of the conversion values of each data set.

## Crystallographic Data

*Data Collection and Processing.* The sample of **2-1b** was mounted on a Mitegen polyimide micromount with a small amount of Paratone N oil. All X-ray measurements were made on a Bruker Kappa Axis Apex2 diffractometer at a temperature of 110 K. The unit cell dimensions were determined from a symmetry constrained fit of 9671 reflections with  $5.6^\circ < 2\theta < 68.64^\circ$ . The data collection strategy was a number of  $\omega$  and  $\varphi$  scans which collected data up to  $72.808^\circ$  ( $2\theta$ ). The frame integration was performed using SAINT.<sup>1</sup> The resulting raw data was scaled and absorption corrected using a multi-scan averaging of symmetry equivalent data using SADABS.<sup>2</sup>

*Structure Solution and Refinement.* The structure was solved by using a dual space methodology using the SHELXT program.<sup>3</sup> All non-hydrogen atoms were obtained from the initial solution. The hydrogen atoms were introduced at idealized positions and were allowed to ride on the parent atom. The asymmetric unit contained a region of electron density which was presumably due to disordered solvent molecule(s). However, attempts to derive a chemically sensible disorder model were unsuccessful. The SQUEEZE routine from PLATON was therefore applied to the data.<sup>4</sup> The structural model was fit to the data using full matrix least-squares based on  $F^2$ . The calculated structure factors included corrections for anomalous dispersion from the usual tabulation. The structure was refined using the SHELXL-2014 program from the SHELXL suite of crystallographic software.<sup>3</sup> Graphic plots were produced using the NRCVAX program suite.<sup>5</sup> Additional information and other relevant literature references can be found in the reference section of this website (<http://xray.chem.uwo.ca>).

- 1 Bruker-Nonius, SAINT version 2012.12, **2012**, Bruker-Nonius, Madison, WI 53711, USA
- 2 Bruker-Nonius, SADABS version 2012.1, **2012**, Bruker-Nonius, Madison, WI 53711, USA
- 3 Burla, M. C.; Caliendo, R.; Camalli, M.; Carrozzini, B.; Cascarano, G. L.; Giacovazzo, C.; Mallamo, M.; Mazzone, A.; Polidori, G.; Spagna, R. *J. Appl. Cryst.* **2012**, *45*, 357-361
- 4 Sheldrick, G. M., *Acta Cryst.* **2008**, *A64*, 112-122
- 5 Gabe, E. J.; Le Page, Y.; Charland, J. P.; Lee, F. L. and White, P. S. *J. Appl. Cryst.* **1989**, *22*, 384-387

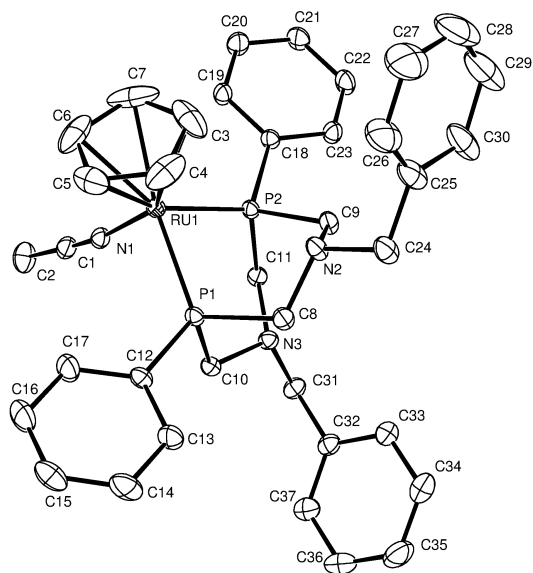


**Figure A-23.** ORTEP drawing of **2-1b** showing naming and numbering scheme. Ellipsoids are at the 50% probability level. Hydrogen atoms,  $[\text{PF}_6]^-$  counter-ion and diethyl ether molecule of solvation were omitted for clarity.

Table A-1: Summary of Crystal Data for **2-1b**

Formula	$C_{41}H_{50}F_6N_3OP_3Ru$ ( <b>2-1b</b> )
CCDC Number	1418495
Formula Weight ( <i>g/mol</i> )	908.82
Crystal Dimensions ( <i>mm</i> )	$0.288 \times 0.186 \times 0.090$
Crystal Color and Habit	colourless prism
Crystal System	triclinic
Space Group	$P\bar{1}$
Temperature, K	110
<i>a</i> , Å	10.832(3)
<i>b</i> , Å	13.759(3)
<i>c</i> , Å	15.524(5)
$\alpha$ , °	99.505(7)
$\beta$ , °	94.478(10)
$\gamma$ , °	104.276(5)
<i>V</i> , Å <sup>3</sup>	2194.3(10)
Number of reflections to determine final unit cell	9671
Min and Max $2\theta$ for cell determination, °	5.6, 68.64
<i>Z</i>	2
F(000)	936
$\rho$ ( <i>g/cm</i> )	1.375
$\lambda$ , Å, (MoK $\alpha$ )	0.71073
$\mu$ , ( <i>cm</i> <sup>-1</sup> )	0.526
Diffractometer Type	Bruker Kappa Axis Apex2
Scan Type(s)	$\Omega$ and $\phi$ scans
Max $2\theta$ for data collection, °	72.808
Measured fraction of data	0.997
Number of reflections measured	115317
Unique reflections measured	19679
$R_{merge}$	0.0356
Number of reflections included in refinement	19679
Cut off Threshold Expression	$I > 2\sigma(I)$
Structure refined using	full matrix least-squares using $F^2$
Weighting Scheme	$w=1/[\sigma^2(F_o^2)+(0.0464P)^2+0.3723P]$ where $P=(F_o^2+2F_c^2)/3$
Number of parameters in least-squares	499
$R_1$	0.0393
w $R_2$	0.0889



R <sub>1</sub> (all data)	0.0564
wR <sub>2</sub> (all data)	0.0958
GOF	1.056
Maximum shift/error	0.004
Min & Max peak heights on final ΔF Map (e <sup>-</sup> /Å)	-0.668, 0.786

Where:

$$R_1 = \sum (|F_o| - |F_c|) / \sum F_o$$

$$wR_2 = [ \sum w (F_o^2 - F_c^2)^2 / \sum w F_o^4 ]^{1/2}$$

$$GOF = [ \sum w (F_o^2 - F_c^2)^2 / (\text{No. of reflns.} - \text{No. of params.}) ]^{1/2}$$

## Appendices B: Supplementary Information for Chapter 3

### NMR Spectra

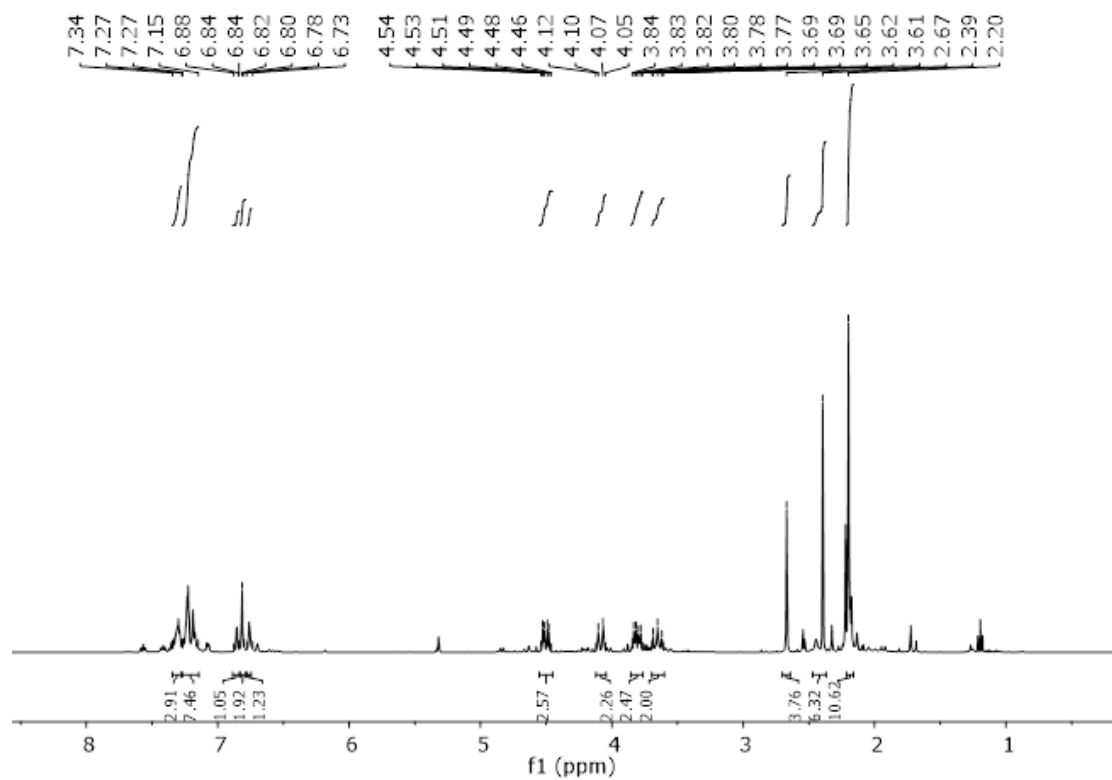


**Figure B-1.** <sup>1</sup>H NMR spectrum of (P<sup>Ph</sup><sub>2</sub>N<sup>Me</sup><sub>2</sub>) (3-1b) in CD<sub>2</sub>Cl<sub>2</sub>.

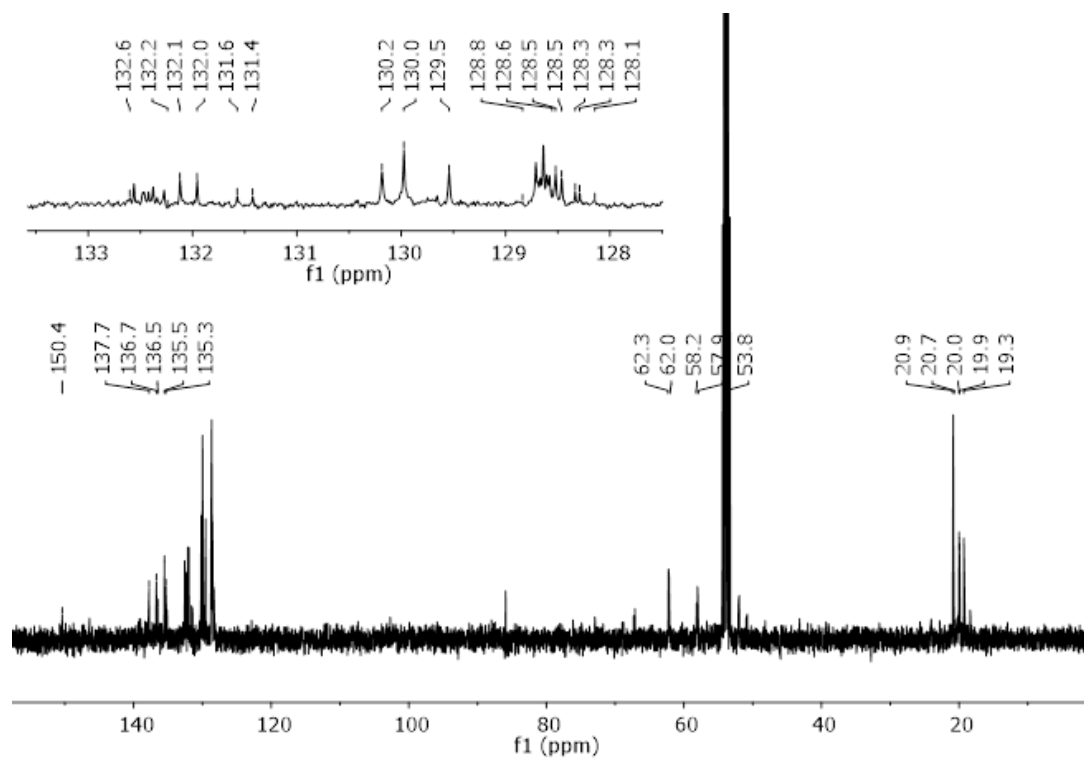


**Figure B-2.**  $^{13}\text{C}$   $\{^1\text{H}\}$  NMR spectrum of  $(\text{P}^{\text{Ph}}_2\text{N}^{\text{Mes}}_2)$  (**3-1b**) in  $\text{CD}_2\text{Cl}_2$ .

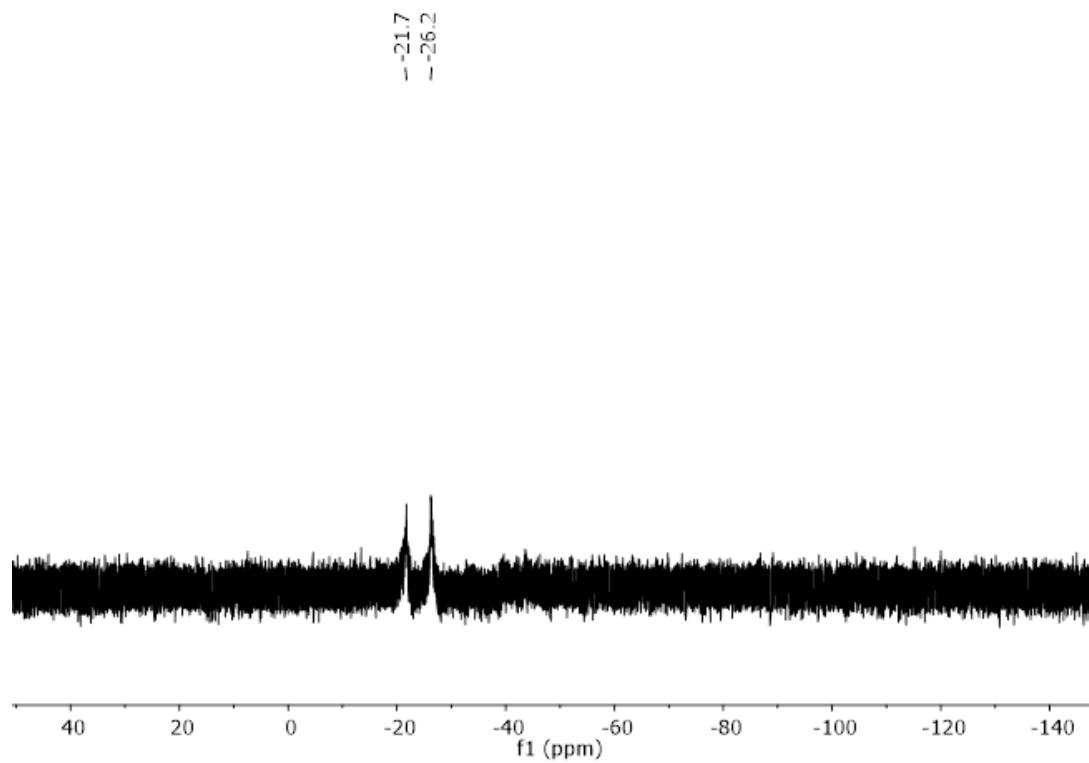


**Figure B-3.**  $^{31}\text{P}$   $\{^1\text{H}\}$  NMR spectrum of  $\text{P}^{\text{Ph}}_2\text{N}^{\text{Bn}}_2$  (**3-1b**) in  $\text{CD}_2\text{Cl}_2$ .

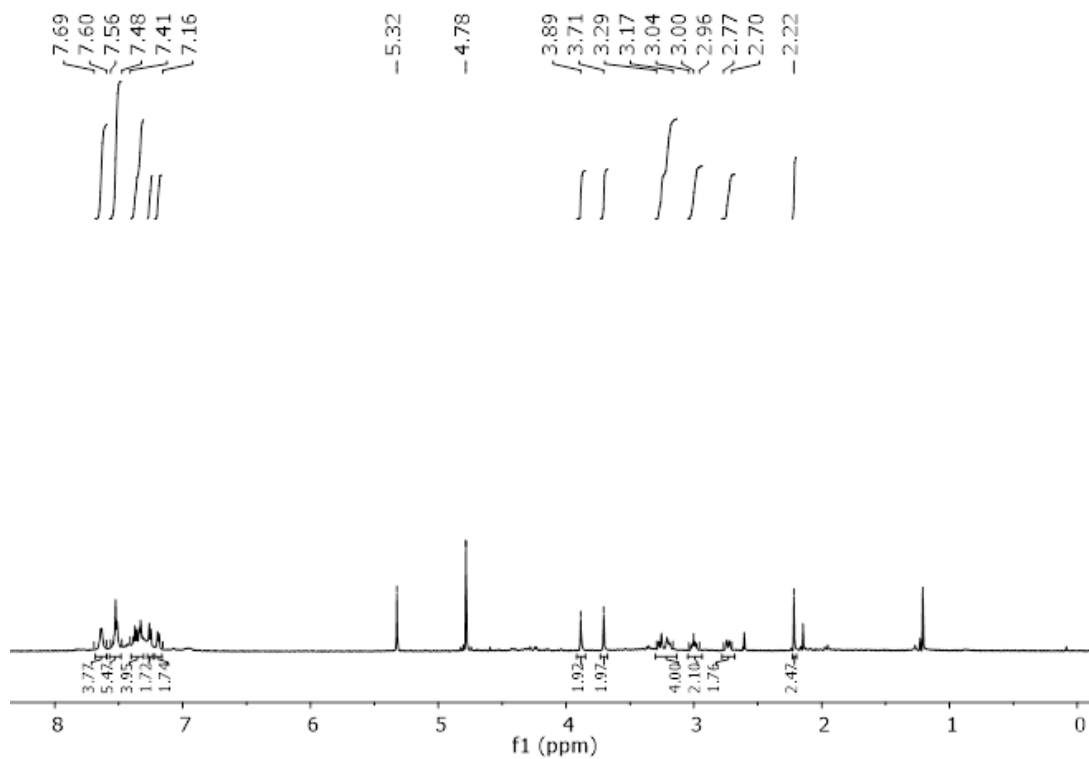


**Figure B-4.**  $^1\text{H}$  NMR spectrum of  $[\text{Ru}(\text{Cp})(\text{P}^{\text{Ph}}_2\text{N}^{\text{Bn}}_2)(\text{NCMe})]\text{PF}_6$  (**2-1b**) in  $\text{CD}_2\text{Cl}_2$ .

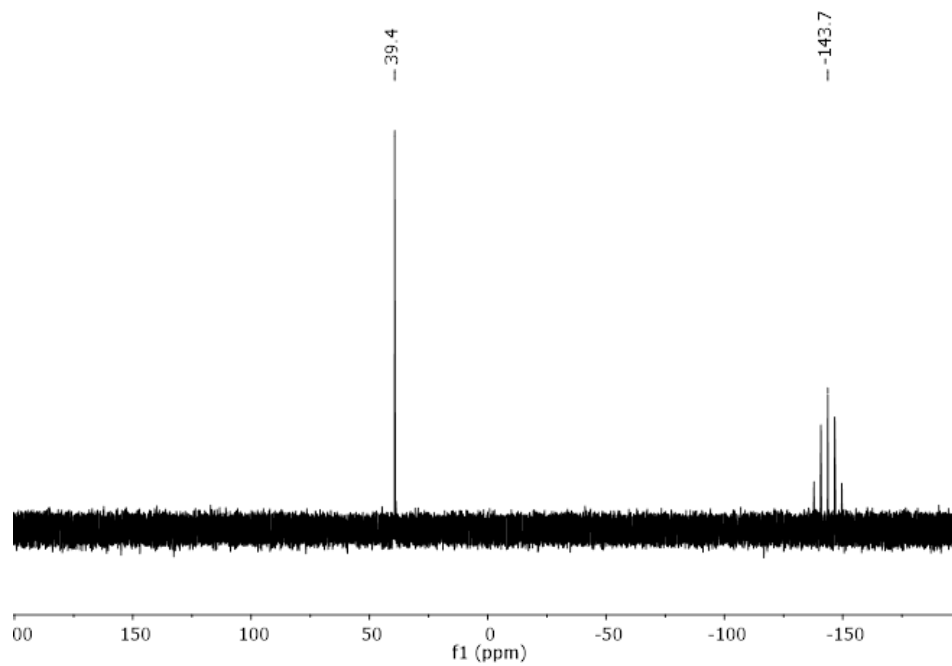


**Figure B-5.**  $^{31}\text{P}$   $\{^1\text{H}\}$  NMR spectrum of  $[\text{Ru}(\text{Cp})(\text{P}^{\text{Ph}}_2\text{N}^{\text{Bn}}_2)(\text{NCMe})]\text{PF}_6$  (**2-1b**) in  $\text{CD}_2\text{Cl}_2$ .

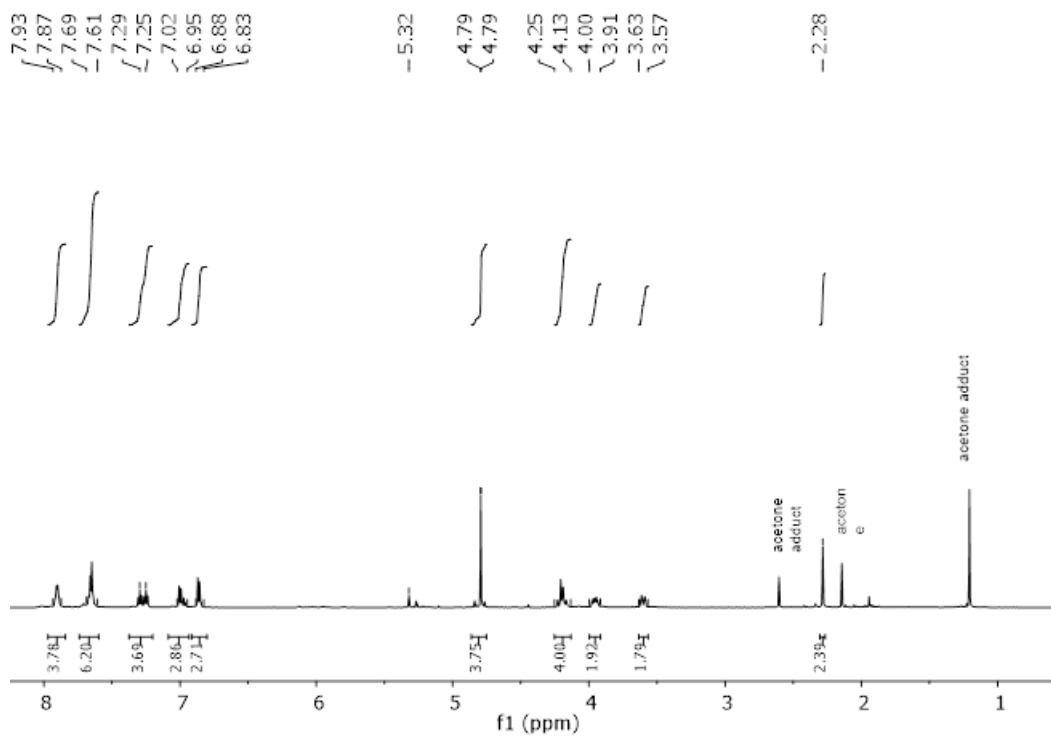


**Figure B-6.**  $^1\text{H}$  NMR spectrum of  $[\text{Ru}(\text{Cp})(\text{P}^{\text{Ph}}_2\text{N}^{\text{Ph}}_2)(\text{NCMe})]\text{PF}_6$  (**3-2a**) in  $\text{CD}_2\text{Cl}_2$ .

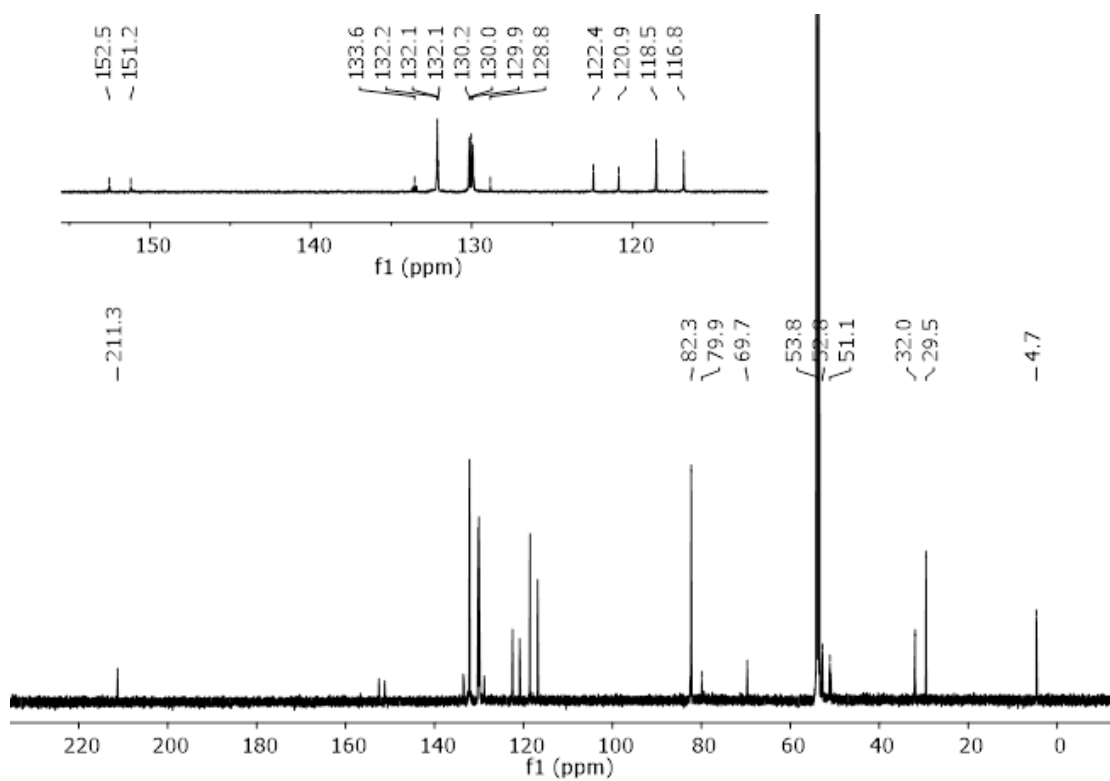


**Figure B-7.**  $^{13}\text{C}$   $\{^1\text{H}\}$  NMR spectrum of  $[\text{Ru}(\text{Cp})(\text{P}^{\text{Ph}}_2\text{N}^{\text{Ph}}_2)(\text{NCMe})]\text{PF}_6$  (**3-2a**) in  $\text{CD}_2\text{Cl}_2$ .

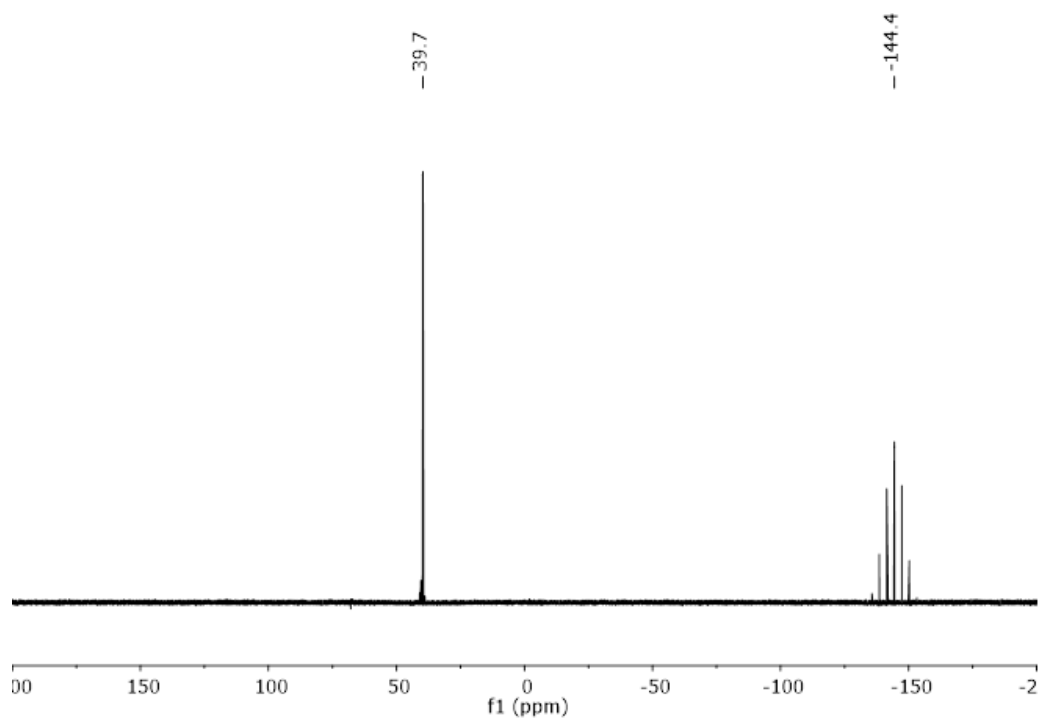


**Figure B-8.** <sup>31</sup>P {<sup>1</sup>H} NMR spectrum of [Ru(Cp)(P<sup>Ph</sup><sub>2</sub>N<sup>Ph</sup><sub>2</sub>)(NCMe)]PF<sub>6</sub> (**3-2a**) in CD<sub>2</sub>Cl<sub>2</sub>.

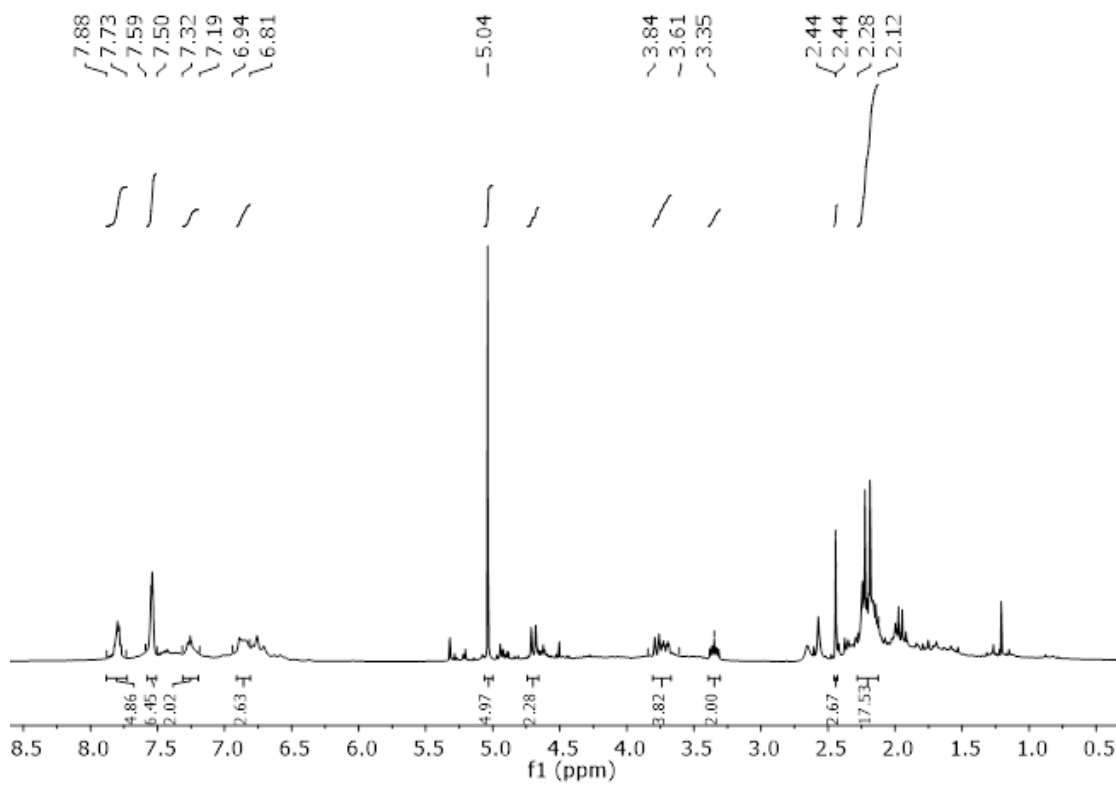


**Figure B-9.** <sup>1</sup>H NMR spectrum of [Ru(Cp)(P<sup>Ph</sup><sub>2</sub>N<sup>Mes</sup><sub>2</sub>)(NCMe)]PF<sub>6</sub> (**3-2b**) in CD<sub>2</sub>Cl<sub>2</sub>.

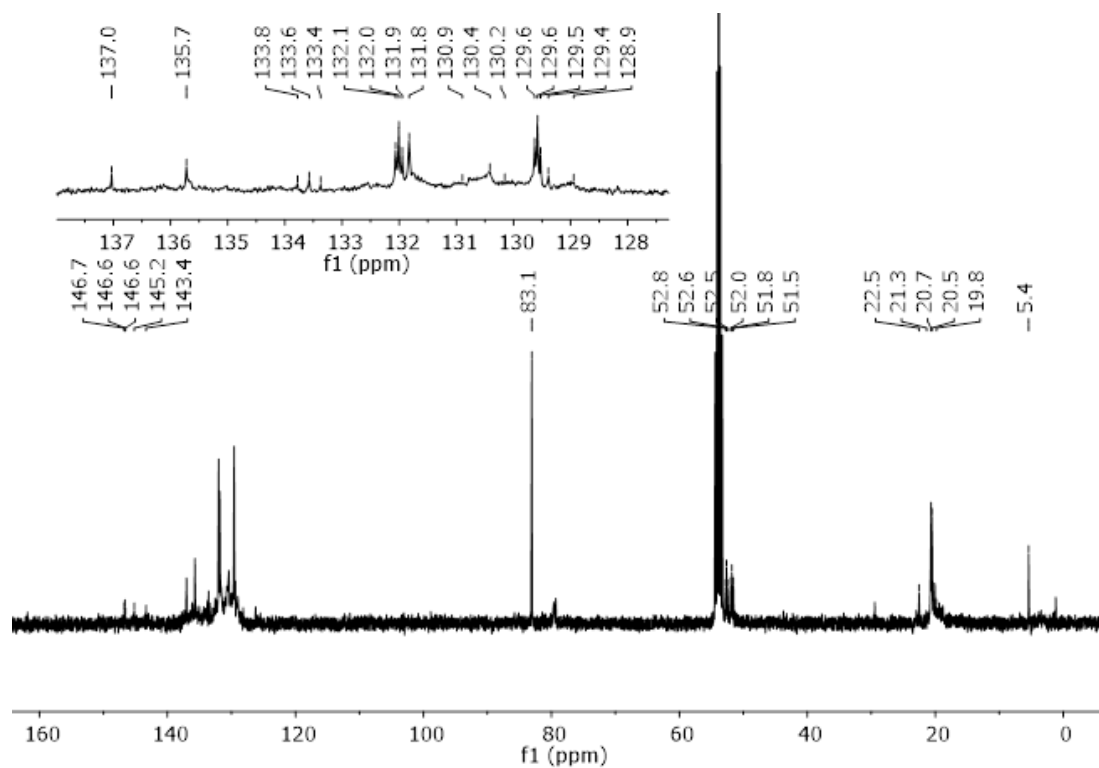


**Figure B-10.**  $^{13}\text{C}$   $\{^1\text{H}\}$  NMR spectrum of  $[\text{Ru}(\text{Cp})(\text{P}^{\text{Ph}}_2\text{N}^{\text{Mes}}_2)(\text{NCMe})]\text{PF}_6$  (**3-2b**) in  $\text{CD}_2\text{Cl}_2$ .

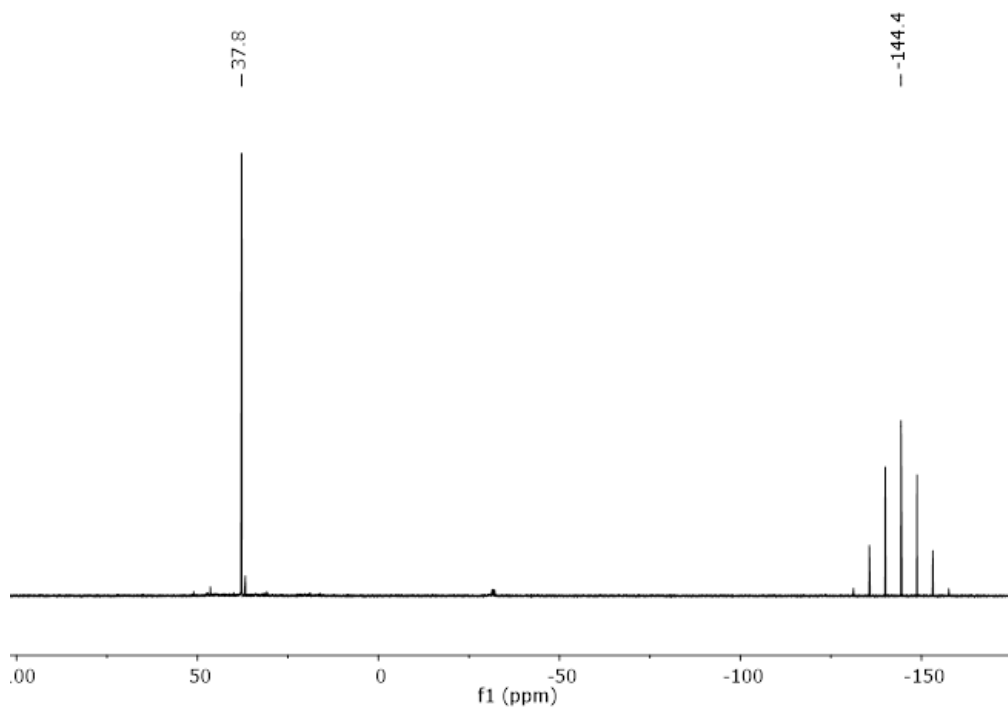


**Figure B-11.**  $^{31}\text{P}$   $\{^1\text{H}\}$  NMR spectrum of  $[\text{Ru}(\text{Cp})(\text{P}^{\text{Ph}}_2\text{N}^{\text{Mes}}_2)(\text{NCMe})]\text{PF}_6$  (**3-2b**) in  $\text{CD}_2\text{Cl}_2$ .

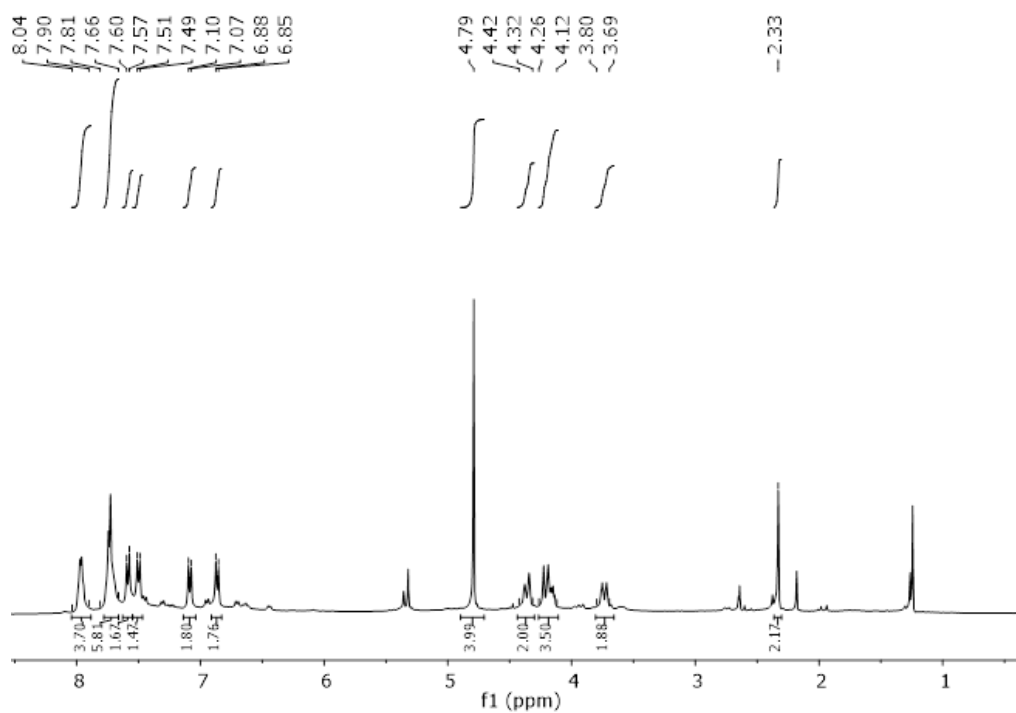


**Figure B-12.**  $^1\text{H}$  NMR spectrum of  $[\text{Ru}(\text{Cp})(\text{P}^{\text{Ph}_2\text{N}^{\text{p-CF}_3\text{-C}_4\text{H}_4}_2)(\text{NCMe})]\text{PF}_6$  (**3-2c**) in  $\text{CD}_2\text{Cl}_2$ .

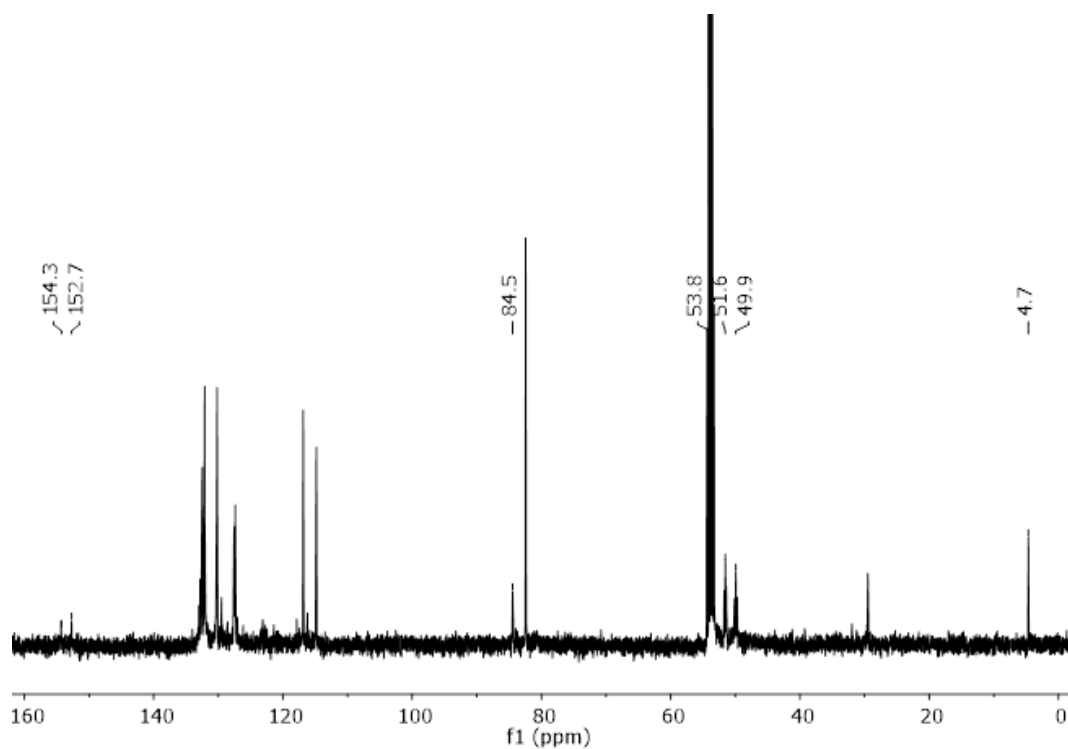


**Figure B-13.**  $^{13}\text{C}$   $\{^1\text{H}\}$  NMR spectrum of  $[\text{Ru}(\text{Cp})(\text{P}^{\text{Ph}_2\text{N}^{\text{p-CF}_3\text{-C}_4\text{H}_4}_2)(\text{NCMe})]\text{PF}_6$  (**3-2c**) in  $\text{CD}_2\text{Cl}_2$ .



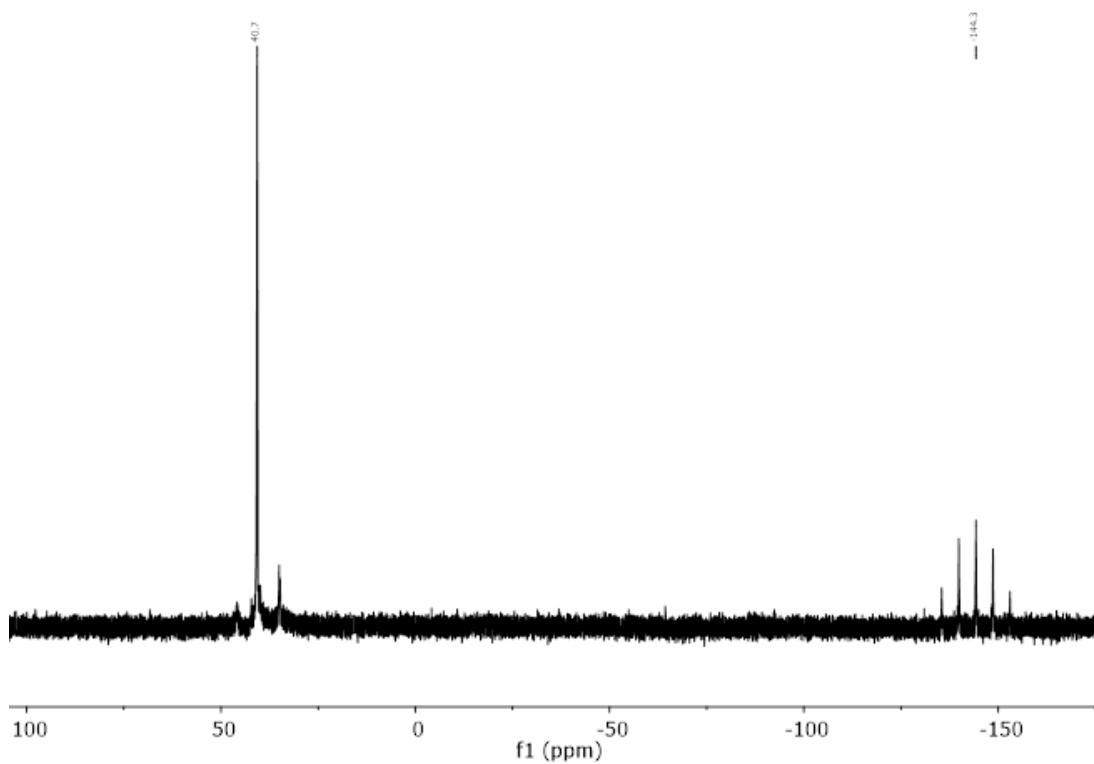


**Figure B-14.**  $^{31}\text{P}$  { $^1\text{H}$ } NMR spectrum of  $[\text{Ru}(\text{Cp})(\text{P}^{\text{Ph}}_2\text{N}^{p\text{-CF}_3\text{-C}_4\text{H}_4}_2)(\text{NCMe})]\text{PF}_6$  (**3-2c**) in  $\text{CD}_2\text{Cl}_2$ .

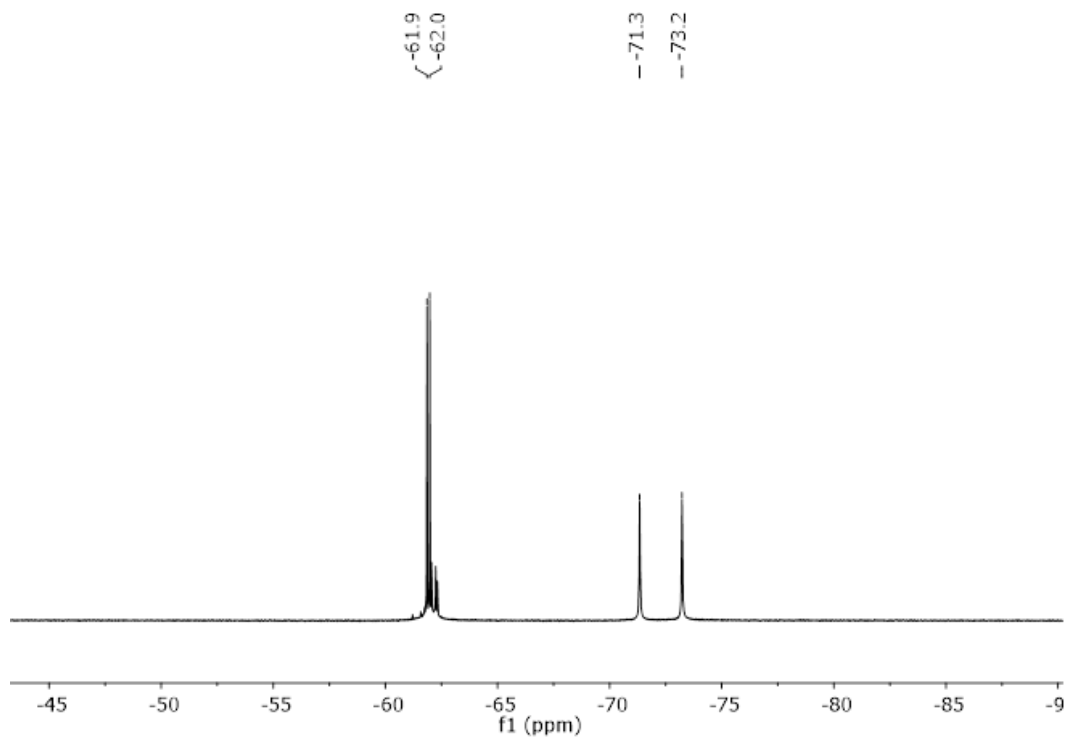


**Figure B-15.**  $^{19}\text{F}$  { $^1\text{H}$ } NMR spectrum of  $[\text{Ru}(\text{Cp})(\text{P}^{\text{Ph}}_2\text{N}^{p\text{-CF}_3\text{-C}_4\text{H}_4}_2)(\text{NCMe})]\text{PF}_6$  (**3-2c**) in  $\text{CD}_2\text{Cl}_2$ .

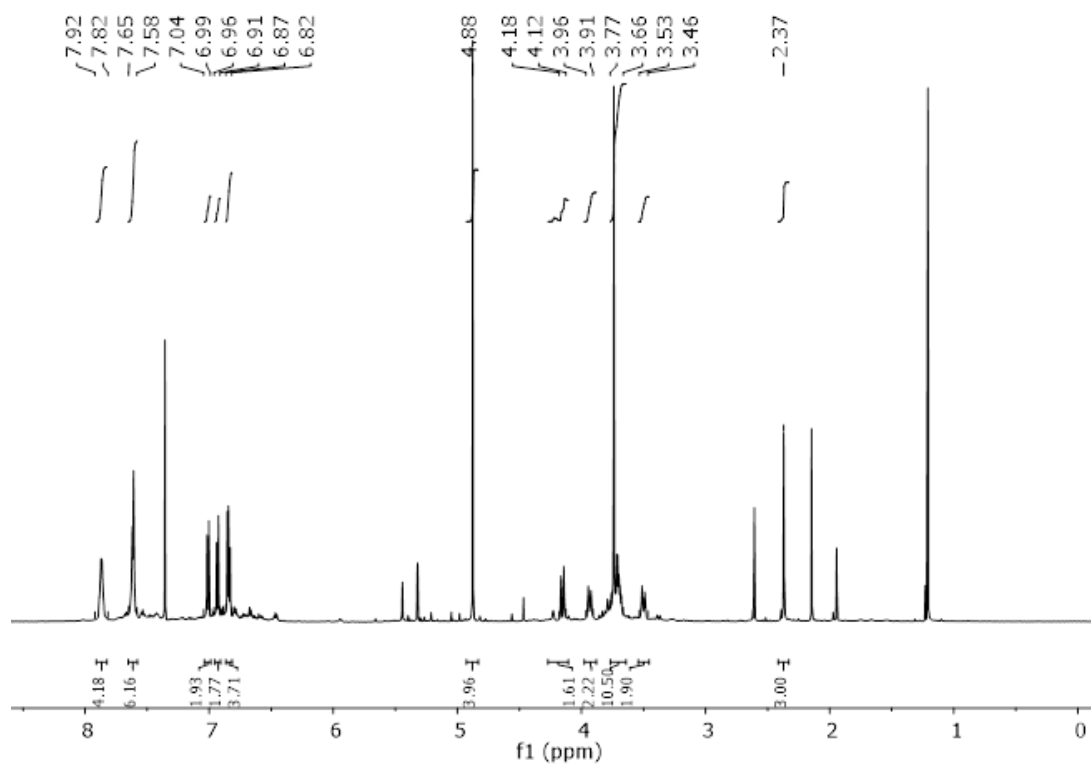


**Figure B-16.**  $^1\text{H}$  NMR spectrum of  $[\text{Ru}(\text{Cp})(\text{P}^{\text{Ph}}_2\text{N}^{p\text{-MeO-C}_4\text{H}_4}_2)(\text{NCMe})]\text{PF}_6$  (**3-2d**) in  $\text{CD}_2\text{Cl}_2$ .

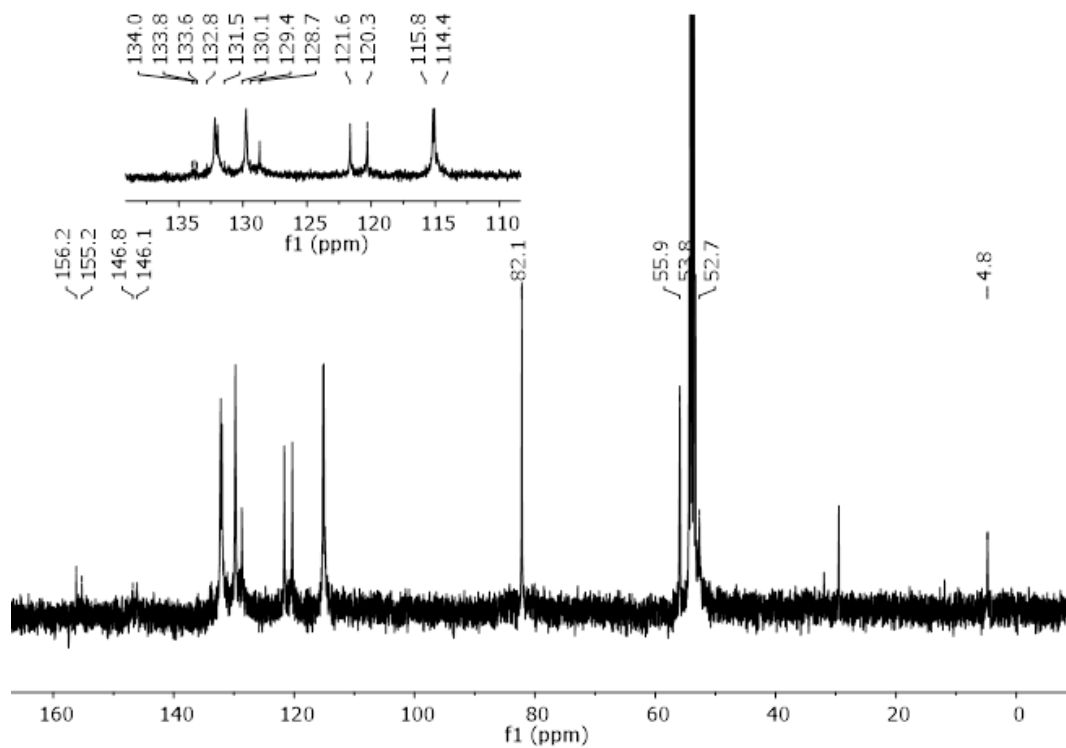


**Figure B-17.**  $^{13}\text{C}$   $\{^1\text{H}\}$  NMR spectrum of  $[\text{Ru}(\text{Cp})(\text{P}^{\text{Ph}}_2\text{N}^{p\text{-MeO-C}_4\text{H}_4}_2)(\text{NCMe})]\text{PF}_6$  (**3-2d**) in  $\text{CD}_2\text{Cl}_2$ .

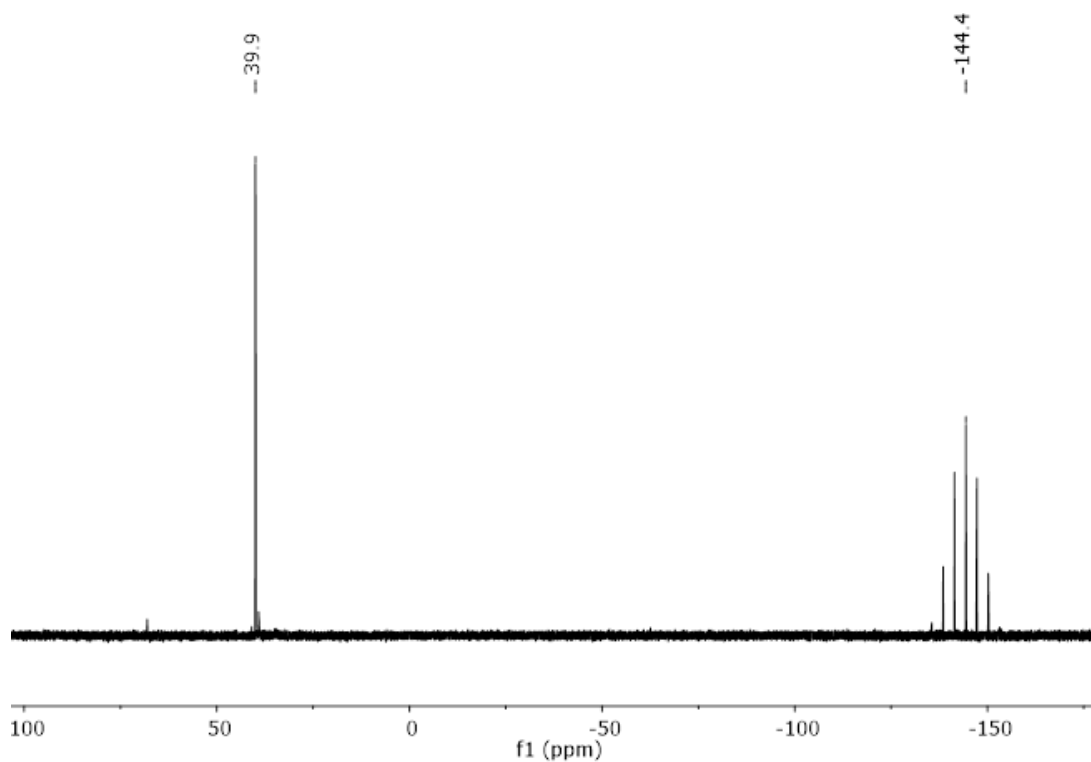


**Figure B-18.**  $^{31}\text{P} \{^1\text{H}\}$  NMR spectrum of  $[\text{Ru}(\text{Cp})(\text{P}^{\text{Ph}}_2\text{N}^{p\text{-MeO-C}_4\text{H}_4}_2)(\text{NCMe})]\text{PF}_6$  (**3-2d**) in  $\text{CD}_2\text{Cl}_2$ .

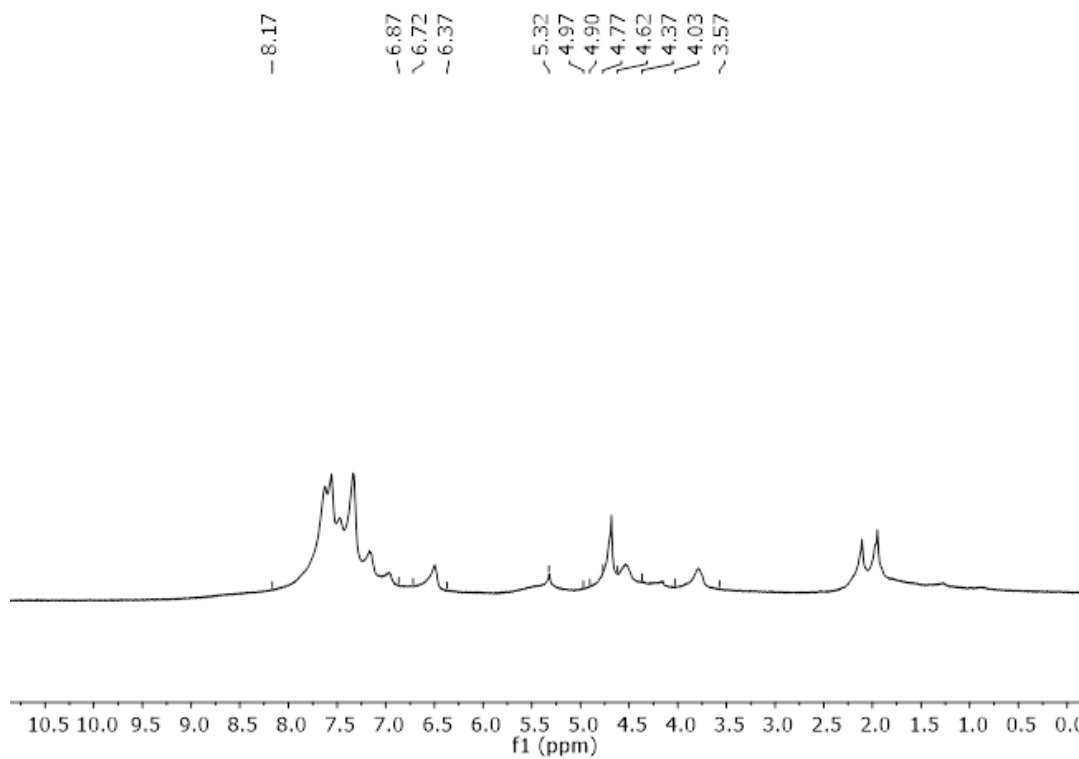


**Figure B-19.**  $^1\text{H}$  NMR spectrum of  $[\text{Ru}(\text{Cp})(\text{P}^{\text{Ph}}_2\text{N}^{\text{Ph}}_1)]\text{PF}_6$  (**3-4**) in  $\text{CD}_2\text{Cl}_2$ .

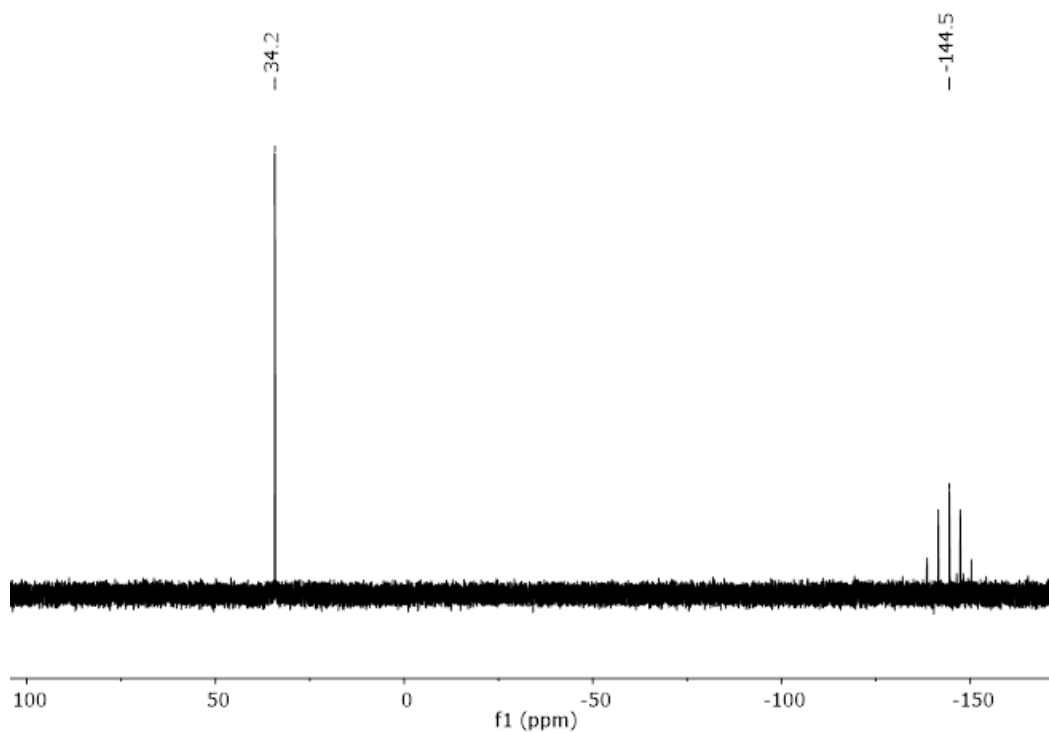


**Figure B-20.**  $^{31}\text{P}$   $\{^1\text{H}\}$  NMR spectrum of  $[\text{Ru}(\text{Cp})(\text{P}^{\text{Ph}}_2\text{N}^{\text{Ph}}_1)]\text{PF}_6$  (**3-4**) in  $\text{CD}_2\text{Cl}_2$ .

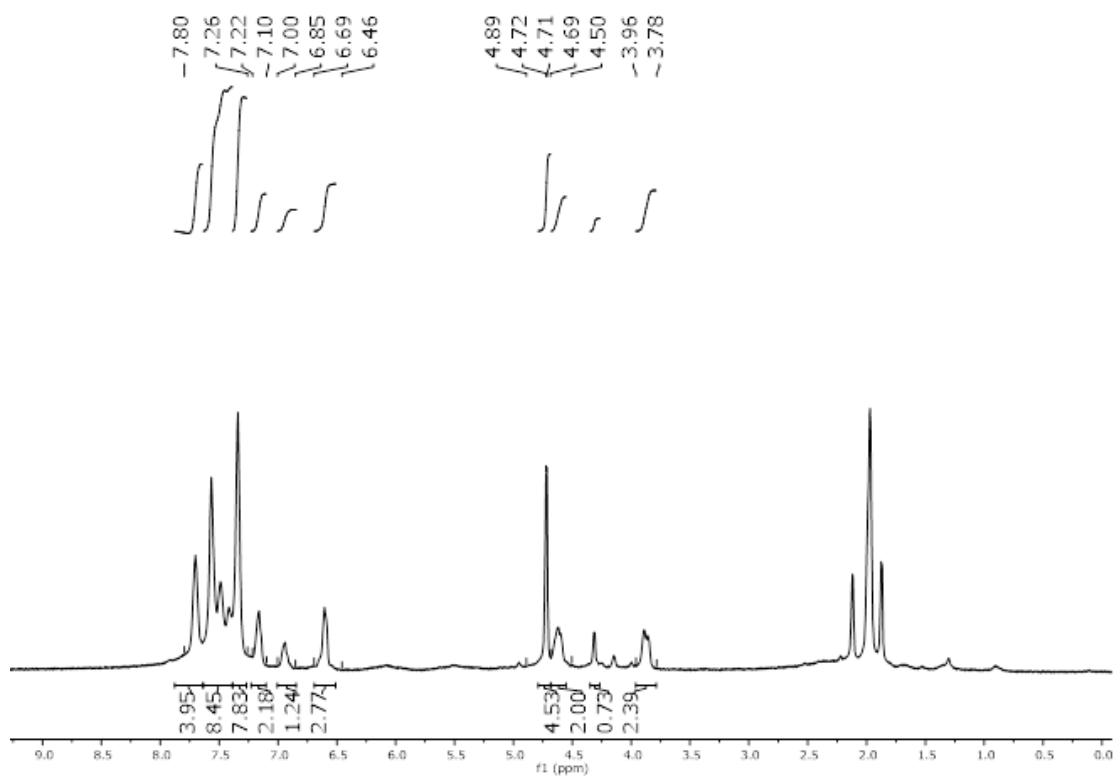


**Figure B-21.**  $^1\text{H}$  NMR spectrum of  $[\text{Ru}(\text{Cp})(\text{P}^{\text{Ph}}_2\text{N}^{\text{Ph}}_1)(\text{NCCD}_3)]\text{PF}_6$  (**3-3**) in  $\text{CD}_3\text{CN}$ .

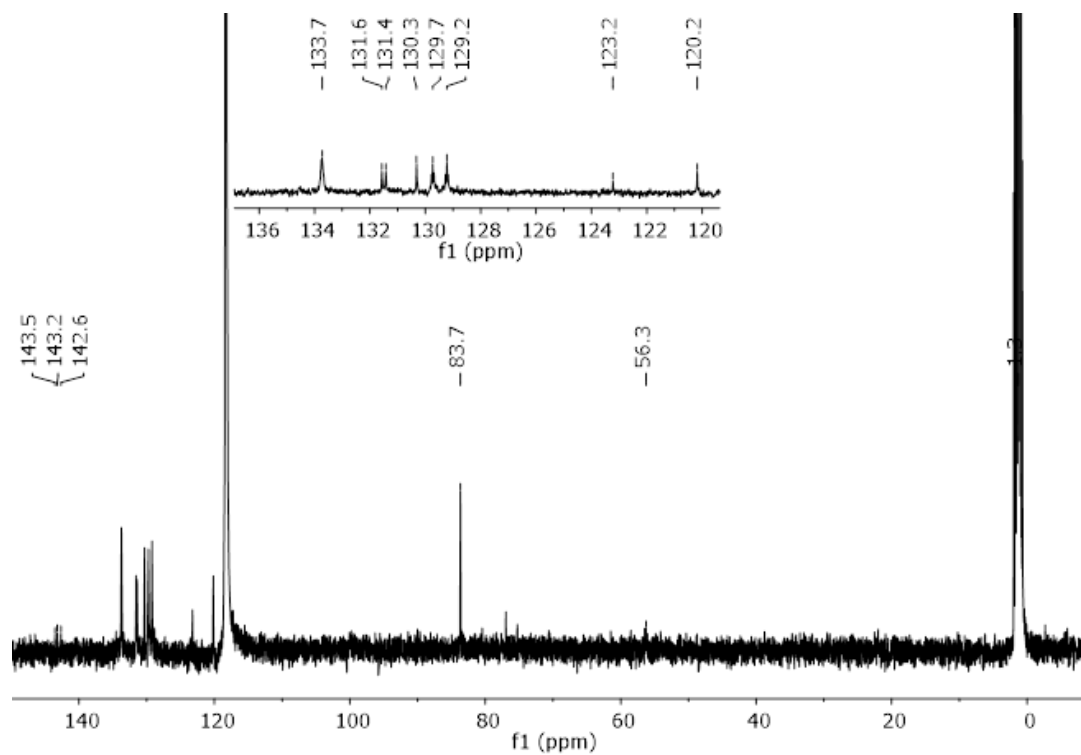


**Figure B-22.**  $^{13}\text{C}$   $\{^1\text{H}\}$  NMR spectrum of  $[\text{Ru}(\text{Cp})(\text{P}^{\text{Ph}}_2\text{N}^{\text{Ph}}_1)(\text{NCCD}_3)]\text{PF}_6$  (**3-3**) in  $\text{CD}_3\text{CN}$ .

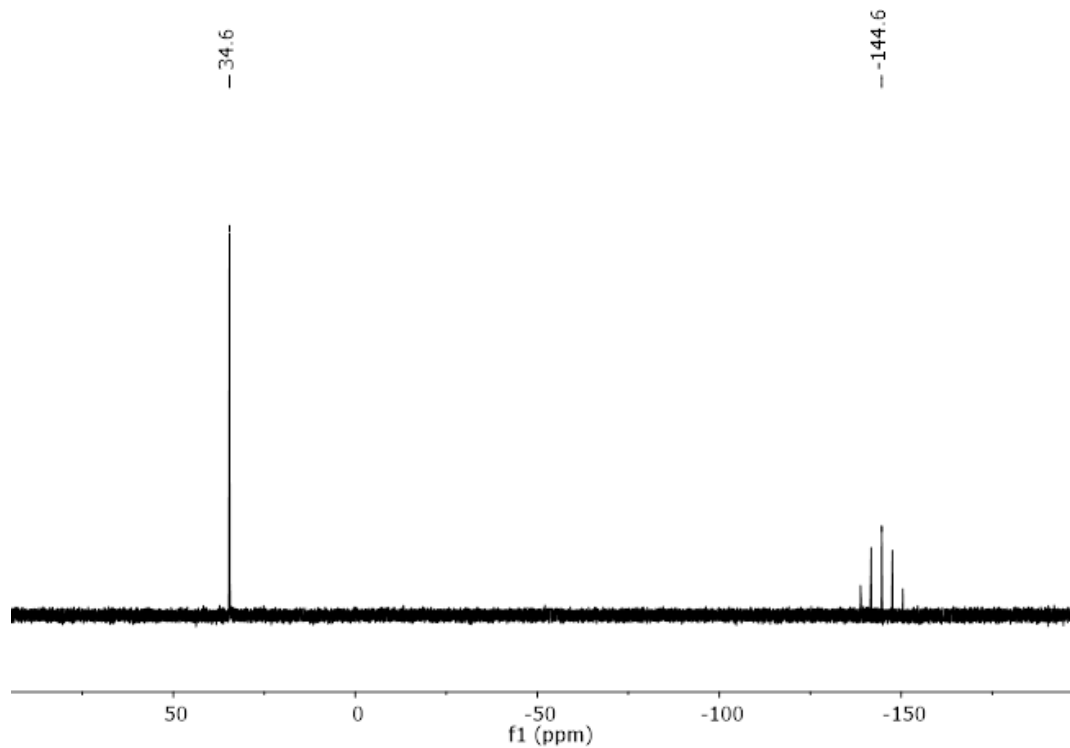


**Figure B-23.**  $^{31}\text{P}$   $\{^1\text{H}\}$  NMR spectrum of  $[\text{Ru}(\text{Cp})(\text{P}^{\text{Ph}}_2\text{N}^{\text{Ph}}_1)(\text{NCCD}_3)]\text{PF}_6$  (**3-3**) in  $\text{CD}_3\text{CN}$ .

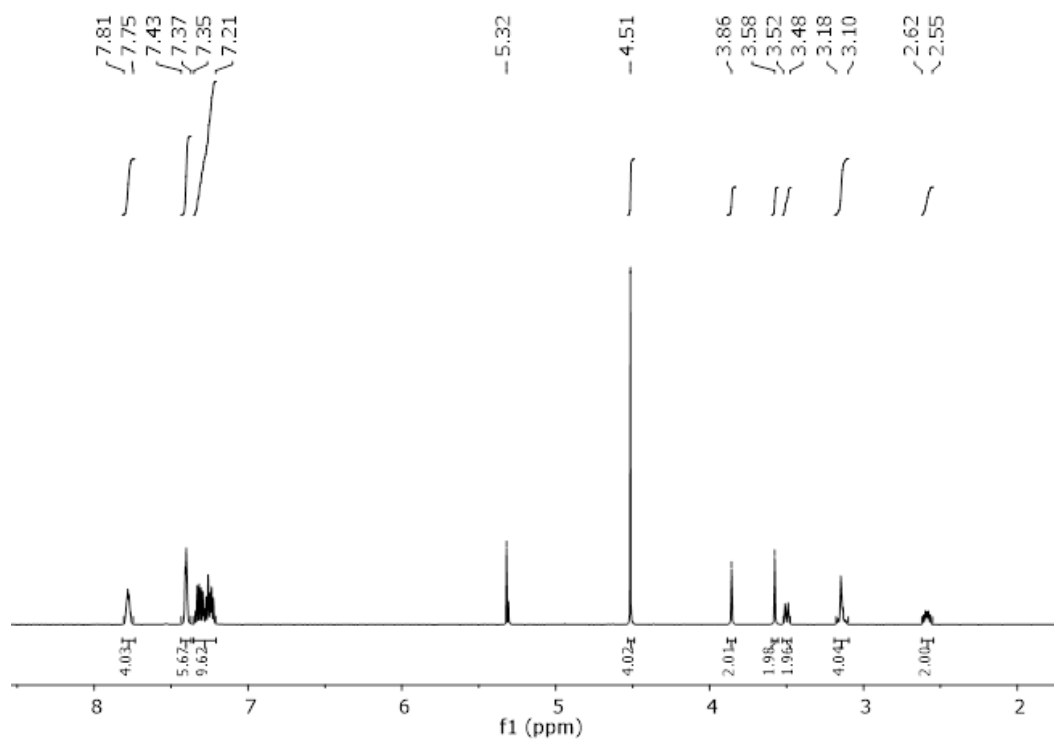


**Figure B-24.**  $^1\text{H}$  NMR spectrum of  $\text{Ru}(\text{Cp})(\text{Cl})(\text{P}^{\text{Ph}}_2\text{N}^{\text{Bn}}_2)$  (**3-5**) in  $\text{CD}_2\text{Cl}_2$ .

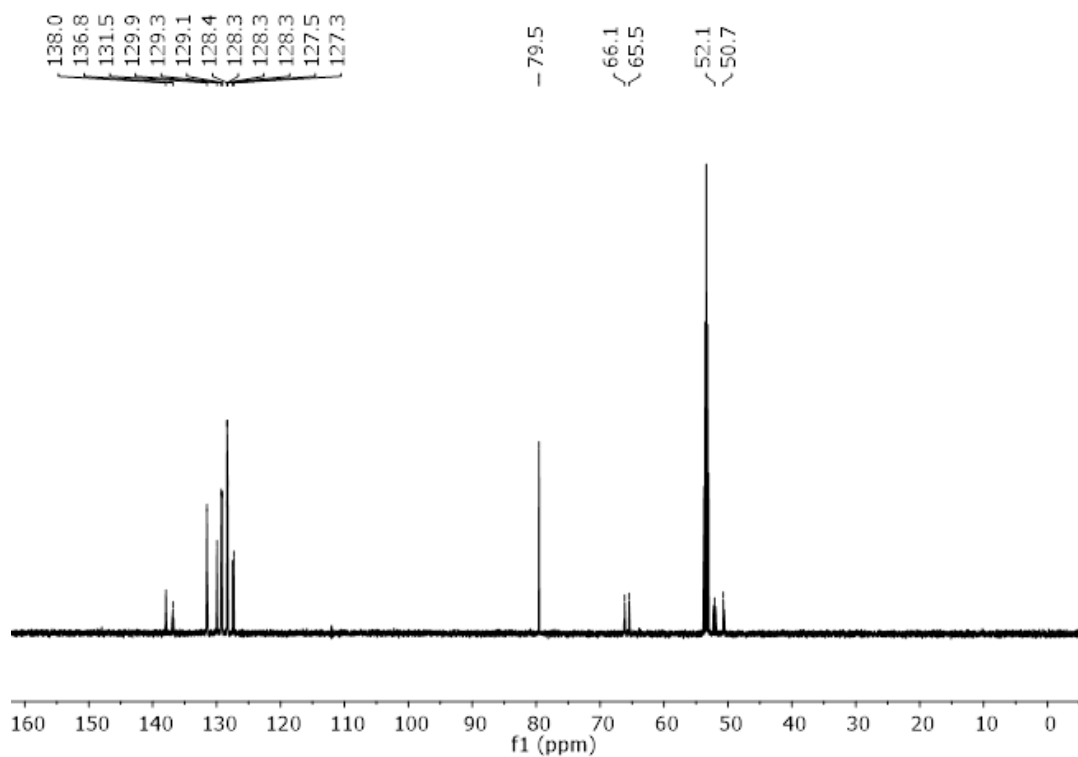


**Figure B-25.**  $^{13}\text{C}$   $\{^1\text{H}\}$  NMR spectrum of  $\text{Ru}(\text{Cp})(\text{Cl})(\text{P}^{\text{Ph}}_2\text{N}^{\text{Bn}}_2)$  (**3-5**) in  $\text{CD}_2\text{Cl}_2$ .

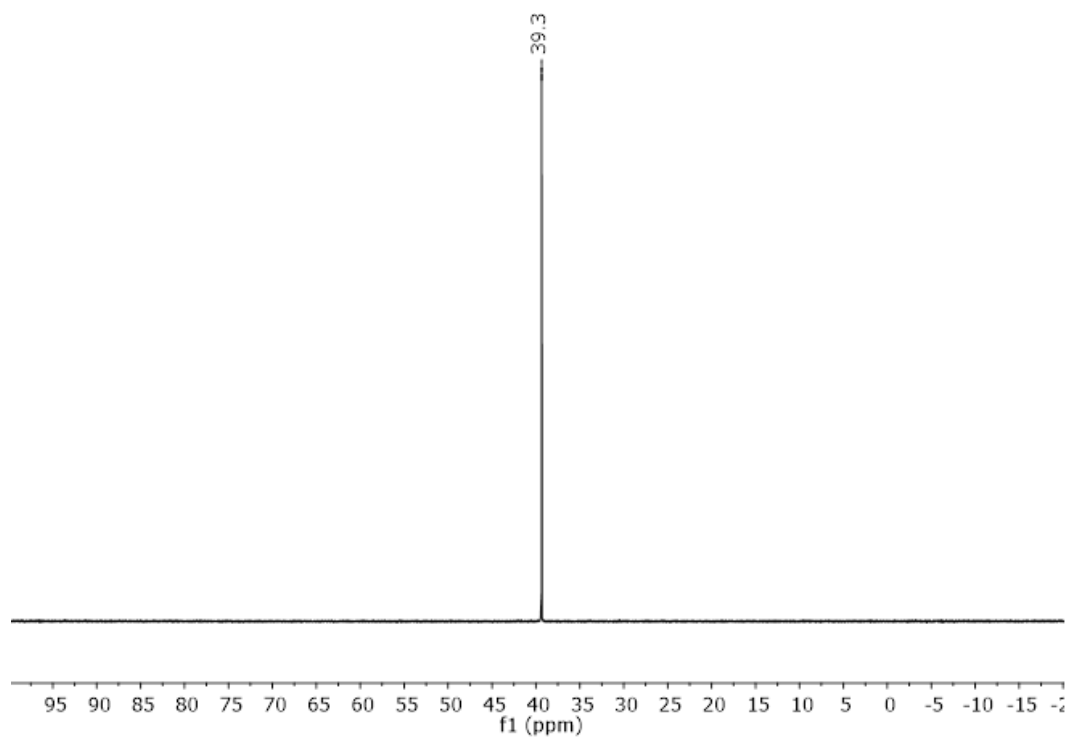


**Figure B-26.**  $^{31}\text{P}$   $\{^1\text{H}\}$  NMR spectrum of  $\text{Ru}(\text{Cp})(\text{Cl})(\text{P}^{\text{Ph}}_2\text{N}^{\text{Bn}}_2)$  (**3-5**) in  $\text{CD}_2\text{Cl}_2$ .

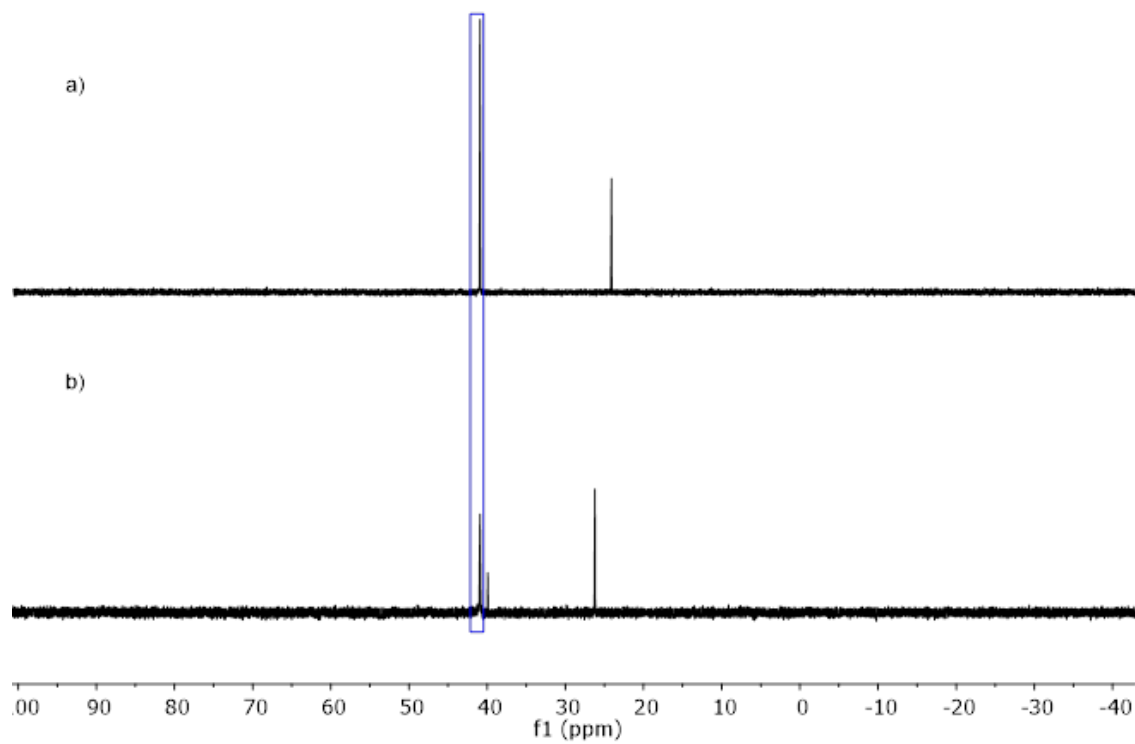


**Figure B-27.**  $^{31}\text{P}$   $\{^1\text{H}\}$  NMR stack plot of  $\text{Ru}(\text{Cp})(\text{Cl})(\text{P}^{\text{Ph}}_2\text{N}^{\text{Bn}}_2)$  (**3-5**) with indole in *proteo*-THF.

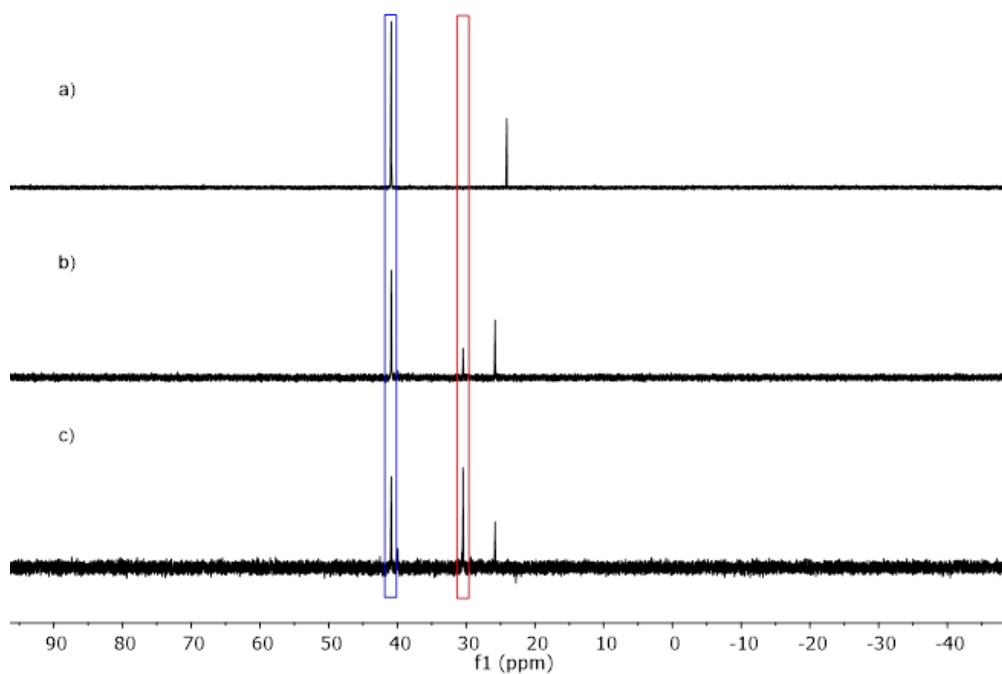
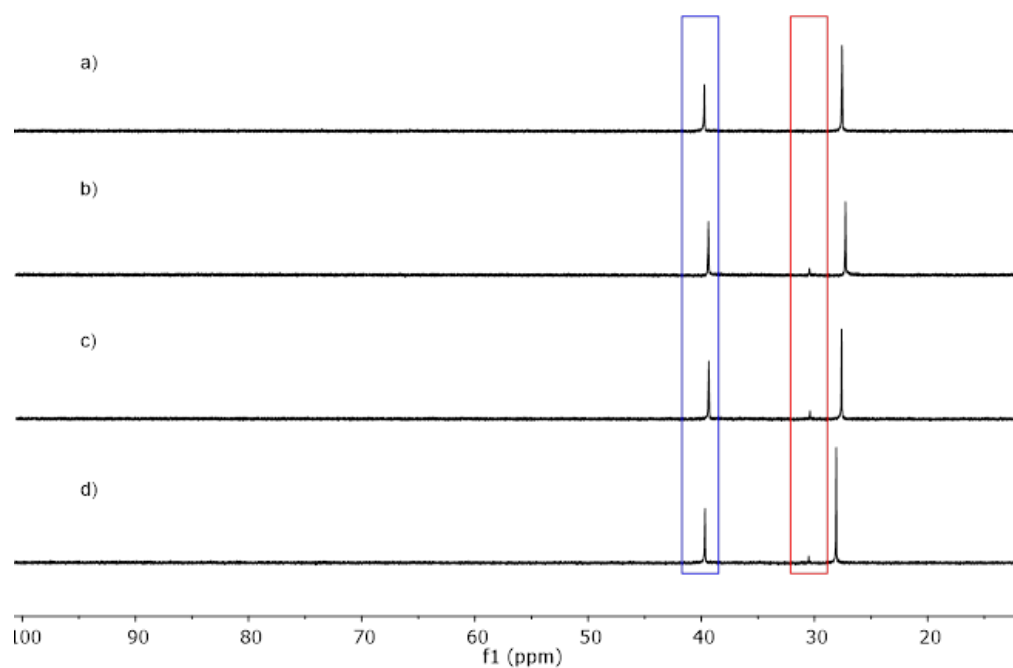
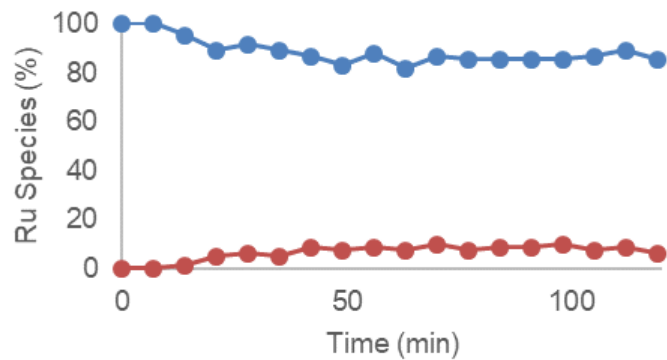


Figure S28:  $^{31}\text{P} \{^1\text{H}\}$  NMR stack plot of  $\text{Ru}(\text{Cp})(\text{Cl})(\text{P}^{\text{Ph}}_2\text{N}^{\text{Bn}}_2)$  (**3-5**) with aniline in proteo-THF.



**Figure B-29.**  $^{31}\text{P} \{^1\text{H}\}$  NMR stack plot of  $[\text{Ru}(\text{Cp})(\text{P}^{\text{Ph}}_2\text{N}^{\text{Bn}}_2)(\text{NCMe})]\text{PF}_6$  (**2-1b** – blue) with 2-ethynylaniline producing a new singlet at 30.6 ppm (red) in *proteo*-THF at a)  $T = 0$ ; b) 15 min; c) 1 h; d) 2 h.





**Figure B-30.** Graph of species present during the reaction of  $[\text{Ru}(\text{Cp})(\text{P}^{\text{Ph}}_2\text{N}^{\text{Bn}}_2)(\text{NCMe})]\text{PF}_6$  (**2-1b**) (blue) with 2-ethynylaniline monitored by  $^{31}\text{P}\{^1\text{H}\}$  NMR in *proteo*-THF producing a new singlet at 30.4 ppm (red).

### IR Spectra

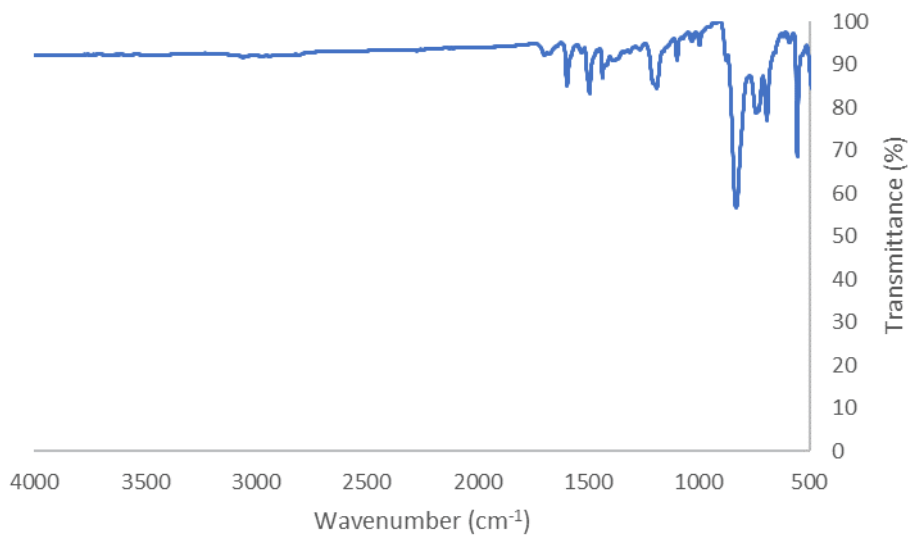
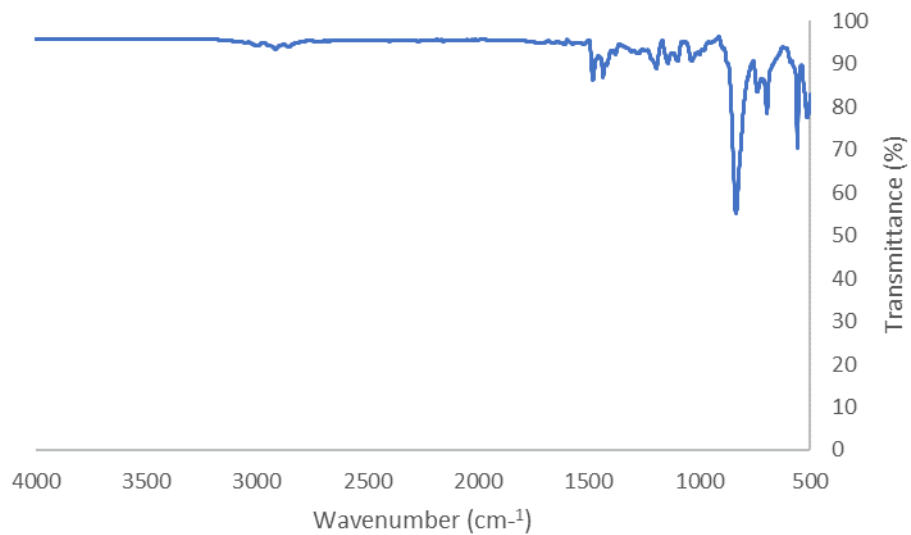
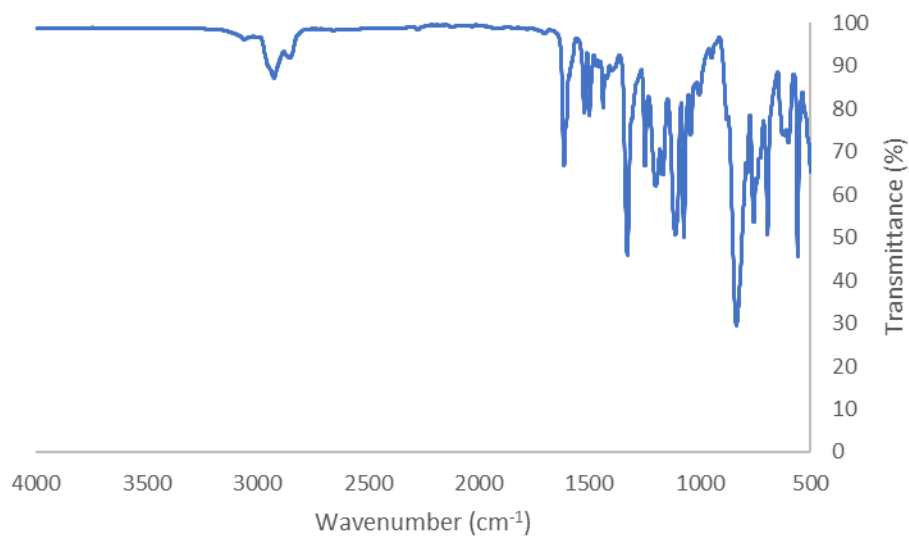


Figure B-31 A solid IR spectrum of  $[\text{Ru}(\text{Cp})(\text{P}^{\text{Ph}}_2\text{N}^{\text{Ph}}_2)(\text{NCMe})]\text{PF}_6$  (**3-2a**) collected with a PerkinElmer UATR Two FT-IR Spectrum Two



**Figure B-32.** A solid IR spectrum of  $[\text{Ru}(\text{Cp})(\text{P}^{\text{Ph}}_2\text{N}^{\text{Mes}}_2)(\text{NCMe})]\text{PF}_6$  (**3-2b**) collected with a PerkinElmer UATR Two FT-IR Spectrum Two



**Figure B-33.** A solid IR spectrum of  $[\text{Ru}(\text{Cp})(\text{P}^{\text{Ph}}_2\text{N}^{p\text{-CF}_3\text{-C}_4\text{H}_4}_2)(\text{NCMe})]\text{PF}_6$  (**3-2c**) collected with a PerkinElmer UATR Two FT-IR Spectrum Two

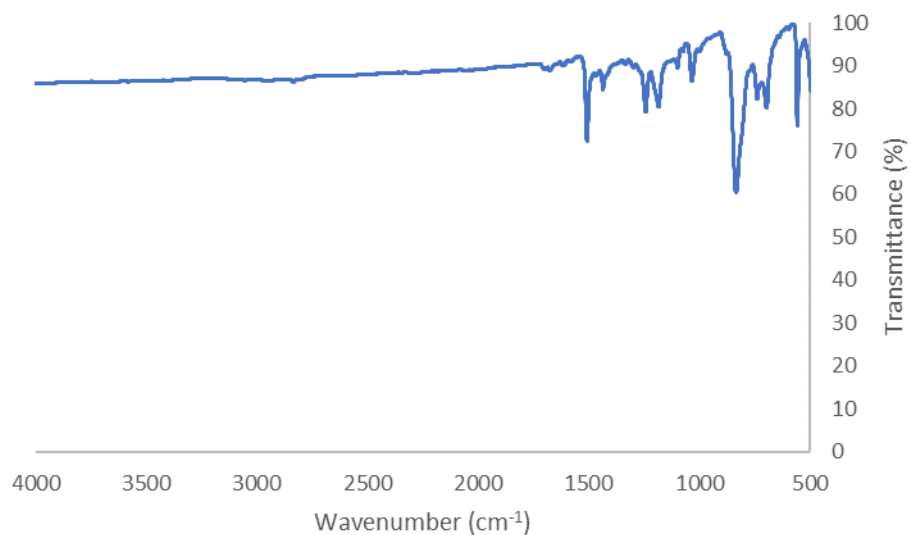


**Figure B-34.** A solid IR spectrum of  $[\text{Ru}(\text{Cp})(\text{P}^{\text{Ph}}_2\text{N}^{p\text{-MeO-C}_4\text{H}_4}_2)(\text{NCMe})]\text{PF}_6$  (**3-2d**) collected with a PerkinElmer UATR Two FT-IR Spectrum Two

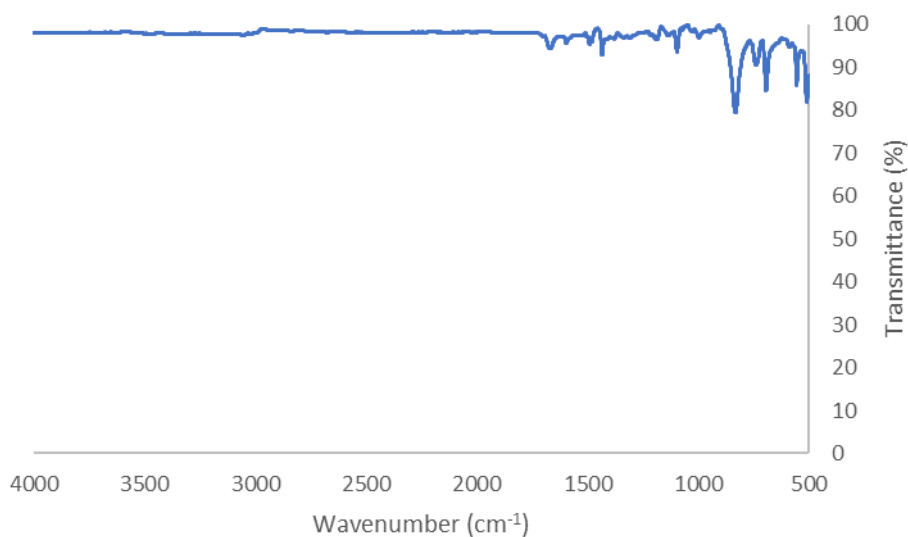


**Figure B-35.** A solid IR spectrum of  $[\text{Ru}(\text{Cp})(\text{P}^{\text{Ph}}_2\text{N}^{\text{Ph}}_1)]\text{PF}_6$  (**3-4**) collected with a PerkinElmer UATR Two FT-IR Spectrum Two

## MALDI Mass Spectrometry Data

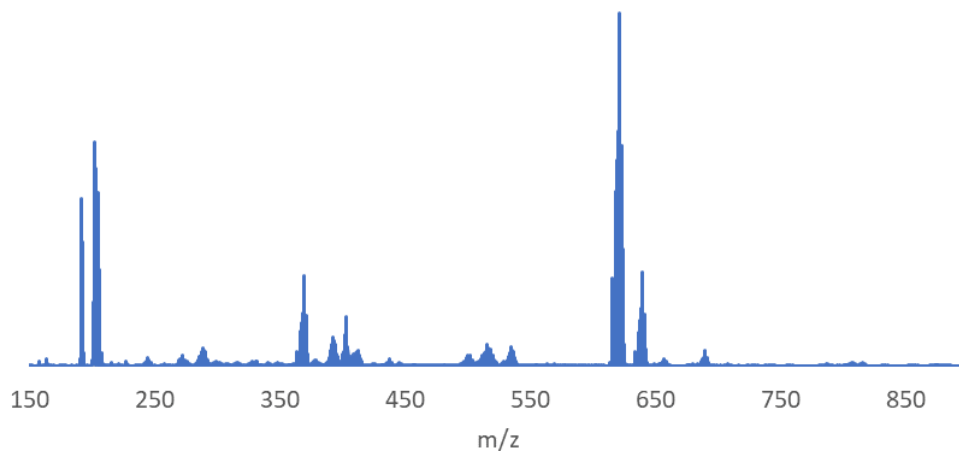


**Figure B-36.** MALDI-TOF mass spectrometry of  $[\text{Ru}(\text{Cp})(\text{P}^{\text{Ph}_2}\text{N}^{\text{Ph}_2})(\text{NCMe})]\text{PF}_6$  (**3-2a**) in a 1:20 ratio of pyrene, the matrix.

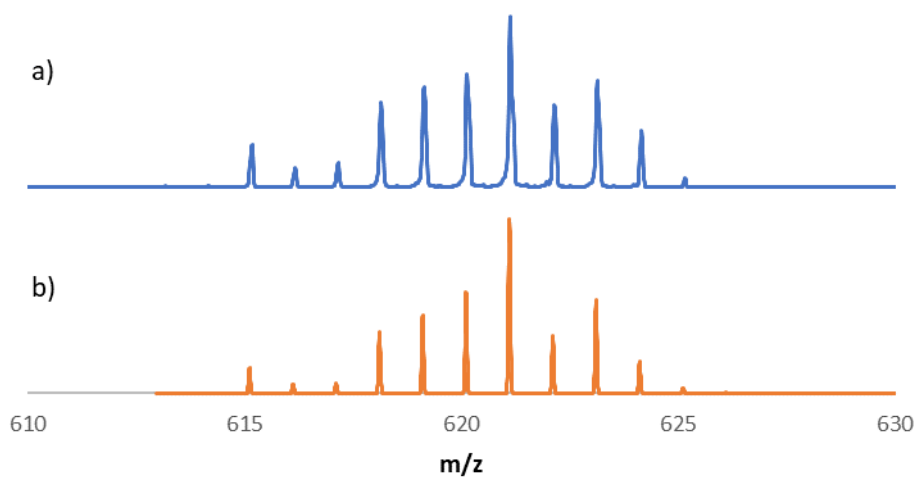


**Figure B-37.** a) Zoom-in of MALDI-TOF mass spectrometry of  $[\text{CpRu}(\text{P}^{\text{Ph}_2}\text{N}^{\text{Bn}_2})]^{+\bullet}$  generated from **3-2a** in a 1:20 ratio of pyrene, the matrix. b) Simulation of MALDI-TOF mass spectrometry of  $[\text{CpRu}(\text{P}^{\text{Ph}_2}\text{N}^{\text{Ph}_2})]^{+\bullet}$ .

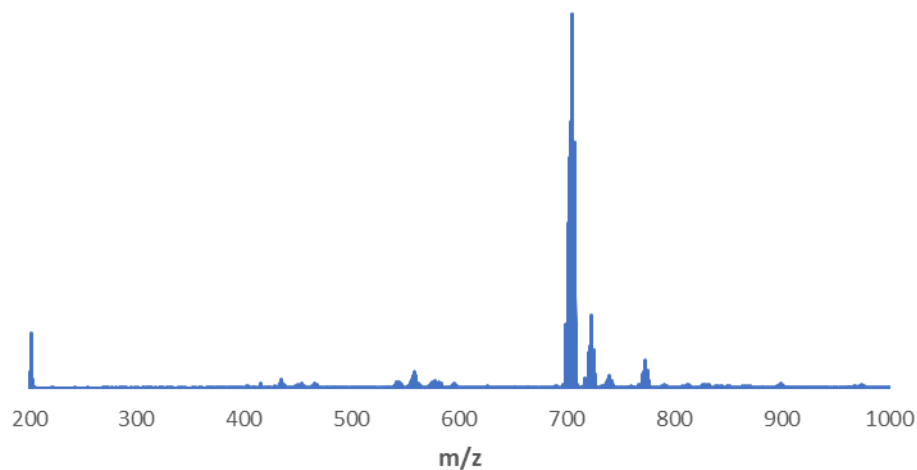


**Figure B-38.** MALDI-TOF mass spectrometry of  $[\text{Ru}(\text{Cp})(\text{P}^{\text{Ph}}_2\text{N}^{\text{Mes}}_2)(\text{NCMe})]\text{PF}_6$  (**3-2b**) in a 1:20 ratio of pyrene, the matrix.

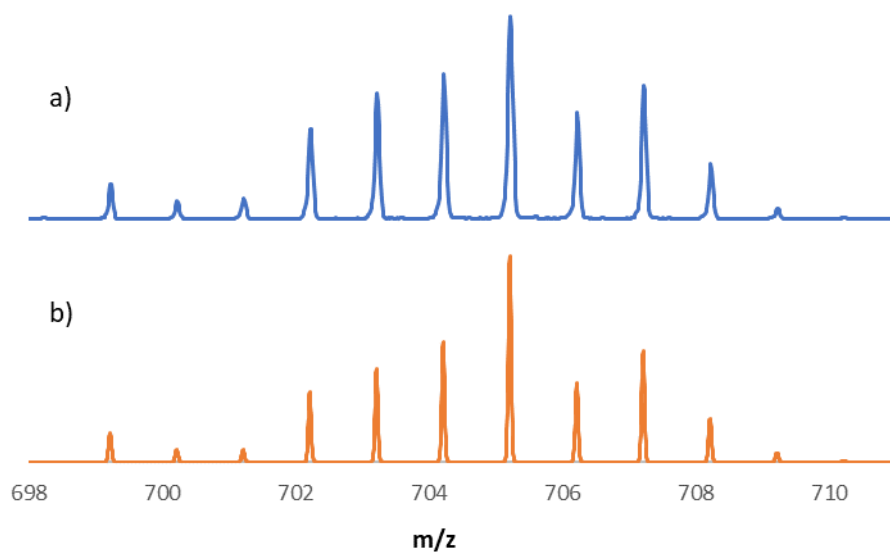


**Figure B-39.** a) Zoom-in of MALDI-TOF mass spectrometry of  $[\text{CpRu}(\text{P}^{\text{Ph}}_2\text{N}^{\text{Mes}}_2)]^{+\bullet}$  generated from  $[\text{Ru}(\text{Cp})(\text{P}^{\text{Ph}}_2\text{N}^{\text{Mes}}_2)(\text{NCMe})]\text{PF}_6$  (**3-2b**) in a 1:20 ratio of pyrene, the matrix. b) Simulation of MALDI-TOF mass spectrometry of  $[\text{CpRu}(\text{P}^{\text{Ph}}_2\text{N}^{\text{Mes}}_2)]^{+\bullet}$ .

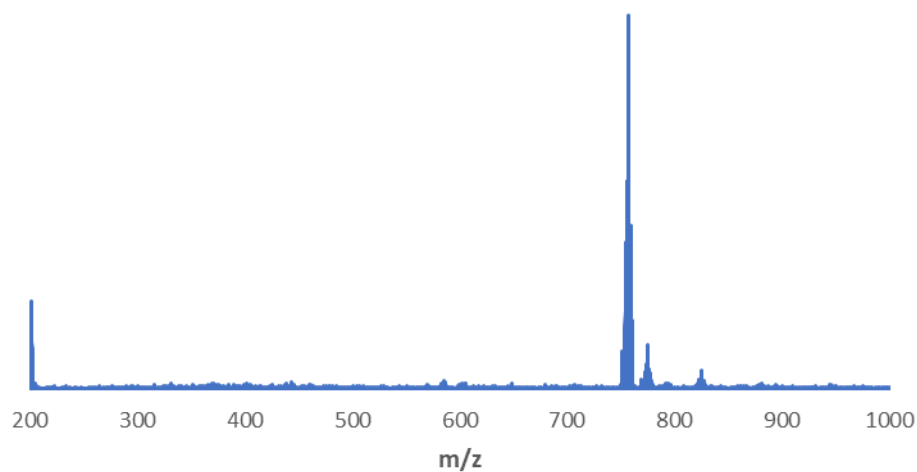


**Figure B-40.** MALDI-TOF mass spectrometry of  $[\text{Ru}(\text{Cp})(\text{P}^{\text{Ph}_2\text{N}^{\text{p-CF}_3\text{-C}_4\text{H}_4_2})(\text{NCMe})]\text{PF}_6$  (**3-2c**) in a 1:20 ratio of pyrene, the matrix.

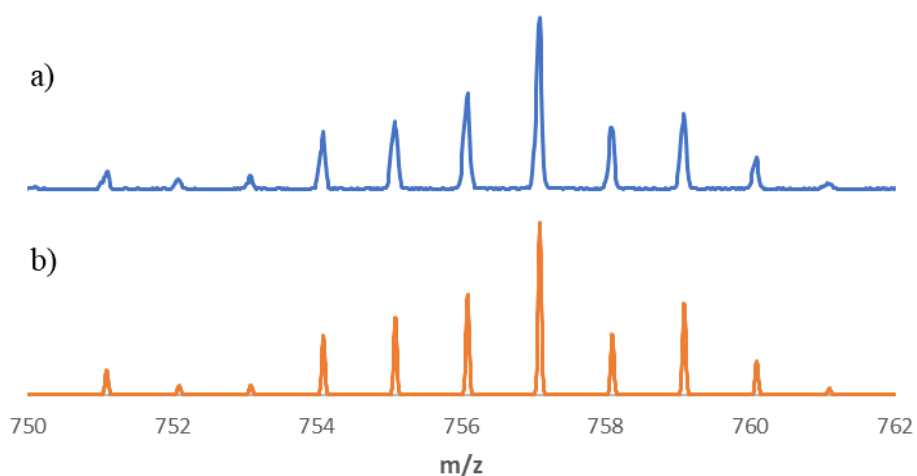


**Figure B-41.** a) Zoom-in of MALDI-TOF mass spectrometry of  $[\text{CpRu}(\text{P}^{\text{Ph}_2\text{N}^{\text{p-CF}_3\text{-C}_4\text{H}_4_2})]^{\bullet+}$  generated from  $[\text{Ru}(\text{Cp})(\text{P}^{\text{Ph}_2\text{N}^{\text{p-CF}_3\text{-C}_4\text{H}_4_2})(\text{NCMe})]\text{PF}_6$  (**3-2c**) in a 1:20 ratio of pyrene, the matrix. b) Simulation of MALDI-TOF mass spectrometry of  $[\text{CpRu}(\text{P}^{\text{Ph}_2\text{N}^{\text{p-CF}_3\text{-C}_4\text{H}_4_2})]^{\bullet+}$ .

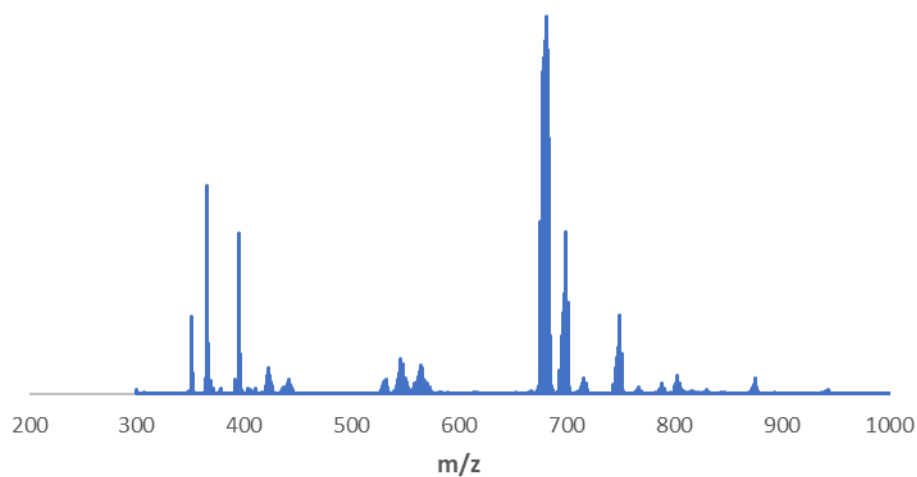


**Figure B-42.** MALDI-TOF mass spectrometry of  $[\text{Ru}(\text{Cp})(\text{P}^{\text{Ph}_2\text{N}^{\text{MeO}_2})(\text{NCMe})]\text{PF}_6$  (**3-2d**) in a 1:20 ratio of pyrene, the matrix.

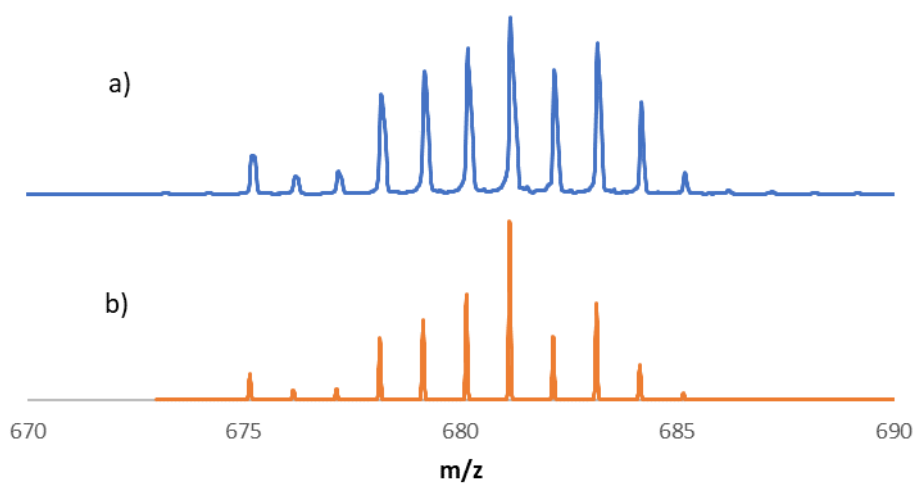


**Figure B-43.** a) Simulation of MALDI-TOF mass spectrometry of  $[\text{CpRu}(\text{P}^{\text{Ph}_2\text{N}^{\text{p-MeO-C}_4\text{H}_4_2})]^{+\bullet}$  b) Zoom-in of MALDI-TOF mass spectrometry of  $[\text{CpRu}(\text{P}^{\text{Ph}_2\text{N}^{\text{MeO}_2})]^{+\bullet}$  generated from  $[\text{Ru}(\text{Cp})(\text{P}^{\text{Ph}_2\text{N}^{\text{MeO}_2})(\text{NCMe})]\text{PF}_6$  (**3-2d**) in a 1:20 ratio of pyrene, the matrix.

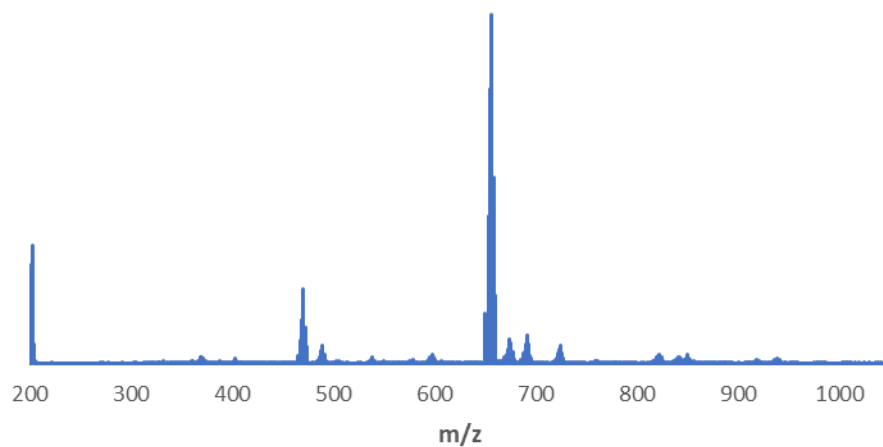


**Figure B-44.** MALDI-TOF mass spectrometry of  $[\text{Ru}(\text{Cp})(\text{P}^{\text{Ph}}_2\text{N}^{\text{Ph}}_1)]\text{PF}_6$  (**3-4**) in a 1:20 ratio of pyrene, the matrix.

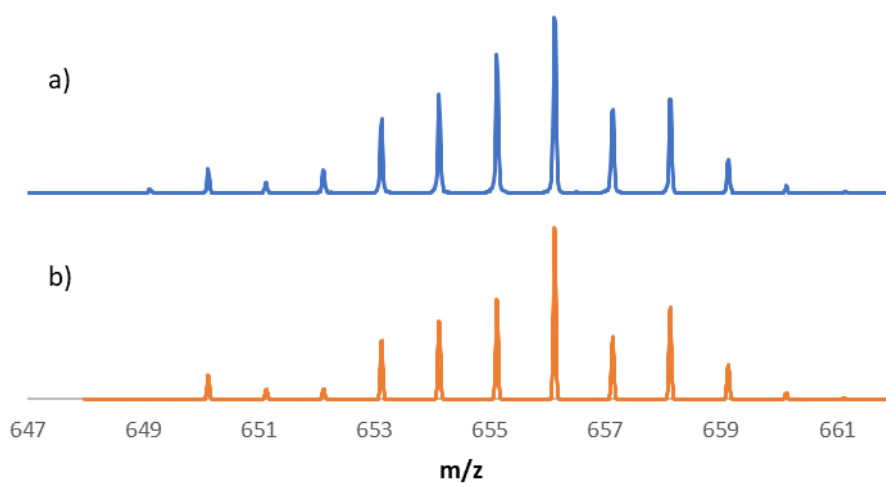


**Figure B-45.** a) Zoom-in of MALDI-TOF mass spectrometry of  $[\text{CpRu}(\text{P}^{\text{Ph}}_2\text{N}^{\text{Bn}}_1)]^+ \cdot$  generated from  $[\text{Ru}(\text{Cp})(\text{P}^{\text{Ph}}_2\text{N}^{\text{Ph}}_1)]\text{PF}_6$  (**3-4**) in a 1:20 ratio of pyrene, the matrix. b) Simulation of MALDI-TOF mass spectrometry of  $[\text{CpRu}(\text{P}^{\text{Ph}}_2\text{N}^{\text{Ph}}_1)]^+ \cdot$ .



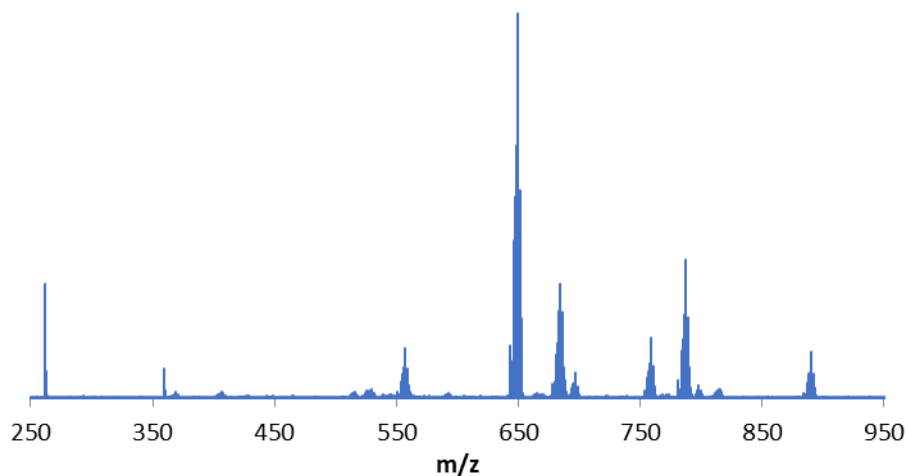


**Figure B-46.** MALDI-TOF mass spectrometry of Ru(Cp)(Cl)(P<sup>Ph<sub>2</sub>N<sup>Bn<sub>2</sub></sup>) (3-5) in a 1:20 ratio of pyrene, the matrix.</sup>

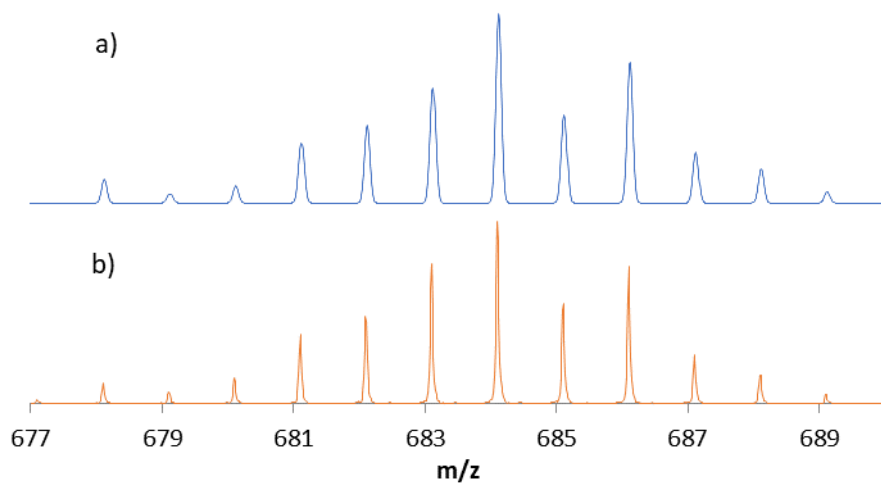


**Figure B-47.** a) Simulation of MALDI-TOF mass spectrometry of [CpRu(P<sup>Ph<sub>2</sub>N<sup>Bn<sub>2</sub></sup>)Cl]<sup>+</sup>. b) Zoom-in of MALDI-TOF mass spectrometry of [CpRu(P<sup>Ph<sub>2</sub>N<sup>Bn<sub>2</sub></sup>)Cl]<sup>+</sup> generated from Ru(Cp)(Cl)(P<sup>Ph<sub>2</sub>N<sup>Bn<sub>2</sub></sup>) (3-5) in a 1:20 ratio of pyrene, the matrix.</sup></sup></sup>

## Crystallographic Details

*Data Collection and Processing.* The sample of **3-5** was mounted on a Mitegen polyimide micromount with a small amount of Paratone N oil. All X-ray measurements were made on a Bruker Kappa Axis Apex2 diffractometer at a temperature of 110 K. The unit cell dimensions were determined from a symmetry constrained fit of 9928 reflections with  $5.6^\circ < 2\theta < 67.98^\circ$ . The data collection strategy was a number of  $\omega$  and  $\varphi$  scans which collected data up to  $74.154^\circ$  ( $2\theta$ ). The frame integration was performed using SAINT.<sup>5</sup> The resulting raw data was scaled and absorption corrected using a multi-scan averaging of symmetry equivalent data using SADABS.<sup>6</sup>

*Structure Solution and Refinement.* The structure was solved by direct methods using the SIR2011 program.<sup>7</sup> All non-hydrogen atoms were obtained from the initial solution. The hydrogen atoms were introduced at idealized positions and were allowed to ride on the parent atom. The structural model was fit to the data using full matrix least-squares based on  $F^2$ . The calculated structure factors included corrections for anomalous dispersion from the usual tabulation. The structure was refined using the SHELXL-2013 program.<sup>8</sup> Graphic plots were produced using the NRCVAX program suite.<sup>9</sup> Additional information and other relevant literature references can be found in the reference section of this website (<http://xray.chem.uwo.ca>).

---

5. Bruker-Nonius, SAINT version 2012.12, **2012**, Bruker-Nonius, Madison, WI 53711, USA

6. Bruker-Nonius, SADABS version 2012.1, **2012**, Bruker-Nonius, Madison, WI 53711, USA

7. Burla, M. C.; Caliendo, R.; Camalli, M.; Carrozzini, B.; Cascarano, G. L.; Giacovazzo, C.; Mallamo, M.; Mazzone, A.; Polidori, G.; Spagna, R. *J. Appl. Cryst.* **2012**, *45*, 357-361

8. Sheldrick, G. M., *Acta Cryst.* **2008**, *A64*, 112-122

9. Gabe, E. J.; Le Page, Y.; Charland, J. P.; Lee, F. L. and White, P. S. *J. Appl. Cryst.* **1989**, *22*, 384-387

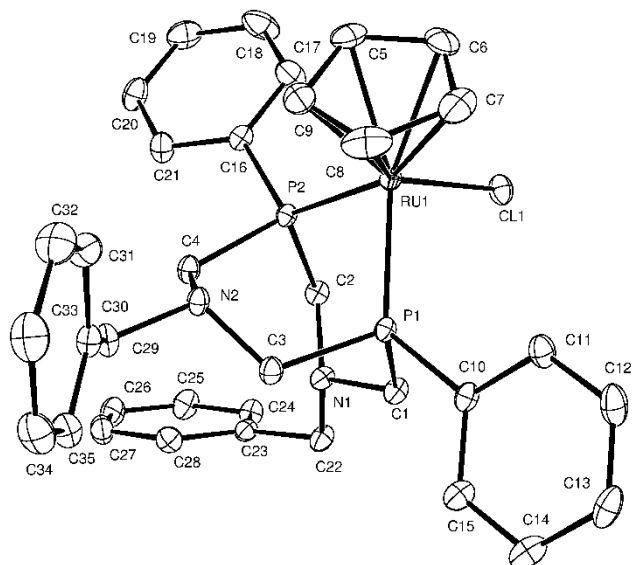


**Figure B-48.** ORTEP drawing of **3-5** showing naming and numbering scheme. Ellipsoids are at the 50% probability level and hydrogen atoms were omitted for clarity.

*Data Collection and Processing.* The sample (**3-2a**) was mounted on a Mitegen polyimide micromount with a small amount of Paratone N oil. All X-ray measurements were made on a Bruker Kappa Axis Apex2 diffractometer at a temperature of 110 K. The unit cell dimensions were determined from a symmetry constrained fit of 6781 reflections with  $4.46^\circ < 2\theta < 51.02^\circ$ . The data collection strategy was a number of  $\omega$  and  $\phi$  scans which collected data up to  $48.498^\circ$  ( $2\theta$ ). The frame integration was performed using SAINT.<sup>1</sup> The resulting raw data was scaled and absorption corrected using a multi-scan averaging of symmetry equivalent data using SADABS.<sup>2</sup>

*Structure Solution and Refinement.* The structure was solved by using a dual space methodology using the SHELXT program.<sup>3</sup> All non-hydrogen atoms were obtained from the initial solution. The hydrogen atoms were introduced at idealized positions and were allowed to ride on the parent atom. The structural model was fit to the data using full matrix least-squares based on  $F^2$ . The calculated structure factors included corrections for anomalous dispersion from the usual tabulation. The structure was refined using the SHELXL program from the SHELXTL suite of crystallographic software.<sup>4</sup> Graphic plots were produced using the SHELXP XP program suite.<sup>ref</sup> Additional information and other relevant literature references can be found in the reference section of this website (<http://xray.chem.uwo.ca>).

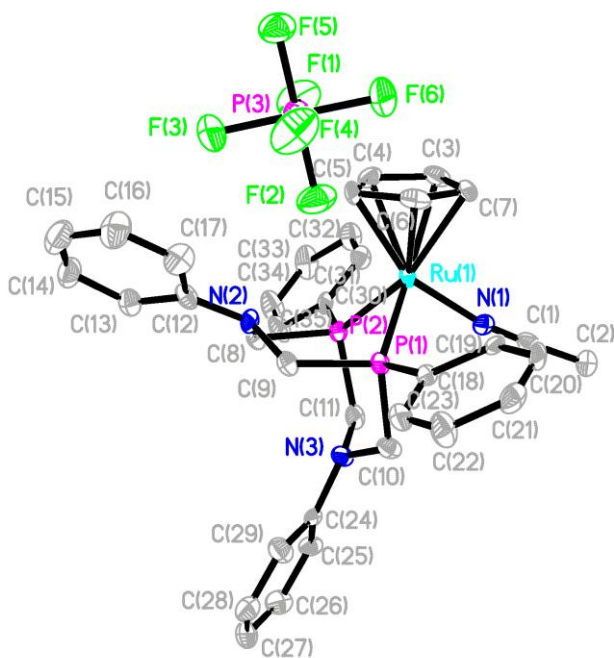


**Figure B-49.** ORTEP drawing of **3-2a** showing naming and numbering scheme. Ellipsoids are at the 50% probability level and hydrogen atoms were omitted for clarity.

**Table B-1.** Summary of Crystal Data for **3-5** and **3-2a**

Formula	C <sub>35</sub> H <sub>37</sub> ClN <sub>2</sub> P <sub>2</sub> Ru ( <b>3-5</b> )	C <sub>41</sub> H <sub>48</sub> F <sub>6</sub> N <sub>3</sub> P <sub>3</sub> Ru ( <b>3-2a</b> )
Formula Weight ( <i>g/mol</i> )	684.12	890.80
Crystal Dimensions ( <i>mm</i> )	0.164 × 0.104 × 0.079	0.219 × 0.064 × 0.062
Crystal Color and Habit	yellow prism	colourless needle
Crystal System	monoclinic	monoclinic
Space Group	P 2 <sub>1</sub> /c	C 2/c
Temperature, K	110	110
<i>a</i> , Å	12.957(4)	36.600(17)
<i>b</i> , Å	14.386(5)	9.698(5)
<i>c</i> , Å	20.061(6)	19.048(8)
α, °	90	90
β, °	122.986(9)	93.569(11)
γ, °	90	90
<i>V</i> , Å <sup>3</sup>	3136.7(17)	6748(5)
Number of reflections to determine final unit cell	9928	6781
Min and Max 2θ for cell determination, °	5.6, 67.98	4.46, 51.02
<i>Z</i>	4	8
F(000)	1408	3664
ρ ( <i>g/cm</i> )	1.449	1.754
λ, Å, (MoKα)	0.71073	0.71073
μ, ( <i>cm</i> <sup>-1</sup> )	0.714	0.680
Diffractometer Type	Bruker Kappa Axis Apex2	Bruker Kappa Axis Apex2
Scan Type(s)	omega and phi scans	phi and omega scans
Max 2θ for data collection, °	74.154	48.498
Measured fraction of data	0.998	0.999
Number of reflections measured	168549	42618
Unique reflections measured	16004	5443
R <sub>merge</sub>	0.0683	0.1767
Number of reflections included in refinement	16004	5443
Cut off Threshold Expression	I > 2σ(I)	I > 2σ(I)
Structure refined using	full matrix least-squares using F <sup>2</sup>	full matrix least-squares using F <sup>2</sup>
Weighting Scheme	w=1/[σ(Fo <sup>2</sup> )+(0.0286P) <sup>2</sup> +1.3265P] ] where P=(Fo <sup>2</sup> +2Fc <sup>2</sup> )/3	w=1/[σ(Fo <sup>2</sup> )+(0.1107P) <sup>2</sup> ] where P=(Fo <sup>2</sup> +2Fc <sup>2</sup> )/3
Number of parameters in least-squares	370	435
R <sub>1</sub>	0.0360	0.0646
wR <sub>2</sub>	0.0692	0.1581

R <sub>1</sub> (all data)	0.0665	0.1005
wR <sub>2</sub> (all data)	0.0788	0.1796
GOF	1.030	0.995
Maximum shift/error	0.001	0.001
Min & Max peak heights on final ΔF Map (e <sup>-</sup> /Å)	-0.922, 0.883	-1.354, 1.759

Where:

$$R_1 = \sum (|F_o| - |F_c|) / \sum F_o$$

$$wR_2 = [ \sum (w(F_o^2 - F_c^2))^2 / \sum (w F_o^4) ]^{1/2}$$

$$GOF = [ \sum (w(F_o^2 - F_c^2))^2 / (\text{No. of reflns.} - \text{No. of params.}) ]^{1/2}$$

*Data Collection and Processing.* The sample (**3-1d**) was mounted on a Mitegen polyimide micromount with a small amount of Paratone N oil. All X-ray measurements were made on a Bruker Kappa Axis Apex2 diffractometer at a temperature of 120 K. The unit cell dimensions were determined from a symmetry constrained fit of 9990 reflections with  $5.76^\circ < 2\theta < 64.44^\circ$ . The data collection strategy was a number of  $\omega$  and  $\phi$  scans which collected data up to  $66.52^\circ$  ( $2\theta$ ). The frame integration was performed using SAINT.<sup>1</sup> The resulting raw data was scaled and absorption corrected using a multi-scan averaging of symmetry equivalent data using SADABS.<sup>2</sup>

*Structure Solution and Refinement.* The structure was solved by using a dual space methodology using the SHELXT program.<sup>3</sup> All non-hydrogen atoms were obtained from the initial solution. The hydrogen atoms were introduced at idealized positions and were allowed to ride on the parent atom. The structural model was fit to the data using full matrix least-squares based on  $F^2$ . The calculated structure factors included corrections for anomalous dispersion from the usual tabulation. The structure was refined using the SHELXL program from the SHELXTL suite of crystallographic software.<sup>4</sup> Graphic plots were produced using the SHELXL XP program suite.<sup>6</sup> Additional information and other relevant literature references can be found in the reference section of this website (<http://xray.chem.uwo.ca>).

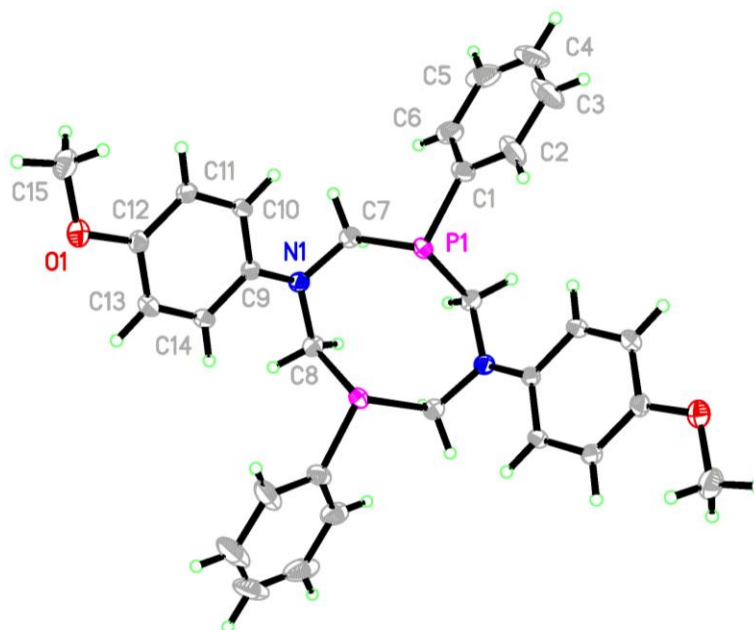


**Figure B-50.** ORTEP drawing of **3-1d** showing naming and numbering scheme. Ellipsoids are at the 50% probability level and hydrogen atoms were omitted for clarity

*Data Collection and Processing.* The **3-1c** was mounted on a Mitegen polyimide micromount with a small amount of Paratone N oil. All X-ray measurements were made on a Bruker Kappa Axis Apex2 diffractometer at a temperature of 110 K. The unit cell dimensions were determined from a symmetry constrained fit of 9974 reflections with  $6.2^\circ < 2\theta < 53.92^\circ$ . The data collection strategy was a number of  $\omega$  and  $\varphi$  scans which collected data up to  $56.634^\circ$  ( $2\theta$ ). The frame integration was performed using SAINT.<sup>1</sup> The resulting raw data was scaled and absorption corrected using a multi-scan averaging of symmetry equivalent data using SADABS.<sup>2</sup>

*Structure Solution and Refinement.* The structure was solved by using a dual space methodology using the SHELXT program.<sup>3</sup> All non-hydrogen atoms were obtained from the initial solution. The hydrogen atoms were introduced at idealized positions and were allowed to ride on the parent atom. The structural model was fit to the data using full matrix least-squares based on  $F^2$ . The calculated structure factors included corrections for anomalous dispersion from the usual tabulation. The structure was refined using the SHELXL program from the SHELXTL suite of crystallographic software.<sup>4</sup> Graphic plots were produced using the SHELXL XP program suite.<sup>6</sup> Additional information and other relevant literature references can be found in the reference section of this website (<http://xray.chem.uwo.ca>).



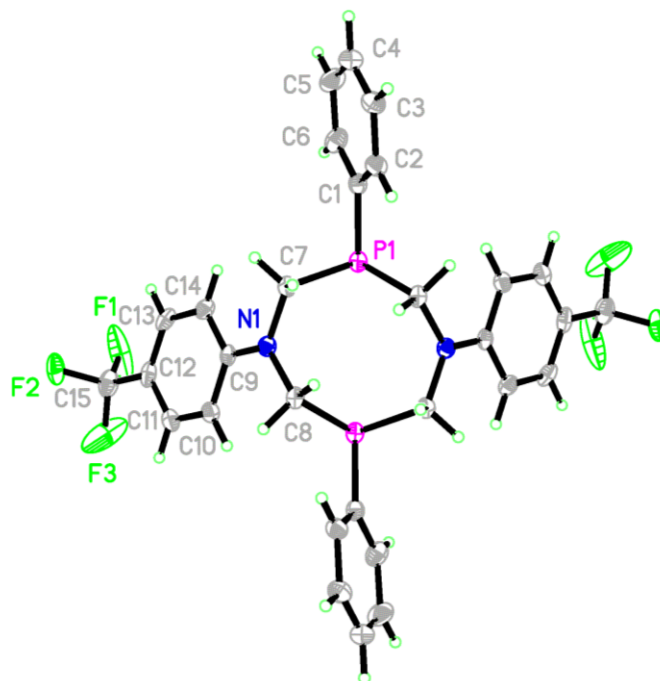


**Figure B-51.** ORTEP drawing of **3-1c** showing naming and numbering scheme. Ellipsoids are at the 50% probability level and hydrogen atoms were omitted for clarity.

**Table B-2.** Summary of Crystal Data for **3-1c** and **3-1d**

Formula	$C_{30}H_{32}N_2O_2P_2$ ( <b>3-1d</b> )	$C_{30}H_{26}F_6N_2P_2$ ( <b>3-1c</b> )
Formula Weight ( <i>g/mol</i> )	514.51	590.47
Crystal Dimensions ( <i>mm</i> )	$0.270 \times 0.206 \times 0.069$	$0.283 \times 0.131 \times 0.092$
Crystal Color and Habit	colourless prism	colourless prism
Crystal System	orthorhombic	orthorhombic
Space Group	<i>P c c n</i>	<i>P c c n</i>
Temperature, K	120	110
<i>a</i> , Å	11.441(4)	13.131(4)
<i>b</i> , Å	23.296(10)	20.176(5)
<i>c</i> , Å	9.784(4)	10.300(3)
$\alpha$ , °	90	90
$\beta$ , °	90	90

$\gamma, ^\circ$	90	90
V, $\text{\AA}^3$	2607.8(18)	2728.8(14)
Number of reflections to determine final unit cell	9990	9974
Min and Max $2\theta$ for cell determination, $^\circ$	5.76, 64.44	6.2, 53.92
Z	4	4
F(000)	1088	1216
$\rho$ (g/cm <sup>3</sup> )	1.310	1.437
$\lambda$ , $\text{\AA}$ , (MoK $\alpha$ )	0.71073	0.71073
$\mu$ , (cm <sup>-1</sup> )	0.198	0.224
Diffractometer Type	Bruker Kappa Axis Apex2	Bruker Kappa Axis Apex2
Scan Type(s)	$\psi$ and $\omega$ scans	$\psi$ and $\omega$ scans
Max $2\theta$ for data collection, $^\circ$	66.52	56.634
Measured fraction of data	0.998	0.999
Number of reflections measured	71376	48779
Unique reflections measured	4998	3394
R <sub>merge</sub>	0.0536	0.0462
Number of reflections included in refinement	4998	3394
Cut off Threshold Expression	$I > 2\sigma(I)$	$I > 2\sigma(I)$
Structure refined using	full matrix least-squares using $F^2$	full matrix least-squares using $F^2$
Weighting Scheme	$w=1/[\sigma^2(F_o^2)+(0.0457P)^2+1.7318P]$ where $P=(F_o^2+2F_c^2)/3$	$w=1/[\sigma^2(F_o^2)+(0.0416P)^2+2.7116P]$ where $P=(F_o^2+2F_c^2)/3$
Number of parameters in least-squares	164	181
R <sub>1</sub>	0.0429	0.0403
wR <sub>2</sub>	0.1014	0.0957
R <sub>1</sub> (all data)	0.0632	0.0531
wR <sub>2</sub> (all data)	0.1131	0.1036
GOF	1.017	1.038
Maximum shift/error	0.002	0.001

Min & Max peak heights on final  
 $\Delta F$  Map ( $e/\text{\AA}$ )

-0.601, 0.563

-0.677, 0.678

Where:

$$R_1 = \frac{\sum (|F_o| - |F_c|)}{\sum F_o}$$

$$wR_2 = \left[ \frac{\sum (w(F_o^2 - F_c^2))^2}{\sum (w F_o^4)} \right]^{1/2}$$

$$\text{GOF} = \left[ \frac{\sum (w(F_o^2 - F_c^2))^2}{(\text{No. of reflns.} - \text{No. of params.})} \right]^{1/2}$$

## Appendices C: Supplementary Information for Chapter 4

### NMR Spectra

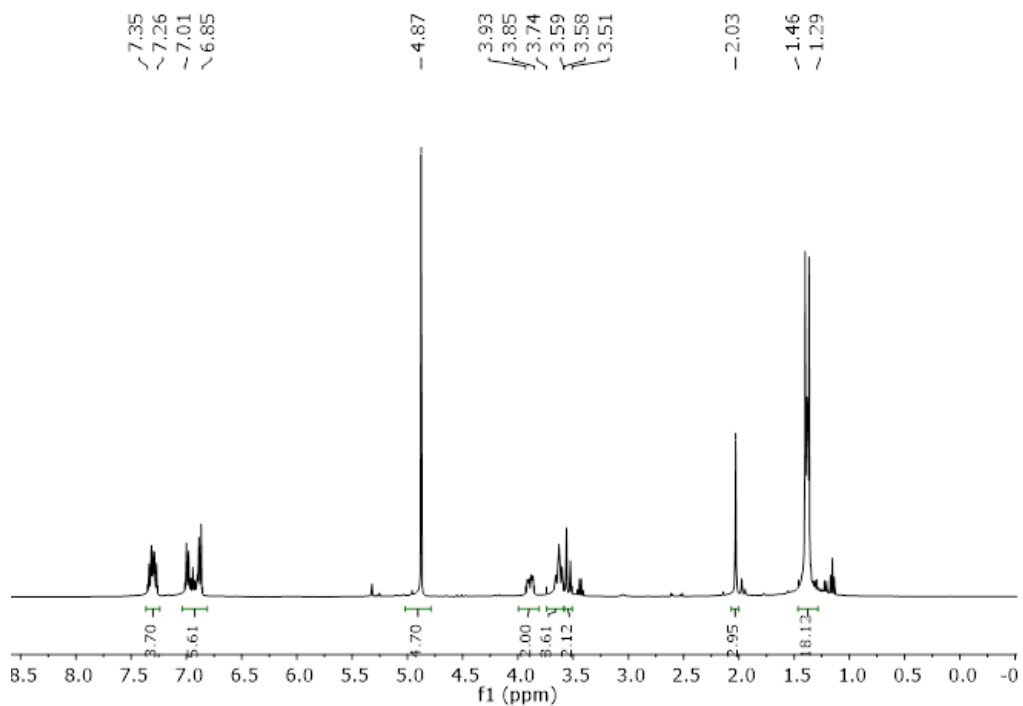


**Figure C-1.** <sup>1</sup>H NMR spectrum of [Ru(Cp)(P<sup>t</sup>Bu<sub>2</sub>N<sup>Ph</sup><sub>2</sub>)(NCCH<sub>3</sub>)]PF<sub>6</sub> (**4-1b**) in CD<sub>2</sub>Cl<sub>2</sub>.

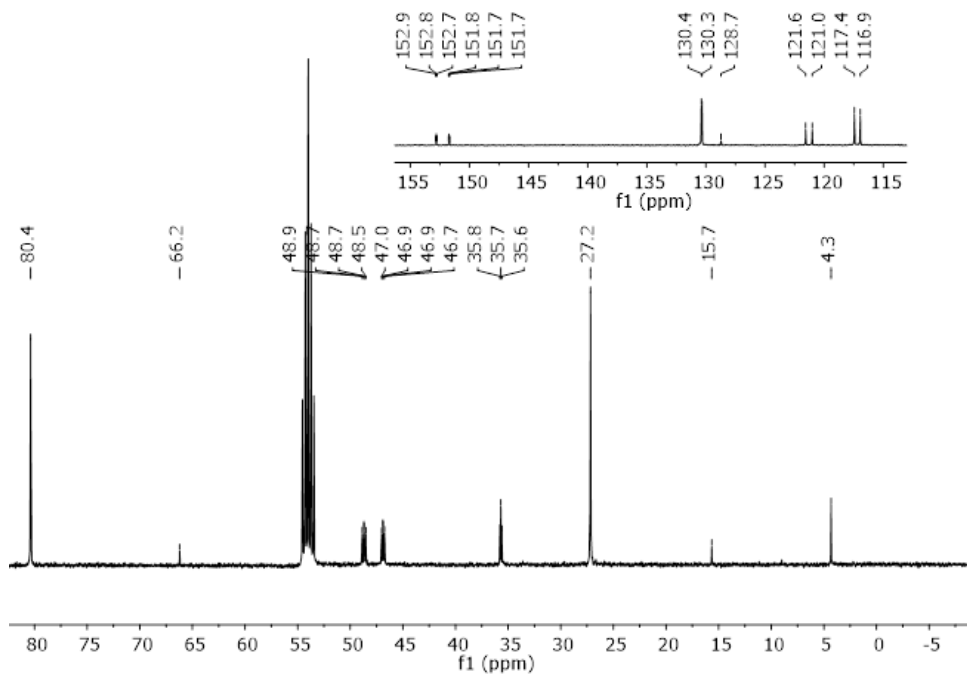


**Figure C-2.**  $^{13}\text{C}$   $\{^1\text{H}\}$  NMR spectrum of  $[\text{Ru}(\text{Cp})(\text{P}^{\text{tBu}}_2\text{N}^{\text{Ph}}_2)(\text{NCCH}_3)]\text{PF}_6$  (**4-1b**) in  $\text{CD}_2\text{Cl}_2$ .

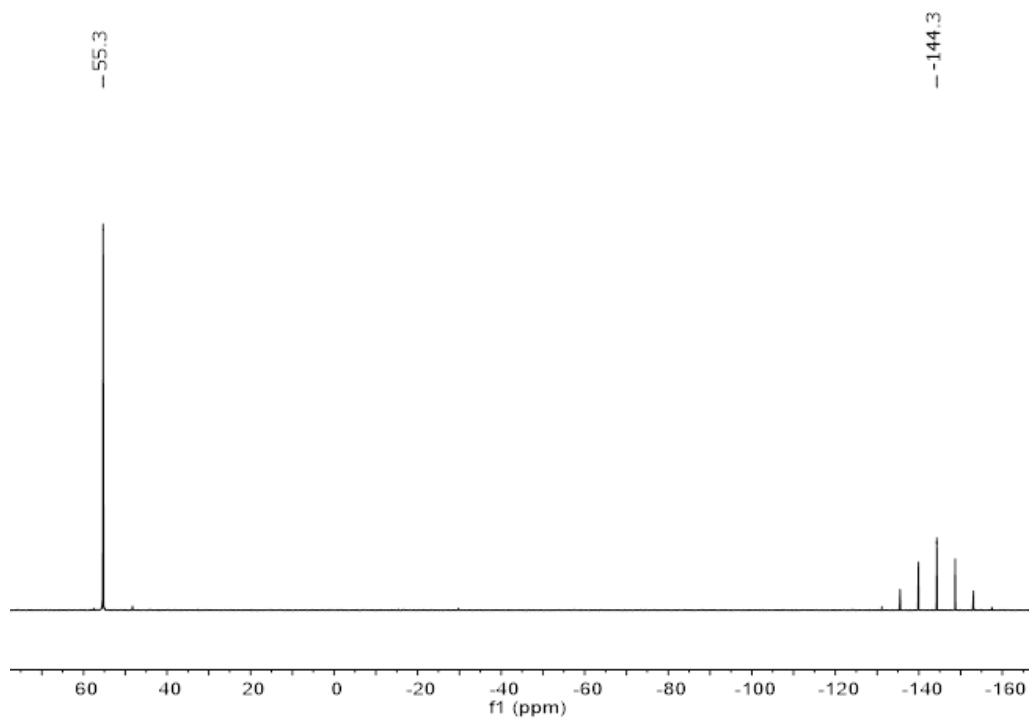


**Figure C-3.**  $^{31}\text{P}$   $\{^1\text{H}\}$  NMR spectrum of  $[\text{Ru}(\text{Cp})(\text{P}^{\text{tBu}}_2\text{N}^{\text{Ph}}_2)(\text{NCCH}_3)]\text{PF}_6$  (**4-1b**) in  $\text{CD}_2\text{Cl}_2$ .

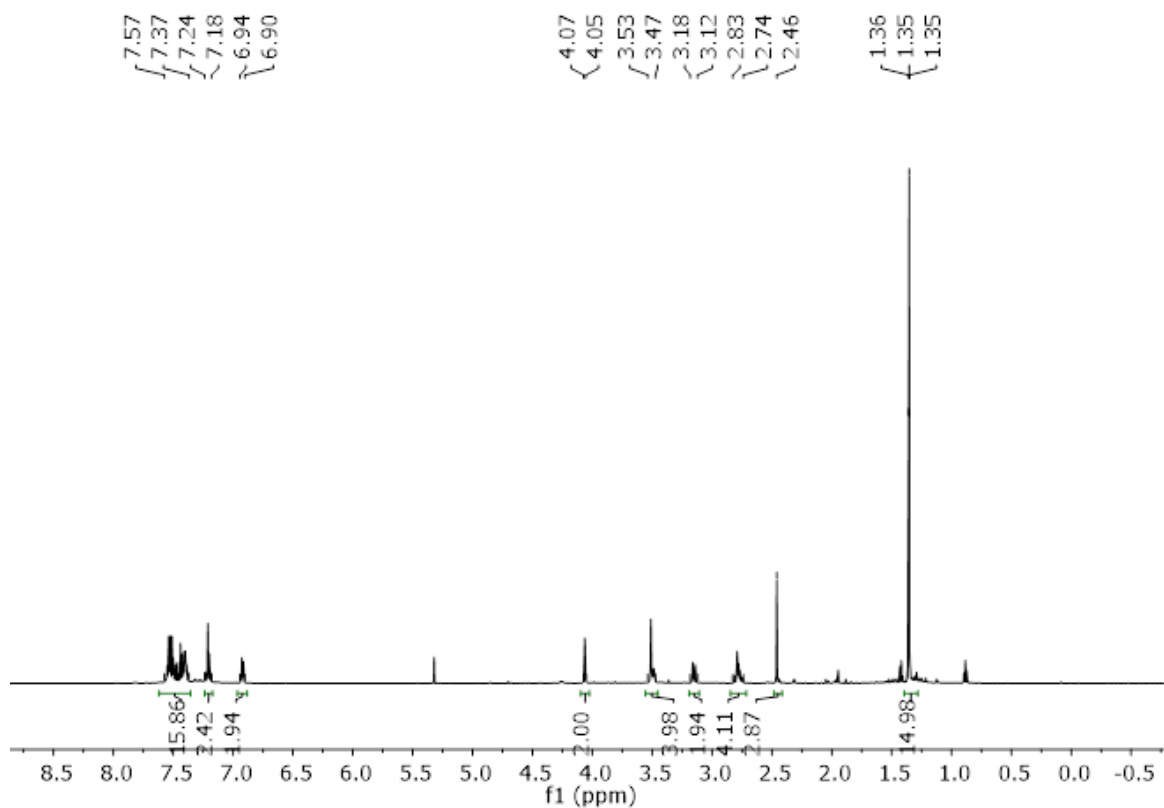


**Figure C-4.**  $^1\text{H}$  NMR spectrum of  $[\text{Ru}(\text{Cp}^*)(\text{P}^{\text{Ph}}_2\text{N}^{\text{Bn}}_2)(\text{NCMe})]\text{PF}_6$  (**4-2a**) in  $\text{CD}_2\text{Cl}_2$ .

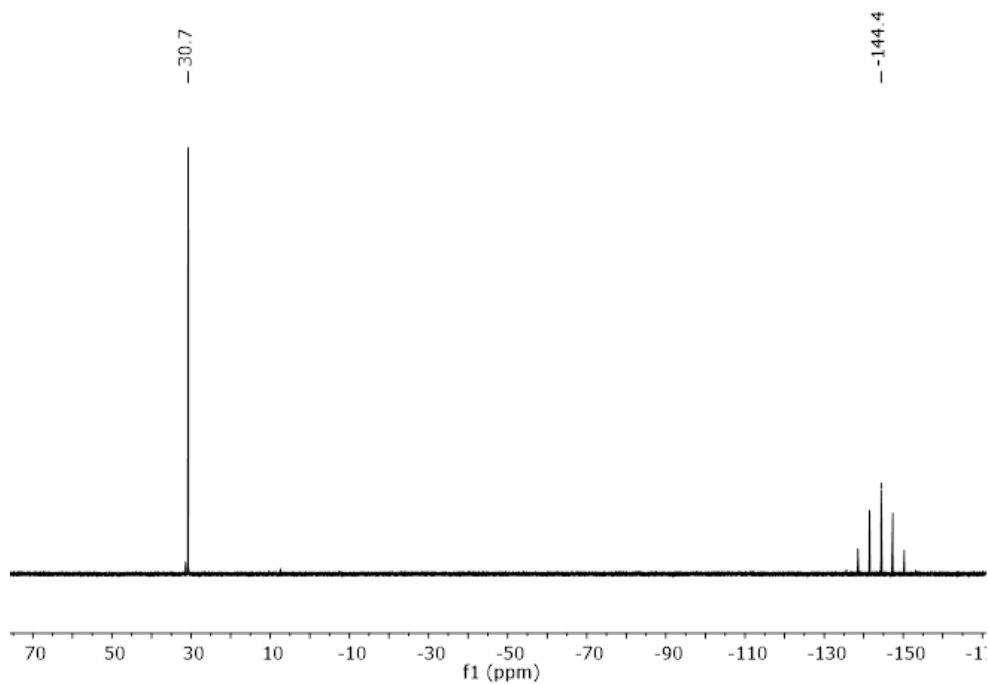


**Figure C-5.**  $^{31}\text{P}$   $\{^1\text{H}\}$  NMR spectrum of  $[\text{Ru}(\text{Cp}^*)(\text{P}^{\text{Ph}}_2\text{N}^{\text{Bn}}_2)(\text{NCMe})]\text{PF}_6$  (**4-2a**) in  $\text{CD}_2\text{Cl}_2$ .

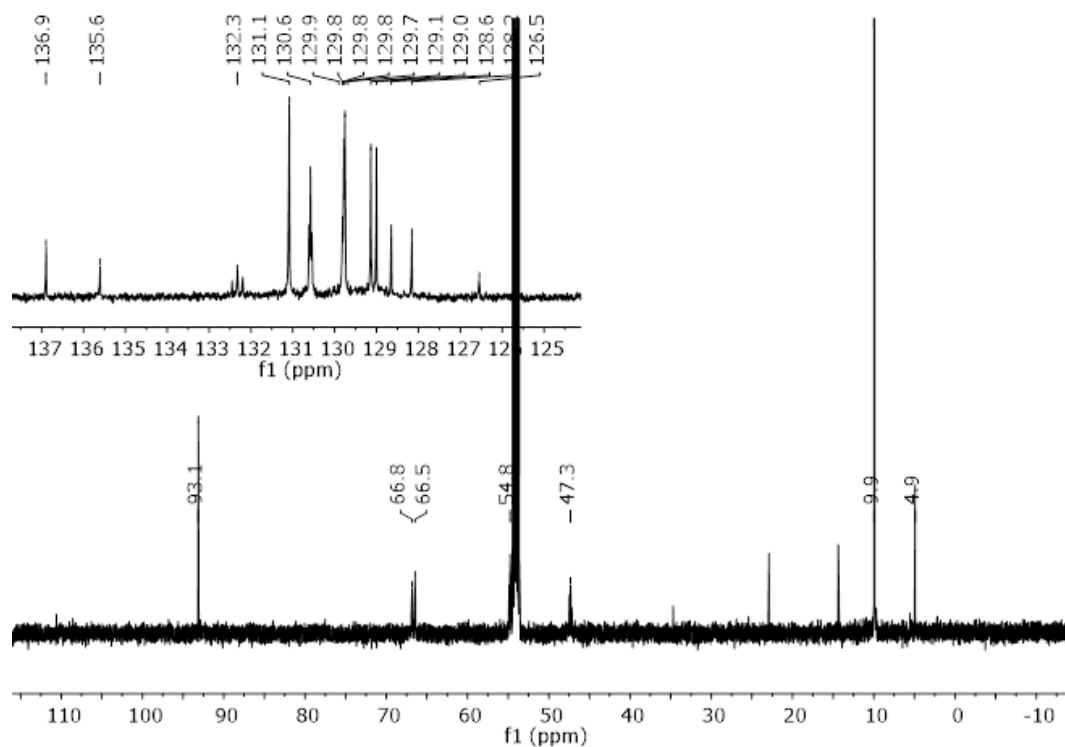


**Figure C-6.**  $^{13}\text{C}$   $\{^1\text{H}\}$  NMR spectrum of  $[\text{Ru}(\text{Cp}^*)(\text{P}^{\text{Ph}}_2\text{N}^{\text{Bn}}_2)(\text{NCMe})]\text{PF}_6$  (**4-2a**) in  $\text{CD}_2\text{Cl}_2$ .

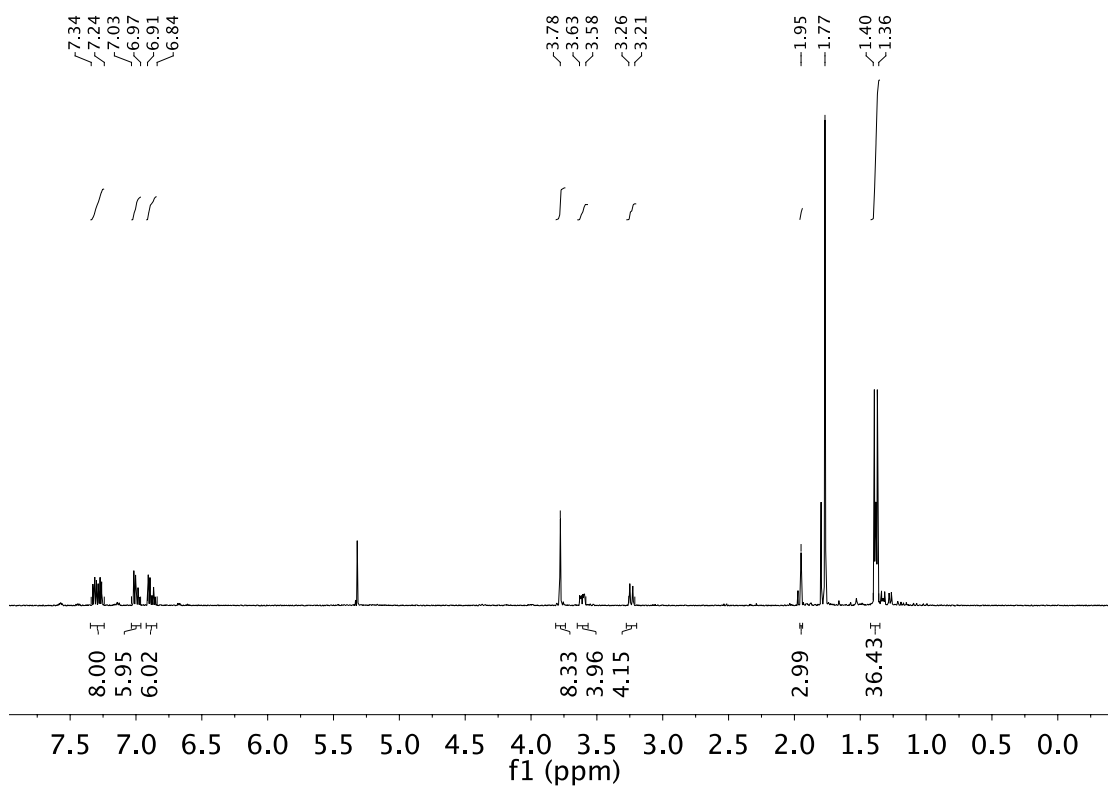


**Figure C-7.**  $^1\text{H}$  NMR spectrum of  $[\text{Ru}(\text{Cp}^*)(\text{P}^{\text{tBu}}_2\text{N}^{\text{Ph}}_2)(\text{NCMe})]\text{PF}_6$  (**4-2b**) in  $\text{CD}_2\text{Cl}_2$ .

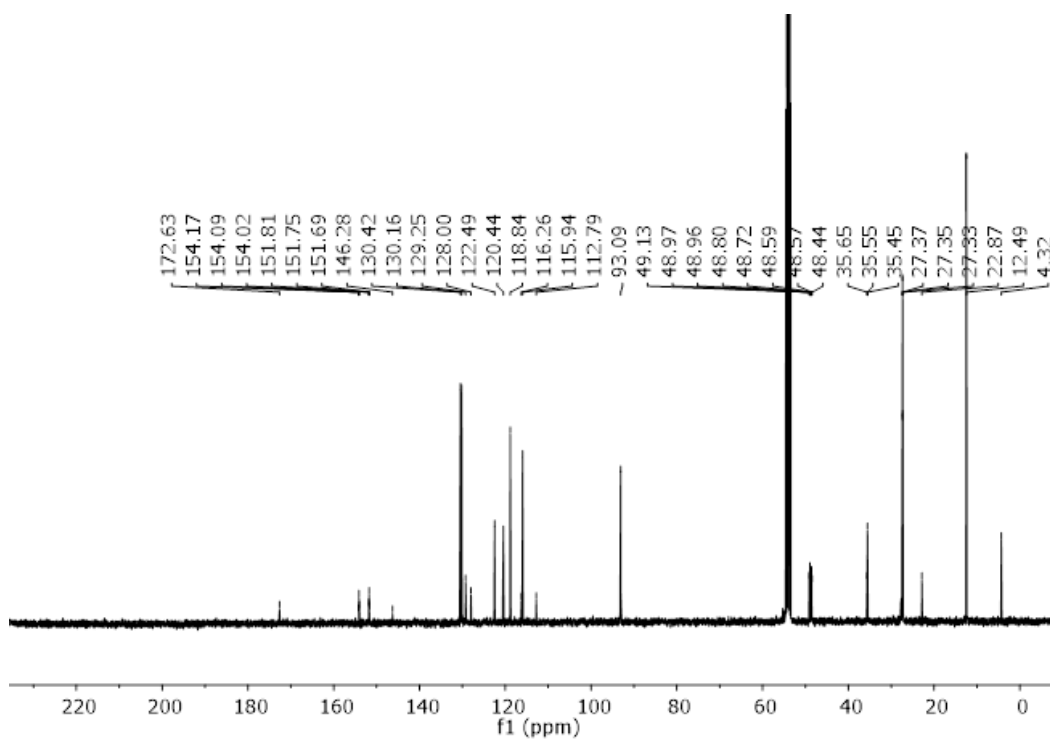


**Figure C-8.**  $^{13}\text{C}$   $\{^1\text{H}\}$  NMR spectrum of  $[\text{Ru}(\text{Cp})(\text{P}^{\text{tBu}}_2\text{N}^{\text{Ph}}_2)(\text{NCMe})]\text{PF}_6$  (**4-2b**) in  $\text{CD}_2\text{Cl}_2$ .

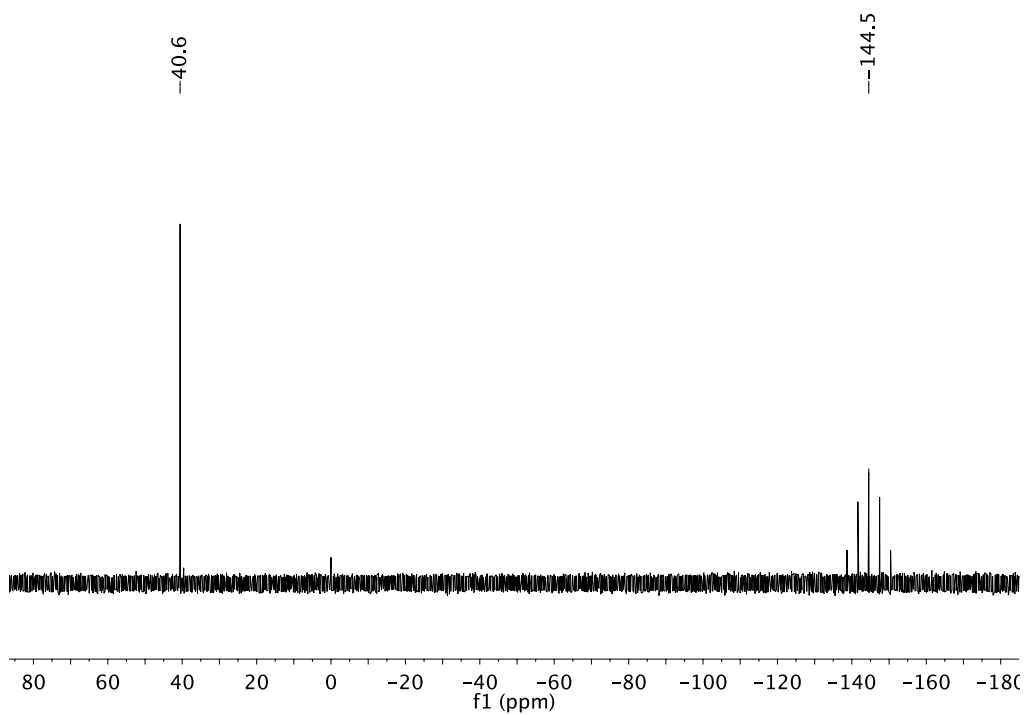




**Figure C-9.**  $^{31}\text{P} \{^1\text{H}\}$  NMR spectrum of  $[\text{Ru}(\text{Cp})(\text{P}^{\text{tBu}}_2\text{N}^{\text{Ph}}_2)(\text{NCMe})]\text{PF}_6$  (**4-2b**) in  $\text{CD}_2\text{Cl}_2$ .

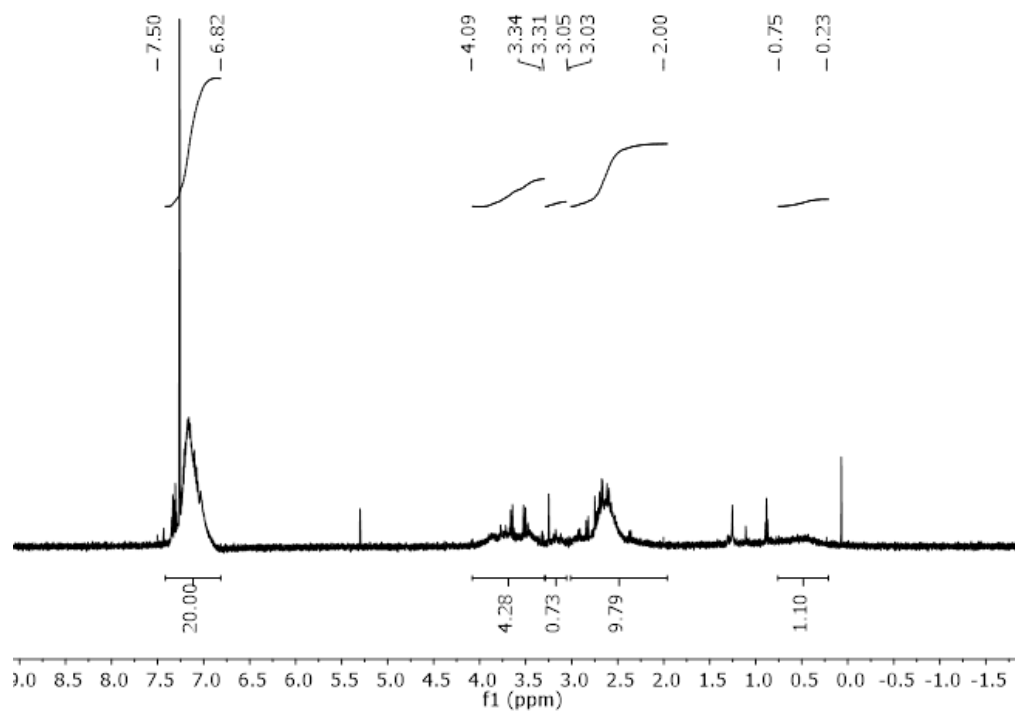


**Figure C-10.**  $^1\text{H}$  NMR spectrum of  $\text{P}^{\text{Bn}}_2\text{N}^{\text{Bn}}_2$  in  $\text{CDCl}_3$ .

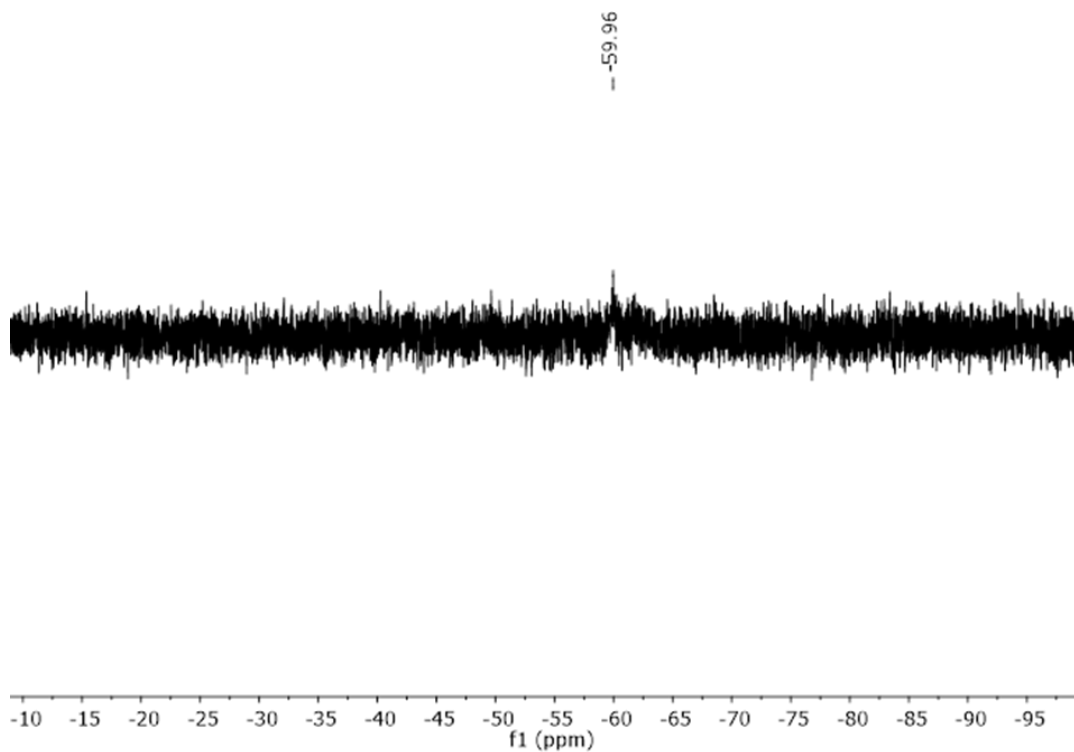


**Figure C-11.**  $^{31}\text{P}$   $\{^1\text{H}\}$  NMR spectrum of  $\text{P}^{\text{Bn}}_2\text{N}^{\text{Bn}}_2$  in  $\text{CDCl}_3$ .

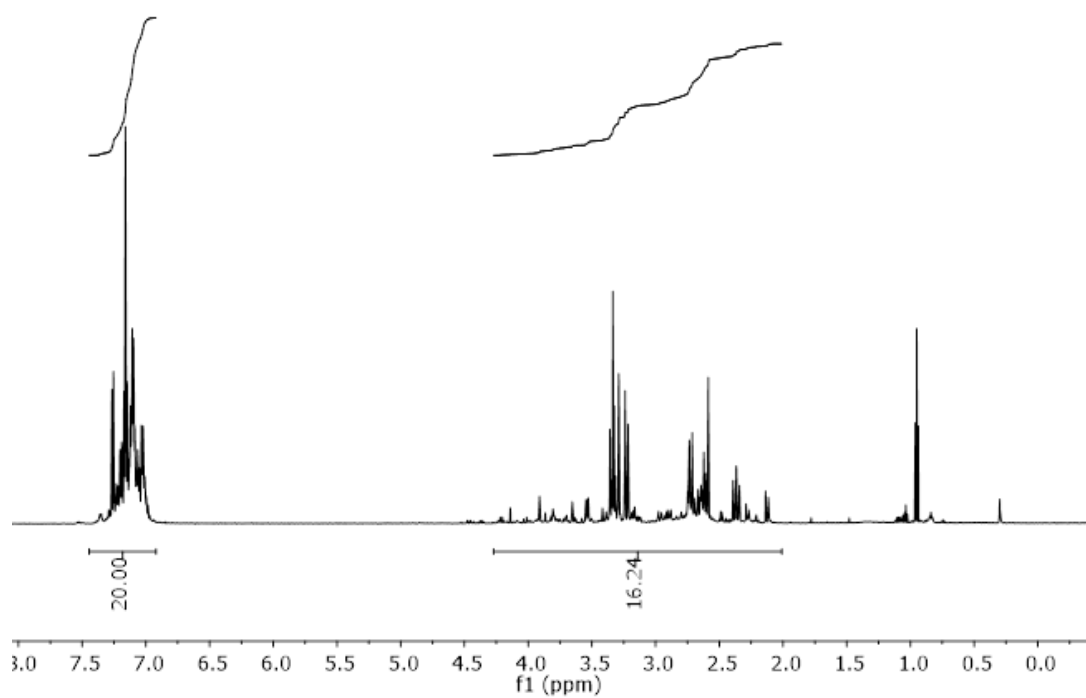


**Figure C-12.**  $^1\text{H}$  NMR spectrum of  $\text{P}^{\text{Bn}}_2\text{N}^{\text{Bn}}_2$  in  $\text{C}_6\text{D}_6$ .

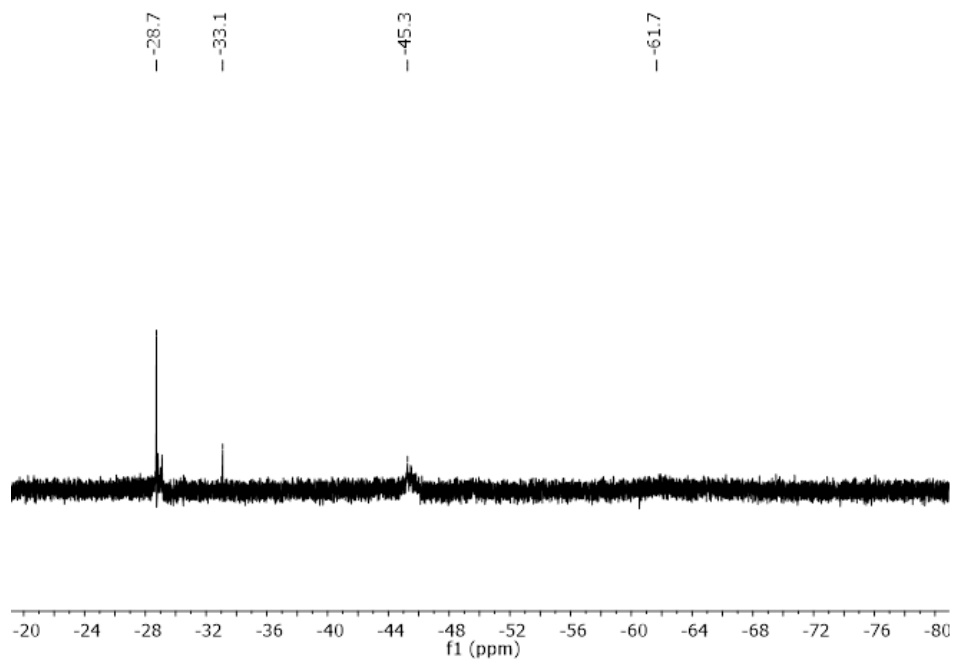


**Figure C-13.**  $^{31}\text{P}$   $\{^1\text{H}\}$  NMR spectrum of  $\text{P}^{\text{Bn}}_2\text{N}^{\text{Bn}}_2$  in  $\text{C}_6\text{D}_6$ .

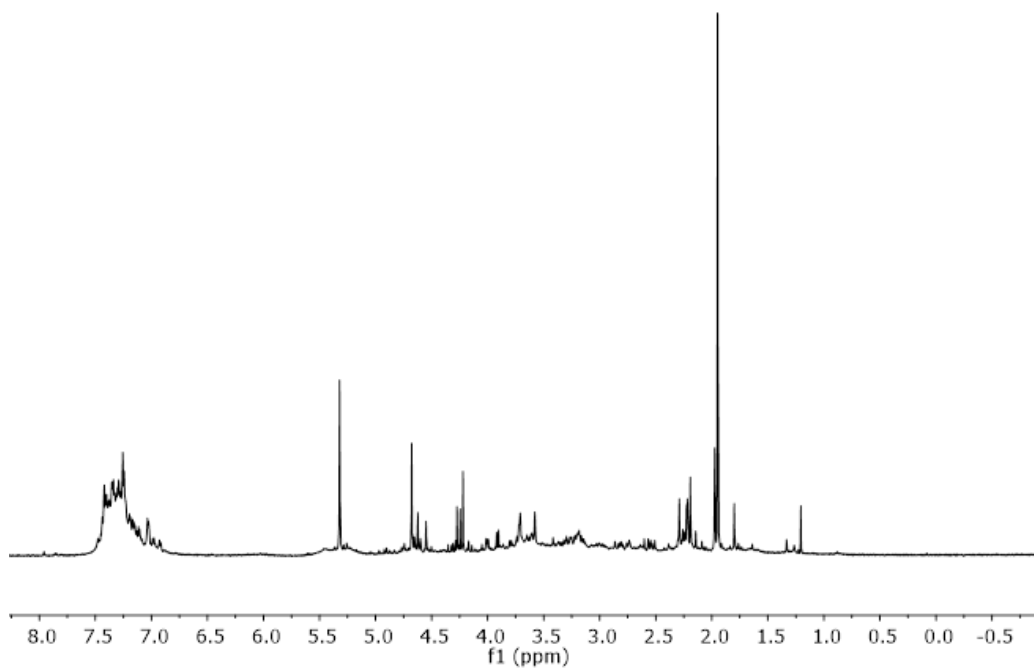


**Figure C-14.**  $^1\text{H}$  NMR spectrum of  $[\text{Ru}(\text{Cp})(\text{P}^{\text{Bn}_2\text{N}^{\text{Bn}_2})(\text{NCMe})]\text{PF}_6$  (**4-1a**) in  $\text{CD}_2\text{Cl}_2$ .

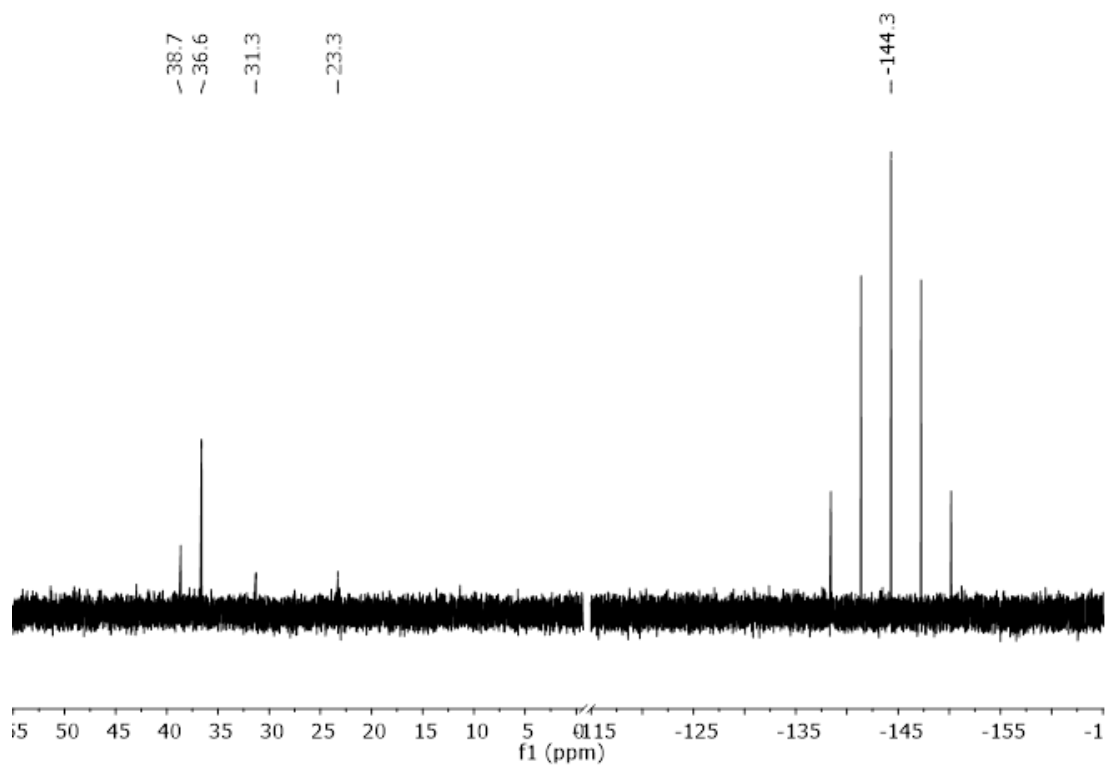


**Figure C-15.**  $^{31}\text{P}$   $\{^1\text{H}\}$  NMR spectrum of  $[\text{Ru}(\text{Cp})(\text{P}^{\text{Bn}_2\text{N}^{\text{Bn}_2})(\text{NCMe})]\text{PF}_6$  (**4-1a**) in  $\text{CD}_2\text{Cl}_2$ .

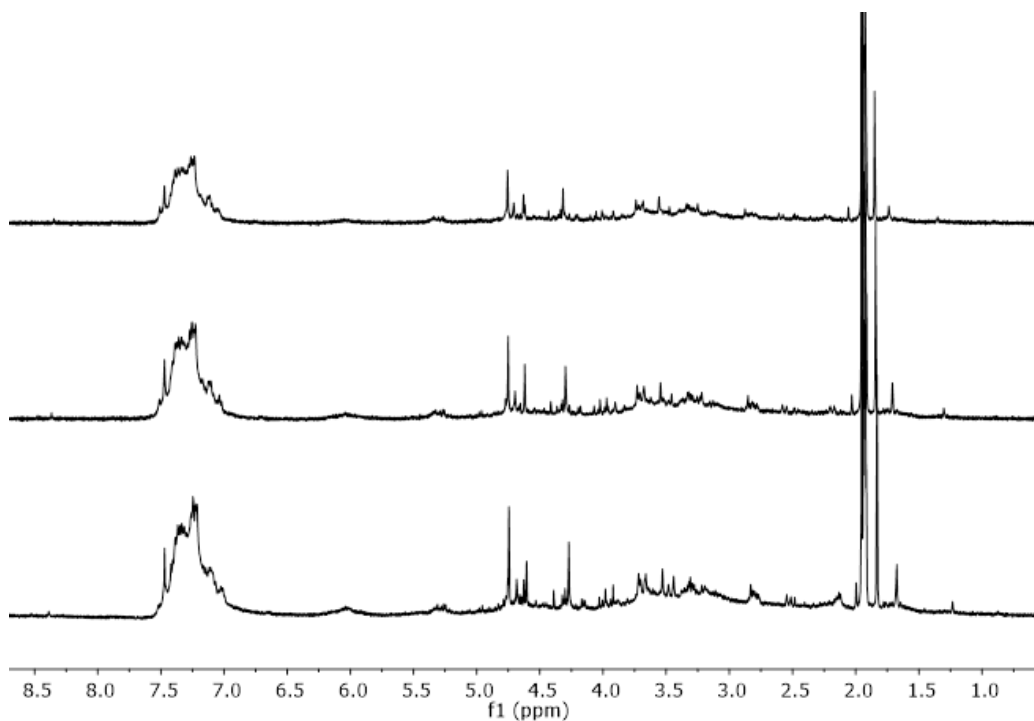


**Figure C-16.**  $^1\text{H}$  NMR stack plot of  $[\text{Ru}(\text{Cp})(\text{P}^{\text{Bn}_2\text{N}^{\text{Bn}_2})(\text{NCCH}_3)]\text{PF}_6$  (**4-1a**) in  $\text{CD}_3\text{CN}$  at various temperatures – a) 70 °C; b) 50 °C; c) 25 °C.

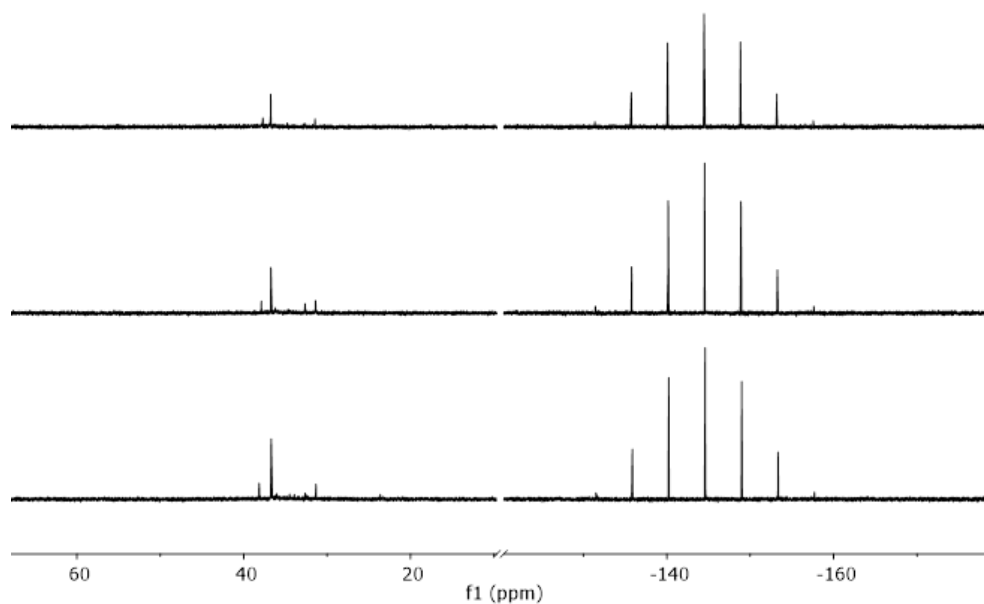


**Figure C-17.**  $^{31}\text{P} \{^1\text{H}\}$  NMR stack plot of  $[\text{Ru}(\text{Cp})(\text{P}^{\text{Bn}_2\text{N}^{\text{Bn}_2})(\text{NCCH}_3)]\text{PF}_6$  (**4-1a**) in  $\text{CD}_3\text{CN}$  at various temperatures – a) 70 °C; b) 50 °C; c) 25 °C.

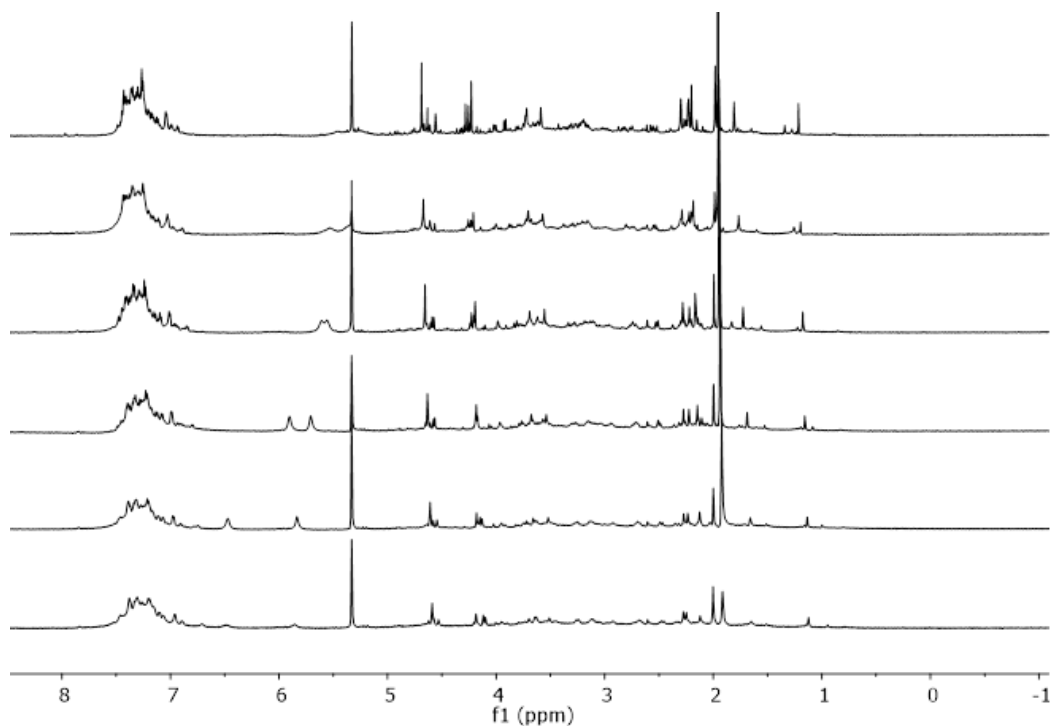


**Figure C-18.**  $^1\text{H}$  NMR stack plot of  $[\text{Ru}(\text{Cp})(\text{P}^{\text{Bn}_2\text{N}^{\text{Bn}_2})(\text{NCCH}_3)]\text{PF}_6$  (**4-1a**) in  $\text{CD}_2\text{Cl}_2$  at various temperatures – a) 25 °C; b) 0 °C; c) – 25 °C; d) – 50 °C; e) – 75 °C; f) – 90 °C.

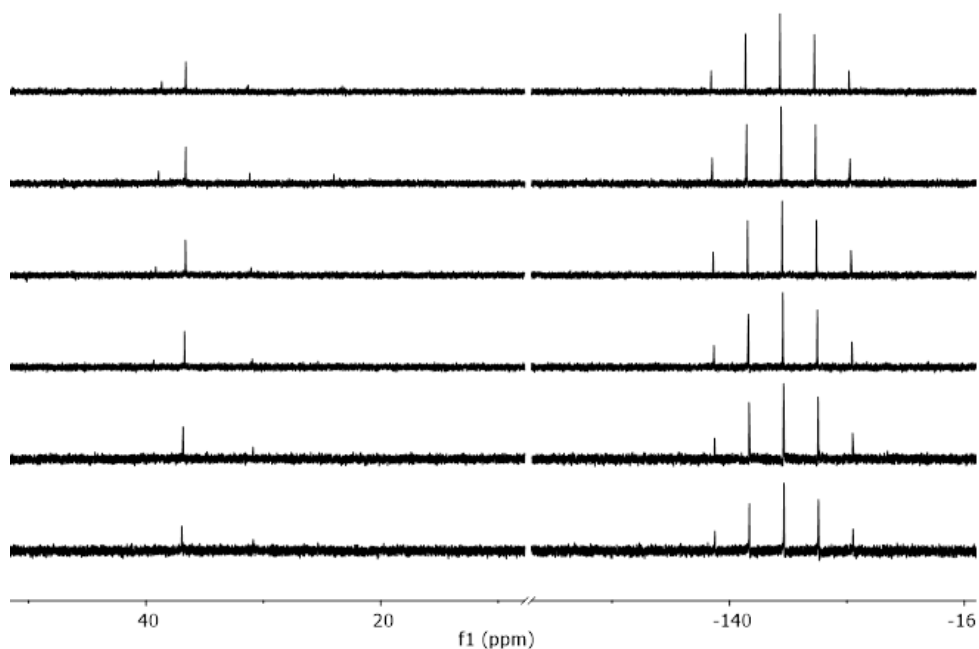


**Figure C-19.**  $^{31}\text{P} \{^1\text{H}\}$  NMR stack plot of  $[\text{Ru}(\text{Cp})(\text{P}^{\text{Bn}_2\text{N}^{\text{Bn}_2})(\text{NCCH}_3)]\text{PF}_6$  (**4-1a**) in  $\text{CD}_2\text{Cl}_2$  at various temperatures – a) 25 °C; b) 0 °C; c) – 25 °C; d) – 50 °C; e) – 75 °C; f) – 90 °C.

## IR Spectra

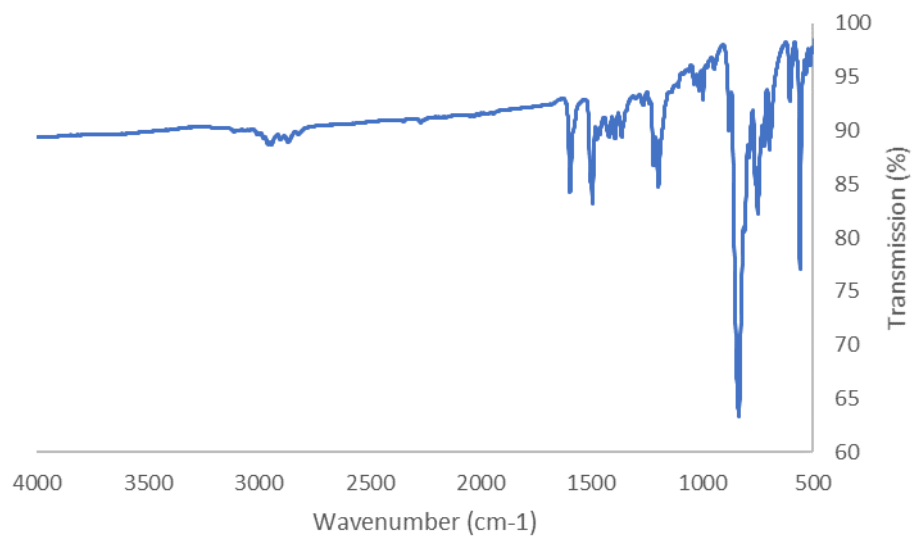


**Figure C-20.** A solid IR spectrum of  $[\text{Ru}(\text{Cp})(\text{P}^{\text{tBu}}_2\text{N}^{\text{Ph}}_2)(\text{NCMe})]\text{PF}_6$  (**4-1b**) collected with a PerkinElmer UATR Two FT-IR Spectrum Two

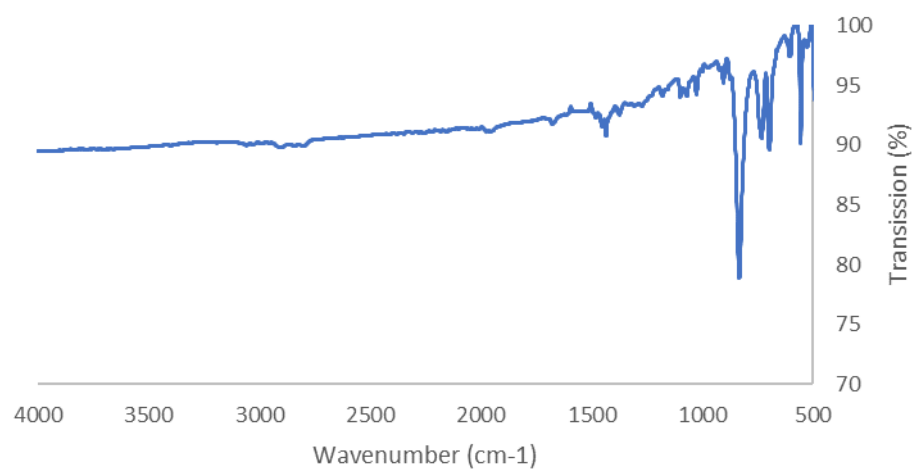


**Figure C-21.** A solid IR spectrum of  $[\text{Ru}(\text{Cp}^*)(\text{P}^{\text{Ph}}_2\text{N}^{\text{Bn}}_2)(\text{NCMe})]\text{PF}_6$  (**4-2a**) collected with a PerkinElmer UATR Two FT-IR Spectrum Two

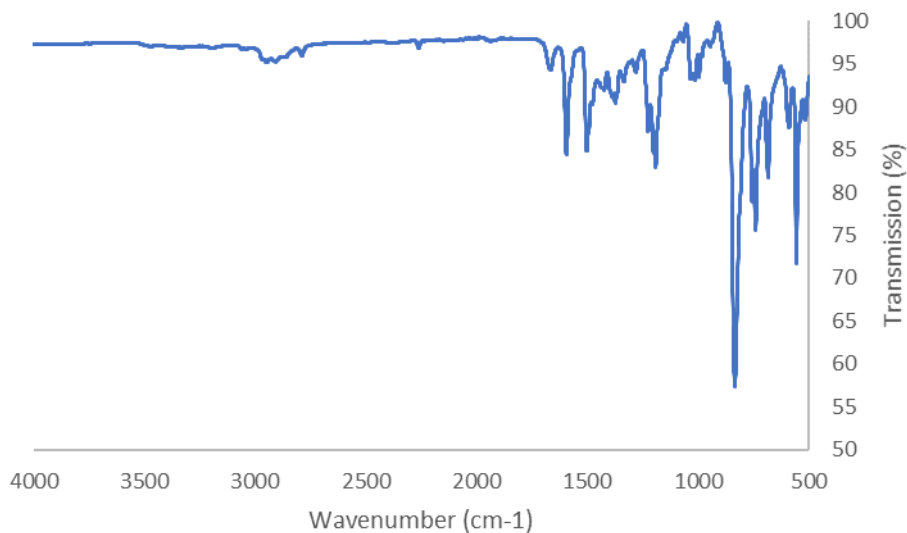


**Figure C-22.** A solid IR spectrum of  $[\text{Ru}(\text{Cp}^*)(\text{P}^{\text{tBu}}_2\text{N}^{\text{Ph}}_2)(\text{NCMe})]\text{PF}_6$  (**4-2b**) collected with a PerkinElmer UATR Two FT-IR Spectrum Two

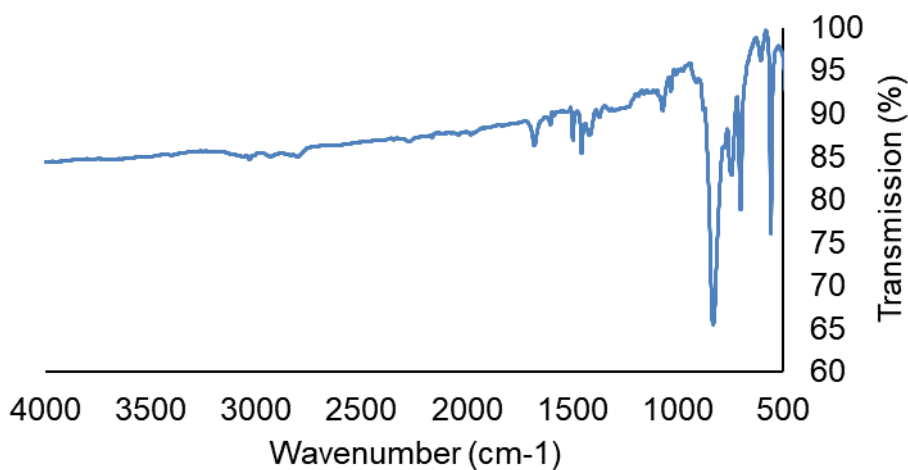


**Figure C-23.** A solid IR spectrum of  $[\text{Ru}(\text{Cp})(\text{P}^{\text{Bn}}_2\text{N}^{\text{Ph}}_2)(\text{NCMe})]\text{PF}_6$  (**4-1a**) collected with a PerkinElmer UATR Two FT-IR Spectrum Two

## MALDI Mass Spectrometry Data

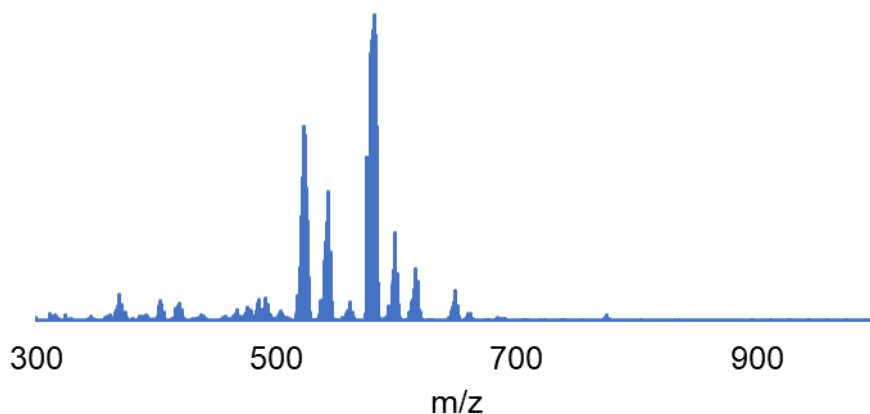


**Figure C-24.** MALDI-TOF mass spectrometry of  $[\text{Ru}(\text{Cp})(\text{P}^{\text{tBu}}_2\text{N}^{\text{Ph}}_2)(\text{NCMe})]\text{PF}_6$  (**4-1d**) in a 1:20 ratio of pyrene, the matrix.

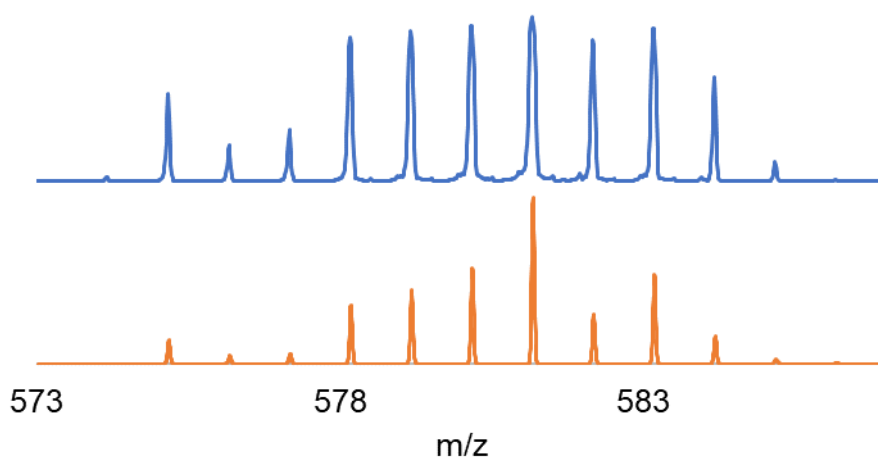


**Figure C-25.** a) Zoom-in of MALDI-TOF mass spectrometry of  $[\text{Ru}(\text{Cp})(\text{P}^{\text{tBu}}_2\text{N}^{\text{Ph}}_2)]^+$  generated from **4-1d** in a 1:20 ratio of pyrene, the matrix. b) Simulation of MALDI-TOF mass spectrometry of  $[\text{Ru}(\text{Cp})(\text{P}^{\text{tBu}}_2\text{N}^{\text{Ph}}_2)]^+$ .



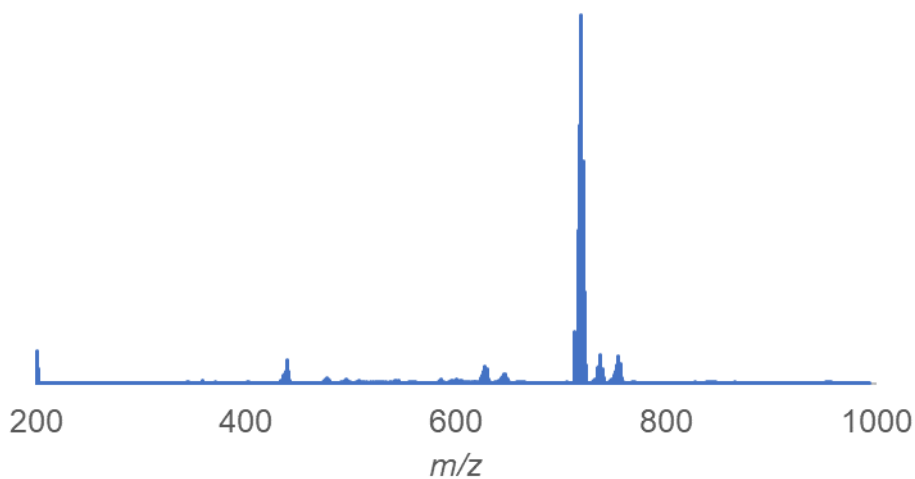


**Figure C-26.** MALDI-TOF mass spectrometry of  $[\text{Ru}(\text{Cp}^*)(\text{P}^{\text{Ph}_2\text{N}^{\text{Bn}_2})(\text{NCMe})]\text{PF}_6$  (**4-2a**) in a 1:20 ratio of pyrene, the matrix.

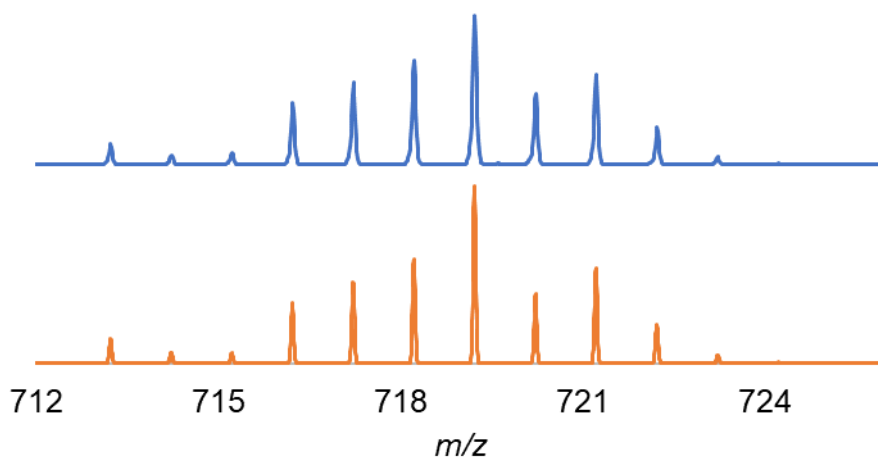


**Figure C-27.** a) Zoom-in of MALDI-TOF mass spectrometry of  $[\text{Ru}(\text{Cp}^*)(\text{P}^{\text{Ph}_2\text{N}^{\text{Bn}_2})}]^{+\bullet}$  generated from  $[\text{Ru}(\text{Cp}^*)(\text{P}^{\text{Ph}_2\text{N}^{\text{Bn}_2})(\text{NCMe})]\text{PF}_6$  (**4-2a**) in a 1:20 ratio of pyrene, the matrix. b) Simulation of MALDI-TOF mass spectrometry of  $[\text{Ru}(\text{Cp}^*)(\text{P}^{\text{Ph}_2\text{N}^{\text{Bn}_2})}]^{+\bullet}$ .

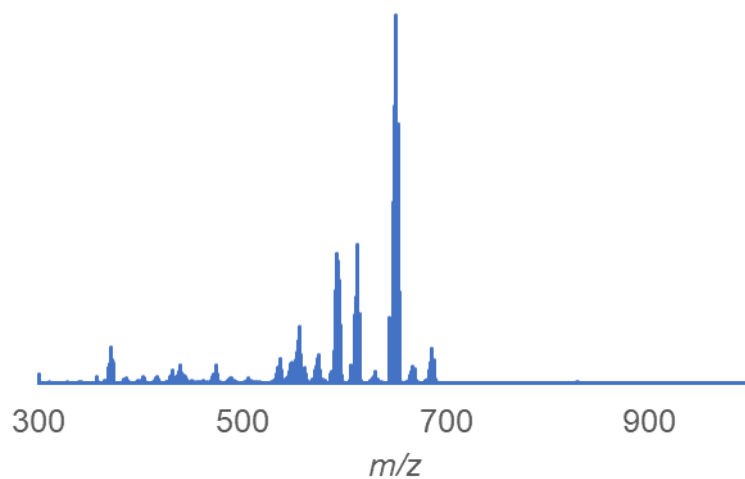


**Figure C-28.** MALDI-TOF mass spectrometry of  $[\text{Ru}(\text{Cp}^*)(\text{P}^{\text{tBu}}_2\text{N}^{\text{Ph}}_2)(\text{NCMe})]\text{PF}_6$  (**4-2b**) in a 1:20 ratio of pyrene, the matrix.

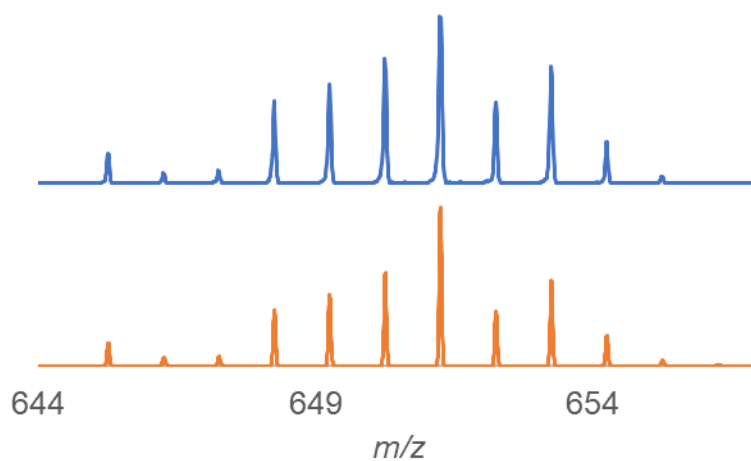


**Figure C-29.** a) Zoom-in of MALDI-TOF mass spectrometry of  $[\text{Ru}(\text{Cp}^*)(\text{P}^{\text{tBu}}_2\text{N}^{\text{Ph}}_2)]^{+\bullet}$  generated from  $[\text{Ru}(\text{Cp}^*)(\text{P}^{\text{tBu}}_2\text{N}^{\text{Ph}}_2)(\text{NCMe})]\text{PF}_6$  (**4-2b**) in a 1:20 ratio of pyrene, the matrix. b) Simulation of MALDI-TOF mass spectrometry of  $[\text{Ru}(\text{Cp}^*)(\text{P}^{\text{tBu}}_2\text{N}^{\text{Ph}}_2)]^{+\bullet}$ .

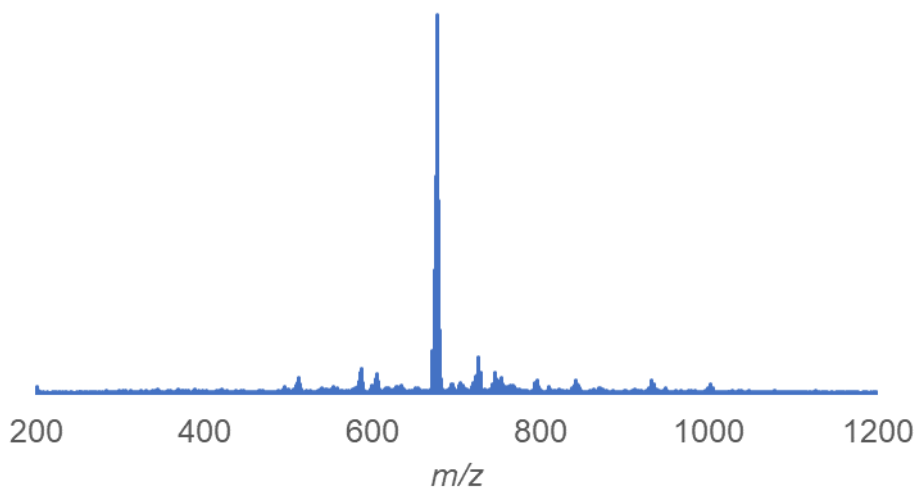


**Figure C-30.** MALDI-TOF mass spectrometry of  $[\text{Ru}(\text{Cp})(\text{P}^{\text{Bn}_2\text{N}^{\text{Bn}_2}})(\text{NCMe})]\text{PF}_6$  (**4-1a**) in a 1:20 ratio of pyrene, the matrix.

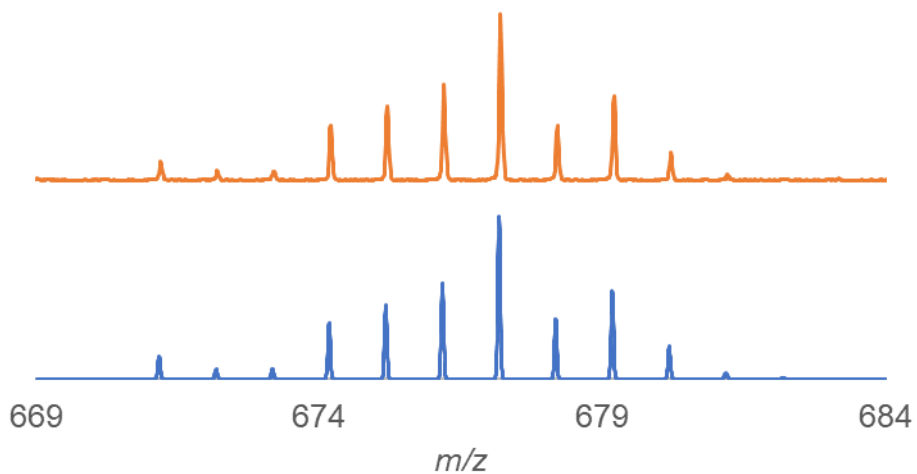


**Figure C-31.** a) Zoom-in of MALDI-TOF mass spectrometry of  $[\text{Ru}(\text{Cp})(\text{P}^{\text{Bn}_2\text{N}^{\text{Bn}_2}})]^{+\bullet}$  generated from  $[\text{Ru}(\text{Cp})(\text{P}^{\text{Bn}_2\text{N}^{\text{Bn}_2}})(\text{NCMe})]\text{PF}_6$  (**4-1a**) in a 1:20 ratio of pyrene, the matrix. b) Simulation of MALDI-TOF mass spectrometry of  $[\text{Ru}(\text{Cp})(\text{P}^{\text{Bn}_2\text{N}^{\text{Bn}_2}})]^{+\bullet}$ .

## Catalytic Data

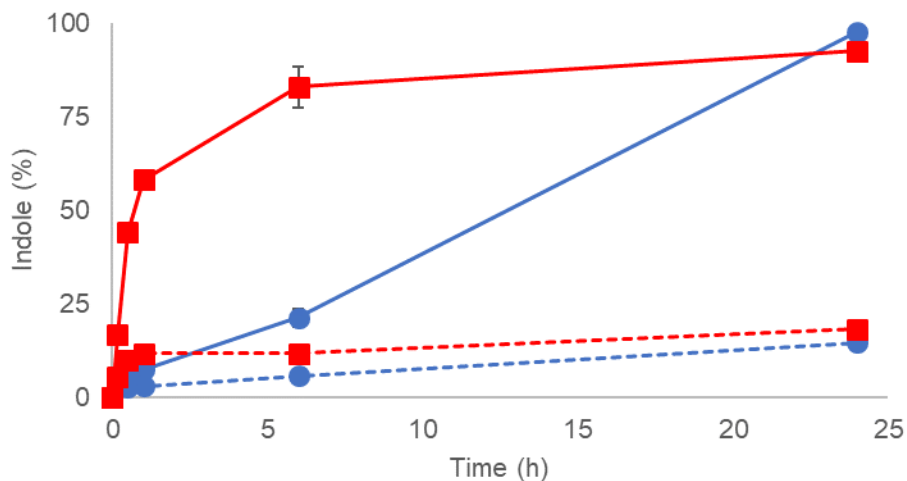


**Figure C-32.** Comparison of  $[\text{Ru}(\text{Cp})(\text{P}^{\text{tBu}}_2\text{N}^{\text{Ph}}_2)(\text{NCCH}_3)]\text{PF}_6$  (**4-1b** – blue) and  $[\text{Ru}(\text{Cp}^*)(\text{P}^{\text{tBu}}_2\text{N}^{\text{Ph}}_2)(\text{NCCH}_3)]\text{PF}_6$  (**4-2b** – red) at 0.1 (dashed) and 0.5 (solid) mol% for the cyclization of 2-ethynylaniline (150 mM) at 55 °C in THF. Results were monitored by GC-FID relative to tetralin (50 mM).

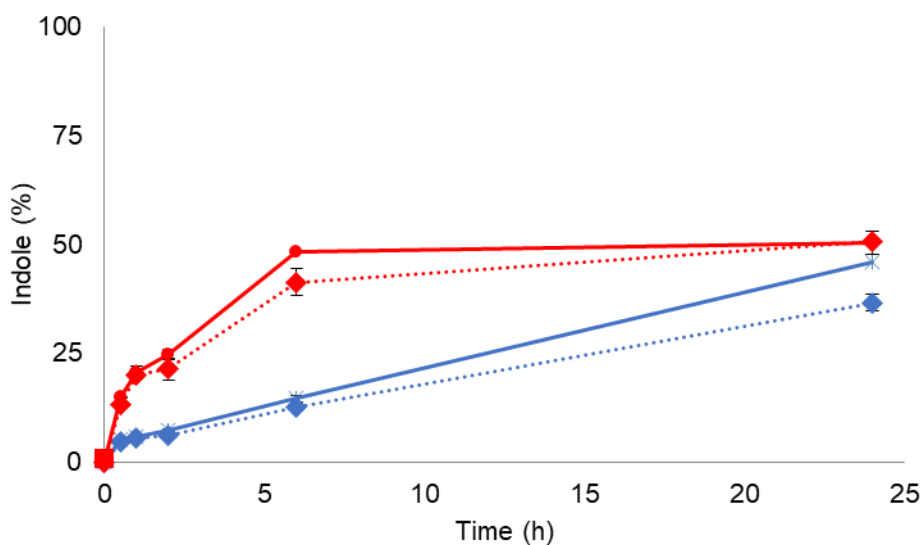


**Figure C-33.** Comparison of  $[\text{Ru}(\text{Cp})(\text{P}^{\text{tBu}}_2\text{N}^{\text{Ph}}_2)(\text{NCCH}_3)]\text{PF}_6$  (**4-1b** – blue) and  $[\text{Ru}(\text{Cp}^*)(\text{P}^{\text{tBu}}_2\text{N}^{\text{Ph}}_2)(\text{NCCH}_3)]\text{PF}_6$  (**4-2b** – red) at 0.2 mol% for the cyclization of 2-ethynylaniline

(150 mM) with 5 equivalents of water (dashed) and without water (solid) at 55 °C in THF. Results were monitored by GC-FID relative to tetralin (50 mM).

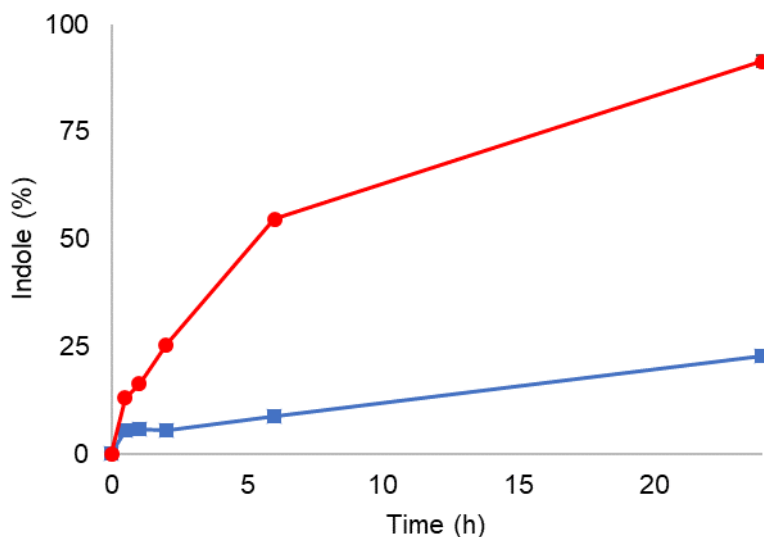


**Figure C-34.** Comparison of  $[\text{Ru}(\text{Cp})(\text{P}^{\text{tBu}}_2\text{N}^{\text{Ph}}_2)(\text{NCCH}_3)]\text{PF}_6$  (**4-1b** – blue) and  $[\text{Ru}(\text{Cp}^*)(\text{P}^{\text{tBu}}_2\text{N}^{\text{Ph}}_2)(\text{NCCH}_3)]\text{PF}_6$  (**4-2b** – red) at 0.5 mol% for the cyclization of 2-ethynylaniline (150 mM) at 40 °C in THF. Results were monitored by GC-FID relative to tetralin (50 mM).

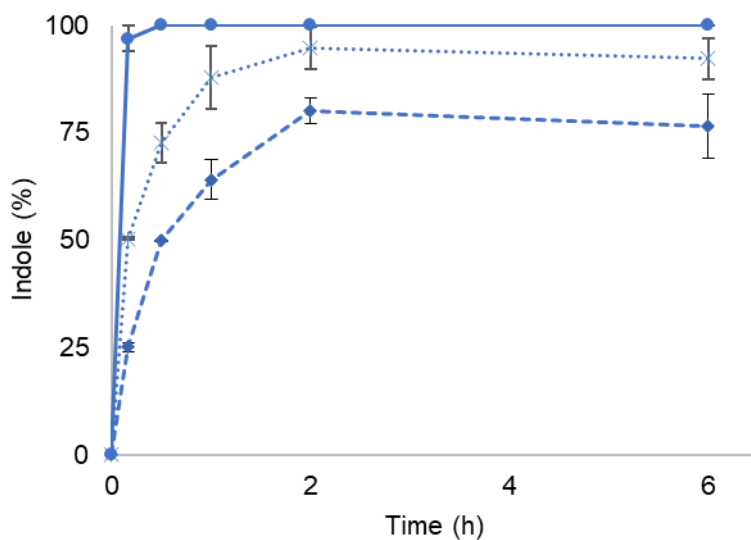


**Figure C-35.** Comparison of 0.1 (dashed), 0.2 (dotted) and 0.5 (solid) mol% of  $[\text{Ru}(\text{Cp})(\text{P}^{\text{tBu}}_2\text{N}^{\text{Ph}}_2)(\text{NCCH}_3)]\text{PF}_6$  (**4-1b**) for the cyclization of 2-ethynylaniline (150 mM) at 70 °C in MeTHF. Results were monitored by GC-FID relative to tetralin (50 mM).

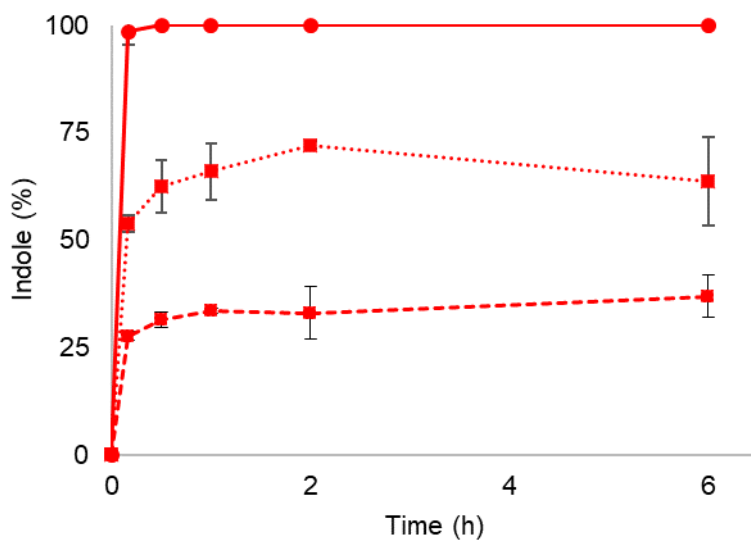


**Figure C-36.** Comparison of 0.1 (dashed), 0.2 (dotted) and 0.5 (solid) mol% of  $[\text{Ru}(\text{Cp}^*)(\text{P}^{\text{tBu}}_2\text{N}^{\text{Ph}}_2)(\text{NCCH}_3)]\text{PF}_6$  (**4-2b**) for the cyclization of 2-ethynylaniline (150 mM) at 70 °C in MeTHF. Results were monitored by GC-FID relative to tetralin (50 mM).

## Crystallographic Details

*Data Collection and Processing.* The sample (**4-2b**) was submitted by James of the Blacquiere research group at the University of Western Ontario. The sample was mounted on a Mitegen polyimide micromount with a small amount of Paratone N oil. All X-ray measurements were made on a Bruker Kappa Axis Apex2 diffractometer at a temperature of 110 K. The unit cell dimensions were determined from a symmetry constrained fit of 9997 reflections with  $5.12^\circ < 2\theta < 60.32^\circ$ . The data collection strategy was a number of  $\omega$  and  $\varphi$  scans which collected data up to  $48.5^\circ$  ( $2\theta$ ). The frame integration was performed using SAINT.<sup>10</sup> The resulting raw data was scaled and absorption corrected using a multi-scan averaging of symmetry equivalent data using SADABS.<sup>11</sup>

*Structure Solution and Refinement.* The structure was solved by using a dual space methodology using the SHELXT program.<sup>12</sup> All non-hydrogen atoms were obtained from the initial solution. The hydrogen atoms were introduced at idealized positions and were allowed to ride on the parent atom. The structural model was fit to the data using full matrix least-squares based on  $F^2$ . The calculated structure factors included corrections for anomalous dispersion from the usual tabulation. The structure was refined using the SHELXL program from the SHELXTL suite of crystallographic software.<sup>13</sup> Graphic plots were produced using the SHELXL XP program suite.<sup>5</sup> Additional information and other relevant literature references can be found in the reference section of this website (<http://xray.chem.uwo.ca>).

## Acknowledgment

- 
- 10 Bruker-AXS, SAINT version 2013.8, **2013**, Bruker-AXS, Madison, WI 53711, USA  
11 Bruker-AXS, SADABS version 2012.1, **2012**, Bruker-AXS, Madison, WI 53711, USA  
12 Sheldrick, G. M., *Acta Cryst.* **2015**, *A71*, 3-8  
13 Sheldrick, G. M., *Acta Cryst.* **2015**, *C71*, 3-8  
10 Gabe, E. J.; Le Page, Y.; Charland, J. P.; Lee, F. L. and White, P. S. *J. Appl. Cryst.* **1989**, *22*, 384-387

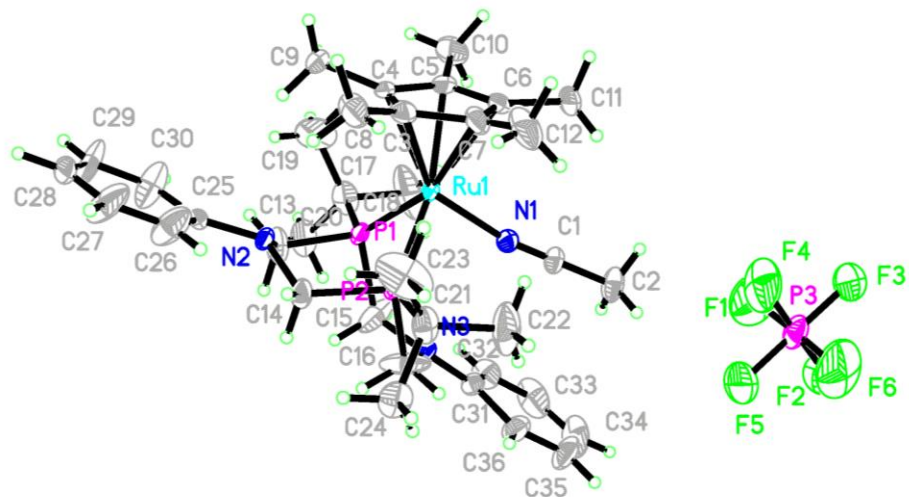


**Figure C-37.** ORTEP drawing of **4-2b** showing naming and numbering scheme. Ellipsoids are at the 50% probability level.

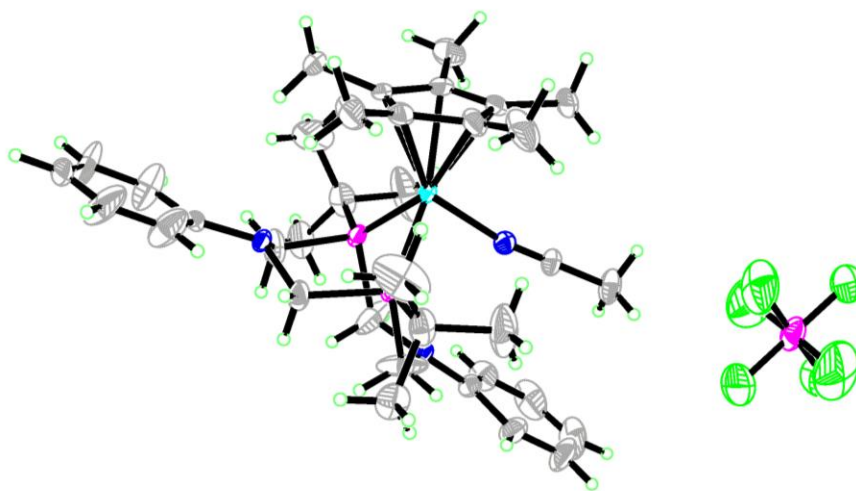


**Figure C-38.** ORTEP drawing of **4-2b**. Ellipsoids are at the 50% probability level.



**Table C-1.** Summary of Crystal Data for **4-2b**

Formula	C <sub>36</sub> H <sub>54</sub> F <sub>6</sub> N <sub>3</sub> P <sub>3</sub> Ru
Formula Weight ( <i>g/mol</i> )	836.80
Crystal Dimensions ( <i>mm</i> )	0.380 × 0.047 × 0.031
Crystal Color and Habit	colourless needle
Crystal System	monoclinic
Space Group	P 2 <sub>1</sub> /c
Temperature, K	110
<i>a</i> , Å	10.021(5)
<i>b</i> , Å	19.421(9)
<i>c</i> , Å	19.200(10)
α, °	90
β, °	92.243(14)
γ, °	90
<i>V</i> , Å <sup>3</sup>	3734(3)
Number of reflections to determine final unit cell	9997
Min and Max 2θ for cell determination, °	5.12, 60.32
<i>Z</i>	4
F(000)	1736
ρ ( <i>g/cm</i> )	1.489
λ, Å, (MoKα)	0.71073
μ, ( <i>cm</i> <sup>-1</sup> )	0.609
Diffractometer Type	Bruker Kappa Axis Apex2
Scan Type(s)	φ and ω scans

Max 2θ for data collection, °	48.5
Measured fraction of data	0.998
Number of reflections measured	65667
Unique reflections measured	6050
R <sub>merge</sub>	0.0499
Number of reflections included in refinement	6050
Cut off Threshold Expression	I > 2σ(I)
Structure refined using	full matrix least-squares using F <sup>2</sup>
Weighting Scheme	w=1/[σ <sup>2</sup> (Fo <sup>2</sup> )+(0.0520P) <sup>2</sup> +11.8552 P] where P=(Fo <sup>2</sup> +2Fc <sup>2</sup> )/3
Number of parameters in least-squares	454
R <sub>1</sub>	0.0459
wR <sub>2</sub>	0.1138
R <sub>1</sub> (all data)	0.0557
wR <sub>2</sub> (all data)	0.1190
GOF	1.088
Maximum shift/error	0.001
Min & Max peak heights on final ΔF Map (e <sup>-</sup> /Å)	-0.833, 0.931

Where:

$$R_1 = \sum (|F_o| - |F_c|) / \sum F_o$$

$$wR_2 = [ \sum (w(F_o^2 - F_c^2))^2 / \sum (w F_o^4) ]^{1/2}$$

$$GOF = [ \sum (w(F_o^2 - F_c^2))^2 / (\text{No. of reflns.} - \text{No. of params.}) ]^{1/2}$$

# Appendices D: Supplementary Information for Chapter 5

## NMR Spectra

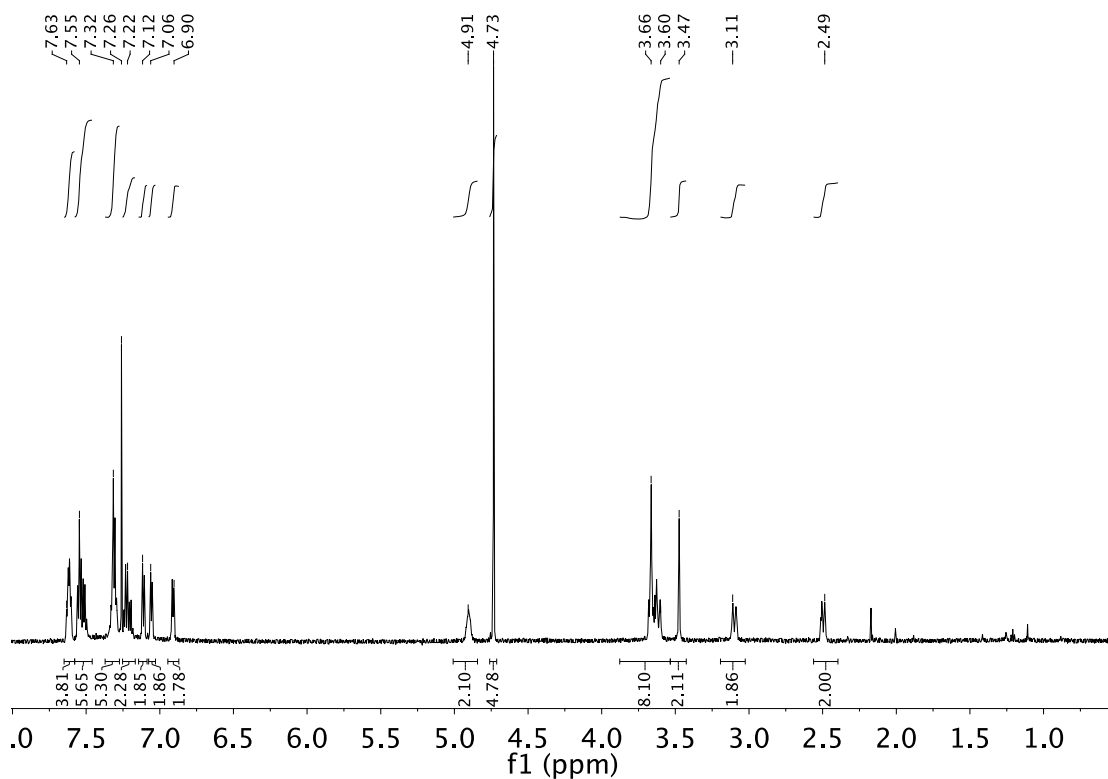


**Figure D-1.**  $^1\text{H}$  NMR spectrum of  $[\text{Ru}(\text{Cp})(\text{P}^{\text{Ph}}_2\text{N}^{\text{Bn}}_2)(\text{benzylamine})]\text{PF}_6$  (**5-1**) in  $\text{CDCl}_3$ .

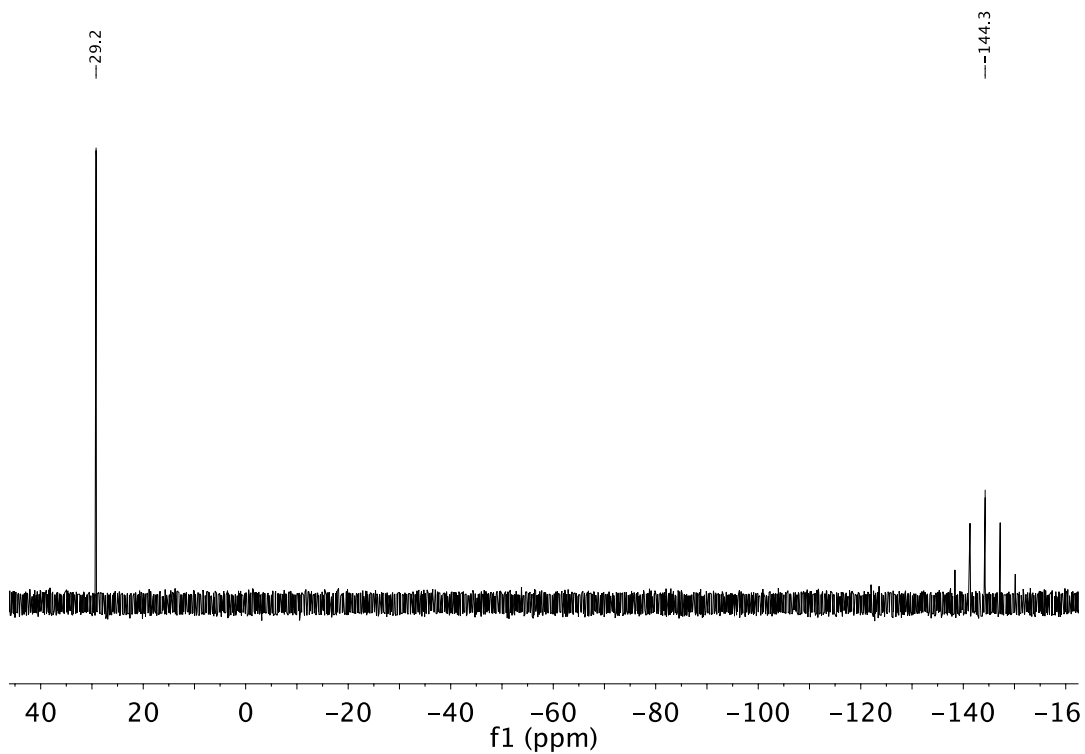


**Figure D-2.**  $^{31}\text{P}\{^1\text{H}\}$  NMR spectrum of  $[\text{Ru}(\text{Cp})(\text{P}^{\text{Ph}}_2\text{N}^{\text{Bn}}_2)(\text{benzylamine})]\text{PF}_6$  (**5-1**) in  $\text{CDCl}_3$ .

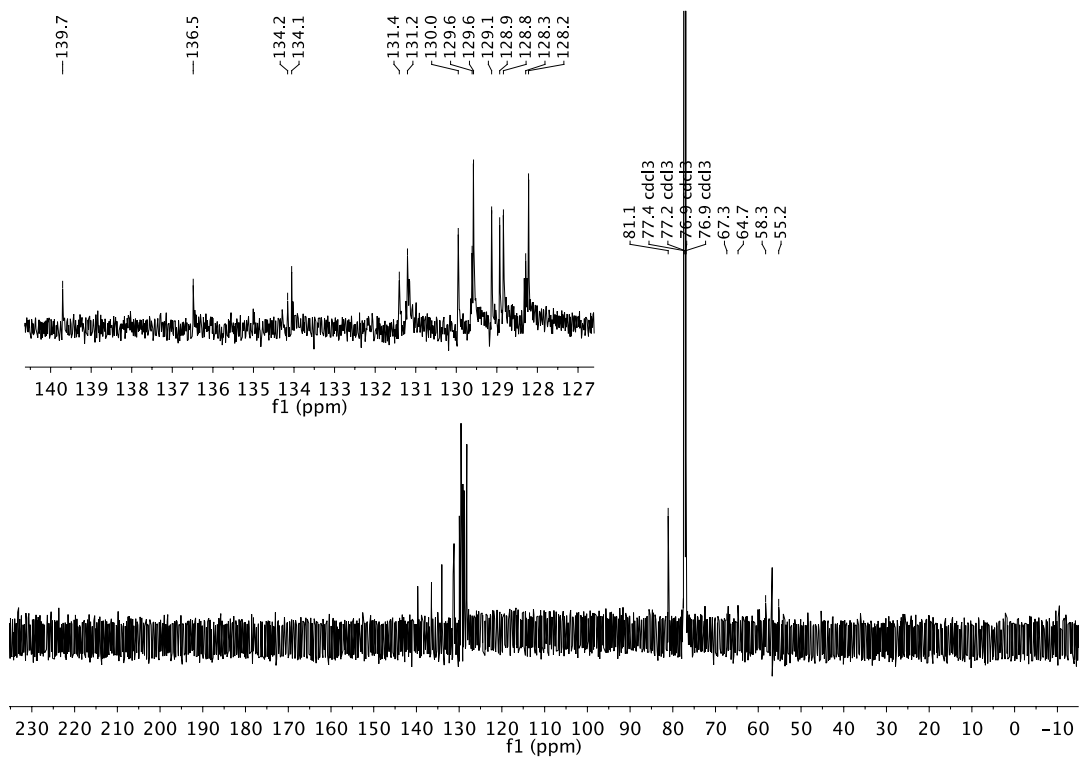


**Figure D-3.**  $^{13}\text{C}\{^1\text{H}\}$  (top) NMR spectrum of  $[\text{Ru}(\text{Cp})(\text{P}^{\text{Ph}}_2\text{N}^{\text{Bn}}_2)(\text{benzylamine})]\text{PF}_6$  (**5-1**) in  $\text{CDCl}_3$ .

The inset displays a zoom-in of the aromatic carbon region.

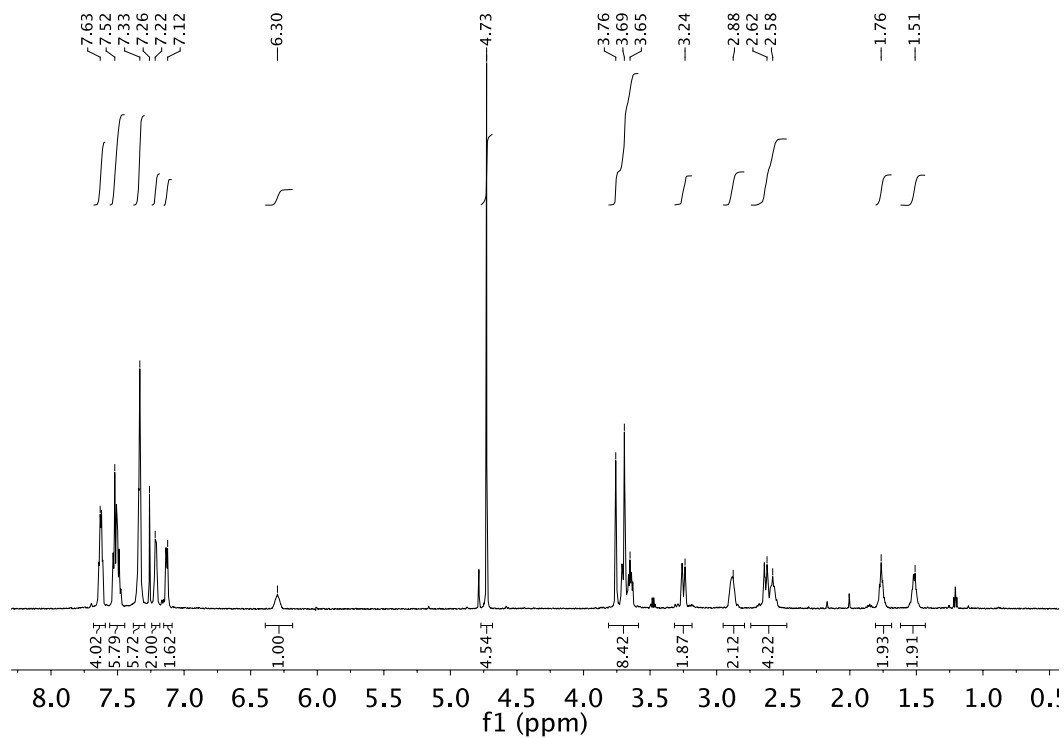


**Figure D-4.**  $^1\text{H}$  NMR spectrum of  $[\text{Ru}(\text{Cp})(\text{P}^{\text{Ph}}_2\text{N}^{\text{Bn}}_2)(\text{pyrrolidine})]\text{PF}_6$  (**5-2**) in  $\text{CDCl}_3$ .

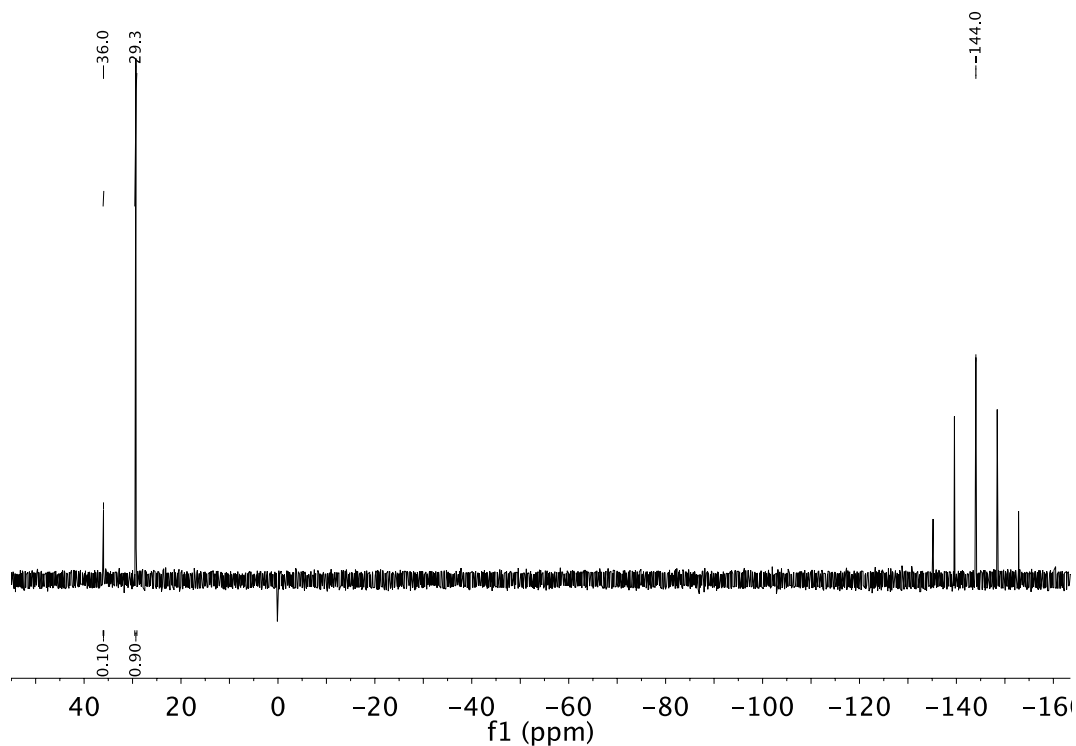


**Figure D-5.**  $^{31}\text{P}\{^1\text{H}\}$  NMR spectrum of  $[\text{Ru}(\text{Cp})(\text{P}^{\text{Ph}}_2\text{N}^{\text{Bn}}_2)(\text{pyrrolidine})]\text{PF}_6$  (**5-2**) in  $\text{CDCl}_3$ . Decomposition (36.0 ppm) is formed after analytically pure sample is dissolved in solution.

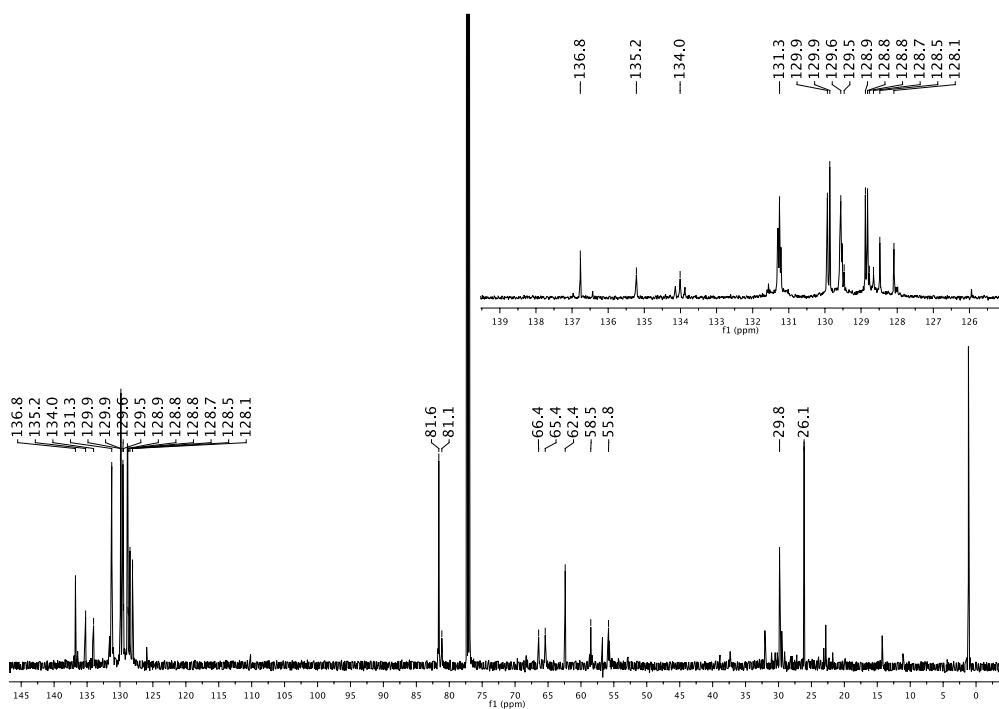


**Figure D-6.**  $^{13}\text{C}\{^1\text{H}\}$  NMR spectrum of  $[\text{Ru}(\text{Cp})(\text{P}^{\text{Ph}}_2\text{N}^{\text{Bn}}_2)(\text{pyrrolidine})]\text{PF}_6$  (**5-2**) in  $\text{CDCl}_3$ . The inset is a zoom-in of the aromatic carbon region.

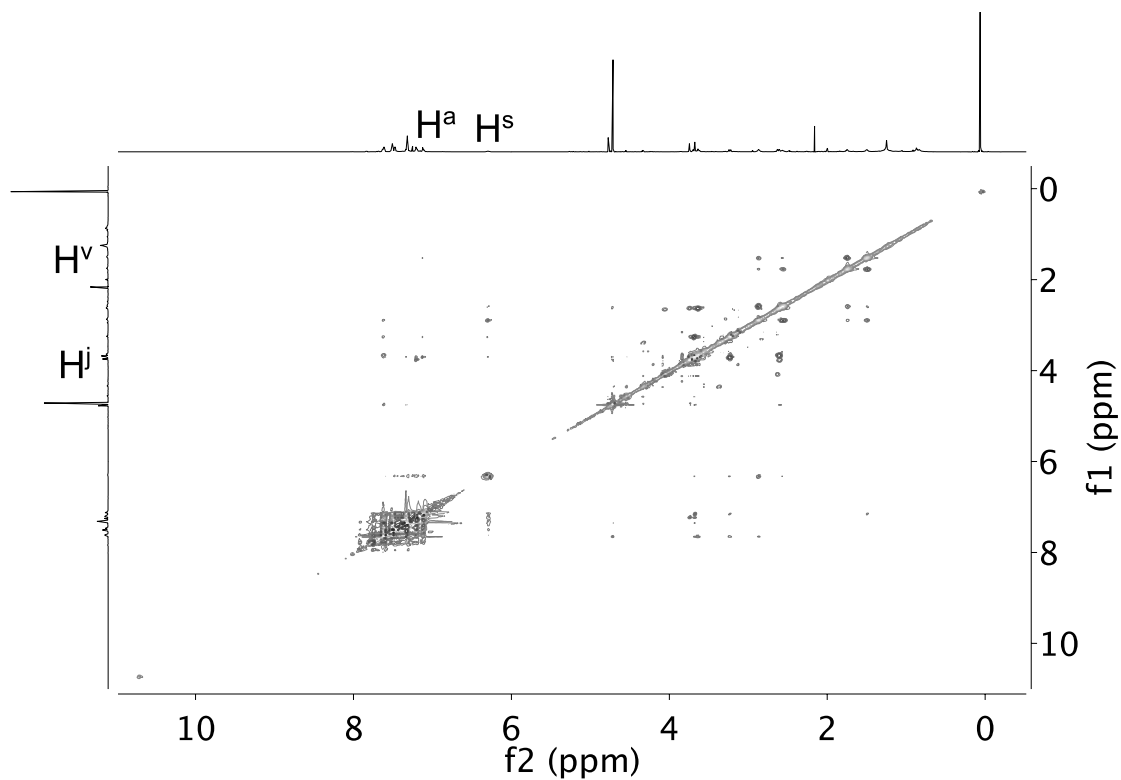


**Figure E-7.**  $^1\text{H}-^1\text{H}$  ROESY NMR spectrum of  $[\text{Ru}(\text{Cp})(\text{P}^{\text{Ph}}_2\text{N}^{\text{Bn}}_2)(\text{pyrrolidine})]\text{PF}_6$  (**5-2**) in  $\text{CDCl}_3$ .

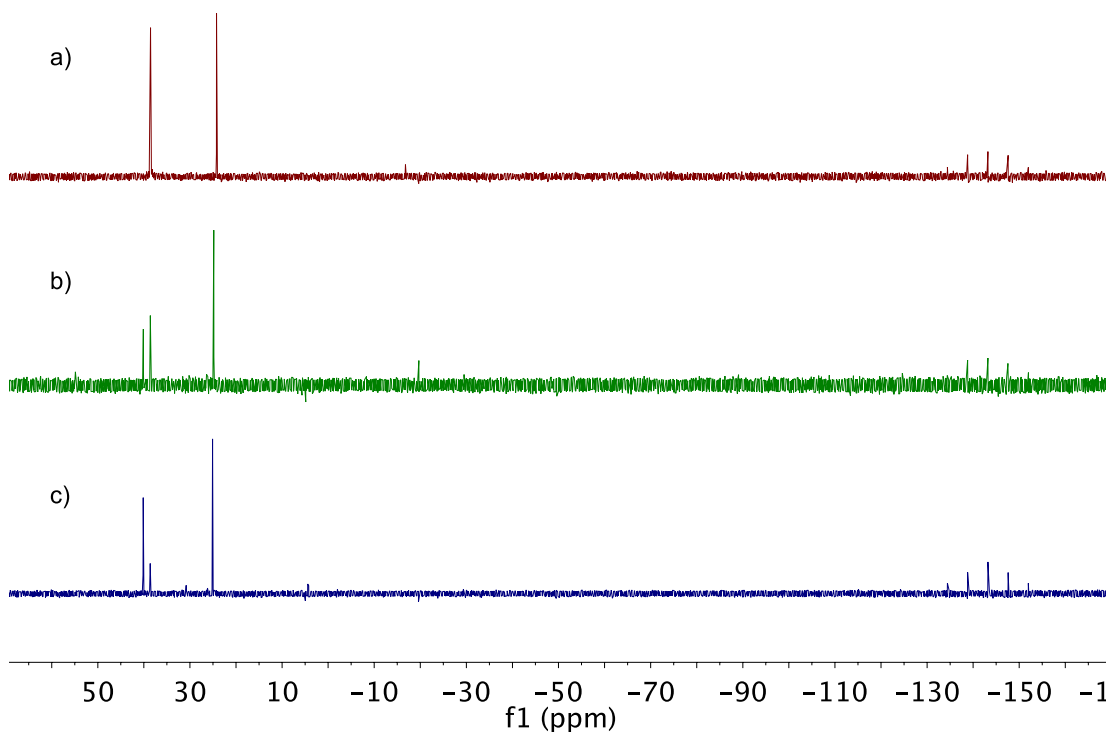


**Figure D-8.**  $^{31}\text{P}\{^1\text{H}\}$  NMR stacked spectra (proteo-THF) of a)  $[\text{Ru}(\text{Cp})(\text{dppp})(\text{NCMe})]\text{PF}_6$  (**2-3**) with  $\text{O}=\text{PPh}_3$ ; and after addition of 5 eq. pyrrolidine at b) 4 h, **2** (38.6 ppm, 35%), **5-3** (40.1 ppm, 27%), missing (38%); and c) 21 h: **2-3** (38.6 ppm, 15%), **5-3** (40.1 ppm, 50%), missing (35%). Species at 40.1 ppm assigned to  $[\text{Ru}(\text{Cp})(\text{dppp})(\text{pyrrolidine})]\text{PF}_6$ , **5-3**, is not stable to isolation.

## Catalysis Graphs

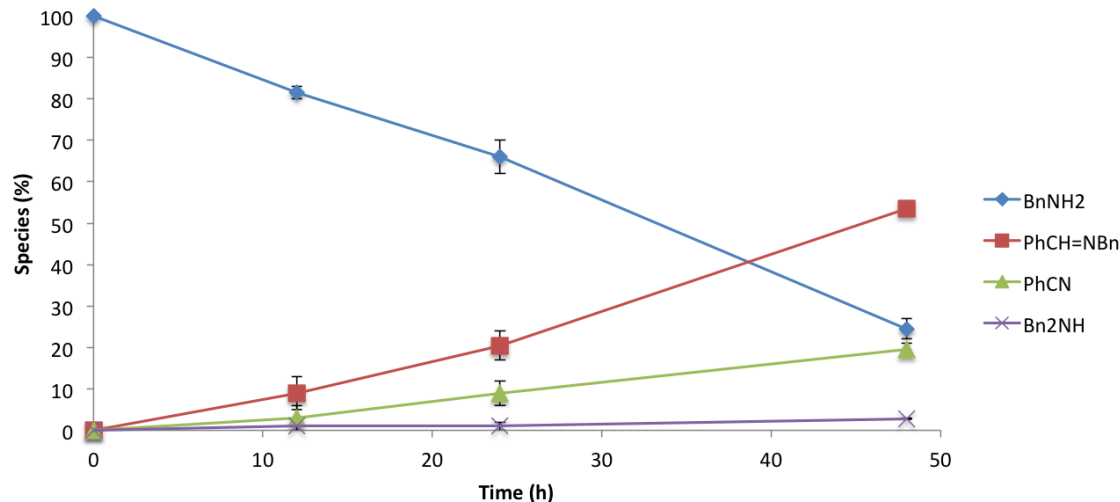


**Figure D-9.** Acceptorless dehydrogenation of benzylamine (250 mM) with 3 mol% **2-1b** at 110 °C in anisole monitored over 48 h. Amounts were determined by GC-FID by area count of calibrated signals relative to an internal standard. Reactions were conducted in duplicate. Data points represent the average of the two runs and the error bars give the span of the conversion values of each data set.

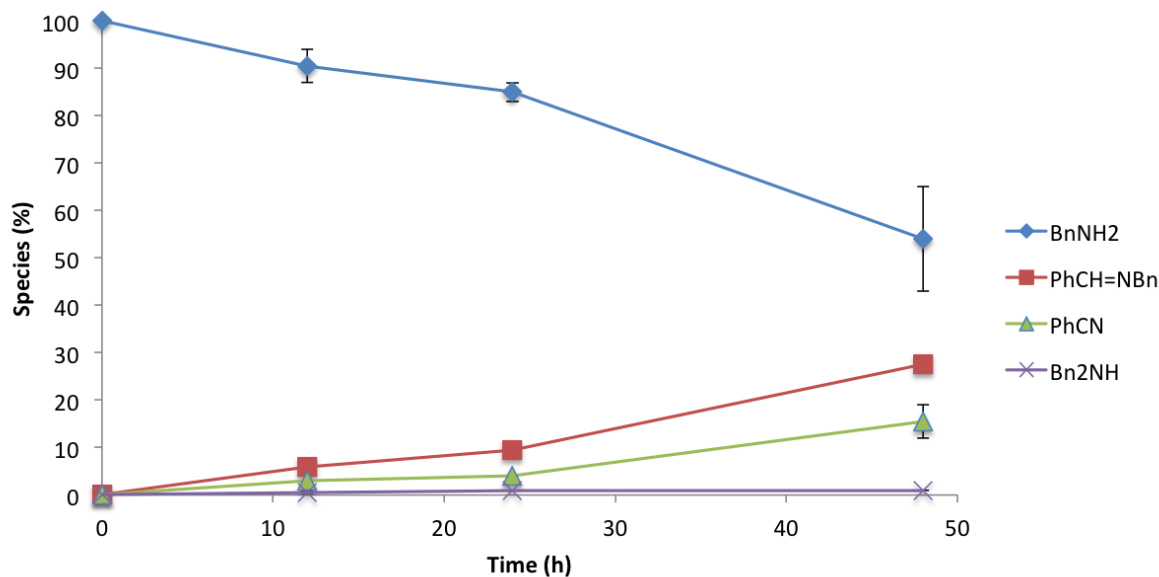


**Figure D-10.** Acceptorless dehydrogenation of benzylamine (250 mM) with 3 mol% **5-1** at 110 °C in anisole monitored over 48 h. Amounts were determined by GC-FID by area count of calibrated signals relative to an internal standard. Reactions were conducted in duplicate. Data points represent the average of the two runs and the error bars give the span of the conversion values of each data set.



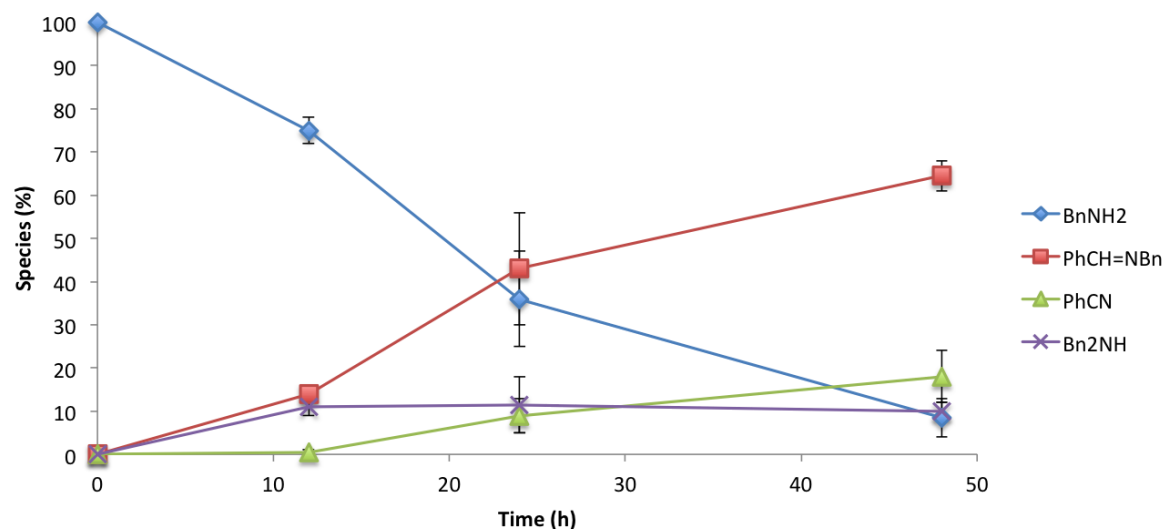


**Figure D-11.** Acceptorless dehydrogenation of benzylamine (250 mM) with 3 mol% **2-3** at 110 °C in anisole monitored over 48 h. Amounts were determined by GC-FID by area count of calibrated signals relative to an internal standard. Reactions were conducted in duplicate. Data points represent the average of the two runs and the error bars give the span of the conversion values of each data set.

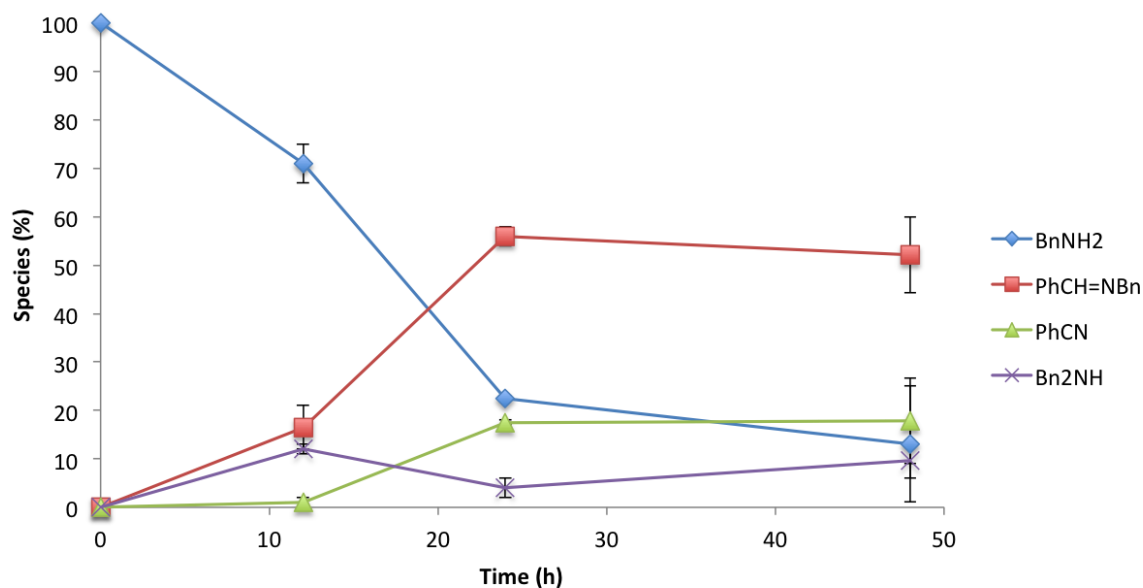


**Figure D-12.** Acceptorless dehydrogenation of benzylamine (250 mM) with 3 mol% **2-3** and 5 equiv.  $\text{NEt}_3$  at 110 °C in anisole monitored over 48 h. Amounts were determined by GC-FID by area count of calibrated signals relative to an internal standard. Reactions were conducted in duplicate. Data points represent the average of the two runs and the error bars give the span of the conversion values of each data set.

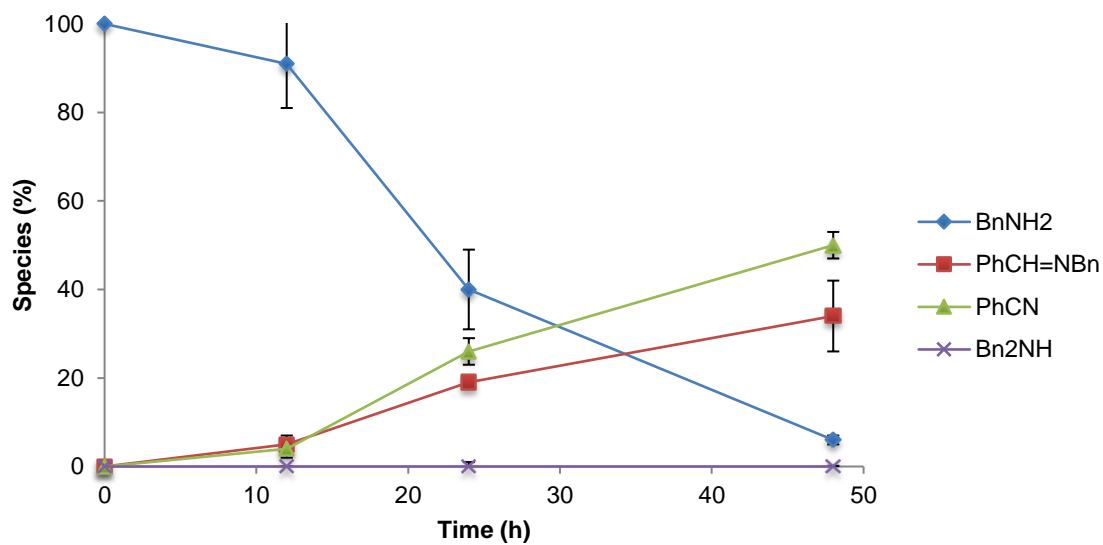


**Figure D-13.** Acceptorless dehydrogenation of benzylamine (250 mM) with 3 mol% **2-3** with 100  $\mu$ L of mercury at 110  $^{\circ}$ C in anisole monitored over 48 h. Amounts were determined by GC-FID by area count of calibrated signals relative to an internal standard. Reactions were conducted in duplicate. Data points represent the average of the two runs and the error bars give the span of the conversion values of each data set.

## MALDI Mass Spectrometry Data

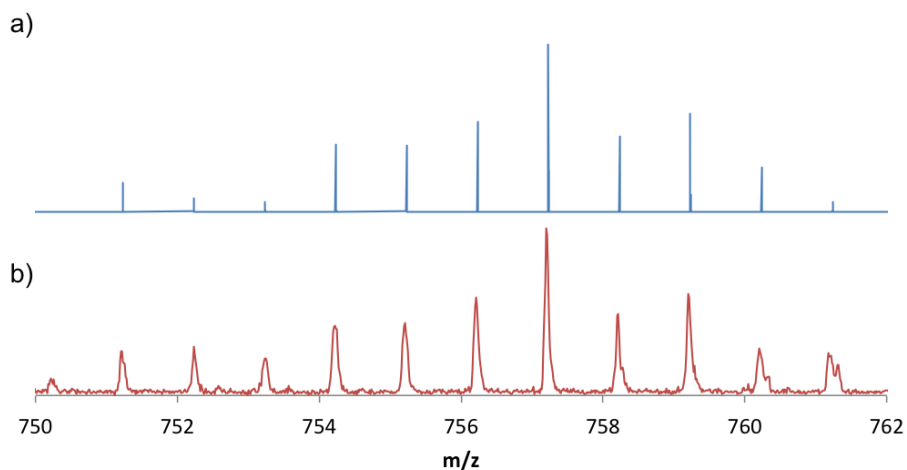


**Figure D-14.** a) Simulation<sup>7</sup> of the mass spectrometry signal for  $[5-1 - PF_6 + H]^+$ . b) Zoom-in of MALDI-TOF mass spectrometry analysis of **5-1** with pyrene as the matrix.

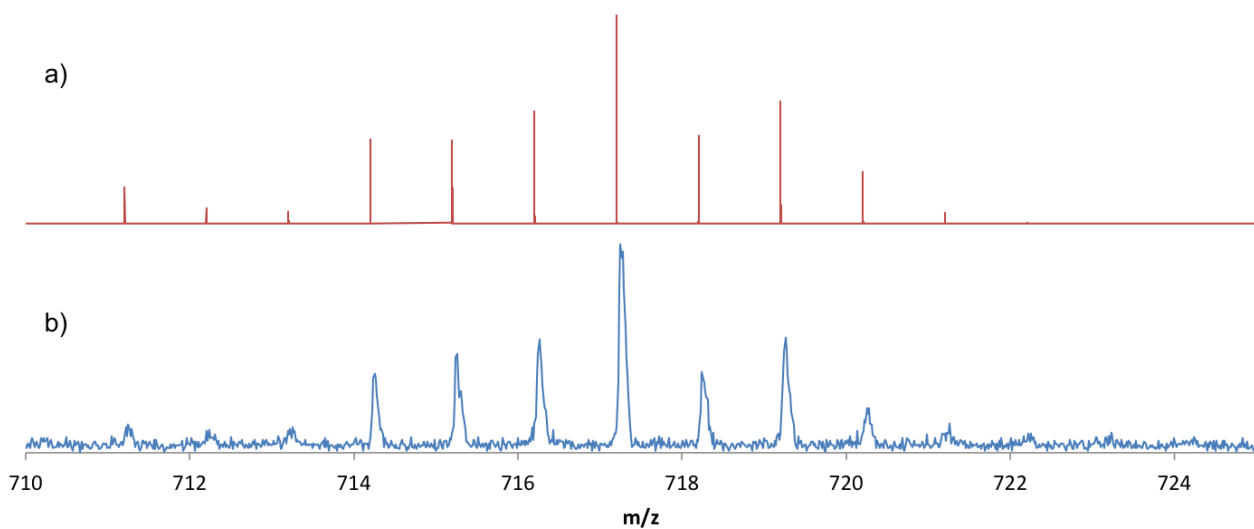


**Figure D-15.** a) Simulation<sup>7</sup> of the mass spectrometry analysis for  $[5-2 - PF_6 - 3H]^+$ . b) Zoom-in of MALDI-TOF mass spectrometry analysis of **5-2** with anthracene as the matrix.

## Crystallographic Details

### Experimental for C<sub>39</sub>H<sub>46</sub>F<sub>6</sub>N<sub>3</sub>P<sub>3</sub>Ru (**5-2**)

*Data Collection and Processing.* The sample was mounted on a Mitegen polyimide micromount with a small amount of Paratone N oil. All X-ray measurements were made on a Bruker Kappa Axis Apex2 diffractometer at a temperature of 110 K. The unit cell dimensions were determined from a symmetry constrained fit of 9960 reflections with  $5.16^\circ < 2\theta < 51.32^\circ$ . The data collection strategy was a number of  $\omega$  and  $\phi$  scans which collected data up to  $51.722^\circ$  ( $2\theta$ ). The frame integration was performed using SAINT.<sup>2</sup> The resulting raw data was scaled and absorption corrected using a multi-scan averaging of symmetry equivalent data using SADABS.<sup>3</sup>

*Structure Solution and Refinement.* The structure was solved by using a dual space methodology using the SHELXT program.<sup>4</sup> All non-hydrogen atoms were obtained from the initial solution. The hydrogen atoms were introduced at idealized positions and were allowed to ride on the parent atom. The structural model was fit to the data using full matrix least-squares based on  $F^2$ . The calculated structure factors included corrections for anomalous dispersion from the usual tabulation. The structure was refined using the SHELXL-2014 program from the SHELX suite of crystallographic software.<sup>5</sup> Graphic plots were produced using the NRCVAX program suite.<sup>6</sup>

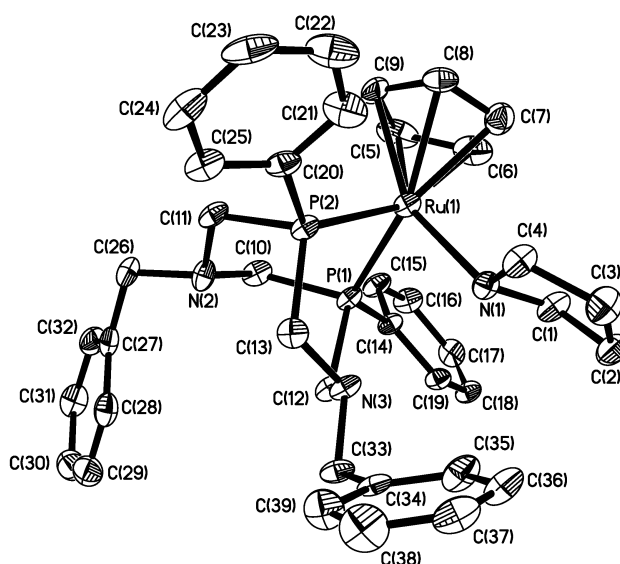


**Figure D-16.** ORTEP drawing of **5-2** showing naming and numbering scheme. Ellipsoids are at the 50% probability level and hydrogen atoms were omitted for clarity. PF<sub>6</sub> counter-ion was omitted for clarity.

**Table D-1.** Summary of Crystal Data for **5-2**

Formula	$C_{39}H_{46}F_6N_3P_3Ru$
Formula Weight ( <i>g/mol</i> )	864.77
Crystal Dimensions ( <i>mm</i> )	$0.165 \times 0.069 \times 0.037$
Crystal Color and Habit	yellow plate
Crystal System	monoclinic
Space Group	$P 2_1/n$
Temperature, K	110
<i>a</i> , Å	10.564(3)
<i>b</i> , Å	23.741(9)
<i>c</i> , Å	15.120(6)
$\alpha$ , °	90
$\beta$ , °	90.179(13)
$\gamma$ , °	90
<i>V</i> , Å <sup>3</sup>	3792(2)
Number of reflections to determine final unit cell	9960
Min and Max 2 $\theta$ for cell determination, °	5.16, 51.32
<i>Z</i>	4
F(000)	1776
$\rho$ ( <i>g/cm</i> )	1.515
$\lambda$ , Å, (MoK $\alpha$ )	0.71073
$\mu$ , ( <i>cm</i> <sup>-1</sup> )	0.603
Diffractometer Type	Bruker Kappa Axis Apex2
Scan Type(s)	$\varphi$ and $\omega$ scans
Max 2 $\theta$ for data collection, °	51.722
Measured fraction of data	0.998
Number of reflections measured	63314
Unique reflections measured	7239
$R_{merge}$	0.1119
Number of reflections included in refinement	7239
Cut off Threshold Expression	$I > 2\sigma(I)$
Structure refined using	full matrix least-squares using $F^2$
Weighting Scheme	$w=1/[\sigma^2(F_o^2)+(0.0841P)^2+5.2475P]$ where $P=(F_o^2+2F_c^2)/3$
Number of parameters in least-squares	469
$R_1$	0.0653
$wR_2$	0.1478

R <sub>1</sub> (all data)	0.1124
wR <sub>2</sub> (all data)	0.1718
GOF	1.056
Maximum shift/error	0.001
Min & Max peak heights on final ΔF Map (e <sup>-</sup> /Å)	-1.363, 2.418

Where:

$$R_1 = \sum (|F_o| - |F_c|) / \sum F_o$$

$$wR_2 = [ \sum (w(F_o^2 - F_c^2))^2 / \sum (w F_o^4) ]^{1/2}$$

$$GOF = [ \sum (w(F_o^2 - F_c^2))^2 / (\text{No. of reflns.} - \text{No. of params.}) ]^{1/2}$$

## References

1. Stubbs, J. M.; Bow, J. P. J.; Hazlehurst, R. J.; Blacquiere, J. M., *Dalton Trans.* **2016**, 45, 17100-17103.
2. Bruker-Nonius; SAINT; version; 2012.12, **2012**, Bruker-Nonius, Madison, WI 53711, USA
3. Bruker-Nonius; SADABS; version; 2012.1, **2012**, Bruker-Nonius, Madison, WI 53711, USA.
4. Sheldrick, G., *Acta Crystallogr. Sect. A* **2015**, A71, 3-8.
5. Sheldrick, G., *Acta Crystallogr. Sect. C* **2015**, C71, 3-8.
6. Gabe, E. J.; Le Page, Y.; Charland, J. P.; Lee, F. L.; White, P. S., *J. Appl. Crystallogr.* **1989**, 22, 384-387.
7. Patiny, L.; Borel, A., *J. Chem. Inf. Model.* **2013**, 53, 1223-1228.

## Appendices E: Supplementary Information for Chapter 6

### NMR Spectra

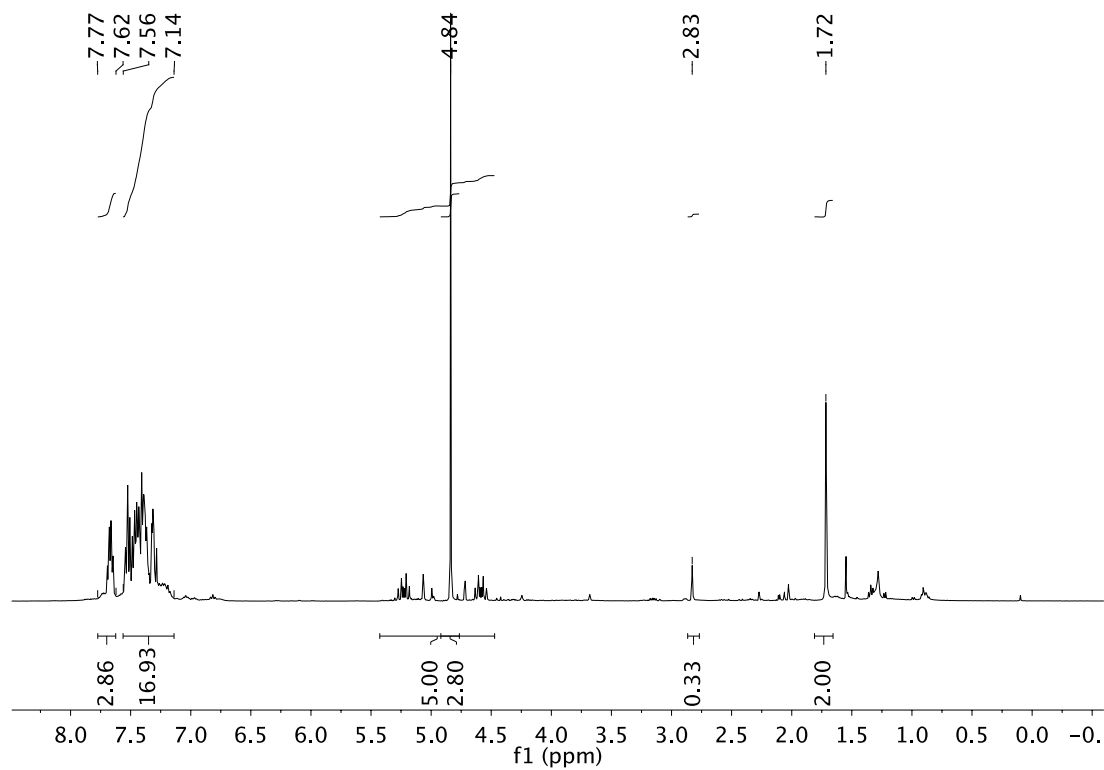


**Figure E-1.** <sup>1</sup>H NMR spectrum of [Ru(Cp)(dppm)(NCCH<sub>3</sub>)]PF<sub>6</sub> (**6-1a**) in CDCl<sub>3</sub>.





**Figure E-3.**  $^{31}\text{P}\{^1\text{H}\}$  NMR spectrum of  $[\text{Ru}(\text{Cp})(\text{dppm})(\text{NCCH}_3)]\text{PF}_6$  (**6-1a**) in  $\text{CDCl}_3$ .

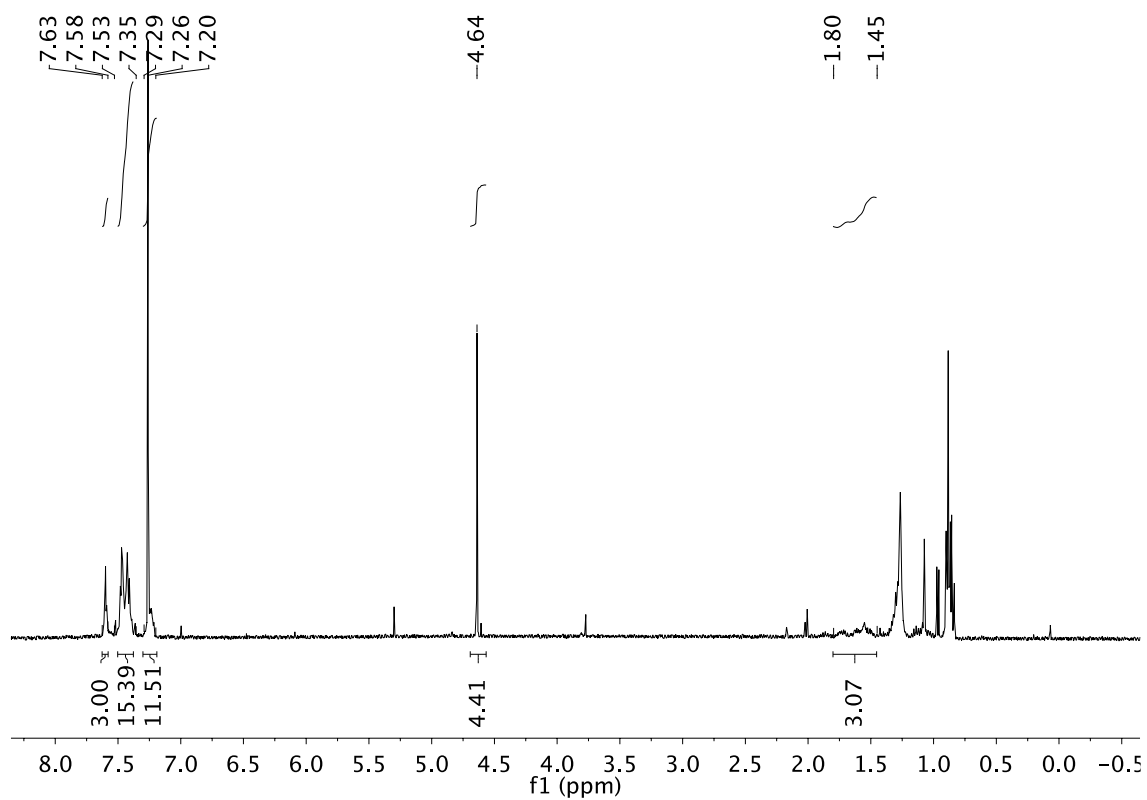


**Figure E-4.**  $^1\text{H}$  NMR spectrum of  $[\text{Ru}(\text{Cp})(\text{dpbz})(\text{NCCH}_3)]\text{PF}_6$  (**6-1c**) in  $\text{CDCl}_3$ .

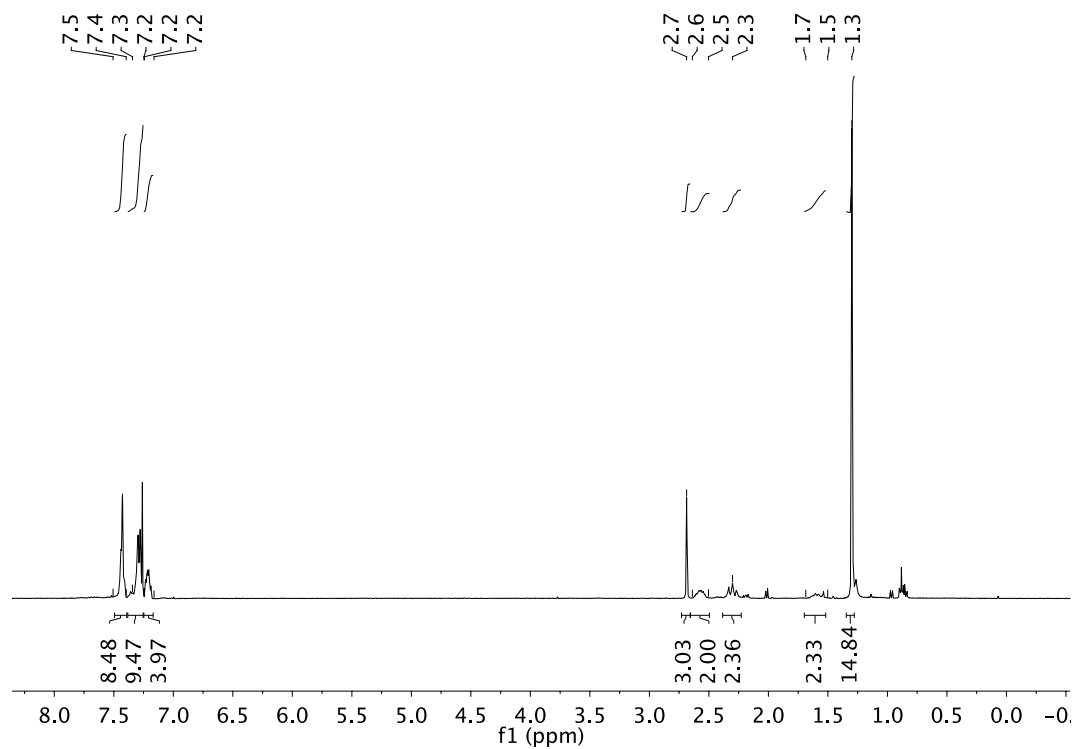


**Figure E-5.**  $^1\text{H}$  NMR spectrum of  $[\text{Ru}(\text{Cp}^*)(\text{dppp})(\text{NCCH}_3)]\text{PF}_6$  (**6-2**) in  $\text{CDCl}_3$ .

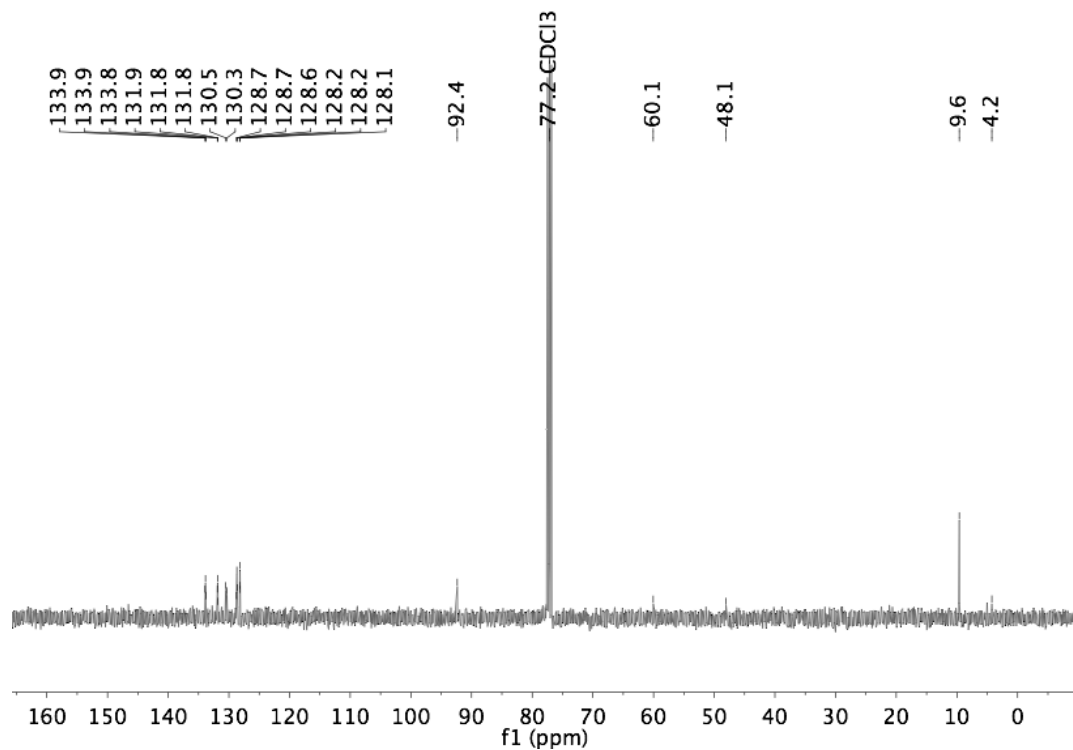


**Figure E-6.**  $^{13}\text{C}$   $\{^1\text{H}\}$  NMR spectrum of  $[\text{Ru}(\text{Cp}^*)(\text{dppp})(\text{NCCH}_3)]\text{PF}_6$  (**6-2**) in  $\text{CDCl}_3$ .

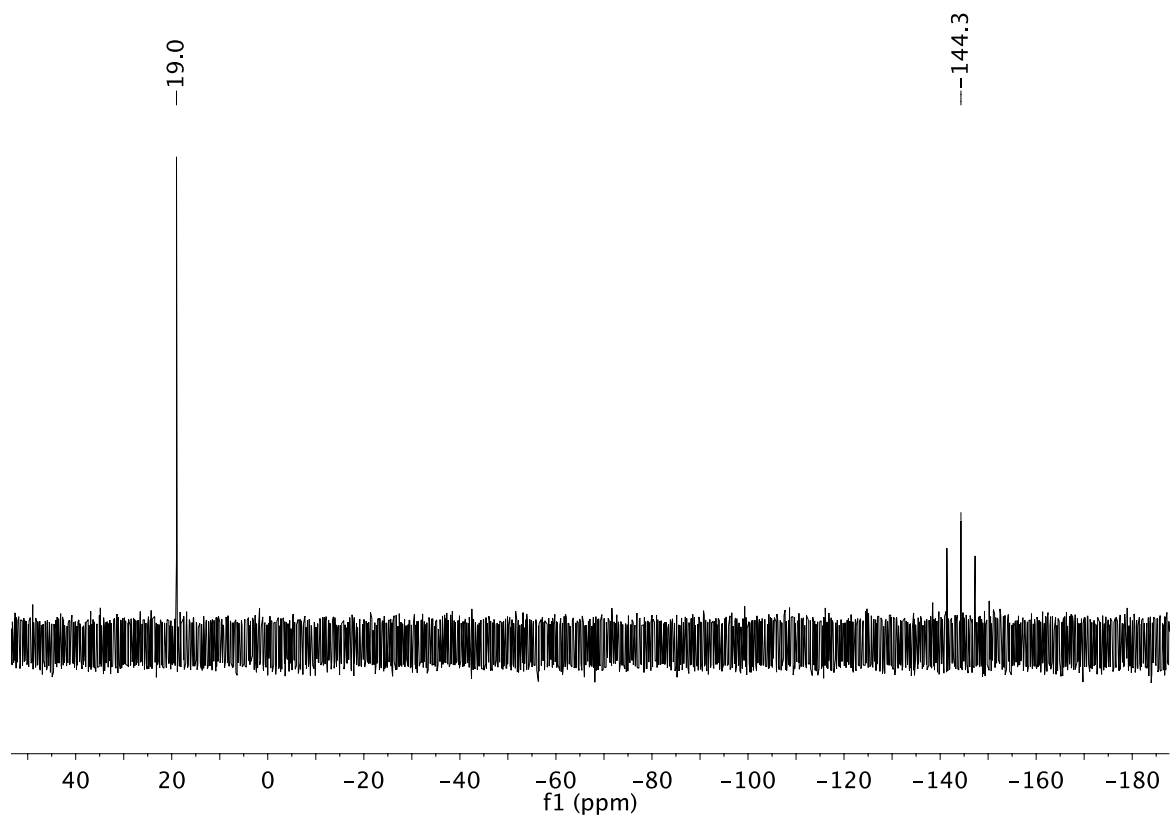


**Figure E-7.**  $^{31}\text{P}$   $\{^1\text{H}\}$  NMR spectrum of  $[\text{Ru}(\text{Cp}^*)(\text{dppp})(\text{NCCH}_3)]\text{PF}_6$  (**6-2**) in  $\text{CD}_2\text{Cl}_2$ .

## MALDI Spectra

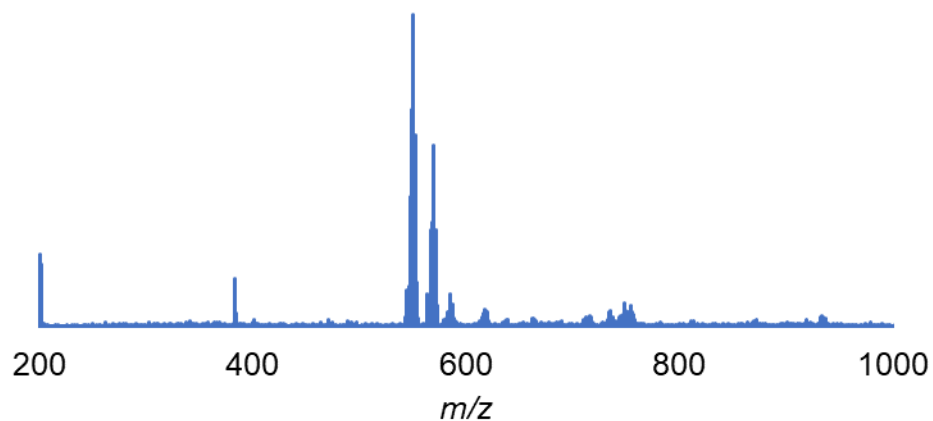


**Figure E-8.** MALDI-TOF mass spectrometry of  $[\text{Ru}(\text{Cp})(\text{dppm})(\text{NCMe})]\text{PF}_6$  (**6-1a**) in a 1:20 ratio of pyrene, the matrix.

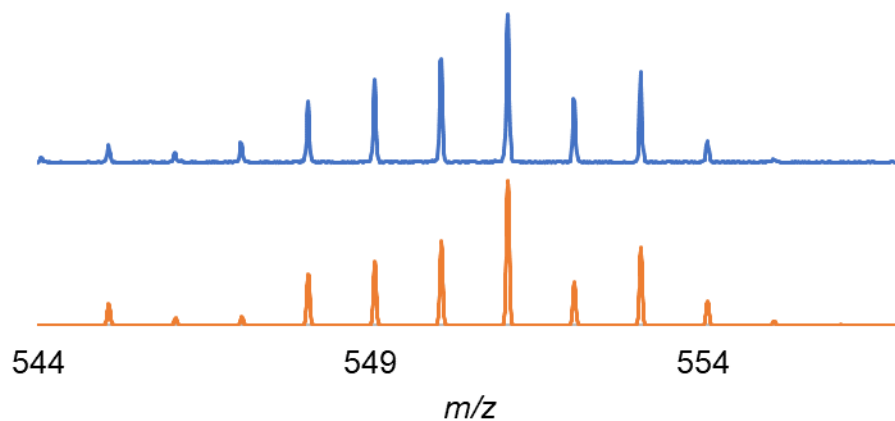


**Figure E-9.** a) Zoom-in of MALDI-TOF mass spectrometry of  $[\text{Ru}(\text{Cp})(\text{dppm})]^+ \cdot$  generated from **6-1a** in a 1:20 ratio of pyrene, the matrix. b) Simulation of MALDI-TOF mass spectrometry of  $[\text{Ru}(\text{Cp})(\text{dppm})]^+ \cdot$ .

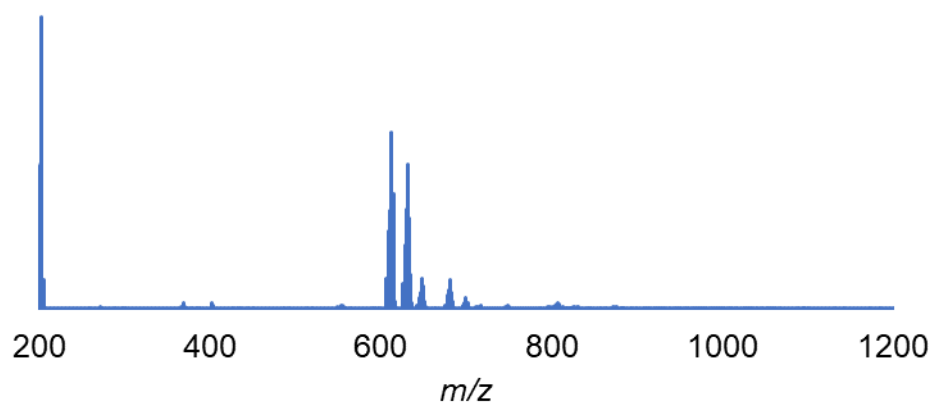


**Figure E-10.** MALDI-TOF mass spectrometry of  $[\text{Ru}(\text{Cp})(\text{dpbz})(\text{NCMe})]\text{PF}_6$  (**6-1c**) in a 1:20 ratio of pyrene, the matrix.

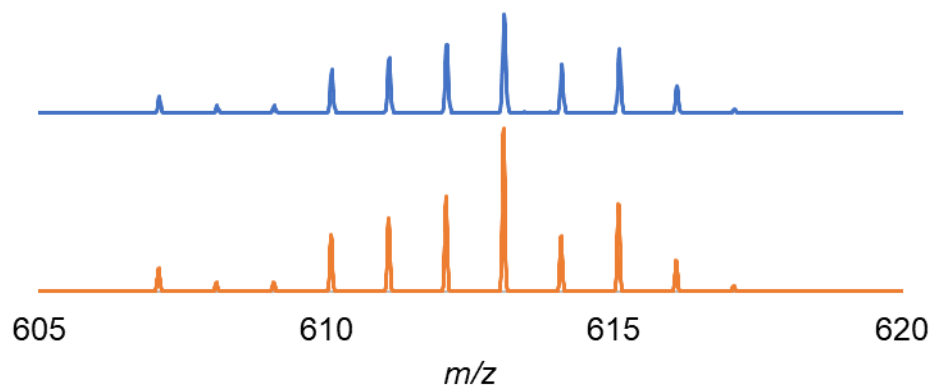


**Figure E-11.** a) Zoom-in of MALDI-TOF mass spectrometry of  $[\text{Ru}(\text{Cp})(\text{dpbz})]^{+\bullet}$  generated from **6-1c** in a 1:20 ratio of pyrene, the matrix. b) Simulation of MALDI-TOF mass spectrometry of  $[\text{Ru}(\text{Cp})(\text{dpbz})]^{+\bullet}$ .

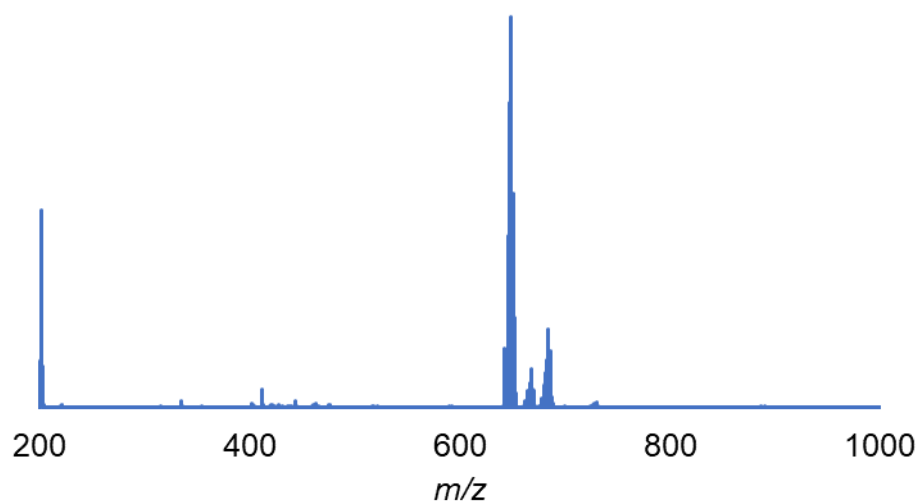


**Figure E-12.** MALDI-TOF mass spectrometry of  $[\text{Ru}(\text{Cp}^*)(\text{dppp})(\text{NCMe})]\text{PF}_6$  (**6-2**) in a 1:20 ratio of pyrene, the matrix.

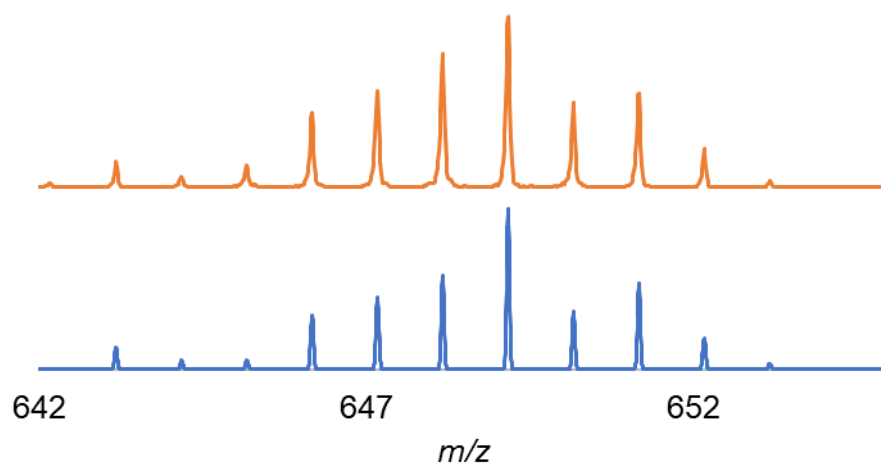


**Figure E-13.** a) Zoom-in of MALDI-TOF mass spectrometry of  $[\text{Ru}(\text{Cp}^*)(\text{dppp})]^+ \cdot$  generated from **6-2** in a 1:20 ratio of pyrene, the matrix. b) Simulation of MALDI-TOF mass spectrometry of  $[\text{Ru}(\text{Cp}^*)(\text{dppp})]^{++}$ .

## Bures Analysis

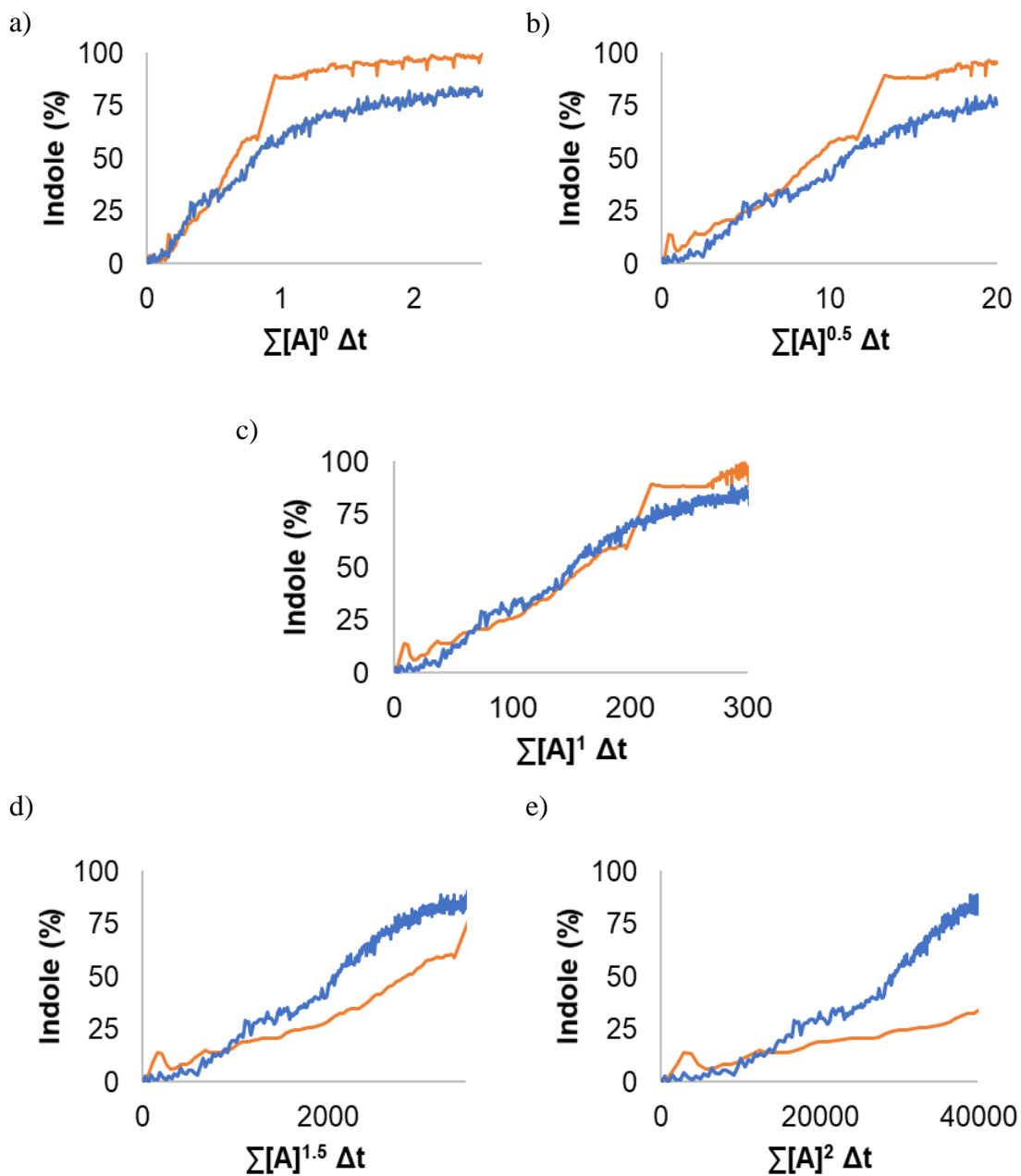


**Figure E-14.** Substrate Bures Analysis Profile at a) 0<sup>th</sup> order; b) 0.5<sup>th</sup> order; c) 1<sup>st</sup> order; d) 1.5<sup>th</sup> order; and e) 2<sup>nd</sup> order for the acceptorless dehydrogenation of indoline (250 mM – blue; 375 mM – orange) using 1 mol% of complex **3-2a** at 97 °C in anisole monitored by REACTIR.

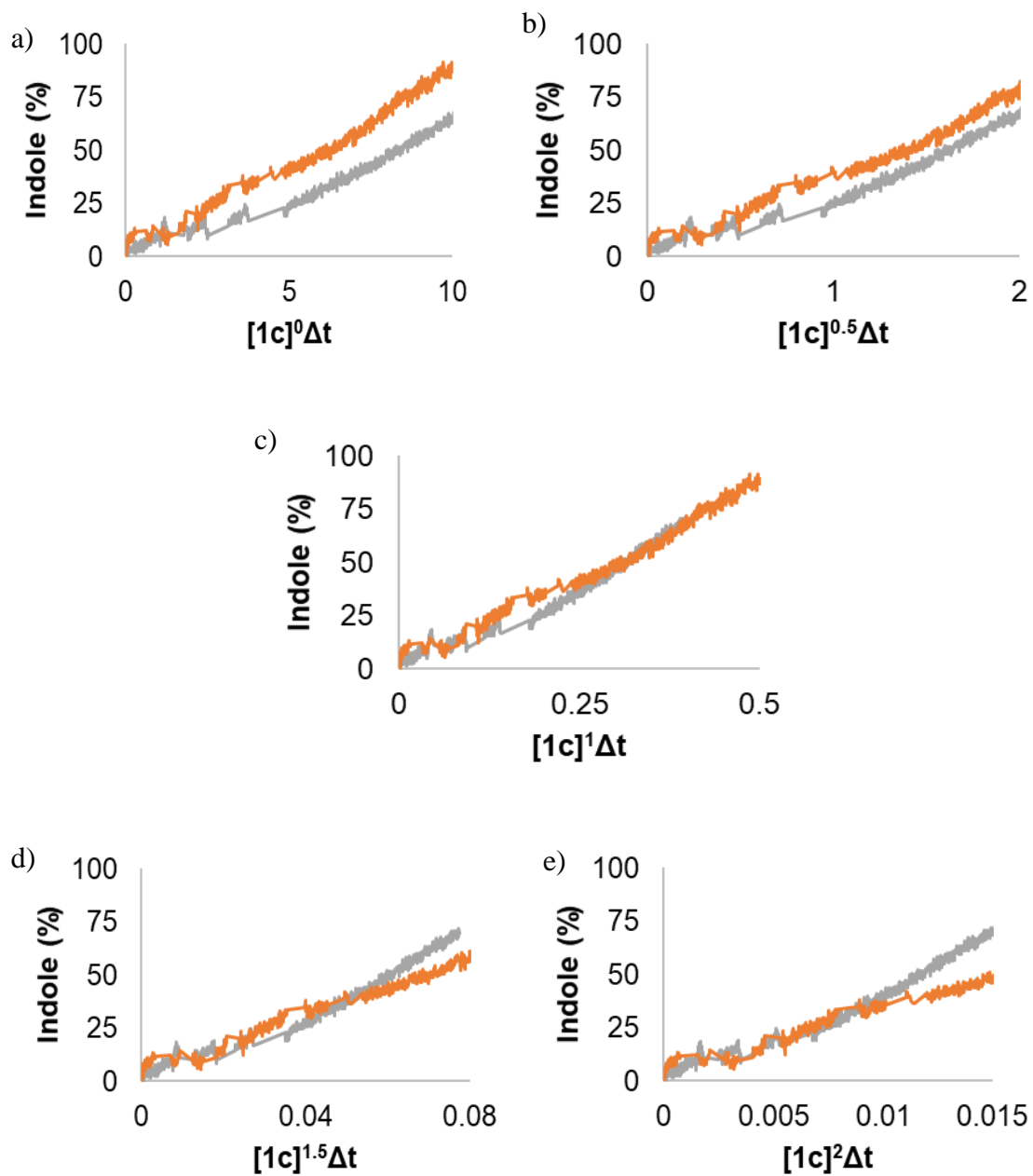


**Figure E-15.** Catalyst Bures analysis profile at a) 0<sup>th</sup> order; b) 0.5<sup>th</sup> order; c) 1<sup>st</sup> order; d) 1.5<sup>th</sup> order; and e) 2<sup>nd</sup> order for the acceptorless dehydrogenation of indoline (250 mM) using complex **3-2a** (grey – 1 mol%; orange – 2 mol%) at 82 °C in anisole monitored by REACTIR.



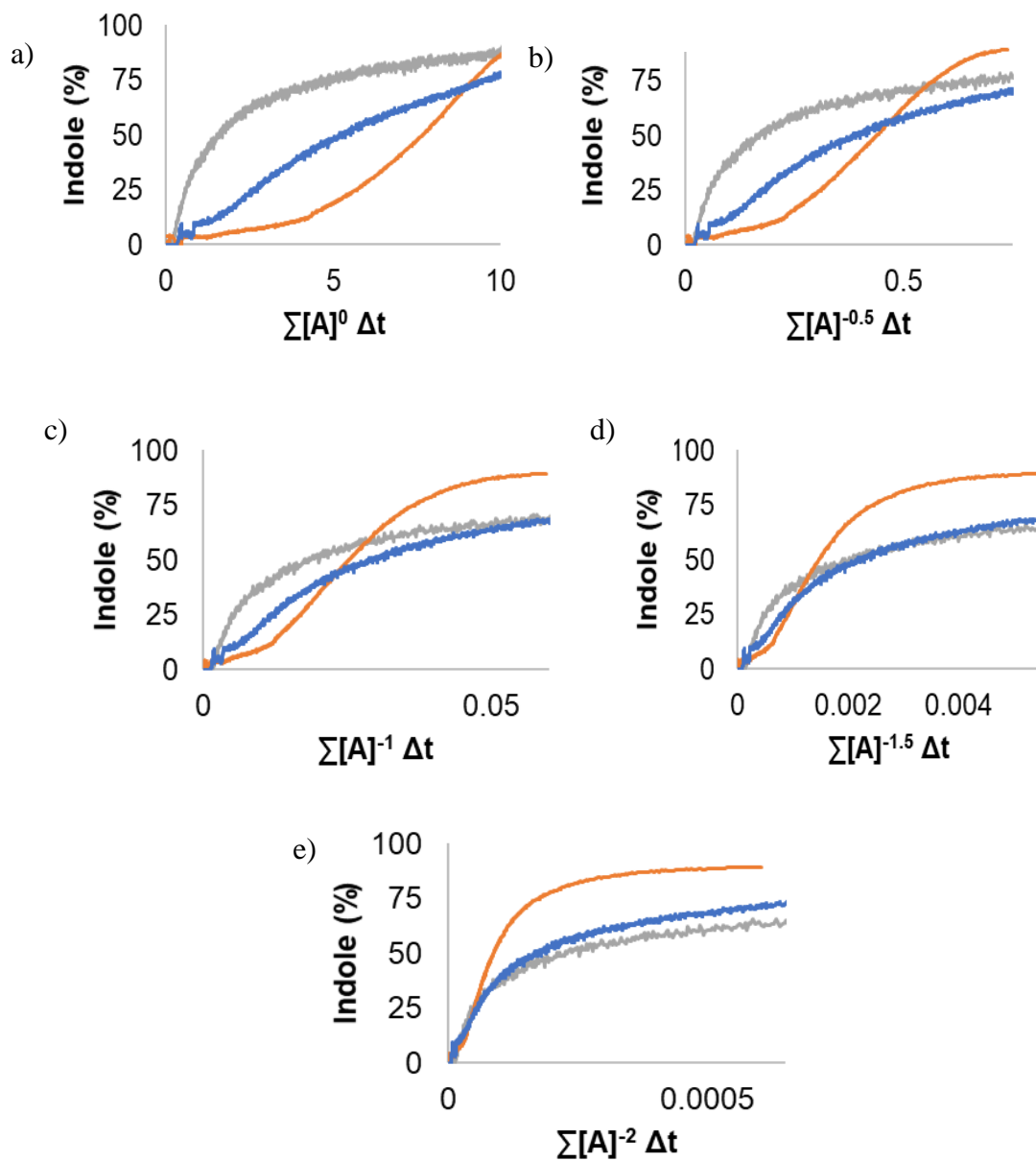


**Figure E-16.** Substrate Bures Analysis Profile at a) 0<sup>th</sup> order; b) -0.5<sup>th</sup> order; c) -1<sup>st</sup> order; d) -1.5<sup>th</sup> order; and e) -2<sup>nd</sup> order for the acceptorless dehydrogenation of indoline (125 mM – grey; 250 mM – blue; 375 mM – orange) using 1 mol% of complex **2-3** at 97 °C in anisole monitored by REACTIR.

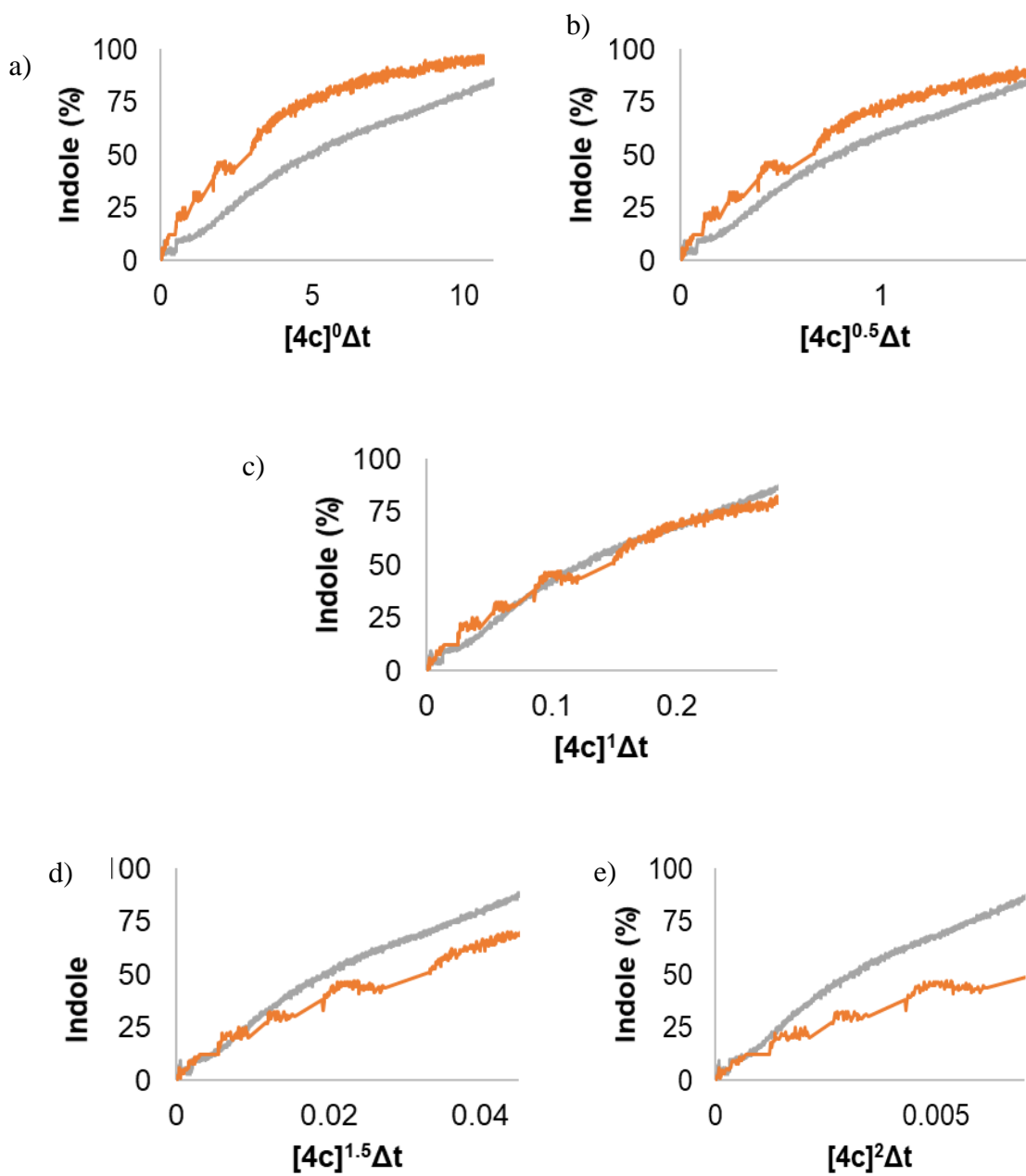


**Figure E-17.** Catalyst Bures analysis profile at a) 0<sup>th</sup> order; b) 0.5<sup>th</sup> order; c) 1<sup>st</sup> order; d) 1.5<sup>th</sup> order; and e) 2<sup>nd</sup> order for the acceptorless dehydrogenation of indoline (250 mM) using complex **2-3** (grey – 1 mol%; orange – 2 mol%) at 100 °C in anisole monitored by REACTIR.

## Catalytic Profiles of Substrate

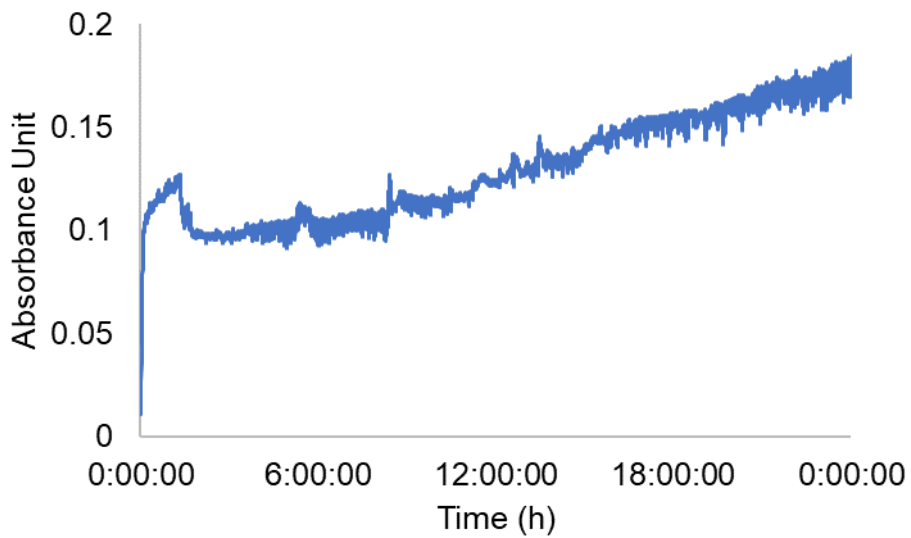


**Figure E-18.** Reaction profile of the acceptorless dehydrogenation of 4-chloroindoline using 1 mol% of complex **3-2a** at 125 °C in anisole monitored by REACTIR at 816  $\text{cm}^{-1}$ .

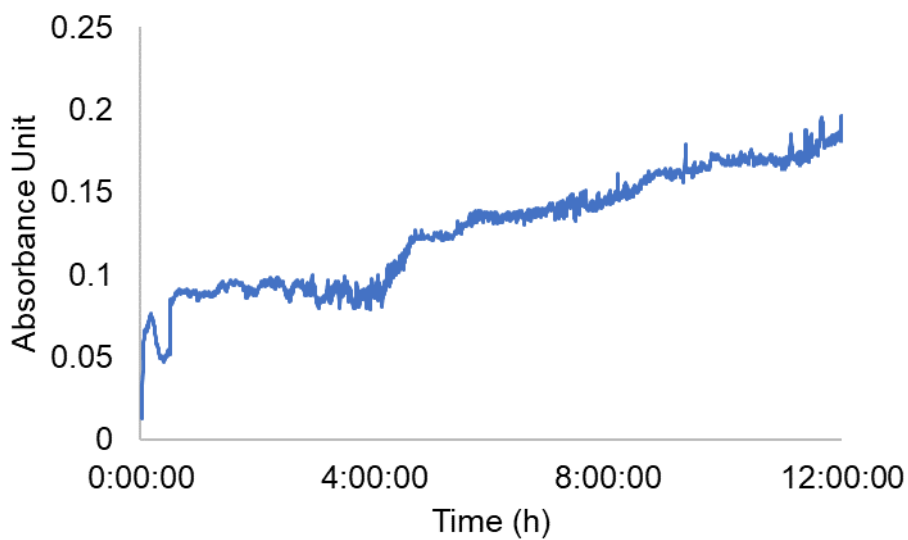


**Figure E-19.** Reaction profile of the acceptorless dehydrogenation of 5-chloroindoline using 1 mol% of complex **3-2a** at 125 °C in anisole monitored by REACTIR at 897 cm<sup>-1</sup>.

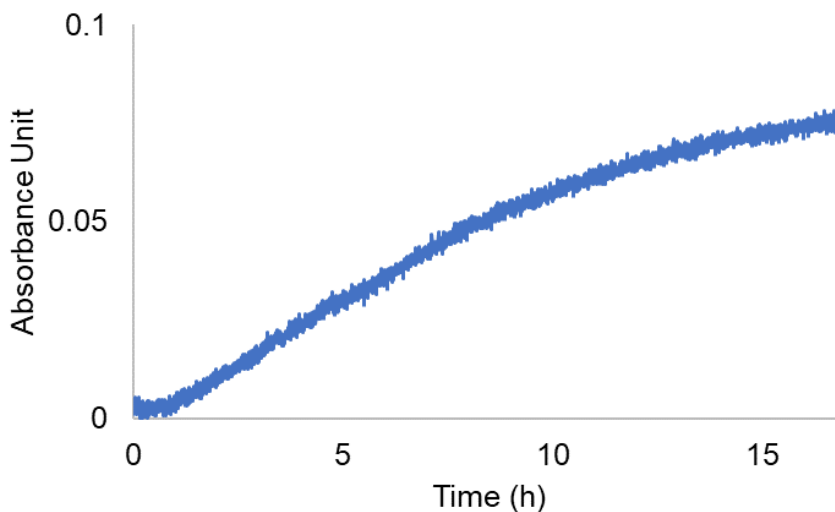


**Figure E-20.** Reaction profile of the acceptorless dehydrogenation of 6-chloroindoline using 1 mol% of complex **3-2a** at 125 °C in anisole monitored by REACTIR at 1005 cm<sup>-1</sup>.

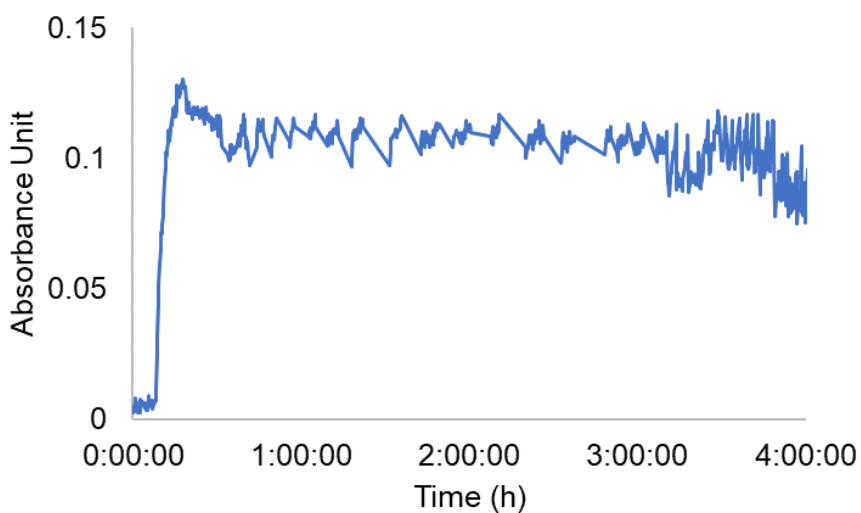


**Figure E-21.** Reaction profile of the acceptorless dehydrogenation of 5-bromoindoline using 1 mol% of complex **3-2a** at 125 °C in anisole monitored by REACTIR at 770 cm<sup>-1</sup>.

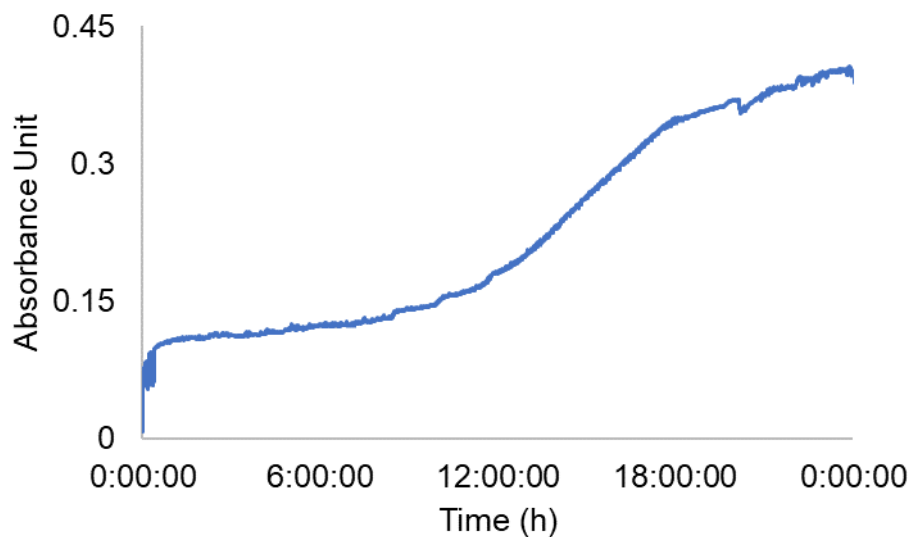


**Figure E-22.** Reaction profile of the acceptorless dehydrogenation of 5-fluoroindoline using 1 mol% of complex **3-2a** at 125 °C in anisole monitored by REACTIR at 899  $\text{cm}^{-1}$ .

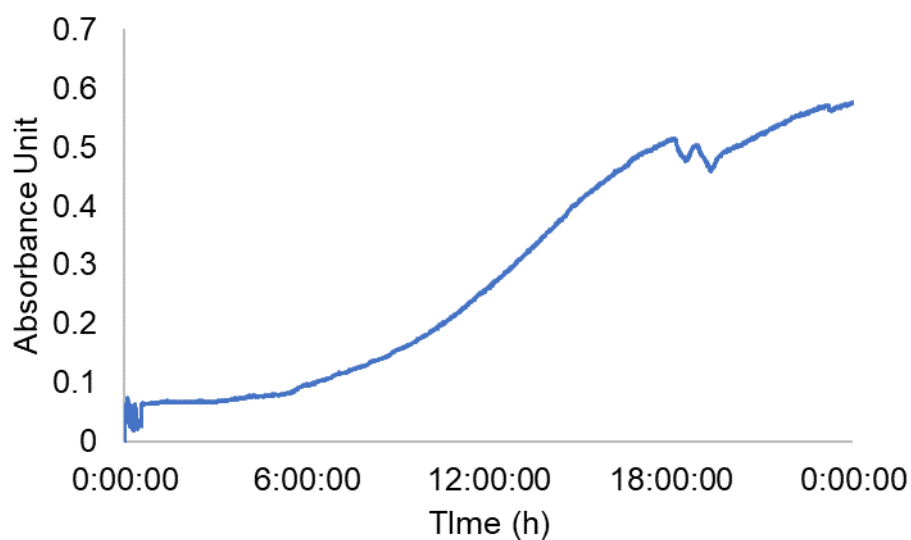


**Figure E-23.** Reaction profile of the acceptorless dehydrogenation of 5-methoxyindoline using 1 mol% of complex **3-2a** at 125 °C in anisole monitored by REACTIR at 898  $\text{cm}^{-1}$ .

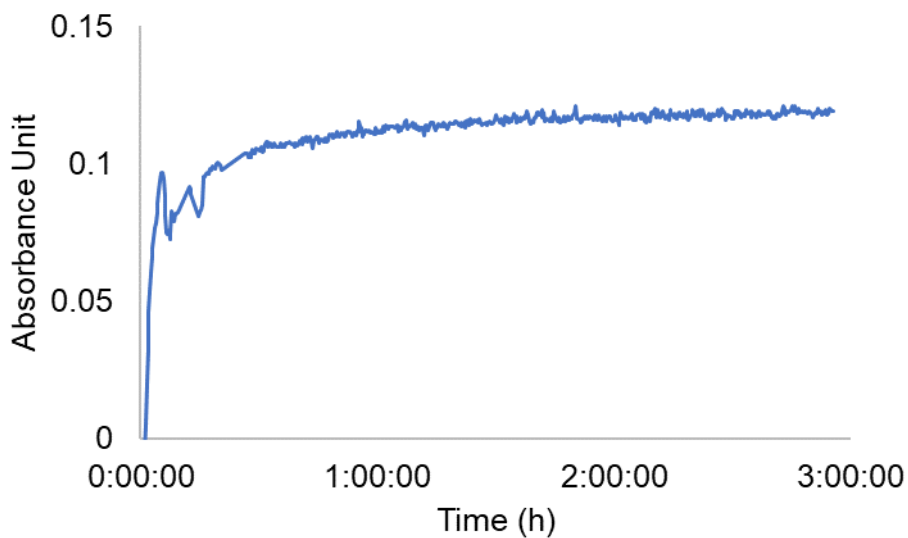


**Figure E-24.** Reaction profile of the acceptorless dehydrogenation of 5-methylindoline using 1 mol% of complex **3-2a** at 125 °C in anisole monitored by REACTIR at 791  $\text{cm}^{-1}$ .

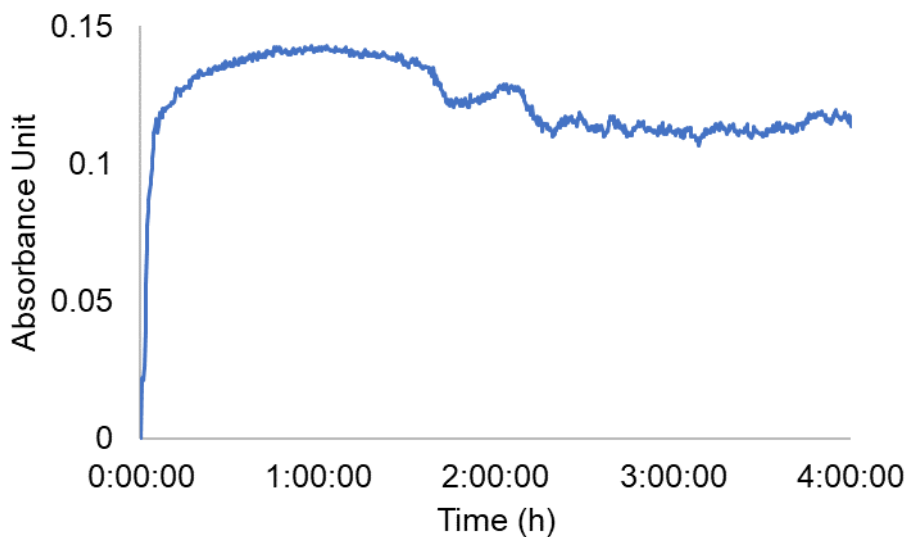


**Figure E-25.** Reaction profile of the acceptorless dehydrogenation of methyl indoline-5-carboxylate using 1 mol% of complex **3-2a** at 125 °C in anisole monitored by REACTIR at 869  $\text{cm}^{-1}$ .

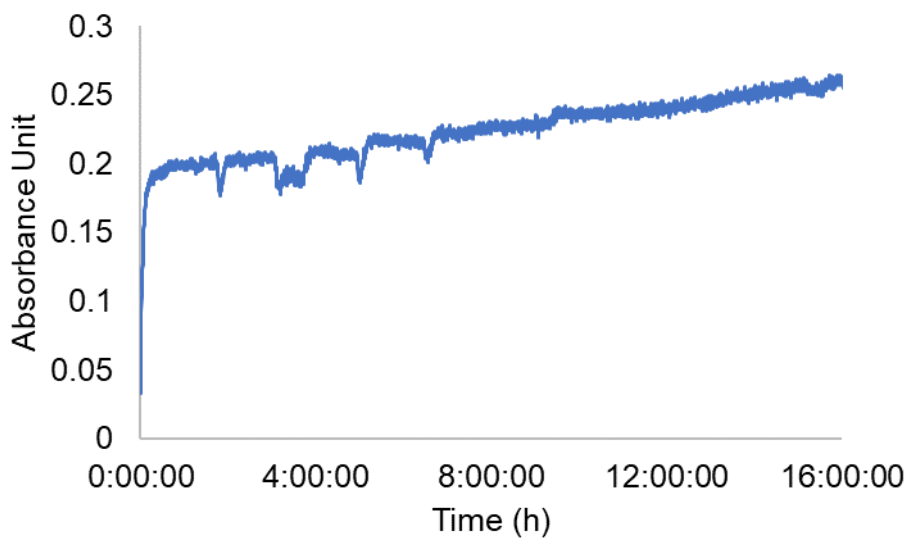


**Figure E-26.** Reaction profile of the acceptorless dehydrogenation of 5-nitroindoline using 1 mol% of complex **3-2a** at 125 °C in anisole monitored by REACTIR at 775  $\text{cm}^{-1}$ .

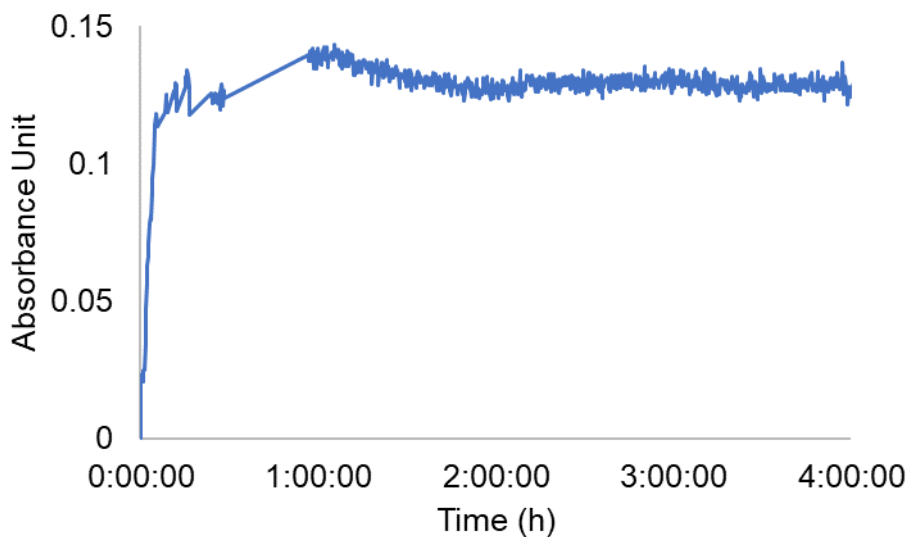


**Figure E-27.** Reaction profile of the acceptorless dehydrogenation of 2-methylindoline using 1 mol% of complex **3-2a** at 125 °C in anisole monitored by REACTIR at 703  $\text{cm}^{-1}$ .

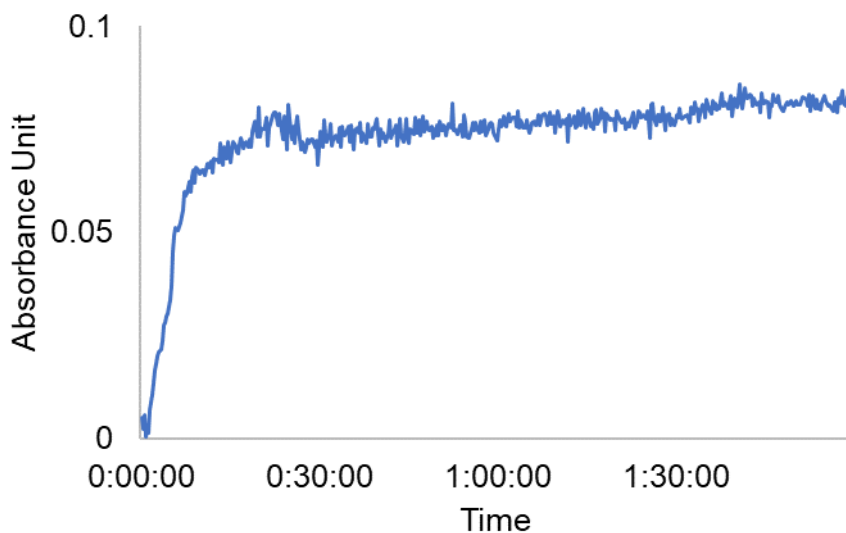


**Figure E-28.** Reaction profile of the acceptorless dehydrogenation of tetrahydroquinoline using 1 mol% of complex **3-2a** at 125 °C in anisole monitored by REACTIR at 765  $\text{cm}^{-1}$ .

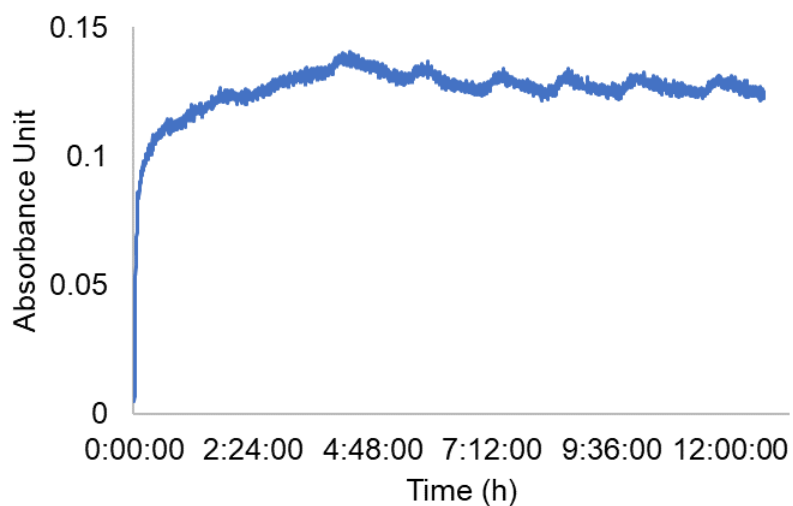


**Figure E-29.** Reaction profile of the acceptorless dehydrogenation of tetrahydroisoquinoline using 1 mol% of complex **3-2a** at 125 °C in anisole monitored by REACTIR at 779  $\text{cm}^{-1}$ .



## Appendices F: Copyright Material and Permissions

**Chapter 2** – Reproduced from J. M. Stubbs, J.-P. J. Bow, R. J. Hazlehurst and J. M. Blacquiere, *Dalton Trans.*, **2016**, 45, 17100-17103 with permission from The Royal Society of Chemistry.

### **Chapter 3** – John Wiley and Sons' Policy on Theses and Dissertations

This Agreement between James M. Stubbs and John Wiley and Sons consists of your license details and the terms and conditions provided by John Wiley and Sons and Copyright Clearance Center.

License Number	4491380388326
License date	Dec 17, 2018
Licensed Content Publisher	John Wiley and Sons
Licensed Content Publication	ChemCatChem
Licensed Content Title	Catalyst Pendent-Base Effects on Cyclization of Alkynyl Amines
Licensed Content Author	James M. Stubbs, Devon E. Chapple, Paul D. Boyle, et al
Licensed Content Date	Jul 6, 2018
Licensed Content Volume	10
Licensed Content Issue	17
Licensed Content Pages	9
Type of use	Dissertation/Thesis
Requestor type	Author of this Wiley article
Format	Print and electronic
Portion	Full article
Will you be translating?	No
Title of your thesis / dissertation	Structure-Activity Relationships (SARs) for Metal-Ligand-Cooperative (MLC) Complexes using PR <sub>2</sub> NR <sub>2</sub> Ligands
Expected completion date	Dec 2018
Expected size (number of pages)	300
Publisher Tax ID	EU826007151
Total	0.00 CAD

## TERMS AND CONDITIONS

This copyrighted material is owned by or exclusively licensed to John Wiley & Sons, Inc. or one of its group companies (each a "Wiley Company") or handled on behalf of a society with which a Wiley Company has exclusive publishing rights in relation to a particular work (collectively "WILEY"). By clicking "accept" in connection with completing this licensing transaction, you agree that the following terms and conditions apply to this transaction (along with the billing and payment terms and conditions established by the Copyright Clearance Center Inc., ("CCC's Billing and Payment terms and conditions"), at the time that you opened your RightsLink account (these are available at any time at <http://myaccount.copyright.com>).

### Chapter 5 – American Chemical Society's Policy on Theses and Dissertations

Title: Catalytic Acceptorless Dehydrogenation of Amines with  $\text{Ru}(\text{P}^{\text{R}}_2\text{N}^{\text{R}'_2})$  and  $\text{Ru}(\text{dppp})$  Complexes

Author: James M. Stubbs, Richard J. Hazlehurst, Paul D. Boyle, et al

Publication: Organometallics

Publisher American Chemical Society

Date: May 1, 2017

Copyright © 2017, American Chemical Society

### **PERMISSION/LICENSE IS GRANTED FOR YOUR ORDER AT NO CHARGE**

This type of permission/license, instead of the standard Terms & Conditions, is sent to you because no fee is being charged for your order. Please note the following:

- Permission is granted for your request in both print and electronic formats, and translations.
- If figures and/or tables were requested, they may be adapted or used in part.
- Please print this page for your records and send a copy of it to your publisher/graduate school.
- Appropriate credit for the requested material should be given as follows:  
"Reprinted (adapted) with permission from (COMPLETE REFERENCE

CITATION). Copyright (YEAR) American Chemical Society." Insert appropriate information in place of the capitalized words.

One-time permission is granted only for the use specified in your request. No additional uses are granted (such as derivative works or other editions). For any other uses, please submit a new request.

# Curriculum Vitae

**Name:** James M. Stubbs

## Education

**Doctorate of Philosophy in Chemistry**, Western University

2014 – Present

Doctoral Thesis: *Developing Structure-Activity-Relationships (SARs) for Metal-Ligand-Cooperative (MLC) Complexes using  $P^{R_2}N^{R'_2}$  Ligands*

Supervisor: Professor Johanna M. Blacquiere

**Bachelor of Science, Honours Specialization in Chemistry**, Western University

2010 – 2014

Undergraduate Thesis: *The Development of Tunable Catalysts Incorporating Proton Shuttling for the Anti-Markovnikov Hydration of Alkynes*

Supervisor: Johanna M. Blacquiere

## Publications

1. K.M.K. Jackman, A.A. Fogh, J.M. Stubbs, J.M. Blacquiere\*. “Synthesis of Pd Phosphine-Imine Complexes and their Reactivity with Base”, *J. Organomet. Chem.*, **2019**, 880, 56.
2. J.M. Stubbs, D.E. Chapple, P.D. Boyle, J.M. Blacquiere.\* “Catalyst Pendent Amine Effects on the Cyclization of Alkynyl Amines”, *ChemCatChem*, **2018**, (DOI: 10.1002/cctc.201800713).
3. Z. Ding, J.M. Stubbs, S. Mittler. “Au-nanoparticles strip-loaded channel waveguide”, *Optimal Engineering*, **2018**, Au-nanoparticles strip-loaded channel waveguide, ID: 180864L.
4. K.M.K. Jackman, B.J. Bridge, E. Sauvé, C. Rowley, C. Zheng, J.M. Stubbs, P.D. Boyle, J.M. Blacquiere.\* “Agostic Stabilization of a Tri-Coordinate Pd(II)-Me Complex”, *Organometallics*, **2018**, submitted, ID: om-2018-00581d.
5. K.M.K. Jackman, A.A. Fogh, J.M. Stubbs, J.M. Blacquiere.\* “Synthesis of Pd Phosphine-Imine Complexes and their Reactivity with Base”, *J. Organomet. Chem.*, **2018**, submitted.
6. Z. Ding, J.M. Stubbs, D. McRae, J.M. Blacquiere, F. Lagugné-Labarthe, S. Mittler.\* “A Mass-Produced and Versatile Sensing System: Localized Surface Plasmon Resonance Excited by Individual Waveguide Modes”, *ACS Sensors*, **2018**, Accepted, DOI: 10.1021/acssensors.7b00736.
7. J.M. Stubbs, K.F. Firth, B.J. Bridge, K.J. Berger, R.J. Hazlehurst, P.D. Boyle, J.M. Blacquiere.\* “Phosphine-Imine and –Enamido Ligands for Acceptorless Dehydrogenation Catalysis”, *Dalton Trans.*, **2017**, 46, 647.

8. J.M. Stubbs, R.J. Hazlehurst, P.D. Boyle, J.M. Blacquiere.\* “Acceptorless Dehydrogenation of Amines with Ru(P<sup>R</sup><sub>2</sub>R'<sup>R</sup><sub>2</sub>) and Ru(dppp) Complexes”, *Organometallics*, **2017**, 36, 1692.
9. Z. Ding, J.M. Stubbs, S. Mittler.\* “Narrowing of Plasmon Resonance Peaks as an Ensemble Effect”, *J. Phys. Chem. Lett.* **2017**, Submitted.
10. T.J. Cuthbert, E. Evoy, J-P.J. Bow, R. Guterman, J.M. Stubbs, E.R. Gillies, P.J. Ragnogna\*, J.M. Blacquiere.\* “CapturePhos – A Phosphorus-Rich Polymer as a Homogeneous Catalyst Scavenger”, *Catal. Sci. Tech.*, **2017**, 2685.
11. J.M. Stubbs, J-P.J. Bow, R.J. Hazlehurst, J.M. Blacquiere.\* “Catalytic Cyclization and Competitive Deactivation with Ru(P<sup>R</sup><sub>2</sub>R'<sup>R</sup><sub>2</sub>) Complexes”, *Dalton Trans.*, **2016**, 45, 17100.

**Conferences** (OP – Oral Presentation, PP – Poster Presentation; Presenter)

- OP4: J.M. Stubbs, B.J. Bridge, E. El-Zouki, J.M. Blacquiere\*. ‘Metal-Ligand-Cooperative Dehydrogenation Catalysis: Investigating the Role of the Pendent Amine’, *21<sup>st</sup> International Symposium of Homogeneous Catalysis Pre-Conference*, Amsterdam, The Netherlands, July 2018.
- PP6: J.M. Stubbs, B.J. Bridge, E. El-Zouki, J.M. Blacquiere\*. ‘Metal-Ligand-Cooperative Dehydrogenation Catalysis: Investigating the Role of the Pendent Amine’, *21<sup>st</sup> International Symposium of Homogeneous Catalysis*, Amsterdam, The Netherlands, July 2018.
- OP3: J.M. Stubbs, D.E. Chapple, J.M. Blacquiere\*. ‘Reactivity of the Secondary Coordination Sphere: Structure Activity Relationship for Intramolecular Cyclization’, *50<sup>th</sup> Inorganic Discussion Weekend*, Toronto, ON, November 2017.
- OP2: J.M. Stubbs, B.J. Bridge, D.E. Chapple, J.M. Blacquiere\*. ‘Structure Performance Relationships of Ru(P<sup>R</sup><sub>2</sub>R'<sup>R</sup><sub>2</sub>) Cyclization Catalysts’, *100<sup>th</sup> Canadian Chemistry Conference and Exhibition*, Toronto, ON, June 2017.
- PP5: K. Jackman, A.A. Fogh, J.M. Stubbs, P.D. Boyle, J.M. Blacquiere\*. ‘Design of Ligands with Flexible and Dynamic Bond Coordination Modes’, *100<sup>th</sup> Canadian Chemistry Conference and Exhibition*, Toronto, ON, June 2017.
- PP4: J.M. Stubbs, J.M. Blacquiere\*. ‘Acceptorless Dehydrogenation of Amines by Cooperative [CpRu(P<sup>R</sup><sub>2</sub>N<sup>R</sup><sup>R</sup><sub>2</sub>)(MeCN)]<sup>+</sup> Complexes’, *The International Chemical Congress of Pacific Basin Societies*, Honolulu, HI, December 2015.
- OP1: J.M. Stubbs, J.M. Blacquiere\*. ‘Acceptorless Dehydrogenation of Amines by Cooperative [CpRu(P<sup>R</sup><sub>2</sub>N<sup>R</sup><sup>R</sup><sub>2</sub>)(MeCN)]<sup>+</sup> Complexes’, *98<sup>th</sup> Canadian Chemistry Conference and Exhibition*, Ottawa, ON, June 2015.
- PP3: J.M. Stubbs, J-P.J. Bow, and J.M. Blacquiere\*. ‘Investigations into the Cooperative Nature of [CpRu(P<sup>R</sup><sub>2</sub>N<sup>R</sup><sup>R</sup><sub>2</sub>)(MeCN)]<sup>+</sup> Complexes’, *Interdisciplinary Research Showcase*, London, ON, December 2014.
- PP2: J.M. Stubbs, J-P.J. Bow, and J.M. Blacquiere\*. ‘Investigations into the Cooperative Nature of [CpRu(P<sup>R</sup><sub>2</sub>N<sup>R</sup><sup>R</sup><sub>2</sub>)(MeCN)]<sup>+</sup> Complexes’, *Inorganic Discussion Weekend*, Montreal, QC, November 2014.

- PP1: J.M. Stubbs, J.M. Blacquiere\*. ‘Development of Proton Shuttling Catalysts’, *Southern Ontario Undergraduate Student Chemistry Conference*, Windsor, ON, March 2014.

### Awards and Scholarships

- CSC Travel Award 2018
- Dr. Joseph Soltys Graduate Award in Chemistry 2018
- Queen Elizabeth II Graduate Scholarship in Science and Technology 2017–2018
- Ontario Graduate Scholarship (awarded twice) 2014 – 2016
- Dean’s Honor List (average >80%) 2010 – 2014
- Laurene Paterson Scholarship (awarded twice) 2012 – 2014
- Caroline and Bradley 125<sup>th</sup> Alumni Scholarship 2013 – 2014
- Ray Leroi Allen Scholarship 2011 – 2012
- Entrance Scholarship (average >90%) 2010 – 2011

### Mentoring/Volunteering

#### **4491E and Volunteer Mentor**, Western University

2015 – Present

- Provide support and transfer laboratory techniques to three 4491E students and four volunteers

#### **Laboratory and Marking Teaching Assistant (Head TA 2017 for 2271A and 2281G)**, Western University

- Chemistry 2281G: Inorganic Chemistry of the Main Group Elements 2015 – 2017
- Chemistry 2271A: Structure and Bonding in Inorganic Chemistry 2014 – 2018
- Chem 1302B: Discovering Chemical Energetics 2018

#### **Inorganic Chemistry Exchange Program Conference Volunteer**, Western University Aug 2016

Assist in the organization of the event

#### **Outreach Program Volunteer**, Western University

2014 - 2018

- Provide a positive hands on laboratory experience for high school students and day camp children

#### **International Symposium of Homogenous Catalysis Volunteer**, Ottawa, Ontario July 2014

- Assist in the registration of the attendants
- Provide technical support to presenters

### Courses

9603S – Advanced NMR Spectroscopy II – 95%; 9541A – Crystallography I – 91%; 9651T – Organometallic Bond Activation – 90%; 9521S – Catalysis – 89%; 9823R – Heterocycles – 88%; 9531Q – Molecular Energy Conversion – 88%; 9503S – Advanced NMR Spectroscopy I – 84%; 9658Y – Seminar – 84%